Influence of mix parameters, and exposure solution and duration on chloride ingress, microstructure, and steel reinforcement corrosion in concrete exposed to chloride and composite chloride-sulfate environment

A thesis submitted in partial fulfillment of the requirements
for the award of

DOCTOR OF PHILOSOPHY

In

Civil Engineering

By

Arya Anuj Jee

(Roll No. 136104012)

Under the supervision of

Prof. Bulu Pradhan

Department of Civil Engineering

Indian Institute of Technology Guwahati

May 2020

Dedicated to

All members of my family, especially to my parents,

Jitendra Prasad Arya

(Father)

&

Prabhavati Devi

(Mother)

DEPARTMENT OF CIVIL ENGINEERING

INDIAN INSTITUTE OF TECHNOLOGY GUWAHATI

GUWAHATI - 781039, ASSAM, INDIA

Dr. Bulu Pradhan
Professor
Email: bulu@iitg.ac.in
Phone: +91-361-258-2425

CERTIFICATE

It is certified that the work contained in the thesis entitled "**Influence of mix parameters, and exposure solution and duration on chloride ingress, microstructure, and steel reinforcement corrosion in concrete exposed to chloride and composite chloride-sulfate environment**" submitted by **Mr. Arya Anuj Jee (Roll No. 136104012)** to the Indian Institute of Technology Guwahati for the award of the degree of **Doctor of Philosophy** has been carried out under my supervision in the Department of Civil Engineering, Indian Institute of Technology Guwahati. This work has not been submitted elsewhere for the award of any other degree or diploma.

Place: IIT Guwahati **(Dr. Bulu Pradhan)**

ACKNOWLEDGEMENT

Undertaking this PhD has been a truly life-changing experience for me, and it was not possible to complete this alone without the support and guidance of many people whom I am indebted to. I take this opportunity to extend my sincere gratitude and appreciation to all people who helped me directly or indirectly to make this journey possible.

First and foremost, I would like to extend my sincere gratitude to my supervisor *Prof. Bulu Pradhan* for his dedicated help, advice, inspiration, encouragement and continuous support throughout my research work. His enthusiasm, integral view on research and his accountability for providing high-quality work has made a deep impression on me. He is my mentor and a better advisor for my doctorate study beyond the imagination and I am delighted to be associated with a person like him.

Apart from my Supervisor, I will not forget to express the gratitude to the honorable members of my doctoral committee: *Prof. Arbind Kumar Singh* (Chairman), *Prof. Teiborlang Lyngdoh Ryntathiang* and *Prof. Mihir Kumar Purkait* for giving the encouragement and sharing insightful suggestions towards improving the quality of my research work from various perspectives. Their endless guidance is hard to forget throughout my life.

I also express my sincere thanks to the Head of the Department, *Prof. Chandan Mahanta* and all respected faculties of the Dep. of Civil Engineering. I appreciate the staff members of Structural Engineering/Infrastructural Engineering Laboratory of the Dept. of Civil Engineering: *Mr. Pranab Hazarika*, *Mr. Nripen Kalita*, and *Mr. Saurabh Kumar Mudoi* for the help, they provided whenever it was required. I wish to express my appreciation to *Mr. Om Prakash Prasad* for being there to help me during the preparation of test specimens. I also wish to express my gratitude to the Dep. of Physics and Central Instruments Facility, IIT Guwahati, for providing access to the various modern instruments, which makes this research work a bit easier. I would also like to take this opportunity to thanks all the other departments of IIT Guwahati, who have supported me directly or indirectly in various aspects. They all mean a lot to me.

I warmly thank to my colleague *Dr. Smrati Jain* for all her supports in a special way during my PhD journey. Especially, I would like to thanks: *Sathishraj Mani*, *Jyotish Kumar Das*, *Jnyanendra Kumar Prusty*, *Kunal Pradhan*, *Sai Rao Maradani*, and *Shehnaazdeep Kaur*

not only for the fun-time, we spent together but also for their support in my research work and my personal life in this journey, which is unforgettable for me. I would also like to thanks all my lab mates from Infrastructural Engineering Laboratory for their support in various manners.

In daily life of my PhD journey, I have been blessed with a family of seniors and juniors: *Dr. Shivshankar Kumar*, *Dr. Suchit Kumar Patel*, *Dr. Pawan Kumar*, *Dr. Awnish Kumar*, *Mr. Chandrabhanu Gupt*, *Mr. Pawan Kishor Sah*, *Mr. Rajan Singh*, *Mr. Prashant Kumar Jha*, *Mr. Shashikant Kumar*, and *Mr. Ravi Kumar*. I would like to thanks all of them for being with me, because of them I never felt far from home during this long journey.

In this precious moment of my life, I am grateful to my two lifelines 'my parents' and my family members: *Mr. Arya Prabhat Jee*, *Mr. Arya Prakash Jee*, *Ms. Vineeta Kumari* and *Ms. Sukanya Kumari*, for giving me lots of love, best wishes, moral support, encouragement and motivation to accomplish the personal goals.

Arya Anuj Jee

ABSTRACT

In reinforced concrete structures, concrete generally provides physical and chemical protection to the steel reinforcement during the service life. The reinforced concrete structures, located in coastal areas, and in the areas where the soil and groundwater are contaminated with chloride and sulfate salts, generally experience durability problems that result in deterioration of concrete. Among the durability problems, corrosion of steel reinforcement is the most serious one that is encountered in reinforced concrete structures around the world. The corrosion of steel reinforcement reduces the service life of reinforced concrete structures, and results in huge repair and maintenance costs. Chloride ions are considered to be the primary cause of reinforcing steel corrosion in concrete. The service life of reinforced concrete structures exposed to chloride environment includes two phases i.e. corrosion initiation period, and corrosion propagation period. The chloride penetration modelling based on Fick's second law of diffusion is a conventional approach to forecast the rebar corrosion in concrete caused by chloride ingress. The estimated chloride diffusion coefficient can be used for predicting the service life of reinforced concrete structures. In case of exposure to sulfate-bearing soil and ground water, and marine environment, the penetration of sulfate ions into the structures results in sulfate attack. The sulfate ions react with the hydrated cement phases, and result in the formation of expansive products leading to expansion and cracking of the concrete. In case of ingress of both chloride and sulfate ions concomitantly (from marine environment, and sulfate-bearing soil and groundwater), the reaction mechanism becomes more complex as a result of simultaneous reaction of both chloride and sulfate ions with the hydrated cement phases of concrete. Thus, the concomitant presence of both chloride and sulfate ions may influence the ingress of chloride ions, and chloride induced corrosion of steel reinforcement as well as sulfate attack in concrete.

The present research work focused on evaluating the influence of mix parameters (i.e. binder type, and w/b ratio), exposure solution, and exposure duration on chloride ingress, chloride binding, microstructure, and corrosion of steel reinforcement in concrete exposed to chloride and composite chloride-sulfate environment. For this purpose, prismatic reinforced concrete specimens with a centrally embedded reinforcing steel bar were prepared from different types of binder, and w/b ratio, and exposed to chloride and composite chloride-sulfate solutions of varying concentrations for different exposure periods. The chloride ingress in concrete was evaluated by determining the free chloride content profile, and apparent chloride diffusion coefficient. In addition, the chloride

binding in concrete was evaluated from the measured free and total chloride contents. The microstructure of concrete was analyzed by performing X-ray diffraction (XRD) analysis, field emission scanning electron microscope (FESEM) analysis, and thermo-gravimetry analysis (TGA). The corrosion behaviour of steel reinforcement in concrete was evaluated through corrosion parameters such as half-cell potential, and corrosion current density. The reinforced concrete specimen, and test setup used in the present research work were designed in such a way that all the parameters i.e. half-cell potential (E_0), corrosion current density (I_{corr}), apparent chloride diffusion coefficient (D), and rebar surface chloride concentration (C_{rs}) were determined from the same specimen. After obtaining these parameters, the empirical relationships were developed between corrosion current density (I_{corr}), and the parameters such as half-cell potential (E_0), apparent chloride diffusion coefficient (D), and rebar surface chloride concentration (C_{rs}) of concrete.

The concrete mixes were prepared from different types of binder such as ordinary Portland cement (OPC), OPC replaced with 20% fly ash (OPC+ 20% FA), and Portland pozzolana cement (PPC) at w/b ratios of 0.45, 0.50, and 0.55. Tempcore TMT (Thermomechanically treated) steel bar was used as the steel reinforcement. From each concrete mix, cube specimens of size 150 mm were prepared for determining the compressive strength of concrete at different curing ages. Similarly, from each concrete mix, prismatic reinforced concrete specimens of size 62 mm × 62 mm × 300 mm with a centrally embedded steel bar of diameter 12 mm were prepared for determining the corrosion parameters, chloride content, and apparent chloride diffusion coefficient of concrete. For exposure to different solutions, a plastic reservoir was attached on a longitudinal face of each prismatic specimen by epoxy coating along with epoxy coating on four vertical faces of the prismatic specimen to avoid any loss of moisture from the concrete. The prismatic specimens were exposed to chloride, and composite chloride-sulfate solutions. Sodium chloride (NaCl) of different concentrations i.e. 1%, 3%, and 5% was used in the preparation of chloride solutions. Similarly, NaCl concentrations of 1%, 3%, and 5%, and magnesium sulfate ($MgSO_4$), and sodium sulfate (Na_2SO_4) concentrations of 2%, and 4% each were used in the preparation of composite chloride-sulfate solutions i.e. NaCl with $MgSO_4$, and NaCl with Na_2SO_4. Thus, a total of fifteen exposure solutions i.e. three chloride solutions, and twelve composite chloride-sulfate solutions were used in the study. The prismatic specimens were exposed to these solutions with alternate wetting-drying cycles till the exposure period of 27 months. Half-cell potential measurement, and corrosion current density by linear polarization resistance (LPR) measurement were carried out on the prismatic specimens at

the start of wetting period of wetting-drying cycle at every 3-month interval of exposure till the exposure period of 27 months. At the end of exposure periods i.e. 9, 15, 21, and 27 months, the concrete powder samples were collected by drilling throughout the exposure surface of prismatic specimens at five depth intervals each of 5 mm i.e. 0-5 mm, 5-10 mm, 10-15 mm, 15-20 mm, and 20-25 mm from the exposure surface of concrete up to the level of embedded reinforcing steel bar. The collected concrete powder samples were used for determining the free chloride content, and total chloride content, and for carrying out the microstructure analysis (XRD analysis, FESEM analysis, and TGA) of concrete. After determining the free chloride content over different depth intervals from the exposure surface of concrete, the apparent chloride diffusion coefficient was estimated using Fick's second law of diffusion by keeping in view the convection zone observed in some cases. From the obtained XRD patterns, the weight percentages of compounds formed in concrete were estimated semi-quantitatively using the reference-intensity ratio (RIR) matrix-flushing method. The surface morphology of concrete powder samples collected at different depth intervals from the prismatic specimens were analyzed using the obtained FESEM images. From the obtained results of thermo-gravimetry analysis (TGA), the mass loss of concrete due to decomposition of various compounds over different temperature ranges were determined. Further, the calcium hydroxide content in concrete was estimated using Taylor's formula from the mass loss obtained from thermo-gravimetry analysis (TGA).

The results of compressive strength test indicated that the concrete made with OPC exhibited higher compressive strength as compared to that made with OPC + 20% FA followed by PPC at all w/b ratios and curing ages. However, the rate of increase in compressive strength with curing age was higher in PPC and OPC + 20% FA concrete as compared to that in OPC concrete. The results of free chloride content indicated the presence of convection zone near the exposure surface region of concrete, which was dependent on binder type, w/b ratio, exposure solution, and exposure duration. The presence of sulfate ions reduced the penetration of chloride ions into concrete exposed to composite chloride-sulfate solutions as compared to chloride solutions, and the free chloride content in concrete decreased with increase in concentration of $MgSO_4$ or Na_2SO_4 in the composite chloride-sulfate solutions. Further, the free chloride content was lower in the concrete exposed to composite solutions of NaCl + Na_2SO_4 as compared to composite solutions of NaCl + $MgSO_4$ at all depth intervals. Among binder type, the free chloride content was higher in PPC concrete at lower depth intervals (i.e. near the exposure surface)

as compared to OPC + 20% FA followed by OPC concrete whereas at higher depth intervals the free chloride content was higher in OPC concrete as compared to OPC + 20% FA followed by PPC concrete. Further, the concrete made with PPC exhibited higher resistance against chloride ingress as compared to OPC + 20% FA followed by OPC concrete. The estimated apparent chloride diffusion coefficient of concrete varied with the concentrations of chloride, and sulfate ions, and the cation type associated with sulfate ions in the exposure solution. The presence of sulfate ions reduced the apparent chloride diffusion coefficient of concrete exposed to composite chloride-sulfate solutions as compared to chloride solutions, and the chloride diffusion coefficient was mostly higher in the concrete exposed to composite solutions of NaCl with $MgSO_4$ as compared to composite solutions of NaCl with Na_2SO_4. Among binder type, the concrete made with OPC exhibited higher apparent chloride diffusion coefficient as compared to OPC + 20% FA followed by PPC. In addition, the apparent chloride diffusion coefficient was lower in the concrete made with lower w/b ratio as compared to higher w/b ratio. The presence of sulfate ions in the exposure solution altered the chloride binding in concrete during early, and later exposure periods. Among binder type, the concrete made with OPC exhibited higher chloride binding as compared to that made with OPC + 20% FA followed by PPC at all exposure periods.

The obtained XRD patterns indicated the formation of various compounds such as ettringite (E), calcium chloroaluminate (CCA), calcium hydroxide (CH), gypsum (G), thaumasite (T), and magnesium hydroxide (MH) in the concrete subjected to different exposure solutions. Similarly, the presence of quartz (Q), calcite (CC), and feldspar (F) in the concrete were also identified from the XRD patterns. The formations of these compounds as indicated by the results of XRD analysis varied with the depth from exposure surface of concrete, type of exposure solution, concentration of chloride and sulfate ions in the exposure solution, cation associated with sulfate ions, binder type, and w/b ratio. The variations in the formation of ettringite, calcium chloroaluminate, and calcium hydroxide, as indicated by the peak intensity and wt. % from XRD analysis, in the concrete exposed to chloride, and composite chloride-sulfate solutions were consistent with the variations in the obtained free chloride content of concrete. The formations of ettringite, calcium chloroaluminate, calcium hydroxide, gypsum, and magnesium hydroxide in the concrete as indicated by the XRD patterns were also confirmed from the obtained FESEM images. The formation of compacted microstructure due to production of more amount of C-S-H gel in OPC + 20% FA, and PPC concrete as compared to OPC concrete was evident from the obtained FESEM images. Further, the formation of M-S-H (magnesium silicate hydrate)

gel in the concrete exposed to composite solutions of NaCl with $MgSO_4$ was evident from the FESEM images. The mass loss of concrete associated with the decomposition of various compounds in different temperature ranges as observed from thermo-gravimetry analysis (TGA) varied with the depth interval from exposure surface, exposure solution, binder type, and w/b ratio. As observed from the results of TGA, the total mass loss was mostly higher in OPC concrete as compared to that in OPC + 20% FA, and PPC concrete in case of exposure to chloride and composite chloride-sulfate (for both cations i.e. Mg^{2+} and Na^{+}) solutions. Further, the variations in mass loss of concrete due to dehydration of calcium hydroxide, ettringite, calcium chloroaluminate, and gypsum were mostly consistent with the variations in the peak intensity and wt. % of these compounds obtained from XRD analysis.

The obtained results of corrosion monitoring of steel reinforcement in concrete indicated that the half-cell potential of steel reinforcement was more negative in case of exposure to chloride and composite chloride-sulfate solutions with higher concentration of NaCl as compared to the solutions with lower concentration of NaCl during the entire exposure period. The variation in corrosion potential of steel reinforcement was unsystematic among exposure solutions for OPC and OPC + 20% FA concrete during the early exposure period. However, during the later exposure period, the corrosion potential of steel reinforcement was more negative in case of exposure to NaCl solutions as compared to composite solutions of NaCl + Na_2SO_4 followed composite solutions of NaCl + $MgSO_4$ in OPC, and OPC + 20% FA concrete. In PPC concrete, the variation in corrosion potential was unsystematic among exposure solutions during the entire exposure period. Further, there was mostly unsystematic variation in corrosion potential of steel reinforcement with increase in concentration of $MgSO_4$ or Na_2SO_4 in the composite chloride-sulfate solutions. The corrosion potential values were more negative than -270 mV (SCE) in case of exposure to chloride solutions with higher concentrations of NaCl i.e. 3% and 5% in OPC and OPC + 20% FA concrete, and in case of exposure to composite chloride-sulfate solutions with higher concentrations of NaCl in only OPC concrete, during the later exposure period thereby indicating greater probability of occurrence of reinforcing steel corrosion in concrete. However, in PPC concrete, the corrosion potential values were less negative than -270 mV (SCE) irrespective of NaCl concentration in chloride and composite chloride-sulfate solutions during the entire exposure period, thereby indicating lower probability of occurrence of reinforcing steel corrosion in concrete.

The corrosion current density of steel reinforcement in concrete increased with increase in concentration of NaCl in chloride solution for all binders and w/b ratios during the entire exposure period. Between composite chloride-sulfate solutions, the corrosion current density was higher in the concrete exposed to composite solutions of NaCl + Na_2SO_4 as compared to composite solutions of NaCl + $MgSO_4$ for all binders, and w/b ratios during the entire exposure period. Among binder type, the concrete made with PPC exhibited higher corrosion current density during early exposure period whereas during later exposure period it showed lower corrosion current density as compared to OPC, and OPC + 20% FA concrete for exposure against chloride and composite chloride-sulfate solutions. While analyzing the effect of w/b ratio, it is observed that the variation in corrosion current density of steel reinforcement with w/b ratio was mostly unsystematic for all binders except the cases wherein, the corrosion current density increased with increase in w/b ratio for exposure to chloride solutions during the entire exposure period in OPC and OPC + 20% FA concrete, and for exposure to composite chloride-sulfate solutions during the later exposure period in OPC concrete. Overall, from the viewpoint of corrosion behaviour of steel reinforcement evaluated through half-cell potential, and corrosion current density, the concrete made with PPC showed better performance than OPC + 20% FA, and OPC concrete against exposure to chloride, and composite chloride-sulfate solutions. Similarly, the concrete made with lower w/b ratio exhibited better corrosion performance than that made with higher w/b ratio against exposure to chloride, and composite chloride-sulfate solutions.

The empirical relationships developed between corrosion current density (I_{corr}) and the parameters i.e. half-cell potential (E_0), apparent chloride diffusion coefficient (D), and rebar surface chloride concentration (C_{rs}) for OPC, and PPC concrete exposed to chloride and composite chloride-sulfate solutions predicted the corrosion current density of steel reinforcement for OPC + 20% FA concrete with greater accuracy, which was independent of the empirical model development. Further, the developed empirical relationship between corrosion current density (I_{corr}), and half-cell potential (E_0) predicted well the corrosion current density (I_{corr}) values reported in the literature for chloride exposure conditions.

TABLE OF CONTENTS

LIST OF FIGURES

LIST OF TABLES

LIST OF SYMBOLS AND ABBREVIATIONS

C_3A	Tricalcium aluminate
C-S-H	Calcium silicate hydrate
C_4AF	Tetracalcium aluminoferrite
C_3S	Tricalcium silicate
C_2S	Dicalcium silicate
M-S-H	Magnesium silicate hydrate
LPR	Linear polarization resistance
OPC	Ordinary Portland cement
PPC	Portland pozzolana cement
FA	Fly ash
XRF	X-ray fluorescence
MSA	Maximum size of aggregate
IS	Indian standards
TMT	Thermomechanically treated
EDX	Energy-dispersive X-ray
w/b	Water-to-binder
NC	NaCl
MS	$MgSO_4$
NS	Na_2SO_4
SCE	Saturated calomel electrode
I_{corr}	Corrosion current density
E_0	Half-cell potential (corrosion potential)
B	Stern-Geary constant
R_p	Polarization resistance of steel reinforcement
β_a	Anodic Tafel constant
β_c	Cathodic Tafel constant
C_f	Free chloride content
C_t	Total chloride content
D	Apparent chloride diffusion coefficient
C_s	Apparent surface chloride content
t	Exposure time
x	Depth from exposure surface

x_1	Depth of convection zone
XRD	X-ray diffraction
FESEM	Field emission scanning electron microscope
TGA	Thermo-gravimetry analysis
θ	Diffraction angle of X-rays
λ	Wave length of X-ray
PDF	Powder diffraction file
ICDD	International centre for diffraction data
DTG	Derivative thermo-gravimetry
RIR	Reference-intensity ratio
CH	Calcium hydroxide or Portlandite
E	Ettringite
CCA	Calcium chloroaluminate or Friedel's salt
G	Gypsum
Q	Quartz
CC	Calcium carbonate or Calcite
F	Feldspar
T	Thaumasite
MH	Magnesium hydroxide or Brucite
C_{rs}	Rebar surface chloride concentration

CHAPTER 1

INTRODUCTION

1.1. General

Concrete is the most widely used construction material because of its long-term durability properties, and versatile applications. Concrete generally provides both physical and chemical protection to the embedded steel reinforcement during the service life [1]. During the service life, the reinforced concrete structures are subjected to various durability problems that results in deterioration of concrete. The deterioration of concrete can be due to physical causes, chemical causes, or due to mechanical damages. The physical causes of deterioration include the effects such as cracking due to crystallization of salts in the pores of concrete, and exposure to extreme temperatures such as fire or frost action that influence the durability of concrete [2, 3]. The chemical causes of deterioration include the effects such as leaching of cement paste by acidic solutions, expansive reactions due to sulfate attack, alkali-aggregate reaction, and corrosion of embedded steel reinforcement in concrete [2, 3]. The mechanical damage of concrete is caused by the impact, abrasion, erosion, or cavitation [3]. Among the durability problems, the corrosion of reinforcing steel is the most serious one, which is encountered in reinforced concrete structures around the world that affects the service life of structures. The corrosion of steel reinforcement (i.e. rebar) in concrete occurs either due to carbonation or due to presence of chloride ions near the steel reinforcement. The presence of chloride ions near rebar level is the primary cause of steel reinforcement corrosion in concrete than that due to carbonation. Chloride ions can initiate the corrosion when its amount near the steel reinforcement reaches the threshold value. The occurrence of steel reinforcement corrosion reduces the service life of reinforced concrete structures, and results in huge repair and maintenance costs. In case of structures located in the coastal areas, and in the areas where the soil and ground water are contaminated with chloride salts, and in case of application of deicing salts on the structures, the penetration of chloride ions to the rebar level results in corrosion of steel reinforcement, and progressively leads to deterioration of reinforced concrete structures. Therefore, the study on chloride ingress in reinforced concrete is important from the viewpoint of estimating the service life along with the qualitative and quantitative information required for maintenance and rehabilitation of reinforced concrete structures located in aggressive environment [4]. Further, in case of exposure to sulfate-bearing soil and ground water, and marine environment, the penetration of sulfate ions into the concrete

structures results in sulfate attack. The sulfate ions react with the hydrated cement phases, and form expansive products that results in expansion and cracking of the concrete.

1.2. Durability issues in concrete

1.2.1. Chloride ingress

The sources of chloride in concrete can be categorized into two types namely internal and external. The internal sources of chloride ions are from concrete ingredients such as use of chloride contaminated mixing water, aggregates and chloride bearing admixtures in the preparation of concrete mixes. The external sources include the penetration of chloride ions into concrete during the service life from the external exposure environment. During the service life, the chloride ions penetrate into reinforced concrete structures from different sources such as seawater, contaminated groundwater, and application of deicing salts on the structures etc. The different processes through which, the chloride ions penetrate into concrete are absorption, capillary suction or diffusion [3, 5]. Among these processes, diffusion is considered to be the primary mechanism of transport of chloride ions into concrete from external exposure environment [5]. In case of exposure to external environment, the adsorption of chloride ions occurs on the concrete surface layers exposed to wetting-drying cycles [6]. Beyond the adsorption zone (also known as convection zone), the diffusion process is dominated, wherein a net flow of chloride ions occurs from higher concentration region to lower concentration region as result of mass transfer by random movement of free chloride ions in the pore solution [7, 8]. This results in increase of chloride concentration in concrete and subsequently near the surface of embedded steel bar. The prediction of corrosion initiation time of steel bar embedded in concrete structures is a challenging task. The corrosion initiation phase depends, from amongst many parameters, mainly on chloride ingress through the concrete matrix, environmental loading, and chloride threshold level, which is influenced by the physical and chemical properties of concrete [9-11]. The chloride penetration modelling based on Fick's second law of diffusion is a conventional approach to forecast the steel reinforcement corrosion in concrete caused by chloride ingress. The estimated chloride diffusion coefficient can be used for service life prediction of reinforced concrete structures. The value of chloride diffusion coefficient depends on various parameters such as mix quantities and microstructure of concrete, exposure solutions, period of exposure, environmental

conditions etc., and different models have been developed by various researchers to estimate the chloride diffusion coefficient as a function of various parameters [12-21].

1.2.1.1. Chloride binding

In concrete, the hydrated cement has the capability to bind the chloride ions as a result of chemical binding of chloride ions by hydrated C_3A, and by physical adsorption of chloride ions on the surface of C-S-H [22]. Chloride ions react chemically with hydrated cement phases and form Friedel's salt through two mechanisms. The first mechanism includes the reaction of residual C_3A with $Ca(OH)_2$ and water, resulting in the formation of metastable C_4AH_{13} ($4CaO \cdot Al_2O_3 \cdot 13H_2O$), which further forms Friedel's salt through ionic exchange between Cl^- and OH^- ions [23]. The reactions involved in the formation of Friedel's salt due to reaction with hydrated C_3A are as follows;

$$Ca(OH)_2 + 3CaO \cdot Al_2O_3 + 13H_2O \rightarrow 4CaO \cdot Al_2O_3 \cdot 13H_2O \quad (1.1)$$

$$2NaCl + 4CaO \cdot Al_2O_3 \cdot 13H_2O \rightarrow 3CaO \cdot Al_2O_3 \cdot CaCl_2 \cdot 10H_2O + 2NaOH + 2H_2O \quad (1.2)$$

The second mechanism involves the reaction of AFm (monosulfoaluminate: $3CaO \cdot Al_2O_3 \cdot CaSO_4 \cdot 12H_2O$) phase with chloride ions through ionic exchange process, which results in the formation of Friedel's salt [23]. The reaction involved in the formation of Friedel's salt due to reaction with AFm phase is as follows;

$$2NaCl + 3CaO \cdot Al_2O_3 \cdot CaSO_4 \cdot 12H_2O \rightarrow 3CaO \cdot Al_2O_3 \cdot CaCl_2 \cdot 10H_2O + Na_2SO_4 + 2H_2O \quad (1.3)$$

The physical binding takes place through the adsorption of chloride ions by calcium silicate hydrate (C-S-H) gel formed in concrete [22]. When the surface of hydration product (C-S-H gel) comes in contact with a polar solution such as water, they become electrically charged, which adsorbs the free chloride ions from the pore solution of concrete [22].

In cementitious materials, the binding of chloride ions depends on various parameters such as chloride concentration, composition of cement, hydroxyl ion concentration, cation type associated with chloride salts, types of supplementary cementitious materials, presence of sulfate ions, etc. [24]. A higher concentration of external chloride results in higher amount of chloride ions in the concrete pore solution and consequently higher extent of chloride binding. The higher content of C_3A and C_4AF in cement results in higher extent of chemical binding of chloride ions in concrete. Similarly, the higher content of C_3S and C_2S in cement

results in higher extent of physical binding due to production of more amount of C-S-H gel in concrete. The SO_3 content in cement leads to reduction in chloride binding as a result of formation of ettringite or monosulfate (due to reaction of sulfates with C_3A and C_4AF) especially at lower concentration of chloride ions. However, at higher chloride concentration, the negative effect on chloride binding reduces due to transformation of ettringite and monosulfate into Friedel's salt. The use of supplementary cementitious materials as part replacement of cement also affect the chloride binding due to their different chemical composition, and physical properties. The higher concentration of hydroxyl ions results in lower chloride binding. The pH of concrete depends on the concentration of hydroxyl ions in the pore solution that influence the chloride binding, as the increase in pH of concrete increases the solubility of Friedel's salt. The cation type associated with chloride ions has significant effect on solubility of Friedel's salt as well as on the accessibility of chloride ions to the adsorption sites on the C-S-H gel. The presence of sulfate ions along with chloride ions also influence the binding of chloride in concrete, as both the ions react with hydrated C_3A [24].

1.2.2. Corrosion of steel reinforcement

Corrosion is an electrochemical process, which involves the chemical reactions through gain and loss of electrons, and the electrical current due to flow of charges through a conductor [25]. The reactions involved in the corrosion of embedded steel bar in concrete are as follows [1];

$$Fe \rightarrow Fe^{++} + 2e^{-} \text{ (anodic reaction)} \quad (1.4)$$

$$4e^{-} + O_2 + 2H_2O \rightarrow 4(OH)^{-} \text{ (cathodic reaction)} \quad (1.5)$$

$$Fe^{++} + 2(OH)^{-} \rightarrow Fe(OH)_2 \text{ (ferrous hydroxide)} \quad (1.6)$$

$$4Fe(OH)_2 + 2H_2O + O_2 \rightarrow 4Fe(OH)_3 \text{ (ferric hydroxide)} \quad (1.7)$$

The schematic diagram of the electrochemical process of corrosion of steel reinforcement in concrete is shown in Figure 1.1.

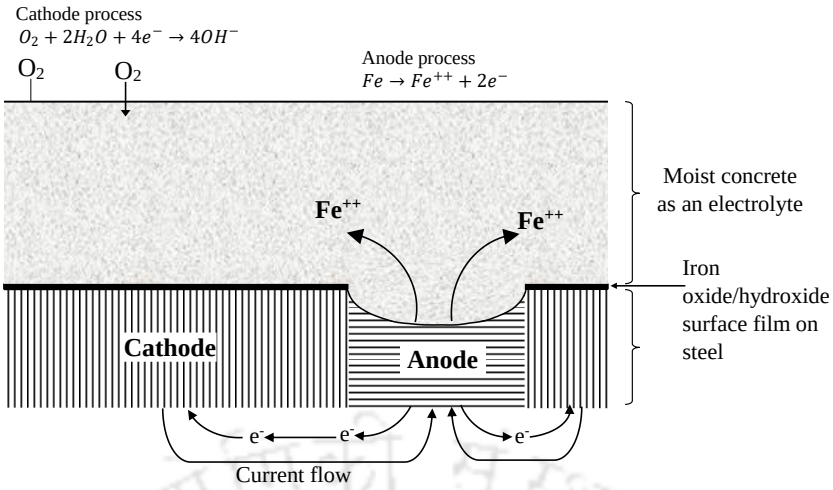

Figure 1.1 Schematic diagram of electrochemical process of corrosion of steel reinforcement in concrete [2]

In the highly alkaline environment of concrete, a passive layer (i.e. a thin layer of iron oxide) is formed over the surface of rebar, which protects it from corrosion. However, the presence of chloride ions near the steel reinforcement destroys the passive layer and initiates the corrosion. As stated earlier, in case of chloride exposure conditions (in marine environment, and in the areas where the soil and ground water are contaminated), the reinforced concrete structures deteriorate primarily because of chloride-induced rebar corrosion. In the presence of chloride ions, the electrochemical reactions of corrosion process are as follows [1];

$$Fe^{++} + 2Cl^- \rightarrow FeCl_2 \qquad (1.8)$$

$$FeCl_2 + 2H_2O \rightarrow Fe(OH)_2 + 2HCl \qquad (1.9)$$

The other reactions, and particularly the cathodic reactions are same as that in the absence of chloride ions, which are mentioned earlier [1]. The presence of chloride ions in the surrounding of steel-concrete interface forms hydrochloric acid (HCl) at the anodic site, which destroys the passive layer over the steel surface, and initiates the corrosion of steel reinforcement [1, 26]. It is important to mention here that both in the absence as well as in the presence of chloride ions, the electrochemical corrosion process proceeds only when water and oxygen are available [1]. The corrosion initiation of steel reinforcement embedded in concrete occurs mainly due to the presence of free chloride ions. The volume of corrosion products formed on steel surface is about 2 to 6 times higher than the volume of solid steel, which induces cracks in concrete matrix, reduces bond strength between the embedded steel bar and concrete, and consequently reduces the shear and flexural strength

of structural members that causes the deterioration of reinforced concrete structures [12, 27, 28].

The service life of reinforced concrete structures with respect to deterioration caused by corrosion of steel reinforcement (due to carbonation or chloride ions) involves two distinct phases as shown in Figure 1.2. The first phase is known as the initiation phase, which represents the time required for chloride ions to reach near the steel-concrete interface (for chloride induced corrosion), and initiate the corrosion activity. The amount of chloride ions required to initiate the corrosion of steel reinforcement is known as threshold chloride content. The value of threshold chloride content depends on various parameters such as cement type, concrete mix proportion, water/cement ratio (w/c ratio), C_3A content of cement, blended materials, chloride binding, steel type/steel surface condition, concentration of hydroxyl ions, temperature, relative humidity, and source of chloride ions [29]. The second phase is known as the propagation phase. During the propagation phase, the cross-sectional area of the steel reinforcement is gradually decreased, and the bond between the steel reinforcement and concrete is reduced. This in turn results in the reduction of effective cross-sectional area of concrete as a result of spalling of concrete cover [30]. The appearance of first corrosion crack in concrete is normally used to define the end of functional service life, and necessitates the rehabilitation of corroding structural elements [31].

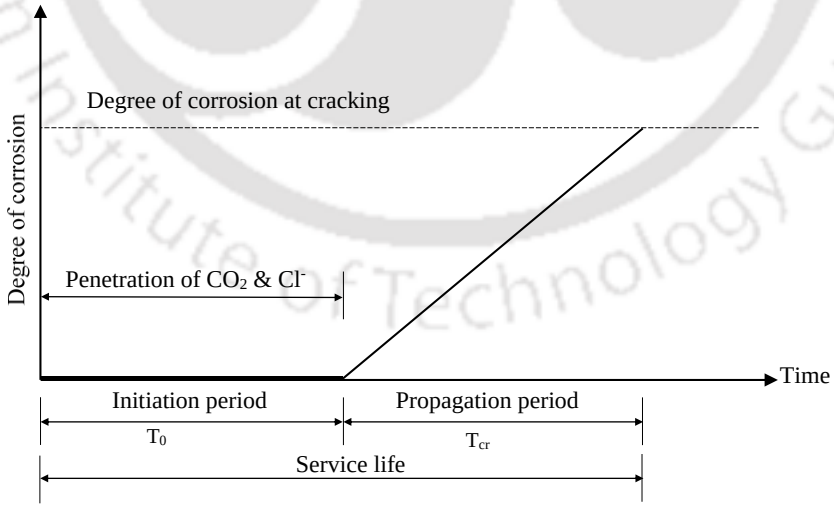

Figure 1.2 Service life of reinforced concrete structures [31]

1.2.3. Effect of sulfate ions on durability of concrete

The sulfate ions enter into the concrete structures from the exposure environment, and react with the hydrated cement phases of concrete, leading to the formation of expansive products, which induces cracks in the concrete matrix. In most of the soil and groundwater, the sulfate salts are present in the form of magnesium sulfate, sodium sulfate, potassium sulfate, calcium sulfate, and ammonium sulfate. In addition, the sulfate slats are also present in seawater. The sulfate attack of concrete is caused primarily through the formation of ettringite, and secondarily through the formation of gypsum [32]. The cation type associated with sulfate ions affects the mechanism of sulfate attack and, subsequently the deterioration process. When the sulfate ions enter into concrete, the monosulfate hydrate (alumina-containing hydrate) is converted to ettringite in the presence of calcium hydroxide according to the following chemical reaction [32].

$$3CaO \cdot Al_2O_3 \cdot CaSO_4 \cdot 12H_2O + 2Ca(OH)_2 + 2Me_xSO_4 \xrightarrow{H_2O} 3CaO \cdot Al_2O_3 \cdot 3CaSO_4 \cdot 32H_2O + 2Me(OH)_y \quad (1.10)$$

If $Me = Na$ or K, $x = 2$ and $y = 1$; if $Me = Mg$, $x = 1$ and $y = 2$.

If the cation type associated with sulfate ions is Na or K, then $Me(OH)_y$ is NaOH or KOH. Since, these compounds are highly soluble, the pH of concrete increases as a result of decalcification. On the other hand, if the cation type associated with sulfate ions is Mg, then in the presence of $MgSO_4$, $Ca(OH)_2$ gets converted into $Mg(OH)_2$, which decreases the pH of concrete [32]. Both sodium sulfate and magnesium sulfate attack result in the formation of expansive products in concrete. In addition, the magnesium sulfate attack results in reduction of strength of concrete [33] to a comparatively greater extent due to conversion C-S-H into M-S-H (magnesium silicate hydrate). The microcracks caused by the expansive products due to sulfate attack provide additional transport channels for the aggressive ions to enter into the concrete, and accelerate the deterioration process of concrete structures [34].

1.2.4. Effect of combined presence of chloride and sulfate ions on durability of concrete

In marine environment, and contaminated soil and groundwater, chloride and sulfate ions exist concomitantly, which may enter into the concrete and cause deterioration of reinforced concrete structures. In reinforced concrete structures, the presence of chloride

ions affects the durability by initiating the corrosion of embedded steel reinforcement whereas the presence of sulfate ion affects the durability by deteriorating the concrete matrix. In the concomitant presence of chloride and sulfate ions, the reaction mechanism becomes more complex due to simultaneous reaction of both the ions with the hydrated cement phases. The C_3A content of cement plays a major role in chloride binding, and sulfate attack. When both chloride and sulfate ions penetrate simultaneously into the concrete, the binding of both the ions with C_3A influences this multi-ion transport [33]. The ingress of chloride ions, and chloride induced corrosion of steel reinforcement in the concomitant presence of sulfate ions are affected by the cation type associated with sulfate ions, concentration of chloride and sulfate salts in the exposure solution, duration of exposure, types of binder, chloride binding behaviour of concrete, and exposure temperature [32, 33, 35-38]. Similarly, the concomitant presence of chloride ions with sulfate ions affects the sulfate attack by altering the extent of reactions of sulfate ions with the hydrated cement phases of concrete.

1.3. Corrosion monitoring techniques

Various electrochemical techniques are used for corrosion monitoring of steel reinforcement in concrete structures. These techniques seem to be easy in monitoring the corrosion of steel reinforcement through measurement of different corrosion parameters. However, the measured corrosion parameters of steel reinforcement may be affected by different factors such as high resistivity of concrete electrolyte, microenvironmental conditions at steel-concrete interface i.e. moisture content, availability of oxygen, chloride content, and pH value etc., and undefined testing area of the steel reinforcement [39]. In addition, the corrosion monitoring of steel reinforcement also necessitates the techniques to be non-destructive to maintain the integrity of the steel-concrete interface [39].

The corrosion parameters, which are generally determined for corrosion monitoring of steel reinforcement are half-cell potential (corrosion potential) and corrosion current density. Different non-destructive techniques are used for measuring these corrosion parameters. The different techniques used for determining the corrosion current density (corrosion rate) of steel reinforcement are polarization resistance techniques, Tafel plot technique, and gravimetric (mass loss) measurement etc. The polarization resistance techniques used for determining the corrosion current density of steel reinforcement are linear polarization resistance (LPR) measurement, AC impedance spectroscopy, galvanostatic pulse technique

etc. Among these polarization techniques, the LPR technique is most widely used for determining the instantaneous corrosion current density of steel reinforcement in concrete.

The half-cell potential measurement is a simple technique for measuring the corrosion potential of steel reinforcement in concrete, and is commonly used for diagnosing the corrosion risk of reinforced concrete structures [40]. The measured half-cell potential values provide information about the probability of occurrence of steel reinforcement corrosion in concrete. In reinforced concrete, the concrete acts as the electrolyte, and half-cell potential develops at the interface of embedded steel bar and concrete, which in turn depends on the concrete environment [39]. The potential measured across two electrodes is defined as the cell potential, which is the sum of two half-cell potentials [39]. It is impossible to determine either the absolute value or a single interface potential difference without completing the electrical circuit. A second electrode i.e. reference electrode needs to be introduced to complete the electrical circuit. In half-cell potential test, the potential difference across two electrodes i.e. rebar (working electrode), and standard reference electrode is measured. The test procedure for measuring the half-cell potential of steel reinforcement embedded in concrete is described in ASTM C876 [41]. The more negative value of half-cell potential signifies a higher tendency of the metal to lose its electrons [25], thereby indicating relatively higher probability of occurrence of reinforcing steel corrosion. As per ASTM C876 [41], the potential values more negative than -350 mV ($Cu/CuSO_4$ electrode)/ –270 mV (saturated calomel electrode) indicate greater than 90% probability of occurrence of steel reinforcement corrosion. Half-cell potential measurement is a widely used electrochemical technique because it is non-destructive, easy to perform, and provides information about the occurrence of steel reinforcement corrosion instantaneously. In addition, the half-cell potential data may assist in deciding whether to perform other corrosion monitoring techniques as well as can be used to validate the corrosion measurement obtained by other techniques. However, the factors such as moisture content, availability of oxygen, chloride content, positioning of reference electrode, electrical continuity, temperature etc. can significantly influence the half-cell potential data, which pose difficulty in interpreting the variations in measured potential values for evaluation of rebar corrosion [39]. The half-cell potential values can be more negative without the significant presence of corrosion, which may be attributed to the polarization phenomena induced by limited oxygen diffusion [42-44]. Thus, the potential values may sometimes not indicate the actual state of corrosion of rebar embedded in concrete.

The linear polarization resistance (LPR) technique is the most widely used non-destructive, relatively fast, and quantitative approach for measurement of corrosion rate of rebar in concrete. The LPR technique involves measuring the change in open-circuit potential (corrosion potential) of the short-circuited electrolytic cell by applying a small perturbation through an auxiliary electrode [25]. For a small perturbation about the open-circuit potential, a linear relationship is obtained between change in potential, and change in applied current per unit area of the steel bar. The ratio of change in potential to the change in applied current per unit area of the steel bar (i.e. the slope of linear relationship) gives the polarization resistance of the steel reinforcement [25]. The obtained polarization resistance of steel reinforcement is further used for determining the corrosion rate (expressed as corrosion current density) using the Stern-Geary equation. In this method, it is necessary to determine the area of steel bar over which the external perturbation is confined to eliminate the uncertainty in the obtained results. The obtained corrosion current density from linear polarization resistance technique indicates the instantaneous corrosion rate of steel reinforcement. The measured corrosion current density (corrosion rate) depends on various factors such as availability of oxygen, moisture content of concrete, and temperature. Thus, it is difficult to extrapolate the service life of reinforced concrete structures based on only one measurement of corrosion rate. Therefore, the measurement of corrosion rate needs to be carried out adequate number of times under different seasonal conditions to understand the variation in corrosion rate over a long period of time [25].

1.4. Novelty of the present research work

Study on chloride ingress and chloride induced corrosion of steel reinforcement in concrete in the presence of chloride ions and that in the concomitant presence of sulfate ions are essential from the viewpoint of evaluating the durability of reinforced concrete structures exposed to different exposure environment. In this regard, various research works have been carried out by the researchers in the literature to evaluate the effect of different mix parameters, and exposure conditions on chloride ingress, microstructure, and corrosion of steel reinforcement in concrete in the presence of chloride ions, however very few studies have been reported in the literature on microstructure and corrosion of steel reinforcement in concrete in the combined presence of chloride and sulfate ions along with the effect of cation type associated with the sulfate ions over a longer exposure period. In addition, the studies on variation in microstructure with depth interval from the exposure surface concrete exposed to chloride and composite chloride-sulfate solutions are scanty in the

literature. Further, it is also essential to establish the relationship between the corrosion parameters (such as corrosion current density) and the parameters related to chloride (such as apparent chloride diffusion coefficient, chloride content at rebar level etc.) to interpret the variations between these parameters in concrete in the presence of chloride ions, and that in the combined presence of chloride and sulfate ions. In the reported literature, very few studies have been carried out on the development of empirical relationships between the corrosion parameters and the parameters related to chloride obtained from the same concrete specimen exposed to chloride and composite chloride-sulfate solutions. Keeping these observations in view, the objectives of the present research work have been formulated to study the effect of mix parameters and exposure condition (exposure solution and exposure period) on chloride ingress, microstructure, and corrosion of steel reinforcement in concrete made from different types of binder and w/b ratio, and exposed to chloride and composite chloride-sulfate solutions of varying concentrations. In addition, an attempt has been made to establish the empirical relationships between corrosion current density and the parameters i.e. half-cell potential, apparent chloride diffusion coefficient, and free chloride content at rebar level obtained from the same concrete specimen exposed to chloride and composite chloride-sulfate solutions.

1.5. Organization of the thesis

The research work carried out in the present investigation has been organized in seven chapters as mentioned below.

- **Chapter 1** - Chapter 1 presents the introduction of the research area as well as the organization of the thesis.
- **Chapter 2** - In this chapter, the review of literature related to the present research work is described. The literature review on the effect of binder type, w/b ratio, and exposure condition on chloride ingress (chloride content profile, and chloride diffusion coefficient), chloride binding, and microstructure of concrete is presented. In addition, the review of literature on corrosion of steel reinforcement in concrete subjected to different exposure environment is also presented. Besides, the research gap in the literature followed by the need and objectives of the present research work are presented in Chapter 2.
- **Chapter 3** - In this chapter, the details of the experimental investigation are presented. The details of materials, mix proportion, preparation of test specimens,

exposure solutions, and different tests carried out on the test specimens are presented in this chapter.

- **Chapter 4** - In this chapter, the results of compressive strength of concrete made with different types of binder and w/b ratio are presented and discussed. Further, the results of free chloride content, estimated apparent chloride diffusion coefficient, and chloride binding in concrete are presented. The effects of depth from the exposure surface of concrete, exposure solution and duration, binder type, and w/b ratio on variations in free chloride content of concrete are analyzed and discussed. In addition, the effects of exposure solution, binder type, w/b ratio, and exposure duration on variations in apparent chloride diffusion coefficient, and chloride binding in concrete are also analyzed and discussed in this chapter.

- **Chapter 5** - In this chapter, the results of microstructure study (through XRD, FESEM, and TGA analyses) on concrete exposed to chloride and composite chloride-sulfate solutions are presented. The effects of depth from exposure surface of concrete, exposure solution, binder type, and w/b ratio on variations in microstructure of concrete are analyzed and discussed in this chapter.

- **Chapter 6** – In this chapter, the obtained results of half-cell potential, and corrosion current density of steel reinforcement in the prismatic reinforced concrete specimens exposed to chloride, and composite chloride-sulfate solutions for different exposure periods are presented. The variations in half-cell potential and corrosion current density of steel reinforcement with exposure solution, binder type, w/b ratio, and exposure duration are analyzed and discussed in this chapter. Further, the empirical relationships developed between the experimentally obtained corrosion current density (I_{corr}), and the parameters i.e. half-cell potential (E_0), apparent chloride diffusion coefficient (D), and rebar surface chloride concentration (C_{rs}) in concrete exposed to chloride and composite chloride-sulfate solutions are also presented and discussed in this chapter.

- **Chapter 7** – In this chapter, the conclusions obtained from the present research work are presented. In addition, the significance of research outcome from the present study, and the suggestions for further research work are also presented in this chapter.

CHAPTER 2

LITERATURE REVIEW

2.1. General

In this chapter, the research work carried out by various researchers in the literature on chloride ingress (chloride content profile and chloride diffusion coefficient) in concrete are presented wherein the effect of different parameters such as binder type, w/b ratio, and exposure condition (exposure solution, exposure duration, wetting-drying cycle etc.) on chloride ingress are discussed. In addition, the reported research work on chloride binding in concrete are presented and the effect of above parameters on variations in chloride binding are discussed. Further, the reported research work on the effect of binder type, w/b ratio, and exposure condition on variations in microstructure of concrete are described. Subsequently, the research work carried out by various researchers on corrosion of steel reinforcement in concrete subjected to different exposure environment are presented, and the effect of binder type, w/b ratio, and exposure condition on corrosion behaviour of steel reinforcement in concrete are discussed. Finally, the summary of literature review with the research gap in the literature followed by the need and objectives of the present research work are presented in this chapter.

2.2. Effect of different parameters on chloride ingress, chloride binding and microstructure of concrete

The research work carried out by various researchers describing the effect of mix parameters (binder type i.e. cement type and supplementary cementitious materials, and w/b ratio), and exposure condition (exposure solution, exposure duration, wetting-drying cycle etc.) on chloride ingress, and chloride binding in concrete are presented in this section. In addition, the reported research work on the variations in microstructure of concrete with respect to mix parameters, and exposure condition are also discussed in this section.

2.2.1. Effect of mix parameters

Gjorv and Vennesland [45] have studied the diffusion of chloride ions from seawater into mortar made with ordinary Portland cement (OPC), sulfate resisting Portland cement (SRPC), two Portland slag cements containing various percentages of slag (30% and 80%) and Portland trass cement (26% trass). Three w/c ratios (0.40, 0.50, and 0.60) and aggregate of maximum size 3 mm were used in the preparation of mortar specimens. Cylindrical specimens of size 2.5 cm in diameter and 10 cm in length, and another type with 10 cm in

diameter and 28 cm in length with a centrally embedded steel rod of diameter 10 mm were prepared for different tests. The mortar specimens were exposed to fresh circulating seawater for different durations. The cylindrical mortar specimens embedded with steel rod were subjected to different polarization levels, i.e. -780 mV, -1050 mV, and -1350 mV (SCE) for evaluating the effect of cathodic protection on chloride penetration. The parameters such as chloride penetration in terms of total chloride content, and pore size distribution using mercury porosimetry were determined. The results indicated that the chloride content increased with exposure time. The effect of w/c ratio on the chloride content was limited to surface layer for short exposure durations. However, for longer exposure durations and greater depths of penetration, cement type showed significant influence on depth of chloride penetration as compared to w/c ratio. Portland cements showed 2-5 times higher chloride penetration than the blended cements. Chloride penetration was not influenced by the C_3A content in the Portland cement while comparing between OPC and SRPC. The results indicated that diffusion of chloride ions into mortar was dependent on permeability, and chloride binding as well as on the ion exchange capacity of the system. The applied cathodic protection reduced the chloride penetration into mortar specimens and the reduction was higher in case of the applied potential with more negative value.

Midgley and Illston [46] have studied the penetration of chloride ions in hardened cement paste by chemical analysis, X-Ray diffraction and thermal analyses. Pore size distribution of hardened cement paste was also determined in this study. Cylindrical paste specimens were prepared from w/c ratios of 0.23, 0.47, and 0.71. After demoulding, the specimens were stored in saturated solution of $Ca(OH)_2$ for one month. After one month, the specimens were placed in solutions containing $Ca(OH)_2$ with 30 g/l of NaCl and 150 g/l of NaCl. The above mentioned tests were conducted on the hardened cement paste after six months and one year of storage in saturated solution of $Ca(OH)_2$ containing chloride ions. The test results indicated that the penetration of chloride ions did not affect the quantity of complex calcium aluminate salt hydrates or ettringite. However, calcium monochloroaluminate hydrate was formed in the hardened cement paste due to reaction of chloride ions with anhydrous tricalcium aluminate in unhydrated cement. The quantity of calcium monochloroaluminate hydrate formed was dependent on time and permeability but not on the concentration of chloride ion in the storage solution. However, the concentration of chloride ion in the hardened cement paste was dependent on the concentration of chloride

ion in the surrounding solution. The chloride penetration was more at higher w/c ratio. The penetration of chloride ions reduced the pore sizes in the hardened cement paste.

Byfors [47] has studied the influence of silica fume and fly ash on chloride diffusion and pH of cement paste. In this study, cylindrical cement paste specimens of diameter 19 mm and length 50 mm were prepared for chloride diffusion and pH measurement, and concrete cube specimens of size 15 cm were prepared for compressive strength test. Ordinary Portland cement (OPC) was partially replaced with silica fume (10% and 20%) and fly ash (15% and 40%), and w/b ratios of 0.40, 0.50 and 0.60 were used for preparation of paste specimens. After demoulding, the cement paste specimens were stored in saturated $Ca(OH)_2$ solution for 14 months. The rate of diffusion of chloride ions was determined using two-chamber method containing 1 M NaCl in saturated $Ca(OH)_2$ solution in one chamber and saturated $Ca(OH)_2$ solution in another chamber. The pore solution was pressed out from hardened cement paste under higher pressure and the pH value of the extracted pore solution was measured. The obtained results indicated that the addition of silica fume increased the strength while addition of fly ash reduced the strength at a constant w/b ratio. The chloride diffusion coefficient significantly reduced with increase in quantity of mineral admixture and with reduction in w/b ratio. The pH value reduced with the addition of mineral admixture in OPC, which has a negative effect on the resistance of cement paste against corrosion of steel reinforcement.

Arya et al. [48] have studied the factors influencing chloride binding in cement paste by considering the effect of cement type, cement extenders, water/cement ratio, hydration time, curing temperature, concentrtaion of chloride ion and associated cation type. For this purpose, cement pastes mixes were prepared using ordinary Portland cement (OPC), sulfate resistance Portland cement (SRPC) and OPC replaced with pulverized fuel ash (PFA), ground granulated blast furnace slag (GGBS), and silica fume (SF) with 15-35%, 70% and 15% respectively at three w/c ratios of 0.4, 0.5, and 0.6. This experimental investigation was conducted in two phases; Phase I was for internal chloride and Phase II was for external chloride. For the internal chloride, chloride was introduced into the paste mix by dissolving NaCl and $CaCl_2$ in mixing water, and cylindrical specimens of 45 mm diameter and 58 mm height were cast and cured at different curing temperatures for different periods. For the external chloride, the same paste mixes without chloride were cast into cylindrical specimens (size 49 mm diameter and 10 mm length) and cured for different periods and cut into 6 mm ± 0.5 mm disks and exposed to various concentrations of chloride solutions

($MgCl_2$, NaCl, and $CaCl_2$). At the end of the curing period (Phase I) or exposure period (Phase II), the pore solution was extracted from cement paste specimens using pore press method and pore solution was tested for chloride content using potentiometric titration. Based on the obtained results from experimental work, the authors concluded that the cement type, proportion and type of cement replacement materials, associated cation type and total chloride content are most important factors for chloride binding when chloride is introduced at the time of mixing. In addition, OPC with higher alkali content or replaced with PFA and GGBS increased the level of chloride binding however, the chloride binding reduced in case of SF replacement and SRPC cement. The binding of internal chloride increased with an increase in w/b ratio, curing temperature and age. In case of external chloride ingress, SRPC and OPC exhbited similar chloride binding behaviour and showed that C_3A content has little effect on chloride binding. The w/c ratio and curing time exhibited little effect on chloride binding in case of external exposure, but the binding increased with exposure time and chloride concentration. The paste exposed to calcium chloride and magnesium chloride exhibited higher chloride binding as compared to sodium chloride.

Thomas et al. [49] have studied the effect of ternary cementitious blends of Portland cement with silica fume and fly ash on durability property of concrete by incorporating the data from different research projects. Different properties such as compressive strength, diffusion coefficient (from electrical migration test), alkali-silica reactivity (ASR), and sulfate resistance (ASTM C 1012) were considerd in this study. Portland cement, silica fume, and fly ash with different CaO contents from low to high were used in the preparation of concrete mixes. The authors found that the use of silica fume increased the compressive strength at all ages while, low CaO fly ash contributed little strength at early ages and significantly enhanced the strength at later ages. Further, combination of silica fume and low CaO fly ash showed improved early age strength and long-term strength development. The solutions used for the chloride diffusion test were 1 M NaCl with 10.3 M NaOH solution as the catholyte and 0.3 M NaOH solution as the anolyte. The reduction in chloride diffusion coefficient with time was higher in case of low CaO fly ash as compared to silica fume concrete. However, ternary blends had benefit of low diffusivity at early ages and large reduction in diffusion coefficient with time. The low CaO fly ash exhibited less expansion due to ASR, and also higher sulfate resistance as compared to high CaO fly ash. However, the combinations of 3 to 5% silica fume with 20 to 30% high CaO fly ash showed

adequate performance in alkali-silica reaction (ASR) and sulfate expansion test. The authors suggested that most of these benefits are due to the reduction in permeability and ionic diffusivity of concrete.

Poon et al. [50] have studied to relate the mechanical and durability properties of high-performance metakaolin (MK) and silica fume (SF) concrete to their microstructure characteristics. Two types of concrete mix were prepared using w/b ratios of 0.30 and 0.50 with ASTM Type I Portland cement, MK (with replacement levels of 5%, 10%, and 20%) and SF (with replacement levels of 5% and 10%). The cube concrete specimens of side 100 mm and cylindrical specimens of 100 mm in diameter and 200 mm in height were prepared from concrete mixes. The compressive strength test on cube specimens, and chloride penetrability (ASTM C1202-94) and pore size distribution (through mercury intrusion porosimetry (MIP)) on cylindrical specimens were conducted after 3, 7, 28 and 90 days of curing. The results showed that the performance of MK concrete was superior to SF concrete in terms of the strength development of concrete. The MK replacement level of 10% performed best among different replacement levels in terms of maximum strength at all the testing ages. The increase in strength development in SF concrete was observed at the age of 7 days and thereafter. In chloride penetration test, both MK and SF concrete showed lower extent of total charges passed as compared to control concrete while, MK concrete performed similar to SF concrete. The MK blended concrete resulted in smaller pore diameters and lower porosity as compared to control concrete and SF blended concrete. The authors used the results of porosity and pore size distribution of cement pastes from an earlier research work [51] and correlated with concrete porosity measured from MIP test, and found strong dependence of the concrete transport properties on the microstructure properties of both cement matrix and matrix-aggregate interface. The authors also reported that the compressive strength of concrete correlates better with paste porosity than that with concrete porosity.

Chindaprasirt et al. [52] have studied the effect of fineness of fly ash on chloride penetration in concrete. Three concrete mix series i.e. low, normal and high-strength concrete mixes were prepared in the study. ASTM Type I Portland cement (PC), and ASTM class F lignite fly ash (FA) with three different fineness such as coarse fly ash (100% original fly ash), medium fly ash (45% fine portion of original fly ash) and fine fly ash (10% fine portion of original fly ash) were used in the preparation of concrete mixes. The compressive strength test of normal concrete was performed on cylindrical specimens of

100 mm diameter and 200 mm height at the ages of 7, 28, and 90 days. Different types of chloride penetration test such as rapid chloride permeability, full immersion test, and partial immersion test were performed on cylindrical specimens made with all three mixes of series i.e. low, normal and high-strength concrete. Immersion tests were performed using the solution containing 3% NaCl. From the obtained results, it was observed that the addition of fly ash reduced the water requirement for workability and reduction was more for low-strength concrete series. The compressive strength of fly ash concrete was reasonably higher than Portland cement concrete, and the use of finer fly ash reduced the water content and further enhanced the strength of concrete. The resistance against chloride ion penetration into concrete was considerably increased with the addition of fly ash and with increase in fineness of fly ash. The chloride penetration depth decreased with an increase in strength, i.e. high-strength concrete showed less chloride penetration depth. The effect of fly ash replacement and its fineness on resistance against chloride penetration in concrete was more dominant in low and normal-strength concrete as compared to high-strength concrete.

Song et al. [53] have reviewed various literatures to study the factors influencing chloride transport in concrete structures exposed to marine environment in terms of diffusion coefficient (D) and surface chloride content (C_s), and proposed a refined model for D and C_s by considering time-dependent chloride transport. The authors considered concrete mix proportion, exposure condition, curing condition and other physical properties as different factors, which influence the transport of chloride ions in concrete. In that published data, the measurement of chloride profile was in terms of total chloride content by acid-soluble extraction in nitric acid at different depth intervals. Fick's 2nd law was used for determining D and C_s of concrete. From the obtained results, it was observed that the value of D increased and C_s decreased with increase in w/b ratio. Addition of mineral admixture (pulverized fuel ash (PFA), ground granulated blast-furnace slag (GGBS) and silica fume (SF) reduced the value of D and increased the value of C_s due to refinement of concrete pores. For the concrete exposed to tidal and splash zones, the values of D and C_s were affected by height from sea level and as height from sea level increased, both D and C_s increased. Aerated curing was found to beneficial for OPC and SF concrete while, in case of PFA and GGBS concrete, water curing was found to beneficial in reducing C_s. However, curing duration did not affect the value of D significantly. The concrete exposed to marine environment near the Equator showed remarkably higher C_s as compared to high latitudes.

The increase in air voids resulted in increased D and decreased C_s. The time-dependency of both D and C_s were observed, where D decreased and C_s increased with time. Considering the initial build-up of chlorides on the surface of concrete, the authors proposed the refined model for time-dependent C_s in terms of logarithmic function. After comparison with linear and square root build-up models, the authors found that the refined model for time-dependent C_s considers a more realistic build-up of chlorides and chloride binding.

Shekarchi et al. [16] have conducted long-term chloride diffusion test on silica fume concrete, which was exposed to tidal zone exposure condition in the Persian Gulf. Four types of concrete mix were prepared with w/c ratios of 0.35, 0.40, 0.45, and 0.50 by using Portland cement (ASTM Type II) and silica fume (SF) with the replacement levels of 5%, 7.5%, 10%, and 12.5% by mass of cement. From these concrete mixes, cube specimens (side 150 mm) were prepared for compressive strength test and prismatic specimens (150 × 150 × 600 mm) were prepared for chloride diffusion test. After exposure, the sampling was done at the ages of 3, 9 and 36 months, and acid-soluble chloride was determined for chloride concentration profile and apparent chloride diffusion coefficient. Fick's 2nd law of diffusion equation was used for estimating the apparent chloride diffusion coefficient of concrete. The obtained results indicated that the rate of strength development in silica fume concrete was more as compared to that made without silica fume. However, the ultimate strength of silica fume concrete did not improve significantly. The replacement of cement with silica fume showed lower diffusion of chloride in concrete and the chloride diffusion coefficient can be expressed as an exponential function of silica fume content. The time-dependent chloride diffusion coefficient was expressed as a power function proposed by Mangat and Molloy [54] and it was found that the time-dependent reduction coefficient was lower in the concrete containing higher amount of silica fume.

Chung et al. [55] have studied the durability of concrete containing fly ash and silica fume exposed to combined mode of deterioration (freeze-thaw and chloride ion penetration). Freeze-thaw (F-T) and chloride ion diffusivity tests were performed on concrete specimens as per ASTM C 666 (rapid freezing in air and thawing in water) and ASTM C 1202 respectively. The concrete mixes were prepared at w/cm (water to cementitious material) ratios of 0.4, 0.5, and 0.6, and 2%, 4% and 6% of air were entrained in the concrete mixes. In this study, ASTM Type-1 Portland cement, ASTM class-F fly ash (20% by mass of binder) and condensed silica fume (10% by mass of binder) were used as cementitious

materials. The fatty acid-based air-entraining admixture and naphthalene sulfonate-based superplasticizer were used for achieving proper air content and workability. Cylinders of 100 mm diameter and 200 mm height were prepared for both tests. The concrete specimens were placed in F-T chamber after 28 days of curing and continued for 300 F-T cycles or until the relative dynamic modulus of elasticity of specimen reached 60% of its initial value. The relative dynamic modulus of elasticity (RDME) of each specimen was estimated using ultrasonic pulse velocity (UPV) values at the end of every 30 cycles. The durability factor was determined based on RDME. In addition, the specimens were further cured up to 91 days to investigate the effect of curing period on the chloride ion diffusivity of concrete. The chloride diffusion test was performed on concrete exposed to F-T cycles as well as on those not exposed to F-T cycles concrete. To determine the diffusivity of concrete, 3% NaCl and 0.3 N NaOH solutions were used on opposite sides of the specimen in the testing shell, and 30 V DC current was applied. The results indicated that the proper curing of concrete showed good durability factor irrespective of the amount of air content. The coefficient of chloride ion diffusivity increased after exposure to F-T cycles. Further, the coefficient of chloride ion diffusivity increased with increase in w/cm ratio and air content. The concrete containing silica fume showed lowest coefficient of chloride ion diffusivity and highest durability factor. In addition, the fly ash concrete made with low w/cm ratio and proper amount of entrained air, and cured properly also exhibited good resistance against chloride ion diffusion before and after F-T cycles.

Cheewaket et al. [56] have studied the effect of w/b ratio, exposure time and fly ash content on chloride binding capacity of concrete exposed to the marine environment for longer periods. For this purpose, the authors prepared control concrete mixes using Type I and Type V Portland cements and fly ash concrete mixes using Type I Portland cement replaced with class F fly ash at replacement levels of 15%, 25%, 35%, and 50% by weight of binder at w/b ratios of 0.65, 0.55, and 0.45. From each concrete mix, concrete cube specimens of size 200 mm were prepared and exposed to the tidal zone of a marine site located in the Gulf of Thailand after 28 days of water curing for different periods of 3, 4, 5 and 7 years. After the end of the different exposure periods, cylindrical core of 100 mm diameter was cut from each concrete cube specimen and the top 10 mm from the surface was ground into concrete powder sample. The concrete powder samples were used for determining the free (water-soluble method) and total (acid-soluble method) chloride contents. The obtained free and total chloride contents were used for determining the chloride binding capacity of

concrete specimens. Based on the results obtained from chloride binding capacity, the authors reported that the percentage of chloride binding capacity decreased with decrease in fly ash replacement level, and increase in exposure period of concrete as compared to total chloride content. Further, the authors also observed that w/b ratio had no noticeable effect on chloride binding capacity of concrete. The authors proposed a linear relationship between free and total chloride of concrete exposed to field marine exposure site.

Panesar et al. [57] have carried out an experimental study to investigate the effect of temperature (ranging from 22° C to -3° C) on chloride binding capacity and the apparent chloride diffusion coefficient of cement paste containing varying percentages of ground granulated blast furnace slag (GGBFS) as cement replacement. The authors have prepared cement paste specimens of size 10 × 20 × 2.5 mm using Type 10 OPC cement and varying percentages (0%, 25%, 50%, and 60%) of GGBFS as cement replacement at a w/b ratio of 0.31. The specimens were demoulded after 1 day and cured in lime-saturated water for 13 days followed by air curing for 14 days in the presence of soda lime. At the end of 28 days, the samples were conditioned for 2 weeks in a desiccator containing saturated lithium chloride, silica gel, and soda lime. After that, the samples weighing approximately 2.5 gm were stored in approximately 5 ml NaCl solution of five initial concentrations such as 0.1, 0.5, 0.75, 1, and 3 M and the equilibrium was reached after approximately 55 days of storage in NaCl solution. The chloride-binding isotherms were measured at temperatures of -3°C, 5°C, 13°C and 22°C. The authors used the equilibrium approach developed by Tang and Nilsson [58] to establish the chloride-binding isotherms. The equilibrious free chloride concentration of cement paste specimens was determined by potentionmetric titration using a 0.01 M $AgNO_3$ electrode. From the obtained results, the authors reported the chloride binding capacity as a function of exposure temperature was in the order of 22°C > -3°C > 13°C > 5°C. The authors observed a direct proportionality between chloride binding capacity and exposure temperature for the temperature range of 5°C to 22°C. A decrease in the exposure temperature from 22°C to 13°C or 22°C to 5°C or 22°C to -3°C had a greater effect on chloride binding capacity as compared to GGBFS replacement level at low (0.5 M) and higher (1 and 3 M) free chloride concentrations. The chloride binding capacity as a function of percentage of GGBFS as cement replacement was in the order: 60% > 50% > 25% > 0%. The authors reported that the ratio of apparent diffusion coefficient to effective diffusion coefficient was not influenced by the GGBFS replacement level at temperatures of -3°C, and 22°C whereas at temperatures of 5°C, and 13°C, the ratio

of apparent diffusion coefficient to effective diffusion coefficient decreased with increase in GGBFS replacement level.

Zhang et al. [59] have studied the influence of fly ash replacement level and repeated loading on chloride diffusion coefficient of concrete. The concrete mixes were prepared using a constant w/b ratio of 0.35 with ordinary Portland cement (OPC 42.5) and fly ash (FA) with replacement levels of 20%, 30%, and 40% by total mass of binder. Cylindrical specimens (of size 95 mm diameter and 300 mm height) were prepared and cured for 28 days in an alkaline solution to ensure the saturation of specimens and to avoid leaching phenomena. The compressive strength test (at 28 days) and repeated loading test (for elastic modulus of concrete) were performed on the cylindrical specimens. A disk of 95 mm diameter and 10 mm length was cut from loaded and nonloaded cylindrical specimens for chloride migration test using migration cell having upstream chamber (that contains 1.5 l of 0.5 mol/l NaCl and 0.3 mol/l NaOH) and downstream chamber (that contains 0.6 l of 0.3 mol/l NaOH dissolved in distilled water) by applying 12 V voltage between two chambers. The diffusion coefficient was determined using Nernst-Planck equation. Further, the impacts of fly ash and repeated loading on the service life of concrete were predicted using Life-365 model. The results indicated that the replacement of cement with fly ash resulted in lower compressive strength and higher diffusion coefficient as compared to OPC concrete mixes at the age of 28 days and these effects increased with increase in fly ash replacement. The results also showed that repeated loading increased the diffusion coefficient and decreased the service life of all concrete mixes. The addition of fly ash in concrete exposed to chloride environment increased the service life as predicted from Life-365 model, however the enhancement of service life was not significant in the concrete prepared with 40% fly ash replacement level. The authors have concluded that the addition of fly ash and the application of service loading should be considered in combination with environmental conditions and material proportions to obtain a rational service life prediction.

Radlinski and Olek [60] have studied the synergistic effect of ternary cementitious systems containing ordinary Portland cement (ASTM C 150 Type I), class C fly ash (FA) and silica fume (SF). The paste and mortar mixes were prepared using four types of binder systems such as plain cement mixture (OPC), binary mixture with 20% FA (20FA), binary mixture with 5% SF (5SF) and ternary mixture with 20% FA and 5% SF (20FA/5SF) at constant water-to-cementitious materials ratio (w/cm) of 0.41. The authors have prepared

paste specimens (cubes of size 51 mm) for compressive strength test (at the ages of 0.5, 1, 3, 7, 28 and 180 days), isothermal calorimetry and thermogravimetric analysis whereas, mortar specimens (of size 51 mm diameter and 102 mm height) for rapid chloride permeability (at the ages of 7, 28 and 180 days) and sorptivity tests (at the ages of 7, 28 and 180 days). The curing procedure adopted was 0-7 days of moist curing at 23°C followed by 7-56 days of moist curing at 38°C by assuming that the specimens had reached a maturity level equivalent to at least 180 days of continuous curing at 23°C. The test results indicated that in the ternary mixture i.e. 20FA/5SF, the synergistic effect was mostly observed at later ages (7 days and onward), which resulted in increase in compressive strength and resistance to chloride ion penetration, and reduction in rate of water absorption as compared to binary mixes (i.e. 20FA and 5SF). The synergy observed for the ternary mix was attributed to both chemical and physical effects. The chemical effect was in the form of an increased amount of hydration products whereas, the physical effect was a result of smaller initial inter-particle spacing resulting from lower specific gravity of both fly ash and silica fume. The authors have finally concluded that application of ternary cementitious systems was beneficial as compared to the binary cementitious systems.

Chidiac et al. [61] have studied the effect of chloride-binder interactions on the physical pore structure of concrete containing ground granulated blast furnace slag (GGBFS). Cylindrical concrete specimens of size 100 mm in diameter and 200 mm in height were prepared using CSA type 10 OPC cement and GGBFS replacement levels of 0, 25, 40 and 60 % for pore structure characterization test. The pore size distribution of concrete was evaluated using a mercury intrusion porosimeter with a maximum pressure of 207 MPa. In addition, two sets of cement paste samples were prepared. The first set of paste samples were prepared using CSA type 10 OPC cement and up to 60 % GGBFS (0, 25, 50 and 60%) as cement replacement. The second set of cement paste samples were prepared with Taiheiyo cement and Taiheiyo cement with 40% GGBFS. The cement paste samples were used for establishing chloride binding isotherms, scanning electron microscopy (SEM) and backscattered electron (BSE) microscopy analysis. The chloride binding isotherms were established using the equilibrium method developed by Tang and Nilsson [58] using different concentrations of NaCl ranging from 0.1 M to 3 M. To determine the chemical binding contribution, the quantity of Friedel's salt present in the samples was determined using differential scanning calorimetry (DSC). The physical binding capacity was determined as a difference between total binding capacity obtained from the chloride

binding isotherms, and chemical binding capacity. From the obtained results, the authors reported that for chloride concentration up to 0.5 M, the physically and chemically bound chloride contribute equally to total bound chloride for mixtures containing 0 and 40% GGBFS. However, at chloride concentrations greater than 0.5 M and less than 1 M, the total bound chloride is predominantly chemically bound chloride for the mixture containing 40% GGBFS. The authors observed that the differences in concrete microstructure are not linearly dependent on GGBFS content, but are influenced conjointly by the total bound chloride content, percentage of chemically bound chlorides, and the pore size distribution of the concrete.

Uysal and Akyuncu [62] have studied the effect of partial replacement of cement with class F and class C fly ash on mechanical and durability properties of concrete. The concrete mixes were prepared using Portland cement, class C fly ash and class F fly ash. Three different cement contents (260 kg/m^3, 320 kg/m^3 and 400 kg/m^3), two different ratios (10% and 17%) of reduced cement from the control concrete and three different ratios (depending on cement reduction ratio) of fly ash were used in the preparation of concrete mixes. In total 39 series of concrete mixes (36 containing class C and class F fly ash, and 3 control series) were prepared for the compressive strength test. After that, out of 36, the mixes that have similar 28 days compressive strength to control mixes were further used for durability tests (i.e. rapid chloride ion permeability, sorptivity and freezing-thawing resistance tests). For compressive strength test, concrete cube specimens of size 150 mm were prepared and tested at the ages of 28 and 90 days. For durability test, different specimens such as cylindrical specimens of size 100 mm diameter and 200 mm height (for rapid chloride ion permeability as per ASTM C 1202-97), prismatic specimens of size 70 × 70 × 280 mm (for freezing-thawing cycle test) and cubes of size 100 mm (for sorptivity test as per ASTM C1585) were prepared. Freezing-thawing test was done as per ASTM C 666 procedure 'B'. The resistance to freezing-thawing cycling was determined in terms of change in mass and ultrasonic pulse velocity after completion of 300 freezing-thawing cycles. The flexural test was also performed on the prismatic specimens at the end of freezing-thawing cycles and deterioration of concrete specimens was determined in terms of loss of flexural strength. The obtained results indicated that the class C fly ash concrete mixes showed higher compressive strength than class F fly ash concrete mixes. The chloride ion permeability and sorptivity decreased with increase in fly ash (both class C and class F) content. Further, the rate of weight loss of concrete increased with increase in replacement level of cement

with fly ash and with increase in cement content. In addition, the control concrete mixes showed lower weight loss values as compared to the concrete mixes containing class C and class F fly ash. Freezing-thawing cycle significantly reduced the ultrasonic pulse velocity in all concrete mixes. The incorporation of fly ash in the concrete mixes resulted reduction in flexural strength loss as compared to the mixes containing only Portland cement.

Simcic et al. [63] have studied the chloride ion penetration in fly ash concrete subjected to alternate wetting-drying cycles in simulated tidal zone. Five concrete mixes were prepared at a constant water-to-binder ratio of 0.45 by using Portland cement (PC) type CEM I 42.5R (EN 197-1) and two types of fly ash namely siliceous fly ash (FA I) and calcareous fly ash (FA II) at replacement levels of 0%, 20% and 50% by weight of binder. Five replicate cylindrical specimens of size 230 mm diameter and 70 mm thickness from each concrete mixture were prepared for cyclic immersion and drying method. Similarly, six replicate cylindrical specimens of size 100 mm in diameter and 50 mm thickness were prepared from each concrete mixture for non-steady state migration (NSSM) test. For determining compressive strength, six replicate concrete cube specimens of size 150 mm from each concrete mixture were prepared and tested after 7, 28 and 90 days of curing. The cyclic immersion and drying test on concrete specimens were performed in a 10% NaCl solution with cyclically alternate wetting (immersion in the solution during one third of the time) and drying (exposed to air for two thirds of the time) condition by maintaining one cyclic rotation per hour. After exposure of 21, 42, 84, 105 and 126 days in wetting-drying cycles, water-soluble and total-soluble chloride profiles were determined by potentiometric titration on 10 successive layers of freshly split section with each layer of 2 mm thickness obtained from cylindrical specimens of size 230 mm diameter and 70 mm thickness. The porosity of concrete specimens was determined after 84 and 126 days of alternate wetting-drying cycles and also on the specimens removed from cube tested for compressive strength. For NSSM test, chloride ions were migrated into the concrete specimens from a catholyte solution of 10% NaCl and anolyte solution of 0.3 N NaOH were used. Afterward, the chloride penetration depth was measured visually by colour change on split half sprayed sample with 0.1 M silver nitrate, induced by the precipitation of white silver chloride. Based on the results obtained from different tests, the authors concluded that the fly ash concrete (at replacement levels of 20% and 50 % by weight of binder) exhibited lower chloride penetration depths as compared to control concrete (at 0% replacement level of PC) due to lower effective porosity in fly ash concrete. The authors also concluded that, not only the

porosity but also the chemical composition of the fly ash plays a key role on chloride diffusion in concrete. The siliceous fly ash concrete (with lower CaO content) showed better resistance to chloride penetration up to 90 days than the calcareous fly ash concrete (with higher CaO content). However, after 126 days, calcareous fly ash concrete showed better chloride resistance characteristics than siliceous fly ash concrete due to slower pozzolanic reactivity of calcareous fly ash concrete upto 90 days of hydration. The trend of decreasing chloride diffusion values for all concrete specimens was in good agreement with the results of the cyclic immersion and drying tests, and that of non-steady state migration test.

Tadayon et al. [64] have investigated the effect of water-to-binder (w/b) ratio (0.35, 0.40, 0.45 and 0.50) in plain concrete specimens made with Type II Portland cement, and the effect of different pozzolans (5% silica fume, 5% metakaolin and 10% natural zeolite by weight of binder) at a constant w/b ratio of 0.40, on chloride ion penetration in concrete under laboratory and tidal in-situ exposure conditions. The plain concrete specimens were prepared with Type II Portland cement and different pozzolans (5% silica fume, 5% metakaolin and 10% natural zeolite by weight of binder). The cube specimens of size 150 mm were prepared for 28 days compressive strength and laboratory chloride ingress test. Prismatic specimens of size 600 × 150 × 150 mm were prepared for field exposure in tidal conditions. The acid-soluble chloride concentration profiles of powdered samples from concrete specimens were determined at different depth intervals after 3 months of laboratory submerged exposure and after 3, 9, 27 and 50 months of exposure in the field tidal zone. The chloride diffusion coefficient and surface chloride content were estimated using Fick's 2nd law of diffusion. From the obtained results, the authors reported that compressive strength improved with incorporation of all three pozzolans with natural zeolite giving slightly better performance than silica fume and metakoalin in the concrete. In addition, the incorporation of pozzolans in concrete was much more significant and efficient than reducing the w/b ratio for the same concrete in terms of durability performance and enhancing the mechanical properties. The chloride diffusion coefficient and surface chloride concentration of all the mixes became close to each other after long exposure time. Further, no improvement i.e. no decrease in chloride diffusion coefficient was observed after 27-50 months of exposure. However, surface chloride concentration increased with time. The performance of 5 % silica fume and 5% metakaolin by weight of

binder in terms of chloride diffusion coefficients over time was slightly better than 10% natural zeolite as Portland cement replacement.

Gao et al. [65] have carried out an experimental study to evaluate the influence of pore solution on chloride diffusion in concrete made with supplementary cementing materials. For this purpose, concrete, mortar, and paste specimens were prepared using Portland cement and Portland cement replaced with fly ash, granulated blast furnace slag and ground limestone at different w/b ratios. Concrete and mortar specimens were used for chloride diffusion test (Rapid chloride migration test (RCM) as per Standard NT Build 49) and electrical resistivity measurement). The paste specimens were used for extraction of simulated concrete pore solution (SCPS), and electrical conductivity of the SCPS was measured by a conductivity meter. The water absorption of concrete specimens was also measured as per ASTM C1585. Based on the results obtained from different tests, the authors reported that the electrical conductivity decreased with an increase in the amount of granulated blast furnace slag and fly ash, and more noticeable in fly ash compared to granulated blast furnace slag. With an increase in the amount of supplementary cementing materials, the electrical resistivity increased and the chloride diffusion coefficient decreased for both mortar and concrete specimens. Based on the relationship between the electrical resistivity and chloride diffusion coefficient, the authors modified the chloride diffusion coefficients of mortar and concrete specimens and found an almost identical relationship in the case of mortar specimens and higher than the initially measured chloride diffusion coefficient in case of concrete specimens. The relative water absorption, relative water absorption rate, and relative chloride diffusion coefficient decreased with an increase in proportion of supplementary cementing materials. The authors concluded that to evaluate the permeability of concrete, the modified chloride diffusion coefficient was a more general parameter as compared to the initially measured chloride diffusion coefficient by the RCM test since the influence of electrical conductivity of pore solution can be eliminated using the modified technique.

Liu et al. [66] have experimentally investigated the chloride transport property and microstructure of concrete with/without fly ash under atmospheric chloride environment. The concrete mixes were prepared at three w/c ratios of 0.53, 0.47 and 0.38 using ordinary Portland cement (OPC) and class F fly ash (15% and 30% by weight of total binder) as partial replacement of OPC. The authors have prepared concrete cubes of size 100 mm from each mix and cured for 56 days. After curing, five surfaces of the cube specimens

were sealed with epoxy resin to facilitate one-dimensional ingress of chloride ions. To simulate the marine atmospheric environment, the concrete cubes were subjected to salt spray test for a period of 28 days using 5% NaCl solution. The salt spray test was carried out by using cyclic drying-wetting action that consisted of 10 h of chloride aerosol spraying and 14 h of drying. Concrete powder samples were obtained by grinding layer-by-layer from the exposed surface at an interval of 1 mm up to the depth of 10 mm followed by 2 mm interval up to the depth 30 mm to determine free and total chloride concentrations (as per AASHTO T260-97). The pore size distribution and morphological surface of concrete subjected to chloride exposure were studied by Mercury intrusion porosimetry (MIP) test and scanning electron microscopy (SEM) analysis respectively. The chloride concentrations were used for estimating the chloride binding capacity and chloride diffusion coefficient (using Fick's 2nd law of diffusion equation) of concrete. The test results showed that in marine environment, a build-up of chloride ion content occurred at the convection region of concrete due to the effect of capillary suction and water evaporation. Further, the authors have observed a linear relationship between free and total chloride in concrete (with/without fly ash) subjected to chloride aerosol ingress. The w/c ratio and fly ash content had significant impact on chloride binding capacity and chloride diffusion coefficient of concrete. The chloride binding capacity and chloride diffusion coefficient increased with an increase in w/c ratio in the concrete mixes. The addition of fly ash in concrete decreased the chloride diffusion coefficient and increased the chloride binding capacity of concrete exposed to chloride aerosol ingress. Fly ash addition reduced the proportion of large capillary pores while increased the proportion of medium capillary pores in concrete.

Zhang et al. [67] have studied the effect of w/b ratio, admixtures and exposure time on age reduction factor of apparent diffusion coefficient and instantaneous diffusion coefficient of concrete exposed to marine tidal environment. In total, nine concrete mixes were prepared that included five concrete mixes from Portland cement (P.C 32.5) at different w/b ratios such as 0.40, 0.45, 0.50, 0.55, and 0.60 and four concrete mixes prepared by admixing Portland cement with different admixtures namely chopped basalt fiber, silica fume, and grade I fly ash at a w/b ratio of 0.50. Cylindrical specimens (size: 100 mm diameter and 50 mm height) and cube specimens (size: 150 mm) were prepared for chloride diffusion test and compressive strength test respectively. For chloride diffusion test, epoxy coating was applied (except for one circular surface) before exposing to natural tidal environment up to

600 days. The free chloride concentration of concrete powder samples collected from different depths were measured at different exposure times i.e. 60, 120, 240, 360, 480 and 600 days. The apparent chloride diffusion coefficient was calculated using Fick's 2nd law of diffusion. The time dependency of apparent chloride diffusion coefficient was represented by power function. Further, the analytical method of instantaneous diffusion coefficient was studied considering the time dependency of apparent chloride diffusion coefficient in concrete. From the obtained results, the authors have observed that there was a convection zone appeared in the concrete after 120 days of exposure in marine tidal environment. The addition of mineral admixtures in concrete reduced the chloride concentration in concrete mixes and the concrete admixed with silica fume and fly ash showed best results among all the concrete mixes. The authors also observed that for the same exposure time, the instantaneous chloride diffusion coefficient was smaller than apparent chloride diffusion coefficient. However, the difference between instantaneous chloride diffusion coefficient and apparent chloride diffusion coefficient decreased with increase in w/b ratio. The chloride diffusion coefficient and age reduction factor of ordinary concrete tend to be stable at 360 days of exposure time.

Panesar and Ching [68] have studied the coupled effect of low temperature on chloride binding capacity, ion-binder interactions and the effect on service life estimate. The cylindrical cement paste specimens of 50 mm diameter and 100 mm height were prepared using general use cement (GU) along with supplementary cementitious materials such as 40% of ground granulated blast furnace slag (GGBFS), 10% of metakaolin (MK), and 10% of silica fume (SF) and cured for 56 days at 23±2 ºC. After completion of curing, the cylindrical paste specimens were broken into smaller pieces of particle size between 0.25 mm and 2.0 mm. The chloride binding capacity was determined by equilibrium method based on Tang and Nilsson method [58]. For this purpose, chloride concentrations of 0.1 M, 0.5 M, 1.0 M, 2.0 M and 3.0 M with 3 g/l of calcium hydroxide were used as exposure solutions. Different temperatures of -15 ºC, -10 ºC, 0 ºC, 5 ºC and 23 ºC were used for isothermal temperature exposure and temperature cycle exposure. The results showed that the chloride binding in different cement paste mixes was in the order: GGBFS > GU > MK > SF. The chloride binding capacity decreased with decrease in exposure temperature. Further, the authors also reported that the seasonal temperature variations have an effect on chloride binding capacity such as the samples initially exposed to chlorides at 0 °C followed by exposure at 23 °C had a higher binding capacity compared to the samples exposed to

chlorides initially at 23 °C followed by the exposure at 0 °C. The service life estimated from Life 365 software indicated that a decrease in temperature coupled with the chloride exposure correspond to either a decrease in relative service life or similar relative service life for 100% GU and 40% GGBFS samples when compared with the sample exposed to 23 °C. In case of 10% MK and 10% SF samples, the decrease in temperature coupled with the chloride exposure resulted either an increase in relative service life or similar relative service life. Further, the service life estimates from Life 365 indicated that the chloride binding capacities determined at 23 °C or room temperature may not be conservative when estimating the service life in colder climates.

Ukpata et al. [69] have carried out an experimental study to investigate the influence of curing duration of specimen, temperature and slag composition on expansion of CEM I cement and composite slag-cement mortars exposed to a combined NaCl and Na_2SO_4 solution. The mortar specimens were prepared using a plain CEM I 42.5 R cement and CEM I 52.5 R cement blended with two slags of different basicity ratios (1.28 and 1.18) at a cement replacement level of 30% by weight, and w/b ratio of 0.5 for expansion and sorptivity tests. The specimens were wet-cured at either 20 °C or 38 °C for 7 or 28 days and then soaked for 24 hours in deionised water prior to immersion in a combined salt solution (NaCl (30 g/l) and Na_2SO_4 (3 g/l)) at a temperature of either 20 °C or 38 °C for up to 664 days. Corresponding reference specimens were stored in saturated limewater at 20 °C. In addition, paste specimens were prepared, cured and exposed under similar conditions for the study of microstructural development and development of the phase assemblages using XRD, TGA and SEM-EDX analyses. From the obtained results, the authors reported that the slag blend mortar specimens cured and exposed at the temperature of 38 °C showed significant resistance to sulphate-induced expansion at both curing ages. In addition, for slag blended specimens, the influence of exposure temperature was found to be more pronounced than curing duration against sulphate-induced expansion. Further, differences in slag composition and curing duration also played important roles on the expansion resistance of mortar specimens. The sorptivity of specimens decreased with increase in curing age and curing temperature in all plain and slag blended mortars. The presence of chloride in the exposure solution reduced the sulphate expansion of CEM I 42.5 R cement mortar. The expansion of the specimen was attributed to the formation of ettringite crystals, although Friedel's salt and Kuzel's salt were also formed.

2.2.2. Effect of exposure condition

Enevoldsen et al. [70] have studied the degree of chloride binding in cement mortar for different chloride exposure conditions such as admixed with chloride, exposed to chloride environment, and combined effect of these two. For this purpose, four mortar mixes with/without admixed sodium chloride (2% by mass of cement) and with/without an air-entraining agent were prepared and used for casting cylindrical specimens (size: 51 mm diameter and 102 mm height) with a centrally embedded steel reinforcement bar of 8 mm diameter. After curing of 2 months, half of each set of specimens were immersed in saturated $Ca(OH)_2$ solution and other half in saturated $Ca(OH)_2$ + 1 mol/l of NaCl solution for one year. After this period, the specimens were subjected to electrochemical chloride removal by placing the specimens in individual cells containing an external graphite anode and the supporting electrolyte of saturated $Ca(OH)_2$, and applying a constant potential of 15 volts for 5 weeks. The concentration of chloride in each cell was measured daily using a chloride selective electrode until it reaches a stable level. Afterward, the mortar specimens were used for chemical analysis by differential scanning calorimetry (DSC) analysis along with the determination of free and total chloride by potentiometric titration. Based on the obtained results, the authors concluded that the admixed chloride in the mortar does not prevent the ingress of external chloride ions and the quantities arising from two sources are additive. Further, the admixed chloride was immediately chemically bound with cement hydrates as monochloroaluminate, and the chloride ingress from external environment may also bound chemically to a certain extent. From the results of electrochemical chloride removal test, the efficiency of removal of free chloride was greater in case of chloride penetrated from the external environment as compared to admixed chloride in hardened cement mortar. The authors suggested that the electrochemical chloride removal of existing structures may be a valid method for stopping the ongoing corrosion, however, the nondestructive nature of the test must be determined.

Al-Khaja [71] has evaluated the influence of temperature, cement type and level of consolidation on chloride ingress into conventional and high-strength concrete. For chloride ingress, two high-strength concrete mixes (71.2 MPa and 68.3 MPa) were compared with two conventional concrete mixes (42.9 MPa and 40.2 MPa) made with ordinary Portland cement (OPC), and sulphate-resisting cement (SRPC) and exposed to similar aggressive environment. The high-strength and conventional concrete mixes were prepared at w/b ratios of 0.39 and 0.48, respectively. From each concrete mix, cylindrical

concrete specimens of size 150 mm in diameter and 300 mm in height were prepared using different levels of consolidation (50% and 100%). The cylindrical specimens were coated with epoxy leaving only the top and bottom surfaces and exposed to 5% NaCl solution by maintaining different exposure temperatures of 20 ºC and 45 ºC for 180 days. After exposure to chloride solution, the acid-soluble chloride content was determined at different depth intervals of the specimens from the exposed surface to a depth of 70 mm toward the center of specimens. From the obtained results, the author reported that the chloride ingress in concrete increased with an increase in temperature especially at small depth intervals and the effect of temperature was more pronounced in conventional concrete as compared to high-strength concrete. The chloride diffusion was more in SRPC as compared to OPC for both conventional and high-strength concrete. The chloride ingress in concrete increased with decrease in consolidation in both conventional and high-strength concrete. In addition, the performance of high-strength concrete in terms of decreasing chloride diffusion was better as compared to conventional concrete.

Suryavanshi et al. [72] have studied the chloride penetration in concrete to evaluate the amount and direction of chloride that diffuses through concrete. The concrete mixes were prepared from ASTM Type I normal Portland cement at w/c ratios of 0.45, 0.60, and 0.75. To simulate the large exposed area, such as bridge decks, the reinforced concrete slab specimens of different sizes (1000 × 1000 × 150 mm and 1000 × 500 × 150 mm) were prepared from each concrete mix. The specimens were embedded with high tensile strength reinforcing steel bar of diameter 20 mm with an effective cover depth of 125 mm. After 28 days of curing, out of six slab specimens, the entire surface of three slab specimens were coated whereas another three slab specimens were coated only half of their surface, with the acrylic-based surface coating system. After coating, the slab specimens were exposed to 4% sodium chloride solution with wetting (three days) and drying (seven days) cycles up to 10, 30, 50, and 70 cycles. After completion of alternate wetting and drying cycles, the slab specimens were left in drying environment for an additional 6 years. After that, the concrete cores of different thickness were sliced from the exposed surface of slab specimens to the depth of 105 mm and crushed to concrete powder samples. The concrete powder samples were used for determining the acid-soluble chloride content for obtaining the chloride profile. Based on the obtained results, the authors concluded that, in large surface area of concrete, chloride diffuses both in the direction of depth and a direction lateral to the depth. The concrete made with higher w/c ratio showed favorable condition

for diffusion of chloride in the direction of lateral to the depth. The amount and depth of chloride diffusion were directly influenced by w/c ratio of the concrete, exposure regime, and duration of exposure. Further, increase in amount of chloride and depth of diffusion were observed with an increase in w/c ratio. In addition, reducing the w/c ratio from 0.60 to 0.45 was far more effective in decreasing chloride penetration than that achieved by reducing the w/c ratio from 0.75 to 0.60. The acrylic-based surface coating system was found highly resistance to chloride penetration.

Costa and Appleton [73] have studied the chloride penetration in three different concrete mixes (two for cast-in-situ and one for shotcrete) subjected to five exposure conditions over a period of five years. A total of 54 concrete panels of size 1.0 × 0.5 × 0.12 m were cast and subjected to 7 days of humid curing. In order to allow chloride penetration through one surface only, all faces except top surface of the concrete panel were protected with an epoxy paint. After two weeks, the concrete panels were subjected to various exposure conditions such as spray zone, tidal zone, atmospheric zone, dockyard 20 (filling up of the dock with estuary water), and dockyard 21 (more frequent filling up cycles than dockyard 20). The chloride penetration profile was determined in terms of total chloride (acid-soluble chloride) content measured from drilled concrete powder samples. The chloride diffusion coefficient was estimated using Fick's 2nd law of diffusion. From the obtained results, it was observed that the penetration of chloride into concrete depends on concrete quality and exposure conditions. The concrete panels exposed to tidal zone exhibited higher penetration of chloride ions as compared to other exposure conditions. Further, the concrete panels subjected to atmospheric zone showed much lower chloride penetration. Moreover, the chloride diffusion coefficient varied significantly with concrete quality, exposure conditions and exposure period. The surface chloride content was not influenced by the concrete quality but considerably affected by exposure conditions that reduced from tidal zone to atmospheric zone.

Hong and Hooton [74] have studied the effect of cyclic exposure (wetting and drying) with sodium chloride solution on chloride ingress in concrete (bridge decks exposed to deicing salts in the Toronto area). Out of three different concrete mixes, for one mix, Portland cement was replaced with 25% of slag whereas for other two mixes, Portland cement was replaced with 25% of slag and 8% of silica fume. The concrete mixes were prepared with two water to cementitious materials (w/cm) ratios of 0.3 and 0.4. The concrete specimens were exposed to two different exposure lengths of wetting-drying

cycles, which consists of 6 hours of wetting with 18 hours (1-day series) or 66 hours (3-day series) of drying. The chloride solution with 1.0 M NaCl concentration was used for wetting of specimens. The effect of number of cycles was evaluated using six pairs of specimens in 1-day series for 1, 4, 9, 16, 25, and 36 cycles, and five sets in 3-day series for 1, 4, 9, 16, and 25 cycles. The test results showed that the increased drying period resulted in deeper sorption. Therefore, for the concrete samples subjected to wetting and drying cycles with 3-day drying periods accelerated the chloride penetration more than that of 1-day drying cycles. It was also observed that during the drying phase of wetting-drying cycle, the diffusion of chlorides continuously occurred in saturated pores at greater depths of concrete. Further, the rate of drying was dependent on the concrete pore structure hence, the rate of drying was slower for high quality concrete. The rate of chloride penetration was found to be linearly related to the square root of the number of cycles of wetting and drying.

Zuquan et al. [38] have studied the effect of interaction between sulfate and chloride ions on concrete made with and without fly ash. Out of two sets of concrete, one set of concrete was prepared with Portland cement (Chinese standard 42.5 R(II)) and another set of concrete was prepared by replacing Portland cement with 20% and 30% of fly ash. The concrete mixes were prepared with w/b ratios of 0.35 and 0.45. The concrete specimens (size: 40 mm × 40 mm × 160 mm) were exposed to three types of exposure solution such as 3.5% NaCl, 5% Na_2SO_4, and a composite solution of 3.5% NaCl and 5% Na_2SO_4 with two types of exposure regime i.e. natural immersion (stored in corrosion solution for long duration), and drying-immersion cycles. The relative dynamic modulus of elasticity (RDME) measurement and test for chloride diffusion coefficient test were carried out on the concrete specimens. The XRD and SEM analyses were performed on the concrete powder samples collected at different depth intervals after the end of the exposure. The experimental results showed that the resistance to chloride ingress in concrete increased at the early exposure period whereas it decreased at the latter exposure period, due to the presence of sulfate ions in the composite solution. The presence of chloride ions in the composite solution reduced the damage of concrete due to sulfate ion. The fly ash addition in concrete considerably improved the resistance to chloride ingress and the resistance to sulfate erosion. From RDME measurement, it was observed that the concrete specimens were severely damaged in 5% Na_2SO_4 solution as compared to that in the composite solution. The presence of chloride ions in the composite solution retarded the deterioration of concrete due to sulfate attack. The authors also reported that the concrete prepared with

low w/b ratio and suitable fly ash content could retard the deterioration due to sulfate attack. From the results of XRD and SEM analyses, the concrete specimens exposed to sulfate solutions or composite solutions, gypsum, and ettringite were found only corrosion crystalline and concentration of these compounds were higher in case of exposure to sulfate solution as compared to composite solution.

Guimaraes et al. [75] have measured the diffusion coefficient of chloride ions through non-saturated and partially saturated (with water) concrete with a simplified procedure based on the interaction of the concrete surface with solid NaCl. The authors have compared the results with previous literature, those obtained from the experiments based on an instantaneous HCl deposition on the tested concrete surface. Five concrete mixes were designed to obtain 28 days medium compressive strength of 30-45 MPa using high early strength and sulfate resistance cement and w/c ratios between 0.48 and 0.66. The specimens for compressive strength test were cast from each concrete mix. From each mix, 50 cylindrical specimens of size 50 mm in height and 30 mm in diameter were prepared using sieved mortar (sieved through a 9.5 mm sieve) and cured for 28 days in a wet chamber. Further, the mortar specimens were kept in the laboratory environment for 150 days from the day of casting before conducting mercury intrusion porosimetry (MIP), bulk density, water absorption, and chloride diffusion test. Chloride diffusion test was performed for the duration of 7, 16, 21 and 130 days after 199 days of casting for varying degrees of saturation (SD) of 100%, 90%, 75% and 50% respectively. For exposure to NaCl, the deposited NaCl was protected with waterproof tape, and after that, the specimens were again closed with three plastic layers for non-saturated specimens. However, for the saturated specimens, a pool of plastic tube was attached to the top, and the solid NaCl was deposited within the pool. For determination of chloride diffusion coefficient and surface chloride concentration, the experimentally obtained chloride profiles were fitted to the error-function solution of Fick's 2nd law of diffusion. The authors established a polynomial relationship for dependency of diffusion coefficient on the degree of water saturation. The authors concluded that the estimation of the chloride diffusion coefficient through concrete at water saturation degrees of 50% to 100% was possible using a simplified methodology based on putting solid NaCl in contact with the concrete surface. The results obtained from five high-early-strength Portland cement mortar showed a strong dependence of diffusion coefficient on the degree of saturation. The authors found that the proposed test

methodology, and the HCl deposition method had comparable results i.e. similar dependence on chloride diffusion with water saturation degree.

Sotiriadis et al. [76] have studied the sulfate resistance of limestone cement concrete exposed to sulfate and composite chloride and sulfate solutions at 5°C temperature. The concrete mixes were prepared using Portland cement clinker replaced with limestone of high calcite content ($CaCO_3$ - 97.5%) with 0%, 15%, and 30% by weight as binder, w/c ratio of 0.52 and calcareous aggregates with a maximum size of 16 mm. The concrete cube specimens (of size 100 mm) were prepared from each concrete mix and cured for 28 days. After completion of curing, the specimens were immersed in solutions (water, 20 g/l of sulfate ($MgSO_4$) solution, and 21.14 g/l of chloride (NaCl) with 20 g/l of sulfate ($MgSO_4$) as composite solution) and stored in industrial refrigerator at 5°C ± 1°C for 2 years. Visual inspection, change in mass of specimens, compressive strength test and XRD measurement were performed at regular intervals for the entire period of exposure. Based on the results obtained from the experimental investigation, it was observed that the deterioration of concrete due to sulfate attack was more intensive for the specimens stored in only sulfate solution as compared to the composite chloride-sulfate solution. The concrete containing limestone deteriorated with higher degree as compared to the concrete without limestone. The concrete having limestone either in the form of cement or aggregate suffered from the thaumasite form of sulfate attack at 5°C. In the deterioration zone of concrete, thaumasite was formed along with the brucite and secondary ettringite whereas, no ettringite and/or portlandite were detected in this zone as observed from XRD analysis.

Safehian and Ramezanianpour [77] have analyzed the effect of basic parameters namely the construction method (in situ and precast) and the exposure conditions (atmospheric, splash and tidal zones) on five-year-old concrete jetties under long-term chloride penetration subjected to harsh marine environmental conditions. In the investigated parts of the structure, Type I (PM) blended cement (conforming to ASTM C595) and silica fume (conforming to ASTM C1240) with pozzolanic activity index 103% were used as cementitious materials. The concrete mixes were prepared to have water to binder (w/b) ratio of 0.35 and high range water reducing superplasticizer meeting the requirements of Type-F as per ASTM C494 was used. The error function solution of Fick's 2nd law was fitted to determine the apparent chloride diffusion coefficient (D_{app}) and the surface chloride content (C_s) using nonlinear regression analysis. The results showed that the exposure conditions did not significantly influence the apparent chloride diffusion

coefficient. However, the construction method and w/b ratio have considerably affected the concrete quality and expected service life. From chloride penetration aspect, the tidal zone has shown the most aggressive exposure condition followed by the splash zone and atmospheric zone. The geographical parameters i.e. location of the structure in a marine environment, degree of exposure to chloride environment, and weathering condition concerning prevailing winds, currents and rainfall, have attributed to the varied surface chloride content values. The authors also concluded that the various uncertainties in the parameters of chloride penetration still exist, and long-term field investigation is needed for calibrating various irregularities.

Xu et al. [78] have studied about the release of bound chloride in cement paste made with ordinary Portland cement (OPC), and OPC partially replaced with 10% silica fume (SF), 30% pulverised fly ash (PFA) and 50% ground granulated blastfurnace (GGBS) and subjected to Na_2SO_4, K_2SO_4 and $MgSO_4$ solutions. Paste specimens (size 40 mm × 40 mm × 160 mm) were prepared using different binders at w/cm ratios of 0.22, 0.32 and 0.42 and admixed with four concentrations of sodium chloride ranging from 0.5% to 3.0% and cured for 4 months at 20 ±2 ºC in sealed storage chamber. After curing, the cement paste was ground into 0.16 mm powder sample and dried at a temperature of 60 ºC. Subsequently, 20 gm of dried concrete powder samples were added to 200 ml of sulfate solutions (5% Na_2SO_4, 5% K_2SO_4 or 5% $MgSO_4$) and also in distilled water as a control suspension. The powder solution was stirred for a period to reach steady-state condition, which was identified by measuring the pH of the solution. After reaching a steady-state condition of powder solutions, the suspension was filtered and used for determining the free chloride content of the suspension solution. The filtered powder samples were used for XRD analysis to investigate the chemical phases of the powder sample. Based on the results obtained from different tests, the authors reported that the chloride binding of cement pastes increased with an increase in w/cm ratio and total chloride content in cement paste. In addition, the partial replacement of SF reduced the chloride binding, on the contrary PFA and GGBS increased the chloride binding. The presence of sulfate in exposure solutions released the bound chloride and tendency of release of bound chloride was lower in the cement paste made with higher w/b ratio, containing lower total chloride content and partially replaced with SF, PFA and GGBS. On comparing the type of sulfate solution, the $MgSO_4$ solution resulted in release of less bound chloride as compared to Na_2SO_4, and K_2SO_4 solutions. The authors also concluded that the release of bound chloride in case of

exposure to sulfate solutions was mainly due to transformation of Friedel's salt into ettringite.

Maes and Belie [33] have examined the effect of multi-ion transport (chloride and sulfate) to investigate the influence of sulfate ion on chloride attack by diffusion test, and influence of chloride ion on sulfate attack by measuring the length and mass change of specimens. The concrete (influence of sulfate on chloride penetration) and mortar (influence of chloride on sulfate attack) mixes were prepared using ordinary Portland cement (OPC), high-sulphate resistant (HSR) cement, and blast-furnace slag (BFS) at 50% and 70% replacement levels by weight of binder having water to binder (w/b) ratio of 0.45. The cement paste samples were also prepared using the same binder type and w/b ratio for the XRD analysis. The specimens were exposed to different test solutions with varying concentrations of sodium chloride and sodium sulfate for different exposure periods. After exposure, for diffusion test, colour change boundaries (ccb) using 0.1 M $AgNO_3$ solution, and acid-soluble as well as water-soluble chlorides were determined to evaluate the influence of sulfate on chloride penetration. From the obtained results, it was observed that the presence of sodium sulfate in the exposure solution increased the free chloride penetration of OPC concrete for immersion period between 7 weeks and 14 weeks. However, the chloride penetration depth decreased in high-sulphate resistant cement concrete for an immersion period of 7 weeks and this effect disappeared at a more extended exposure period i.e. 14 weeks. The presence of chloride in the exposure solution delayed the sulfate deterioration as chlorides have mitigating effects on sodium sulfate attack. The authors also concluded that over time Friedel's salt starts disappearing due to the formation of ettringite and gypsum (as observed from XRD analysis) leading to the deterioration of mortar exposed to chloride and sulfate containing environment. The use of blast-furnace slag as a binder in OPC improved the resistance of concrete against chloride and sulfate attack.

Weerdt et al. [79] have carried out a study on chloride binding in Portland cement paste in the presence of magnesium and sulfate in seawater. In this study, the cement paste was prepared using Portland cement (CEM I 42.5) at w/c ratio of 0.40 and cured in the water bath at 5 ºC for 3 days and at 20 ºC for 4 days. After 7 days of curing, the cement paste was crushed into 1 mm fine particles and mixed with 40% of water by weight of powdered cement paste and stored in airtight polypropylene bottles at 20 ºC for additional 7 days. Afterward, the moist hardened cement paste was crushed in plastic bag converted into moist

sand and stored in airtight polypropylene bottles until analysis of the sample. The free water present and degree of hydration of wet paste were determined using TG analysis. To determine the chloride binding isotherm of cement paste, different chloride-containing solutions made with NaCl, $MgCl_2$, $MgCl_2$ + NaCl, $MgCl_2$ + $MgSO_4$, and sweater (using technical grade salts: $MgSO_4 \cdot 7H_2O$, $MgCl_2 \cdot 6H_2O$, NaCl, $CaCl_2 \cdot 6H_2O$ and KCl) were used. For this purpose, 15 ml of chloride-containing solution was added to 30 g of the hydrated cement paste in a plastic centrifuge bottle and stored for 2 months at 20 ºC. Afterw ard, the samples were taken out for analysis, and pH and chloride content of supernatant were analyzed. The free chloride content was determined from the chloride concentration of the added solution and bound chloride was determined from the measured equilibrium chloride concentration in the liquid phase. Some of the cement paste samples were further used for microstructure study using SEM-EDS and TG analyses. Based on the results obtained from different tests, the authors found that the Portland cement paste exposed to seawater or NaCl, NaCl + $MgCl_2$ and $MgSO_4$ + $MgCl_2$ showed similar chloride binding. However, the chloride binding was higher in the specimens exposed to $MgCl_2$ solution as compared to other chloride-containing solutions because of the reduced pH of concrete in the presence of $MgCl_2$. In addition, the presence of sulfate in seawater resulted in the reduction of chloride binding in cement paste due to the conversion of a part of the AFm phases into ettringite. The authors concluded that the increased chloride binding in case of exposure solutions of $MgCl_2$ due to decreased pH is not valid for the exposure solution containing varying sulfate contents.

Song et al. [80] have studied the influence of cation type (K^+, Na^+, Ca^{2+} and Mg^{2+}) associated with chloride ion on chloride diffusion behaviour in concrete structures exposed to chloride environment. The concrete mix was prepared using Type II Portland cement at a w/c ratio of 0.50. The slab specimens were prepared from the concrete mix, and cylindrical samples were drilled out from the slab specimens. The side and bottom surfaces of cylindrical specimens were sealed with epoxy and top surface was exposed to 0.5 mol/l $NaCl_{aq.}$, 0.5 mol/l $KCl_{aq.}$, 0.25 mol/l $CaCl_{2aq.}$ and 0.25 mol/l $MgCl_{2aq.}$ solutions for 6 months duration. After the end of exposure, concrete powder samples were collected layer by layer to determine the water-soluble and total chloride concentrations. The XRD analysis was performed on the powder sample made up of paste in the depth of 1-3 mm of concrete surface. The chloride diffusion coefficient was estimated using Fick's 2nd law of diffusion. The authors have used finite difference method to simulate the ionic diffusion processes

occurred in the immersion test. Based on the results obtained from the experimental data, it was observed that the cation associated with chloride ions influenced the diffusion of chloride ions into concrete mainly due to difference in chloride binding capacity. The chloride binding capacity of the associated cations were found in the order of $Ca^{2+} > Mg^{2+} > Na^{+} \approx K^{+}$. Due to chloride binding capacity, the apparent diffusion coefficients of chloride ions were found in the order of $K^{+} \approx Na^{+} > Ca^{2+} > Mg^{2+}$. From the results of XRD analysis, the formation of M-S-H gel was observed in case of $MgCl_2$ exposure. From the improved chloride diffusion model, the authors have concluded that the cation type and the contact duration are the two major factors, which vary with the range of distance because of which the chloride binding capacity also vary significantly.

Lu et al. [81] have studied the mechanism of chloride penetration in concrete made with ordinary Portland cement (OPC) and fly ash, and subjected to NaCl solution under drying-wetting cycles. The authors evaluated the effect of mix proportion, a period ratio of drying to wetting, and exposure time. In this experimental study, prismatic specimens of size 150 × 150 × 400 mm were prepared using OPC and OPC with 0%, 15%, and 30% replacement levels of fly ash at w/b ratios of 0.43 and 0.385. For one-dimensional transport of chloride ions, five faces of prismatic specimens were coated with epoxy resin, and exposed to 5% NaCl solution under different drying-wetting period. The free chloride concentration was determined on concrete powder samples collected from a different locations and different depth intervals up to 60 mm from the surface, using a distilled water extraction. After obtaining free chloride content, the apparent chloride diffusion coefficient was determined using a modified Fick's 2^{nd} law of diffusion by considering the depth of the convection zone. Based on the obtained results, the authors concluded that the transport of chloride ions represents a combination of diffusion and convection for the concrete exposed to drying-wetting cycles. The depth of convection zone mainly varied from 6 to 15 mm and was mainly dependent on environmental conditions, material properties, and exposure time. By taking into account the depth of convection zone, the modified one-dimensional diffusion model described well the chloride profile in the inner part of the concrete with a high goodness of fit. Finally, the time-dependent chloride diffusion coefficient (D_{cl}) was calculated by the apparent chloride diffusion coefficient (D_{app}) and the obtained time exponent (m). The authors found that the value of time-dependent chloride diffusion coefficient (D_{cl}) decreased with an increase in fly ash content.

Farahani et al. [17] have studied and developed the chloride diffusion model based on age, temperature, water-to-binder ratio, and pozzolanic materials used for concrete mix design. The concrete mixes were prepared using Type II Portland cement with 5%, 7.5%, 10% and 12.5% of silica fume by weight of cement at w/b ratios of 0.35, 0.40, 0.45 and 0.50. The prismatic specimens of size 150 mm × 150 mm × 600 mm were prepared from all concrete mixes. To ensure one-dimensional ingress of chloride ions, four sides of the prismatic specimens were sealed using epoxy polyurethane coating. The specimens were exposed to tidal zone in an investigation marine site for periods of 3, 9, 36 and 60 consecutive months. After the end of the exposure, acid-soluble chloride content was determined at different depth intervals. Fick's 2nd law of diffusion was used to fit the chloride profile obtained from the experimental study. The authors have developed a model as a function of time, temperature and relative humidity by considering the diffusion coefficient at three months of exposure as reference diffusion coefficient. The reference diffusion coefficient was predicted as a function of w/b ratio and silica fume content. The function of time was considered as an inverse power function. Similarly, the proposed model by Saetta et al. [82] was used to estimate the influence of temperature and relative humidity on chloride diffusion. The obtained model was validated with the experimentally obtained data and the empirical models, and was found in good agreement. The authors concluded that lower w/b ratio with a higher silica fume replacement (up to 10%) reduces the chloride diffusion coefficient of concrete in a marine environment. In addition, the chloride diffusion coefficient decreased with exposure duration and increased with an increase in temperature.

Chen et al. [83] have studied the resistance of concrete made with ordinary Portland cement (OPC) and OPC replaced with fly ash and slag against individual and combined chloride and sulfate attack under drying-wetting cycles. For this purpose, prismatic concrete specimens of size 70 mm × 70 mm × 280 mm were prepared using OPC and OPC replaced with 30% and 50% of fly ash or slag (GBFS) at a w/b ratio of 0.35. After curing, epoxy resin was applied on all four surfaces of the prismatic specimen except two opposite vertical surfaces (70 × 280 mm). After that, the coated prismatic specimens were exposed to combined solutions of sodium chloride (5% NaCl) and sodium sulfate (5% and 10% Na_2SO_4) with drying-wetting cycle for 300 days. Each drying-wetting cycle continued for 72 hours, which involved immersion of concrete specimen in the exposure solution at room temperature for 21 hours followed by 3 hours of drying in air, and again drying at a temperature of 60 ºC for 45 hours followed by cooling down at room temperature for 3

hours. Dynamic modulus of elasticity, mass change, and total chloride content were determined at the end of the exposure. To study the alteration in the microstructure, MIP, XRD, and TG/DSC analyses were performed on the paste samples made with same binder type as used in the concrete and exposed to the same combined chloride and sulfate solutions. From the obtained values of dynamic modulus of elasticity and mass change, it was observed that the concrete specimens made with fly ash and GBFS showed better resistance as compared to those made with OPC against the combined attack of chloride and sulfate under drying-wetting cycle. From total chloride profile, it was observed that the addition of fly ash and GBFS exhibited better resistance against chloride ingress under combined chloride-sulfate attack, and less porous concrete as compared to OPC concrete specimens. In terms of chloride ingress, the composite solutions were less aggressive as compared to only chloride solution. From the results of XRD and TG/DSC analyses, the formation of Friedel's salt, and sulfate products such as ettringite in the presence of combined chloride and sulfate solutions may be retarded as compared to the individual solutions.

Wu et al. [84] have studied the effects of exposure condition on chloride ingress in concrete, and time-dependent chloride diffusivity of concrete. In this study, three existing coastal reinforced concrete structures located in the Beibu Gulf were selected, and having the same concrete mix proportion with w/c ratio of 0.40 and concrete strength grade of C40. These structures were located in different exposure conditions such as tidal, splash and atmospheric zones for different periods. For determination of chloride content profile, concrete powder samples were taken from the external wall of the structure at different depth intervals each of 7 mm up to the depth of 56 mm, and the chloride concentration was determined through rapid chloride concentration tester (RCT). The obtained chloride concentration at different depth intervals was fitted with Fick's 2nd law of diffusion to estimate the apparent chloride diffusion coefficient and surface chloride concentration. The estimated apparent chloride diffusion coefficient at different ages was used to determine the time-dependency properties of the diffusion coefficient. The authors also predicted the probabilistic corrosion initiation time by using different corrosion models such as DuraCrete 2000 model, Life 365 model and LNEC E465 model. Based on the obtained results, the authors reported that the reinforced concrete structure exposed to the splash zone had higher chloride concentration as compared to tidal and atmospheric zones. The time-dependency properties of the diffusion coefficient revealed that the apparent chloride

diffusion coefficient decreased with exposure time and must be considered for durability assessment of reinforced concrete structures. Further, the age factor was found as normally distributed random parameter and mean value of the age factor for atmospheric, tidal and splash zones were evaluated as 0.19, 0.36 and 0.43, respectively. After the comparison of different corrosion models, the authors found that the DuraCrete 2000 model can characterize the chloride transport better in the concrete located in Biebu Gulf as compared to the Life 365 model and the LNEC E465 model.

Zuquan et al. [85] have studied the chloride ion transport and chloride binding capacity of different concrete mixes exposed in marine atmospheric zone, splash zone, tidal zone, and submerged zone. In this study, the concrete mixes were prepared using Portland cement (59.8 MPa) and mineral admixtures (Class I fly ash and GGBS) at a w/b ratio of 0.35. The different replacement levels of fly ash and GGBS used for the preparation of concrete mixes were 32% GGBS with 17% Fly ash (LF50) and 15-65 % GGBS or fly ash by weight of the binder. From each concrete mix, concrete cube specimens of size 100 mm, and from control concrete and LF50 concrete mixes, reinforced concrete specimens of size 150 mm × 200 mm × 1000 mm were cast and cured for 28 days. After curing, the four sides of cube specimens were sealed for one-dimensional ingress of chloride ions. The sealed cube specimens were exposed to marine exposure fields of separate corrosion zones including atmospheric zone, splash zone, tidal zone and submerged zone. The reinforced concrete specimens were exposed throughout to all exposure zones longitudinally in such a way that 300 mm length in the submerged zone, 400 mm length in the tidal zone, 150-200 mm length in the splash zone, and the remaining length of the specimen lie in the atmospheric zone. After the end of the exposure, the carbonation depth and compressive strength was determined on core cylindrical specimens cut from reinforced concrete specimens. Water-soluble chloride (free chloride) and acid-soluble chloride (total chloride) were determined on concrete powder samples collected at different depth intervals from cube specimens and core cylindrical specimens cut from reinforced concrete specimens. Further, the obtained free and total chloride contents were used to determine the chloride binding capacity of concrete and free chloride was used for estimation of apparent chloride diffusion coefficient (using Fick's 2nd law of diffusion). The paste sample was also prepared from a control mix for XRD and DSC-TG analyses and also exposed to the different exposure zones. From the results of chloride content, the authors reported that the chloride content was highest in the submerged zone as compared to the atmospheric zone in case of exposure to separate

corrosion zones. However, in case of exposure to throughout corrosion zone, the chloride ion content in case of atmospheric zone and splash zone was higher compared to the submerged zone due to seawater capillary absorption. Further, the chloride ion content was lower in fly ash and GGBS concrete as compared to control concrete, and apparent chloride diffusion coefficient was also less in the same concrete. The convection zone was observed in concrete specimens exposed to the tidal zone and splash zone. From the results of chloride binding capacity, the lowest chloride binding capacity of concrete was noted in case of concrete specimens exposed to atmospheric zone as compared to other zones and sulfate ions in seawater reduced the chloride binding capacity with time. Further, the chloride binding capacity reduced with an increase in replacement level of GGBS and fly ash. From the results of XRD and DSC-TG analyses, the lowest $Ca(OH)_2$ content was found in the concrete exposed to tidal zone, which was caused by the washing effect due to tidal action.

Qiao et al. [23] have studied the influence of salt type i.e. NaCl and $MgCl_2$ on chloride transport in concrete due to diffusion and wicking. The effects of w/c ratio and supplementary cementitious materials (fly ash and slag) on chloride transport were also evaluated. For this purpose, cement paste and concrete mix were prepared using Type I cement and Type I cement replaced with class C fly ash and ground blast furnace slag at replacement levels of 20%, 35%, and 50% of fly ash or slag by mass of total binder. The concrete specimens were used for porosity test (ASTM C642-13), chloride ponding test and wicking test whereas, the paste specimens were used for chloride binding test. Chloride ponding test was conducted on cylindrical concrete specimens where all surfaces were coated with epoxy except the face being exposed to 5 mol/l NaCl solution for 4 months. After the end of ponding, the concrete powders were obtained by grinding 2-mm layers for the first 10 mm and 3-mm layers for depths greater than 10 mm from the exposure surface and the total chloride content of each layer was determined by the automatic titration device. For wicking test, the cylindrical concrete specimens with the uncoated face at bottom were exposed to a 5 mol/l NaCl solution or 2.5 mol/l $MgCl_2$ and top surface was in contact with air for 5 months. For the chloride binding test, the powder samples of cement paste specimens immersed in different concentrations of NaCl solutions (all mixes of cement paste) and $MgCl_2$ solutions (plain cement pastes) were used. Based on the obtained results, the authors concluded that the chloride binding capacity increased due to the addition of fly ash and slag among binder type and higher chloride binding was observed

in cement paste specimens exposed to $MgCl_2$ solution among solution type. The results indicated that wicking resulted in a greater penetration depth in the concrete than that of diffusion alone and their difference was more at higher w/c ratio. The chloride transport was significantly influenced by the salt type wherein the specimens exposed to $MgCl_2$ solutions showed lower penetration depth as compared to NaCl solutions.

Zhang et al. [86] have studied the effect of field exposure and accelerated exposure conditions on the time-dependent characteristic of the diffusion coefficient. In this study, five concrete mixes were prepared using Portland cement (PC 32.5) at w/c ratios of 0.40, 0.45, 0.50, 0.55 and 0.60. From each concrete mix, cylindrical specimens of diameter 100 mm and height 50 mm were cast and kept for 28 days of curing. After curing, all the surfaces except one circular surface of cylindrical specimens were sealed using epoxy resin for one-dimensional ingress of chloride ions. The sealed cylindrical specimens were exposed to different environmental conditions (simulating the field exposure) and accelerated condition. The four environmental conditions were set for varying temperatures (from 14 ºC to 52 ºC) and humidity levels (73% to 85%) at a chloride (NaCl) concentration of 2.1%. However, for accelerated condition, the simulated temperature was set as twice the average temperature of one season and exposed to mist spray (4 hours) and drying (44 hours) with 12.5% concentration of sodium chloride in exposure solution. After the end of expected exposure time (40 days, 80 days, 120 days, 160 days and 200 days), the concrete powder samples were collected at depth intervals of 2 mm from the exposed surface. The concrete powder samples were used for determining the free chloride concentration at different depth intervals of concrete. The obtained free chloride concentration at different depth intervals was fitted with Fick's 2^{nd} law of diffusion by considering the convection zone, to estimate the chloride diffusion coefficient of concrete. The estimated values of chloride diffusion coefficient from different exposure periods were further used for determining the time-dependent characteristics of diffusion coefficient using a power function. Based on the obtained results, the authors reported that the convection zone in the profile of free chloride concentration exists both in the simulated accelerated condition and simulated field exposure. Additionally, the depth of the convection zone was affected little by the w/c ratio and increased with an increase in exposure time in the simulated accelerated condition. From the results of the time dependency of chloride diffusion coefficient, the authors reported that with an increase in w/c ratio, the chloride diffusion coefficient in a reference time (D_0) increased and age factor (m) decreased, and the relationship between

D_0, m and w/c ratio was fitted by quadratic polynomials in case of simulated accelerated condition. The age factor at 200 days of exposure time was about three times higher in simulated accelerated condition as compared to simulated field exposure for the same mix proportion of concrete.

Cao et al. [36] have investigated the effect of sulfate ion on chloride diffusion mechanism in mortar. For this purpose, mortars specimens of size 40 mm × 40 mm × 160 mm were prepared using Portland cement (P.I 52.5) at a w/c ratio of 0.48 and cured for 28 days. After curing, the specimens were sealed using epoxy to ensure one-dimensional diffusion. The sealed mortar specimens were exposed to chloride (25% NaCl) and composite chloride-sulfate (25% NaCl + 5% Na_2SO_4) solutions for different exposure periods. After the end of exposure, chloride diffusion depth analysis using colorimetric method along with total chloride content, and the microscopic analysis using X-ray diffraction (XRD) analysis, scanning electron microscopy (SEM-EDS) and mercury intrusion porosimetry (MIP) were performed. Based on the results obtained from different tests, the authors reported that the chloride diffusion in mortar specimens increased in short-term exposure due to the presence of sulfate ions in the exposure solution, whereas, in long-term exposure, the chloride diffusion decreased. In addition, the chloride binding of mortar specimens reduced in the presence of sulfate ions in the exposure solutions due to conversion of Friedel's salt to ettringite (as observed from XRD analysis). Further, due to ingress of sulfate, the porosity of mortar specimens reduced due to presence of large amount of unreacted sulfate in the form of calcium sulfate. From the results of total chloride content, the authors found that the impact of sulfate ions on chloride diffusion changed from outside to the inside and turns from inhibition to promotion.

Cheng et al. [87] have investigated the effect of sulfate and magnesium ions on chloride diffusion behavior of Portland cement mortar. For this purpose, the authors have prepared mortar mixes using Portland cement and Portland cement replaced with 30 wt. % of fly ash (FA) and 50 wt. % of ground granulated blast furnace slag (GGBFS) at a w/b ratio 0.50. From the mortar mixes, specimens of size 40 mm × 40 mm × 160 mm were prepared and cured for 28 days. After the end of curing, all the surfaces except the exposed surface (40 mm × 40 mm) of the specimen were sealed by epoxy resin and exposed NaCl, NaCl + $MgCl_2$, NaCl + Na_2SO_4 and NaCl + Na_2SO_4 + $MgCl_2$ solutions with a fixed chloride concentration for 60 days and 90 days. Chloride binding capacity, apparent chloride diffusion coefficient, and pH of mortar were determined. Phase composition using XRD

and TGA analyses, and microstructure by SEM-EDS analysis and MIP (mercury intrusion porosimetry) were conducted. The results indicated that the presence sulfate ions in NaCl + Na_2SO_4 solution increased the chloride binding capacity and decreased the apparent chloride diffusion coefficient of mortar whereas the presence magnesium ions and combined presence of sulfate and magnesium ions in chloride solution reduced the chloride binding capacity and increased the apparent chloride diffusion coefficient after 90 days of exposure. The mortar prepared with GGBFS showed lower chloride content, and decrease in chloride binding capacity and apparent diffusion coefficient as compared to control mortar. Further, the mortar prepared with GGBFS was more effective in reducing the apparent chloride diffusion coefficient as compared to that made with fly ash when compared with the control mortar. The authors observed that the combined presence of sulfate and chloride ions increases the porosity of mortar as a result of formation of more micro-cracking in the pore structure.

Cheng et al. [35] have studied the effects of sulfate, and magnesium ions on chloride ion transport behaviour and binding capacity of Portland cement mortar made with and without fly ash (FA) and ground blast furnace slag (BFS). For this purpose, the authors have prepared mortar mixes using Portland cement and Portland cement replaced with 30 wt. % of fly ash and 50 wt. % of ground blast furnace slag at w/b ratios of 0.40, 0.45 and 0.50. From mortar mixes, specimens of size 40 mm × 40 mm × 160 mm were cast and cured for 7 days. After curing, the mortar specimens were sealed using epoxy to ensure one-dimensional ingress and exposed to different concentrations of NaCl, NaCl + $MgCl_2$, NaCl + Na_2SO_4 and NaCl + $MgCl_2$ + Na_2SO_4 solutions for 60 days. After end of exposure, the concrete powder samples were collected at different depth intervals to determine the free chloride (water-soluble) and total chloride (acid-soluble) contents. Further, the chloride binding capacity and apparent chloride diffusion coefficient (using Fick's 2nd law) was determined using chloride contents. X-Ray diffraction (XRD) analysis and thermogravimetric analysis (TGA) were performed on powdered samples to study the hydration product formed in the exposed mortar specimens. The pore structure of exposed mortar was determined using micromeritics mercury porosimeter. Based on results of different tests, the authors reported that the mortar specimens exposed to NaCl + $MgCl_2$ solutions showed highest chloride content at the outmost layer (0-5 mm) as compared to other chloride and composite chloride-sulfate solutions. Further, the presence of magnesium ions, and combined sulfate and magnesium ions in the chloride solution

accelerated the chloride ingress, while the sulfate ions limits the chloride penetration. Further, the presence of sulfate ions in NaCl + Na_2SO_4 solution reduced the apparent chloride diffusion coefficient and enhanced the chloride binding capacity. However, magnesium ion and combined of sulfate and magnesium ions in chloride solution reduced the chloride binding and increased the apparent chloride diffusion coefficient of mortar. From the results of XRD and TG analyses, it was observed that the sulfate ions in presence of chloride promoted the formation of Friedel's salt while magnesium ions induced the formation of hemicarboaluminate phases except in the outermost layer. The replacement of Portland cement with fly ash and ground blast furnace slag decreased the apparent chloride diffusion coefficient. Moreover, ground blast furnace slag resulted a decrease in chloride binding capacity and pore size however, fly ash seems to have no clear effect on chloride ion profile and chloride binding capacity.

Balestra et al. [4] have carried out a study on the modeling of chloride profile obtained from concrete structures existing for more than 40 years in tidal, splash and marine atmosphere zones under natural degradation. Concrete cores of diameter of 75 mm with variable length were extracted from the existing structures in different exposure zones. Some of the cores were ground into powder samples at different depth intervals for determining the chloride concentration using the X-Ray Fluorescence Spectroscopy method and potentiometric titration technique. Subsequently, the authors developed a relationship between these two techniques, and found a good degree of correlation, and further used for determination of chloride content. The obtained chloride profiles were analyzed using Fick's 2nd law equation and modified Holliday equation. In addition, the physical and mechanical characterization of the core concrete samples were carried out using trace reconstitution, mercury intrusion porosimetry and compressive strength. Based on the results obtained from chloride profile, the authors reported that the convection zone exists in concrete after that diffusion zone started. From the analysis of different models, it was observed that both Fick's 2nd law and modified Holliday equation presented a strong similarity to represent chloride concentration in diffusion zone even in more advanced (longer) ages of structure. However, in the presence of convection zone, only the modified Holliday equation was able to represent the chloride concentration in both the convection and diffusion zones, regardless of the age of structure and marine aggressive zone. From the analysis, it was concluded that it is possible to represent the chloride concentration by considering the convection zone through a simple empirical model using different variables

such as the apparent diffusion coefficient, age of structure, and the peak value of chloride concentration.

Weerdt et al. [37] have studied the chloride ingress in mortar from seawater and NaCl solution to investigate the effect of ions other than sodium and chloride in seawater on chloride ingress. For this purpose, mortar specimens (125 ml cylindrical sealed plastic bottles) were prepared using ordinary Portland cement (PC) with 6% silica fume (SF) at a w/b ratio of 0.40. The cylindrical specimens were coated with epoxy before exposure. The coated specimens were exposed to seawater and NaCl solution with the same chloride concentration as the seawater for 21, 90, and 180 days. After the end of the exposure, the chloride ingress depth (sprayed with 0.1 M $AgNO_3$) was determined by splitting the sample. Also, the profile grinding was performed at different depth intervals up to 23 mm and chloride analysis (total chloride content), thermogravimetric analysis (TGA), and induced coupled plasma mass spectrometry (ICP-MS) were performed on collected concrete powder samples. Thermodynamic modeling was also done using the Gibbs free energy minimization software GEMS3 to assess the change in hydration products after exposure to chloride and seawater. SEM-EDS elemental maps were used to illustrate the elemental changes taking place in the outer 100 μm of the mortar exposed to seawater and NaCl exposed samples. Based on the results obtained from different tests, the authors reported that the only 1 mm of mortar specimens exposed to seawater was enriched with sulfur and magnesium, which did not limit the chloride ingress in mortar within 180 days of exposure. The reduction in the amount of portlandite was due to carbonation in top exposure surface and due to leaching of portlandite in mortar specimens at deeper uncarbonated sections. A clear diffusion profile of chlorine and potassium was noted until 10-20 mm depth, whereas the diffusion of sodium, sulfur, and magnesium was limited to the outer surface of 1 mm. The authors also concluded that the chloride ingress in marine exposed concrete could be evaluated using NaCl solutions.

Zhao et al. [88] have investigated the degradation mechanism of concrete against combined sulfate-chloride attack. The concrete mix was prepared at a w/b ratio of 0.486 with ASTM Type I Portland cement. Cylindrical specimens (size: 100 × 200 mm) were cast and after 8 hrs of curing, epoxy resin was used to seal the top and bottom sides of the specimens. Then, the specimens were placed in eight different exposure solutions (3% Na_2SO_4, 5% Na_2SO_4, 10% Na_2SO_4, 3% NaCl, 3% NaCl + 3% Na_2SO_4, 3% NaCl + 5% Na_2SO_4, 3% NaCl + 10% Na_2SO_4, and distilled water). The properties such as dimension

change, weight loss, compressive strength, sulfate concentration, and mineral and chemical composition of concrete were determined after 1, 3, 6, 9, and 12 months of immersion in the exposure solutions. The microstructural analysis was performed using SEM, EDS, XRD, TG-DTG and DSC analyses. The test results showed that the concrete specimens suffered more physical damage and strength loss when subjected to combined chloride-sulfate solutions as compared to only sulfate solutions. The chloride ions accelerated the diffusion of sulfate ions due to severe damage induced by the combined sulfate-chloride attack, by resulting in more cracks in the concrete matrix and providing more paths for ingress of sulfate ions.

Cheng et al. [89] have studied the influence of multiple ions present in seawater on the degradation process of Portland cement mortar under drying-wetting cycles. For this purpose, the authors have prepared mortar and cement paste specimens using Portland cement at a w/b ratio 0.50. From mortar mixes, specimens of size 40 mm × 40 mm × 160 mm and from cement paste, specimens of size 40 mm × 40 mm × 40 mm were prepared and cured for 28 days. After curing, all the surfaces of mortar specimen except the exposed surface (40 × 40 mm) were sealed by epoxy resin and immersed in NaCl, NaCl + $MgCl_2$, NaCl + Na_2SO_4 and NaCl + $MgCl_2$ + Na_2SO_4 solutions of fixed chloride concentration for 30, 60, 90 and 120 days under drying-wetting cycle. The paste specimens were also exposed to same exposure solutions for 6 months and used for determination of phase composition using XRD and TG analyses. After the end of different exposure periods, the free chloride content was determined at different depth intervals from the mortar specimens. From the obtained free chloride profile, apparent chloride diffusion coefficient was estimated using Fick's second law of diffusion. Further, magnesium and sulfur profile, physical degradation (mass change and dynamic modulus of elasticity), microstructure (SEM-EDS analysis) and pore structure characteristics (mercury intrusion porosimetry (MIP)) were also determined for mortar specimens. From the obtained results, the authors concluded that the presence of sulfate ions, and combined presence of sulfate ions with magnesium ions in chloride solution initially decreased and then increased the chloride content and apparent chloride diffusion coefficient of mortar when compared with NaCl solution. The presence of magnesium ions in chloride solution increased the chloride diffusion coefficient of mortar as compared to NaCl solution. Further, the mortar specimens exposed to composite solutions containing magnesium ions showed enrichment of magnesium at the outer layer (0–5 mm) of mortar. From the test results of mass change and dynamic modulus of

elasticity, the presence of sulfate ions and combined presence of sulfate ions with magnesium ions in the exposure solutions accelerated the degradation process, whereas the presence of only magnesium ions had negligible effect on the damage of the samples. From the results of phase composition analysis, the combined presence of sulfate ions with magnesium ions in chloride solution promoted the formation of ettringite but decreased the contents of Friedel's salt and portlandite, and resulted in decalcification of C–S–H. Further, the presence of sulfate ions and combined presence of magnesium and sulfate ions in the chloride solution showed more cracks and pores, which further accelerate the penetration of aggressive ions as compared to only chloride (NaCl) solution.

2.3. Corrosion of steel reinforcement in concrete subjected to different exposure environment

The research work carried out by various researchers on the effect of mix parameters (binder type i.e. cement type, and supplementary cementitious materials, and w/b ratio), and exposure condition (exposure solution, exposure duration, wetting-drying cycle etc.) on corrosion of steel reinforcement in concrete are presented and discussed in this section.

2.3.1. Effect of mix parameters on corrosion of steel reinforcement

Page et al. [90] have studied the effect of binder type on chloride-induced corrosion of reinforcing steel by considering the concentrations of aggressive chloride ions and inhibitive hydroxyl ions in the pore solution, and ionic diffusivity of chloride ions. For this purpose, the experimental investigation involved the expression and analysis of pore solution, determination of chloride diffusivity and measurement of corrosion rate of embedded steel reinforcement. Ordinary Portland cement (OPC) with different C_3A contents (OPC A with C_3A 7.7%, and OPC B with C_3A 14.3%), sulfate resisting Portland cement (SRPC with C_3A 1.9%) and two blended cements (OPC B + 30% PFA (pulverized fuel ash) and OPC B + 65% GGBS (ground granulated blast furnace slag)) were used for the preparation of specimens. For expression and analysis of pore solution, the paste samples were prepared at w/c ratio of 0.50 and admixed with 0.4% chloride ion (NaCl as source of chloride ions) by weight of cement at the time of mixing. The pore solution was expressed using pressure vessel, which was analyzed for hydroxyl ion and chloride ion concentrations. The diffusion of chloride was measured using the diffusion cell method. For corrosion measurement, mild steel reinforcement bar (with exposed area of 10 cm^2) was embedded in the paste specimens (size: 50 mm diameter and 75 mm length) made with or without 0.4% chloride ion and the polarization resistance technique was used for

measurement of corrosion rate. Based on results obtained from different tests, the authors reported that the blending agents resulted in the reduction of alkalinity of the pore solution, and did not reduce the chloride binding capacity. SRPC showed the poorest degree of corrosion protection, whereas slag and PFA blended cements showed the highest degree of corrosion protection as compared to OPC. The diffusion of chloride ions was less in blended cements and more in SRPC as compared to OPC.

Cao and Sirivivatnanon [91] have studied the effectiveness of increase in strength of concrete and the effect of silica fume on the corrosion rate of embedded steel reinforcement in chloride contaminated environment. For this purpose, the authors prepared the concrete mixes using ordinary Portland cement (type A) and silica fume with different replacement levels of 10% and 20% by mass of cement at different w/b ratios. The 28 days compressive strength of different concrete mixes varied from 21 MPa to 71 MPa. From each concrete mix, cylindrical concrete specimens of size 100 mm in diameter and 200 mm in length embedded with two steel rods each of 6 mm diameter were prepared for corrosion monitoring. After 7 days of curing, the cylindrical specimens were partially immersed in lime-saturated water or 4% NaCl solution with a constant DC voltage of 400 ± 25 mV applied across two steel rods. Simultaneously, the corrosion rate of steel in reinforced concrete specimens was measured for different immersion periods till 200 days. After the end of testing, the specimens were broken and the weight of anodic steel rods was measured to determine the weight loss. Additionally, the resistivity of concretes was also measured using the Weiner bridge with a quadrature oscillator in the same exposure solutions. Based on results obtained from different tests, the authors reported that the corrosion of steel reinforcement and chloride penetration could be reduced by increasing the compressive strength of concrete. In addition, the results indicated that OPC with 10% silica fume produced high-strength concrete and showed lower corrosion of steel reinforcement and lower weight loss as compared to other concrete mixes. However, OPC with 20% silica fume also produced high-strength concrete, but on the contrary, the corrosion rate and weight loss of steel were higher as compared to OPC and OPC with 10% silica fume concrete. The authors observed that the chloride threshold level for steel corrosion was lower for 20% silica fume replaced concrete.

Mangat et al. [92] have investigated the relationships between microstructure (porosity and pore structure), chloride diffusion and resistance against steel reinforcement corrosion. For this purpose, cement paste and concrete mixes were prepared using ordinary Portland

cement (OPC) and OPC replaced with pulverized fuel ash, microsilica, and ground granulated blast furnace slag at different w/b ratios. The cubes of cement paste of size 100 mm were prepared at a w/b ratio of 0.45 for porosity and pore structure measurement using mercury-intrusion porosimetry (MIP) test. The concrete specimens were prepared for compressive strength (cube) and chloride diffusion (prism) tests at w/b ratios of 0.45 and 0.58 respectively. For chloride diffusion test, the prismatic specimens were coated with bituminous paint, except one face to allow chloride penetration during exposure to a chloride environment. For corrosion measurement, the prismatic concrete specimens embedded with three replicate rebar electrodes of diameter 12 mm and positioned at a cover of 10 mm from the side face were prepared and sealed using bituminous paint, except one side face. All the concrete test specimens were exposed to a chloride environment using a seawater spray chamber, which provided two wet and dry cycles at every 24 hours for different exposure periods. Subsequently, the corrosion potential and polarization resistance were measured using a potentiostat at different intervals during exposure. After the end of the exposure period, acid-soluble chloride (from concrete powder) and free chloride (from pore fluid expressed from concrete under high pressure) concentrations were determined at different depth intervals. Based on obtained results, the authors reported that the replacement of cement with 10% microsilica exhibited increased intruded pore volume in paste among all binder replacements however, it decreased the chloride penetration and corrosion rate of steel rebar in concrete specimens. Further, the replacement with 20% pulverized fuel ash resulted in higher pore volume and coarser pore-size distribution in hardened cement paste as compared to control paste, which increased the chloride content up to 30 mm depth from the surface and reduced the chloride content beyond 30 mm. The corrosion rate was found to be higher in case of replacement with 20% pulverized fuel ash as compared to the control mix. In case of 40% slag replacement, an increase in intruded pore volume of cement paste was observed as compared to control paste; and the chloride content increased up to 20 mm depth from the surface and reduced beyond 20 mm. Further, the corrosion rate was higher in case of replacement with slag as compared to the control mix. From the study, the authors concluded that the microstructure of cement paste matrix was not necessarily related to chloride diffusion and steel reinforcement corrosion rate in concrete replaced with different supplementary cementitious materials.

Arya and Xu [93] have investigated the relationship between chloride binding and rate of reinforcement corrosion using cement paste and concrete specimens made with ordinary

Portland cement (OPC) and OPC replaced with 65% ground granulated blast furnace slag (GGBS) or 35% pulverized fuel ash (PFA) or 10% silica fume (SF) at a w/b ratio of 0.50. The cement paste specimens were prepared to evaluate the chloride binding in different mixes by dissolving appropriate quantities of NaCl in the mixing water (0.2% to 2.5% Cl^- by mass of cement). The concrete specimens embedded with three (two in chloride-free layer and one in contaminated chloride layer) 8 mm diameter steel electrodes were prepared for corrosion rate measurement The concrete specimens comprised of two 50 mm thick layers in which, the lower layer was contaminated with dosages of 1% and 3% Cl^- (by weight of cement). From the cement paste specimens, the pore solution was extracted using a pore press method and used for measurement of Cl^- and OH^- concentrations. The corrosion of steel in concrete was measured in terms of galvanic current in macro corrosion cells employing a zero resistance ammeter. Based on results obtained from different tests, the authors reported that the chloride binding was not related in any simple way to the corrosion rate of steel reinforcement embedded in concrete. Further, the authors reported that the chloride ion binding for different types of binders occurred in the order of GGBS > PFA> OPC > SF. The amount of free chloride and the corrosion rate increased with an increase in chloride concentration. The corrosion rates occurred in the order of PFA> SF> GGBS > OPC in the concrete admixed with 1% Cl^- concentration, and in the order of PFA> OPC > GGBS > SF in the concrete admixed with 3% Cl^- concentration.

Al-Amoudi [94] has carried out an experimental investigation to evaluate the performance of reinforced concrete in mixed magnesium sulfate and sodium sulfate environment. For this purpose, 15 concrete mixes were prepared using three Portland cements (ASTM C 150 Type I, Type II, and Type V Portland cements), three mineral admixtures (10% silica fume and 20% class F fly ash as replacement of Type I and Type V cements, and 60% blast furnace slag as replacement of Type I cement by weight) and two w/cm ratios of 0.35 and 0.50. For corrosion measurement, cylindrical specimens of size 75 mm in diameter and 150 mm in height with a centrally embedded 12 mm diameter reinforcing steel bar were prepared from different mixes and cured for 14 days. After curing, the specimens were exposed to test solutions containing 2.1% concentration of SO_4^{2-} (50% sodium sulfate and 50% magnesium sulfate) for 44 months. During the exposure period, the physical deterioration due to sulfate attack was evaluated in terms of reduction or increase in weight of the reinforced concrete specimens. The corrosion of steel reinforcement was monitored by measuring half-cell potential (using saturated calomel electrode) and polarization

resistance by linear polarization resistance technique. Based on obtained results, the authors concluded that the plain cement (Type I, II, and V) concretes irrespective of their C_3A content performed well against sulfate attack whereas, they exhibited poor performance against steel reinforcement corrosion. The blended cement concrete mixes made with fly ash, and blast furnace slag showed a higher degree of deterioration in case of both sulfate attack and steel reinforcement corrosion. On the other hand, concrete made with silica fume exhibited the best performance against reinforcement corrosion and poor performance against sulfate attack as compared to other mixes. Further, it was also reported that the reduction in w/cm ratio was generally harmful in the context of sulfate attack in both plain and blended cement concretes.

Asrar et al. [26] have studied the performance of microsilica addition in concrete on chloride permeability and corrosion behaviour of rebar in chloride solution (5% NaCl) and seawater environments. For this purpose, the authors prepared the concrete mixes using ordinary Portland cement (OPC, ASTM Type-I) and sulfate resistant cement (SRC, ASTM Type-V) either alone or in combination with 10% densified or undensified microsilica by weight of cement. From each mix, cylindrical specimens of size 76 mm in diameter and 152 mm in height with a centrally embedded 14 mm diameter steel bar were cast for different tests. On cylindrical specimens, different tests such as salt fog test, salt ingress test, potential measurement and rapid chloride permeability (RCP) test were performed for different periods. Based on the results obtained, the authors reported that the addition of microsilica decreased the chloride permeability of concrete in both OPC and SRC concrete specimens. The blending of microsilica with OPC decreased the corrosion of rebar in case of exposure to chloride solution. On the contrary, it enhanced the corrosion of the steel bar in case of exposure to seawater due to the presence of SO_4^{2+} and Mg^{2+} ions. The authors concluded that the densified microsilica performed better than undensified microsilica against chloride ingress and corrosion of steel bar in concrete, and densified silica fume with SRF may be a better option for controlling rebar corrosion in the marine environment.

Kayali and Zhu [95] have carried out an investigation to study the role of fly ash against the durability of lightweight aggregate concrete exposed to marine environment. Slab specimens of size 470 mm × 470 mm × 150 mm with and without the grid of 12 mm diameter ribbed steel bars were prepared using high-strength lightweight aggregate concrete (LWHS, 7% silica fume + 23% fly ash), normal weight high-strength concrete (HS, 9% silica fume), and normal weight medium-strength concrete (MS). The concrete

cover to steel reinforcement was 25 mm from bottom and 50 mm from side of the slab specimens. From all concrete mixes, cylindrical specimens of size 150 mm diameter and 300 mm height were prepared for measurement of compressive strength. All the slab specimens were partially submerged to a depth of 10 mm from the face near to the reinforcement in chloride solution with a concentration of 20000 ppm (3.5% NaCl). Simultaneously, half-cell potential test (using copper-copper sulphate electrode), linear polarization resistance measurement, and resistivity measurement were carried out on slab specimens during the exposure at various testing periods. The chloride content was also determined every week on non-reinforced slabs at different depth intervals. Based on results obtained, the authors observed that the LWHS concrete with fly ash showed very low concentration of chloride ions after a long exposure period, and very low corrosion activity in terms of half-cell potential and corrosion current density, and high resistivity as compared to HS and MS concrete. The authors developed a relationship between corrosion current density and obtained resistivity values for high-strength concrete slabs and found that the values of resistivity are consistent with the value of corrosion current density.

Kayali and Zhu [96] have studied the corrosion performance of high-strength, and medium-strength reinforced concrete exposed to 3.5% NaCl solution. For this purpose, slab specimens (size: 470 mm × 470 mm × 150 mm) with and without the grid of 12 mm diameter ribbed steel bars were prepared using high-strength (HS, 10% silica fume) and medium-strength (MS) concrete. The cover to the reinforcement was 25 mm from bottom and 50 mm from side of the slab specimens. The slab specimens with rebar were used for corrosion measurement, and slab specimens without rebar were used for chloride ingress test. All the slab specimens were partially submerged to a depth of 10 mm from the face near to the reinforcement in chloride solution with a concentration of 20000 ppm (3.5% NaCl). Simultaneously, half-cell potential test (copper-copper sulfate electrode), and linear polarization resistance measurement were carried out on slab specimens during exposure at various intervals. The chloride content was also determined at different periods on non-reinforced slabs at different depth intervals. Based on obtained results, it was observed that the high-strength concrete with 10% silica fume showed a compressive strength of 70 MPa. From corrosion measurement and chloride ingress test, the high-strength concrete exhibited higher corrosion performance as compared to medium-strength concrete due to lower chloride concentration near the steel bar. Extremely low corrosion current density and half-cell potential values were observed in case of high-strength concrete and these values

remained low after long exposure period. The authors correlated the experimentally obtained half-cell potential and corrosion current density values for medium-strength concrete and reported that the corrosion current density was exponentially related to half-cell potential.

Pradhan and Bhattacharjee [29] have carried out a study to evaluate the corrosion performance of reinforced concrete made with different types of cement, steel, and varying w/c ratios and exposed to chloride solution. For this purpose, the concrete mixes were prepared using ordinary Portland cement (OPC, satisfying ASTM Type I and Indian standards IS 8112:1989), Portland pozzolana cement (PPC) having 20% pozzolana (fly ash) content (satisfying ASTM Type IP and IS 1489:1991-Part I), and Portland slag cement (PSC, satisfying ASTM Type IS and IS 455:1989) at w/c ratios of 0.45, 0.50, and 0.55. The reinforced concrete beam specimens of size 280 mm × 150 mm × 115 mm were prepared as per ASTM G 109 with 12 mm diameter reinforcing steel bars of three types namely cold twisted deformed bars (CTD) and two types of thermomechanically treated (Thermex TMT and Tempcore TMT) ribbed bars. The beam specimens were prepared with two steel bars embedded at the bottom with a cover of 25 mm, and one steel bar centrally at the top with a clear cover depth of 7.5 mm. In addition, the beam specimens having top clear cover depth of 15 mm were also prepared. For compressive strength test, cube specimens of size 150 mm were prepared from each concrete mix and tested after the curing of 28 days. The beam specimens were exposed to 3 % NaCl solution (in a plastic reservoir at the top surface of the specimen) with alternate wetting and drying cycles. For measurement of corrosion parameters, the half-cell potential of the top steel bar was measured with reference to saturated calomel electrode followed by measuring the potential difference between the top steel bar and the common terminal of bottom steel bars across a 100 Ω resistor. The potential values were measured at the beginning of both wetting and drying periods. For all the specimens made with 7.5 mm cover depth at the top, a sudden drop in the half-cell potential (more negative) of the top steel bar was observed. At the same time, the direction of the current flow had changed as indicated by the change in the sign of the potential difference between the top and bottom steel bars. After observing a sudden drop in the potential values, the concrete powder samples were collected at different depth intervals for determining the free chloride and total chloride contents. Based on obtained results, it was demonstrated that for laboratory investigation, the half-cell potential is a stable indicator of corrosion initiation of steel reinforcement in chloride contaminated concrete.

It was observed that the critical chloride level for corrosion initiation is not a unique value, and it depends on steel type, cement type, and w/c ratio. Among binder type, PPC and PSC concrete exhibited higher chloride tolerance and longer corrosion initiation period as compared to OPC concrete. Similarly, among steel type, Tempcore TMT steel exhibited higher chloride tolerance and longer corrosion initiation period as compared to Thermax TMT and CTD steels.

Alghamdi and Ahmad [94] have carried out an experimental investigation to establish a relationship between electrochemically and gravimetrically measured reinforcement corrosion rates. For this purpose, concrete mixes were prepared using ASTM C 150 Type I normal Portland cement with 8% replacement by silica fume at water to cementitious materials ratios (w/cm) of 0.35, 0.40 and 0.45, and fine aggregate to total aggregate ratios of 0.40, 0.45, and 0.50. From these mixes, a total number of 486 reinforced concrete (RC) cylindrical specimens were prepared with a centrally embedded 16 mm diameter steel bar (100 mm exposed length inside the concrete) and three different concrete-cover thicknesses (25 mm, 37.5 mm, and 50 mm). The cylindrical specimens were partially submerged in three varying concentrations of chloride solutions (3%, 7%, and 12% NaCl). The corrosion rate was determined using two methods: electrochemical linear polarization resistance (LPR) method and the gravimetric weight loss method. Based on the relationship between the LPR method and the gravimetric method, the authors reported that a linear correlation exists between two methods irrespective of cover thickness, chloride concentration, and concrete quality. The authors also reported that this correlation could be used to estimate the remaining service life of the reinforced concrete structure by converting electrochemically measured corrosion rate into an equivalent gravimetric corrosion rate.

2.3.2. Effect of exposure condition on corrosion of steel reinforcement

Cheng et al. [98] have studied the role of chloride and sulfate ions on corrosion of steel reinforcement in concrete. For this purpose, concrete mixes were prepared using Type I and Type V Portland cements at a w/c ratio of 0.50. Cylindrical concrete specimens of diameter 50 mm and height 100 mm with a centrally embedded low carbon steel rod (exposed surface area of 38 cm^2) at cover depth of about 15 mm were prepared from each concrete mix. After that, some of the specimens were treated with polymer impregnation to seal the diffusion paths of corrosive ions. The corrosive exposure environment was prepared using artificial seawater and concentrated sulfate solution (220 g of Na_2SO_4, 10 g of NaCl and 10 g of Na_2HPO_4 per liter of water). All the specimens were immersed in

corrosive environment, and the open-circuit potentials (OCPs) were measured using high input impedance electrometer with reference to saturated calomel electrode. Simultaneously, the corrosion rate was determined using the AC impedance technique. From the obtained results, the authors reported that the open-circuit potentials of concrete specimens immersed in concentrated sulfate solution were more positive than those in artificial sea water. Further, the chloride ions were more aggressive than sulfate ions; therefore, the breakdown of the passive layer was caused mainly by the chloride ions. The results of AC impedance measurement indicated that the sulfate ions could change the mechanistic parameter of surface film more significantly, and the sulfate-induced corrosion problems may be more severe. The authors also concluded that the application of polymer impregnation treatment can increase the concrete resistivity greatly and reduce the corrosion activity.

Tayyib and Khan [99] have studied the effect of sulfate and chloride ions on the corrosion performance of steel reinforcement in concrete. For this purpose, concrete mixes were prepared using ASTM Type V (sulfate resistance) Portland cement at a w/c ratio of 0.50 and admixed with or without 0.6, 1.2 and 1.8 kg/m^3 of Na_2SO_4 or NaCl. From each concrete mix, prismatic concrete specimens of size 63 mm × 100 mm × 300 mm with a centrally embedded 12.5 mm diameter plain steel bar were prepared and cured for 28 days. After curing, the prismatic concrete specimens were stored in laboratory conditions for four months, then partially immersed for 808 days in potable water, and transferred to sulfate solution (4.5% Na_2SO_4) and chloride solution (5% NaC1) for 60 days. Simultaneously, the corrosion monitoring of prismatic specimens was performed using half-cell potential measurement (using saturated calomel electrode) and linear polarization resistance measurement. Based on the results obtained from corrosion monitoring, the authors reported that the sulfate ions are corrosive to steel reinforcement, but their corrosivity was less than that of chloride ions. It was also reported that the corrosion rate of chloride-contaminated concrete specimens was 23-35% higher than that of sulfate-contaminated concrete specimens. Further, it was observed that the corrosion activity increased in both solutions, but, in chloride solution, the half-cell potential reached up to active corrosion; however, in sulfate solution it was yet to attain an active potential in 60 days of exposure.

Al-Amoudi and Maslehuddin [100] have studied the effect of chloride, sulfate, and composite chloride-sulfate solutions on corrosion of steel reinforcement embedded in cement paste. For this purpose, cement paste specimens of size 31 mm × 31 mm × 152 mm

and embedded with a 6 mm diameter steel bar were prepared using ordinary Portland cement and cured for 14 days. After curing, the specimens were exposed to four different test solutions (15.7% Cl^-, 2.1% SO_4^{2-}, 0.55% SO_4^{2-} + 15.7% Cl^- and 2.1% SO_4^{2-} + 15.7% Cl^-) for 500 days. Simultaneously, the corrosion parameter of steel reinforcement was evaluated by measuring corrosion potential with reference to saturated calomel electrode and corrosion current density using linear polarization resistance technique. After the end of the exposure, the paste specimens were broken, and paste surrounding to the steel bar was collected to determine the water-soluble chloride content and sulfate content. From the collected paste sample, the water-soluble chloride was determined by titrating against standard mercuric nitrate solution, and sulfate content was determined using spectrophotometric technique. Based on the obtained results, the authors reported that the corrosion activity as time to initiation of corrosion and corrosion current density of steel reinforcement was higher in composite chloride-sulfate solution as compared to only chloride solution followed by sulfate solutions. From visual inspection, the cracks in cement paste were noted in composite solution with high sulfate content, and the surface deterioration in terms of eating away of the surface skin was noted in the specimens exposed to only sulfate solutions. The authors also reported that the corrosion initiation time was 20 days for chloride solution and 56 days for the composite chloride-sulfate solution.

Dehwah et al. [101] have studied the influence of sulfate ion concentration and associated cation type on chloride-induced reinforcement corrosion in concrete. For this purpose, concrete mixes were prepared using ordinary Portland cement (with C_3A contents of 8.5% and 9.65%) and sulfate resisting Portland cement (with C_3A content of 3.6%) at a w/c ratio of 0.45. From the concrete mixes, reinforced concrete specimens of size 75 mm in diameter and 150 mm in height with a centrally embedded 12 mm diameter steel bar were prepared and cured for 28 days. After curing, the concrete specimens were dried in room temperature for one week and then partially immersed (85-90 mm) in chloride and composite chloride-sulfate solutions containing 5% NaCl individual and including 1%, 2.5%, and 4% SO_4^{2-} (sodium sulfate or magnesium sulfate as a source of sulfate ions). Simultaneously, the corrosion potential (with reference to saturated calomel reference electrode) and corrosion current density using linear polarization resistance technique were measured to evaluate the corrosion activity of steel reinforcement in concrete. Based on the obtained results, the authors reported that the time-to-initiation of steel reinforcement corrosion in terms of

corrosion potential was independent of the presence of sulfate ions in the exposure solution and the time-to-initiation of reinforcement corrosion was more in ordinary Portland cement concrete as compared to sulfate resisting Portland cement concrete. The presence of sodium sulfate in the composite chloride-sulfate solution showed higher corrosion current density (I_{corr}) as compared to only chloride solution and increased with an increase in the concentration of sodium sulfate. Similarly, the I_{corr} in the concrete specimens exposed to composite solution with magnesium sulfate increased up to 2.5% concentration of SO_4^{2-} and marginally less for 4% SO_4^{2-} concentration as compared to 2.5% SO_4^{2-} concentration. In addition, the authors reported that the corrosion current density values increased with exposure period and sulfate concentration in the composite solutions and were higher for the composite solution containing magnesium sulfate as compared to sodium sulfate. The authors also reported that the higher C_3A content in cement resulted in lower corrosion current density, which might be due to higher chloride binding.

Dousti et al. [102] have studied several levels of deterioration of existing structure associated with different exposure conditions in the Persian Gulf (atmospheric and splash zones). For this purpose, the jetty structure located in Mahshahr Petrochemical Special Zone complex was taken for the study, which consists of mainly three parts such as reinforced concrete slabs (60 mm cover thickness), steel beams, and steel piles. In this study, investigation of corrosion damage of reinforced concrete slab was reported by visual inspection, and using nondestructive testing to identify an area of extensive degradation for obtaining concrete core and powder for laboratory tests. In laboratory tests, compressive strength test, depth of carbonation, chloride diffusion profile, half-cell potential, level of corrosion (gravimetric mass loss), and XRD analysis were performed on different concrete core and concrete powder samples. Based on the results obtained from different tests, the authors reported that the leading cause of deterioration of the reinforced concrete slab was chloride-induced reinforcement corrosion, and this led to extensive delamination and spalling of the concrete cover. Further, the rate of deterioration was mainly dependent on exposure conditions, and higher deterioration was observed in case of specimens subjected to drying-wetting cycles. From initial inspection, the authors did not find any other deterioration mechanism than corrosion, e.g., alkali-silica reaction in this structure. From the results of carbonation depth, low carbonation depth was found due to high percentage of humidity. From the results of XRD analysis, the authors found weak peaks of portlandite and reported that during sulfate attack, portlandite reacted with sulfate ions and formed

gypsum or other substances. In addition, the depth of sulfate attack was found to be greater than 25 mm depth.

Pradhan [44] has carried out an investigation to study the corrosion behaviour of steel reinforcement in concrete exposed to chloride and composite chloride-sulfate solutions. For this purpose, concrete mixes were prepared with two types of cement, namely ordinary Portland cement (OPC) and Portland pozzolana cement (PPC, fly ash based) and four w/c ratios of 0.45, 0.50, 0.55 and 0.60. From each concrete mix, cube specimens of size 150 mm were prepared for 28 days compressive strength test and slab specimens of size 320 mm × 320 mm × 52 mm with a centrally embedded steel bar of 12 mm diameter at cover thickness of 20 mm both at the top and bottom were prepared for corrosion monitoring. After curing, the slab specimens were kept for 14 days in laboratory exposure condition followed by exposing to 15 chloride and composite chloride-sulfate solutions with alternate drying-wetting cycles for 300 days. The chloride solutions were prepared with NaCl concentrations of 1.5%, 3.5%, and 5% by weight of water. The composite chloride-sulfate solutions were prepared with these concentrations of NaCl combined with $MgSO_4$ or Na_2SO_4 concentrations of 2.5% and 5% of by weight of water. After the end of the exposure, the corrosion parameters such as half-cell potential, relative resistivity, and corrosion current density by linear polarization resistance technique were determined. In addition, analysis of variance (ANOVA) was also carried out to evaluate the effect of chloride ion, sulfate ion, cement type, and w/c ratio on the variations in the corrosion parameters. From the obtained results, it was observed that the half-cell potential values were more negative than -270 mV (saturated calomel electrode) in all exposure solutions (chloride and composite chloride-sulfate) for both types of cement and all w/c ratios thereby indicating the corrosion initiation of steel reinforcement in concrete. It was observed that the concrete made with PPC exhibited higher relative resistivity and lower corrosion current density as compared to OPC concrete in all exposure solutions for all w/c ratios. In addition, for both OPC and PPC, opposite behaviour was observed between composite solutions of sodium chloride with magnesium sulfate, and sodium chloride with sodium sulfate in terms of variations in relative resistivity and corrosion current density. From the results of analysis of variance, it was observed that cement type, w/c ratio, and chloride ion concentration affected both the relative resistivity and corrosion current density in composite solutions of sodium chloride and magnesium sulfate. In case of composite solutions of sodium chloride and sodium sulfate, chloride ion and sulfate ion did not have

significant effect on the variations in relative resistivity, however chloride ion concentration, cement type and w/c ratio had significant effect on the variations in corrosion current density of steel reinforcement in concrete.

Otieno et al. [103] have carried out an investigation to study the long-term corrosion behaviour of concrete exposed to laboratory accelerated (cyclic 3 days wetting with 5% NaCl solution followed by 4 days air-drying), and natural marine environmental (marine tidal zone in Cape Town (Table Bay Harbour)) conditions. The authors considered the crack width 'w_{cr}' (0, incipient crack, 0.4, 0.7 mm), cover depth 'c' (20, 40 mm), binder types (PC (Portland cement), PC/GGBS (ground granulated blastfurnace slag), PC/FA (fly ash)) and w/b ratios (0.40, 0.55) as experimental variables. For this purpose, reinforced concrete beam specimens of size 120 mm × 130 mm × 375 mm and embedded with a high yield strength 10 mm diameter steel bar were prepared with different cover depths for corrosion test. The cracks of different width were introduced on beam specimens using three-point loading. The cracked or un-cracked beam specimens were exposed to laboratory accelerated and natural marine environment, and corrosion parameters were measured using of half-cell potential test and linear polarization resistance measurement up to 2.25 years at successive time intervals. In addition, the diffusion coefficient was also obtained from the measured 28 days chloride conductivity index (CCI) of beam specimens based on the empirical correlation between diffusion coefficient and CCI. Based on the obtained results, the authors reported that the corrosion rate decreased with a decrease in crack width of concrete specimens. Also, the corrosion rate increased with an increase in w/b ratio, and a change in w/b ratio was less effective in concrete made with blended cement as compared to Portland cement and showed similar effect in both laboratory and field exposure conditions. Further, the blended cement resulted in decreased corrosion rate, and no marked difference was observed between laboratory and field exposure conditions. In addition, with an increase in cover depth, the corrosion rate decreased. The authors concluded that in the field under natural condition, corrosion of steel reinforcement in concrete cannot be concluded from its performance in the laboratory under accelerated corrosion, and other factors such as corrosion process should be taken into consideration during evaluation. Finally, the authors have developed a relationship between corrosion rate and half-cell potential and found in good agreement and reported that the high corrosion rate corresponds to a more negative value of half-cell potential.

Otieno et al. [104] have developed chloride-induced corrosion rate prediction model for concrete exposed to laboratory accelerated (cyclic 3 days wetting with 5% NaCl solution followed by 4 days air-drying) and natural marine environments (marine tidal zone in Cape Town (Table Bay Harbour)) conditions. The authors considered the crack width 'w_{cr}' (0, incipient crack, 0.4, 0.7 mm), cover depth 'c' (20, 40 mm), and concrete quality as model variables. The details about the specimens and tests conducted on specimens are already mentioned [103]. The correlation between corrosion rate and concrete quality (quantified using chloride diffusion coefficient) was found in an exponential function, and the correlation between corrosion rate and c/w_{cr} (cover depth/crack width) ratio was found in terms of a power function. Afterward, the authors proposed corrosion rate prediction models for both field and laboratory exposure conditions by considering the concrete quality and c/w_{cr} ratio. Further, using the developed model, the authors predicted the corrosion rate for both field and laboratory conditions and validated with measured corrosion rate and found in good agreement. In addition, the authors suggested that the proposed models provide a novel way to select the concrete durability design parameters (cover depth, concrete quality and crack width) for corrosion affected reinforced concrete structures. Finally, the authors suggested that for model development, the chloride diffusion coefficient could also be determined from the rapid chloride migration test and bulk diffusion test.

Liu et al. [105] have carried out an investigation to study the effect of carbonate and sulfate ions on corrosion initiation and chloride threshold level of reinforcement corrosion in the mortar made with/without fly ash. For this purpose, mortar mixes were prepared using ordinary Portland cement (OPC), and OPC replaced with 15% and 30% fly ash at w/b ratio of 0.53, and binder-sand ratio of 1:3. From each mortar mix, prismatic mortar specimens of size 4 cm × 4 cm × 16 cm with a centrally embedded steel bar of diameter 1 cm and length 6 cm by maintaining a cover depth of 15 mm were prepared and cured for 28 days. After curing, the prismatic mortar specimens were placed in aggressive solutions containing 5% NaCl and 5% NaCl with 2% and 4% of Na_2CO_3 or 2% and 5% Na_2SO_4 for 4 days followed by continuing the exposure in the same solution under drying-wetting cycle until corrosion initiation observed. For measurement of corrosion initiation, electrochemical measurements such as half-cell potential measurement and electrochemical impedance spectroscopy technique were performed at regular intervals. After confirming active corrosion of steel bar, the mortar specimens were broken to analyze

the free chloride and total chloride of mortar samples taken from near the steel bar to evaluate the threshold chloride content. Based on results obtained from corrosion monitoring and chloride content, the authors reported that the time to initiation of active corrosion and chloride threshold level decreased with increase in carbonate concentration in chloride-carbonate solutions. The presence of sulfate ions in chloride-sulfate solution showed little effect on time to initiation of reinforcement corrosion; however, sulfate ions reduced the chloride threshold level. The mortar specimens made with replacement of fly ash exhibited lower chloride threshold level and longer time to initiation of steel reinforcement corrosion.

Sotiriadis et al. [106] have studied the durability performance in terms of reinforcement corrosion and diffusion of chloride in limestone cement-based materials exposed to the chloride and composite chloride-sulfate environment at low temperature. For this purpose, concrete (w/c ratio = 0.52) and mortar (w/c ratio = 0.57) mixes were prepared using Portland cement (PC) and two Portland limestone cement (produced by intergrinding Portland cement clinker and 15% and 35% w/w (weight-to-weight ratio) limestone of high calcite content). From concrete mixes, cylindrical specimens of diameter 100 mm and height 200 mm were prepared for chloride diffusion test. From mortar mixes, cylindrical specimens of diameter 40 mm and height 100 mm with a centrally embedded steel bar of diameter 10 mm were made for reinforcement corrosion test. After curing, the concrete specimens were fully immersed, while mortar specimens were partially immersed up to a depth of 75 mm in chloride (21.14 Cl^- g/l, NaCl) and composite chloride-sulfate (21.14 Cl^- g/l + 20.0 SO_4^{2-} g/l, NaCl + $MgSO_4.7H_2O$) solutions and stored in industrial refrigerator at 5±1ºC for different exposure periods. After the end of exposure of concrete specimens, powder samples were collected from different depth intervals for free (water-soluble) and total (acid-soluble) chloride contents. The chloride contents were used for estimating the chloride diffusion coefficient using Fick's 2nd law of diffusion. Simultaneously, the corrosion test was performed on reinforced mortar specimens using half-cell potential test (copper-copper sulphate electrode) and linear polarization resistance measurement at different intervals. Based on the results obtained from chloride ingress, the authors reported that the free chloride and total chloride contents increased with time and with an increase in limestone content. In addition, the presence of sulfate along with chloride ions in storage solution exhibited higher chloride ion concentrations, less chloride binding and, generally, higher values of chloride diffusion coefficient as compared to only chloride solution. From

the results of corrosion tests, the authors reported that preventing steel reinforcement corrosion was most effective in mortar specimens made of low limestone content cement (15% w/w) in case of exposure to the combined chloride-sulfate solution, however, it showed most severe corrosion in the case of the chloride solution. The authors concluded that at low temperature conditions, the deterioration due to sulfate attack and the ingress of chloride and sulfate ions were enhanced while the corrosion rate was relatively low.

Abdalkader et al. [107] have studied the corrosion performance of steel rebar in cement mortar subjected to chloride and combined chloride-sulfate solutions at temperatures of 5 ºC and 20 ºC. In the study, the mortar mixes were prepared using Portland cement (PC, CEMI (BS EN 197)), and PC blended with 10% limestone filler at a w/c ratio of 0.60. From each mortar mix, cylindrical mortar specimens of diameter 50 mm and height 100 mm with a centrally embedded mild steel bar were prepared for corrosion monitoring. The cylindrical mortar specimens were exposed to chloride (0.5% or 2.0% chloride (NaCl) and combined chloride-sulfate (0.6% sulfate and 0.152% Mg^{+2} ($MgSO_4.7H_2O$) with either 0.5% or 2.0% chloride (NaCl)) solutions at different temperatures for 720 days, and after that, linear polarization resistance (LPR) measurement was conducted. Subsequently, a positive 100 mV DC voltage was applied continuously for an additional 180 days followed by conducting LPR measurement again on the cylindrical mortar specimens. After the second LPR measurement, the specimens were broken and mortar samples were collected from the interfacial steel-mortar zone. The collected mortar samples were used for XRD, SEM, and EDX analyses. Based on the results, the authors reported that the formation of thaumasite exhibited lower corrosion resistance of steel rebar in mortar specimens. In addition, the mortar specimens made with limestone cement and exposed to 0.5% chloride in magnesium sulfate solution at 5 ºC showed higher corrosion rate as compared to other composite solutions and 2% chloride solution. However, at 20 ºC, the limestone cement mortar exposed to composite solution and 2.0% chloride solution showed higher corrosion rate as compared to 0.5% chloride solution. The authors concluded that the thaumasite formation in mortar specimens resulted in lower chloride binding, which contributed as a crucial factor in accelerating the steel reinforcement corrosion.

Kwon et al. [108] have carried out an investigation to study the long-term corrosion performance of steel reinforcement in blended cement concrete exposed to three marine exposure conditions such as atmospheric zone, immersion zone and splash zone. For this purpose, concrete mixes were prepared using ordinary Portland cement (OPC), Portland

pozzolana cement (PPC), and Portland slag cement (PSC) at w/c ratio of 0.55. From each concrete mix, concrete cube specimens were prepared and embedded with/without two steel bars of diameter 12 mm by maintaining the concrete cover of 40 mm. The concrete cube specimens were exposed to different marine exposure conditions for 10 years (at Offshore Platform Marine Electrochemistry Center, Tuticorin, India). After exposure, different tests such as compressive strength, pH measurement, estimation of chloride content, estimation of sulfate content, amount of bio-fouling attachment in concrete, X-ray diffraction (XRD) analysis, scanning electron microscopy (SEM) analysis and electrochemical studies on cube specimens were conducted. Based on the results of compressive strength test, it was observed that the blended cement concrete achieved equal compressive strength as compared to OPC concrete in atmospheric zone and showed a lower strength in the immersion zone and splash zone with a slight decrease in strength. From the results of pH measurement, the alkalinity of the blended cement concrete was relatively equal to that of OPC concrete, and the pH of blended cement concrete was above the threshold limit with respect to depassivation. From the results of chloride and sulfate contents, the blended cement concrete showed lower ingress of chloride ions as compared to OPC concrete in all exposure conditions where PSC showed better performance against chloride ingress, however, the sulfate content in PPC concrete was almost equal to OPC concrete and higher in PSC concrete. As observed from the bio-fouling attachment in concrete, the blended cement concretes exhibited very large bio-fouling attachment as compared to OPC concrete. From the results of electrochemical study, the corrosion rate of the embedded steel bar decreased in the order: PSC < PPC < OPC. From the results of microstructure study, the formation of chloride complex was found lower in atmospheric zone as compared to immersion zone and splash zone, and also lower in blended cement concretes as compared to OPC concrete. Further, the formation of $CaSO_4$ was higher in immersion zone and splash zone as compared to atmospheric zone, and PSC concrete showed more formation of $CaSO_4$ as compared to OPC and PPC concrete. The authors recommended that the blended cements are technically viable from durability point of view rather than OPC and highly recommended for marine environmental exposure conditions.

2.4. Summary of literature review

From the review of literature, it is observed that several studies have been carried out by different researchers to evaluate the influence of mix parameters (binder type i.e. cement type and supplementary cementitious materials, and w/b ratio), and exposure condition

(exposure solution, exposure duration, wetting-drying cycle etc.) on chloride ingress, chloride binding, and microstructure of concrete. The observations from these studies indicated that extent of penetration of chloride ions, chloride binding, and chloride diffusion coefficient of concrete varied with the cement type, supplementary cementitious materials, w/b ratio, and exposure solution (chloride, and composite chloride-sulfate solutions along with the cation type associated with sulfate ions). In addition, the microstructure of concrete also varied with the above mentioned parameters. However, the studies on variations in microstructure with depth interval from the exposure surface of concrete subjected to different exposure solutions are scanty in the literature. From the review of literature, it was observed that the addition of mineral admixtures (supplementary cementitious materials) such as fly ash, ground granulated blast furnace slag (GGBS), and silica fume etc. increased the resistance of concrete against chloride ingress. Further, the review of literature indicated contradicting observations about the variations in chloride binding of concrete wherein in some studies the researchers have observed increase in chloride binding due to addition of mineral admixtures such as fly ash and ground granulated blast furnace slag (GGBS) in concrete whereas in other studies, the opposite variation in chloride binding was observed with the addition of these mineral admixtures in concrete. In addition, contradicting observations about the variations in chloride binding, and chloride diffusion coefficient of concrete between sodium chloride solution, and composite solution of sodium chloride plus sodium sulfate were reported in different studies.

From the literature review, it is observed that several researchers have conducted investigations to study the corrosion behaviour of steel reinforcement embedded in concrete subjected to chloride and composite chloride-sulfate environment. In addition, in some studies the researchers have established the empirical relationship between corrosion parameters such as corrosion potential and corrosion current density of steel reinforcement in concrete exposed to chloride solutions. However, the studies on the development of empirical relationship between corrosion potential and corrosion current density of steel reinforcement in concrete exposed to composite chloride-sulfate solutions are scanty in the literature. Further, in very few studies, the relationship between chloride diffusion coefficient, and corrosion current density of steel reinforcement was established. In addition, in these limited studies, the values of diffusion coefficient and corrosion current density were not determined from the same specimen, i.e. different types of specimen were

used for determining these parameters, and also the diffusion coefficient of chloride was estimated from the empirical correlation between it and the chloride conductivity index obtained from the rapid chloride conductivity test. It may be noted that the relationship between chloride diffusion coefficient, and corrosion current density of steel reinforcement determined from the same specimen may represent the true variation between these parameters as compared to that obtained between these parameters determined from different types of specimen, because the interaction of chloride ions with different phases in concrete may not take place to the same extent in both the cases.

Keeping in view the aforementioned observations from the review of literature, there is a need to study the chloride ingress, chloride binding, microstructure, and corrosion of steel reinforcement in concrete, and establishing the empirical relationships between corrosion parameters and other durability parameters in the concrete subjected to different exposure environment. For this purpose, in the present research work, an investigation has been carried out to study the chloride ingress (free chloride content profile and apparent chloride diffusion coefficient), chloride binding, microstructure, and corrosion of steel reinforcement in concrete exposed to chloride and composite chloride-sulfate solutions for different exposure periods wherein the corrosion parameters (E_0: half-cell potential, and I_{corr}: corrosion current density), and apparent chloride diffusion coefficient (D) were determined from the same concrete specimen, followed by establishing the empirical relationship between I_{corr} and D. In addition, the empirical relationship between the I_{corr} and E_0, and that between I_{corr} and rebar surface chloride concentration (C_{rs}) were also established. Further, the variations in microstructure of concrete exposed to chloride and composite chloride-sulfate solutions were evaluated by performing different microstructure techniques. For these purpose, in this research work, prismatic reinforced concrete specimens embedded centrally with a reinforcing steel bar were prepared from different types of binder such as ordinary Portland cement (OPC), OPC + 20% fly ash (FA), and Portland pozzolana cement (PPC) at w/b ratios of 0.45, 0.50 and 0.55, and exposed to chloride (NaCl), and composite chloride-sulfate (NaCl + $MgSO_4$ and NaCl + Na_2SO_4) solutions of varying concentrations for different exposure periods. It may be noted that in the literature, several investigations have been reported wherein the durability performance of concrete made with fly ash as partial replacement of OPC has been evaluated, however, the reported research work in the literature on durability performance of concrete made with fly ash based blended cement such as PPC (Portland pozzolana cement) is scanty.

Therefore, in the present investigation, the test specimens were prepared from PPC along with those prepared from OPC and OPC plus fly ash. The prismatic reinforced concrete specimen with ponding of chloride, and composite chloride-sulfate solutions was used for natural diffusion test, and also for determining the corrosion parameters of steel reinforcement. The parameters i.e. half-cell potential (E_0), corrosion current density (I_{corr}), chloride content, and apparent chloride diffusion coefficient (D) were determined from the prismatic reinforced concrete specimens at the end of different exposure periods. The specimen and test setup used in the present study were designed in such a way that all the parameters i.e. half-cell potential (E_0), corrosion current density (I_{corr}), rebar surface chloride concentration (C_{rs}), and apparent chloride diffusion coefficient (D) were determined from the same specimen. Further, in this research work, X-ray diffraction (XRD) analysis, field emission scanning electron microscope (FESEM) analysis, and thermo-gravimetry analysis (TGA) were conducted on the concrete powder samples collected from the prismatic reinforced concrete specimens to analyze the microstructure of concrete exposed to chloride and composite chloride-sulfate solutions.

2.5. Objectives of the present research work

By keeping in view the research needs identified from the review of literature, the objectives of the present research work have been formulated as follows:

- To evaluate the effect of mix parameters, chloride ion concentration, sulfate ion concentration and its associated cation type in the exposure solution, and exposure duration on free chloride content profile, apparent chloride diffusion coefficient, and chloride binding in concrete.
- To analyze the microstructure of concrete exposed to chloride and composite chloride-sulfate solutions of varying concentrations.
- To determine the effect of mix parameters, chloride ion concentration, sulfate ion concentration and its associated cation type, and exposure duration on steel reinforcement corrosion in concrete exposed to chloride and composite chloride-sulfate solutions of varying concentrations.
- To establish the empirical relationships between corrosion current density, and the parameters such as half-cell potential, apparent chloride diffusion coefficient, and rebar surface chloride concentration of concrete.

CHAPTER 3

EXPERIMENTAL WORK

3.1. General

In this chapter, the details about the materials, mix proportion of concrete, test specimens, and different tests conducted on the test specimens are presented.

3.2. Materials

Different materials, which were used in this experimental work are presented below.

3.2.1. Binder

In this experimental study, the concrete test specimens were prepared using three types of binder such as ordinary Portland cement (OPC) of 43 grade conforming to IS: 8112-2013 [109] and ASTM Type I [110], Portland pozzolana cement (PPC) conforming to IS: 1489-1991(part-1) [111] and ASTM Type IP [112], and OPC plus 20% Class F fly ash conforming to ASTM C618 [113]. Fly ash was used as a mineral admixture at a replacement level of 20% by mass of binder content. The measured values of specific gravity of OPC, PPC, and fly ash (FA) were 3.12, 2.78, and 2.10 respectively. The chemical composition (oxide composition) of OPC, PPC, and fly ash determined from XRF (X-ray fluorescence) analysis are presented in Table 3.1. The mineral composition or Bogue composition of OPC and PPC are presented in Table 3.2.

Table 3.1 Chemical composition of OPC, PPC, and fly ash

Compound (wt. %)	OPC	PPC	FA
Calcium oxide (CaO)	65.26	63.1	16.57
Silicon dioxide (SiO_2)	21.46	23.11	53.24
Aluminium oxide (Al_2O_3)	4.98	3.14	25.30
Ferric oxide (Fe_2O_3)	1.46	1.94	1.20
Magnesium oxide (MgO)	2.83	2.41	1.15
Sulphur trioxide (SO_3)	2.09	1.90	0.20
Potassium oxide (K_2O)	0.41	1.12	0.40
Sodium oxide (Na_2O)	0.83	2.53	0.13

Table 3.2 Bogue composition of OPC and PPC

Mineral composition (wt. %)	OPC	PPC
C_3S	61.08	51.96
C_2S	15.45	27.06
C_3A	10.73	5.04
C_4AF	4.44	5.90

3.2.2. Aggregate

Aggregates of size 20 mm MSA (maximum size of aggregate) and 10 mm MSA as coarse aggregate and locally available river sand as fine aggregate were used in the preparation of concrete mixes.

3.2.2.1. Sieve analysis of coarse aggregate and fine aggregate

The sieve analysis of 20 mm MSA and 10 mm MSA coarse aggregates, and sand were carried out as per the guidelines mentioned in IS: 2386 - 1963 (part-1) [114]. Particle size distribution curves of all the aggregates are shown in Figure 3.1. From the obtained cumulative percentage passing values, it was observed that the sand is conforming to ASTM C33-16 [115], and grading Zone-II as per IS: 383-1970 [116].

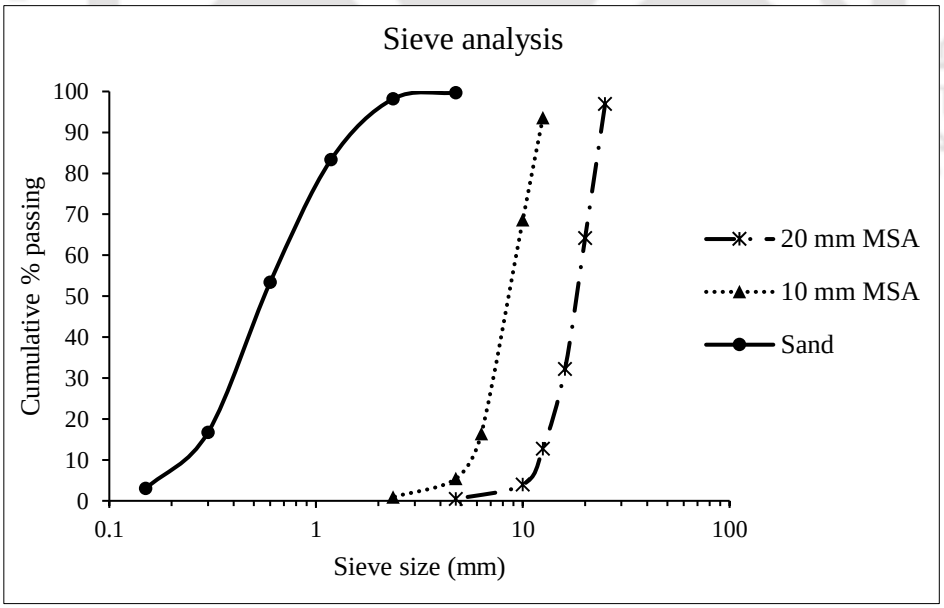

Figure 3.1 Particle size distribution curves of 20 mm MSA and 10 mm MSA coarse aggregates, and sand

3.2.2.2. Specific gravity of coarse aggregate and fine aggregate

The specific gravity of 20 mm MSA coarse aggregate was determined using wire basket method as per the guidelines mentioned in IS: 2386-1963 (part-3) [117]. The obtained value of specific gravity of 20 mm MSA coarse aggregate was 2.65. Similarly, the specific gravity of 10 mm MSA coarse aggregate and sand were determined using pycnometer method as per the guidelines mentioned in IS: 2386-1963 (part-3) [117]. The obtained values of specific gravity for 10 mm MSA coarse aggregate, and sand were 2.65 and 2.62 respectively.

3.2.3. Steel reinforcement

Tempcore TMT (Thermomechanically treated) deformed steel bars of diameter 12 mm were used as the steel reinforcement. The weight % (wt. %) of the chemical elements of steel reinforcement determined by energy-dispersive X-ray (EDX) analysis is presented in Table 3.3.

Table 3.3 Chemical composition of steel reinforcement (wt. %)

Chemical element	Mn	Si	Ni	Cr	Cu	S	P	C	Fe
wt. %	1.2	0.6	0.2	0.2	0.1	0.2	0.1	<0.1	Balance

3.3. Mix proportioning of concrete

The mix proportioning of the ingredients of concrete mix was carried out as per DOE (British mix design method) method with some modification [118]. In the present investigation, the concrete mixes were prepared with water-to binder (w/b) ratios of 0.45, 0.50 and 0.55. These w/b ratios were selected to evaluate the performance of concrete against different exposure conditions such as severe, moderate and mild [119]. Based on trial tests, all the concrete mixes were prepared at a mixing water content of 205 kg/m^3 with slump value varying from 30 mm to 60 mm. The wet density of concrete was calculated corresponding to the specific gravity of combined aggregate and the water content as per SP: 23-1982 [118]. The total aggregate content was calculated by subtracting the total mass of water and binder content from the wet density of concrete. The proportion of sand (fine aggregate) was taken as 37% of total aggregate content by mass for all w/b ratios based on the trial tests carried out for the desired range of slump value. After that, coarse aggregate content was determined, and the proportion of 20 mm MSA and 10 mm MSA coarse

aggregates were 62% and 38% respectively by mass of total coarse aggregate content. The mix quantities of the concrete mixes are presented in Table 3.4.

3.4. Preparation of test specimens

Two types of specimens were prepared from each concrete mix. Cube specimens of size 150 mm were prepared for the compressive strength test. Prismatic reinforced concrete specimens of size 62 mm × 62 mm × 300 mm with a centrally embedded steel bar of diameter 12 mm were prepared for determining the corrosion parameters and for estimating the apparent chloride diffusion coefficient of concrete. The steel bars were cut to a length of 380 mm and cleaned with wire brush to remove any surface scale. Insulating tape followed by epoxy coating was applied over the steel rebar for a certain length, to prevent crevice corrosion, at the locations of discontinuity of steel bar with the concrete. The concrete cover to the steel bar in the prismatic specimen was 25 mm, and the exposed length of the steel bar in it was 200 mm. Three replicate cube specimens were prepared from each concrete mix for each curing age i.e. 28 days, 90 days and 180 days. Separate replicate prismatic reinforced concrete specimens were prepared from each concrete mix for different exposure periods of 9, 15, 21 and 27 months. The schematic diagram along with the photograph of the steel specimen, and schematic diagram of the prismatic reinforced concrete specimen are shown in Figure 3.2 and Figure 3.3 respectively.

Table 3.4 Mix quantities of concrete mixes at different w/b ratios

Binder type	w/b ratio	Cement (kg/m^3)	Fly ash (kg/m^3)	Coarse aggregate (kg/m^3)	Sand (kg/m^3)
OPC	0.45	455.55	…	1073.80	630.64
OPC + 20%FA*		364.44	91.11		
PPC		455.55	…		
OPC	0.50	410.00	…	1102.50	647.00
OPC + 20%FA		328.00	82.00		
PPC		410.00	…		
OPC	0.55	372.72	…	1125.98	661.29
OPC + 20%FA		298.18	74.54		
PPC		372.72	…		

* FA: Fly ash

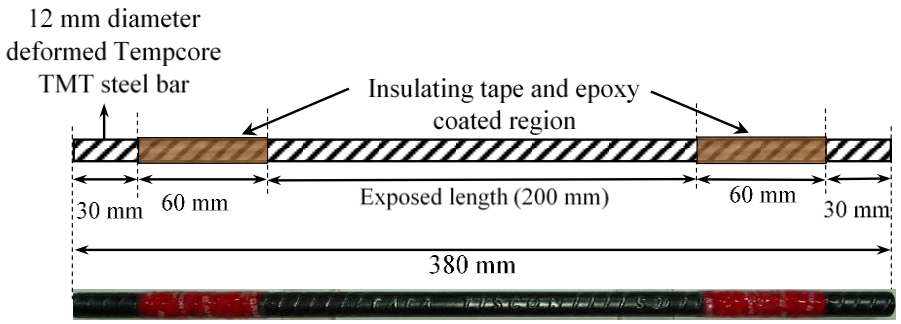

Figure 3.2 Schematic diagram and photograph of the steel bar

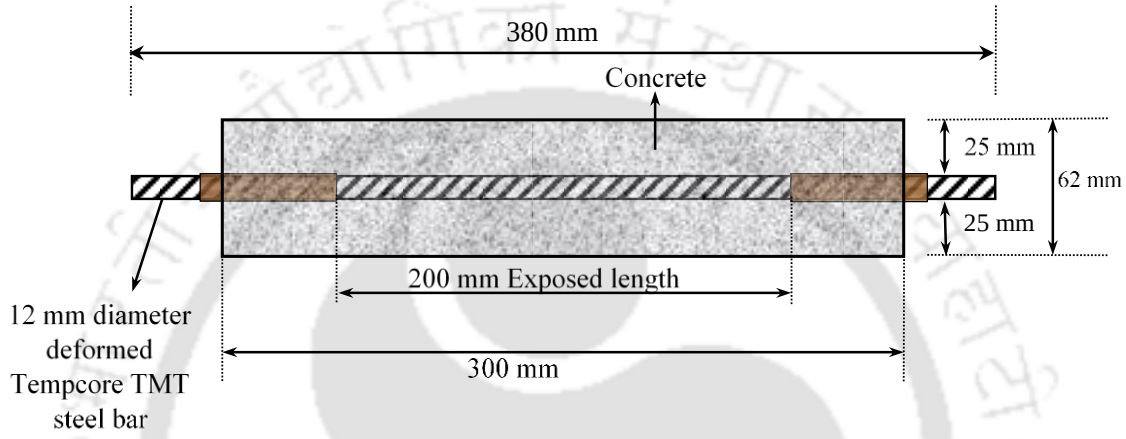

Figure 3.3 Schematic diagram of prismatic reinforced concrete specimen of size 62 mm × 62 mm × 300 mm

The mixing of the ingredients of concrete mix was carried out in a laboratory drum mixer and the compaction of concrete mix inside the moulds was carried out on a vibrating table. After 24 hours of preparation, the cube and prismatic specimens were demoulded and were then subjected to water curing in curing tank. The cube specimens were removed from the curing tank at the end of different curing ages, i.e. of 28 days, 90 days and 180 days from the day of preparation for conducting compressive strength test. The prismatic reinforced concrete specimens were removed from the curing tank at the age of 28 days from the day of preparation and were then kept under ambient laboratory condition for next 14 days. After laboratory drying, the prismatic reinforced concrete specimens were cleaned to remove any dust present on the surface. For storage of exposure solution during the wetting period of exposure cycle (i.e. wetting-drying cycle), a plastic (acrylic sheet) reservoir of size (internal dimension) 50 mm (height) × 42 mm (width) × 200 mm (length) was placed over a longitudinal face of the prismatic specimen and was then joined with the concrete surface by applying epoxy coating. After that, epoxy coating was applied on four vertical faces, and remaining portion of the longitudinal face (outside of the plastic reservoir) of

each prismatic specimen to avoid any loss of moisture from concrete. The schematic diagram, and photograph of the prismatic reinforced concrete specimen with the plastic reservoir are shown in Figure 3.4.

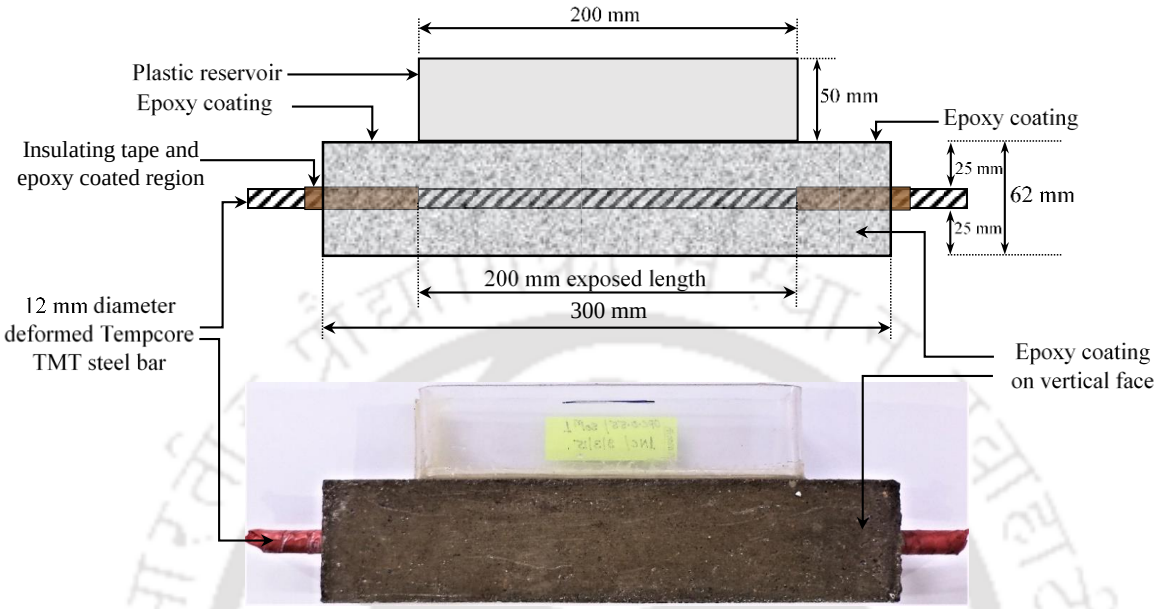

Figure 3.4 Schematic diagram and photograph of prismatic reinforced concrete specimen with the plastic reservoir

3.5. Exposure condition

To evaluate the chloride ingress and chloride-induced corrosion of steel reinforcement in concrete in the presence of sulfate ions in the exposure solutions, the prismatic reinforced concrete specimens were exposed to chloride and composite chloride-sulfate solutions. The prismatic reinforced concrete specimens made from OPC, PPC, and OPC + 20% FA at w/b ratios of 0.45, 0.50, and 0.55 were exposed to external chloride and composite chloride-sulfate solutions for different exposure periods after fixing the plastic reservoir over a longitudinal face of the prismatic specimen, and application of epoxy coating as mentioned in the previous section. Sodium chloride (NaCl) was used as the source of chloride ions whereas, magnesium sulfate ($MgSO_4$) and sodium sulfate (Na_2SO_4) were used as the sources of sulfate ions. The concentrations of chloride and sulfate salts in the exposure solutions were decided by considering the concentrations used by various researchers in the literature, and also the concentrations of the salts present in seawater and groundwater. In this research work, the concentrations of NaCl used were 1%, 3%, and 5%, and those of $MgSO_4$ and Na_2SO_4 used were 2% and 4% each. Three chloride solutions, and twelve

composite chloride-sulfate solutions were prepared by dissolving these dosages (by weight of water) of NaCl, $MgSO_4$, and Na_2SO_4 in water. The composition of exposure solutions are presented in Table 3.5.

Table 3.5 Composition of exposure solutions

Sl. No	Concentrations of exposure solution	Abbreviation
1	1% NaCl	1NC
2	3% NaCl	3NC
3	5% NaCl	5NC
4	1% NaCl + 2% $MgSO_4$	1NC + 2MS
5	1% NaCl + 4% $MgSO_4$	1NC + 4MS
6	3% NaCl + 2% $MgSO_4$	3NC + 2MS
7	3% NaCl + 4% $MgSO_4$	3NC + 4MS
8	5% NaCl + 2% $MgSO_4$	5NC + 2MS
9	5% NaCl + 4% $MgSO_4$	5NC + 4MS
10	1% NaCl + 2% Na_2SO_4	1NC + 2NS
11	1% NaCl + 4% Na_2SO_4	1NC + 4NS
12	3% NaCl + 2% Na_2SO_4	3NC + 2NS
13	3% NaCl + 4% Na_2SO_4	3NC + 4NS
14	5% NaCl + 2% Na_2SO_4	5NC + 2NS
15	5% NaCl + 4% Na_2SO_4	5NC + 4NS

The prismatic reinforced concrete specimens were subjected to above exposure solutions in ambient laboratory condition (temperature range of 27±3° C) with alternate wetting-drying cycles to accelerate the ingress of ions from exposure solution into the concrete. One alternate wetting and drying cycle consists of filling the plastic reservoir with exposure solution for a height of 40 mm during wetting for five days followed by removing the solution from the reservoir and drying in the ambient laboratory condition for ten days. During the wetting period, the plastic reservoirs filled with the exposure solution were covered with plastic sheets at the top to avoid the evaporation. The exposure solutions in the plastic reservoir were replaced with fresh solutions after two cycles of exposure, i.e. after every month. The prismatic specimens were exposed to NaCl solutions, and composite solutions of NaCl + $MgSO_4$, and NaCl + Na_2SO_4 till the exposure period 27 months. The

photographs of the prismatic reinforced concrete specimens exposed to chloride, and composite chloride-sulfate solutions in the laboratory are shown in Figure 3.5.

Figure 3.5 Photograph of prismatic specimens in the laboratory during exposure to external chloride and composite chloride-sulfate solutions with alternate wetting-drying cycles

3.6. Compressive strength test

Compressive strength test was performed on concrete cube specimens at the curing ages of 28, 90, and 180 days from the day of casting. From each concrete mix, three replicate cube specimens were tested in a compression testing machine at a given curing age, and the average value was reported.

3.7. Monitoring of rebar corrosion in concrete

Half-cell potential and linear polarization resistance (LPR) measurements were conducted on the prismatic specimens at the start of wetting period of wetting-drying cycle at every 3-month interval of exposure period using the instrument: ACM (manufacturer), model: Gill AC and Serial no. 1542, till the exposure period of 27 months. The half-cell potential (E_0) of embedded steel bar in the prismatic specimen was measured with reference to saturated calomel electrode (SCE). The LPR measurement was used for determining the corrosion current density (I_{corr}) of embedded steel bar in the prismatic specimen. During LPR measurement, the embedded steel bar (working electrode: WE) was polarized from the equilibrium potential to ± 20 mV with a scan rate of 0.1 mV per second [39]. The external perturbation was applied through the auxiliary electrode (AE) (a stainless steel plate), which was placed on the exposed surface along with the conducting sponge. During testing, the test solution (same as the exposure solution used during the wetting period) was filled into the plastic reservoir. The schematic diagram and photograph of laboratory experimental setup for corrosion measurement are shown in Figures 3.6 and 3.7 respectively. For determining I_{corr}, it was considered that only upper half exposed surface area of the embedded steel bar in the prismatic specimen was polarized [39]. The Stern-Geary equation was used to calculate the I_{corr} of the steel bar in the prismatic specimen, which is expressed by:

$$I_{corr} = \frac{B}{R_p} \tag{3.1}$$

Where, I_{corr}= corrosion current density; B = Stern-Geary constant; and R_p= polarization resistance of steel bar.

The relationship between Stern-Geary constant (B) and the Tafel constants is as follows;

$$B = \frac{(\beta_a \times \beta_c)}{2.3\,(\beta_a + \beta_c)} \tag{3.2}$$

Where, β_a is anodic Tafel constant and β_c is cathodic Tafel constant. Considering the embedded steel bar in active condition, the value of B was considered as 26 mV in this investigation [44, 120].

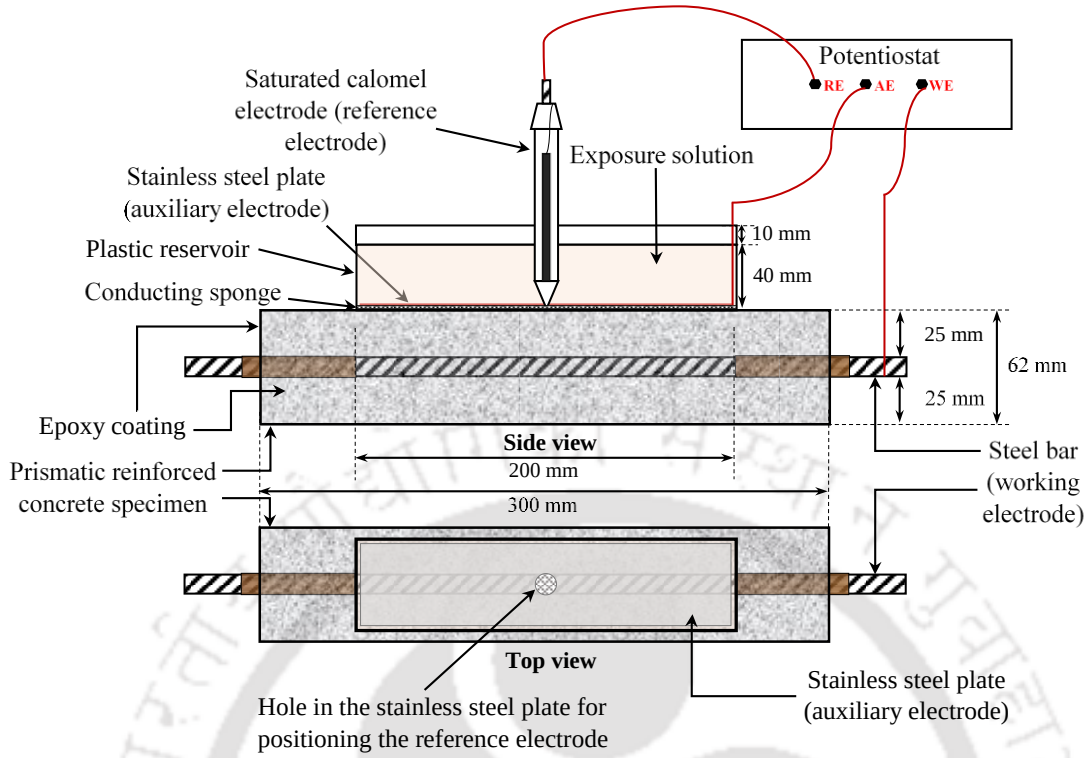

Figure 3.6 Schematic diagram of the experimental setup for half-cell potential and LPR measurements

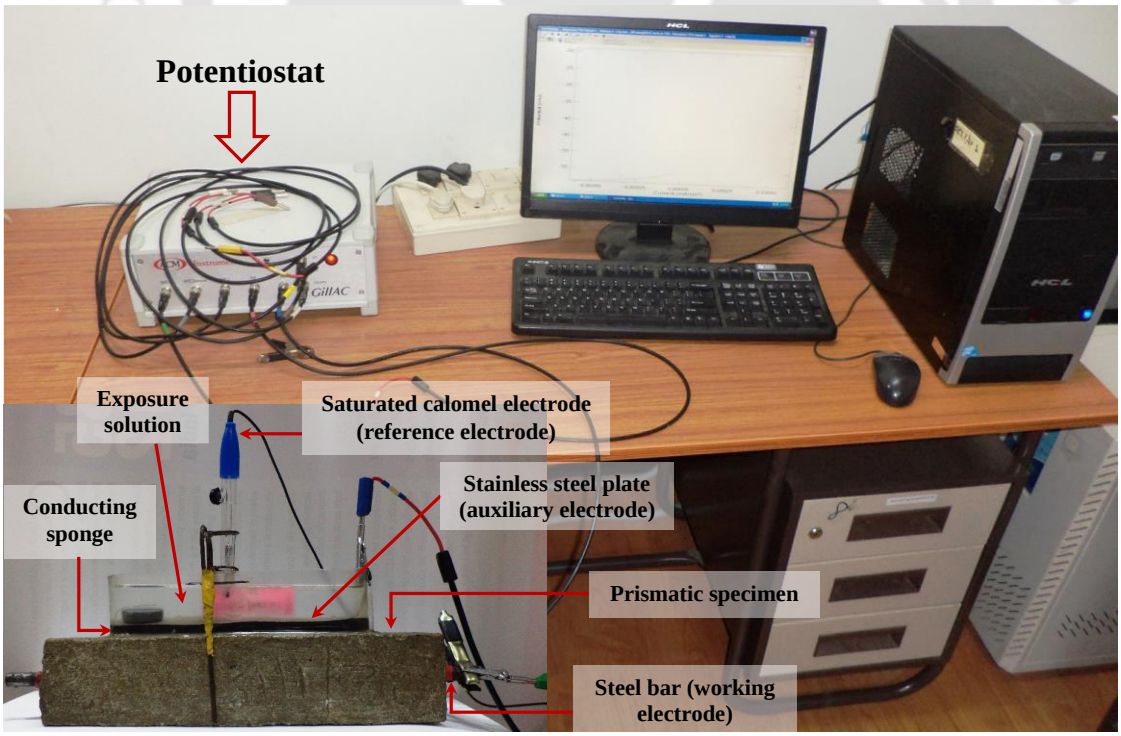

Figure 3.7 Photograph of the experimental setup for half-cell potential and LPR measurements

3.8. Collection of concrete powder samples

At the end of different exposure periods, the concrete powder samples were collected by drilling throughout the exposure surface of prismatic reinforced concrete specimen at five depth intervals each of 5 mm i.e. 0-5 mm, 5-10 mm, 10-15 mm, 15-20 mm, and 20-25 mm, from the exposure surface up to the level of embedded steel bar. The drilled concrete powder samples were stored in airtight containers and were then kept in a desiccator. It is to be noted that the prismatic reinforced concrete specimens exposed to NaCl solutions, and composite solutions of NaCl + $MgSO_4$ were drilled at the end of exposure periods of 9, 15, 21, and 27 months, and those exposed to composite solutions of NaCl + Na_2SO_4 were drilled at the end of exposure periods of 15, 21, and 27 months for collection of concrete powder samples. The collected concrete powder samples were used for determining free chloride content, total chloride content and microstructure analysis of concrete. The photographs of the prismatic reinforced concrete specimen after drilling along with the collected concrete powder samples are shown in Figure 3.8.

Figure 3.8 Photographs of prismatic reinforced concrete specimen after drilling and collected concrete powder samples

3.9. Chloride ingress in concrete

3.9.1. Measurement of chloride content

The chloride ingress in concrete was determined by measuring the free chloride, and total chloride contents of concrete powder samples collected at different depth intervals from

the exposure surface of prismatic specimens at the end of different exposure periods corresponding to the exposure solutions. Potentiometric titration was used for determining the free chloride content (C_f) and total chloride content (C_t) of concrete powder samples using a titrator: Metrohm (manufacturer), and model: 848 Titrino Plus. For determining the free chloride or total chloride content, 3 grams of concrete powder sample collected from a given depth interval was placed into a 100 ml beaker, and 50 ml of the solvent (distilled water for free chloride content, and concentrated nitric acid (3 N) for total chloride content) was added [121, 122]. For determining free chloride content, the concrete powder solution was mixed thoroughly, and heated gently up to boiling, and further continued for boiling for about one minute [123] on a hot plate with a stirrer. Afterward, the concrete powder solution was cooled to room temperature (27±3° C). For determining total chloride content, the concrete powder solution (3 grams of concrete powder in 50 ml of 3N nitric acid) was mixed thoroughly by the stirrer without heating. The free chloride and the total chloride contents were determined by titrating with 0.1 M $AgNO_3$ solution [121]. The measured free chloride and total chloride contents were expressed as % by weight of concrete. The free and total chloride contents for a given depth interval was considered as the average chloride content of the concrete powder samples collected from that depth interval. It is to be noted that the free chloride and total chloride contents were measured separately.

3.9.2. Determination of apparent chloride diffusion coefficient of concrete

After obtaining free chloride content over different depth intervals from the exposure surface of prismatic specimens up to the level of embedded steel bar at the end of different exposure periods i.e. 9, 15, 21, and 27 months, Fick's second law of diffusion was used for estimating the apparent surface chloride content (C_s), and apparent chloride diffusion coefficient (D), and is given by;

$$\frac{\partial C}{\partial t} = D\frac{\partial^2 C}{\partial x^2} \tag{3.3}$$

Where $C = C_{(x,t)}$ = chloride content (%) at depth x from the exposure surface of concrete at time t, x = depth from exposure surface of concrete, t = exposure period, and D = apparent chloride diffusion coefficient.

By considering one-dimensional ingress into a semi-infinite medium, an analytical solution (error function solution) of the Fick's second law of diffusion (Equation 3.3) is given by the following equation [53, 54];

$$C_{(x,t)} = C_s \left[1 - erf\left(\frac{x}{2\sqrt{Dt}}\right)\right] \quad (3.4)$$

Where, C_s = apparent surface chloride content (%), and erf = error function.

In case of exposure of concrete to chloride solutions under alternate wetting-drying conditions, two different zones namely convection zone and diffusion zone are observed with respect to chloride profile [4, 67, 124, 125]. Normally, the convection zone is a thin layer from the exposure surface of concrete to the location corresponding to a peak value of chloride concentration [4, 124]. Beyond convection zone, the diffusion zone is located in which the chloride ingress is governed by the mechanism of ionic diffusion according to the Fick's second law of diffusion.

The chloride ingress in convection zone does not conform to Fick's second law of diffusion. Thus, the chloride concentration data in the convection zone is excluded while applying Fick's second law of diffusion. If x_1 is the depth of convection zone from the exposure surface of concrete, then the chloride concentration profile in the diffusion zone is given by [67, 124, 125];

$$C_{(x,t)} = C_{smax} \left[1 - erf\left(\frac{x-x_1}{2\sqrt{Dt}}\right)\right] \quad (3.5)$$

Where, C_{smax} is the peak value of chloride content at the interface of the convection zone, and diffusion zone.

To estimate the apparent surface chloride content (C_s), and apparent chloride diffusion coefficient (D) of concrete at the end of different exposure periods i.e. 9, 15, 21, and 27 months, the experimentally obtained free chloride content versus depth was fitted with the best-fit relationship obtained from the analytical solution of Fick's second law of diffusion. The best-fit relationship was obtained by minimizing the sum of the squared differences between the actual and fitted data of free chloride content by adjusting the regressor variable. Generalized reduced gradient (GRG) nonlinear solving method was used for obtaining the best-fit relationship by solving the equation using the SOLVER function in Microsoft Excel Spreadsheet [126]. To obtain free chloride content at the embedded rebar level (C_{rs}), the fitted chloride profile was extrapolated to the level of rebar, i.e. to a depth of 25 mm from the exposure surface of concrete.

3.10. Microstructure analysis of concrete

The microstructure analysis of concrete exposed to chloride, and composite chloride-sulfate solutions was carried out using X-ray diffraction (XRD) analysis, field emission scanning electron microscope (FESEM) analysis, and thermo-gravimetry analysis (TGA). The concrete powder samples collected from different depth intervals of prismatic specimens at the end of different exposure periods as mentioned earlier were passed through a sieve having square openings of size 75 µm, and the sieved concrete powder samples were used for performing the microstructure analysis of concrete.

3.10.1. X-ray diffraction (XRD) analysis

The XRD analysis was carried out to identify the phase composition of concrete exposed to chloride and composite chloride-sulfate solutions. The XRD analysis was performed by recording the X-ray diffraction patterns in a X-ray diffractometer (Rigaku high power, TTRAX III model) with CuKα radiation (λ = 1.5405 Å), and operating at 50 kV and 100 mA. In the XRD analysis, the concrete powder sample was scanned from 5º to 60º 2θ at a scan speed of 4º 2θ per minute. From the obtained XRD patterns, the phase composition was identified using the PDF2 reference library (ICDD: International Centre for Diffraction Data), and PANalytical X'Pert HighScore Plus software. From the XRD patterns, the weight percentages of the compounds formed in concrete were determined semi-quantitatively using the reference-intensity ratio (RIR) matrix-flushing method [127-129]. The equation used for estimating the weight percentage (wt. %) of the compounds is given by [130-132];

$$W_i = \frac{\frac{I_i}{RIR_i}}{\sum_{i=1}^{N}\left(\frac{I_i}{RIR_i}\right)} \tag{3.6}$$

$W_1 + W_2 + \cdots + W_N = 1$

Where W_i = relative mass of compound i,

I_i = integral intensity of the highest peak of compound i (calculated using PANalytical X'Pert HighScore Plus software)

RIR_i = reference intensity ratio of compound i (mentioned in PDF reference library of ICDD)

N = number of compounds considered in the sample

The same reference phase was used for each compound for all the samples so that RIR concentrations were used consistently among the samples.

3.10.2. Field emission scanning electron microscope (FESEM) analysis

The morphology of concrete exposed to chloride, and composite chloride-sulfate solutions was analyzed using Zeiss Sigma field emission scanning electron microscope. The concrete powder sample was put into the stub with carbon tape. After that, a thin gold layer coating was applied to the sample by sputtering method. The surface morphology of the concrete powder sample was observed using in-lens mode.

3.10.3. Thermo-gravimetry analysis (TGA)

The thermo-gravimetry analysis (TGA) was performed to evaluate the decomposition of various compounds of concrete over different temperature ranges. The mass loss of a concrete powder sample as a result of decomposition of different compounds over a temperature range was estimated from TGA. Derivative thermo-gravimetry (DTG) was determined as the first derivative of the obtained TGA curve that gives sharp yield peaks at the location (temperature) of substantial mass change. Thermo-gravimetry analysis (TGA) was performed on the concrete powder sample using the instrument NETZSCH STA 449F3. During the test, the concrete powder sample was heated in an aluminum crucible from ambient temperature to temperature of 950 ºC at a rate of 10 ºC per minute in argon environment flowing at 60 ml per minute.

From the mass loss obtained from TGA, the calcium hydroxide content in concrete was determined using Taylor's formula [133] and is given by:

$$CH\ (\%) = W_{CH} \times \frac{M_{CH}}{M_{H_2O}} \tag{3.7}$$

Where $CH\ (\%)$ = calcium hydroxide content, W_{CH} = mass loss during dehydration of calcium hydroxide as a percentage of the ignited mass (%), M_{CH} = molar mass of calcium hydroxide, and M_{H_2O} = molar mass of water.

3.11. Summary

In the experimental work of the present study, different binders such as OPC, OPC plus 20% fly ash, and PPC, and w/b ratios such as 0.45, 0.50 and 0.55 were used in the preparation of concrete mixes. Prismatic specimens embedded centrally with a steel bar of 12 mm diameter were prepared from different concrete mixes, and were exposed to chloride

(NaCl), and composite chloride-sulfate (NaCl + $MgSO_4$ and NaCl + Na_2SO_4) solutions of varying concentrations with alternate wetting-drying cycles for different exposure periods till 27 months. During the exposure period, the corrosion parameters such as half-cell potential, and corrosion current density (by linear polarization resistance measurement) of steel reinforcement in concrete were measured at every 3-month interval. At the end of different exposure periods i.e. 9, 15, 21, and 27 months, concrete powder samples were collected from the prismatic specimens at different depth intervals from the exposure surface for determining the free chloride and total chloride contents. From the obtained free chloride content profile, the apparent chloride diffusion coefficient of concrete was estimated using Fick's second law of diffusion. Further, the microstructure analyses of concrete powder samples collected from different depth intervals of prismatic specimens at the end of different exposure periods were carried out by XRD analysis, FESEM analysis, and thermo-gravimetry analysis (TGA).

CHAPTER 4

CHLORIDE INGRESS AND CHLORIDE BINDING IN CONCRETE EXPOSED TO CHLORIDE AND COMPOSITE CHLORIDE-SULFATE SOLUTIONS

4.1. General

In this chapter, the results of compressive strength of concrete made with different types of binder such as OPC, OPC + 20% FA and PPC, and w/b ratios such as 0.45, 0.50 and 0.55 are presented and discussed for different curing ages. As stated earlier in Chapter 3, the free and total chloride contents of concrete exposed to NaCl solutions, and composite solutions of NaCl + $MgSO_4$ were measured at the end of exposure periods of 9, 15, 21 and 27 months, and those of concrete exposed to composite solutions of NaCl + Na_2SO_4 were measured at the end of exposure periods of 15, 21 and 27 months. Accordingly, the results of free chloride content, apparent chloride diffusion coefficient, and chloride binding of concrete presented in this chapter correspond to the above exposure periods for the respective exposure solution. In this chapter, the effect of different parameters such as depth from the exposure surface of concrete, exposure solution and duration, binder type, and w/b ratio on variations in free chloride content are evaluated and discussed. Subsequently, the results of apparent chloride diffusion coefficient of concrete estimated using Fick's second law of diffusion are presented, and the effect of above parameters on variations in apparent chloride diffusion coefficient are discussed. Further, the influence of exposure solution, binder type, and w/b ratio on variations in chloride binding in concrete at different exposure periods are analyzed and discussed.

4.2. Compressive strength of concrete

The results of average compressive strength (along with the standard deviation) of concrete made with different types of binder, and w/b ratios at curing ages of 28 days, 90 days and 180 days are shown in Figure 4.1. Each value of compressive strength shown in this figure is the average value of three replicate cube specimens. From this figure, it is observed that the compressive strength of concrete made with OPC was higher as compared to those made with OPC + 20% FA and PPC at all w/b ratios and curing ages, which is ascribed to the dominant effect of hydration reaction in OPC concrete as compared to that in OPC + 20% FA and PPC concrete. Further, it is inferred that the compressive strength of concrete made with OPC + 20% FA was mostly higher as compared to that made with PPC. Further,

the compressive strength of concrete increased with increase in curing age irrespective of binder type and w/b ratio as evident from Figure 4.1. This is attributed to the effect of continued hydration reaction in OPC concrete and significant effect of continued pozzolanic reaction in OPC + 20% FA and PPC concrete. The average increase in compressive strength varied from 3.29% to 13.28%, 12.75% to 39.29% and 10.50% to 29.94% for OPC, OPC + 20% FA and PPC respectively irrespective of w/b ratio with increase in curing age from 28 days to 90 days. Similarly, with increase in curing age from 28 days to 180 days, the average increase in compressive strength varied from 15.35% to 21.05%, 30.28% to 57.74% and 28.57% to 59.32% for OPC, OPC + 20% FA and PPC respectively irrespective of w/b ratio. These values indicate that the rate of increase in compressive strength with curing age was more in the concrete made with OPC + 20% FA, and PPC as compared to that made with OPC, which is ascribed to the significant effect of continued pozzolanic reaction in OPC + 20% FA, and PPC concrete.

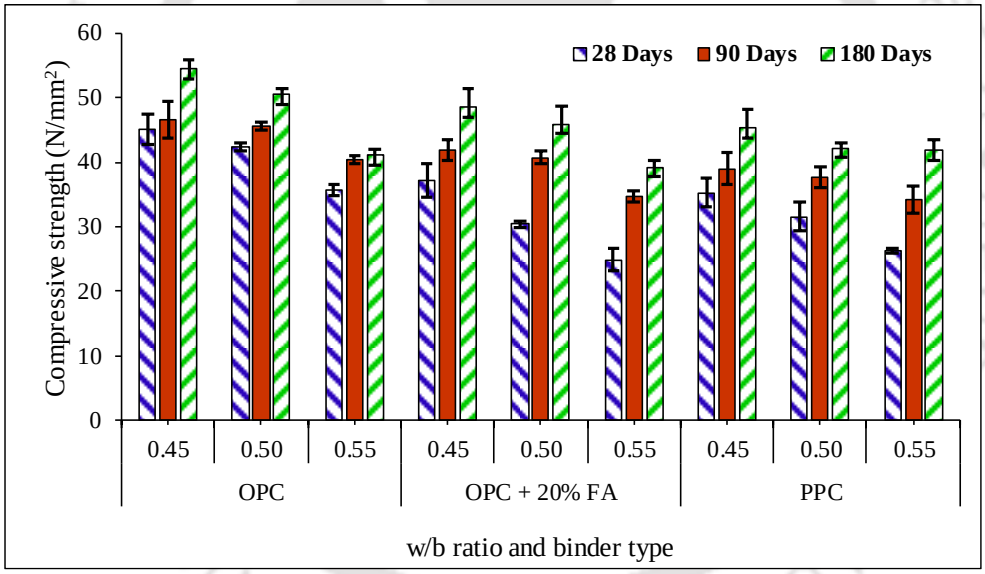

Figure 4.1 Compressive strength of concrete made with OPC, OPC + 20% FA, and PPC, and w/b ratios of 0.45, 0.50, and 0.55, at different curing ages

4.3. Chloride ingress in concrete

4.3.1. Free chloride content profile

As stated earlier in Chapter 3, at the end of different exposure periods, the free chloride content of concrete powder samples collected from depth intervals of 0-5 mm, 5-10 mm, 10-15 mm, 15-20 mm, and 20-25 mm from the exposure surface of prismatic specimens were determined by potentiometric titration. In order to obtain the free chloride content profile, the experimentally determined free chloride content of concrete exposed to

chloride, and composite chloride-sulfate solutions were plotted against the depth interval from the exposure surface of concrete for different exposure periods.

4.3.1.1. Effect of depth from exposure surface of concrete on free chloride content

Typical plots of free chloride content profile of concrete obtained from the prismatic specimens exposed to chloride and composite chloride-sulfate solutions for the exposure period of 27 months are shown in Figure 4.2 to 4.10. The plots of free chloride content profile of concrete obtained for the exposure periods of 9, 15, and 21 months are presented in Appendix A1. As already stated in Chapter 3, the free chloride content for a given depth interval was considered as the average chloride content of the concrete powder samples collected from that depth interval. The free chloride content for a given depth interval is represented at its mid-depth level in the plot of free chloride content profile, i.e. at 2.5 mm, 7.5 mm, 12.5 mm, 17.5 mm, and 22.5 mm for depth intervals of 0-5 mm, 5-10 mm, 10-15 mm, 15-20 mm and 20-25 mm respectively.

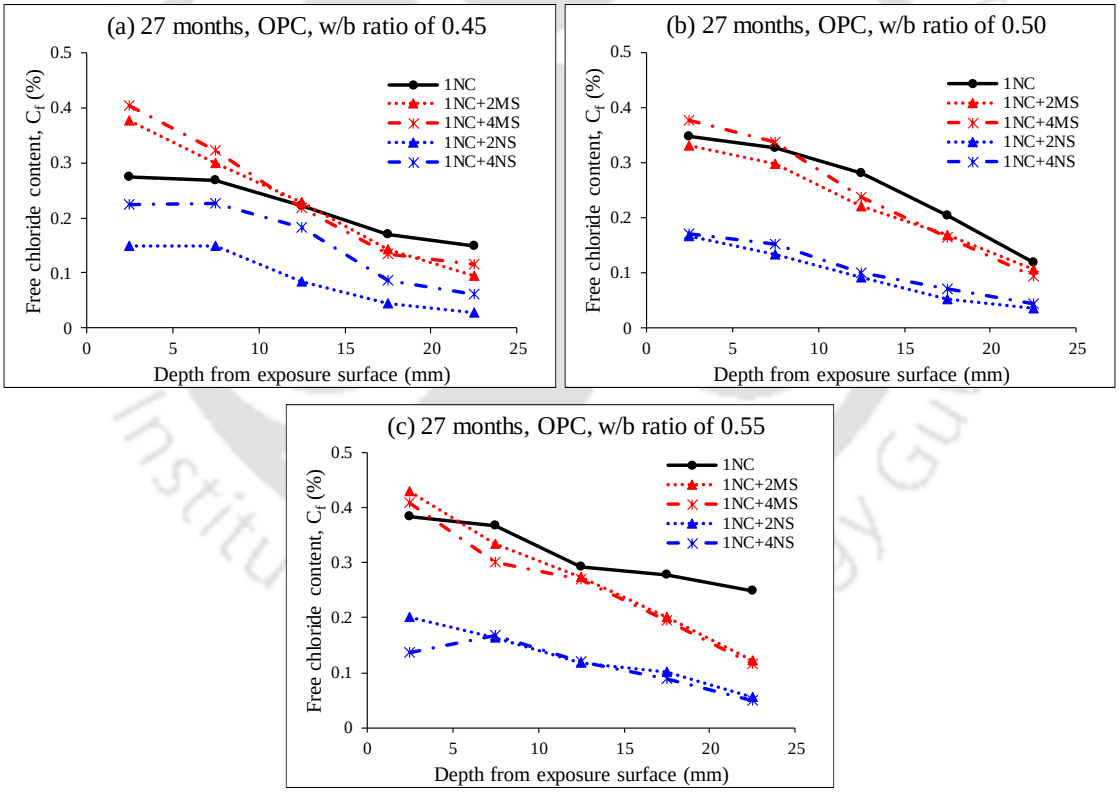

1NC: 1% NaCl, **1NC+2MS:** 1% NaCl + 2% $MgSO_4$, **1NC+4MS:** 1% NaCl + 4% $MgSO_4$

1NC+2NS: 1% NaCl + 2% Na_2SO_4, **1NC+4NS:** 1% NaCl + 4% Na_2SO_4

Figure 4.2 Free chloride content profile of OPC concrete exposed to 1% NaCl, and 1% NaCl with $MgSO_4$ or Na_2SO_4 solutions for 27 months: (a) w/b ratio of 0.45, (b) w/b ratio of 0.50, and (c) w/b ratio of 0.55

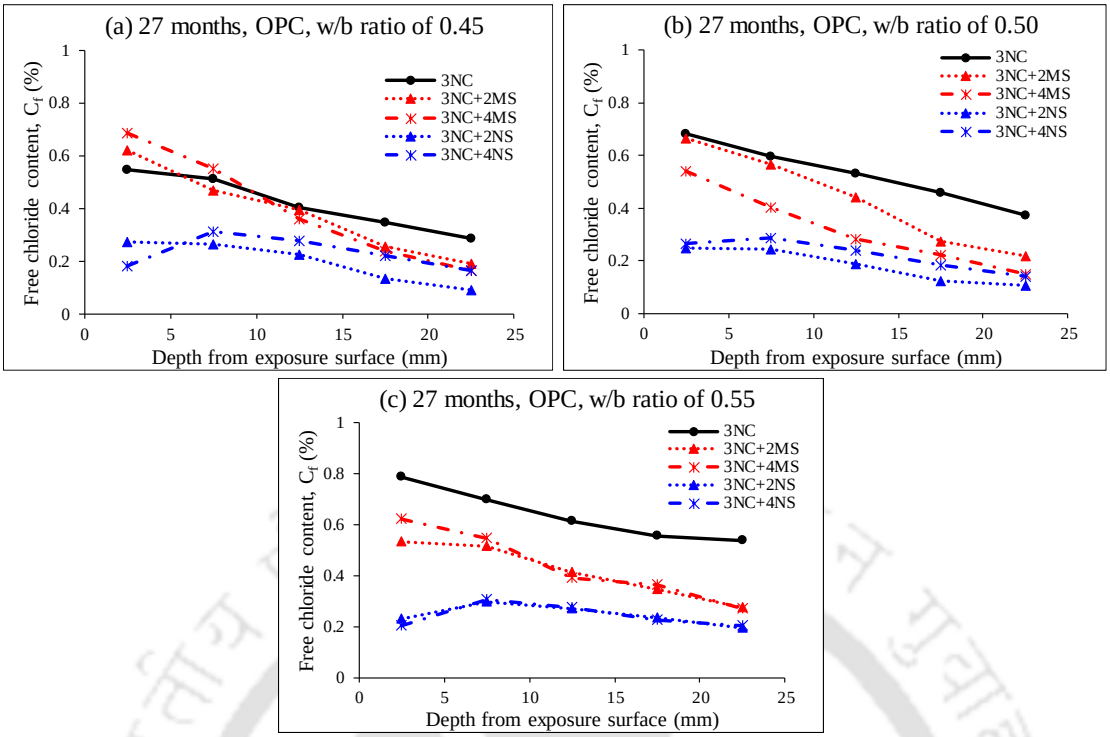

3NC: 3% NaCl, **3NC+2MS:** 3% NaCl + 2% $MgSO_4$, **3NC+4MS:** 3% NaCl + 4% $MgSO_4$
3NC+2NS: 3% NaCl + 2% Na_2SO_4, **3NC+4NS:** 3% NaCl + 4% Na_2SO_4

Figure 4.3 Free chloride content profile of OPC concrete exposed to 3% NaCl, and 3% NaCl with $MgSO_4$ or Na_2SO_4 solutions for 27 months: (a) w/b ratio of 0.45, (b) w/b ratio of 0.50, and (c) w/b ratio of 0.55

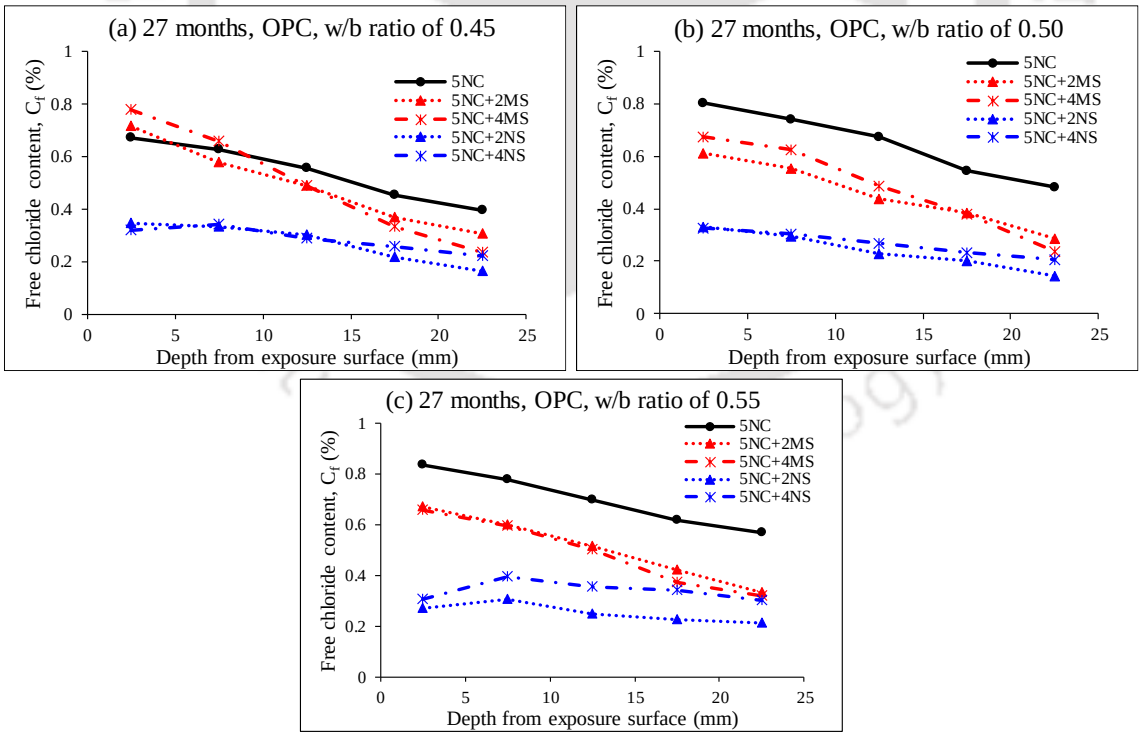

5NC: 5% NaCl, **5NC+2MS:** 5% NaCl + 2% $MgSO_4$, **5NC+4MS:** 5% NaCl + 4% $MgSO_4$
5NC+2NS: 5% NaCl + 2% Na_2SO_4, **5NC+4NS:** 5% NaCl + 4% Na_2SO_4

Figure 4.4 Free chloride content profile of OPC concrete exposed to 5% NaCl, and 5% NaCl with $MgSO_4$ or Na_2SO_4 solutions for 27 months: (a) w/b ratio of 0.45, (b) w/b ratio of 0.50, and (c) w/b ratio of 0.55

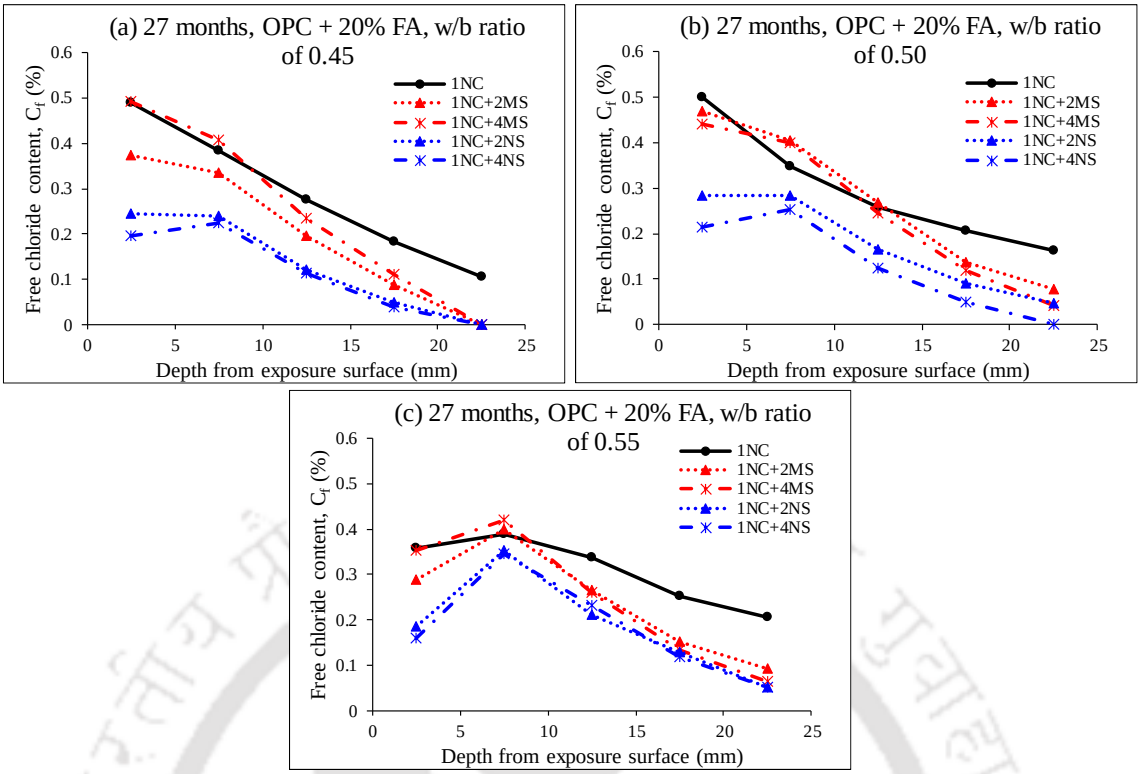

Figure 4.5 Free chloride content profile of OPC + 20% FA concrete exposed to 1% NaCl, and 1% NaCl with $MgSO_4$ or Na_2SO_4 solutions for 27 months: (a) w/b ratio of 0.45, (b) w/b ratio of 0.50, and (c) w/b ratio of 0.55

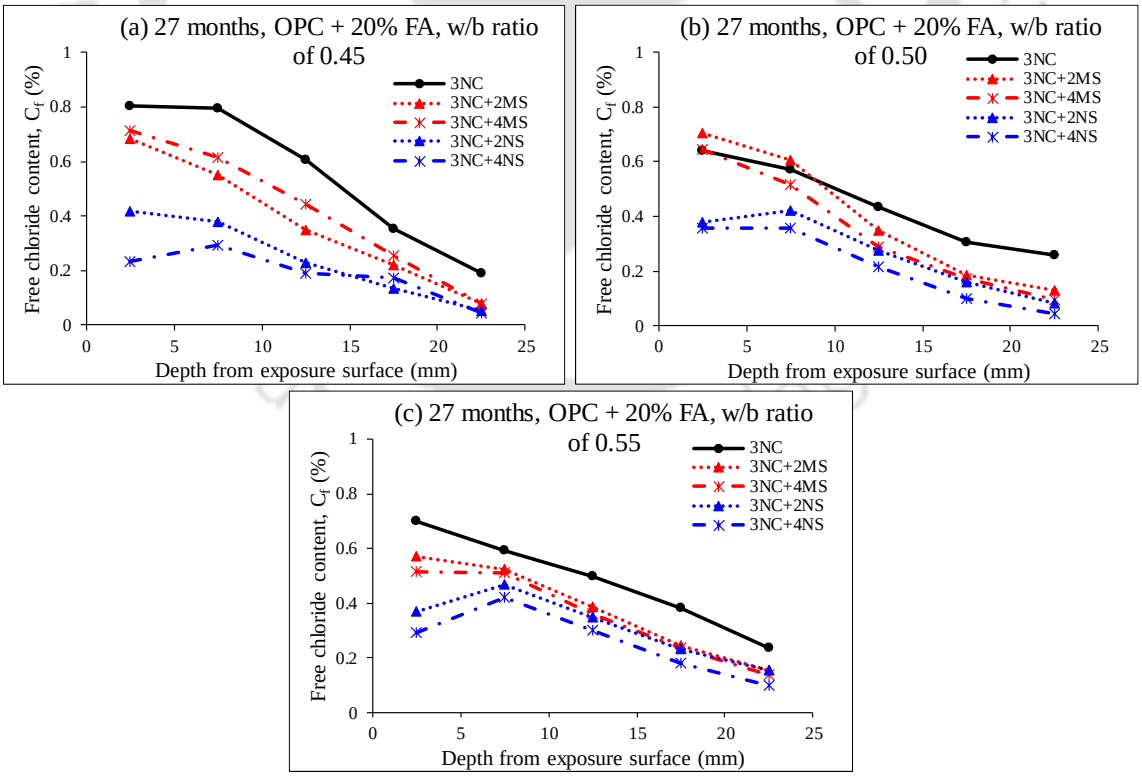

Figure 4.6 Free chloride content profile of OPC + 20% FA concrete exposed to 3% NaCl, and 3% NaCl with $MgSO_4$ or Na_2SO_4 solutions for 27 months: (a) w/b ratio of 0.45, (b) w/b ratio of 0.50, and (c) w/b ratio of 0.55

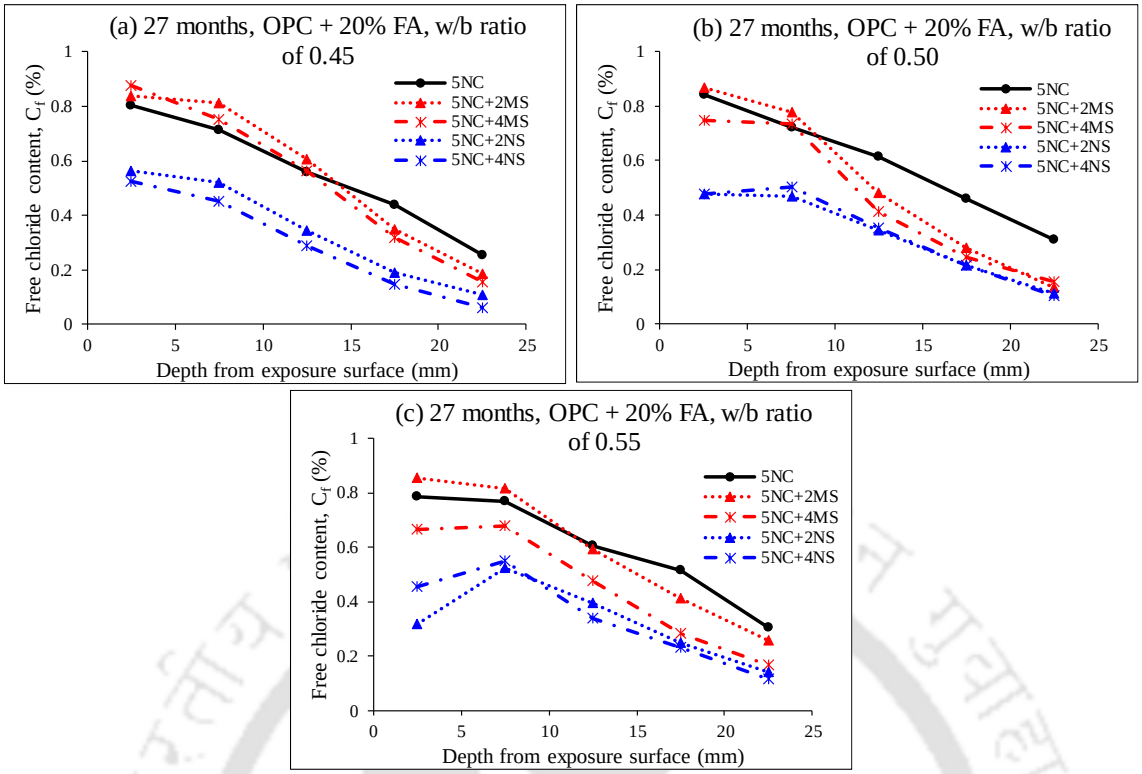

Figure 4.7 Free chloride content profile of OPC + 20% FA concrete exposed to 5% NaCl, and 5% NaCl with $MgSO_4$ or Na_2SO_4 solutions for 27 months: (a) w/b ratio of 0.45, (b) w/b ratio of 0.50, and (c) w/b ratio of 0.55

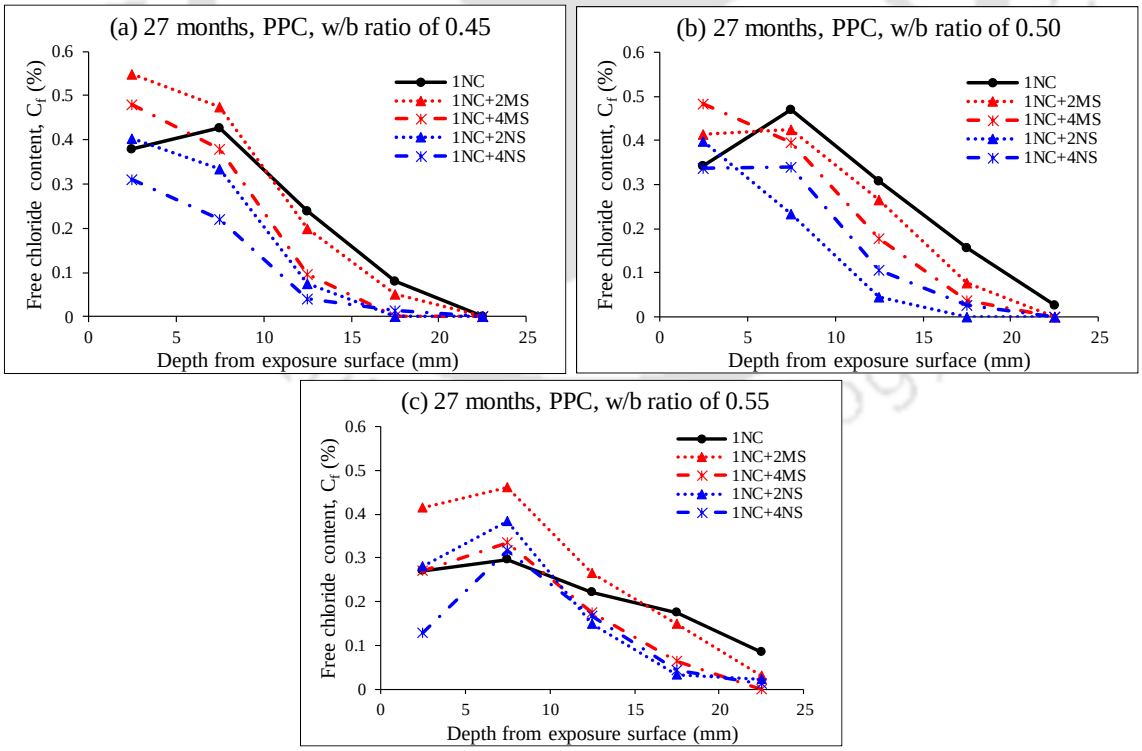

Figure 4.8 Free chloride content profile of PPC concrete exposed to 1% NaCl, and 1% NaCl with $MgSO_4$ or Na_2SO_4 solutions for 27 months: (a) w/b ratio of 0.45, (b) w/b ratio of 0.50, and (c) w/b ratio of 0.55

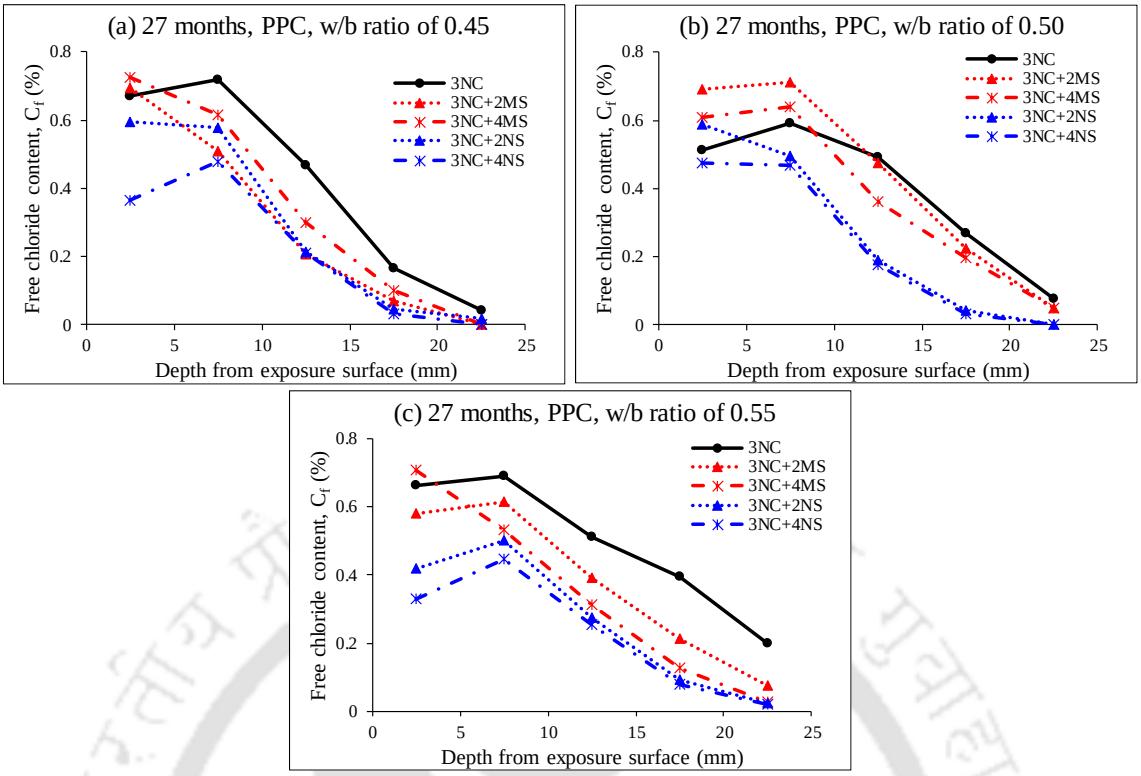

Figure 4.9 Free chloride content profile of PPC concrete exposed to 3% NaCl, and 3% NaCl with $MgSO_4$ or Na_2SO_4 solutions for 27 months: (a) w/b ratio of 0.45, (b) w/b ratio of 0.50, and (c) w/b ratio of 0.55

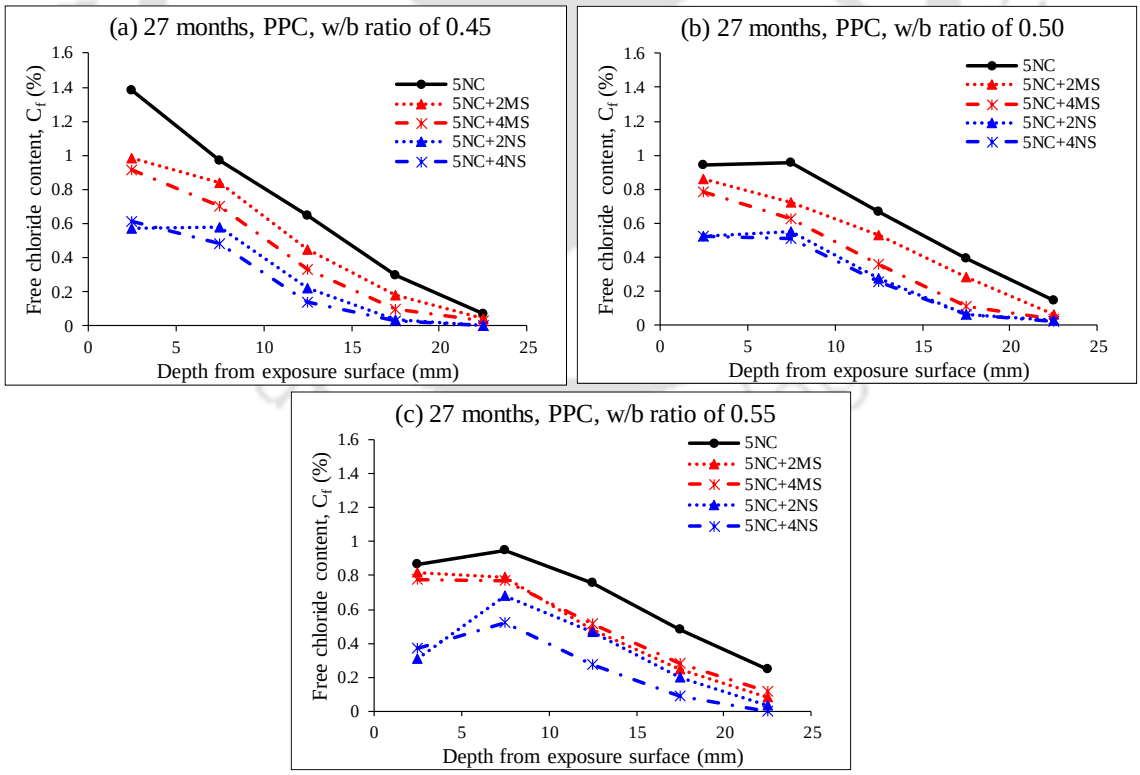

Figure 4.10 Free chloride content profile of PPC concrete exposed to 5% NaCl, and 5% NaCl with $MgSO_4$ or Na_2SO_4 solutions for 27 months: (a) w/b ratio of 0.45, (b) w/b ratio of 0.50, and (c) w/b ratio of 0.55

From Figure 4.2 to 4.10 and the figures shown in Appendix A1, it is observed that the free chloride content decreased with increase in depth beyond the depth interval of 0-5 mm from the exposure surface for all prismatic specimens exposed to chloride and composite chloride-sulfate solutions. The decrease in free chloride content with increase in depth beyond the depth interval of 0-5 mm from the exposure surface is attributed to the penetration of lower amount of chloride ions to higher depth intervals in concrete. In case of some prismatic specimens, the obtained free chloride content in the depth interval of 0-5 mm was less than that obtained in the depth interval of 5-10 mm as observed from Figure 4.2 to 4.10 and figures shown in Appendix A1. The lower chloride content in the depth interval of 0-5 mm near the surface of concrete may be ascribed to the presence of convection zone. As mentioned in Chapter 3, in case of exposure of concrete under alternate wetting-drying conditions, two different zones namely convection zone and diffusion zone are observed with respect to the penetration of chloride ions [4, 67, 124, 125]. The convection zone is a thin layer from the exposure surface of concrete to the location corresponding to a peak value of chloride concentration [4, 124]. In the convection zone, there is dominant effect of capillary absorption through the pore network of concrete. Beyond convection zone, the diffusion zone is located in which the chloride ingress is governed by the mechanism of ionic diffusion according to the Fick's second law of diffusion.

The formation of convection zone depends on exposure duration, binder type, w/b ratio, and exposure solution. The formation of convection zone was more dominant in case of prismatic specimens exposed for longer duration, which may be attributed to the exposure of specimens to the solutions with more number of wetting and drying cycles. Among the binder type, the formation of convection zone was more dominant in the prismatic specimens made with PPC as compared to those made with OPC + 20% FA followed by OPC [134]. This may be attributed to the effect of leaching of calcium hydroxide in the presence of chloride ions as well as due to the effect of lower extent of pozzolanic reaction near the surface zone that might have resulted in alteration of pore structure of PPC and OPC + 20% FA concrete to a greater extent as compared to OPC concrete. The formation of convection zone increased in concrete with increase in w/b ratio [135]. This may be attributed to the influence of local alteration in the pore structure of concrete near the surface with change in w/b ratio that affected capillary absorption through the pore network. In case of exposure to composite solutions of NaCl + Na_2SO_4, the convection

zone was observed in all the specimens till the exposure period of 27 months. However, in case of exposure to NaCl and NaCl + $MgSO_4$ solutions, the formation of convection zone was not systematic and was mostly higher in the specimens exposed to composite solutions of NaCl + $MgSO_4$ as compared to NaCl solutions. In other words, the formation of convection zone was more in the concrete exposed to NaCl + Na_2SO_4 as compared to NaCl + $MgSO_4$ followed by NaCl solutions as observed from Figure 4.2 to 4.10 and figures shown in Appendix A1. This indicates that the differences in the extent of penetration of chloride ions along with the sulfate ions, and also the cation type associated with sulfate ions affect the formation of convection zone in concrete exposed to chloride and composite chloride-sulfate solutions with alternate wetting-drying cycles.

4.3.1.2. Effect of exposure solution and duration on free chloride content in concrete

From Figure 4.2 to 4.10 and figures presented in Appendix A1, it is observed that the free chloride content increased with increase in concentration of chloride ions in the exposure solution at all depth intervals for both chloride (NaCl) and composite chloride-sulfate (NaCl + $MgSO_4$, and NaCl + Na_2SO_4) solutions. In other words, the free chloride content was more in the concrete specimens exposed to 5% NaCl and its associated composite solutions as compared to 3% NaCl followed by 1% NaCl and the associated composite solutions. The increase in free chloride content with increase in the amount of NaCl in the exposure solution is attributed to the ingress of the higher amount of chloride ions because of the formation of porous C-S-H due to leaching of calcium in the presence of chloride ions [136-138]. The formation of porous C-S-H gel in concrete exposed to higher concentration of NaCl solution was observed from the FESEM images of concrete presented in Chapter 5 (discussed in Section 5.2.2).

While evaluating the effect of sulfate ions in the exposure solution on chloride ingress in concrete, it is observed that the free chloride content was mostly lower when exposed to composite chloride-sulfate solutions (NaCl + $MgSO_4$ and NaCl + Na_2SO_4) as compared to chloride solutions (NaCl) at almost all depth intervals as observed from Figure 4.2 to 4.10 and those presented in Appendix A1. Further, the free chloride content decreased with increase in concentration of $MgSO_4$ or Na_2SO_4 in the exposure solution. The lower free chloride content in the prismatic specimens exposed to composite chloride-sulfate solutions may be attributed to the reduction in penetration of chloride ions because of the simultaneous ingress of both chloride and sulfate ions from the exposure solutions, and also due to dominant effect of filling of pores with ettringite in concrete when exposed to

composite chloride-sulfate solutions that reduced the ingress of chloride ions in concrete. The reaction of chloride, and sulfate ions, with the hydrated tricalcium aluminate (C_3A) forms calcium chloroaluminate and ettringite respectively in concrete. Thus, in case of exposure of concrete to composite chloride-sulfate solutions, there is formation of more amount of ettringite due to reaction of sulfate ions with C_3A, and also due to conversion of calcium chloroaluminate to ettringite in the presence of sulfate ions [36]. The presence of higher amount of ettringite and lower amount of calcium chloroaluminate in the specimens exposed to composite chloride-sulfate solutions was also confirmed from the XRD patterns presented in Chapter 5 (discussed in Section 5.2.2), wherein the peak intensity and wt. % of ettringite were higher whereas those of calcium chloroaluminate were lower in the prismatic specimens exposed to composite chloride-sulfate solutions as compared to those exposed to chloride solutions for all binders, w/b ratios and at all depth intervals. Although, there is conversion of calcium chloroaluminate to ettringite in the presence of sulfate ions in case of exposure of concrete to composite chloride-sulfate solutions, which results in the release of bound chloride, the dominant effect of pore filling with the ettringite resulted in a significant reduction in penetration of chloride ions into concrete. In few cases, higher free chloride content was observed in case of exposure of prismatic specimens to composite chloride-sulfate solutions as compared to chloride solutions, which may be attributed to the effect of local alteration in chloride binding in concrete.

On comparing the effect of cation type associated with sulfate ions on chloride ingress in concrete, it is observed that the prismatic specimens exposed to composite solutions of NaCl + Na_2SO_4 showed lower free chloride content at all depth intervals as compared to those exposed to NaCl + $MgSO_4$ solutions at all exposure periods as observed from Figure 4.2 to 4.10 and those presented in Appendix A1. This is ascribed to the formation of more amount of ettringite in the concrete when exposed to NaCl + Na_2SO_4 solutions as compared to NaCl + $MgSO_4$ solutions that filled the pores in concrete to a relatively higher extent thereby reducing the penetration of chloride ions. The presence of higher amount of ettringite in the specimens exposed to NaCl + Na_2SO_4 solutions as compared to those exposed to NaCl + $MgSO_4$ solutions was confirmed from the XRD patterns presented in Chapter 5 (discussed in Section 5.2.2) wherein the peak intensity and wt. % of ettringite were higher in the prismatic specimens exposed to NaCl + Na_2SO_4 solutions as compared to NaCl + $MgSO_4$ solutions. While analyzing the variation in free chloride content with exposure period, it is inferred that the free chloride content increased with increase in

exposure period irrespective of binder type, w/b ratio, concentration of chloride and sulfate ions in the exposure solutions, and cation type associated with sulfate ions, as observed from Figure 4.2 to 4.10 and those presented in Appendix A1. However, the rate of increase in free chloride content with exposure period decreased after 15 months of exposure, which may be ascribed to the improvement in the microstructure of concrete at later ages due to the continued hydration and pozzolanic reactions with age as well as due to pore filling effect of reaction products formed in concrete in the presence of chloride and sulfate ions, which resulted in a reduction in rate of penetration of chloride ions into concrete.

4.3.1.3. Effect of binder type and w/b ratio on free chloride content in concrete

As stated earlier, the prismatic reinforced concrete specimens were prepared using three types of binder (OPC, OPC + 20% FA and PPC) and three w/b ratios (0.45, 0.50 and 0.55). The experimentally obtained free chloride contents were plotted in ternary plots in the scale of 0 - 100% for OPC, OPC + 20% FA and PPC irrespective of w/b ratio, and exposure solution, and are shown in Figure 4.11, 4.12, 4.13, and 4.14 for exposure durations of 9, 15, 21, and 27 months, respectively.

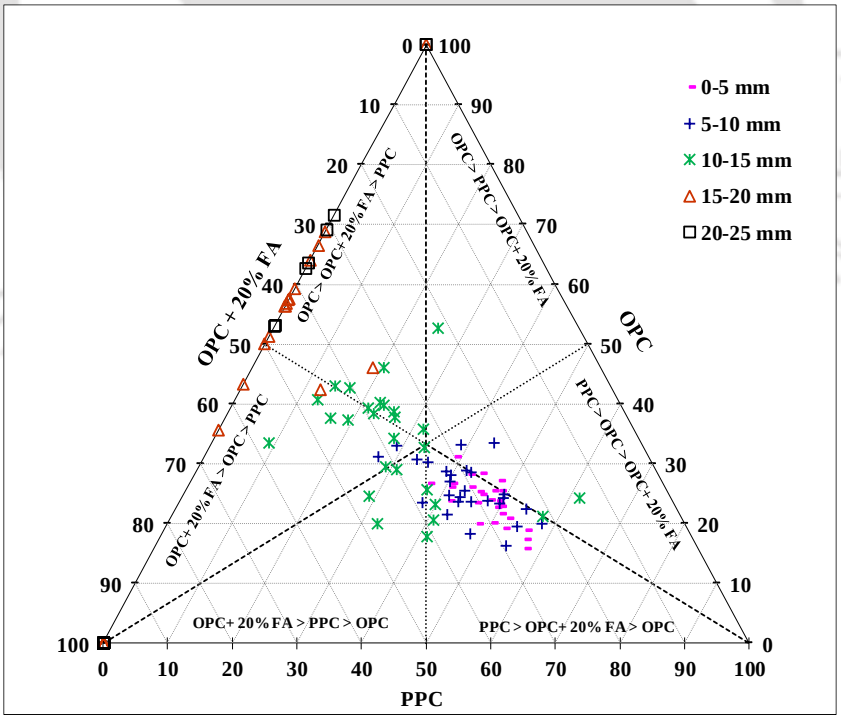

Figure 4.11 Comparison of experimentally obtained free chloride content at different depth intervals from exposure surface of prismatic specimens made with OPC, OPC + 20% FA, and PPC for exposure period of 9 months

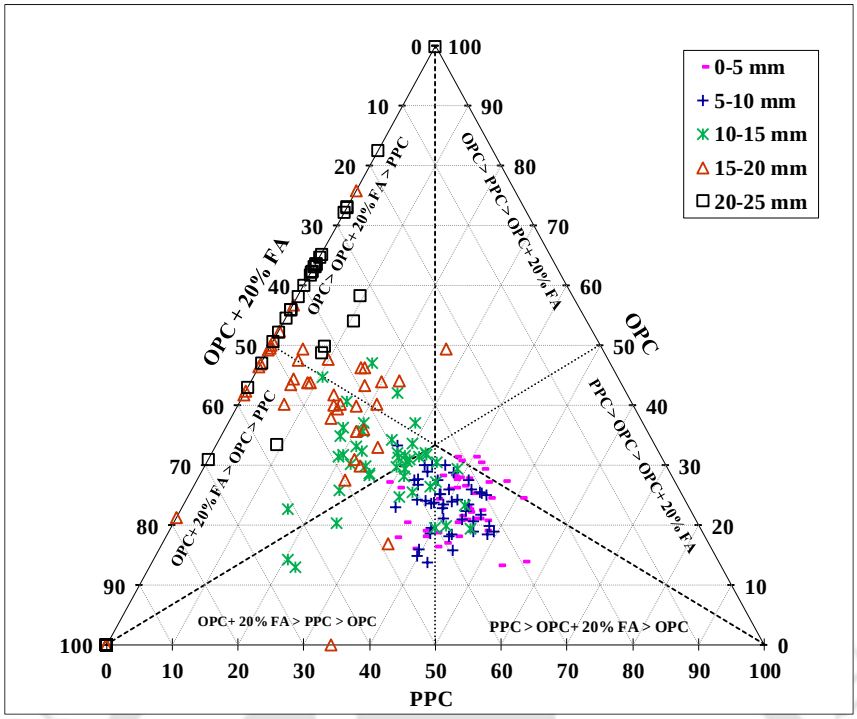

Figure 4.12 Comparison of experimentally obtained free chloride content at different depth intervals from exposure surface of prismatic specimens made with OPC, OPC + 20% FA, and PPC for exposure period of 15 months

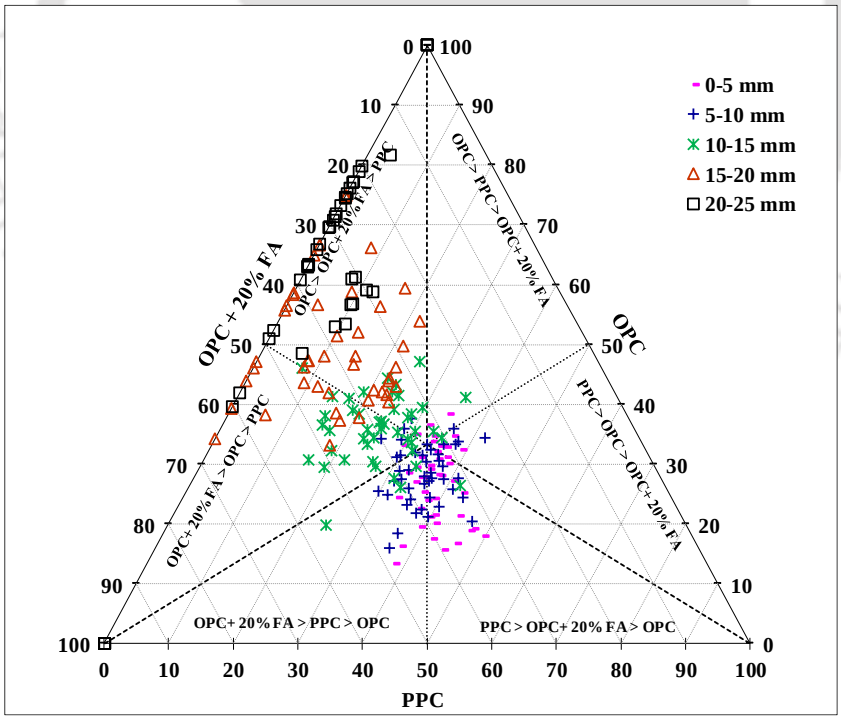

Figure 4.13 Comparison of experimentally obtained free chloride content at different depth intervals from exposure surface of prismatic specimens made with OPC, OPC + 20% FA, and PPC for exposure period of 21 months

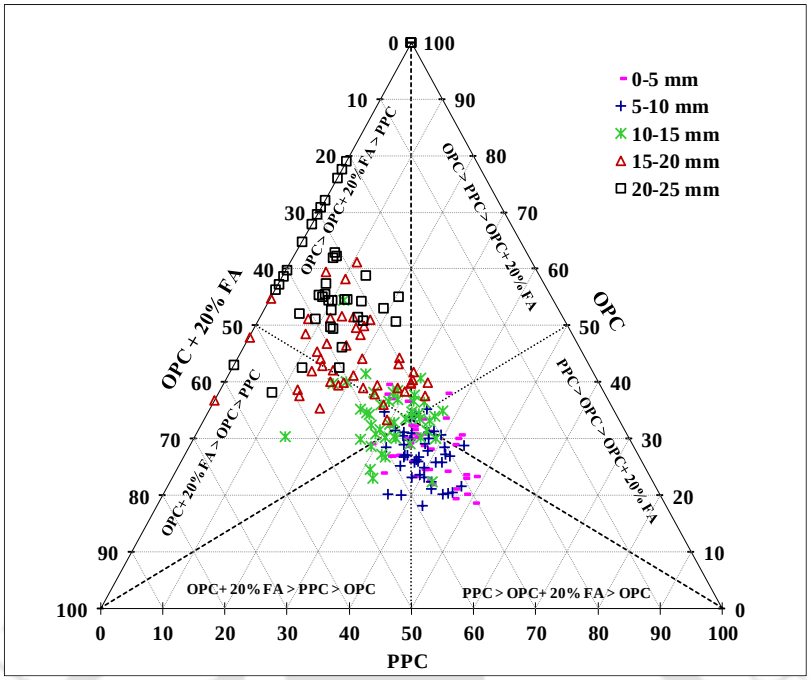

Figure 4.14 Comparison of experimentally obtained free chloride content at different depth intervals from exposure surface of prismatic specimens made with OPC, OPC + 20% FA, and PPC for exposure period of 27 months

From Figure 4.11 to 4.14, it is observed that the amount of free chloride content varied with the type of binder at different depth intervals. The prismatic specimens made with PPC mostly exhibited higher free chloride content as compared to OPC + 20% FA followed by OPC at depth intervals of 0-5 mm and 5-10 mm from the exposure surface for all exposure periods. At depth interval of 10-15 mm, the prismatic specimens made with OPC + 20% FA mostly exhibited higher free chloride content as compared to OPC followed by PPC for the exposure periods of 9, 15 and 21 months. However, for exposure period of 27 months, there is no systematic variation in free chloride content in the depth interval of 10-15 mm from the exposure surface among binder type. At depth intervals of 15-20 mm and 20-25 mm, the prismatic specimens made with OPC mostly showed higher free chloride content as compared to OPC + 20% FA followed by PPC specimens for all exposure periods. From the aforementioned observations, it is inferred that the free chloride content was higher in OPC + 20% FA and PPC concrete at lower depth intervals i.e. near the surface as compared to that in OPC concrete whereas at higher depth intervals the free chloride content was higher in OPC concrete as compared to that in OPC + 20% FA and PPC concrete for all w/b ratios, exposure solutions, and exposure periods. The higher free chloride content near the exposure surface i.e. at lower depth intervals (0-5 mm and 5-10 mm from the surface) in OPC + 20% FA and PPC specimens is attributed to the dominant effect of gradual

accumulation of chloride ions in the region near the surface of concrete during wetting-drying cycles due to the formation of denser pore structure at relatively greater depth in OPC + 20% FA and PPC concrete [134]. The formation of denser pore structure in OPC + 20% FA and PPC concrete reduced the penetration of chloride ions to higher depths thereby decreasing the free chloride content at higher depth intervals (beyond 10 mm from the surface). Further, as observed from Figure 4.2 to 4.10 and the figures shown in Appendix A1, the resistance against chloride penetration i.e. rate of decrease of free chloride content with depth from the exposure surface was higher in PPC concrete as compared to that in OPC + 20% FA followed by OPC concrete for all w/b ratios, exposure solutions and exposure periods. The higher resistance against penetration of chloride ions in PPC and OPC + 20% FA concrete than that in OPC concrete may be ascribed to the formation of compacted microstructure in OPC + 20% FA and PPC concrete due to the production of additional C-S-H gel because of pozzolanic reaction. The formation of compacted microstructure due to production of more amount of C-S-H gel in OPC + 20% FA and PPC concrete as compared to that in OPC concrete is evident from the typical FESEM images shown in Chapter 5 (discussed in Section 5.2.3). Between OPC + 20% FA and PPC, the resistance against penetration of chloride ions was higher in PPC concrete as compared to that in OPC + 20% FA concrete. This may be attributed to the effect of uniform blending of fly ash with OPC clinker during the manufacture of PPC that has resulted in formation of improved microstructure in PPC concrete as compared to that in OPC + 20% FA concrete, thereby reducing the penetration of chloride ions to higher depths. Thus, overall PPC concrete exhibited better performance against penetration of chloride ions as compared to OPC + 20% FA followed by OPC concrete when exposed to chloride and composite chloride-sulfate solutions.

While evaluating the effect of w/b ratio on free chloride content, it is noted that the specimens made with lower w/b ratio (w/b ratio of 0.45) mostly exhibited higher free chloride content at depth intervals of 0-5 mm and 5-10 mm from the exposure surface as compared to those made with higher w/b ratios (0.50 and 0.55) for all binders, exposure solutions, and exposure periods as observed from Figure 4.2 to 4.10 and the figures shown in Appendix A1. The higher free chloride content at lower w/b ratio near the exposure surface may be attributed to the alteration in pore structure of concrete near the surface region that might have altered capillary absorption through the pore network. At depth intervals of 10-15 mm, 15-20 mm, and 20-25 mm from the surface of concrete, the

prismatic specimens made with lower w/b ratio mostly exhibited lower free chloride content as compared to those made with higher w/b ratio for all binders, exposure solutions, and exposure periods. This is attributed to the ingress of lower amount of chloride ions in concrete at lower w/b ratio due to formation of denser microstructure than that at higher w/b ratio. Further, the resistance against chloride ion penetration (rate of decrease of free chloride content with depth) was mostly higher at lower w/b ratio as compared to that at higher w/b ratio.

4.3.2. Apparent chloride diffusion coefficient

The apparent chloride diffusion coefficient (D) of concrete was estimated by fitting the best-fit relationship of the analytical solution of Fick's second law of diffusion to the experimentally obtained free chloride content (C_f) at different depth intervals, which was stated earlier in Section 3.9.2. In some cases, the convection zone was observed in the depth interval of 0-5 mm from the exposure surface of concrete, and chloride content in the convection zone was excluded from the free chloride content profile for estimating the apparent chloride diffusion coefficient (as stated in Section 3.9.2). Typical plots of experimentally obtained, and fitted free chloride content profile indicating the convection zone, and diffusion zone are shown in Figure 4.15 (a, and b). Figure 4.15 (a) shows the free chloride content profile of concrete where the convection zone is not present, and Fick's second law of diffusion was used for estimating the apparent chloride diffusion coefficient by considering free chloride content of all the depth intervals from the exposure surface of concrete. Figure 4.15 (b) shows the free chloride content profile where the convection zone is observed in the depth interval of 0-5 mm from the exposure surface of concrete. As stated earlier, the convection zone is a thin layer from the exposure surface of concrete to the location of peak value of chloride concentration. In Figure 4.15 (b), where the convection zone was observed in the depth interval of 0-5 mm, the peak value of free chloride content was observed in the depth interval of 5-10 mm from the exposure of concrete, and this peak value of free chloride content for the depth interval of 5-10 mm is represented at the mid-depth level i.e. at 7.5 mm in the free chloride content profile. It may be noted that (as stated earlier), the free chloride contents for depth intervals of 0-5 mm, 5-10 mm, 10-15 mm, 15-20 mm, and 20-25 mm from the exposure surface of concrete were represented at the respective mid-depth levels i.e. at 2.5 mm, 7.5 mm, 12.5 mm, 17.5 mm, and 22.5 mm in the plot of free chloride content profile.

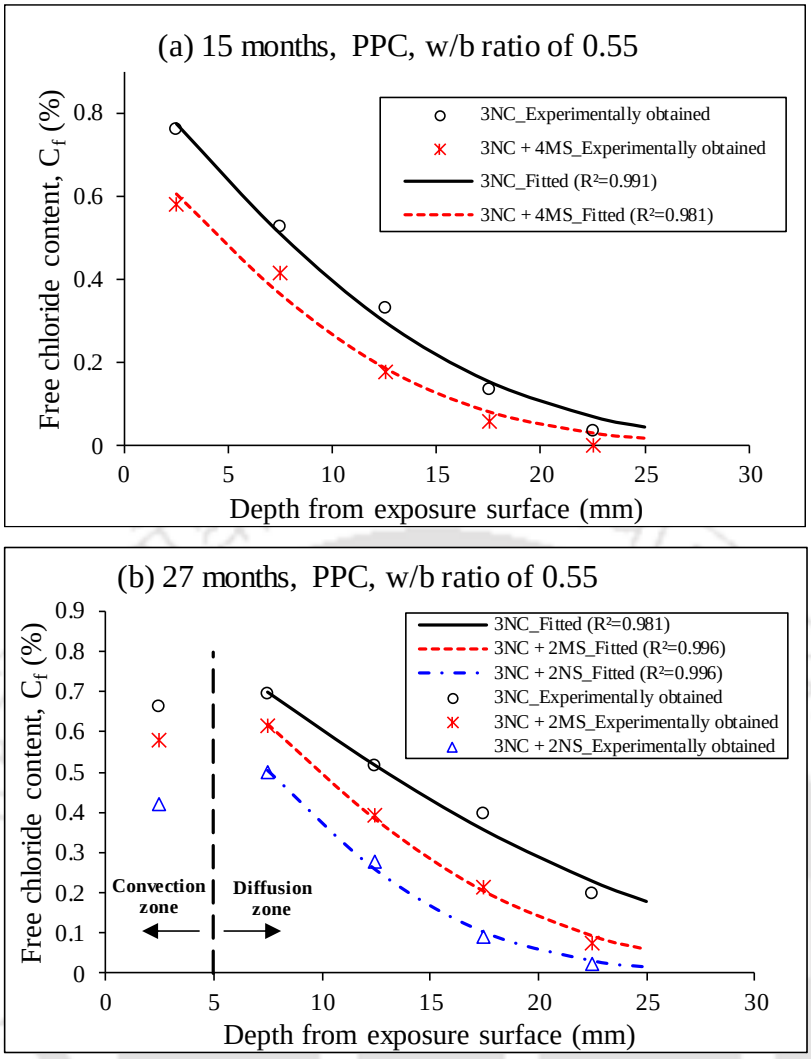

Figure 4.15 Plot of experimentally obtained, and fitted free chloride content profile of concrete made with PPC at w/b ratio of 0.55 and exposed to chloride and composite chloride-sulfate solutions: (a) 15 months (convection zone is not present), and (b) 27 months (convection zone is present in the depth interval of 0-5 mm from the exposure surface)

As stated earlier in Chapter 3, the free chloride content of concrete exposed to NaCl solutions, and composite solutions of NaCl + $MgSO_4$ was determined at the end of exposure periods of 9, 15, 21 and 27 months, and that of concrete exposed to composite solutions of NaCl + Na_2SO_4 was determined at the end of exposure periods of 15, 21 and 27 months. Accordingly, the apparent chloride diffusion coefficient of concrete was estimated at the end of above exposure periods corresponding to the respective exposure solution.

4.3.2.1. Effect of exposure solution on apparent chloride diffusion coefficient

The estimated apparent chloride diffusion coefficient (D) of concrete made with w/b ratios of 0.45, 0.50 and 0.55 and exposed to chloride and composite-chloride-sulfate solutions are

shown in Figure 4.16, 4.17, 4.18 and 4.19 for exposure periods of 9, 15, 21 and 27 months respectively.

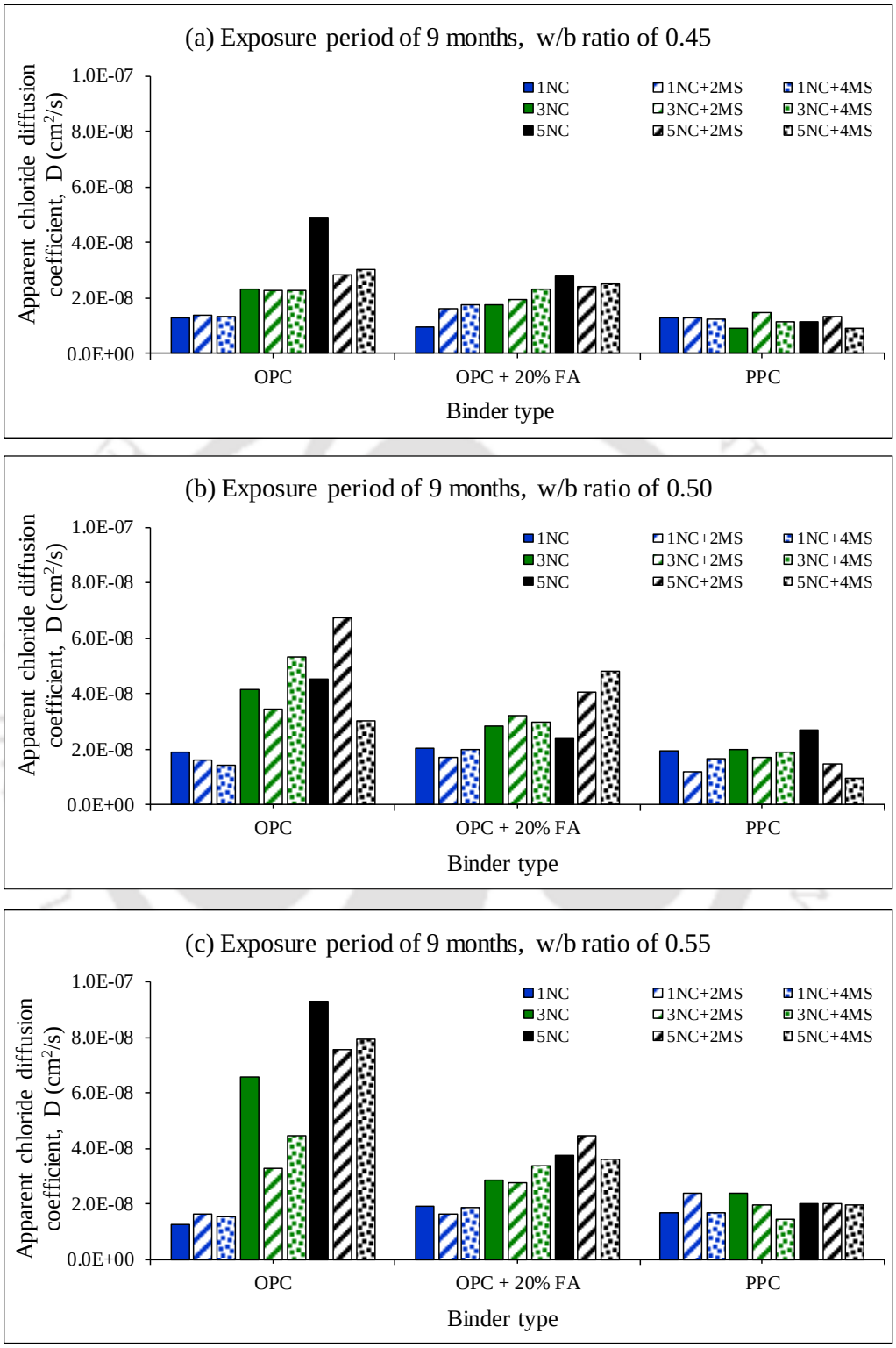

Figure 4.16 Apparent chloride diffusion coefficient (D) of concrete exposed to chloride (NaCl) and composite chloride-sulfate (NaCl + $MgSO_4$) solutions for 9 months: (a) w/b ratio of 0.45, (b) w/b ratio of 0.50, and (c) w/b ratio of 0.55

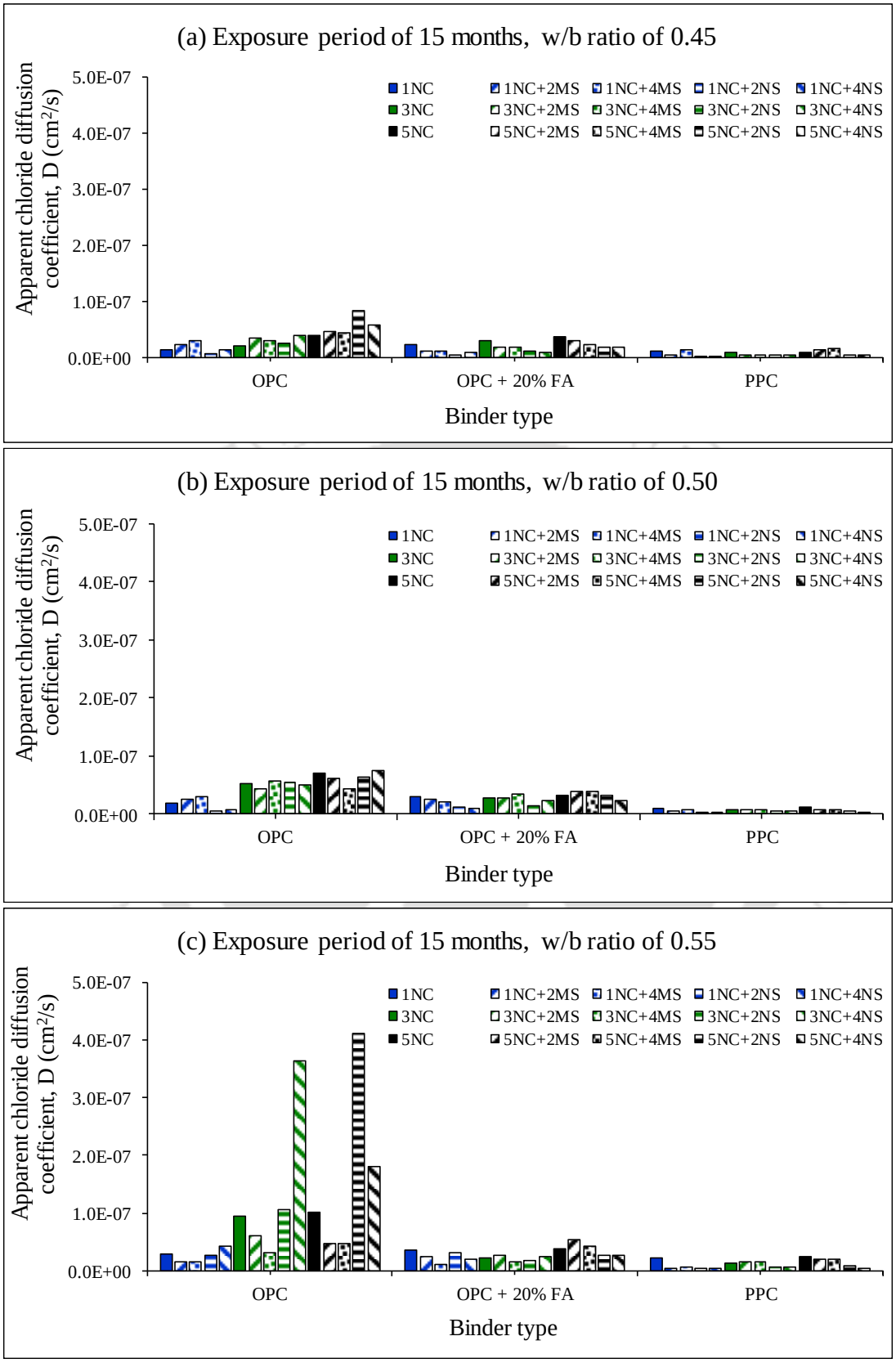

Figure 4.17 Apparent chloride diffusion coefficient (D) of concrete exposed to chloride (NaCl) and composite chloride-sulfate (NaCl + $MgSO_4$ and NaCl + Na_2SO_4) solutions for 15 months: (a) w/b ratio of 0.45, (b) w/b ratio of 0.50, and (c) w/b ratio of 0.55

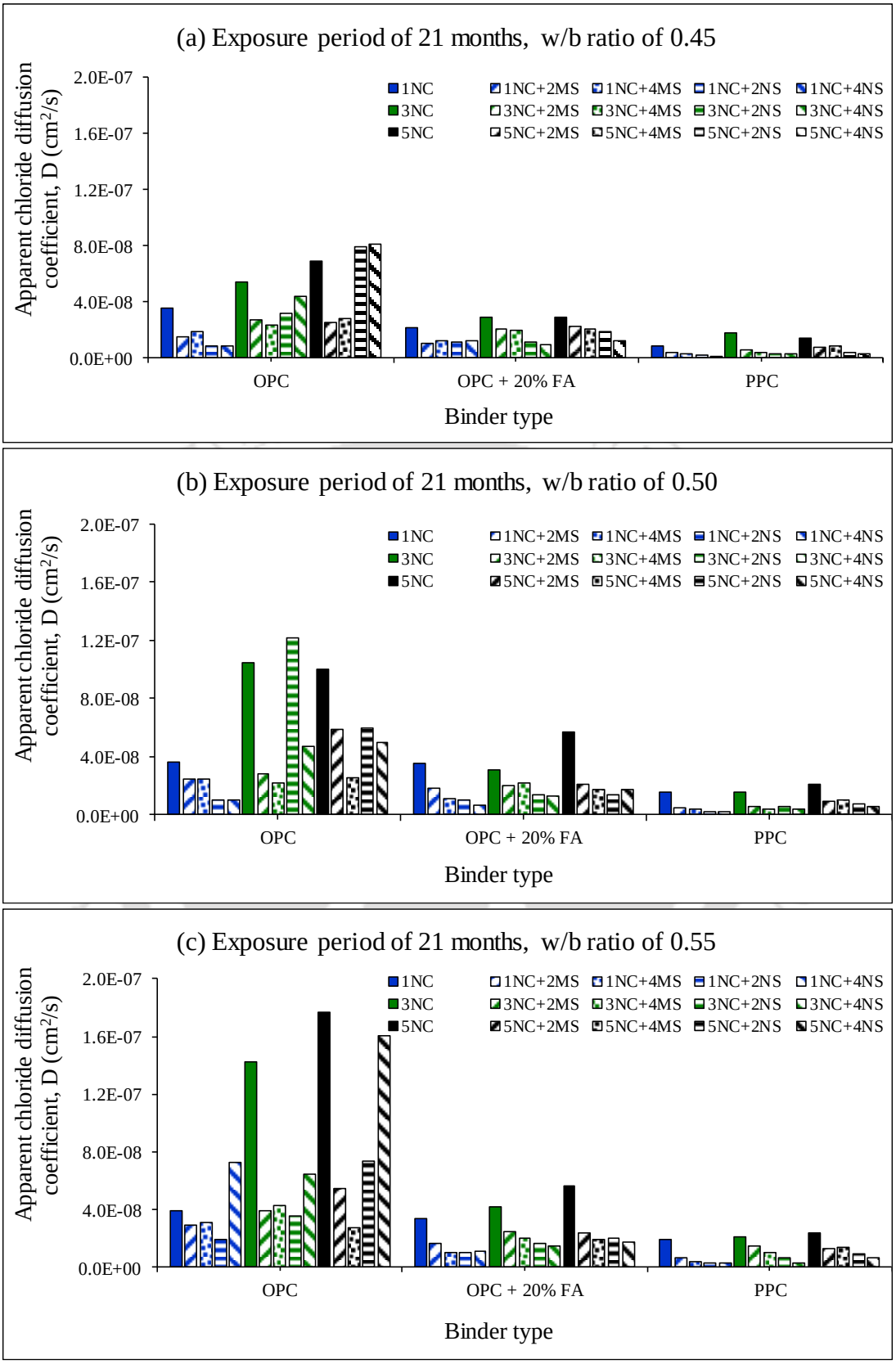

Figure 4.18 Apparent chloride diffusion coefficient (D) of concrete exposed to chloride (NaCl) and composite chloride-sulfate (NaCl + $MgSO_4$ and NaCl + Na_2SO_4) solutions for 21 months: (a) w/b ratio of 0.45, (b) w/b ratio of 0.50, and (c) w/b ratio of 0.55

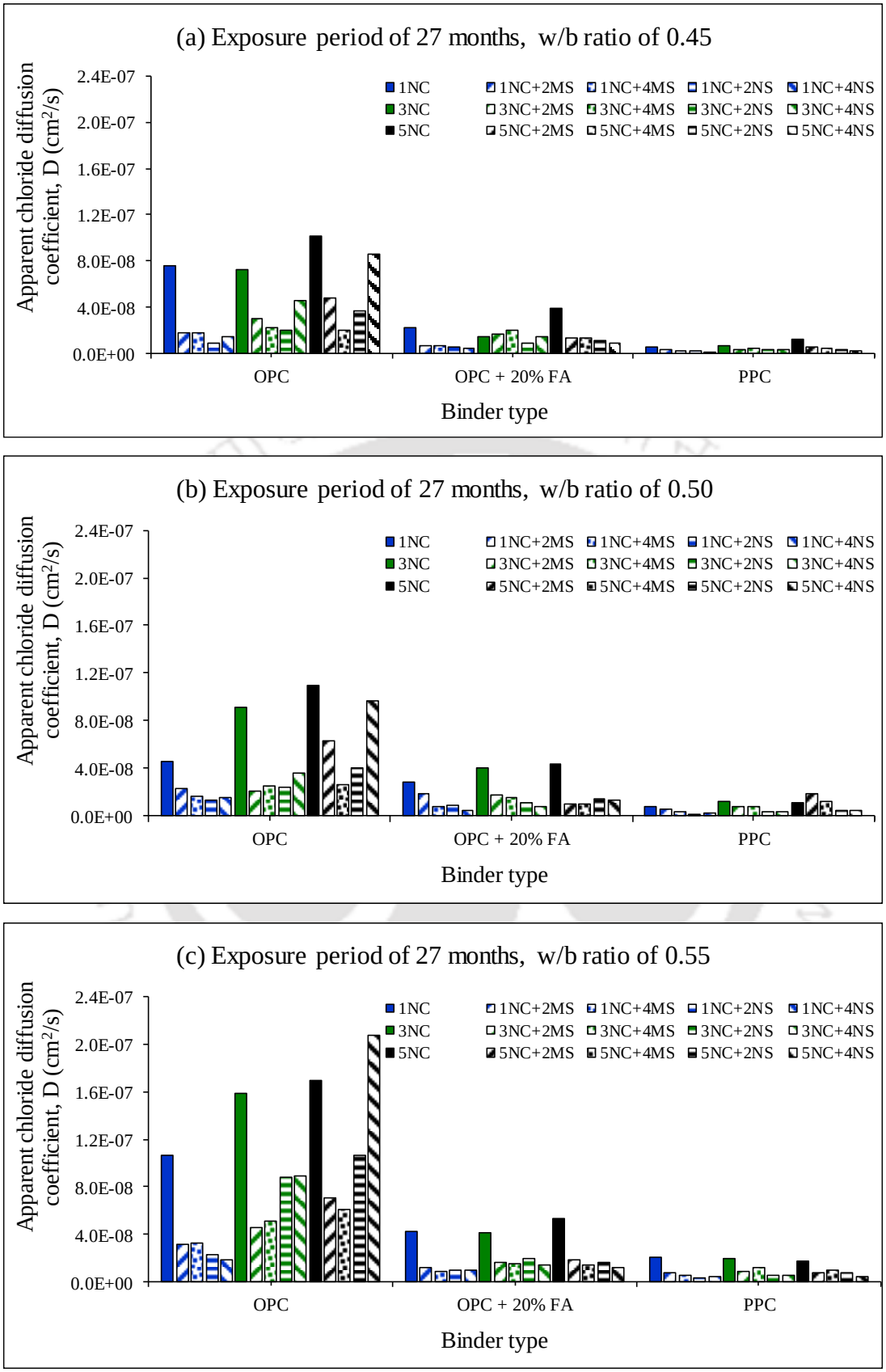

Figure 4.19 Apparent chloride diffusion coefficient (D) of concrete exposed to chloride (NaCl) and composite chloride-sulfate (NaCl + $MgSO_4$ and NaCl + Na_2SO_4) solutions for 27 months: (a) w/b ratio of 0.45, (b) w/b ratio of 0.50, and (c) w/b ratio of 0.55

From the estimated apparent chloride diffusion coefficient (D) shown in Figure 4.16 - 4.19, it is observed that the apparent chloride diffusion coefficient mostly increased with increase in concentration of NaCl in the chloride and composite chloride-sulfate solutions for OPC irrespective w/b ratio and exposure duration. This is ascribed to a higher concentration gradient of chloride ions in the concrete specimens exposed to higher concentration of NaCl in chloride and composite chloride-sulfates solutions than that exposed to lower concentration of NaCl in chloride and composite chloride-sulfates solutions. In addition, the formation of porous C-S-H as a result of leaching of calcium because of the presence of chloride ions might have resulted in a comparatively porous concrete microstructure, thereby increasing the ingress of chloride ions into the concrete exposed to a higher concentration of NaCl in chloride and composite chloride-sulfates solutions. For OPC, the apparent chloride diffusion coefficient of concrete exposed to 5% NaCl and 3% NaCl solutions were 3 and 2.7 times greater respectively than that in the concrete exposed to 1% NaCl solution, irrespective of w/b ratio, and exposure duration till 27 months of exposure. Similarly for OPC, the apparent chloride diffusion coefficient of concrete exposed to composite solutions of 5% NaCl with $MgSO_4$ (2% and 4%), and 3% NaCl with $MgSO_4$ (2% and 4%) were 2.3 and 1.8 times greater respectively than that in the concrete exposed to composite solutions of 1% NaCl with $MgSO_4$ (2% and 4%), irrespective of w/b ratio, concentration of $MgSO_4$ and exposure duration till 27 months of exposure. Further, in case of exposure of OPC concrete to composite chloride (NaCl)-sulfate (Na_2SO_4) solutions, the apparent chloride diffusion coefficient was 7 and 4.5 times greater respectively in the concrete exposed to composite solutions of 5% NaCl with Na_2SO_4 (2% and 4%), and 3% NaCl with Na_2SO_4 (2% and 4%) as compared to that exposed to composite solutions of 1% NaCl with Na_2SO_4 (2% and 4%), irrespective of w/b ratio, concentration of Na_2SO_4 and exposure duration.

In case of OPC + 20% FA and PPC, the apparent chloride diffusion coefficient of concrete exposed to chloride and composite chloride-sulfate solutions with 3% NaCl concentration was higher as compared to that exposed to chloride and composite chloride-sulfate solutions with 1% NaCl concentration in majority of the cases as observed from Figure 4.16 - 4.19. Similarly, in majority of the cases, apparent chloride diffusion coefficient in case of exposure to chloride and composite chloride-sulfate solutions with 5% NaCl concentration was higher as compared to that exposed to chloride and composite chloride-sulfate solutions with 3% NaCl concentration. However, in some cases, the apparent

chloride diffusion coefficient was higher in the concrete exposed to lower concentration of NaCl in chloride and composite chloride-sulfate solutions as compared to that exposed to higher concentration of NaCl in chloride and composite chloride-sulfate solutions for OPC + 20% FA and PPC concrete, which may be attributed to the dominant effect of formation of denser microstructure in OPC + 20% FA and PPC concrete over the effect of concentration of NaCl in the exposure solution that might have affected the ingress of chloride ions into concrete.

The apparent chloride diffusion coefficient of concrete exposed to 5% NaCl and 3% NaCl solutions were 1.3 and 1.1 times; and 1.6 and 1.2 times higher for PPC and OPC + 20% FA respectively than that in the concrete exposed to 1% NaCl solution, irrespective of w/b ratio and exposure duration till 27 months. Similarly, the apparent chloride diffusion coefficient of concrete exposed to composite solutions of 5% NaCl with $MgSO_4$ (2% and 4%), and 3% NaCl with $MgSO_4$ (2% and 4%) were 2 and 1.5 times; and 1.9 and 1.6 times higher for PPC and OPC + 20% FA respectively than that in the concrete exposed to composite solutions of 1% NaCl with $MgSO_4$ (2% and 4%), irrespective of w/b ratio, concentration of $MgSO_4$ and exposure duration. In case of exposure to composite solutions of NaCl with Na_2SO_4, the apparent chloride diffusion coefficient of concrete exposed to composite solutions of 5% NaCl with Na_2SO_4 (2% and 4%), and 3% NaCl with Na_2SO_4 (2% and 4%) were 2.1 and 1.7 times; and 1.9 and 1.5 times higher for PPC and OPC + 20% FA respectively as compared to that exposed to composite solutions of 1% NaCl with Na_2SO_4 (2% and 4%).

While observing the effect of sulfate ions in the exposure solution on apparent chloride diffusion coefficient of concrete (Figure 4.16 - 4.19), it is inferred that the apparent chloride diffusion coefficient was mostly lower in the presence of sulfate ions for both cations i.e. Na^+ and Mg^{2+} for all binders, w/b ratios and all exposure periods, except few cases till the exposure period of 15 months. The lower apparent chloride diffusion coefficient in case of exposure to composite chloride-sulfate solutions as compared to chloride solutions may be attributed to the reduced penetration of chloride ions into the concrete mixes. The reason for reduction in the penetration of chloride ions in case of exposure to composite chloride-sulfate solutions is already stated in Section 4.3.1.2. In few cases, the higher apparent chloride diffusion coefficient in case of exposure to composite chloride-sulfate solutions as compared to chloride solutions till the exposure period of 15 months may be attributed to the presence of higher amount of free chloride in the concrete due to release of bound

chloride as a results of decomposition of Friedel's salt (formed due to chloride binding) in the presence of sulfate ions. Further, the apparent chloride diffusion coefficient decreased with increase in concentration of sulfate ions in the exposure solution for both cations (Mg^{2+} and Na^{+}) in majority of the cases for exposure to composite chloride-sulfate solutions. Overall, the concrete specimens exposed to NaCl solutions exhibited 1.95 and 2.95 times higher apparent chloride diffusion coefficient as compared to those exposed to composite chloride-sulfate solutions of NaCl with $MgSO_4$, and NaCl with Na_2SO_4 respectively irrespective of binder type, w/b ratio, concentration of chloride and sulfate ions, and exposure duration.

On comparing the effect of cation type associated with sulfate ions in the exposure solution, it is observed that the specimens exposed to composite solutions of NaCl with $MgSO_4$ mostly exhibited higher apparent chloride diffusion coefficient as compared to those exposed to composite solutions of NaCl with Na_2SO_4 irrespective of binder type, w/b ratio, concentration of chloride and sulfate ions, and exposure duration except in few cases (in case of OPC exposed to composite solutions with NaCl concentrations of 3% and 5%, and Na_2SO_4 concentrations of 2% and 4%), as observed from Figure 4.17 - 4.19. The higher chloride diffusion coefficient in case of composite solutions of NaCl with $MgSO_4$ is attributed to the penetration of higher amount of chloride ions into the concrete exposed to composite solutions of NaCl with $MgSO_4$ as compared to composite solutions of NaCl with Na_2SO_4. It may be noted that the free chloride content was higher in the concrete specimens exposed to NaCl + $MgSO_4$ solutions as compared to those exposed to NaCl + Na_2SO_4 solutions at all depth intervals (discussed in Section 4.3.1.2). The higher chloride diffusion coefficient in case of OPC concrete exposed to composite solutions of NaCl (3% and 5%) with Na_2SO_4 (2% and 4%) may be attributed to the effect of less difference in the free chloride content between lower and higher depth intervals of the prismatic specimens as observed from the free chloride content profile shown in Figure 4.3 and 4.4, although the free chloride contents in case of exposure to NaCl + Na_2SO_4 solutions were lower as compared to NaCl + $MgSO_4$ solutions at all depth intervals. In other words, in these specimens, the resistance against chloride penetration i.e. rate of decrease of free chloride content with depth was lower in OPC concrete exposed to composite solutions of NaCl with Na_2SO_4 as compared to composite solutions of NaCl with $MgSO_4$.

4.3.2.2. Effect of binder type and w/b ratio on apparent chloride diffusion coefficient

To evaluate the effect of binder type and w/b ratio on apparent chloride diffusion coefficient (D) of concrete, the estimated values were plotted in ternary plots in the scale of 0 - 100% for different exposure periods. The ternary plots for comparison of apparent chloride diffusion coefficient among binder type (irrespective of w/b ratio, and exposure solution), and w/b ratio (irrespective of binder type, and exposure solution) are shown in Figure 4.20 and 4.21 respectively.

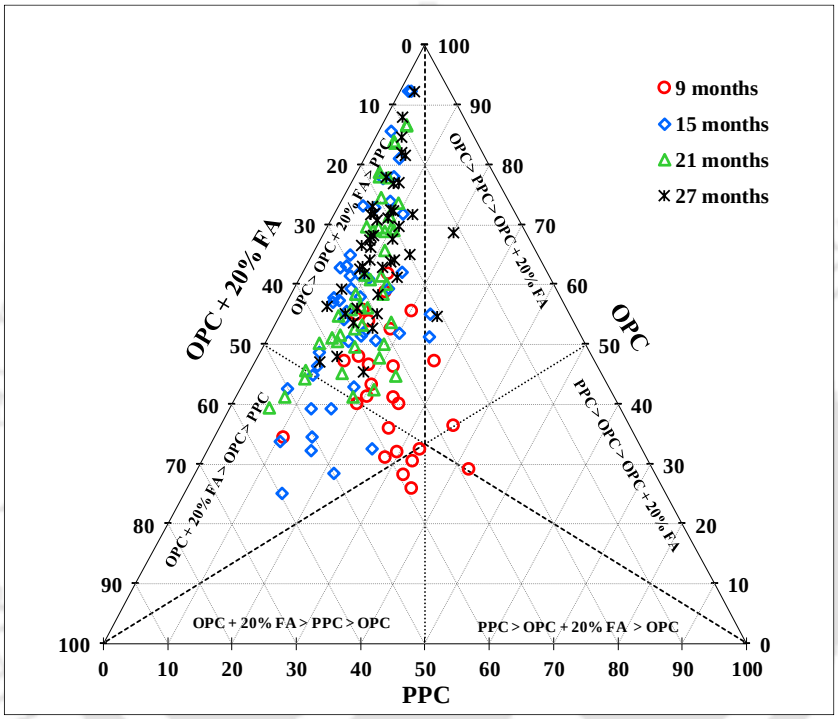

Figure 4.20 Comparison of estimated apparent chloride diffusion coefficient of concrete made with OPC, OPC + 20% FA, and PPC at different exposure periods

From Figure 4.20, it is inferred that the concrete specimens made with OPC exhibited higher apparent chloride diffusion coefficient as compared to those made with OPC + 20% FA followed by PPC irrespective of w/b ratio, exposure solution, and exposure duration. The lower diffusion coefficient in the concrete made with PPC, and OPC + 20% FA may be ascribed to the higher resistance against penetration of chloride ions because of formation of compacted microstructure as a result of pozzolanic reaction. The apparent chloride diffusion coefficient of concrete made with OPC was 2.09 times and 4.87 times higher than those made with OPC + 20% FA, and PPC respectively for exposure against NaCl solutions, irrespective of w/b ratio, concentration of NaCl in the exposure solution, and exposure duration. As reported by Al-Sodani et al. [139] the concrete made with OPC showed higher chloride diffusion coefficient as compared to that made with OPC plus 20%

fly ash in case of exposure to chloride solution in the laboratory and exposed in the tidal zone of a marine exposure site located on the Arabian Gulf coast. Further in the present study, the apparent chloride diffusion coefficient was 1.79 times and 4.14 times higher for the concrete made with OPC as compared to those made with OPC + 20% FA, and PPC respectively for exposure against composite solutions of NaCl with $MgSO_4$, irrespective of w/b ratio, concentration of NaCl and $MgSO_4$ in the exposure solution, and exposure duration. Further, the apparent chloride diffusion coefficient of concrete made with OPC was 4.23 times and 14.69 times higher than those made with OPC + 20% FA, and PPC respectively for exposure against composite solutions of NaCl with Na_2SO_4, irrespective of w/b ratio, concentration of NaCl and Na_2SO_4 in the exposure solution, and exposure duration.

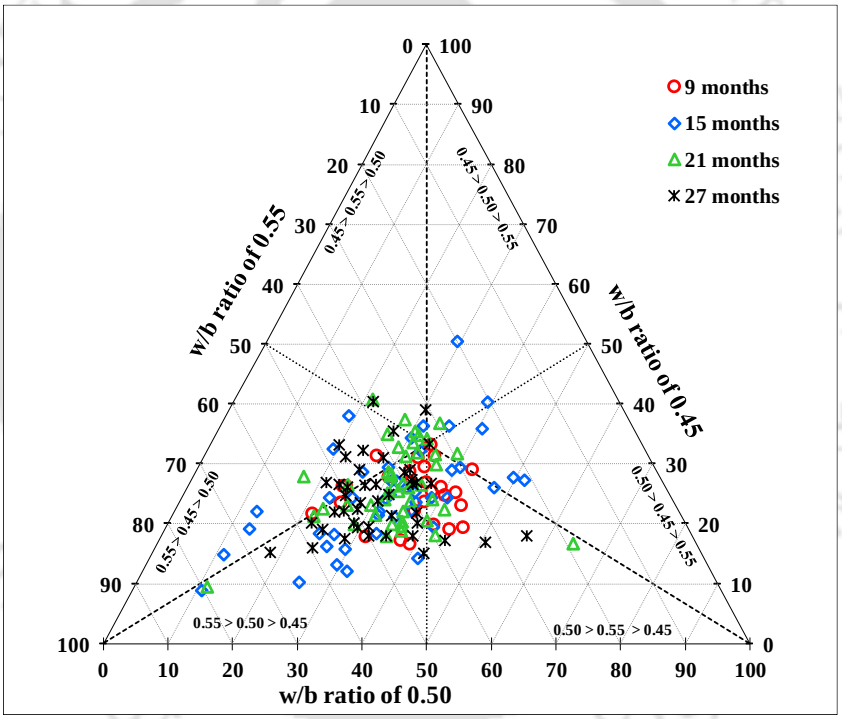

Figure 4.21 Comparison of estimated apparent chloride diffusion coefficient of concrete made with w/b ratios of 0.45, 0.50 and 0.55

From Figure 4.21 it is observed that the apparent chloride diffusion coefficient of concrete mostly decreased with decrease in w/b ratio, irrespective of binder type, exposure solution, and exposure duration. This is attributed to the formation of denser microstructure in concrete at lower w/b ratio thereby reducing the penetration of chloride ions as compared to that at higher w/b ratio. In case of exposure to NaCl solution, the concrete made with w/b ratios of 0.50 and 0.55 showed 1.46 times and 1.98 times respectively higher apparent chloride diffusion coefficient than that made with w/b ratio of 0.45, irrespective of type of

binder, concentration of NaCl in the exposure solution, and exposure duration. Similarly, the apparent chloride diffusion coefficient was 1.37 times and 1.60 times higher in the concrete made with w/b ratios of 0.50 and 0.55 respectively as compared to that made with w/b ratio of 0.45 for exposure against composite solutions of NaCl with $MgSO_4$, irrespective of binder type, concentration of NaCl and $MgSO_4$ in the exposure solution, and exposure duration. Further, in case of exposure to composite solutions of NaCl with Na_2SO_4, the apparent chloride diffusion coefficient of concrete made with w/b ratios of 0.50 and 0.55 were 1.32 times and 2.36 times higher than that made with w/b ratio of 0.45 irrespective of type of binder, concentration of NaCl and Na_2SO_4 in the exposure solution, and exposure duration.

4.3.2.3. Effect of exposure duration on apparent chloride diffusion coefficient

From Figure 4.16 and 4.19 it is observed that the estimated apparent chloride diffusion coefficient mostly decreased with increase in exposure period in the concrete mixes exposed to composite chloride-sulfate solutions irrespective of binder type, w/b ratio, concentration of chloride and sulfate ions in the exposure solution, and cation type associated with sulfate ions. This may be attributed to the decrease in rate of penetration of chloride ions into the concrete with increase in exposure period due to the improvement in microstructure of concrete as a result of continued hydration and pozzolanic reactions as well as due to pore filling effect of reaction products formed in concrete in the presence of chloride and sulfate ions. As stated earlier (Section 4.3.1.2), the rate of increase in the observed free chloride content decreased during the later ages for exposure against both chloride and composite chloride-sulfate solutions. In case of exposure to chloride solutions, the variation in the estimated apparent chloride diffusion coefficient with exposure period was mostly unsystematic till 21 months followed by a decrease at the exposure period of 27 months in majority of the cases. This variation in apparent chloride diffusion coefficient of concrete may be ascribed to the non-uniform variation in the free chloride content at different depth intervals with increase in exposure period in the concrete exposed to chloride solutions. The non-uniform variation in free chloride content at different depth intervals of concrete with increase in exposure period may be attributed to the effect of variations in the microstructure due to alterations in the filling of pores with reaction products formed in concrete in the presence of chloride ions, as well as due to the variations in the degree of saturation of concrete with exposure period [140].

4.4. Chloride binding in concrete

To evaluate the chloride binding in concrete exposed to chloride and composite chloride-sulfate solutions, the experimentally obtained free chloride and total chloride contents were plotted for different binders, w/b ratios, and exposure solutions at different exposure periods. The plots of free chloride content (C_f) versus total chloride content (C_t) for different binders irrespective of w/b ratio, exposure solution, and depth interval from the exposure surface of prismatic specimen are shown in Figure 4.22 - 4.24. Similarly, the plots for w/b ratio (irrespective of binder type, exposure solution and depth interval), and exposure solution (irrespective of concentrations of NaCl, $MgSO_4$ and Na_2SO_4 in the exposure solution, binder type, w/b ratio and depth interval) are provided in the Appendix A2. In addition, the typical plots of free chloride content (C_f) versus total chloride content (C_t) for different concentrations of NaCl in case of chloride solutions, and for different concentrations of NaCl, $MgSO_4$ and Na_2SO_4 in case of composite chloride-sulfate solutions irrespective of depth interval from the exposure surface of concrete are also provided in Appendix A2.

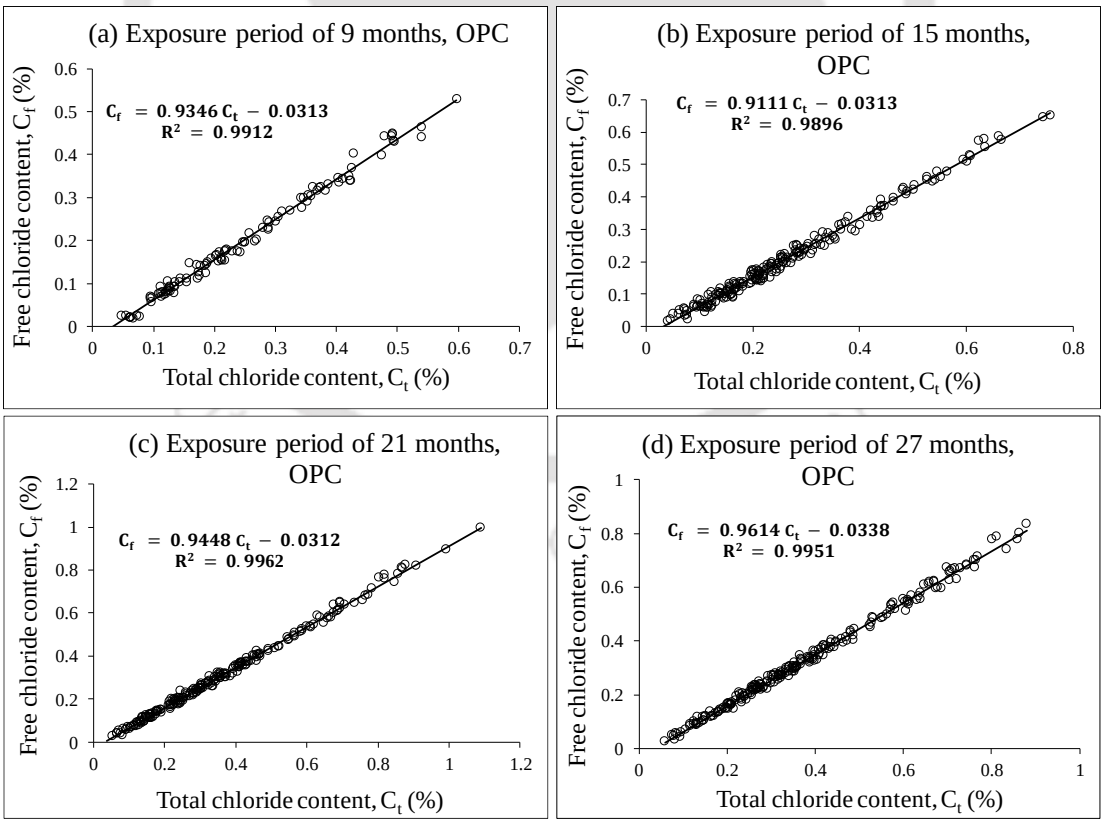

Figure 4.22 Free chloride content (C_f) versus total chloride content (C_t) of OPC concrete for exposure periods of: (a) 9 months, (b) 15 months, (c) 21 months and (d) 27 months

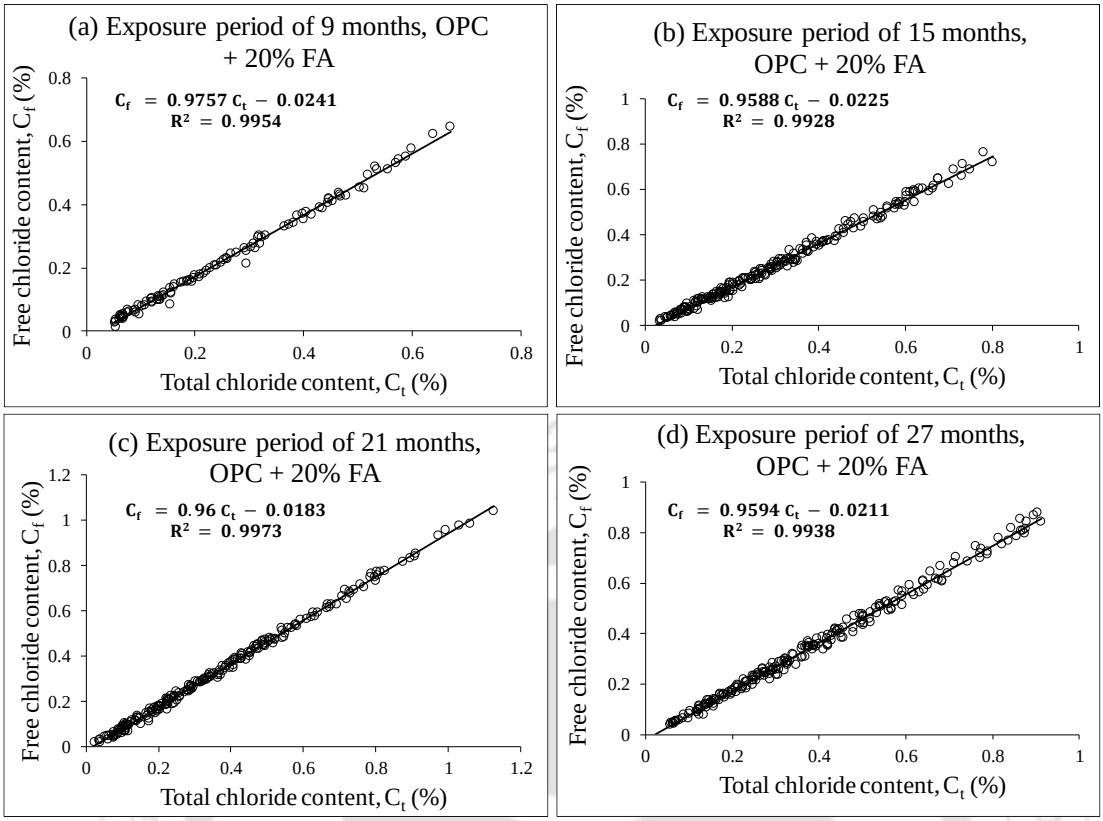

Figure 4.23 Free chloride content (C_f) versus total chloride content (C_t) of OPC + 20% FA concrete for exposure periods of: (a) 9 months, (b) 15 months, (c) 21 months and (d) 27 months

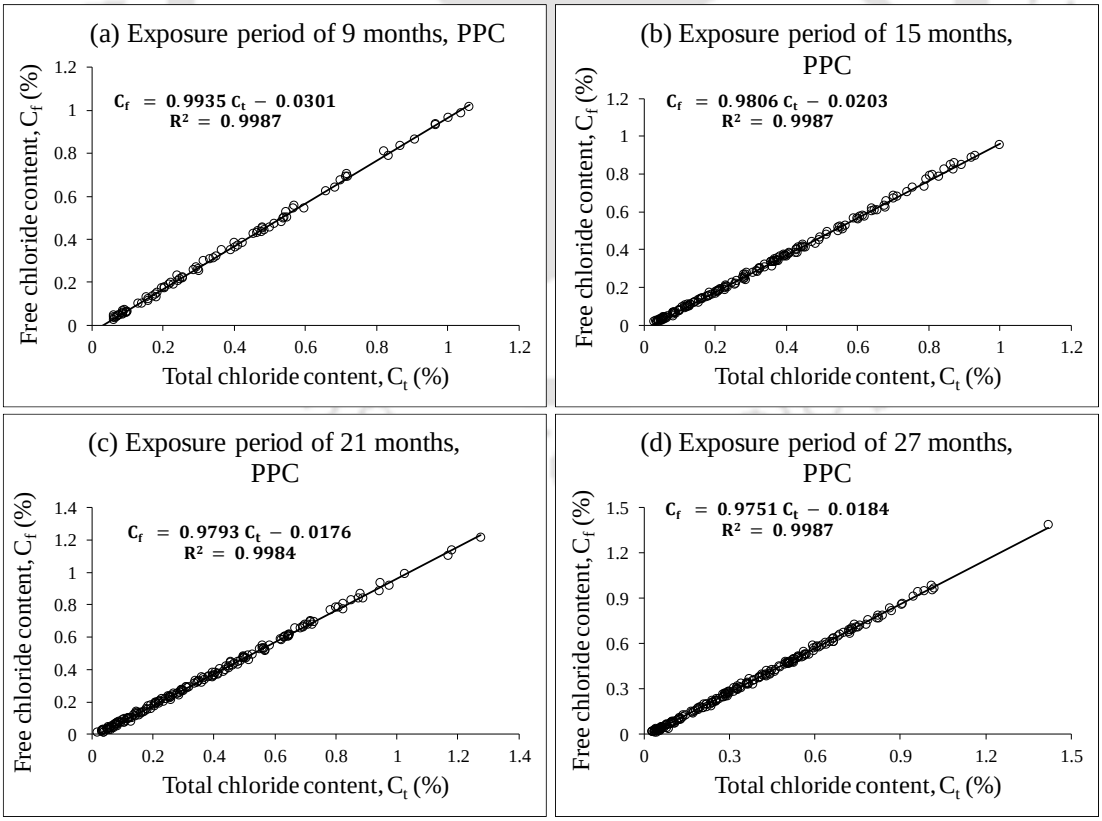

Figure 4.24 Free chloride content (C_f) versus total chloride content (C_t) of PPC concrete for exposure periods: (a) 9 months, (b) 15 months, (c) 21 months and (d) 27 months

In these plots, the developed relationship between free chloride and total chloride contents is shown along with the coefficient of correlation (R^2). From Figure 4.22-4.24, it is observed that there exists a linear relationship between free chloride and total chloride contents. The obtained linear relationship is presented below;

$$C_f = m \times C_t - n \quad (4.1)$$

Where C_f and C_t are free chloride content (%) and total chloride content (%) respectively. 'm' and 'n' are the coefficients. The coefficient 'm' in the above equation represents the rate of increase of free chloride content with total chloride content. The obtained values of coefficient 'm' are shown in Figure 4.25 (a, b), 4.26 and 4.27 for exposure solution, binder type, and w/b ratio respectively. The higher value of 'm' indicates higher rate of increase in free chloride content with total chloride content, thereby indicating lower chloride binding in the concrete.

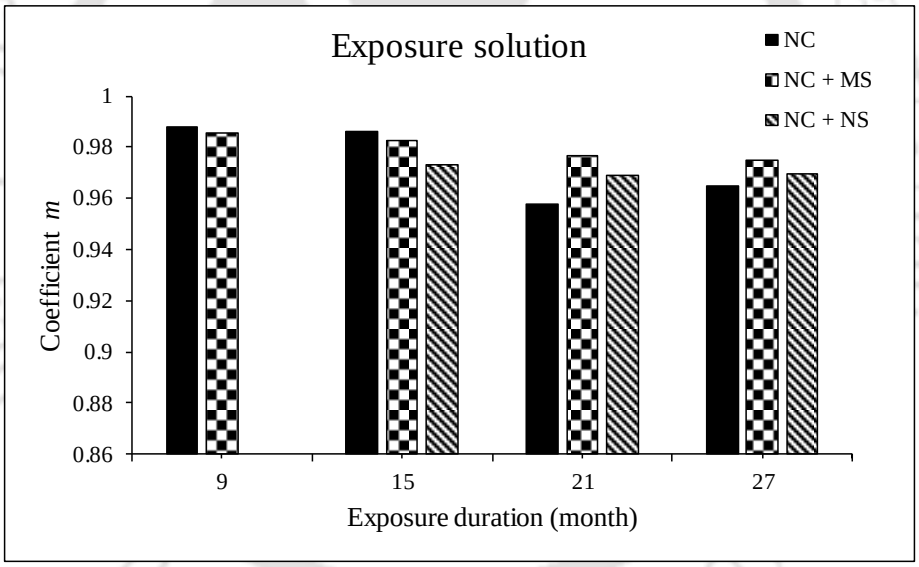

NC: NaCl, **NC + MS:** NaCl + $MgSO_4$, **NC + NS:** NaCl + Na_2SO_4

Figure 4.25 (a) Rate of increase of free chloride content with total chloride content (Coefficient 'm') among exposure solutions irrespective of concentrations of NaCl, $MgSO_4$ and Na_2SO_4 in the exposure solution, binder type, w/b ratio and depth interval

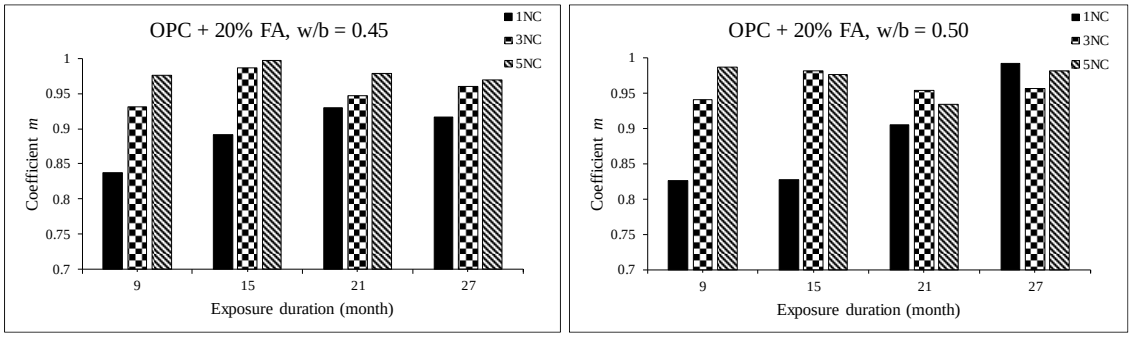

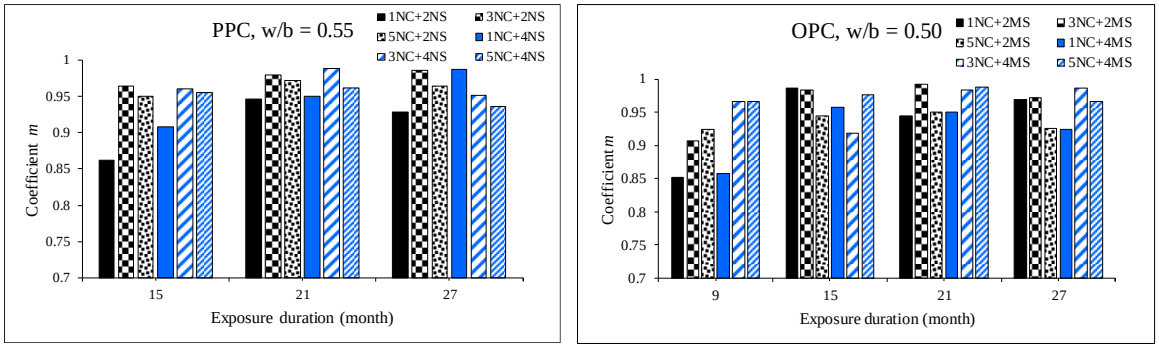

Figure 4.25 (b) Typical plot of rate of increase of free chloride content with total chloride content (Coefficient 'm') among exposure solutions irrespective of depth interval from exposure surface

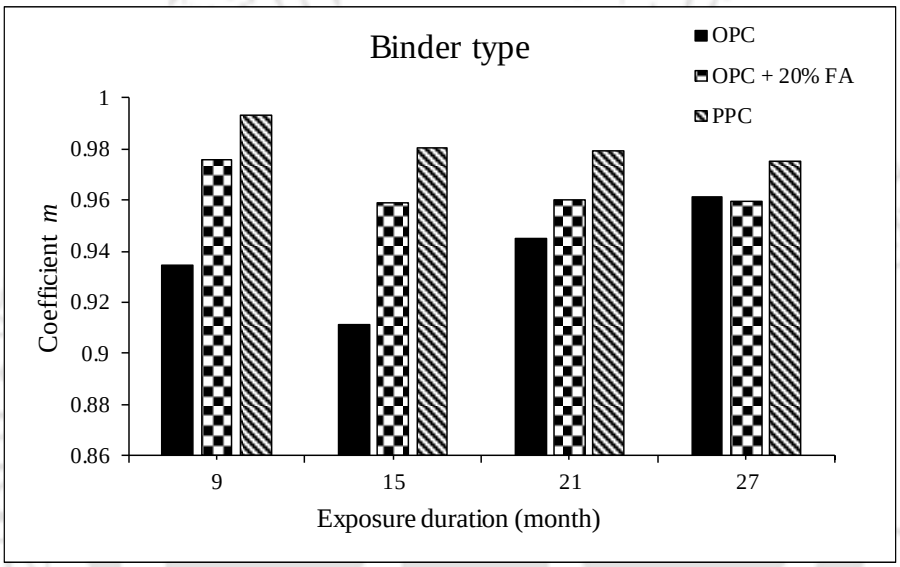

Figure 4.26 Rate of increase of free chloride content with total chloride content (Coefficient 'm') among binder type

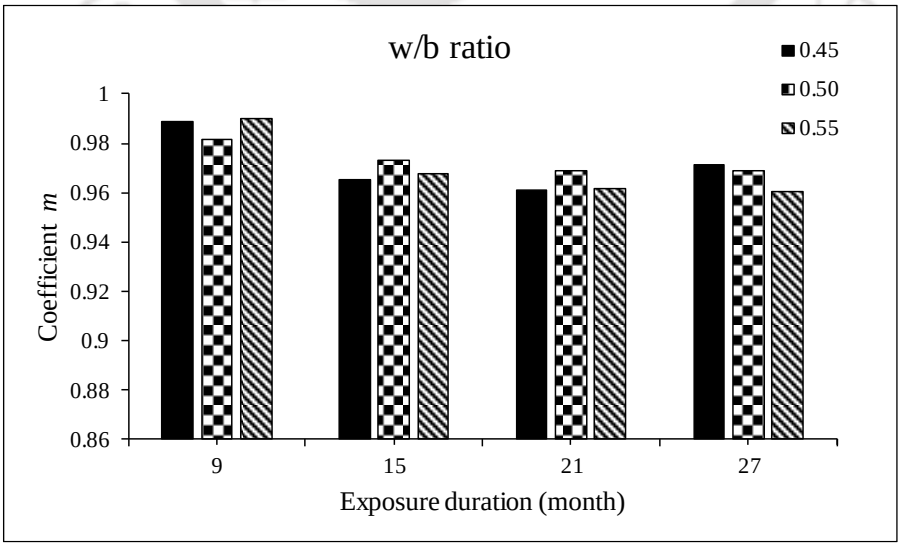

Figure 4.27 Rate of increase of free chloride content with total chloride content (Coefficient 'm') among w/b ratio

From Figure 4.25 (a), it is observed that the value of coefficient 'm' was lower in case of exposure to composite chloride-sulfate solutions as compared to chloride solutions till the exposure period of 15 months, which indicates higher chloride binding in the concrete exposed to composite chloride-sulfate solutions. As stated earlier, the free chloride content was mostly lower when exposed to composite chloride-sulfate solutions (NaCl + $MgSO_4$ and NaCl + Na_2SO_4) as compared to chloride solutions (NaCl) at all exposure durations. Further, the formation of calcium chloroaluminate (formed due to the reaction of chloride ions with hydrated C_3A) was lower in the concrete exposed to composite chloride-sulfate solutions as compared to chloride solutions as observed from the results of XRD analysis presented in Chapter 5 (discussed in Section 5.2.2). The formation of lower calcium chloroaluminate indicates lower extent of chemical binding of chloride ions in the concrete exposed to composite chloride-sulfate solutions. However, higher chloride binding in the concrete exposed to composite chloride-sulfate solutions during the early exposure periods (i.e. till 15 months of exposure) may be attributed to the dominant effect of higher extent of physical binding of chloride ions with C-S-H gel in the concrete. The physical binding occurs as a result of adsorption of chloride ions on the surface of calcium silicate hydrate (C-S-H). The factors that influence the physical binding of chloride ions include the amount of C-S-H in concrete, Ca/Si ratio (calcium to silica ratio) of C-S-H, composition of concrete pore solution, temperature, sulfate attack, carbonation etc. [24, 141]. During the later exposure periods (i.e. after 15 months of exposure), the rate of increase in free chloride content with total chloride content was less in the concrete exposed to chloride solutions as compared to composite chloride-sulfate solutions as evident from Figure 4.25 (a). This indicates more chloride binding in the concrete exposed to chloride solutions during the later ages, which may be attributed to the dominant effect of higher extent of chemical binding of chloride ions when exposed to chloride solutions as compared to composite chloride-sulfate solutions during the later ages. The lower chloride binding in the concrete exposed to composite chloride-sulfate solutions during the later ages may be ascribed to the release of bound chloride due to the solubility of calcium chloroaluminate (Friedel's salt) in the presence of sulfate ions. While observing the effect of cation type associated with sulfate ions, it is inferred that the chloride binding was higher in case of exposure to composite solution of NaCl with Na_2SO_4 as compared to composite solution of NaCl with $MgSO_4$ at all exposure durations as the value of coefficient 'm' was lower in case of exposure to composite solution of NaCl with Na_2SO_4 as compared to composite solution of NaCl with $MgSO_4$ as evident from Figure 4.25 (a). This may be attributed to the

significant effect of physical binding of chloride ions with C-S-H gel in the concrete exposed to composite solution of NaCl with Na_2SO_4 as compared to composite solution of NaCl with $MgSO_4$. It may be noted that the formation of calcium chloroaluminate was higher in the concrete exposed to composite solution of NaCl with $MgSO_4$ as compared to composite solution of NaCl with Na_2SO_4 (observed from the results of XRD analysis presented in Chapter 5, Section 5.2.2), thereby indicating relatively higher extent of chemical binding of chloride ions in the concrete exposed to composite solution of NaCl with $MgSO_4$. However, the formation of magnesium silicate hydrate (M-S-H) gel in the concrete exposed to composite solution of NaCl with $MgSO_4$ due to conversion of C-S-H gel in the presence of magnesium sulfate might have resulted in a significant decrease in physical binding of chloride ions with C-S-H gel, thereby reducing the chloride binding in case of exposure to composite solution of NaCl with $MgSO_4$ as compared to composite solution of NaCl with Na_2SO_4. The formation of M-S-H gel in the concrete exposed to composite solution of NaCl with $MgSO_4$ was evident from the FESEM images provided in Chapter 5 (Section 5.2.2). While evaluating the effect of concentration of NaCl in chloride and composite chloride-sulfate solutions, it is observed that the variation in chloride binding with increase in concentration of NaCl was mostly unsystematic as indicated by the values of coefficient '*m*' (Figure 4.25 (b)) for all binders, w/b ratios and exposure durations except for the case wherein the chloride binding decreased with increase in concentration of NaCl in chloride solution for OPC + 20% FA concrete at w/b ratio 0.45. As stated earlier, the free chloride content increased with increase in concentration of NaCl in chloride and composite chloride-sulfate solutions. Further, the formation of calcium chloroaluminate mostly increased with increase in concentration of NaCl in chloride and composite chloride-sulfate solutions (observed from the results of XRD analysis presented in Section 5.2.2, Chapter 5), which indicates increase in the extent of chemical binding of chloride ions in concrete with increase in concentration of NaCl in chloride and composite chloride-sulfate solutions. Thus, the unsystematic variation in chloride binding in concrete with increase in concentration of NaCl in chloride and composite chloride-sulfate solutions may be ascribed to the effect of alterations in the extent of physical binding of chloride ions with C-S-H in concrete. Further, there was mostly unsystematic variation in chloride binding in concrete with increase in concentration of $MgSO_4$ and $NaSO_4$ in the composite solutions of NaCl with $MgSO_4$, and NaCl with Na_2SO_4 respectively, as indicated by the values of coefficient '*m*' (Figure 4.25 (b)). As observed from the results of XRD analysis presented in Section 5.2.2 (Chapter 5), the formation of calcium chloroaluminate mostly

increased with increase in concentrations of Na_2SO_4 and $MgSO_4$ in the composite chloride-sulfate solutions, thereby indicating higher extent of chemical binding of chloride ions in concrete. Thus, unsystematic variation in chloride binding in concrete with increase in concentration of $MgSO_4$ and Na_2SO_4 in the composite chloride-sulfate solutions may be due the effect of alterations in the physical binding of chloride ions with C-S-H gel in concrete.

From Figure 4.26, it is observed that the concrete made with OPC exhibited higher chloride binding as compared to that made with OPC + 20% FA followed by PPC at all exposure durations as indicated by lower values of coefficient 'm' for OPC as compared to OPC + 20% FA followed by PPC. As mentioned earlier in Section 4.3.1.3, the free chloride content was mostly higher in PPC concrete as compared to OPC + 20% FA followed by OPC concrete at lower depth intervals whereas at higher depth intervals the free chloride content was mostly higher in OPC concrete than that in OPC + 20% FA followed by PPC concrete for all w/b ratios, exposure solutions, and exposure periods. Further, the formation of calcium chloroaluminate was mostly higher in OPC + 20% FA concrete as compared to PPC followed by OPC concrete at lower depth intervals whereas at higher depth intervals the formation of calcium chloroaluminate was higher in OPC concrete as compared to OPC + 20% FA followed by PPC concrete as observed from the results of XRD analysis (discussed in Section 5.2.3, Chapter 5). Thus, the higher chloride binding in OPC concrete as compared to OPC + 20% FA and PPC concrete may be ascribed to the significant effect of physical binding of chloride ions with C-S-H gel to a greater extent at lower depth intervals and due to the significant effect of chemical binding of chloride ions (i.e. reaction of chloride ions with hydrated C_3A) to a greater extent at higher depth intervals in OPC concrete. The lower extent of physical binding of chloride ions in OPC + 20% FA and PPC as compared to OPC concrete may be attributed to the dominant effect of lower Ca/Si ratio of C-S-H in OPC + 20% FA and PPC than that in OPC concrete [24, 141], although there is formation of more amount of C-S-H gel in OPC + 20% FA and PPC concrete as compared to OPC concrete at later ages. Between OPC + 20% FA and PPC, the higher chloride binding in OPC + 20% FA concrete as compared to PPC concrete may be attributed to the dominant effect of chemical binding of chloride ions i.e. reaction of chloride ions with hydrated C_3A to a greater extent at all depth intervals in OPC + 20% FA concrete than that in PPC concrete as the formation of calcium chloroaluminate was higher in OPC + 20% FA concrete as compared to that in PPC concrete (observed from the results

of XRD analysis discussed in Section 5.2.3, Chapter 5). As stated earlier in Section 4.3.1.3, the resistance against chloride penetration i.e. rate of decrease of observed free chloride content with depth was higher in PPC concrete as compared to that in OPC + 20% FA followed by OPC concrete for exposure against chloride and composite chloride-sulfate solutions. From Figure 4.27, it is observed that the variation in chloride binding in concrete with w/b ratio was mostly unsystematic as indicated by the values of coefficient 'm'. This may be attributed to the effect of variations in the extent of reaction of chloride ions with aluminate hydrates in the concrete mixes, and also due to the alterations in the microstructure of concrete at various depth intervals with change in w/b ratio. As observed from Figure 4.27, although there was less difference in value of the coefficient 'm' with exposure duration, however, for all w/b ratios i.e. 0.45, 0.50 and 0.55, it decreased mostly with increase in exposure duration.

4.5. Summary

The results obtained from the study showed that the concrete made with OPC exhibited higher compressive strength as compared to that made with OPC + 20% FA followed by PPC at all w/b ratios and curing ages. However, the rate of increase in compressive strength with curing age was higher in PPC and OPC + 20% FA concrete as compared to OPC concrete. From the obtained free chloride content profile, it is observed that the free chloride content decreased with increase in depth from the exposure surface of concrete for all binders, w/b ratios, exposure solutions, and exposure periods except for some cases in which the free chloride content in the depth interval of 0-5 mm was less than that in the depth interval of 5-10 mm from the exposure surface. The lower free chloride content in the depth interval of 0-5 mm from the exposure surface of concrete may be ascribed to the presence of convection zone, which was dependent on exposure duration, binder type, w/b ratio, and exposure solution. The free chloride content was less in the concrete exposed to composite chloride-sulfate solutions as compared to chloride solutions, and the free chloride content decreased with increase in concentration of $MgSO_4$ or Na_2SO_4 in the exposure solution. Between composite chloride-sulfate solutions, the free chloride content was lower in the concrete exposed to composite solutions of NaCl + Na_2SO_4 as compared to composite solutions of NaCl + $MgSO_4$ at all depth intervals. Among binder type, the free chloride content was higher in PPC concrete at lower depth intervals i.e. near the exposure surface as compared to OPC + 20% FA followed by OPC concrete whereas at higher depth intervals, the free chloride content was higher in OPC concrete as compared to OPC + 20%

FA followed by PPC concrete for all w/b ratios, exposure solutions and exposure periods. Further, the resistance against chloride penetration was higher in PPC concrete as compared to that in OPC + 20% FA followed by OPC concrete. While evaluating the effect of w/b ratio, it is observed that the free chloride content was higher at lower w/b ratio as compared to higher w/b ratio at lower depth intervals whereas the opposite variation was observed at higher depth intervals i.e. the free chloride content was higher at higher w/b ratio as compared to lower w/b ratio for all binders, exposure solutions, and exposure periods.

The estimated apparent chloride diffusion coefficient of concrete increased with increase in concentration of NaCl in the chloride and composite chloride-sulfate solutions for OPC, OPC + 20% FA and PPC concrete, however in some cases, the apparent chloride diffusion coefficient was higher in the concrete exposed to lower concentration of NaCl in the exposure solutions as compared to higher concentration of NaCl in the exposure solutions for PPC and OPC + 20% FA concrete. The estimated apparent chloride diffusion coefficient was mostly lower in the concrete exposed to composite chloride-sulfate solutions as compared to chloride solution. Further, the chloride diffusion coefficient decreased with an increase in concentration of sulfate ions in the exposure solution for both cations i.e. Mg^{2+} and Na^{+} in case of exposure to composite chloride-sulfate solutions. Between composite chloride-sulfate solutions, the concrete exposed to composite solutions of NaCl + $MgSO_4$ mostly exhibited higher apparent chloride diffusion coefficient as compared to composite solutions of NaCl + Na_2SO_4. Among binder type, the apparent chloride diffusion coefficient was higher in OPC concrete as compared to OPC + 20% FA followed by PPC concrete irrespective of w/b ratio, exposure solution, and exposure duration. Further, the concrete made with lower w/b ratio exhibited lower apparent chloride diffusion coefficient as compared to higher w/b ratio. In addition, the estimated apparent chloride diffusion coefficient mostly decreased with increase in exposure period in the concrete exposed to composite chloride-sulfate solutions. In case of exposure to chloride solutions, the variation in apparent chloride diffusion coefficient with exposure period was mostly unsystematic till 21 months but in majority of the cases, it decreased at the exposure period of 27 months.

From the obtained results of chloride binding, it was observed that the concrete exposed to composite chloride-sulfate (both cations i.e. Mg^{2+} and Na^{+}) solutions exhibited higher chloride binding as compared to chloride solutions during the early exposure periods (i.e. till 15 months of exposure) whereas the opposite variation was observed during the later exposure periods (after 15 months of exposure) i.e. the chloride binding was higher in the

concrete exposed to chloride solutions as compared to composite chloride-sulfate solutions. Further, the concrete exposed to composite solution of NaCl + Na_2SO_4 exhibited higher chloride binding as compared to composite solution of NaCl + $MgSO_4$. Among binder type, OPC concrete exhibited higher chloride binding as compared to OPC + 20% FA followed by PPC concrete at all exposure durations. Further, the variation in chloride binding with w/b ratio was mostly unsystematic in the concrete.

CHAPTER 5

MICROSTRUCTURE ANALYSIS OF CONCRETE EXPOSED TO CHLORIDE AND COMPOSITE CHLORIDE-SULFATE SOLUTIONS

5.1. General

In this chapter, the results of microstructure study on concrete made with different types of binder and w/b ratio, and exposed to chloride and composite chloride-sulfate solutions for different exposure periods are presented. As stated in Chapter 3, the microstructure of concrete exposed to chloride and composite chloride-sulfate solutions was analyzed by carrying out X-ray diffraction (XRD) analysis, field emission scanning electron microscope (FESEM) analysis and thermo-gravimetry analysis (TGA) on the concrete powder samples collected at different depth intervals from the prismatic specimens at the end of different exposure periods. From the obtained results of microstructure study, the effect of depth from the exposure surface of concrete, exposure solution, binder type, and w/b ratio at different exposure periods on the variations in microstructure of concrete are analyzed and discussed.

5.2. XRD and FESEM analyses

From the obtained results of XRD analysis, the phase composition of concrete was analyzed using PDF2 reference library (ICDD) and PANalytical X'pert HighScore Plus software (stated in Chapter 3). The peaks of different compounds formed in concrete were identified in the obtained XRD patterns. The peaks of ettringite (E), and calcium chloroaluminate (CCA) were found at 8.8º 2θ, and 15.75º 2θ; and 11.2º 2θ and 23.2º 2θ respectively. Further, the peaks of calcium hydroxide (CH), and gypsum (G) were identified at 18.1º 2θ, 34.1º 2θ, and 47.2º 2θ; and at 32.1º 2θ and 50.3º 2θ respectively. Similarly, the peaks of quartz (Q), and calcite (CC) were found at 20.78º 2θ, 26.65º 2θ, 39.45º 2θ, 42.45º 2θ, 50.2º 2θ and 54.85º 2θ; and 29.45º 2θ respectively. The peaks of feldspar (F) were found at 27.5º 2θ. Similarly, the peaks of thaumasite (T) were identified at 9.21º 2θ and 15.75º 2θ. In addition, the peaks of magnesium hydroxide (MH) were found at 18.85º 2θ in the concrete exposed to composite solution of NaCl plus $MgSO_4$. As stated in Chapter 3, the weight percentage (wt. %) of different compounds formed in concrete were estimated semi-quantitatively using the reference-intensity ratio (RIR) matrix-flushing method. The details about the compounds such as ettringite, calcium chloroaluminate (Friedel's salt), calcium hydroxide (portlandite), quartz, gypsum, and calcite, obtained from the ICDD reference library are

presented in Table 5.1. The sum of wt. % of the compounds calculated using RIR matrix-flushing method is equal to 100%.

Table 5.1 Details of compounds from PDF2 reference library of ICDD

Ref. code	Compound	Chemical formula	RIR
01-072-0646	Ettringite	$Ca_6(Al(OH)_6)_2(SO_4)_3(H_2O)_{26}$	1.61
01-078-1219	Calcium aluminum chloride hydroxide hydrate (Friedel's salt)	$Ca_2Al(OH)_6Cl(H_2O)_2$	1.36
00-004-0733	Portlandite	$Ca(OH)_2$	1.4
01-079-1910	Quartz	SiO_2	3.07
00-021-0816	Gypsum	$CaSO_4.2H_2O$	1.7
00-005-0586	Calcite	$CaCO_3$	2

The effects of depth from the surface of concrete, exposure solution, binder type, and w/b ratio on the variations in microstructure of concrete exposed to chloride and composite chloride-sulfate solutions of varying concentrations are presented below.

5.2.1. Effect of depth from exposure surface of concrete on variations in microstructure

To analyze the changes in microstructure of concrete with increase in depth from the exposure surface of prismatic specimens exposed to chloride and composite chloride-sulfate solutions, typical plots of the obtained XRD patterns and wt. % of the compounds estimated using RIR method for different depth intervals are shown in Figure 5.1 to 5.5. The remaining figures of XRD patterns and wt. % of the compounds are presented in Appendix B1.

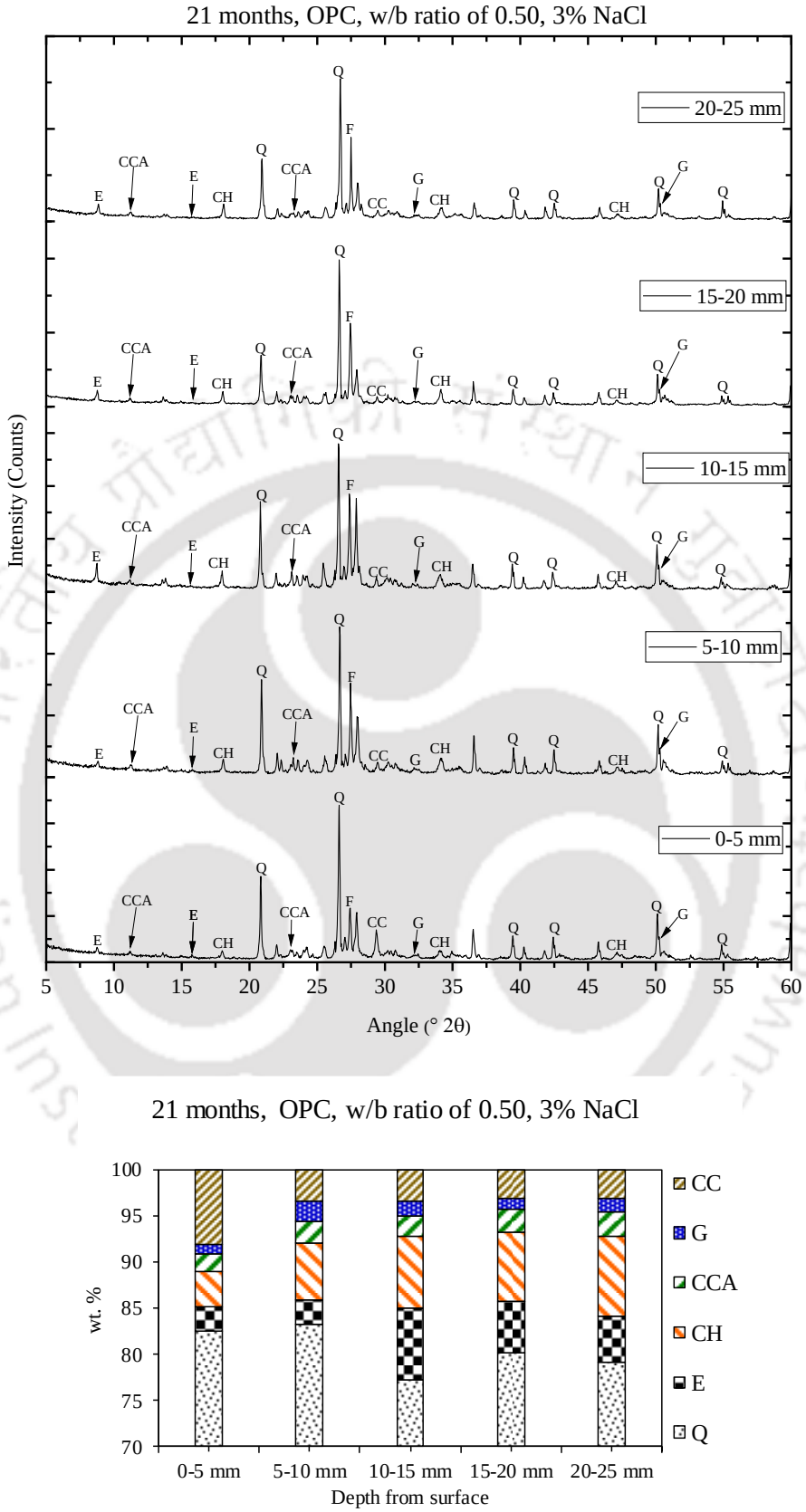

Figure 5.1 XRD patterns and wt. % of compounds of concrete at depth intervals of 0-5 mm, 5-10 mm, 10-15 mm, 15-20 mm and 20-25 mm from the exposure surface of OPC concrete at w/b ratio of 0.50 and exposed to 3% NaCl solution for 21 months

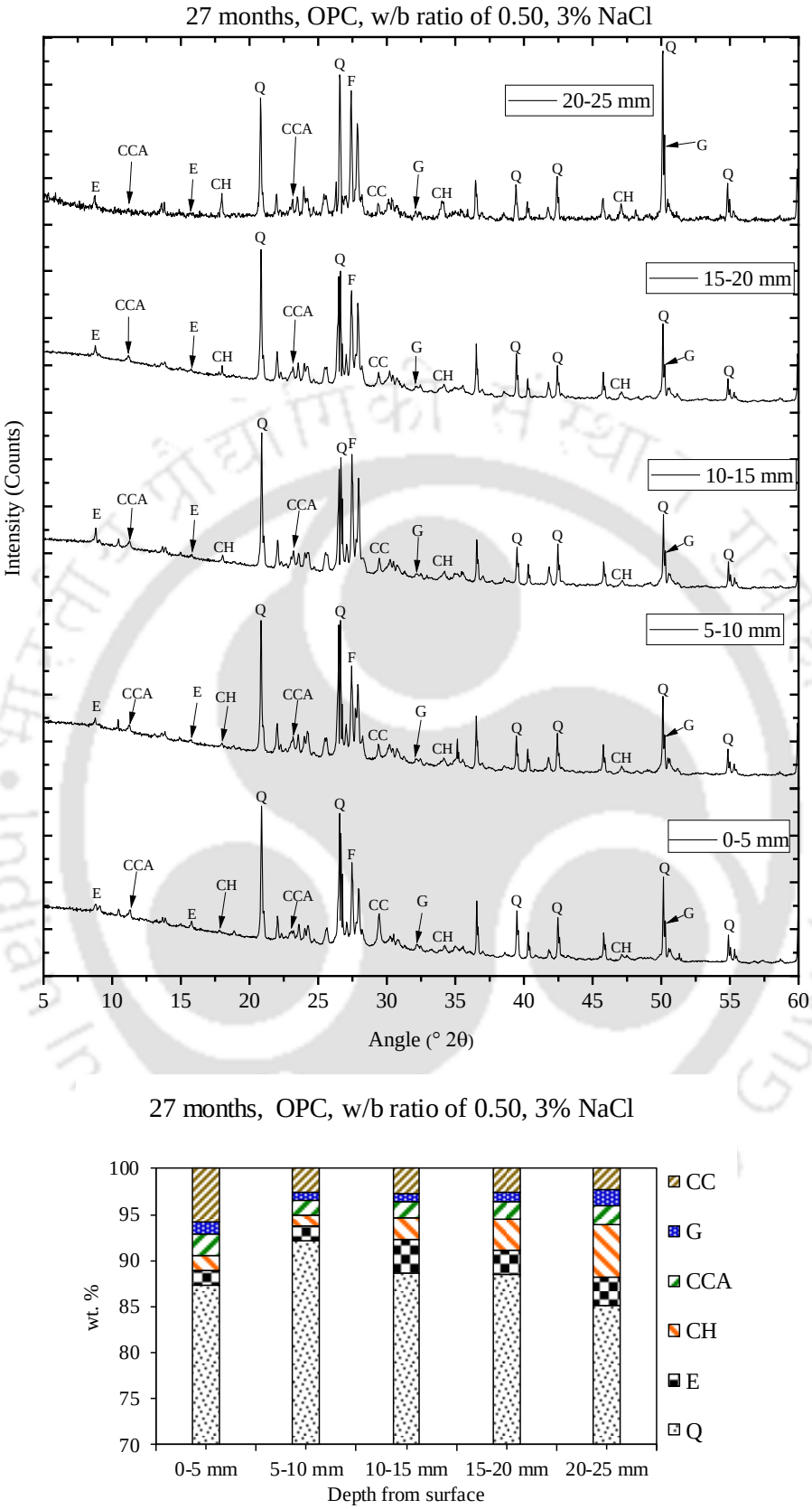

Figure 5.2 XRD patterns and wt. % of compounds of concrete at depth intervals of 0-5 mm, 5-10 mm, 10-15 mm, 15-20 mm and 20-25 mm from the exposure surface of OPC concrete at w/b ratio of 0.50 and exposed to 3% NaCl solution for 27 months

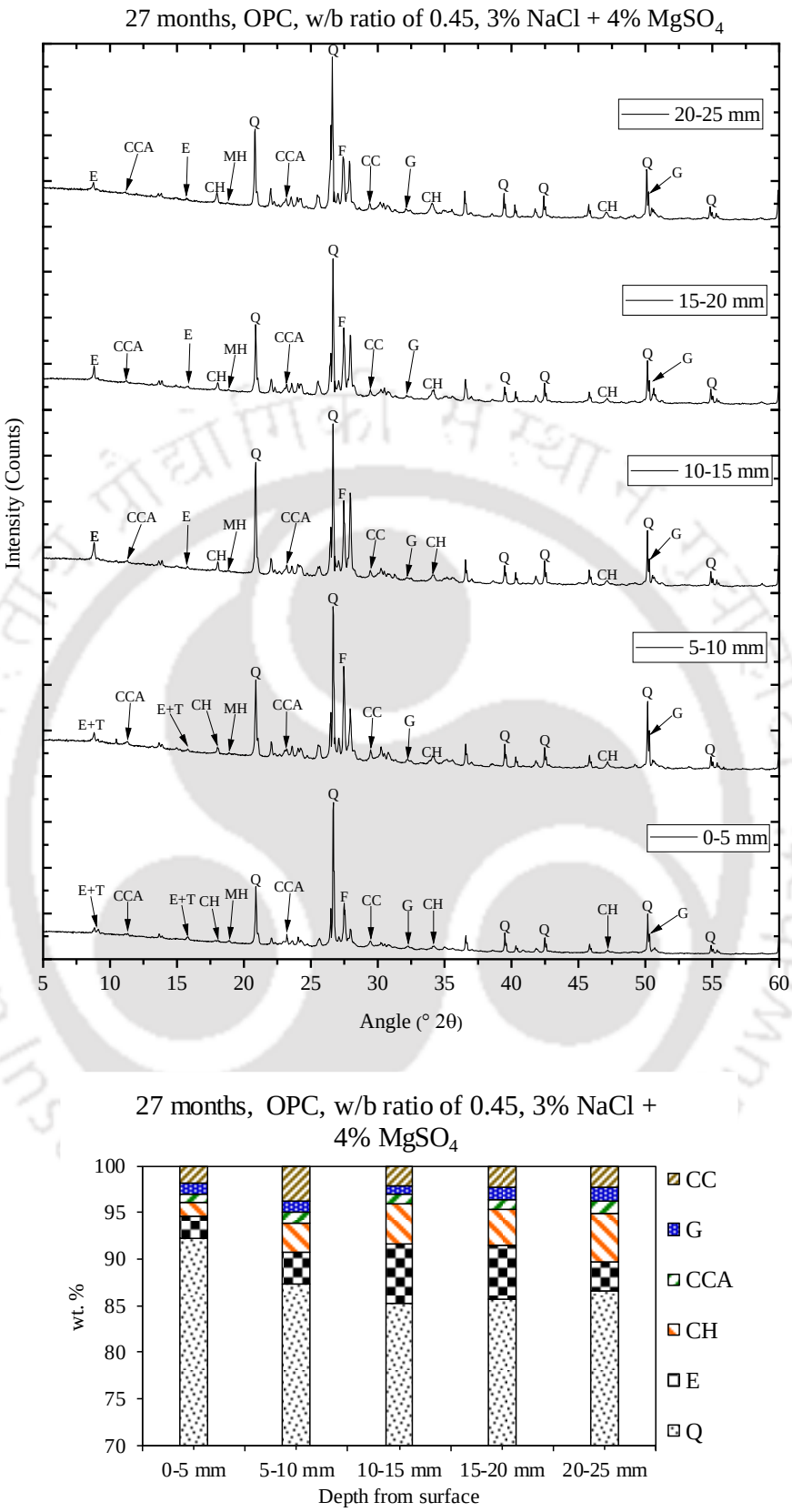

Figure 5.3 XRD patterns and wt. % of compounds of concrete at depth intervals of 0-5 mm, 5-10 mm, 10-15 mm, 15-20 mm and 20-25 mm from the exposure surface of OPC + 20% FA concrete at w/b ratio of 0.45 and exposed to 3% NaCl + 4% $MgSO_4$ solution for 27 months

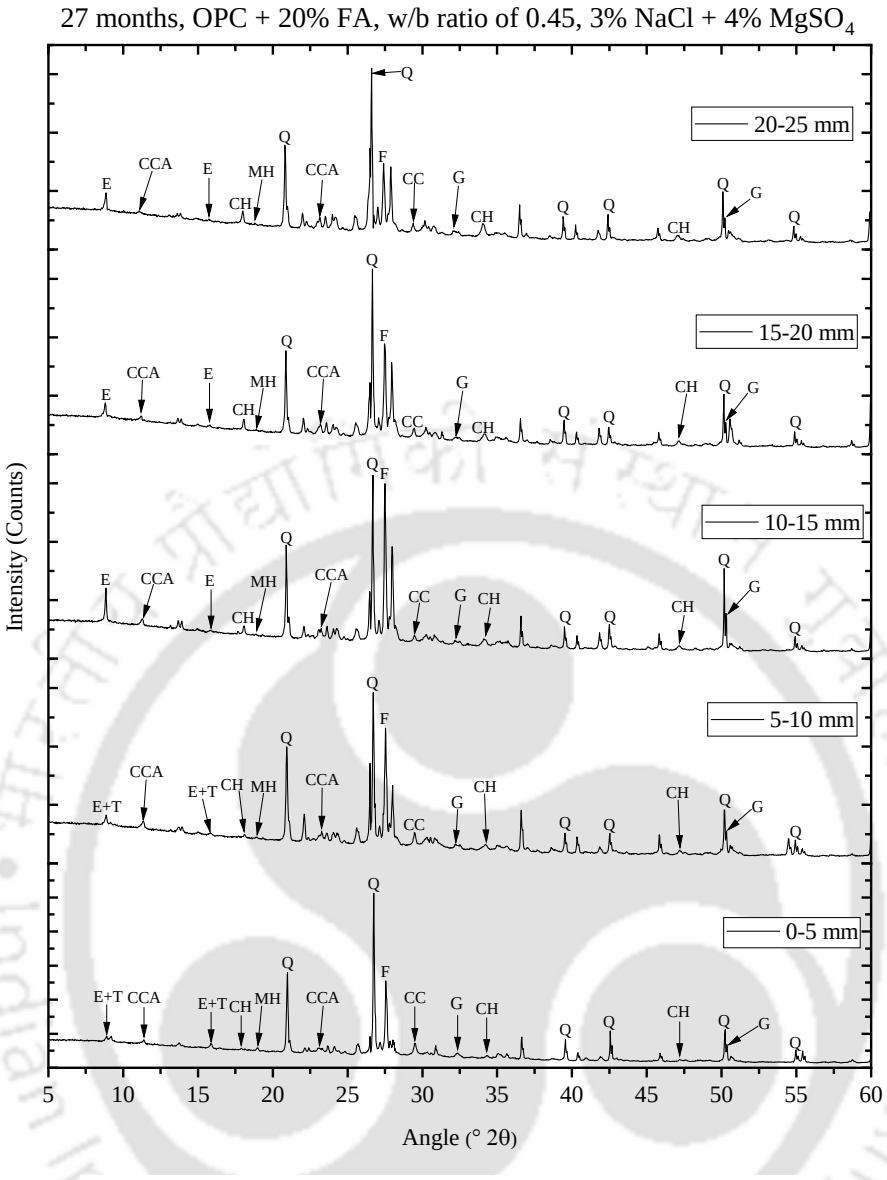

Figure 5.4 XRD patterns and wt. % of compounds of concrete at depth intervals of 0-5 mm, 5-10 mm, 10-15 mm, 15-20 mm and 20-25 mm from the exposure surface of OPC + 20% FA concrete at w/b ratio of 0.45 and exposed to 3% NaCl + 4% $MgSO_4$ solution for 27 months

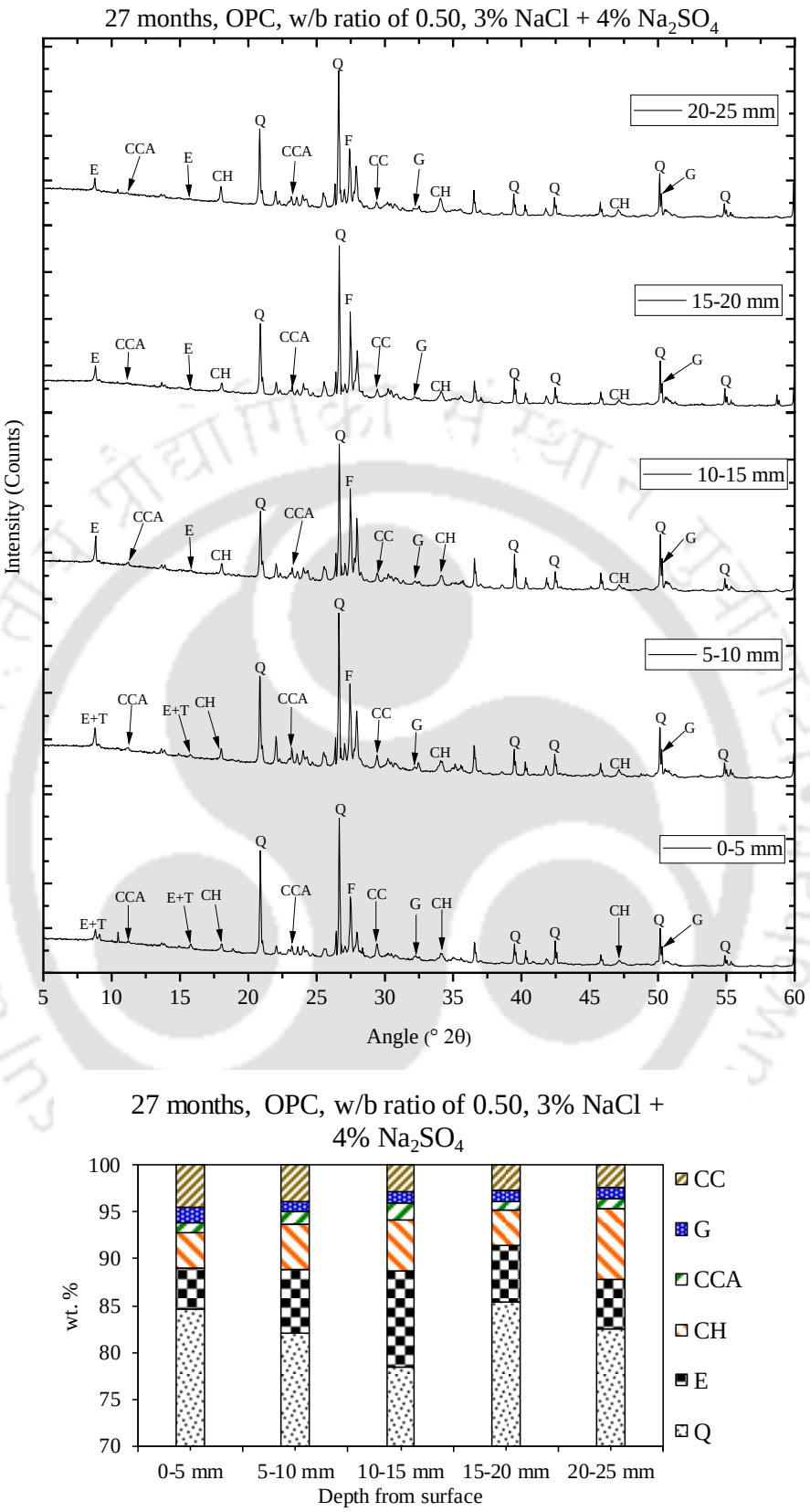

Figure 5.5 XRD patterns and wt. % of compounds of concrete at depth intervals of 0-5 mm, 5-10 mm, 10-15 mm, 15-20 mm and 20-25 mm from the exposure surface of OPC concrete at w/b ratio of 0.50 and exposed to 3% NaCl + 4% Na_2SO_4 solution for 27 months

From the XRD patterns and wt. % of the compounds shown in these figures, it is observed that the peak intensity and wt. % of calcium hydroxide (CH) mostly increased with increase in depth from the exposure surface of concrete exposed to chloride and composite chloride-sulfate solutions. This indicates the presence of more amount of calcium hydroxide at higher depth intervals as compared to that at lower depth intervals from the exposure surface. As stated earlier in Section 4.3.1.1 (Chapter 4), in some of the prismatic specimens the convection zone was observed in the depth interval of 0-5 mm, which might have affected the presence of calcium hydroxide in the depth interval of 0-5 mm. The higher amount of calcium hydroxide (portlandite) in concrete at higher depth intervals is attributed to the effect of its leaching in the presence of chloride ions [136-138] to a lower extent as compared to that at lower depth intervals. The lower extent of leaching of calcium hydroxide at higher depth intervals is ascribed to the penetration of lower amount of chloride ions to higher depths as compared to lower depths from the exposure surface of concrete. It may be noted that due to the penetration of lower amount of chloride ions to higher depth intervals in concrete, the measured free chloride content was lower at higher depth intervals as compared to that at lower depth intervals (discussed earlier in Section 4.3.1.1, Chapter 4).

The formation of calcium hydroxide (CH) in concrete is evident from the typical FESEM images shown in Figures 5.6 and 5.7, wherein the calcium hydroxide crystals were observed in the form of hexagonal shape plates [142].

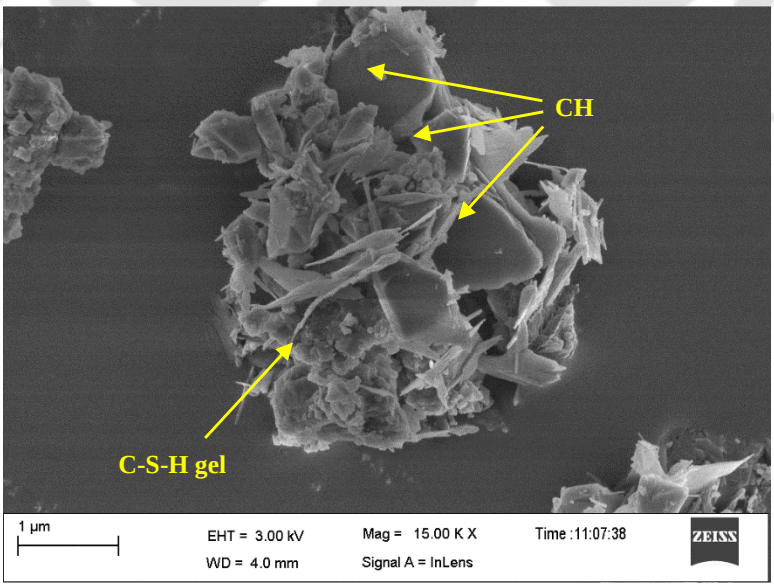

Figure 5.6 FESEM image at depth interval of 20-25 mm from exposure surface of concrete made with OPC at w/b ratio of 0.50 and exposed to 3% NaCl + 4% $MgSO_4$ solution for 27 months

From Figure 5.1 to 5.5 and figures shown in Appendix B1, it is observed that there is no systematic variation in peak intensity and wt. % of ettringite (E) with increase in depth from exposure surface of concrete. From these figures, it is observed that the peak intensity and wt. % of ettringite (E) were mostly higher in the depth interval of 10-15 mm followed by depth intervals of 15-20 mm and 5-10 mm as compared to other depth intervals for all binders, exposure solutions and exposure periods. In other words, the peak intensity and wt. % of ettringite (E) mostly increased with depth till the depth interval of 10-15 mm from the exposure surface followed by a decrease thereafter. This indicates the formation of higher amount of ettringite in the depth interval of 10-15 mm. The primary ettringite is formed in concrete due to reaction of gypsum with hydrated C_3A. Further, the secondary ettringite is formed as a result of reaction of sulfate ions with hydrated C_3A, which is the case for exposure of concrete to composite chloride-sulfate solutions. The formation of ettringite in concrete is substantiated from the typical FESEM images shown in Figure 5.7 wherein the presence of ettringite was observed in the form of needle-shape crystals [143]. The formation of higher amount of ettringite in the depth interval of 10-15 mm may be attributed to the dominant effect of reaction of gypsum with hydrated C_3A to a greater extent in case of exposure to chloride solutions, and due to dominant effect of reaction of sulfate ions with hydrated C_3A to a greater extent in case of exposure to composite chloride-sulfate solutions.

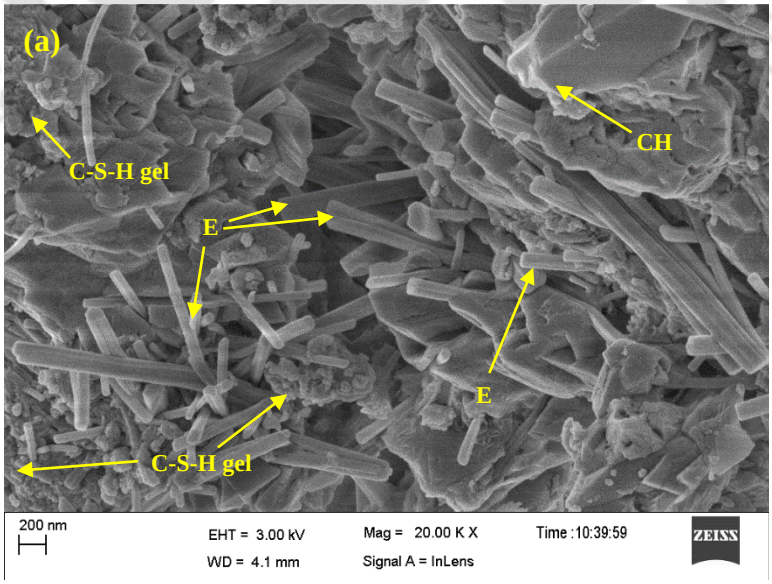

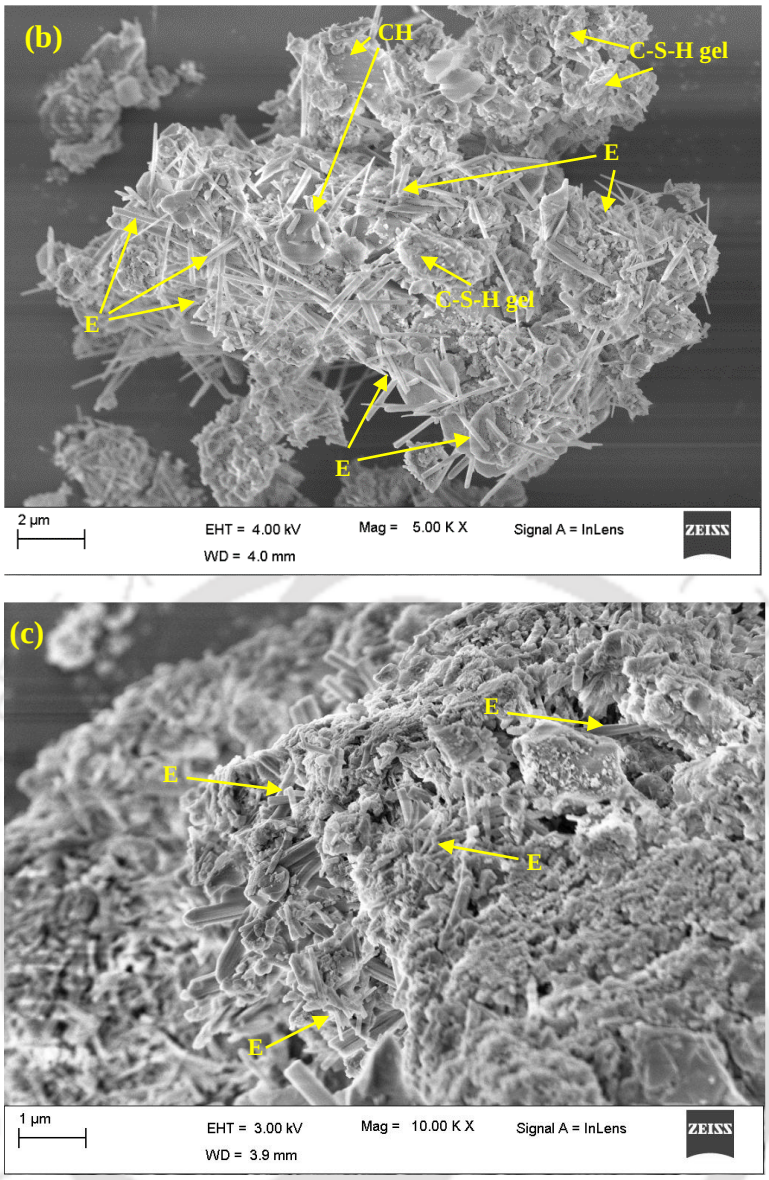

Figure 5.7 FESEM images at depth interval of 20-25 mm from exposure surface of concrete made with w/b ratio of 0.50: (a) OPC concrete exposed to 3% NaCl + 4% Na_2SO_4 solution, (b) OPC + 20% FA concrete exposed to 3% NaCl + 4% Na_2SO_4 solution, and (c) PPC concrete exposed to 3% NaCl + 4% Na_2SO_4 solution, for 27 months

The peak intensity and wt. % of ettringite (E) were mostly lower in the depth interval of 0-5 mm as compared to other depth intervals. The lower amount of ettringite in the depth of interval of 0-5 mm as indicated by the lower peak intensity in the XRD patterns may possibly be attributed to its formation in lower amount, however, as reported by Weerdt et al. [144], the lower peak intensity of ettringite as observed from the XRD patterns in the surface region of concrete may also be attributed to its lower degree of crystallinity in the surface region. Further, the presence of convection zone in the depth interval of 0-5 mm from the exposure surface might have also affected the presence of ettringite. As stated

earlier in Section 4.3.1.1 (Chapter 4), the convection zone was observed in the depth interval of 0-5 mm in some of the prismatic specimens. The presence of comparatively lower amount of ettringite in the depth interval of 5-10 mm as compared to that in the depth interval of 10-15 mm is ascribed to the dominant effect of solubility of ettringite in the presence of chloride ions to a greater extent as the free chloride content was higher in the depth interval of 5-10 mm as compared to that in the depth interval of 10-15 mm for both chloride as well as composite chloride-sulfate exposure solutions (discussed earlier in Section 4.3.1.1, Chapter 4). Further, comparatively lower amount of ettringite in the depth interval of 15-20 mm followed by 20-25 mm as compared to that in the depth interval of 10-15 mm may be attributed to the significant effect of reaction of gypsum, and sulfate ions with hydrated C_3A to a lower extent. The reaction of gypsum with C_3A in case of exposure to chloride solutions and that of sulfate ions with C_3A in case of exposure to composite chloride-sulfate solutions to a lower extent in the depth intervals of 15-20 mm and 20-25 mm may be attributed to the effect of simultaneous reaction of C_3A with gypsum and chloride ions in case of exposure to chloride solutions, and that of penetration of lower amount of sulfate ions to higher depth intervals as well as simultaneous reaction of C_3A with sulfate ions and chloride ions in case of exposure to composite chloride-sulfate solutions. The solubility of ettringite in the presence of chloride ions may not have significant effect on its presence at higher depth intervals because of penetration of lower amount of chloride ions to higher depth intervals. As mentioned earlier in Section 4.3.1.1 (Chapter 4), the free chloride content was lower at higher depth intervals as compared to that at lower depth intervals due to penetration of lower amount of chloride ions to higher depth intervals in concrete.

From Figure 5.1 to 5.5 and the figures shown in Appendix B1, it is observed that there is no systematic variation in peak intensity and wt. % of gypsum (G) with depth from the exposure surface of concrete for all binders, exposure solutions and exposure periods. This may be attributed to the effect of alterations in the extent of reaction of aluminate hydrates with gypsum in the concrete exposed to chloride solutions. It may be noted that when concrete is exposed to solutions containing sulfate salts, the reaction of magnesium sulfate with calcium hydroxide forms gypsum and magnesium hydroxide in concrete. Similarly, the reaction of sodium sulfate with calcium hydroxide results in the formation of gypsum and sodium hydroxide in concrete. Thus, in case of exposure to composite chloride-sulfate solutions, the unsystematic variation in the amount of gypsum with depth from the exposure surface as indicated by the XRD analysis may be ascribed to the significant effect of

variations in the extent of reaction of sulfate ions with calcium hydroxide at different depth intervals.

The peaks of thaumasite (T) were observed in the XRD patterns obtained from the concrete exposed to composite chloride-sulfate solutions and mostly found at lower depth intervals i.e. till 10 mm from the exposure surface, as observed from Figure 5.3 to 5.5 and the figures shown in Appendix B1. In case of exposure to composite chloride-sulfate solutions, the sulfate ions that penetrated into concrete react with hydrated C_3A to form ettringite. The ettringite thus formed reacts with C-S-H, and calcium carbonate in the presence of water to form thaumasite through woodfordite route [145]. As stated earlier, the peak intensity of ettringite was mostly lower at lower depth intervals in the concrete exposed to composite chloride-sulfate solutions, which may also be attributed to its consumption in the formation of thaumasite, in addition to the other reasons mentioned earlier. The formation of thaumasite in the concrete near the surface region is also attributed to the presence of calcium carbonate in higher amount in the surface region as observed from the XRD patterns shown in Figure 5.1 to 5.5 and the figures shown in Appendix B1. From these figures, it is observed that peak intensity and wt. % of calcite (CC) were higher in the depth interval of 0-5 mm from the exposure surface as compared to other depth intervals, which may be attributed to the effect of carbonation that might have taken place near the surface region of concrete during the wetting-drying process of exposure. Further, the aggregates used in the preparation of concrete mixes and the limestone used in the manufacture of Portland cement may also be the sources of calcite (calcium carbonate) in the concrete [145]. From Figure 5.1 to 5.5 and the figures shown in Appendix B1, it is observed that peak intensity and wt. % of calcite (CC) were not systematic with increase in depth interval from the surface of concrete. The presence of quartz as indicated by its peak in the XRD patterns shown in Figure 5.1 to 5.5 and the figures shown in Appendix B1 is mostly due to the presence aggregates in the concrete.

From Figure 5.1 to 5.5 and the figures shown in Appendix B1, it is observed that there is no systematic variation in peak intensity and wt. % of calcium chloroaluminate (CCA) with depth from the surface of concrete for all binders, exposure solutions and exposure periods. In addition, there was minor difference in the peak intensity and wt. % of CCA among different depth intervals. However, in majority of the cases, the peak intensity and wt. % of CCA were slightly higher at lower depth intervals (i.e. till 10 mm from the exposure surface) as compared to that at higher depth intervals. This may be ascribed to the effect of reaction of chloride ions with hydrated C_3A to a greater extent due to ingress of more

amount of chloride ions at lower depth intervals, thereby forming higher amount of CCA as compared to that at higher depth intervals. As mentioned in earlier in Section 4.3.1.1 (Chapter 4), the free chloride content was higher at lower depth intervals as compared to that at higher depth intervals from exposure surface of concrete. The higher free chloride content, and also the formation of slightly higher amount of CCA at lower depth intervals from exposure surface as indicated by the XRD analysis are mainly ascribed to the penetration of more amount of chloride ions into concrete at lower depth intervals from the exposure surface. In few cases, the lower amount of calcium chloroaluminate in the depth interval of 0-5 mm as indicated by the XRD analysis as compared to higher depth intervals may be attributed to the effect of presence of convection zone in this depth interval. The formation of calcium chloroaluminate (CCA) in concrete was also confirmed from the typical FESEM images shown in Figure 5.8, wherein calcium chloroaluminate (CCA) was observed in the form of hexagonal-slice shape crystals [146, 147].

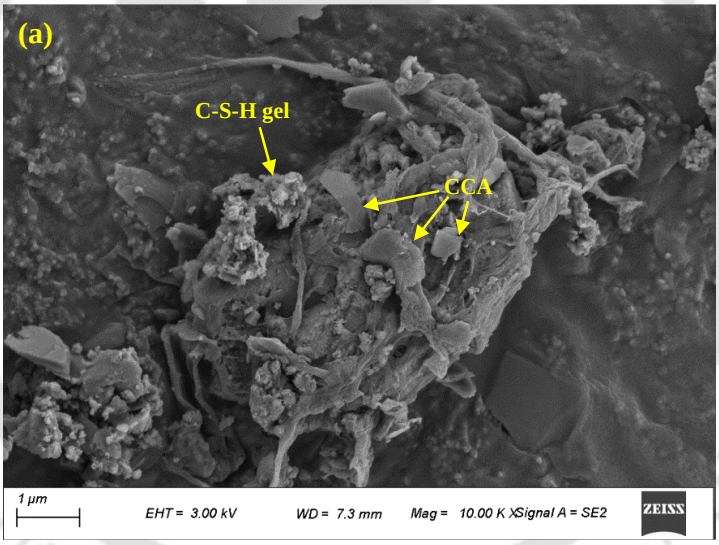

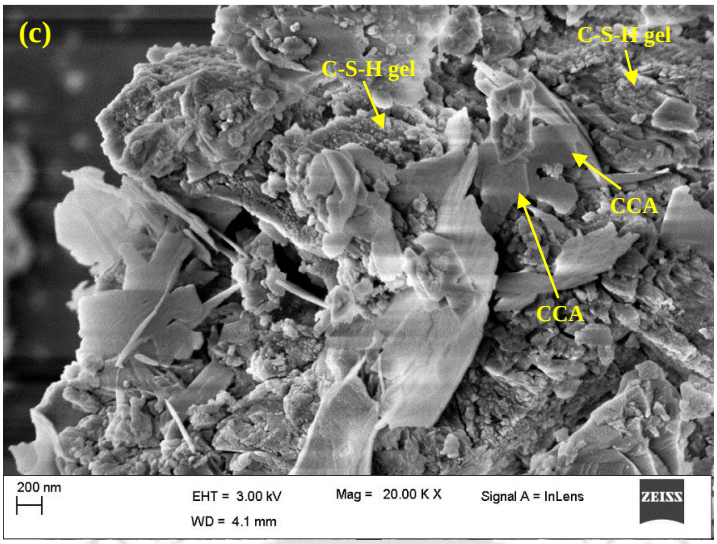

Figure 5.8 FESEM images at depth interval of 20-25 mm from exposure surface of concrete made with w/b ratio of 0.50 for: (a) OPC, (b) OPC + 20% FA, and (c) PPC concrete, exposed to 5% NaCl solution for 27 months

5.2.2. Effect of exposure solution on variations in microstructure of concrete

To study the effect of exposure solution on microstructure of concrete exposed to chloride and composite chloride-sulfate solutions, typical plots of obtained XRD patterns and wt. % of the compounds estimated using RIR method for different exposure solutions are shown in Figure 5.9 to 5.17. The remaining figures are presented in Appendix B2. The XRD patterns shown in Figure 5.9 to 5.17 and Appendix B2 correspond to the concrete powder samples obtained from the depth interval of 20-25 mm from the exposure surface of prismatic specimens. In addition, the XRD patterns shown in Figure 5.1 to 5.5 and the figures shown in Appendix B1 (discussed earlier) for different depth intervals from the exposure surface of concrete are also taken into consideration while evaluating the effect of exposure solution on microstructure of concrete exposed to chloride and composite chloride-sulfate solutions.

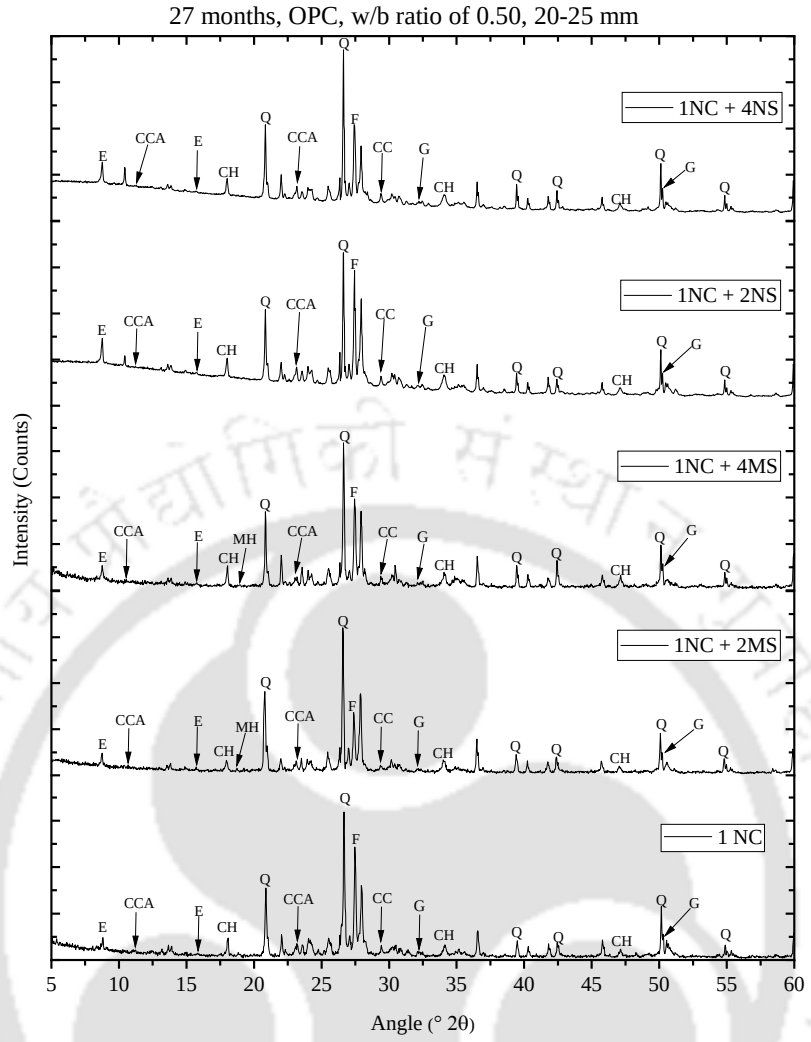

1NC: 1% NaCl, **1NC+2MS:** 1% NaCl + 2% $MgSO_4$, **1NC+4MS:** 1% NaCl + 4% $MgSO_4$
1NC+2NS: 1% NaCl + 2% Na_2SO_4, **1NC+4NS:** 1% NaCl + 4% Na_2SO_4

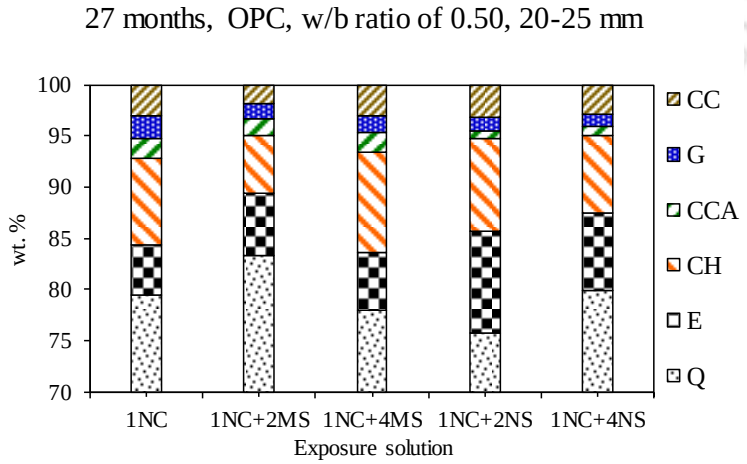

Figure 5.9 XRD patterns and wt. % of compounds of concrete at depth interval of 20-25 mm (i.e. near rebar) from exposure surface of OPC concrete at w/b ratio of 0.50 and exposed to 1% NaCl solution and corresponding composite solutions for 27 months

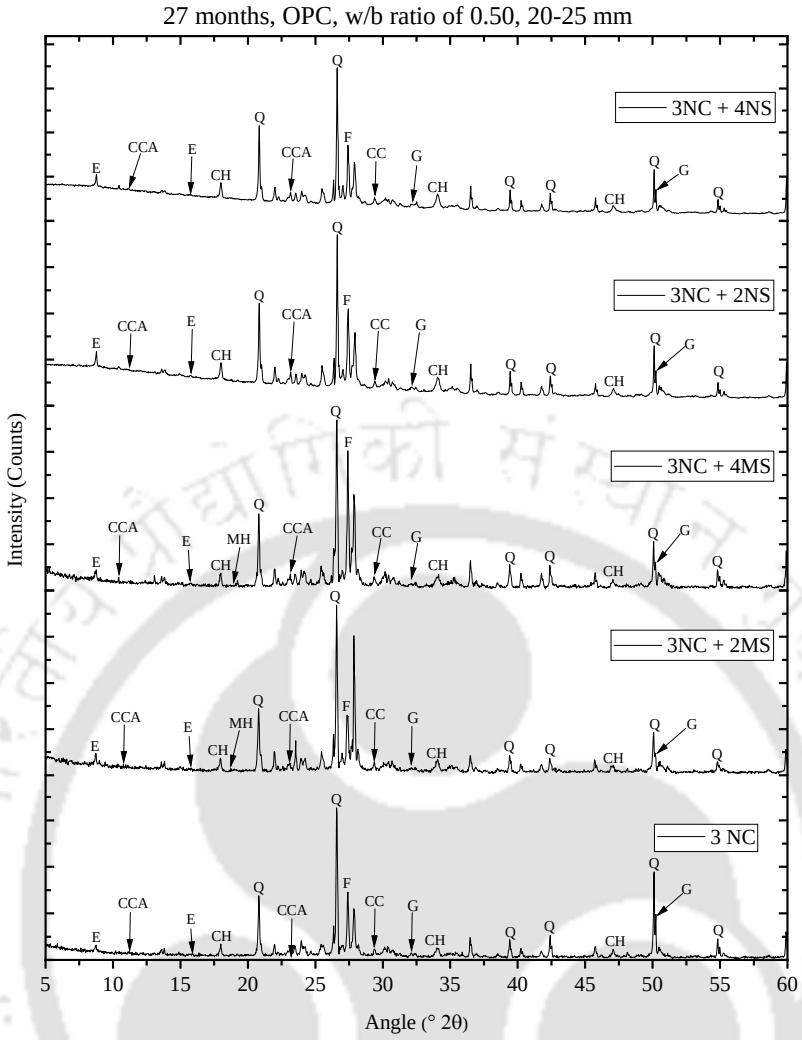

3NC: 3% NaCl, **3NC+2MS:** 3% NaCl + 2% $MgSO_4$, **3NC+4MS:** 3% NaCl + 4% $MgSO_4$
3NC+2NS: 3% NaCl + 2% Na_2SO_4, **3NC+4NS:** 3% NaCl + 4% Na_2SO_4

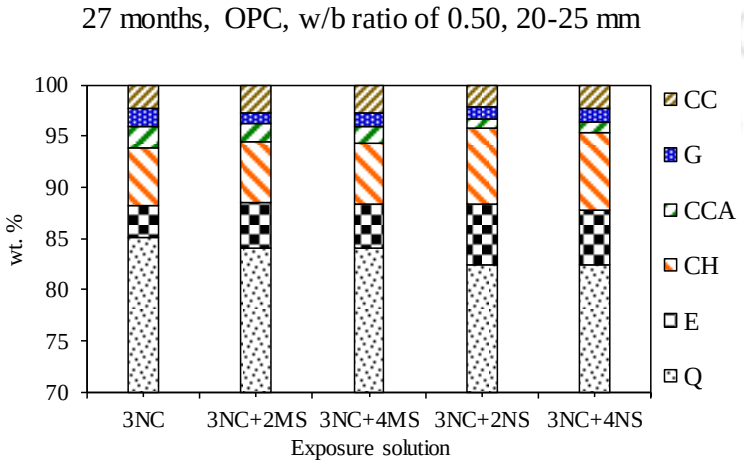

Figure 5.10 XRD patterns and wt. % of compounds of concrete at depth interval of 20-25 mm (i.e. near rebar) from exposure surface of OPC concrete at w/b ratio of 0.50 and exposed to 3% NaCl solution and corresponding composite solutions for 27 months

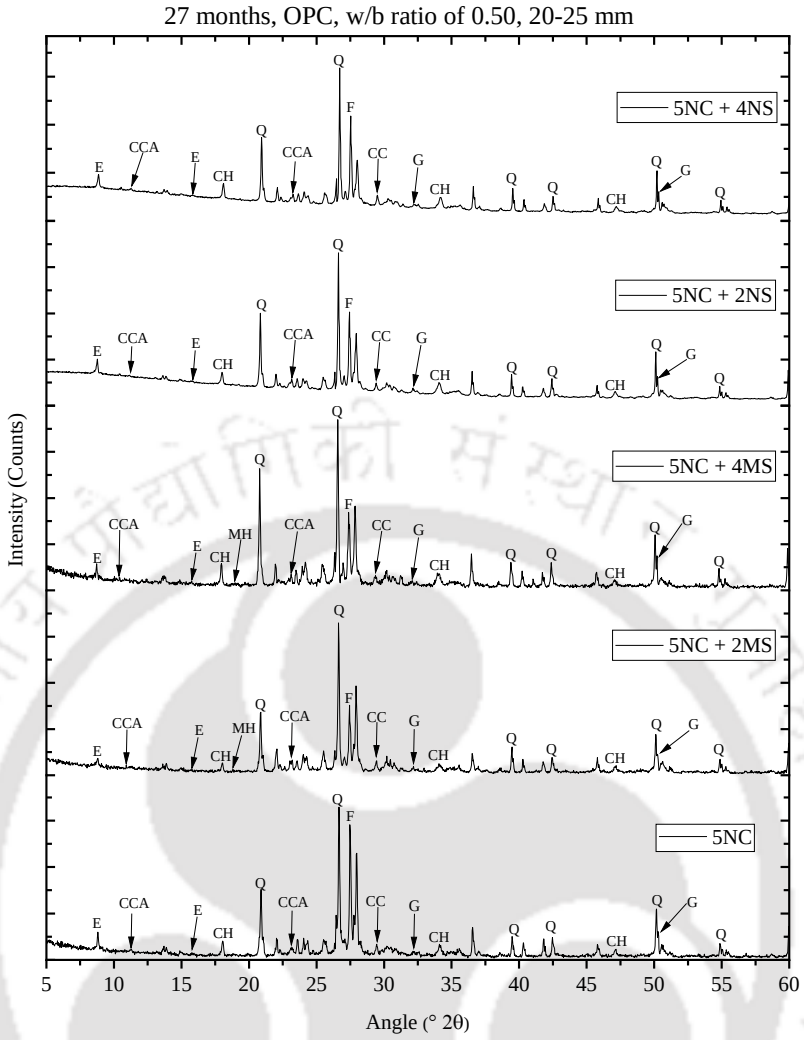

5NC: 5% NaCl, **5NC+2MS:** 5% NaCl + 2% $MgSO_4$, **5NC+4MS:** 5% NaCl + 4% $MgSO_4$
5NC+2NS: 5% NaCl + 2% Na_2SO_4, **5NC+4NS:** 5% NaCl + 4% Na_2SO_4

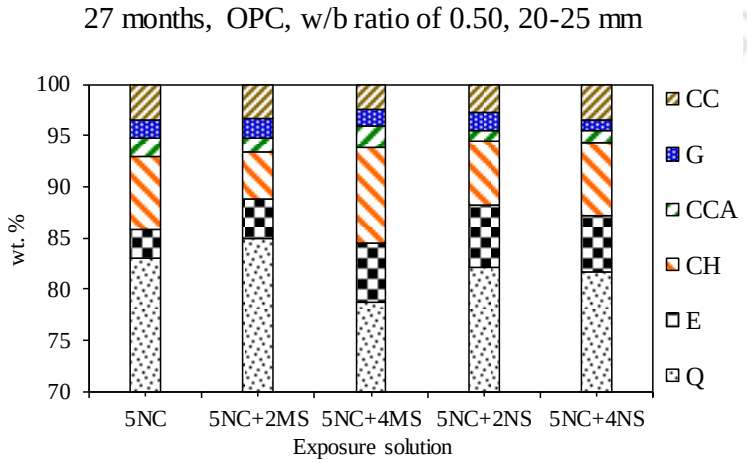

Figure 5.11 XRD patterns and wt. % of compounds of concrete at depth interval of 20-25 mm (i.e. near rebar) from exposure surface of OPC concrete at w/b ratio of 0.50 and exposed to 5% NaCl solution and corresponding composite solutions for 27 months

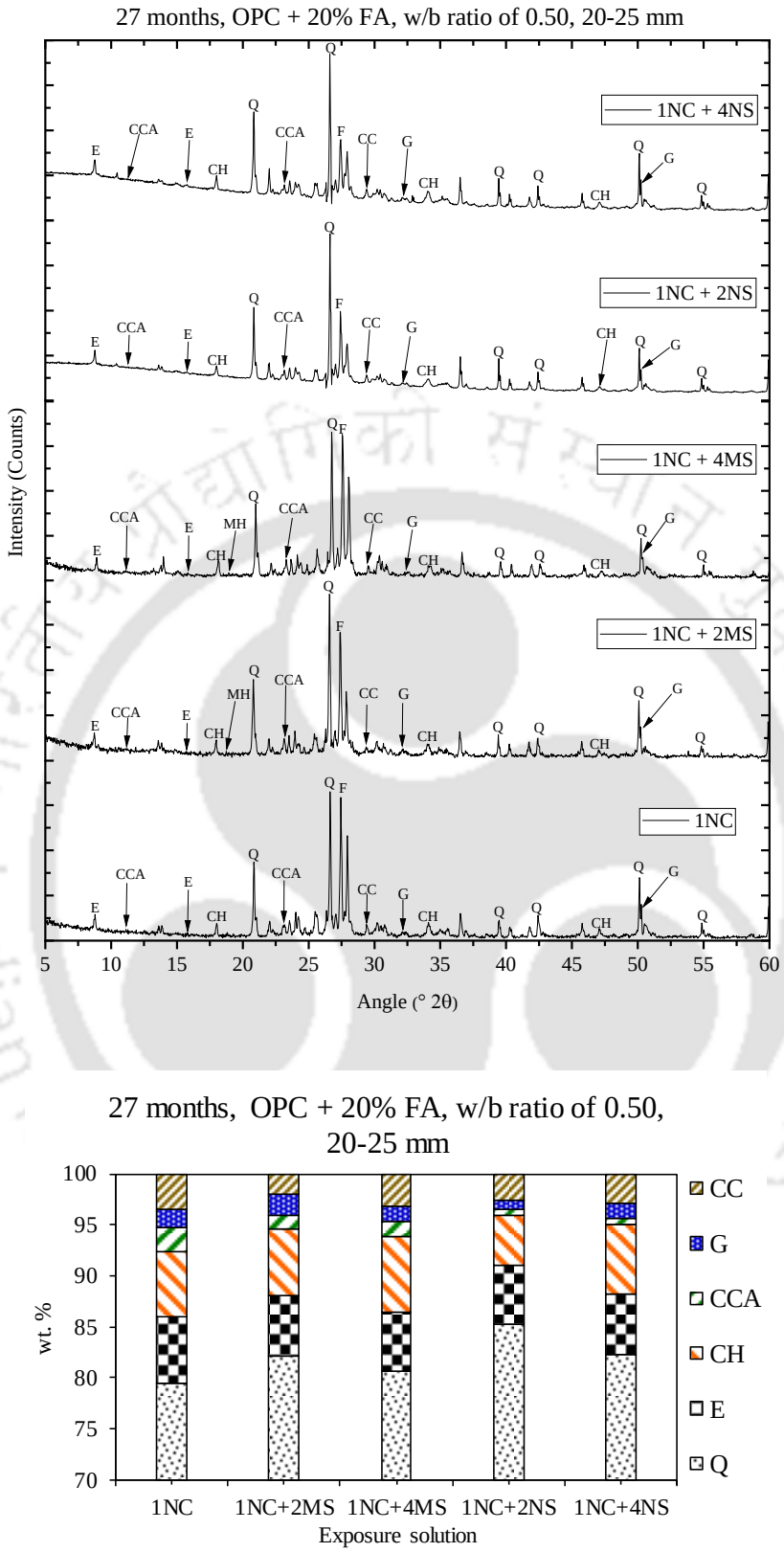

Figure 5.12 XRD patterns and wt. % of compounds of concrete at depth interval of 20-25 mm (i.e. near rebar) from exposure surface of OPC + 20% FA concrete at w/b ratio of 0.50 and exposed to 1% NaCl solution and corresponding composite solutions for 27 months

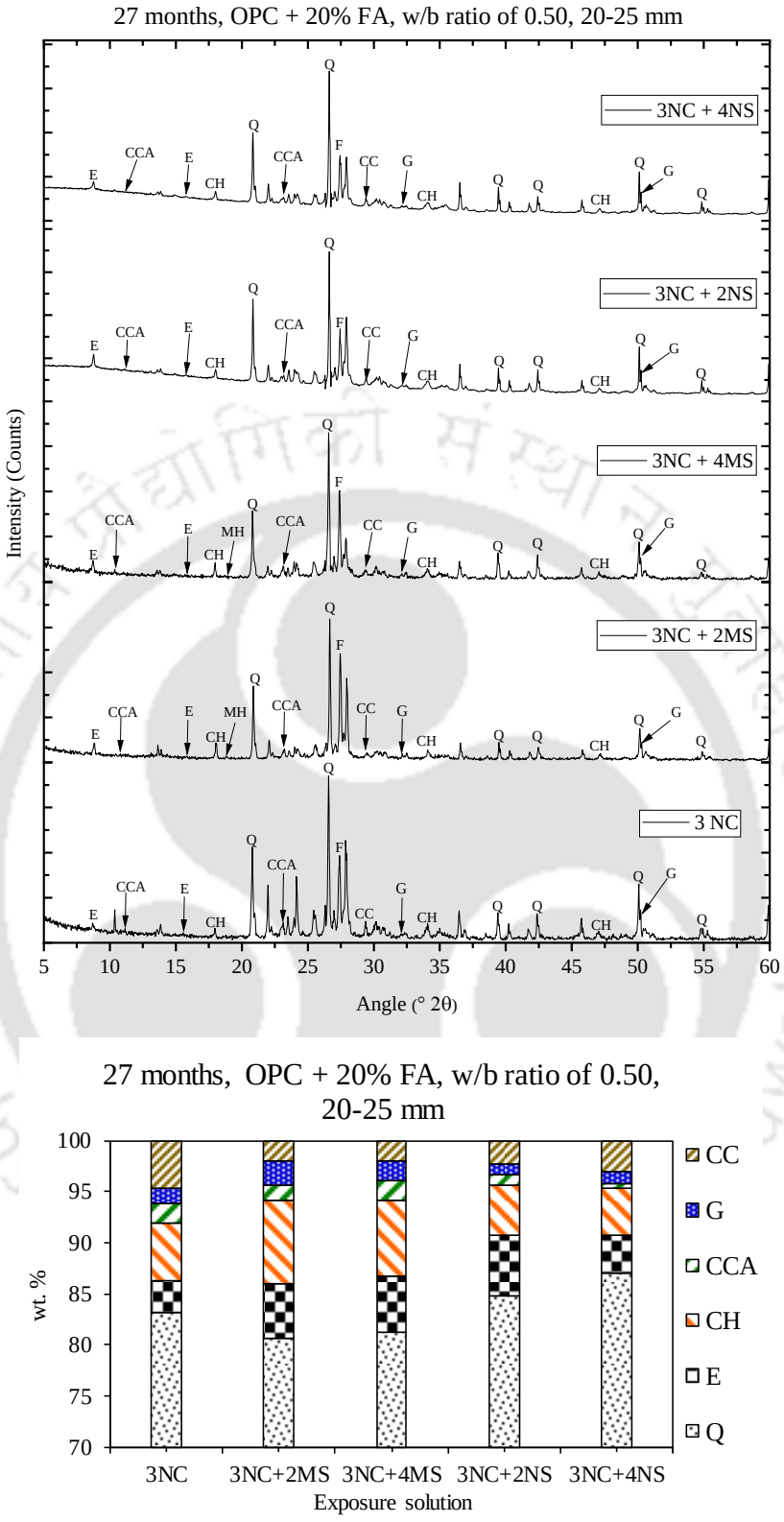

Figure 5.13 XRD patterns and wt. % of compounds of concrete at depth interval of 20-25 mm (i.e. near rebar) from exposure surface of OPC + 20% FA concrete at w/b ratio of 0.50 and exposed to 3% NaCl solution and corresponding composite solutions for 27 months

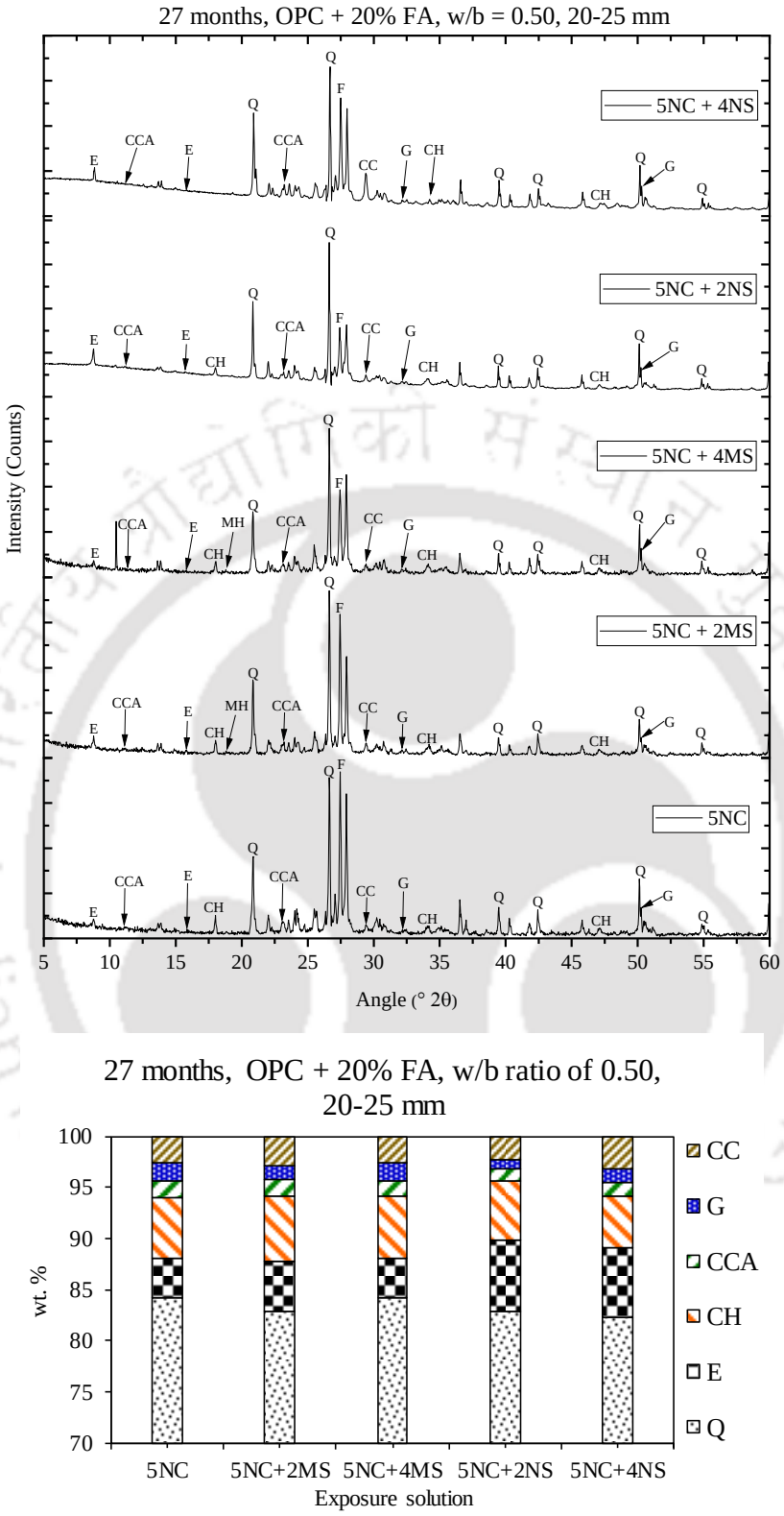

Figure 5.14 XRD patterns and wt. % of compounds of concrete at depth interval of 20-25 mm (i.e. near rebar) from exposure surface of OPC + 20% FA concrete at w/b ratio of 0.50 and exposed to 5% NaCl solution and corresponding composite solutions for 27 months

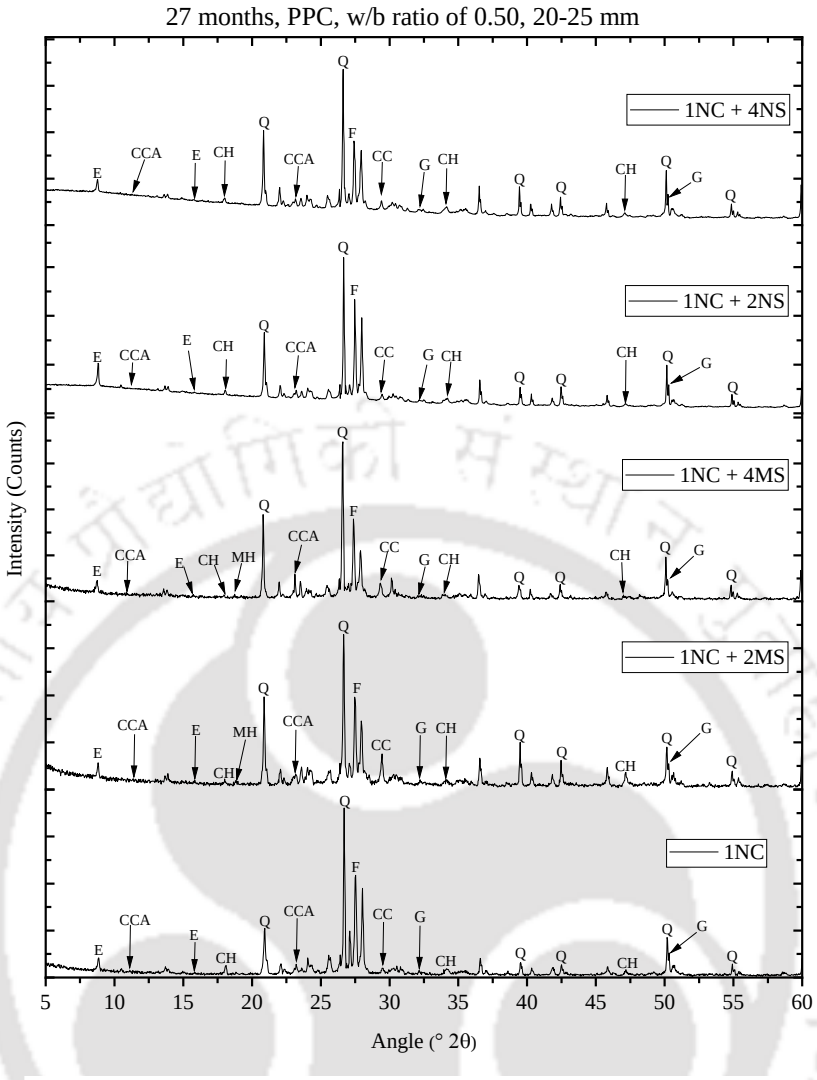

Figure 5.15 XRD patterns and wt. % of compounds of concrete at depth interval of 20-25 mm (i.e. near rebar) from exposure surface of PPC concrete at w/b ratio of 0.50 and exposed to 1% NaCl solution and corresponding composite solutions for 27 months

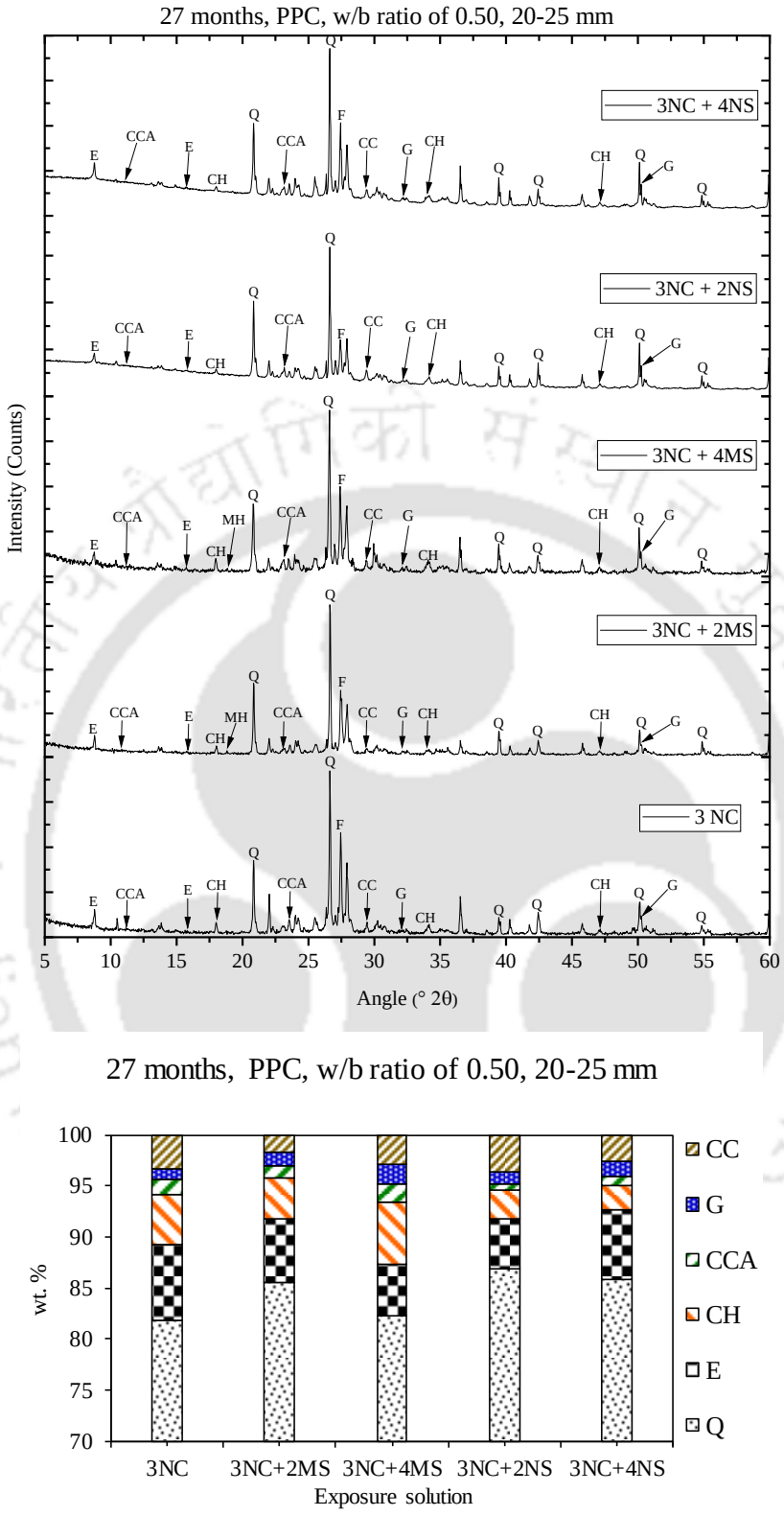

Figure 5.16 XRD patterns and wt. % of compounds of concrete at depth interval of 20-25 mm (i.e. near rebar) from exposure surface of PPC concrete at w/b ratio of 0.50 and exposed to 3% NaCl solution and corresponding composite solutions for 27 months

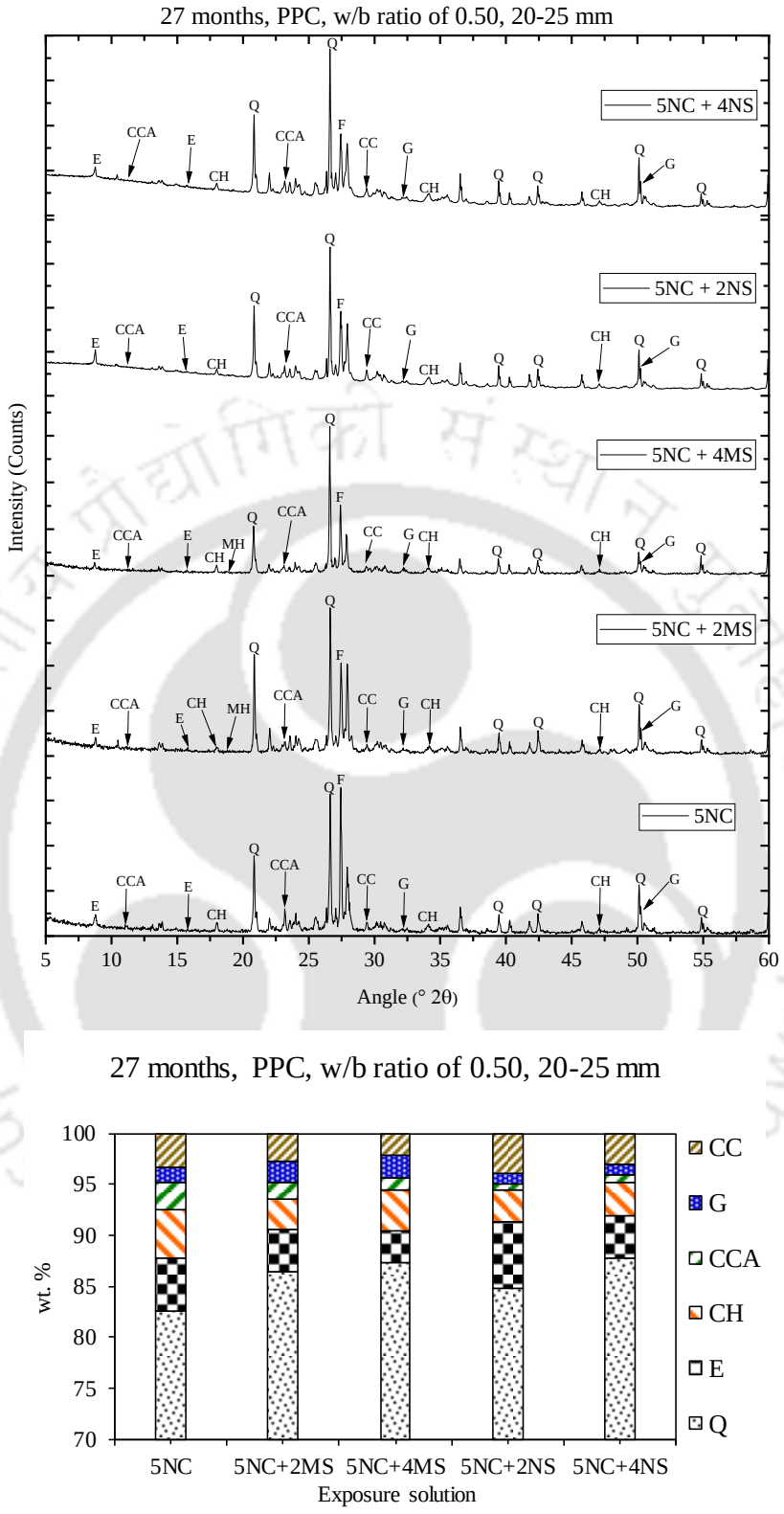

Figure 5.17 XRD patterns and wt. % of compounds of concrete at depth interval of 20-25 mm (i.e. near rebar) from exposure surface of PPC concrete at w/b ratio of 0.50 and exposed to 5% NaCl solution and corresponding composite solutions for 27 months

From Figure 5.1 to 5.5, Appendix B1, Figure 5.9 to 5.17 and Appendix B2, it is observed that the peak intensity and wt. % of ettringite were mostly higher in the concrete exposed to composite solution of NaCl with Na_2SO_4 as compared to composite solution of NaCl with $MgSO_4$ followed by NaCl solution for all concentrations of NaCl, $MgSO_4$ and Na_2SO_4. The formation of higher amount of ettringite in the concrete exposed to composite solutions of NaCl with Na_2SO_4 may be attributed to the reaction of sulfate ions with hydrated C_3A to a greater extent as compared to composite solutions of NaCl with $MgSO_4$. The lower amount of ettringite in the concrete exposed to NaCl solutions as compared to composite chloride-sulfate solutions may be due to the effect of solubility of ettringite in the presence of chloride ions to a greater extent in the concrete exposed to NaCl solutions. The formation of higher amount of ettringite in the concrete exposed to composite solution of NaCl with Na_2SO_4 as compared to composite solution of NaCl with $MgSO_4$ followed by NaCl solution is also observed from the typical FESEM images shown in Figure 5.18. Further, the peak intensity and wt. % of ettringite mostly decreased with increase in concentration of NaCl in both chloride as well as composite chloride-sulfate solutions as observed from Figure 5.1 to 5.5, Appendix B1, Figure 5.9 to 5.17 and Appendix B2. This is attributed to the solubility of ettringite to a higher extent in the presence of more amount of chloride ions in the concrete subjected to exposure solutions with higher concentration of NaCl. While analyzing the effect of sulfate ion concentration, it is inferred that the peak intensity and wt. % of ettringite mostly decreased with increase in concentration of $MgSO_4$ and Na_2SO_4 in the composite chloride-sulfate solutions as observed from Figure 5.9 to 5.17 and Appendix B2. This indicates that in case of exposure to composite chloride-sulfate solutions, the presence of higher concentration of sulfate ions has resulted in lower amount of ettringite in the concrete in the concomitant presence of chloride ions for both cations (Mg^{2+}, and Na^{+}) associated with sulfate ions as compared to lower concentration of sulfate ions. In other words, in the concomitant presence of chloride ions, the formation of ettringite was higher in the presence of lower concentration of sulfate ions. This may be attributed to the fact that in addition to the formation of ettringite due to the reaction of sulfate ions with hydrated C_3A, the dominant effect of conversion of calcium chloroaluminate to ettringite to a greater extent in the presence of lower concentration of sulfate ions has resulted in higher amount of ettringite in the concrete exposed to composite chloride-sulfate solutions with lower concentration of $MgSO_4$ or Na_2SO_4 as compared to higher concentration.

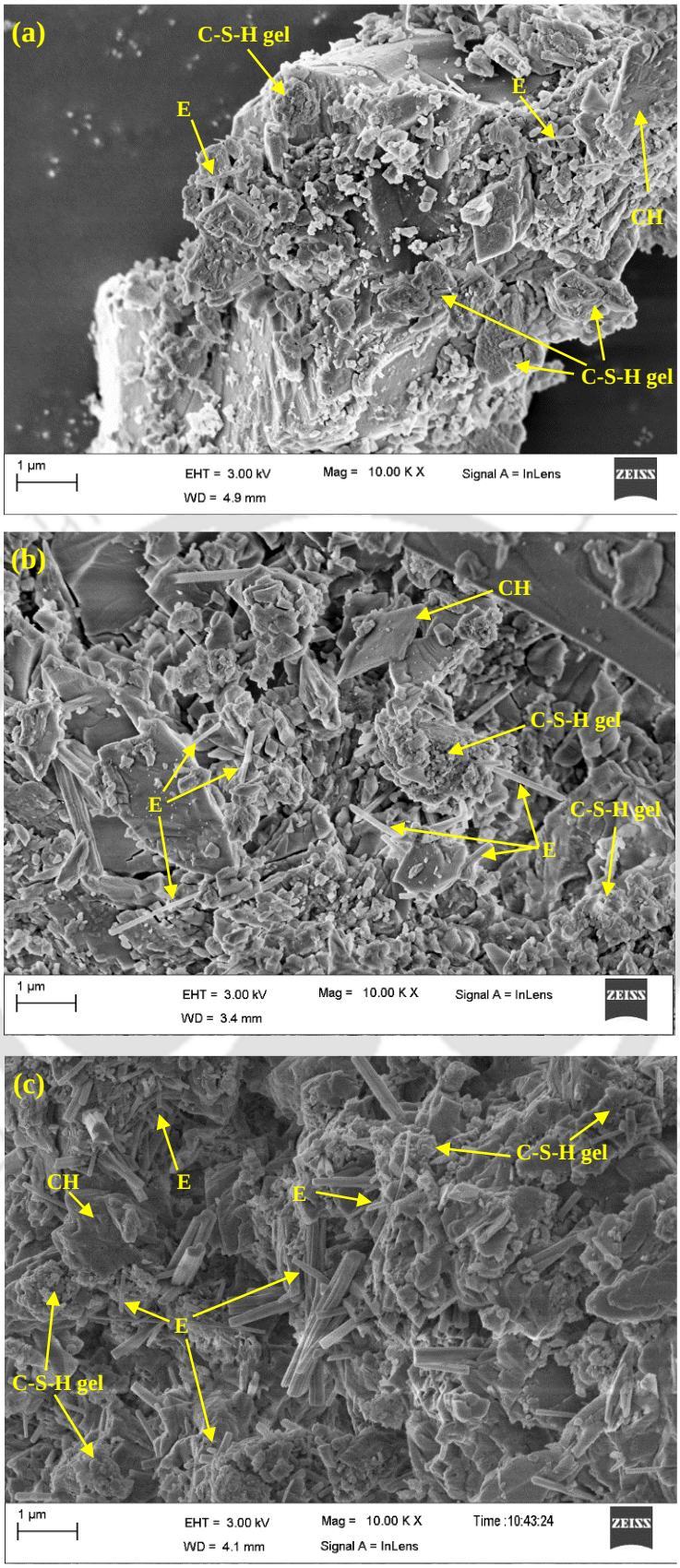

Figure 5.18 FESEM images at depth interval of 20-25 mm from exposure surface of OPC concrete made with w/b ratio of 0.50 and exposed to: (a) 3% NaCl solution, (b) 3% NaCl + 4% $MgSO_4$ solution, and (c) 3% NaCl + 4% Na_2SO_4 solution

From Figure 5.1 to 5.5, Appendix B1, Figure 5.9 to 5.17 and Appendix B2, it is observed that, the peak intensity and wt. % of calcium chloroaluminate (CCA) mostly increased with increase in concentration of NaCl in chloride as well as composite chloride-sulfate solutions for both $MgSO_4$ and Na_2SO_4. This may be attributed to the binding of chloride ions with hydrated C_3A to a greater extent due to ingress of higher amount of chloride ions into the concrete exposed to the solutions containing higher concentration of NaCl. The penetration of higher amount of chloride ions into the concrete exposed to solutions with higher concentration of NaCl is attributed to the formation of porous C-S-H as a result of leaching of calcium in the presence of chloride ions [136-138]. The formation of porous C-S-H gel in the concrete exposed to solutions with higher concentration of NaCl is observed from the FESEM images shown in Figure 5.19 [142, 148].

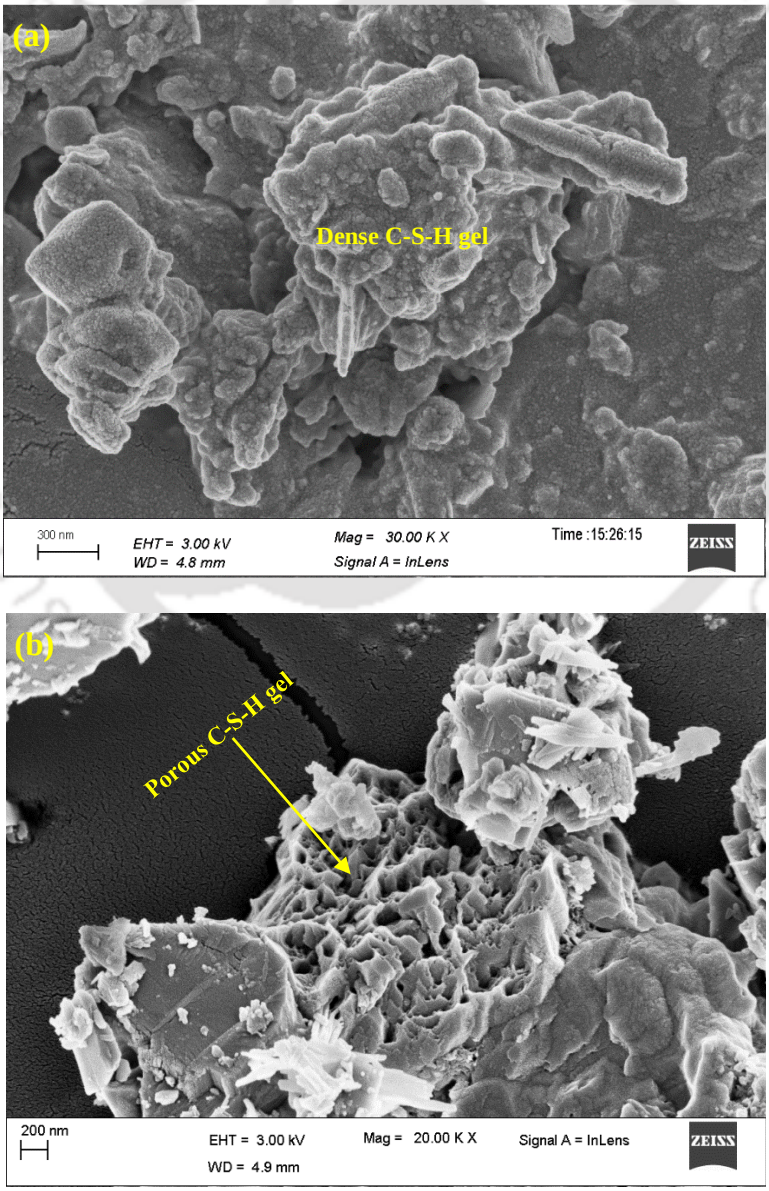

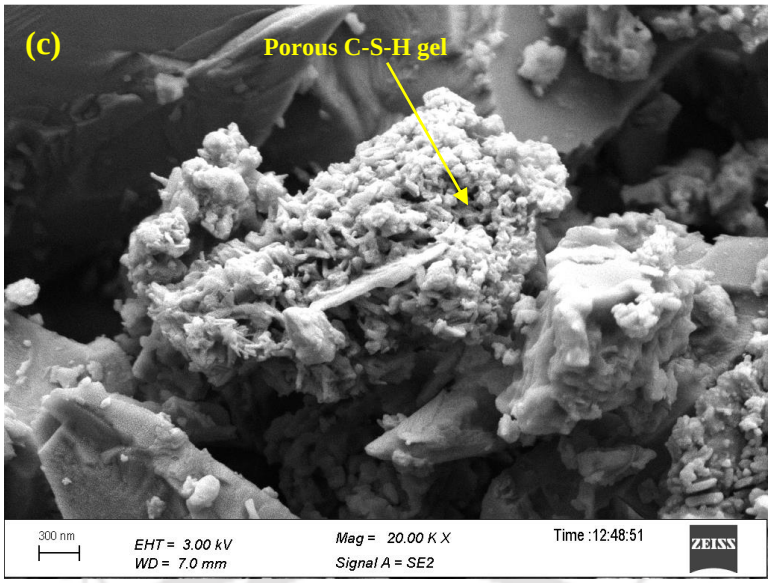

Figure 5.19 FESEM images at depth interval of 20-25 mm from exposure surface of OPC concrete made with w/b ratio of 0.50 and exposed to: (a) 1% NaCl + 4% $MgSO_4$ solution, (b) 5% NaCl solution, and (c) 5% NaCl + 4% $MgSO_4$ solution

On comparing the formation of calcium chloroaluminate (CCA) between chloride and composite chloride-sulfate solutions, it is observed that the specimens exposed to NaCl solutions mostly showed higher peak intensity and wt. % of CCA as compared to those exposed to composite solutions of NaCl with $MgSO_4$ followed by composite solutions of NaCl with Na_2SO_4 for all concentrations of NaCl, $MgSO_4$ and Na_2SO_4. The formation of higher amount of calcium chloroaluminate in the concrete exposed to NaCl solutions as indicated by XRD analysis may be attributed to the preferential reaction of chloride ions with hydrated C_3A. The formation of lower amount of calcium chloroaluminate in case of exposure to composite solutions of NaCl with $MgSO_4$, and NaCl with Na_2SO_4 may be attributed to reaction of chloride ions with hydrated C_3A to a lower extent. The reason for lower extent of reaction of chloride ions with hydrated C_3A is ascribed to the preferential reaction of sulfate ions with hydrated C_3A, thereby forming higher amount of ettringite in the concrete exposed to composite chloride-sulfate solutions. Further, the preferential reaction of sulfate ions than chloride ions with hydrated C_3A has resulted in the formation of higher amount of ettringite and lower amount of calcium chloroaluminate in the concrete exposed to composite solutions of NaCl with Na_2SO_4 as compared to composite solutions of NaCl with $MgSO_4$. As mentioned earlier, more amount of ettringite was formed in the concrete exposed to composite solutions of NaCl with Na_2SO_4, and NaCl with $MgSO_4$ as compared to NaCl solutions, and between composite chloride-sulfate solutions, higher amount of ettringite was formed in the concrete exposed to composite solutions of NaCl

with Na_2SO_4, as compared to composite solutions of NaCl with $MgSO_4$ as indicated by the peak intensity and wt. % of ettringite from the XRD results. While analyzing the effect of sulfate ion concentration, it is inferred that the peak intensity and wt. % of calcium chloroaluminate mostly increased with increase in concentration of $MgSO_4$ and Na_2SO_4 in the composite chloride-sulfate solutions as observed from Figure 5.9 to 5.17 and Appendix B2. This may be ascribed to the effect of conversion of calcium chloroaluminate to ettringite to a lower extent in the presence of higher concentration of sulfate ions thereby resulting in higher amount of calcium chloroaluminate as compared to that in case of lower concentration of sulfate ions.

The XRD patterns shown in Figure 5.3 and 5.4, Appendix B1, Figure 5.9 to 5.17 and Appendix B2 indicated the formation of magnesium hydroxide (MH) through its peaks at 18.85º 2θ in the concrete exposed to composite solution of NaCl with $MgSO_4$. Magnesium hydroxide (brucite) is formed in concrete due to reaction of magnesium sulfate with calcium hydroxide, which is liberated from the hydration reaction of cement. The formation of brucite is also evident from the FESEM images shown in Figure 5.20, as indicated by the crystals of rosette-like clusters [147]. Further, there was formation of M-S-H (magnesium silicate hydrate) gel in the concrete exposed to composite solutions of NaCl with $MgSO_4$ as evident from the FESEM images shown in Figure 5.21 [149]. Due to magnesium sulfate attack, the C-S-H gel is converted to non-cementitious M-S-H (magnesium silicate hydrate) gel in concrete.

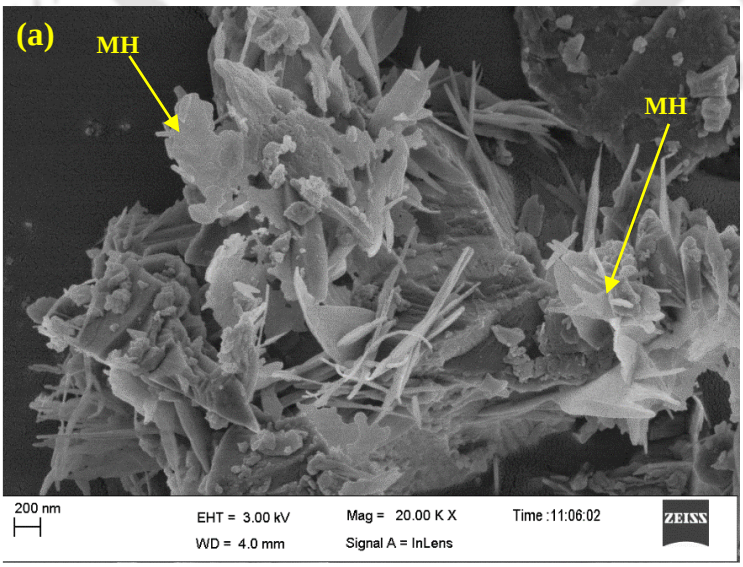

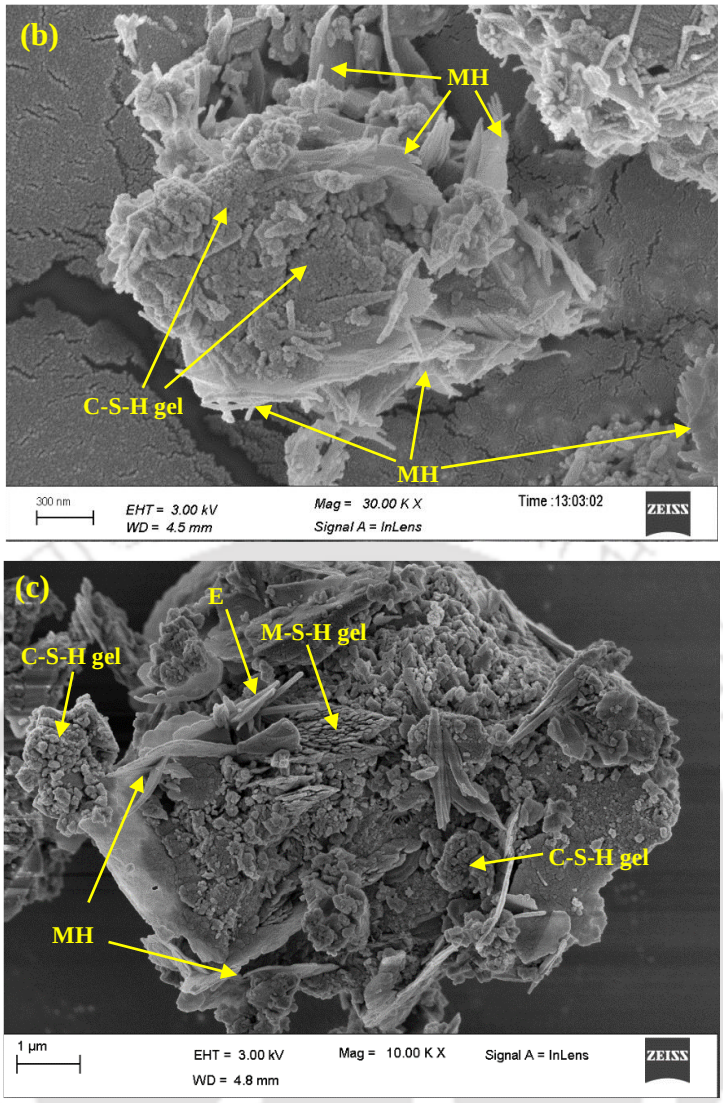

Figure 5.20 FESEM images at depth interval of 20-25 mm from exposure surface of concrete made with w/b ratio of 0.50: (a) OPC exposed to 3% NaCl + 4% $MgSO_4$ solution, (b) OPC + 20% FA exposed to 3% NaCl + 4% $MgSO_4$ solution, and (c) PPC exposed to 1% NaCl + 4% $MgSO_4$ solution for 27 months

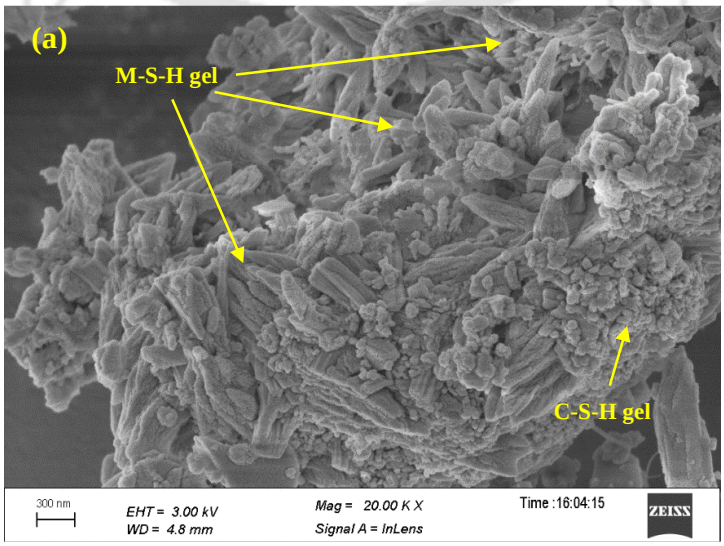

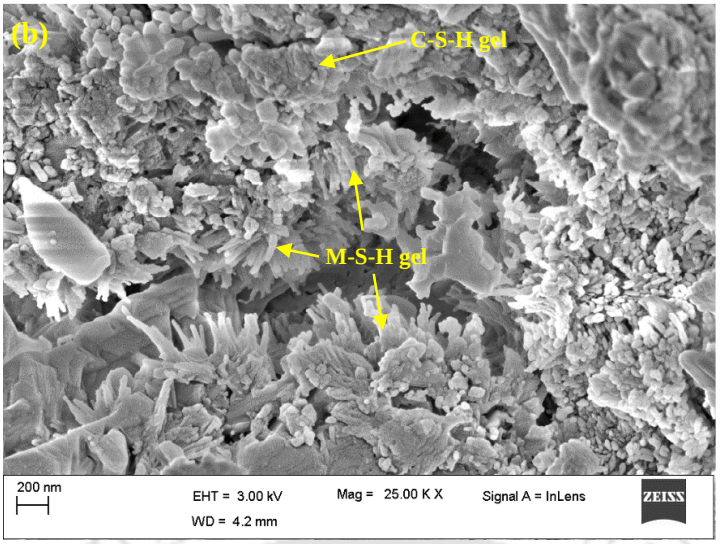

Figure 5.21 FESEM images of concrete made with OPC at w/b ratio of 0.50: (a) 5% NaCl + 4% $MgSO_4$ solution for depth interval of 0-5 mm, and (b) 3% NaCl + 4% $MgSO_4$ solution for depth interval of 10-15 mm from exposure surface of concrete for exposure period of 27 months

From Figure 5.9 to 5.17 and Appendix B2, it is observed that, the peak intensity and wt. % of calcium hydroxide (CH) mostly decreased with increase in concentration of NaCl in chloride as well as composite chloride-sulfate solutions for all binders. The lower peak intensity and wt. % of calcium hydroxide in the concrete exposed to solutions with higher concentration of NaCl may be attributed to its leaching to a greater extent due to the presence of more amount of chloride ions [136-138]. The ingress of chloride ions into concrete results in counter-diffusion of hydroxide ions in order to maintain electroneutrality of the pore solution that leads to the solubility of calcium hydroxide due to the presence of chloride [136-138]. Further, from Figure 5.1 to 5.5, Appendix B1, Figure 5.9 to 5.17 and Appendix B2, it is observed that the peak intensity and wt. % of calcium hydroxide were mostly higher in case of exposure to composite solutions of NaCl with Na_2SO_4 as compared to composite solutions of NaCl with $MgSO_4$ followed by NaCl solutions at all depth intervals for all binders and all concentrations of NaCl, $MgSO_4$ and Na_2SO_4, with unsystematic variation in peak intensity and wt. % of calcium hydroxide among exposure solutions in few cases at depth interval of 20-25 mm. The lower peak intensity and wt. % of calcium hydroxide in case of exposure to NaCl solutions as compared to composite solutions of NaCl with $MgSO_4$ followed by composite solutions of NaCl with Na_2SO_4 is attributed to the effect of leaching of calcium hydroxide to a greater extent in the presence of higher amount of chloride ions in case of exposure to NaCl solutions. It may be noted that the free chloride content was higher in the concrete exposed to NaCl solutions as

compared to composite solutions of NaCl with $MgSO_4$ followed by composite solutions of NaCl with Na_2SO_4 (discussed earlier in Section 4.3.1.2, Chapter 4). In few cases at depth interval of 20-25 mm from the exposure surface, the unsystematic variation in the amount of calcium hydroxide among the exposure solutions as indicated by the XRD analysis may be attributed to the effect of variations in the extent of leaching of calcium hydroxide as well as due to the alterations in the extent of reaction of calcium hydroxide with sulfate ions in the concrete exposed to composite chloride-sulfate solutions. While analyzing the effect of concentration of $MgSO_4$, it is observed that the peak intensity and wt. % of calcium hydroxide mostly increased with increase in concentration of $MgSO_4$ in the composite solution of NaCl with $MgSO_4$ for all binders. This is ascribed to the presence of lower amount of chloride ions in the concrete exposed to composite chloride-sulfate solutions with higher concentration of $MgSO_4$ because of penetration of comparatively lower amount of chloride ions that resulted in leaching of calcium hydroxide to a lower extent as compared to that exposed to composite solution of NaCl with $MgSO_4$ with lower concentration of $MgSO_4$. As stated earlier in Section 4.3.1.2 (Chapter 4), the free chloride content in concrete decreased with increase in concentration of $MgSO_4$ in the composite solution of NaCl with $MgSO_4$. While analyzing the effect of concentration of Na_2SO_4, it is inferred that mostly there is no systematic variation in the peak intensity and wt. % of calcium hydroxide with increase in concentration of Na_2SO_4 in the composite solution of NaCl with Na_2SO_4 for all binders. It may be noted that, the free chloride content in concrete decreased with increase in concentration of Na_2SO_4 in the composite solution of NaCl with Na_2SO_4. Thus, although there was lower extent of leaching of calcium hydroxide in the concrete exposed to composite solution of NaCl with Na_2SO_4 with higher concentration of Na_2SO_4 due to presence of lower amount of chloride ions, the unsystematic variation in the amount of calcium hydroxide with increase in concentration of Na_2SO_4 as indicated by the XRD analysis may be attributed to the alterations in the extent of reaction of calcium hydroxide with sulfate ions due to the simultaneous reaction of sulfate ions with hydrated C_3A in the concrete exposed to composite solutions of NaCl with Na_2SO_4.

From Figure 5.1 to 5.5, Appendix B1, Figure 5.9 to 5.17 and Appendix B2, it is observed that the peak intensity and wt. % of gypsum (G) were mostly higher in case of exposure to composite solutions of NaCl with $MgSO_4$ as compared to NaCl solutions followed by composite solutions of NaCl with Na_2SO_4 for all concentrations of NaCl, $MgSO_4$ and Na_2SO_4. The presence of higher amount of gypsum in the concrete exposed to composite

solutions of NaCl with $MgSO_4$ is attributed to the reaction of magnesium sulfate with calcium hydroxide to a greater extent. In addition, magnesium sulfate attack results in decalcification of C-S-H and forms higher amount of gypsum in concrete. The presence of lower amount of gypsum in the concrete exposed to composite solutions of NaCl with Na_2SO_4 as compared to the amount of gypsum present in the concrete exposed to NaCl solutions may be attributed to the significant effect of lower extent of reaction of sodium sulfate with calcium hydroxide in case of exposure to composite solutions of NaCl with Na_2SO_4. The presence of higher amount of gypsum in the concrete exposed to NaCl solutions as compared to composite solutions of NaCl with Na_2SO_4 may be ascribed to the solubility of primary ettringite in the presence of chloride ions to a greater extent thereby forming higher amount of gypsum as a result of decomposition of ettringite in the concrete exposed to NaCl solutions. The primary ettringite is formed due to reaction of hydrated C_3A with gypsum, which is added in the manufacturing process of Portland cement to control its early setting and hardening behaviour. The presence of gypsum in the concrete is observed in the form of layers of ice like plates as evident from the FESEM images shown in Figure 5.22 [147]. From Figure 5.9 to 7.17 and Appendix B2, it is inferred that there is no systematic variation in the peak intensity and wt. % of gypsum with increase in concentration of NaCl in chloride and composite chloride-sulfate solutions. This may be attributed to the alterations in the extent of reaction of gypsum with hydrated C_3A in case of exposure to chloride solutions, and the effect of alterations in the extent of reaction of sulfate ions with calcium hydroxide in case of exposure to composite chloride-sulfate solutions, with increase in NaCl concentration in the exposure solutions.

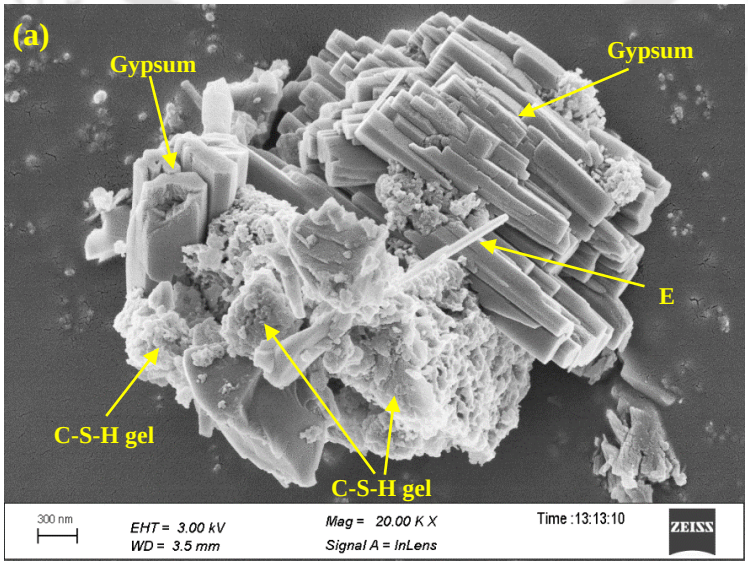

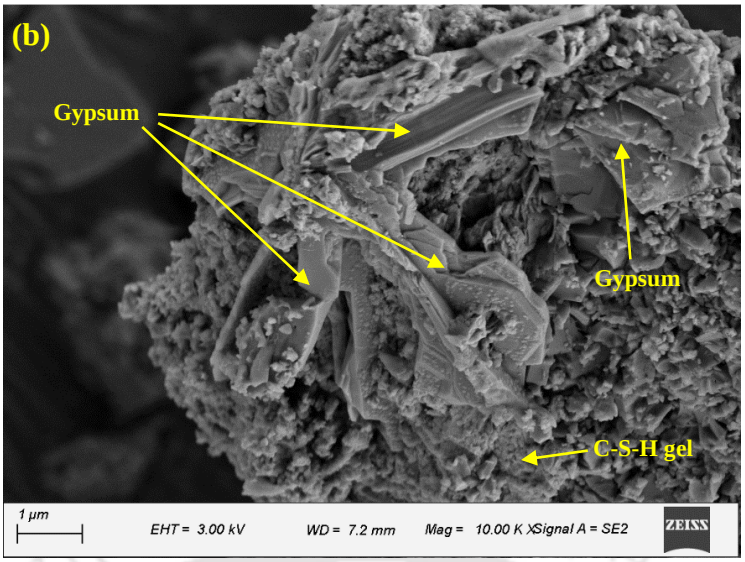

Figure 5.22 FESEM images at depth interval of 20-25 mm from exposure surface of concrete made with OPC at w/b ratio of 0.50 and exposed to: (a) 1% NaCl solution, and (b) 3% NaCl + 4% $MgSO_4$ solution, for 27 months

Further, while analyzing the effect of concentration of $MgSO_4$ and Na_2SO_4, it is observed that the peak intensity and wt. % of gypsum mostly increased with increase in concentration of $MgSO_4$ and Na_2SO_4 in the composite chloride-sulfate solutions. This is ascribed to the effect of reaction of magnesium sulfate or sodium sulfate with calcium hydroxide to a greater extent thereby forming higher amount of gypsum in the concrete exposed to composite chloride-sulfate solutions with higher concentration of $MgSO_4$ or Na_2SO_4 as compared to that in the concrete exposed to composite chloride-sulfate solutions with lower concentration of $MgSO_4$ or Na_2SO_4. As stated earlier, the peak intensity and wt. % of calcium hydroxide mostly increased with increase in concentration of $MgSO_4$ in the composite solution of NaCl with $MgSO_4$ whereas in case of exposure to composite solution of NaCl with Na_2SO_4, there was no systematic variation in the peak intensity and wt. % of calcium hydroxide with increase in concentration of Na_2SO_4 in the composite solution of NaCl with Na_2SO_4. Thus, although there was unsystematic variation in the amount of calcium hydroxide with increase in concentration of Na_2SO_4 as indicated by the XRD analysis, the increase in amount of gypsum with increase in concentration of Na_2SO_4 in the exposure solution may be attributed to the dominant effect of presence of comparatively higher amount of sulfate ions in the concrete exposed to composite solution of NaCl with Na_2SO_4 with higher concentration of Na_2SO_4, which might have resulted in the formation of more amount of gypsum as compared to that in the concrete exposed to composite solution of NaCl with Na_2SO_4 with lower concentration of Na_2SO_4.

5.2.3. Effect of binder type and w/b ratio on variations in microstructure of concrete

To study the effect of binder type and w/b ratio on microstructure of concrete exposed to chloride and composite chloride-sulfate solutions, typical plots of XRD patterns and wt. % of the compounds estimated using RIR method for different binders and w/b ratios are shown in Figure 5.23 to 5.25. The XRD patterns shown in Figure 5.23 to 5.25 correspond to the concrete powder samples collected from the depth interval of 20-25 mm from the exposure surface of prismatic specimens. Further, the XRD patterns shown in Figure 5.1 to 5.5, and Appendix B1 for different depth intervals, and those shown in Figure 5.9 to 5.17 and Appendix B2 for different exposure solutions are also considered while evaluating the effect of binder type on microstructure of concrete exposed to chloride and composite chloride-sulfate solutions. Similarly, the XRD patterns shown in Figure 5.10, 5.13, and 5.16 and Appendix B2 for different exposure solutions are also considered while evaluating the effect of w/b ratio on microstructure of concrete exposed to different exposure solutions.

From Figure 5.1 to 5.5, Appendix B1, Figure 5.9 to 5.17, Appendix B2 and Figure 5.23 to 5.25, it is observed that the peak intensity and wt. % of calcium chloroaluminate (CCA) were mostly higher in the concrete made with OPC + 20% FA as compared to PPC followed by that made with OPC at lower depth intervals (i.e. till 10 mm from the exposure surface) for chloride and composite chloride-sulfate solutions. However at higher depth intervals (i.e. beyond 10 mm from the exposure surface), the peak intensity and wt. % of calcium chloroaluminate (CCA) were mostly higher in OPC concrete as compared to OPC + 20% FA followed by PPC concrete. The formation of higher amount of calcium chloroaluminate in OPC + 20% FA concrete at lower depth intervals may be attributed to the dominant effect of reaction of chloride ions with aluminate hydrates to a greater extent as compared to PPC and OPC concrete. It may be noted that the wt. % of Al_2O_3 was higher in fly ash than that in OPC followed by PPC (observed from Table 3.1, Chapter 3). The formation of higher amount of calcium chloroaluminate in PPC concrete as compared to OPC concrete at lower depth intervals is ascribed to the reaction of chloride ions with hydrated C_3A to a higher extent due to penetration of more amount of chloride ions in PPC concrete than that in OPC concrete at lower depth intervals. As mentioned earlier (Section 4.3.1.3, Chapter 4), the free chloride content was also higher in PPC concrete than that in OPC + 20% FA followed by OPC concrete at lower depth intervals from the exposure surface. The formation of more amount of calcium chloroaluminate in OPC concrete as compared to OPC + 20% FA and PPC concrete at higher depth intervals may be due to the effect of

reaction of chloride ions with hydrated C_3A to a greater extent as a result of penetration of higher amount of chloride ions in OPC concrete as compared to OPC + 20% FA and PPC concrete at higher depth intervals. It may be noted that the free chloride content was also higher in OPC concrete than that in OPC + 20% FA followed by PPC concrete at higher depth intervals from the exposure surface (mentioned earlier Section 4.3.1.3, Chapter 4). The higher amount of calcium chloroaluminate in OPC + 20% FA concrete as compared to PPC concrete at higher depth intervals is attributed to the presence of higher amount of Al_2O_3 in fly ash as well as due to the penetration of more amount of chloride ions in OPC + 20% FA concrete as compared to PPC concrete at higher depth intervals, which resulted in reaction of chloride ions with aluminate hydrates to a greater extent in OPC + 20% FA concrete as compared to PPC concrete.

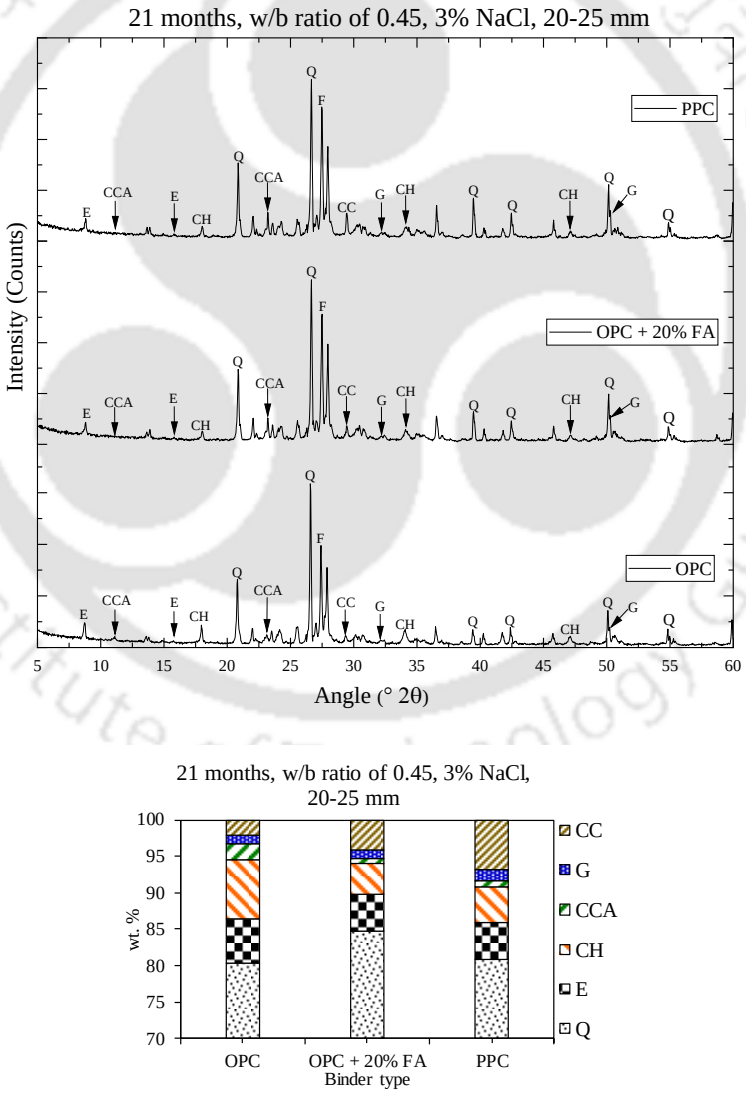

Figure 5.23 XRD patterns and wt. % of compounds at depth interval of 20-25 mm (i.e. near rebar) from exposure surface of concrete made with different types of binder at w/b ratio of 0.45 and exposed to 3% NaCl solution for 21 months

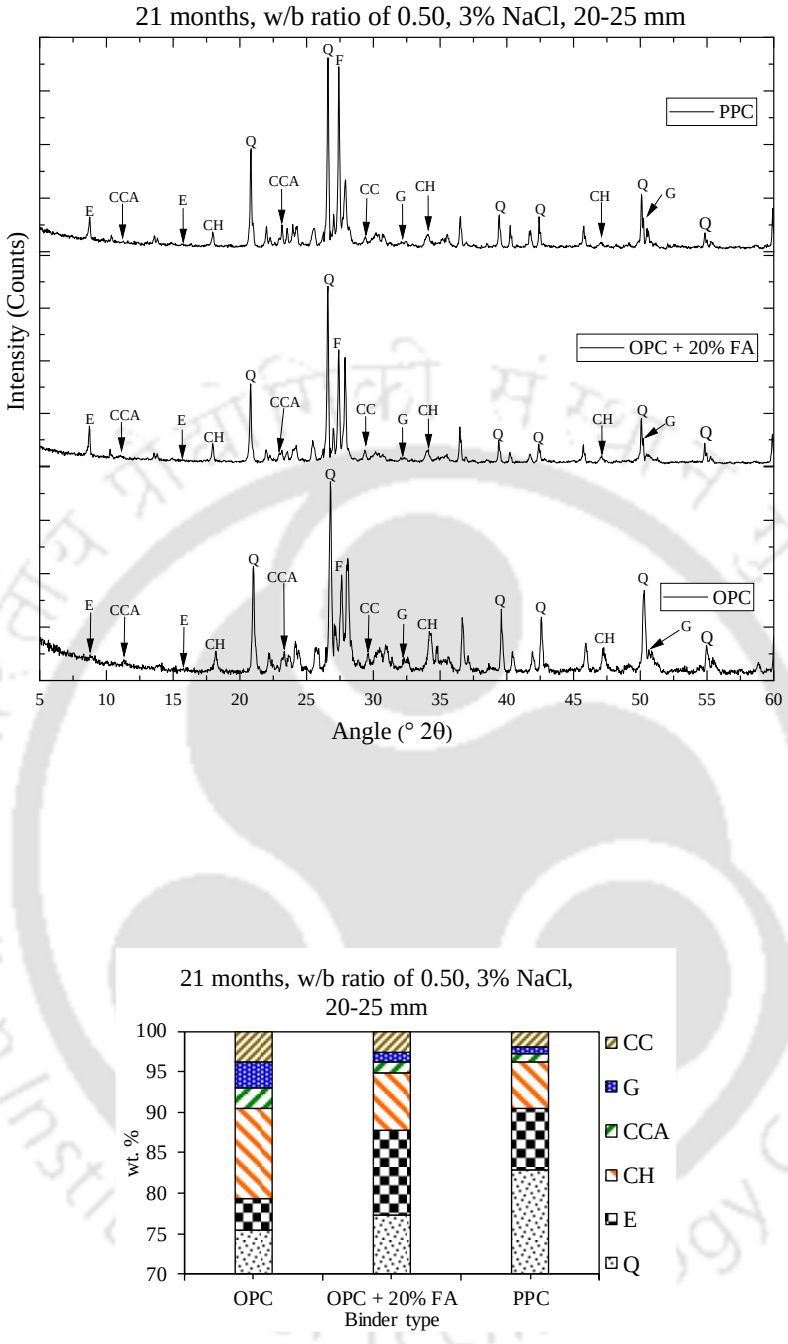

Figure 5.24 XRD patterns and wt. % of compounds at depth interval of 20-25 mm (i.e. near rebar) from exposure surface of concrete made with different types of binder at w/b ratio of 0.50 and exposed to 3% NaCl solution for 21 months

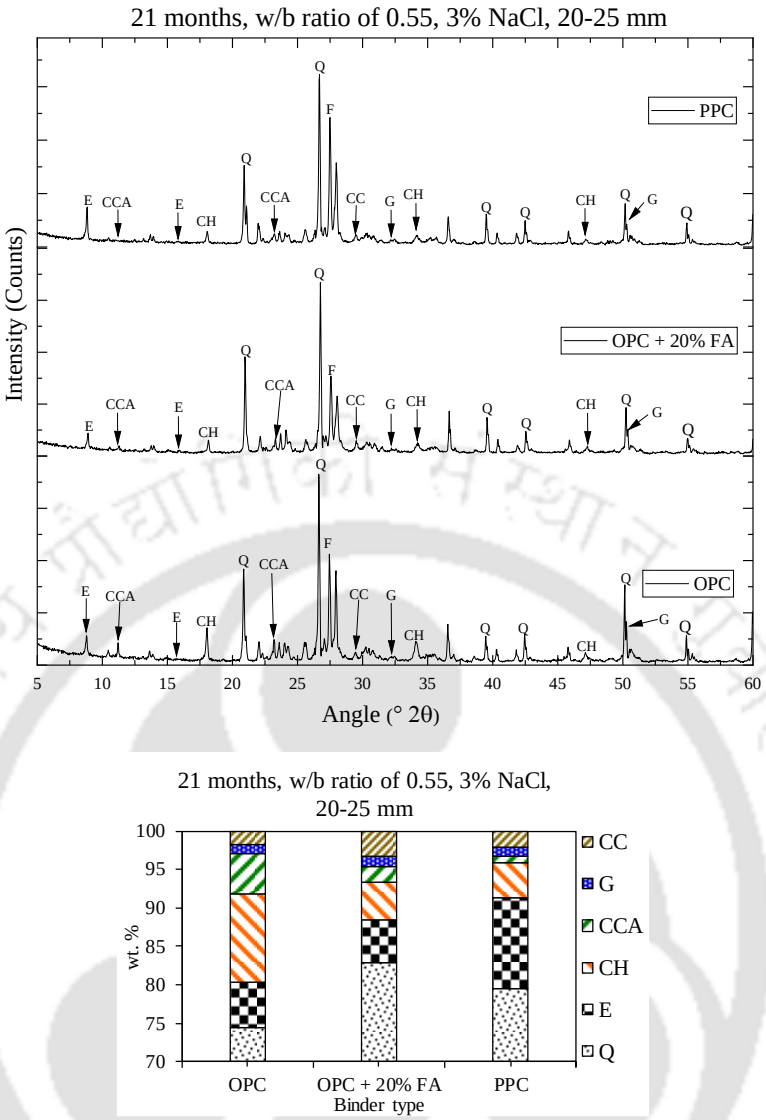

Figure 5.25 XRD patterns and wt. % of compounds at depth interval of 20-25 mm (i.e. near rebar) from exposure surface of concrete made with different types of binder at w/b ratio of 0.55 and exposed to 3% NaCl solution for 21 months

From Figure 5.1 to 5.5, Appendix B1, Figure 5.9 to 5.17, Appendix B2 and Figure 5.23 to 5.25, it is observed that the peak intensity and wt. % of ettringite (E) were lower in OPC concrete as compared to OPC + 20% FA followed by PPC concrete in case of exposure to chloride solutions at all depth intervals. This may be attributed to the reaction of gypsum with hydrated C_3A to a comparatively lower extent in OPC and OPC + 20% FA concrete as compared to that in PPC concrete as well as due to the variations in the extent of solubility of ettringite in the presence of chloride ions among binder type at different depth intervals. It may be noted that the free chloride content was mostly higher in PPC concrete than that in OPC + 20% FA followed by OPC concrete at lower depth intervals from the exposure surface whereas at higher depth intervals the free chloride content was mostly

higher in OPC concrete than that in OPC + 20% FA followed by PPC concrete, as mentioned earlier in Section 4.3.1.3, Chapter 4. In case of exposure to composite solutions of NaCl with $MgSO_4$, the peak intensity and wt. % of ettringite were higher in OPC + 20% FA and PPC concrete as compared to OPC concrete at lower depth intervals whereas at higher depth intervals the peak intensity and wt. % of ettringite were higher in OPC concrete as compared to OPC + 20% FA followed by PPC concrete. In case of exposure to composite solutions of NaCl with Na_2SO_4, the peak intensity and wt. % of ettringite were higher in PPC concrete as compared to OPC followed by OPC + 20% FA concrete at all depth intervals. This indicated that the formation of ettringite in the concrete made with different types of binder was affected by the cation type associated with sulfate ions in the presence of chloride ions. The variations in the amount of ettringite in the concrete exposed to composite chloride-sulfate solutions may be attributed to the effect of alterations in the extent of reaction of sulfate ions with hydrated C_3A due to variations in the penetrations of sulfate ions in concrete at different depth intervals as well as due to the variations in the solubility of ettringite at different depth intervals in the presence of chloride ions for different types of binder.

From Figure 5.1 to 5.5, Appendix B1, Figure 5.9 to 5.17, Appendix B2 and Figure 5.23 to 5.25, it is observed that the peak intensity and wt. % of calcium hydroxide (CH) were lower in OPC + 20% FA and PPC concrete as compared to OPC concrete at all depth intervals in case of specimens exposed to composite chloride-sulfate solutions, and at higher depth intervals in case of specimens exposed to chloride solutions. Between PPC and OPC + 20% FA, the amount of calcium hydroxide was lower in PPC concrete as compared to that in OPC + 20% FA concrete as observed from the XRD analysis. The presence of lower amount of calcium hydroxide in OPC + 20% FA, and PPC than that in OPC concrete as indicated by the XRD analysis is ascribed to its consumption in the pozzolanic reaction with fly ash, which results in the production of additional C-S-H gel in OPC + 20% FA, and PPC concrete. The formation of compacted microstructure due to production of more amount of C-S-H gel in OPC + 20% FA and PPC concrete as compared to that in OPC concrete is evident from the FESEM images shown in Figure 5.26. In the FESEM images shown in Figure 5.26, the C-S-H gel is appeared as reticular network structure [150]. The unsystematic variation in calcium hydroxide (CH) content with binder type as observed from the XRD analysis at lower depth intervals (i.e. till 10 mm from the exposure surface of concrete) in case of exposure to chloride solutions may be attributed to the dominant

effect of variations in its leaching with respect to binder type near the exposure surface of concrete.

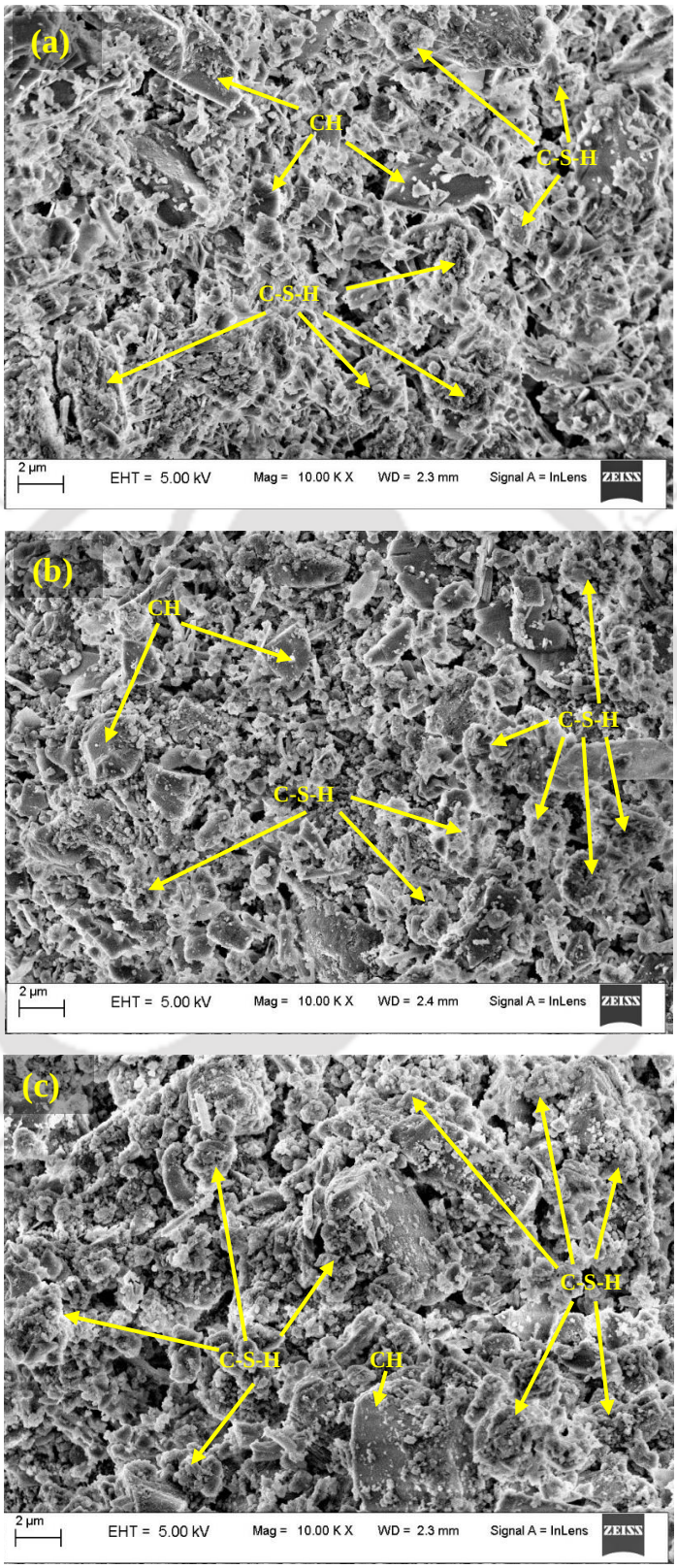

Figure 5.26 FESEM images of concrete near rebar level (i.e. at depth interval of 20-25 mm from exposure surface of concrete) for: (a) OPC, (b) OPC + 20% fly ash, and (c) PPC at w/b ratio of 0.50 and exposed to 3% NaCl solution for 21 months

From Figure 5.1 and 5.2, Appendix B1, Figure 5.9 to 5.17, Appendix B2 and Figure 5.23 to 5.25, it is observed that the peak intensity and wt. % of gypsum (G) were lower in PPC concrete as compared to that in OPC and OPC + 20% FA concrete in case of exposure to NaCl solutions at all depth intervals. The presence of lower amount of gypsum in PPC concrete is attributed to its consumption in the reaction with hydrated C_3A to a comparatively greater extent (although C_3A content of PPC was lower as compared to OPC, Table 3.2, Chapter 3), thereby forming higher amount of ettringite in PPC concrete as compared to that in OPC and OPC + 20% FA concrete (discussed earlier). Similarly, the presence of higher amount of gypsum in OPC and OPC + 20% FA concrete exposed to chloride solutions is ascribed to its reaction with hydrated C_3A to a lower extent. In case of exposure of concrete to the solutions containing sulfate salts, the reaction of magnesium sulfate with calcium hydroxide forms gypsum and magnesium hydroxide. Similarly, the reaction of sodium sulfate with calcium hydroxide results in the formation of gypsum and sodium hydroxide. From Figure 5.3 to 5.5, Appendix B1, Figure 5.9 to 5.17 and Appendix B2, it is observed that the variation in peak intensity and wt. % of gypsum is unsystematic as well as very less with respect to binder type in the concrete exposed to composite chloride-sulfate solutions (for both $MgSO_4$ and Na_2SO_4) at all depth intervals. This may be attributed to the dominant effect of alterations in the extent of reaction of calcium hydroxide with magnesium sulfate or sodium sulfate in the concomitant presence of chloride ions due to variations in the extent of penetration of sulfate ions as well as due to variations in the availability of calcium hydroxide with binder type in concrete at different depth intervals.

From Figure 5.3 and 5.4, Appendix B1, Figure 5.9 to 5.17 and Appendix B2, it is observed that the peak intensity of magnesium hydroxide (brucite) was mostly higher in the concrete made with OPC as compared to that made with OPC + 20% FA followed by PPC in case of exposure to composite solutions of NaCl with $MgSO_4$. The formation of higher amount of magnesium hydroxide in OPC concrete as indicated by the XRD analysis is attributed to the dominant effect of reaction of calcium hydroxide with magnesium sulfate to a greater extent due to availability of higher amount of calcium hydroxide in OPC concrete as compared to that in OPC + 20% FA and PPC concrete.

On comparing the effect of w/b ratio, it is observed that the peak intensity and wt. % of calcium hydroxide (CH) were mostly higher in the concrete made with w/b ratio of 0.50 as compared to those made with w/b ratios 0.45 and 0.55 for all binders and exposure solutions (chloride and composite chloride-sulfate solutions) as evident from Figure 5.10, 5.13, 5.16, Figure 5.23 to 5.25 and Appendix B2. Further, there was minor difference in the peak

intensity and wt. % of calcium hydroxide between w/b ratios of 0.45 and 0.55. These differences in the amount of calcium hydroxide in concrete with change in w/b ratio are attributed to the combined effect of: a) variations in the release of calcium hydroxide from hydration reaction and that in the consumption of calcium hydroxide in the pozzolanic reaction, b) variations in the leaching of calcium hydroxide in the presence of chloride ions, and c) alterations in the extent of reaction of magnesium sulfate or sodium sulfate with calcium hydroxide due to the variations in the penetration of sulfate ions as a result of alterations in the microstructure of concrete with change in w/b ratio.

From Figure 5.10, 5.13, 5.16, Figure 5.23 to 5.25 and Appendix B2, it is inferred that the peak intensity and wt. % of ettringite (E) were higher at w/b ratio of 0.55 as compared to that at w/b ratio of 0.50 followed by w/b ratio of 0.45 for all binders and exposure solutions. In case of exposure to chloride solutions, the presence of higher amount of ettringite in the concrete made with higher w/b ratio as observed from the XRD analysis may be attributed to the preferential reaction of hydrated C_3A with gypsum than that with chloride ions. In case of exposure to composite chloride-sulfate solutions, the presence of higher amount of ettringite in the concrete made with higher w/b ratio is attributed to the reaction of sulfate ions with hydrated C_3A to a greater extent as a result of penetration of more amount of sulfate ions into concrete made with higher w/b ratio.

From Figure 5.10, 5.13, 5.16, Figure 5.23 to 5.25 and Appendix B2, it is inferred that there is unsystematic variation in the peak intensity and wt. % of gypsum (G) with change in w/b ratio for all binders and exposure solutions. In case of exposure to chloride solutions, the unsystematic variation in the amount of gypsum with change in w/b ratio is attributed to the alterations in the extent of its reaction with hydrated C_3A. In case of exposure to composite chloride-sulfate solutions, the unsystematic variation in the amount of gypsum with change in w/b ratio as indicated by the XRD analysis is attributed to the effect of alterations in its formation (due to reaction of sulfate ions with calcium hydroxide) as a result of variations in the availability of calcium hydroxide and in the penetration of sulfate ions with change in w/b ratio.

From Figure 5.10, 5.13, 5.16, Figure 5.23 to 5.25 and Appendix B2, it is observed that the peak intensity and wt. % of calcium chloroaluminate (CCA) were lower at w/b ratio of 0.55 as compared to other w/b ratios for all binders and exposure solutions. The formation of lower amount of calcium chloroaluminate (CCA) at w/b ratio of 0.55 as indicated by the XRD analysis is attributed to the reaction of chloride ions with hydrated C_3A to a lower

extent as a result of preferential reaction of hydrated C_3A with gypsum in case of exposure to chloride solutions and that of hydrated C_3A with sulfate ions in case of exposure to composite chloride-sulfate solutions there by forming higher amount of ettringite at w/b ratio of 0.55 (as stated earlier). Further, the peak intensity and wt. % of calcium chloroaluminate (CCA) were higher at w/b ratio of 0.50 as compared to that at w/b ratio of 0.45 as observed from Figure 5.10, 5.13, 5.16, Figure 5.23 to 5.25 and Appendix B2. The formation of higher amount of calcium chloroaluminate (CCA) at w/b ratio of 0.50 is ascribed to the dominant effect reaction of chloride ions with hydrated C_3A to a greater extent due to penetration of more amount of chloride ions at w/b ratio of 0.50 that that at w/b ratio of 0.45 in case of exposure to both chloride as well as composite chloride-sulfate solutions. The formation of lower amount of calcium chloroaluminate (CCA) at w/b ratio of 0.45 as compared that at w/b ratio of 0.50 is ascribed to the reaction of chloride ions with hydrated C_3A to a lower extent due to penetration of lower amount of chloride ions even though there was availability of comparatively higher amount of C_3A due to lower extent of reaction of hydrated C_3A with gypsum in case of exposure to chloride solutions and that of hydrated C_3A with sulfate ions in case of exposure to composite chloride-sulfate solutions thereby forming lower amount of ettringite at w/b ratio of 0.45 as compared to that at w/b ratio of 0.50 (as stated earlier).

5.3. Thermo-gravimetry analysis (TGA)

Thermo-gravimetry analysis (TGA) was conducted on the concrete powder samples collected at different depth intervals from the prismatic specimens made with OPC, OPC + 20% FA and PPC and exposed to chloride and composite chloride-sulfate solutions for different exposure periods. The first derivative of change of mass (derivative thermo-gravimetry: DTG) obtained from TGA was also plotted along with TGA curve, which indicates sharp yield peaks at the location of change of mass. From the obtained results of TG/DTG analysis, the variations in the decomposition of various compounds at different temperature ranges with depth interval, exposure solution, binder type, and w/b ratio were analyzed. As mentioned in Chapter 3, the calcium hydroxide content (%) in concrete was estimated by Taylor's formula using the mass loss results obtained from TGA [133].

5.3.1. Variations in decomposition of compounds with depth from exposure surface of concrete

Typical plots of TGA and DTG curves obtained for different depth intervals from the exposure surface of prismatic specimens are shown in Figure 5.27 and Figure 5.28. Further,

the mass loss at different temperature ranges and the wt. % of calcium hydroxide estimated using Taylor's formula are presented in Table 5.2 and Table 5.3 respectively.

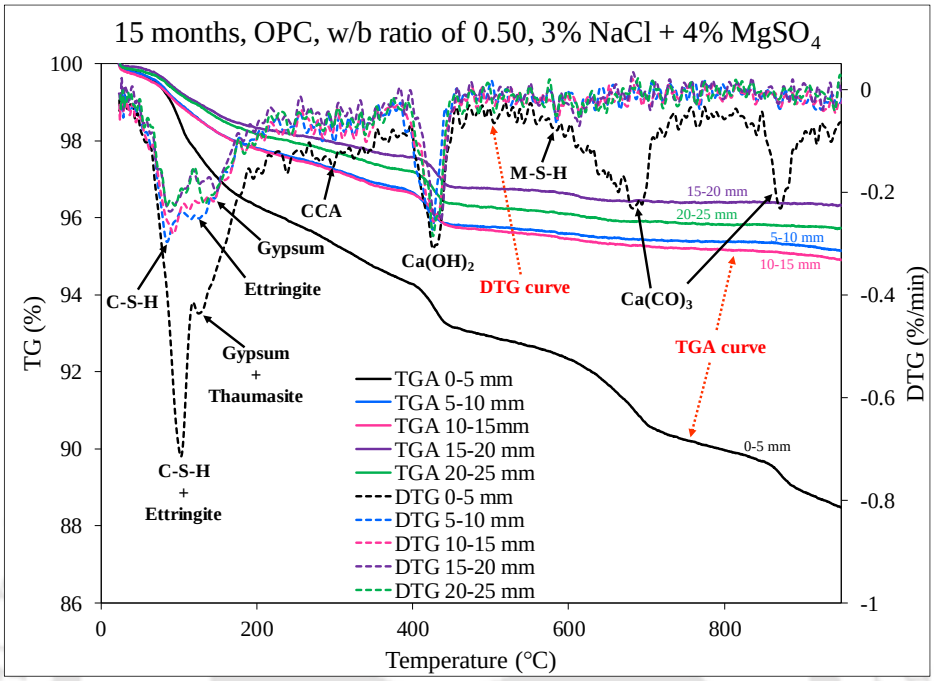

Figure 5.27 TGA and DTG curves of concrete at different depth intervals from exposure surface for OPC at w/b ratio of 0.50 and exposed to 3% NaCl + 4% $MgSO_4$ solution for 15 months

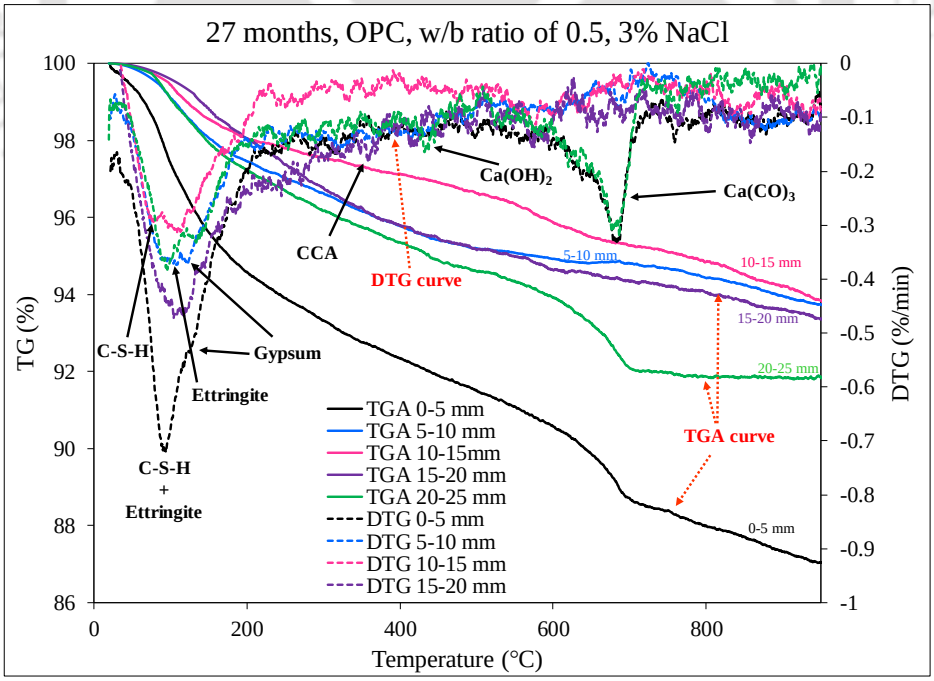

Figure 5.28 TGA and DTG curves of concrete at different depth intervals from exposure surface for OPC at w/b ratio of 0.50 and exposed to 3% NaCl solution for 27 months

In the TGA and DTG curves shown in Figure 5.27 and Figure 5.28 for different depth intervals of concrete from the exposure surface, the mass loss in the temperature range from ambient to 90 °C is due to the loss of free water from concrete. The mass loss in the temperature range of 90 °C - 400 °C is ascribed to the loss of combined water due to dehydration of C-S-H, aluminate hydrates, ferroaluminate hydrates, thaumasite and gypsum [37, 151]. In the DTG curve, in the temperature range of about 90 °C - 103 °C, a relatively more intense endothermic peak was observed, which is due to the loss of combined water in the C-S-H gel [151]. A less intense endothermic peak in the DTG curve observed in the temperature range of about 103 °C - 118 °C is associated with the dehydration of ettringite [151]. Similarly, in the temperature range of about 125 °C - 128 °C, a relatively less intense endothermic peak was observed in the concrete at lower depth intervals i.e. till about 10 mm from the exposure surface for exposure against composite chloride-sulfate solutions (Figure 5.27), which is attributed to the dehydration of thaumasite [151]. As discussed earlier (Section 5.2.1), the thaumasite peaks were observed in the obtained XRD patterns of concrete at lower depth intervals, i.e. till 10 mm from the exposure surface against exposure to composite chloride-sulfate solutions. Further, in the temperature range of about 128 °C - 151 °C in the DTG curve, a relatively less intense endothermic peak was observed, which is associated with the dehydration of gypsum [151]. The mass loss in the temperature range of 280 °C - 341 °C is associated with the dehydration of Friedel's salt (calcium chloroaluminate) [37]. A sharp change in the slope of TGA curve was observed in the temperature range of 400 °C - 460 °C, which is attributed to the mass loss associated with the dehydration of calcium hydroxide (portlandite) [151]. In the same temperature range, a strong intense endothermic peak was also observed in the DTG curve as observed from Figure 5.27 and Figure 5.28. In the temperature range of 460 °C - 950 °C, the mass loss is mostly attributed to the decarbonation of calcium carbonate (calcite), which causes escape of CO_2 from concrete [37]. Further, in the temperature of 573 °C - 600 °C, the mass loss was attributed to the dehydration of magnesium silicate hydrate (M-S-H) gel in the concrete exposed to composite solution of NaCl with $MgSO_4$ [152]. The formation of M-S-H in concrete was evident from the FESEM images shown earlier in Figure 5.21 for the concrete exposed to composite solution of NaCl with $MgSO_4$.

Table 5.2 Mass loss (%) obtained from TGA at various temperature ranges for different depth intervals from exposure surface of concrete

Concrete mix and details of exposure	Depth from exposure surface	Mass loss (%)				Total mass loss (%) (ambient to 950 °C)
		Ambient to 90 °C	90-400 °C	400-460 °C	460-950 °C	
OPC, w/b ratio = 0.50, 3% NaCl + 4% $MgSO_4$ solution, and exposure period of 15 months	0-5 mm	1.00	4.73	1.15	4.65	11.52
	5-10 mm	0.83	2.51	0.84	0.68	4.86
	10-15 mm	0.86	2.52	0.87	0.84	5.09
	15-20 mm	0.55	1.77	0.88	0.47	3.67
	20-25 mm	0.60	2.15	0.89	0.63	4.26
OPC, w/b ratio = 0.50, 3% NaCl solution, and exposure period of 27 months	0-5 mm	2.07	5.59	0.52	4.77	12.95
	5-10 mm	0.66	3.57	0.40	1.64	6.27
	10-15 mm	0.40	2.46	0.29	3.01	6.16
	15-20 mm	0.31	3.90	0.40	2.04	6.65
	20-25 mm	0.63	4.01	0.53	2.99	8.17

Table 5.3 Calcium hydroxide content (% by mass) obtained from TGA at different depth intervals from exposure surface of concrete

Concrete mix and details of exposure	Calcium hydroxide content (% by mass)				
	Depth from exposure surface				
	0-5 mm	5-10 mm	10-15 mm	15-20 mm	20-25 mm
OPC, w/b ratio = 0.50, 3% NaCl + 4% $MgSO_4$ solution, and exposure period of 15 months	4.73	3.45	3.58	3.63	3.66
OPC, w/b ratio = 0.50, 3% NaCl solution, and exposure period of 27 months	2.15	1.66	1.19	1.64	2.18

From Table 5.2, it is observed that the total mass loss in the temperature range of ambient to 950 °C mostly decreased with increase in depth till about 15 mm from the exposure surface followed by an increase thereafter at higher depth intervals. From Table 5.2, it is noted that the total mass loss was higher in the depth interval of 0-5 mm from the exposure surface as compared other depth intervals for both exposure solutions and exposure periods. This is attributed to dominant effect of loss of free water (ambient to 90 °C), loss of combined water due to dehydration of C-S-H, aluminate hydrates, and gypsum (90 °C -

400 °C), and decarbonation of calcium carbonate (460 °C - 950 °C) in concrete. The mass loss in the temperature range of ambient to 90 °C was higher in the depth interval of 0-5 mm and decreased with increase in depth till 20 mm from the exposure surface followed by an increase in the depth interval of 20-25 mm as observed from Table 5.2. This variation in mass loss with increase in depth from the exposure surface of concrete may be attributed to the alterations in the loss of free water from the hydrated cement phases as a result of variations in the absorption of water by the hydrated cement phases at different depth intervals during the wetting-drying process of exposure.

The higher mass loss due to loss of combined water (90 °C - 400 °C) in the depth interval of 0-5 mm may be attributed to the dominant effect of dehydration of calcium chloroaluminate, gypsum and ettringite. As observed from the XRD analysis (Section 5.2.1), the peak intensity and wt. % of calcium chloroaluminate were slightly higher at lower depth intervals i.e. till 10 mm from the exposure surface as compared to other depth intervals. Thus, the dehydration of calcium chloroaluminate in the depth interval of 0-5 mm to a greater extent thereby indicating its presence in higher amount corroborates with the results of XRD analysis. Further, as stated earlier, there was unsystematic variation in peak intensity and wt. % of gypsum in concrete with depth interval from the exposure surface as indicated by the XRD analysis (Section 5.2.1). In the depth interval of 0-5 mm from the exposure surface, the dehydration of ettringite to a comparatively greater extent thereby indicating its presence in higher amount in this depth interval is not in line with the observation obtained from the XRD analysis wherein the peak intensity and wt. % of ettringite were lower in the depth interval of 0-5 mm, which may be attributed possibly to its lower degree of crystallinity in the surface region of concrete [144], as stated earlier in Section 5.2.1.

In case of exposure to composite chloride-sulfate solutions, the higher mass loss due to loss of combined water (90 °C - 400 °C) in the depth interval of 0-5 mm from the exposure surface is also associated with the dehydration of thaumasite, which corroborates with the results of XRD analysis indicating the formation of thaumasite at lower depth intervals i.e. near the surface region of concrete exposed to composite chloride-sulfate solutions. From Table 5.2, it is observed that the mass loss in the temperature range of 90 °C - 400 °C mostly decreased with increase in depth till about 15 mm from the exposure surface followed by an increase at higher depth intervals. This variation in mass loss till a depth of about 15 mm from the exposure surface in the temperature range of 90 °C - 400 °C is

attributed to the dominant effect of variations in the dehydration of calcium chloroaluminate, gypsum and ettringite in the concrete. The increase in mass loss in the temperature range of 90 °C - 400 °C at higher depth interval i.e. beyond a depth of about 15 mm from the exposure surface is attributed to the significant effect of dehydration of C-S-H to a relatively greater extent.

From Table 5.2 it is observed that the mass loss in the temperature range of 400 °C - 460 °C was higher in the depth interval of 0-5 mm from the exposure surface of concrete followed by a decrease in the depth interval of 5-10 mm for both chloride and composite chloride-sulfate solutions. Beyond the depth interval 5-10 mm, the mass loss mostly increased with increase in depth from the exposure surface in case of exposure to chloride solution as well as composite chloride-sulfate solution (although the increase was small) as evident from Table 5.2. The higher mass loss in the depth interval of 0-5 mm is ascribed to dehydration of calcium hydroxide to a greater extent. This is attributed to the presence of higher amount of calcium hydroxide in the depth interval of 0-5 mm as indicated by its amount estimated using Taylor's formula in this depth interval presented in Table 5.3. However, as observed from XRD analysis (Section 5.2.1), the peak intensity and wt. % of calcium hydroxide (CH) were less in the depth interval of 0-5 mm as compared to other depth intervals. In other words, in the depth interval of 0-5 mm, the amount of calcium hydroxide estimated using Taylor's formula from TGA is different from that obtained from XRD analysis. In the depth interval of 0-5 mm from the exposure surface, the presence of higher amount of calcium hydroxide as estimated from TGA using Taylor's formula may be attributed to the fact that due to leaching of calcium hydroxide in the presence of chloride ions from higher depth intervals during the alternate wetting-drying process, the calcium hydroxide might have accumulated near the surface region of concrete. However, the presence of calcium hydroxide might not have been indicated completely by the peak intensity in the XRD patterns, which may be attributed to the lower degree of crystallinity of calcium hydroxide [153] in the surface region of concrete thereby showing its lower peak intensity in the depth interval of 0-5 mm from the exposure surface. Beyond the depth interval of 0-5 mm from the exposure surface, the variation in the amount of calcium hydroxide estimated using Taylor's formula from TGA is similar to the variation in its peak intensity and wt. % obtained from the XRD analysis (Section 5.2.1).

The higher mass loss due to decarbonation of calcium carbonate (460 °C - 950 °C) in the depth interval of 0-5 mm is attributed to its presence due to aggregates as well as may be

due to the occurrence of carbonation near the surface region of concrete during the alternate wetting-drying process of exposure. As mentioned earlier (Section 5.2.1), the peak intensity and wt. % of calcite (CC) were higher in the depth interval of 0-5 mm from the exposure surface as compared to other depth intervals as indicated by the XRD analysis. Thus, the higher mass loss due to decarbonation of calcium carbonate in the depth interval of 0-5 mm thereby indicating its presence in higher amount corroborates with the results of XRD analysis. Further, the higher mass loss in the depth interval of 0-5 mm from the exposure surface is also associated with the dehydration of magnesium silicate hydrate (M-S-H) in the temperature range of 573 °C - 600 °C, wherein a relatively sharp change in the slope of TGA curve was observed in the depth interval of 0-5 mm from the exposure surface of concrete exposed to composite solution of NaCl with $MgSO_4$ as evident from Figure 5.27.

5.3.2. Variations in decomposition of compounds with exposure solution

Typical plots of TGA and DTG curves obtained for different exposure solutions are shown in Figure 5.29 to 5.31. Further, the mass loss corresponding to different temperature ranges and the wt. % of calcium hydroxide estimated using Taylor's formula are presented in Table 5.4 and Table 5.5 respectively. These results of TGA for different exposure solutions correspond to the concrete powder samples collected from the depth interval of 20-25 mm from the exposure surface of concrete.

From Figure 5.29 to 5.31 and Table 5.4, it is observed that in the temperature range of ambient to 90 °C, there is no systematic variation in mass loss with exposure solution for OPC and OPC + 20% FA concrete, whereas in case of PPC concrete the mass loss due to loss of free water was lower in case of exposure to chloride solution as compared to composite chloride-sulfate solutions. These variations in mass loss with exposure solution may be ascribed to the effect of variations in the loss of free water from the hydrated cement phases in the presence of chloride, and combined presence of chloride-sulfate ions. In the temperature range of 90 °C - 400 °C, there is no systematic variation in the mass loss with increase in concentration of NaCl in chloride and composite chloride-sulfate (NaCl with $MgSO_4$) solutions as evident from Figure 5.29 to 5.31 and Table 5.4.

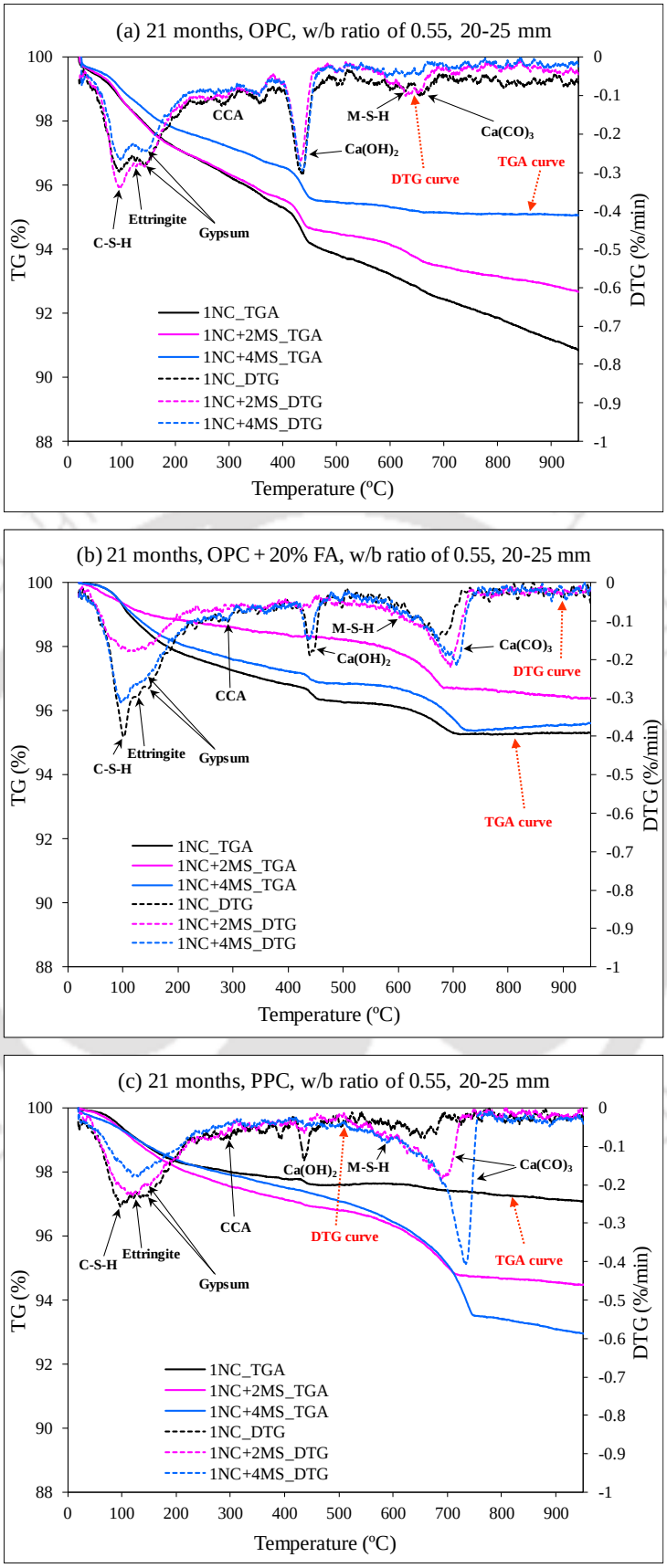

Figure 5.29 TGA and DTG curves of concrete at depth interval of 20-25 mm from exposure surface for 1% NaCl, and 1% NaCl with $MgSO_4$ (2% and 4%) solutions at w/b ratio of 0.55 and exposure period of 21 months: (a) OPC, (b) OPC + 20% FA and (c) PPC

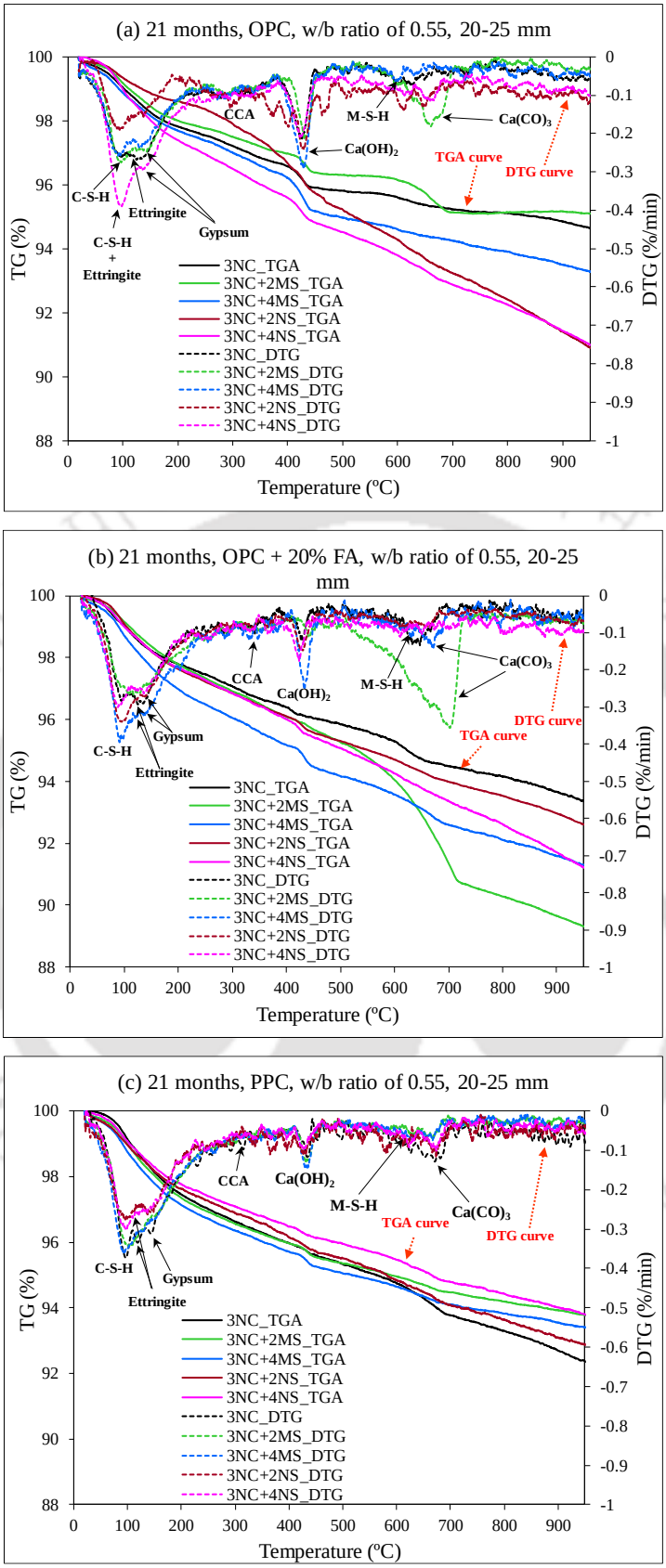

Figure 5.30 TGA and DTG curves of concrete at depth interval of 20-25 mm from exposure surface for 3% NaCl, 3% NaCl with $MgSO_4$ (2% and 4%), and 3% NaCl with Na_2SO_4 (2% and 4%) solutions at w/b ratio of 0.55 and exposure period of 21 months: (a) OPC, (b) OPC + 20% FA and (c) PPC

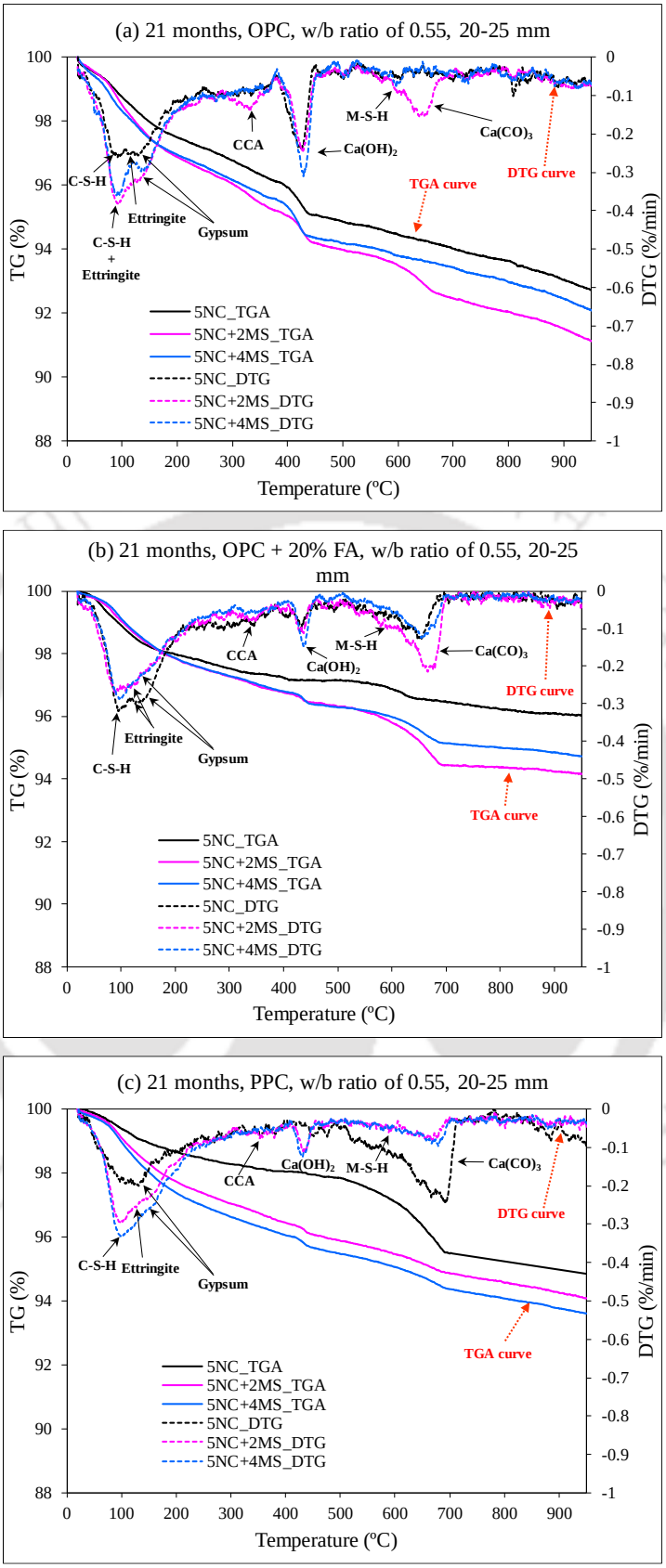

Figure 5.31 TGA and DTG curves of concrete at depth interval of 20-25 mm from exposure surface for 5% NaCl, and 5% NaCl with $MgSO_4$ (2% and 4%) solutions at w/b ratio of 0.55 and exposure period of 21 months: (a) OPC, (b) OPC + 20% FA and (c) PPC

Table 5.4 Mass loss (%) obtained from TGA at various temperature ranges for different binders exposed to chloride and composite chloride-sulfate solutions

Concrete mix and exposure period	Exposure solution	Mass loss (%)				Total mass loss (%) (ambient to 950 °C)
		Ambient to 90 °C	90-400 °C	400-460 °C	460-950 °C	
OPC, w/b ratio = 0.55, depth interval of 20-25 mm, and 21 months	1NC	1.11	3.58	1.20	3.26	9.16
	3NC	0.79	2.64	0.68	1.25	5.37
	5NC	1.07	3.00	0.91	2.30	7.28
	1NC+2MS	1.06	3.39	0.94	1.94	7.33
	1NC+4MS	0.83	2.60	1.04	0.47	4.94
	3NC+2MS	0.64	2.38	0.63	1.25	4.90
	3NC+4MS	0.95	2.84	1.09	1.84	6.72
	5NC+2MS	1.24	3.73	0.90	3.01	8.87
	5NC+4MS	1.49	3.18	1.01	2.23	7.91
	3NC+2NS	0.55	2.80	1.03	4.73	9.10
	3NC+4NS	0.74	3.67	0.83	3.77	9.02
OPC + 20% FA, w/b ratio = 0.55, depth interval of 20-25 mm, and 21 months	1NC	0.50	2.58	0.58	1.04	4.70
	3NC	0.83	2.78	0.37	2.66	6.64
	5NC	0.94	1.83	0.08	1.11	3.96
	1NC+2MS	0.56	1.09	0.06	1.89	3.60
	1NC+4MS	0.48	2.29	0.35	1.27	4.39
	3NC+2MS	0.68	3.24	0.50	6.27	10.69
	3NC+4MS	1.02	3.80	0.80	3.07	8.70
	5NC+2MS	0.79	2.46	0.34	2.25	5.83
	5NC+4MS	0.67	2.53	0.43	1.64	5.28
	3NC+2NS	0.68	3.22	0.58	2.91	7.40
	3NC+4NS	0.81	3.18	0.65	4.15	8.78
PPC, w/b ratio = 0.55, depth interval of 20-25 mm, and 21 months	1NC	0.45	1.77	0.18	0.51	2.91
	3NC	0.63	2.04	0.16	3.61	6.44
	5NC	0.51	1.44	0.12	3.08	5.15
	1NC+2MS	0.56	2.31	0.23	2.43	5.53
	1NC+4MS	0.59	1.90	0.24	4.32	7.04
	3NC+2MS	0.77	3.27	0.47	1.72	6.23
	3NC+4MS	1.00	3.29	0.51	1.79	6.59
	5NC+2MS	0.69	2.87	0.41	1.95	5.92
	5NC+4MS	0.80	3.15	0.43	2.01	6.39
	3NC+2NS	0.86	3.00	0.48	2.77	7.12
	3NC+4NS	0.65	2.84	0.39	2.31	6.18

As observed from XRD analysis (Section 5.2.2), the wt. % of calcium chloroaluminate (CCA) increased whereas that of ettringite (E) decreased with increase in concentration of NaCl in chloride and composite chloride-sulfate solutions. However, there was no

systematic variation in wt. % of gypsum (G) with increase in concentration of NaCl in chloride and composite chloride-sulfate solutions as observed from the XRD analysis. Thus, in the temperature range of 91 °C - 400 °C, the unsystematic variation in the mass loss with increase in concentration of NaCl in the exposure solution is attributed to the variations in the extent of dehydration of calcium chloroaluminate, ettringite and gypsum as a result of variations in the amount of these compounds present in concrete.

While comparing between chloride and composite chloride-sulfate solutions, it is noted that in the temperature range of 90 °C - 400 °C, the mass loss was mostly higher in the concrete exposed to composite chloride-sulfate solutions (for both $MgSO_4$ and Na_2SO_4) as compared to chloride solutions for all binders as evident from Figure 5.29 to 5.31 and Table 5.4. This is attributed to the significant effect of loss of combined water due to dehydration of ettringite to a greater extent in the concrete exposed to composite chloride-sulfate solutions than that exposed to chloride solution. This observation corroborates with the results of XRD analysis wherein the peak intensity and wt. % of ettringite were higher in the concrete exposed to composite chloride-sulfate solutions (for both $MgSO_4$ and Na_2SO_4) as compared to that exposed to chloride solutions (stated earlier in Section 5.2.2).

While comparing between composite solutions of NaCl with $MgSO_4$, and NaCl with Na_2SO_4, it is observed that the mass loss in the temperature range of 90 °C - 400 °C was higher in the concrete exposed to composite solution of NaCl with $MgSO_4$ as compared to composite solution of NaCl with Na_2SO_4 for OPC + 20% FA and PPC concrete, whereas the opposite variation was observed in case of OPC concrete as evident from Table 5.4. The higher mass loss in case of exposure to composite solution of NaCl with $MgSO_4$ for OPC + 20% FA, and PPC concrete is attributed to the dominant effect of loss of combined water due to dehydration of gypsum and calcium chloroaluminate to a higher extent as compared to the composite solution of NaCl with Na_2SO_4. This observation is consistent with the inference drawn from the XRD analysis (Section 5.2.2) wherein the peak intensity and wt. % of both gypsum and calcium chloroaluminate were higher in the concrete exposed to composite solution of NaCl with $MgSO_4$ as compared to composite solution of NaCl with Na_2SO_4 for all binders. The higher mass loss in case of exposure to composite solution of NaCl with Na_2SO_4 for OPC concrete is ascribed to the significant effect of loss of combined water due to dehydration of ettringite to a greater extent as compared to that in the concrete exposed to composite solution of NaCl with $MgSO_4$. As observed from XRD analysis, the peak intensity and wt. % of ettringite were higher in the concrete exposed

to composite solution of NaCl with Na_2SO_4 as compared to composite solution of NaCl with $MgSO_4$ for all binders.

While evaluating the effect of concentration of $MgSO_4$ or Na_2SO_4 in the exposure solution, it is inferred that the mass loss of concrete in the temperature range of 90 °C - 400 °C mostly increased with increase in concentration of $MgSO_4$ in the composite solution of NaCl with $MgSO_4$ whereas it decreased with increase in concentration of Na_2SO_4 in the composite solution of NaCl with Na_2SO_4 for OPC + 20% FA and PPC concrete as observed from Figure 5.29 to 5.31 and Table 5.4. However, in case of OPC concrete, the opposite variation was observed i.e. mass loss in the temperature range of 90 °C - 400 °C mostly decreased with increase in concentration of $MgSO_4$ in the composite solution of NaCl with $MgSO_4$ whereas it increased with increase in concentration of Na_2SO_4 in the composite solution of NaCl with Na_2SO_4. The increase in mass loss with increase in concentration of $MgSO_4$ in the exposure solution for OPC + 20% FA and PPC concrete and that with increase in concentration of Na_2SO_4 in the exposure solution for OPC concrete are attributed to the significant effect of loss of combined water due to dehydration of gypsum and calcium chloroaluminate to a greater extent. Similarly, the decrease in mass loss with increase in concentration of Na_2SO_4 in the exposure solution for OPC + 20% FA and PPC concrete and that with increase in concentration of $MgSO_4$ in the exposure solution for OPC concrete are attributed to the dominant effect of loss of combined water due to dehydration of ettringite to a lower extent. These observations are in line with the inferences drawn from the XRD analysis (stated earlier in Section 5.2.2), wherein the variations in the peak intensity and wt. % of calcium chloroaluminate, gypsum and ettringite are consistent with the variations in the extent of dehydration of calcium chloroaluminate, gypsum and ettringite with increase in concentration of $MgSO_4$ or Na_2SO_4 in the exposure solutions for different types of binder.

From Figure 5.29 to 5.31 and Table 5.4, it is observed that in the temperature range of 400 °C - 460 °C, the mass loss was mostly lower in the concrete exposed chloride (NaCl) solutions as compared to composite chloride-sulfate solutions (both NaCl + $MgSO_4$ and NaCl + Na_2SO_4). This is attributed to lower extent of dehydration of calcium hydroxide in case of exposure to chloride solutions. The lower extent of dehydration is ascribed to the presence of lower amount of calcium hydroxide as indicated by its amount estimated using Taylor's formula (Table 5.5) in the concrete exposed to chloride solutions as compared to composite chloride-sulfate solutions. This variation in mass loss due to dehydration of

calcium hydroxide is consistent with the observations from XRD analysis wherein the peak intensity and wt. % of calcium hydroxide were lower in the concrete exposed to chloride solutions as compared to that exposed to composite chloride-sulfate solutions owing to the variations in its amount present in the concrete mixes.

Table 5.5 Calcium hydroxide content (% by mass) obtained from TGA for different binders exposed to chloride and composite chloride-sulfate solutions

w/b ratio and exposure period	Exposure solution	Calcium hydroxide content (% by mass)		
		Binder type		
		OPC	OPC + 20% FA	PPC
w/b ratio = 0.55, depth interval of 20-25 mm and 21 months	1NC	4.94	2.39	0.74
	3NC	2.80	1.52	0.66
	5NC	3.74	0.33	0.49
	1NC+2MS	3.87	0.25	0.95
	1NC+4MS	4.28	1.44	0.99
	3NC+2MS	2.59	2.06	1.93
	3NC+4MS	4.48	3.29	2.10
	5NC+2MS	3.70	1.40	1.69
	5NC+4MS	4.15	1.77	1.77
	3NC+2NS	4.24	2.39	1.97
	3NC+4NS	3.41	2.67	1.60

From Table 5.4, it is noted that the mass loss in the temperature range of 400 °C - 460 °C decreased with increase in concentration of NaCl in the exposure solution in case of exposure to chloride (NaCl) solutions, which is due to the dehydration of calcium hydroxide to a lower extent as indicated by its amount estimated using Taylor's formula (Table 5.5) from TGA. The lower extent of dehydration of calcium hydroxide with increase in concentration of NaCl in the chloride solutions is substantiated by the lower peak intensity and wt. % of calcium hydroxide (from XRD analysis, Section 5.2.2) in the concrete exposed to chloride solutions with higher concentration of NaCl. Further, as observed from the XRD analysis (Section 5.2.2), the peak intensity and wt. % of calcium hydroxide (CH) mostly decreased with increase in concentration of NaCl in composite chloride-sulfate solutions. From Table 5.4, it is observed that the mass loss due to dehydration of calcium hydroxide mostly increased with increase in concentration of NaCl from 1% to 3% whereas it decreased with increase in concentration of NaCl from 3% to 5% in the concrete exposed to composite solutions of NaCl with $MgSO_4$ (2% and 4%).

From Table 5.4, it is noted that the variation in mass loss in the temperature range of 400 °C - 460 °C between composite solutions of NaCl with $MgSO_4$ and NaCl with Na_2SO_4 is not systematic. This is attributed to the effect of variations in the extent of dehydration of calcium hydroxide in concrete between different exposure solutions. It may be noted that in the depth interval of 20-25 mm, there was also unsystematic variation in the peak intensity and wt. % of calcium hydroxide (from XRD analysis, Section 5.2.2) between composite solutions of NaCl with $MgSO_4$ and NaCl with Na_2SO_4 in few cases, although the peak intensity and wt. % of calcium hydroxide were mostly higher in case of exposure to composite solutions of NaCl with Na_2SO_4 as compared to composite solutions of NaCl with $MgSO_4$ at all depth intervals. While evaluating the effect of concentration of $MgSO_4$, it is observed that the mass loss in the temperature range of 400 °C - 460 °C increased with increase in concentration of $MgSO_4$ in the composite solution of NaCl with $MgSO_4$ for all binders. This is attributed to the dehydration of calcium hydroxide to a greater extent at higher concentration of $MgSO_4$, which is consistent with the observations obtained from XRD analysis wherein the peak intensity and wt. % of calcium hydroxide increased with increase in concentration of $MgSO_4$ in the composite solution of NaCl with $MgSO_4$ (Section 5.2.2). In case of exposure to composite solutions of NaCl with Na_2SO_4, it is observed that the mass loss in the temperature range of 400 °C - 460 °C decreased in OPC and PPC concrete whereas it increased in OPC + 20% FA concrete with increase in concentration of Na_2SO_4 in the composite solution of NaCl with Na_2SO_4 (Table 5.4), which indicates alterations in the extent of dehydration of calcium hydroxide among different types of binder. As stated earlier in Section 5.2.2, the variation in peak intensity and wt. % of calcium hydroxide (from XRD analysis) was mostly unsystematic with increase in concentration of Na_2SO_4 in the composite solution of NaCl with Na_2SO_4 for all binders. Overall, it is inferred that the mass loss of concrete due to departure of combined water i.e. mass loss in the temperature range of 90 °C to 460 °C is mostly higher in the concrete exposed to composite chloride-sulfate solutions (both $MgSO_4$ and Na_2SO_4) as compared to chloride solutions as observed from Table 5.4. This is attributed to the significant effect of dehydration of ettringite and calcium hydroxide to a greater extent in the concrete exposed to composite chloride-sulfate solutions as compared to chloride solutions.

From Figure 5.29 to 5.31 and Table 5.4, it is observed that there is no systematic variation in mass loss in the temperature range of 460°C - 950°C among exposure solutions (chloride and composite chloride-sulfate solutions). Further, the variations in mass loss with increase

in concentration of NaCl in chloride as well as in composite chloride-sulfate solutions, and that with increase in concentration of Na_2SO_4 in composite solution of NaCl with Na_2SO_4 were also not systematic. In addition, it is inferred that the mass loss in the temperature range of 460 °C - 950 °C mostly decreased in OPC and OPC + 20% FA concrete whereas it increased in PPC concrete with increase in concentration of $MgSO_4$ in composite solution of NaCl with $MgSO_4$. This may be attributed to the alterations in the extent of dehydration of magnesium silicate hydrate (M-S-H) with increase in concentration of $MgSO_4$ in composite solution of NaCl with $MgSO_4$ among different binders, in addition to the decarbonation of calcium carbonate. As mentioned earlier, the mass loss in the temperature of 573 °C - 600 °C was due to dehydration of magnesium silicate hydrate (M-S-H) in the concrete exposed to composite solutions of NaCl with $MgSO_4$. From Table 5.4, it is observed that the variation in total mass loss of concrete is mostly unsystematic with respect to exposure solution.

5.3.3. Variations in decomposition of compounds with binder type and w/b ratio

In addition to the plots presented in Figure 5.29 to 5.31, typical plots of TGA and DTG curves obtained for different binders and w/b ratios are shown in Figure 5.32 to 5.34. The mass loss in different temperature ranges and wt. % of calcium hydroxide estimated using Taylor's formula for different binders are already presented in Table 5.4 and Table 5.5 respectively. Further, the mass loss corresponding to different temperature ranges and wt. % of calcium hydroxide estimated using Taylor's formula for different w/b ratios are presented in Table 5.6 and Table 5.7 respectively. These results of TGA for different binders and w/b ratios correspond to the concrete powder samples collected from the depth interval of 20-25 mm from the exposure surface of concrete.

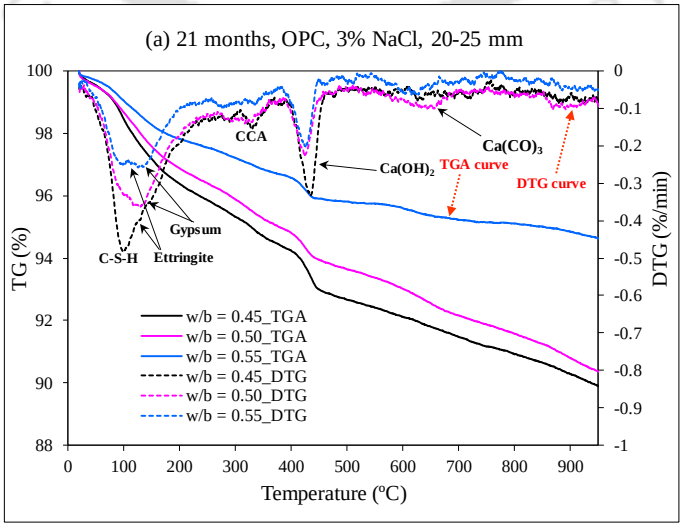

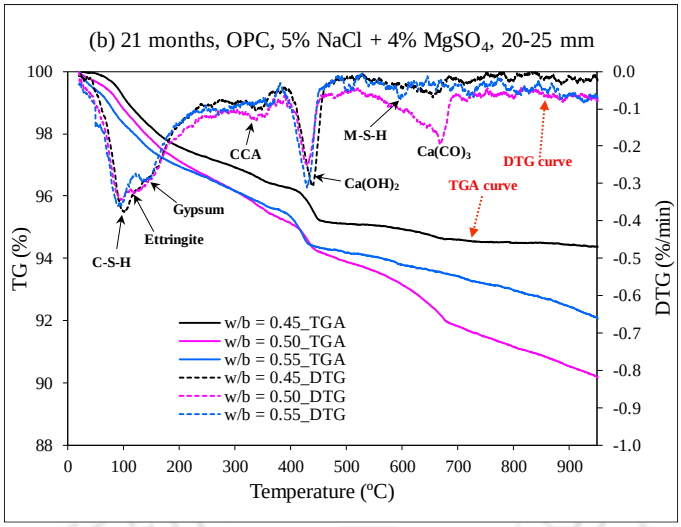

Figure 5.32 TGA and DTG curves at depth interval of 20-25 mm from exposure surface of concrete made with OPC at different w/b ratios, and exposure period of 21 months: (a) 3% NaCl solution and (b) 5% NaCl + 4% $MgSO_4$ solution

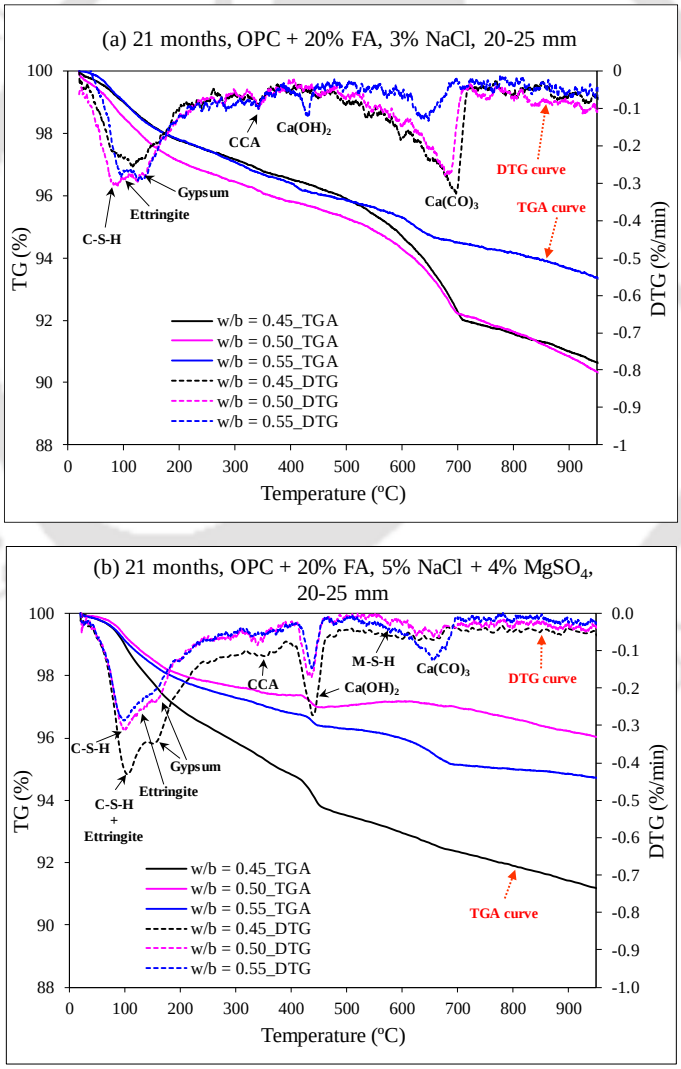

Figure 5.33 TGA and DTG curves at depth interval of 20-25 mm from exposure surface of concrete made with OPC + 20% FA at different w/b ratios, and exposure period of 21 months: (a) 3% NaCl solution and (b) 5% NaCl + 4% $MgSO_4$ solution

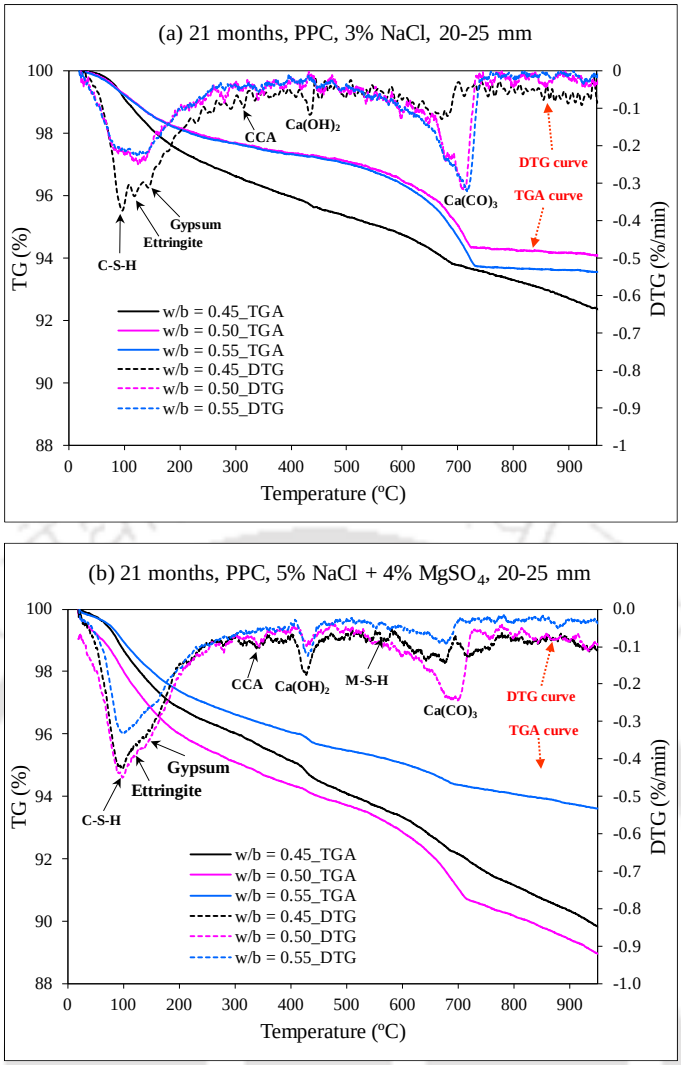

Figure 5.34 TGA and DTG curves at depth interval of 20-25 mm from exposure surface of concrete made with PPC at different w/b ratios, and exposure period of 21 months: (a) 3% NaCl solution and (b) 5% NaCl + 4% $MgSO_4$ solution

From Figure 5.29 to 5.34, Table 5.4, and Table 5.6, it is observed that in the temperature range of ambient to 90 °C, the mass loss was mostly higher in the concrete made with OPC as compared to that made with OPC + 20% FA followed by PPC for all exposure solutions. This may be attributed to the loss of free water from hydrated cement phases to a higher extent in the concrete made with OPC as compared to OPC + 20% FA and PPC as a result of possibly higher amount of absorption of water by the hydrated cement phases in OPC concrete as compared to OPC + 20% FA and PPC concrete during the wetting-drying process of exposure. In the temperature range of 90 °C - 400 °C, the mass loss was mostly higher in the concrete made with OPC as compared to that made with OPC + 20% FA followed by PPC for all exposure solutions as observed from Figure 5.29 to 5.34, Table 5.4, and Table 5.6.

Table 5.6 Mass loss (%) obtained from TGA at various temperature ranges for different w/b ratios for exposure period of 21 months

Binder type and exposure solution	w/b ratio	Mass loss (%)				Total mass loss (%) (ambient to 950 °C)
		Ambient to 90 °C	90-400 °C	400-460 °C	460-950 °C	
OPC, 3% NaCl solution and depth interval of 20-25 mm	0.45	1.22	4.54	1.34	2.98	10.09
	0.50	1.13	4.07	0.94	3.50	9.63
	0.55	0.79	2.64	0.68	1.25	5.37
OPC, 5% NaCl + 4% $MgSO_4$ solution, and depth interval of 20-25 mm	0.45	0.56	3.20	1.06	0.81	5.63
	0.50	0.98	3.91	0.97	3.95	9.81
	0.55	1.49	3.18	1.01	2.23	7.91
OPC + 20% FA, 3% NaCl solution and depth interval of 20-25 mm	0.45	0.88	2.61	0.34	5.53	9.35
	0.50	1.31	2.89	0.30	5.17	9.66
	0.55	0.82	2.79	0.37	2.66	6.64
OPC + 20% FA, 5% NaCl + 4% $MgSO_4$ solution and depth interval of 20-25 mm	0.45	0.71	4.47	1.09	2.56	8.83
	0.50	0.51	2.12	0.39	0.94	3.96
	0.55	0.67	2.53	0.43	1.64	5.28
PPC, 3% NaCl solution and depth interval of 20-25 mm	0.45	0.63	3.40	0.45	3.16	7.63
	0.50	0.62	2.02	0.13	3.14	5.92
	0.55	0.63	2.04	0.16	3.61	6.44
PPC, 5% NaCl + 4% $MgSO_4$ solution and depth interval of 20-25 mm	0.45	1.03	3.84	0.72	4.58	10.17
	0.50	1.68	3.95	0.43	4.97	11.03
	0.55	0.80	3.15	0.43	2.01	6.39

Table 5.7 Calcium hydroxide content (% by mass) obtained from TGA for different w/b ratios for exposure period of 21 months

Binder type and exposure solution	Calcium hydroxide content (% by mass)		
	w/b ratio		
	0.45	0.5	0.55
OPC, 3% NaCl solution and depth interval of 20-25 mm	5.53	3.85	2.81
OPC, 5% NaCl + 4% $MgSO_4$ solution and depth interval of 20-25 mm	4.36	3.98	4.14
OPC + 20% FA, 3% NaCl solution and depth interval of 20-25 mm	1.41	1.23	1.52
OPC + 20% FA, 5% NaCl + 4% $MgSO_4$ solution and depth interval of 20-25 mm	4.50	1.61	1.78
PPC, 3% NaCl solution and depth interval of 20-25 mm	1.84	0.55	0.67
PPC, 5% NaCl + 4% $MgSO_4$ solution and depth interval of 20-25 mm	2.98	1.76	1.78

For chloride (NaCl) solutions, the higher mass loss in OPC concrete as compared to OPC + 20% FA followed by PPC concrete may be attributed to the dominant effect of loss of combined water due to dehydration of calcium chloroaluminate to a greater extent in OPC concrete. This observation is consistent with the inference drawn from XRD analysis wherein the peak intensity and wt. % of calcium chloroaluminate were higher in the OPC concrete as compared to OPC + 20% FA followed by PPC concrete at higher depth intervals from exposure surface (Section 5.2.3). As mentioned earlier, the mass loss values presented in Table 5.4 and Table 5.6 correspond to the concrete powder samples collected from the depth interval of 20-25 mm from the exposure surface of concrete. For composite chloride-sulfate solutions (NaCl with $MgSO_4$ and NaCl with Na_2SO_4), the higher mass loss in the temperature range of 90 °C - 400 °C in OPC concrete may be ascribed to the dominant effect of dehydration of calcium chloroaluminate and ettringite to a higher extent in OPC as compared to OPC + 20% FA followed by PPC concrete, which is mostly in line with the variations in the peak intensity and wt. % of calcium chloroaluminate and ettringite obtained from the XRD analysis (stated earlier in Section 5.2.3) for different types of binder.

From Table 5.4 and Table 5.6, it is observed that the mass loss in the temperature range of 400 °C - 460 °C was higher in the concrete made with OPC as compared to that made with OPC + 20% FA and PPC for all exposure solutions. This is attributed to the effect of dehydration of calcium hydroxide to a greater extent in OPC concrete as compared to OPC + 20% FA and PPC concrete as indicated by the amount of calcium hydroxide (%) estimated using Taylor's formula (Table 5.5 and Table 5.7) from TGA. This observation substantiates the results of XRD analysis wherein the peak intensity and wt. % of calcium hydroxide were higher in OPC concrete as compared to OPC + 20% FA and PPC concrete for all exposure solutions. The mass loss due to departure of combined water (i.e. mass loss in the temperature range of 90 °C to 460 °C) is mostly higher in OPC concrete as compared to OPC + 20% FA followed by PPC concrete for all exposure solutions as evident from Table 5.4 and Table 5.6. Further from Figure 5.29 to 5.34, Table 5.4, and Table 5.6, it is observed that the variations in mass loss in the temperature range of 460 °C - 950 °C is not systematic with binder type for different exposure solutions. From Table 5.4 and Table 5.6, it is observed that the total mass loss was mostly higher in OPC concrete as compared to OPC + 20% FA and PPC concrete.

From Figure 5.32 to 5.34 and Table 5.6, it is observed that the variation in mass loss in the temperature range of ambient to 90 °C is not systematic with w/b ratio, which may be ascribed to the effect of alterations in the extent of loss of free water from the hydrated cement phases in concrete with change in w/b ratio. Further from Figure 5.32 to 5.34 and Table 5.6, it inferred that the mass loss in the temperature range of 90 °C - 400 °C is mostly higher at lower w/b ratio (0.45 and 0.50) as compared that at higher w/b ratio (0.55) for different binders and exposure solutions. Between w/b ratios of 0.45 and 0.50, the mass loss was mostly higher at w/b ratio of 0.45 as compared to that at w/b ratio of 0.50 with opposite variation in some cases, however the increase in mass loss at w/b ratio of 0.45 with respect to w/b ratio of 0.50 was significantly higher. From the XRD analysis (Section 5.2.3), it was observed that peak intensity and wt. % of ettringite increased with increase in w/b ratio, and there was unsystematic variation in the peak intensity and wt. % of gypsum with change in w/b ratio. Further, the peak intensity and wt. % of calcium chloroaluminate were higher at w/b ratio of 0.50 as compared to w/b ratio of 0.45 followed by w/b ratio of 0.55. These observations indicate the variations in the extent of formation of ettringite, gypsum and calcium chloroaluminate in concrete with change in w/b ratio. Thus, the variations in mass loss of concrete in the temperature range of 90 °C - 400 °C with change in w/b ratio may be attributed to the combined effect of variations in the departure of combined water as a result of alterations in the extent of dehydration of ettringite, gypsum and calcium chloroaluminate in concrete with change in w/b ratio. From Table 5.6, it is observed that in the temperature range of 400 °C - 460 °C, the mass loss due to dehydration of calcium hydroxide was mostly higher at w/b ratio of 0.45 as compared to w/b ratio of 0.55 followed by w/b ratio 0.50. From the XRD analysis (Section 5.2.3), it was observed that peak intensity and wt. % of calcium hydroxide were mostly higher at with w/b ratio of 0.50 with minor difference in its peak intensity and wt. % between w/b ratios of 0.45 and 0.55. Thus, the variation in mass loss due to dehydration of calcium hydroxide with change in w/b ratio is mostly not in line with the variations in the peak intensity and wt. % of calcium hydroxide obtained from the XRD analysis for different w/b ratios. Further from Table 5.6, it is inferred that there is no systematic variation in mass loss of concrete due to decarbonation of calcium carbonate (calcite) in the temperature range of 460 °C - 950 °C with change in w/b ratio. From Table 5.6, it is observed that the variation in total mass loss of concrete is not systematic with w/b ratio.

5.4. Summary

From the microstructure study, the obtained results of XRD analysis indicated that the peak intensity and wt. % of calcium hydroxide (CH) in concrete were lower near the exposure surface and increased with increase in depth from the exposure surface of concrete exposed to chloride and composite chloride-sulfate solutions. The formation of calcium hydroxide in concrete was also observed from the obtained FESEM images. There was no systematic variation in the formation of ettringite (E) with increase in depth from exposure surface of concrete as indicated by its peak intensity and wt. % obtained from the XRD analysis. The peak intensity and wt. % of ettringite (E) in concrete were mostly higher in the depth interval of 10-15 mm followed by 15-20 mm and 5-10 mm as compared to other depth intervals for all binders, exposure solutions and exposure periods. The peak intensity and wt. % of gypsum (G) were not systematic with increase in depth from the exposure surface of concrete for all binders, exposure solutions and exposure periods. The peaks of thaumasite (T) in the XRD patterns were observed at lower depth intervals i.e. till 10 mm from the exposure surface of concrete exposed to composite chloride-sulfate solutions. The formation of thaumasite in concrete near the surface region is also attributed to the presence of calcium carbonate in higher amount in the surface region as indicated by the XRD patterns wherein the peak intensity and wt. % of calcite (CC) were higher in the depth interval of 0-5 mm from the exposure surface as compared to other depth intervals. Further there was unsystematic variation as well as minor difference in peak intensity and wt. % of calcium chloroaluminate (CCA) among different depth intervals for all binders, exposure solutions and exposure periods. However, in majority of the cases, the peak intensity and wt. % of CCA were slightly higher at lower depth intervals (i.e. till 10 mm from the surface) than that at higher depth intervals. The formation of calcium chloroaluminate in concrete was also substantiated from the obtained FESEM images.

While analyzing the effect of exposure solution on microstructure of concrete, it was observed that the formation of ettringite (E) was mostly higher in the concrete exposed to composite solutions of NaCl with Na_2SO_4 as compared to composite solutions of NaCl with $MgSO_4$ followed by NaCl solutions for all concentrations of NaCl, $MgSO_4$ and Na_2SO_4 as indicated by the peak intensity and wt. % of ettringite obtained from XRD analysis. This variation in the formation of ettringite in concrete with exposure solution was also observed from the obtained FESEM images. Further, the peak intensity and wt. % of ettringite mostly decreased with increase in concentration of NaCl in both chloride as well as composite

chloride-sulfate solutions and with increase in concentration of $MgSO_4$ and Na_2SO_4 in the composite chloride-sulfate solutions. Among exposure solutions, the formation of calcium chloroaluminate (CCA) was mostly higher in the concrete exposed to NaCl solutions as compared to composite solutions of NaCl with $MgSO_4$ followed by composite solutions of NaCl with Na_2SO_4 for all concentrations of NaCl, $MgSO_4$ and Na_2SO_4 as indicated by the peak intensity and wt. % of CCA. Further, the peak intensity and wt. % of CCA mostly increased with increase in concentration of NaCl in chloride as well as composite chloride-sulfate solutions and with increase in concentration of $MgSO_4$ and Na_2SO_4 in composite chloride-sulfate solutions. The obtained XRD patterns indicated the formation of magnesium hydroxide (MH) in the concrete exposed to composite solution of NaCl with $MgSO_4$, which was also evident from the obtained FESEM images. In addition, the formation of M-S-H (magnesium silicate hydrate) gel in the concrete exposed to composite solutions of NaCl with $MgSO_4$ was evident from the obtained FESEM images. Among exposure solutions, the amount of calcium hydroxide (CH) was mostly higher in the concrete exposed to composite solutions of NaCl with Na_2SO_4 as compared to composite solutions of NaCl with $MgSO_4$ followed by NaCl solutions at all depth intervals for all binders and all concentrations of NaCl, $MgSO_4$ and Na_2SO_4 as indicated by the peak intensity and wt. % of calcium hydroxide obtained from the XRD analysis. Further, the peak intensity and wt. % of calcium hydroxide mostly decreased with increase in concentration of NaCl in both chloride and composite chloride-sulfate solutions for all binders, which may be attributed to the leaching of calcium hydroxide to a greater extent due to presence of more amount of chloride ions in the concrete exposed to solutions with higher concentration of NaCl. The peak intensity and wt. % of calcium hydroxide mostly increased with increase in concentration of $MgSO_4$ whereas there was no systematic variation in its peak intensity and wt. % with increase in concentration of Na_2SO_4 in the respective composite chloride-sulfate solutions for all binders. The obtained XRD results indicated that the peak intensity and wt. % of gypsum were mostly higher in the concrete exposed to composite solutions of NaCl with $MgSO_4$ as compared to NaCl solutions followed by composite solutions of NaCl with Na_2SO_4 for all concentrations of NaCl, $MgSO_4$ and Na_2SO_4. Further, there was no systematic variation in peak intensity and wt. % of gypsum in concrete with increase in concentration of NaCl in chloride and composite chloride-sulfate solutions, whereas the peak intensity and wt. % of gypsum mostly increased with increase in concentration of $MgSO_4$ and Na_2SO_4 in the composite chloride-

sulfate solutions. The presence of gypsum in concrete was also observed from the obtained FESEM images.

While evaluating the effect of binder type on microstructure of concrete, it was observed that the formation of calcium chloroaluminate (CCA) was mostly higher in the concrete made with OPC + 20% FA as compared to PPC followed by OPC at lower depth intervals (i.e. till 10 mm from the exposure surface) whereas at higher depth intervals (i.e. beyond 10 mm from the exposure surface), the formation of CCA was mostly higher in OPC concrete as compared to OPC + 20% FA followed by PPC concrete for chloride and composite chloride-sulfate solutions as indicated by the peak intensity and wt. % of CCA obtained from the XRD analysis. Further the results of XRD analysis indicated that the peak intensity and wt. % of ettringite (E) were lower in OPC concrete as compared to OPC + 20% FA followed by PPC concrete in case of exposure to chloride solutions at all depth intervals. However, with respect to binder type, the formation of ettringite as observed from XRD analysis varied with depth interval from exposure surface of concrete in case of exposure to composite solutions of NaCl with $MgSO_4$ whereas in case of exposure to composite solutions of NaCl with Na_2SO_4, the peak intensity and wt. % of ettringite were higher in PPC as compared to OPC followed by OPC + 20% FA concrete at all depth intervals. Further, the amount of calcium hydroxide (CH) was lower in OPC + 20% FA and PPC as compared to OPC concrete at all depth intervals in case of exposure to composite chloride-sulfate solutions, and at higher depth intervals in case of exposure to chloride solutions as indicated by the results of XRD analysis. The formation of compacted microstructure due to production of more amount of C-S-H gel in OPC + 20% FA and PPC concrete as compared to that in OPC concrete was observed from the FESEM images. In case of exposure to NaCl solutions, the peak intensity and wt. % of gypsum (G) were lower in PPC as compared to that in OPC and OPC + 20% FA concrete, however, the variation in peak intensity and wt. % of gypsum in concrete was unsystematic as well as very less with respect to binder type in case of exposure to composite chloride-sulfate solutions at all depth intervals. The formation of magnesium hydroxide (brucite) was mostly higher in the concrete made with OPC as compared to OPC + 20% FA followed by PPC in case of exposure to composite solutions of NaCl with $MgSO_4$ as indicated by the results of XRD analysis. Further, the formation of ettringite, calcium chloroaluminate, calcium hydroxide, and gypsum in the concrete exposed to chloride and composite chloride-sulfate solutions varied with w/b ratio as indicated by the results of XRD analysis.

From thermo-gravimetry analysis (TGA), the mass loss of concrete associated with the decomposition of various compounds in different temperature ranges were obtained for different depth intervals, exposure solutions, binders, and w/b ratios. From the obtained results of TGA, it was observed that the total mass loss of concrete was higher in the depth interval of 0-5 mm from the exposure surface as compared to other depth intervals for chloride and composite chloride-sulfate solutions. Further, the mass loss of concrete due to departure of combined water was mostly higher in the concrete exposed to composite chloride-sulfate (both cations i.e. Mg^{2+} and Na^{+}) solutions as compared to chloride solutions. Similarly, the mass loss due to departure of combined water was mostly higher in OPC concrete as compared to OPC + 20% FA followed by PPC concrete for all exposure solutions. The total mass loss was mostly higher in the concrete made with OPC as compared to that made with OPC + 20% FA and PPC. However, there was no systematic variation in total mass loss of concrete with respect to exposure solution, and w/b ratio. Further, the variations in mass loss of concrete, obtained from TGA, in different temperature ranges due to dehydration of calcium hydroxide, ettringite, calcium chloroaluminate, and gypsum were mostly consistent with the variations in the peak intensity and wt. % of these compounds obtained from XRD analysis for different binders and exposure solutions.

CHAPTER 6

CORROSION OF STEEL REINFORCEMENT AND DEVELOPMENT OF EMPIRICAL RELATIONSHIPS BETWEEN DURABILITY PARAMETERS OF CONCRETE EXPOSED TO CHLORIDE AND COMPOSITE CHLORIDE-SULFATE SOLUTIONS

6.1. General

In this chapter, the results obtained from corrosion tests conducted on prismatic reinforced concrete specimens made with OPC, OPC + 20% FA and PPC, and w/b ratios of 0.45, 0.50 and 0.55 are presented. The prismatic specimens were exposed to chloride and composite chloride-sulfate solutions till the exposure period of 27 months. The corrosion behaviour of reinforcing steel bar in concrete was evaluated by determining the half-cell potential, and corrosion current density (by LPR measurement). With respect to the exposure period, the variations in corrosion parameters i.e. half-cell potential and corrosion current density were obtained wherein the early exposure period refers to the exposure of prismatic specimens to different exposure solutions till 15 months from the start of exposure and the later exposure period refers to the exposure of specimens to the solutions thereafter (i.e. after 15 months). From the obtained results of half-cell potential, and corrosion current density, the effect of exposure solution, binder type, and w/b ratio on corrosion behaviour of steel reinforcement in concrete were evaluated for different exposure periods. Further, the empirical relationship between the obtained corrosion parameters i.e. between half-cell potential (E_0) and corrosion current density (I_{corr}), and that between apparent chloride diffusion coefficient (D) and corrosion current density (I_{corr}), and between rebar surface chloride concentration (C_{rs}) and corrosion current density (I_{corr}) were established.

6.2. Half-cell potential of steel reinforcement in concrete

The half-cell potential measurement was carried out for determining the probability of occurrence of steel reinforcement corrosion in concrete. As already mentioned in Chapter 3, the half-cell potential of steel reinforcement embedded in prismatic specimens was measured at the start of wetting period (of wetting-drying cycle) at every 3-month interval. The reported half-cell potential values at different testing ages of exposure periods are the average values of replicate prismatic specimens.

6.2.1. Effect of exposure solution and cation type associated with sulfate ions on half-cell potential

As already stated in Chapter 3, to evaluate the effect of chloride and composite chloride-sulfate ions on half-cell potential of steel reinforcement in concrete, the prismatic reinforced concrete specimens were exposed to different exposure solutions containing sodium chloride (1%, 3% and 5%) and combination of sodium chloride with magnesium sulfate (2% and 4%) or sodium sulfate (2% and 4%) for different exposure periods. The obtained half-cell potential values of steel reinforcement were plotted for chloride solutions, and composite chloride-sulfate solutions against exposure duration as shown in Figure 6.1 to Figure 6.9.

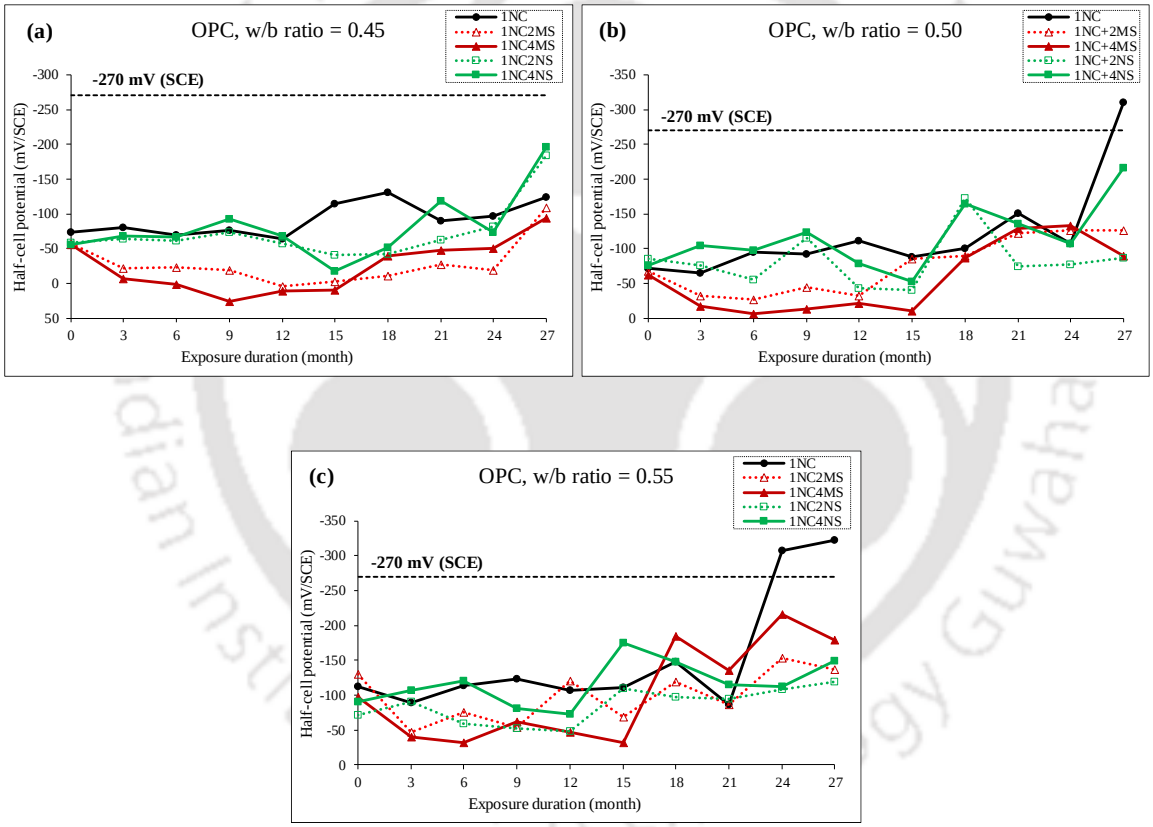

1NC: 1% NaCl, **1NC+2MS:** 1% NaCl + 2% $MgSO_4$, **1NC+4MS:** 1% NaCl + 4% $MgSO_4$
1NC+2NS: 1% NaCl + 2% Na_2SO_4, **1NC+4NS:** 1% NaCl + 4% Na_2SO_4

Figure 6.1 Half-cell potential (E_0) of steel bar in concrete made with OPC and exposed to 1% NaCl and respective composite chloride-sulfate solutions: (a) w/b ratio = 0.45, (b) w/b ratio = 0.50, and (c) w/b ratio = 0.55

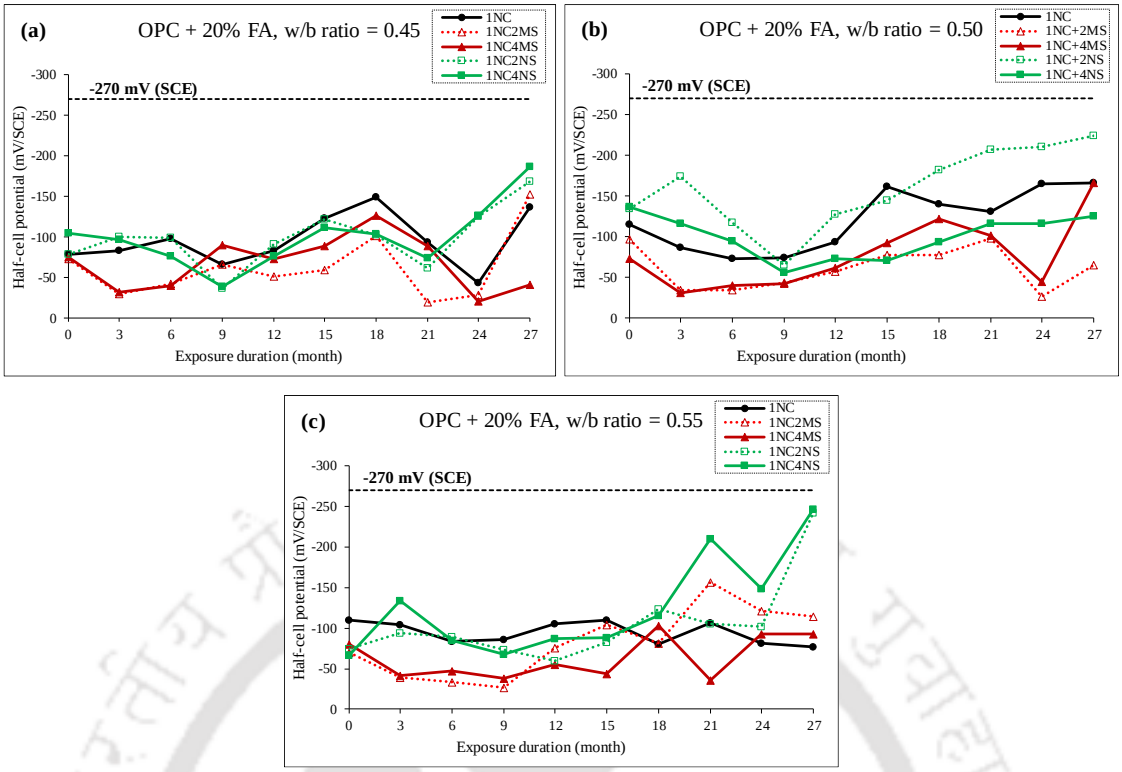

Figure 6.2 Half-cell potential (E_0) of steel bar in concrete made with OPC + 20% FA and exposed to 1% NaCl and respective composite chloride-sulfate solutions: (a) w/b ratio = 0.45, (b) w/b ratio = 0.50, and (c) w/b ratio = 0.55

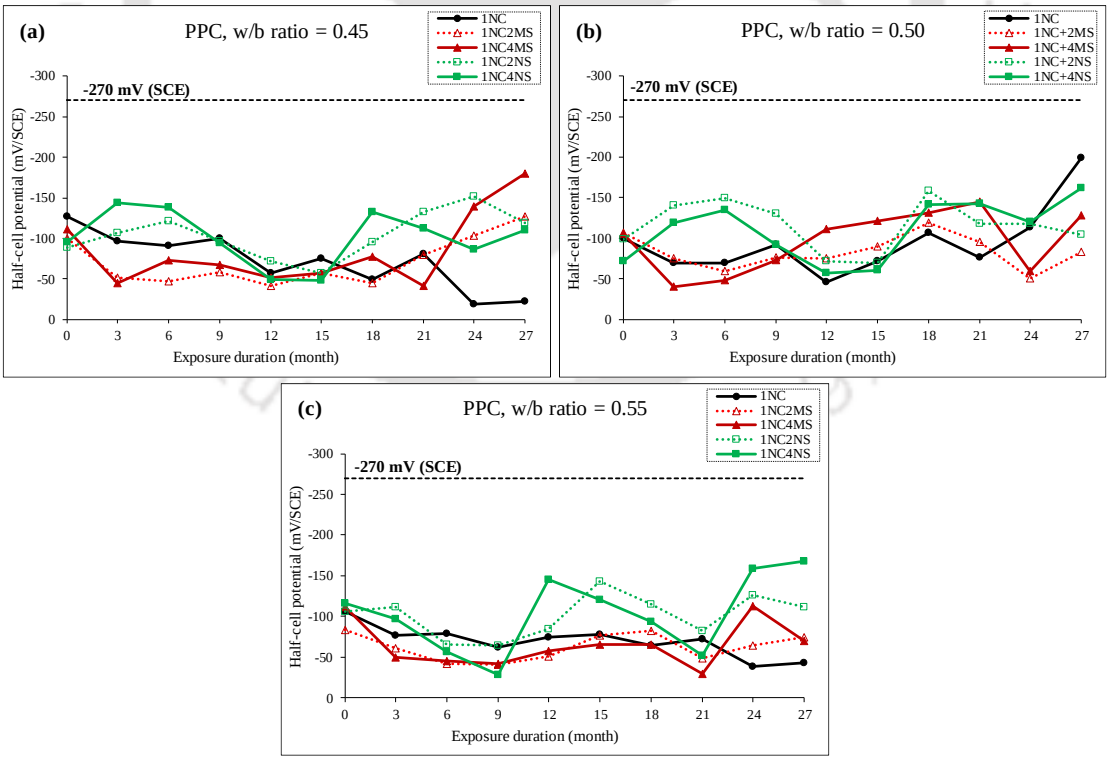

Figure 6.3 Half-cell potential (E_0) of steel bar in concrete made with PPC and exposed to 1% NaCl and respective composite chloride-sulfate solutions: (a) w/b ratio = 0.45, (b) w/b ratio = 0.50, and (c) w/b ratio = 0.55

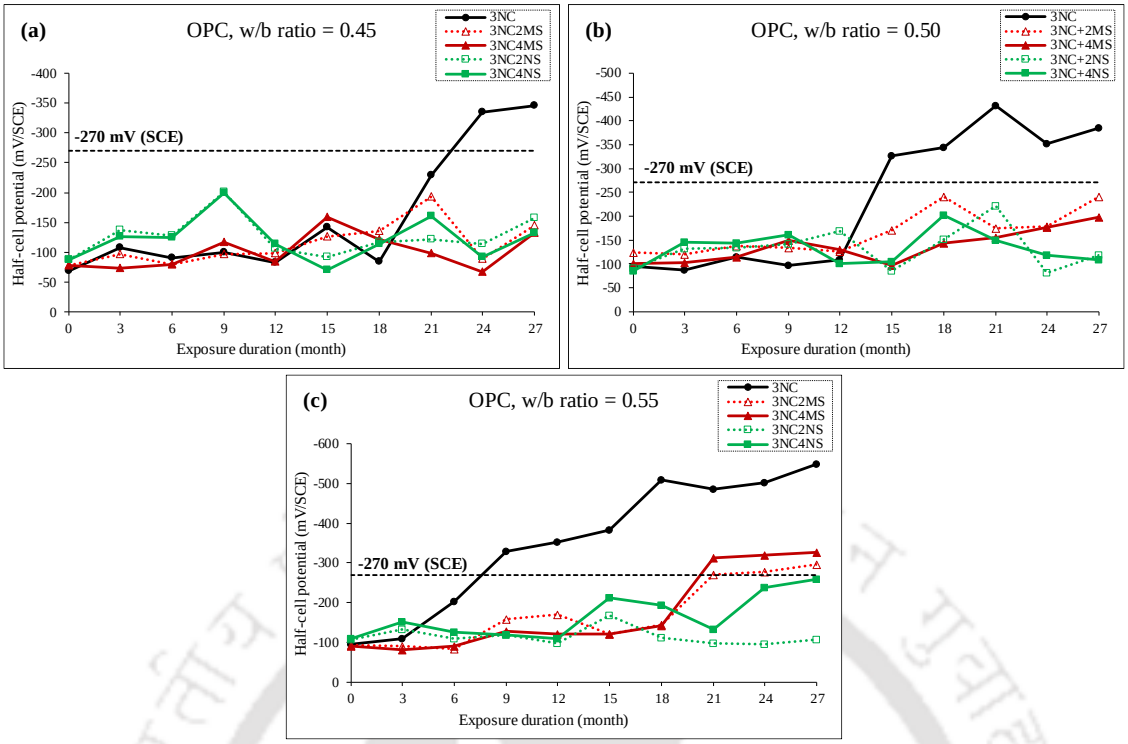

3NC: 3% NaCl, **3NC+2MS:** 3% NaCl + 2% $MgSO_4$, **3NC+4MS:** 3% NaCl + 4% $MgSO_4$
3NC+2NS: 3% NaCl + 2% Na_2SO_4, **3NC+4NS:** 3% NaCl + 4% Na_2SO_4

Figure 6.4 Half-cell potential (E_0) of steel bar in concrete made with OPC and exposed to 3% NaCl and respective composite chloride-sulfate solutions: (a) w/b ratio = 0.45, (b) w/b ratio = 0.50, and (c) w/b ratio = 0.55

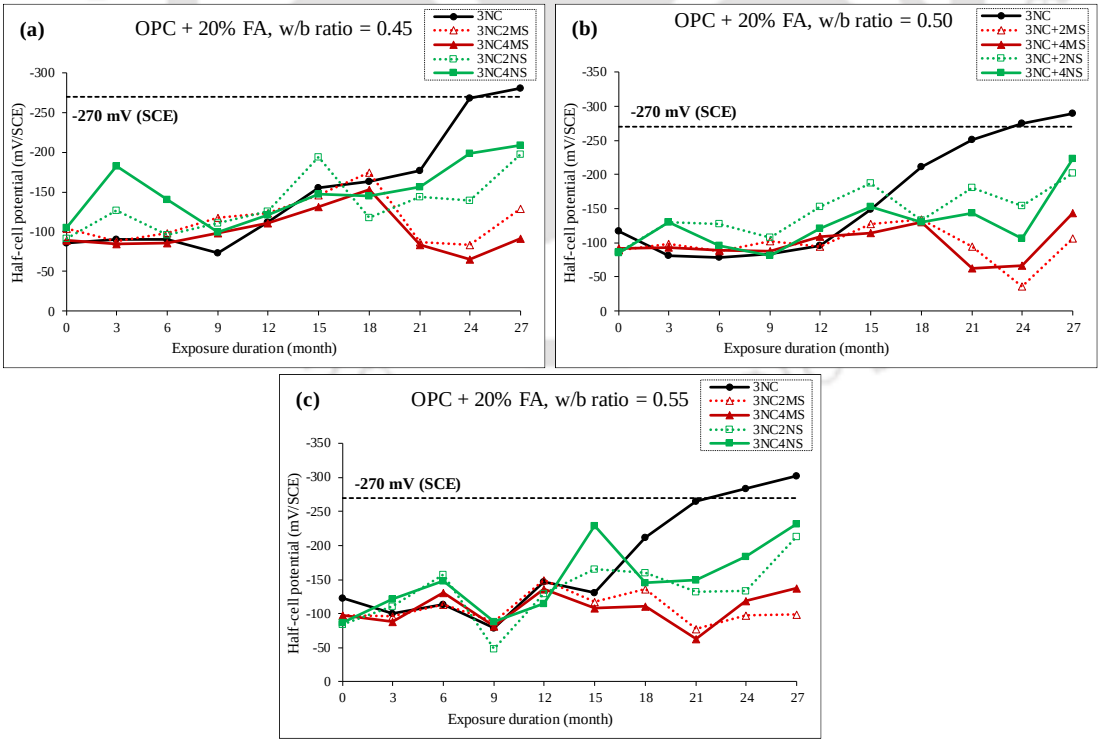

Figure 6.5 Half-cell potential (E_0) of steel bar in concrete made with OPC + 20% FA and exposed to 3% NaCl and respective composite chloride-sulfate solutions: (a) w/b ratio = 0.45, (b) w/b ratio = 0.50, and (c) w/b ratio = 0.55

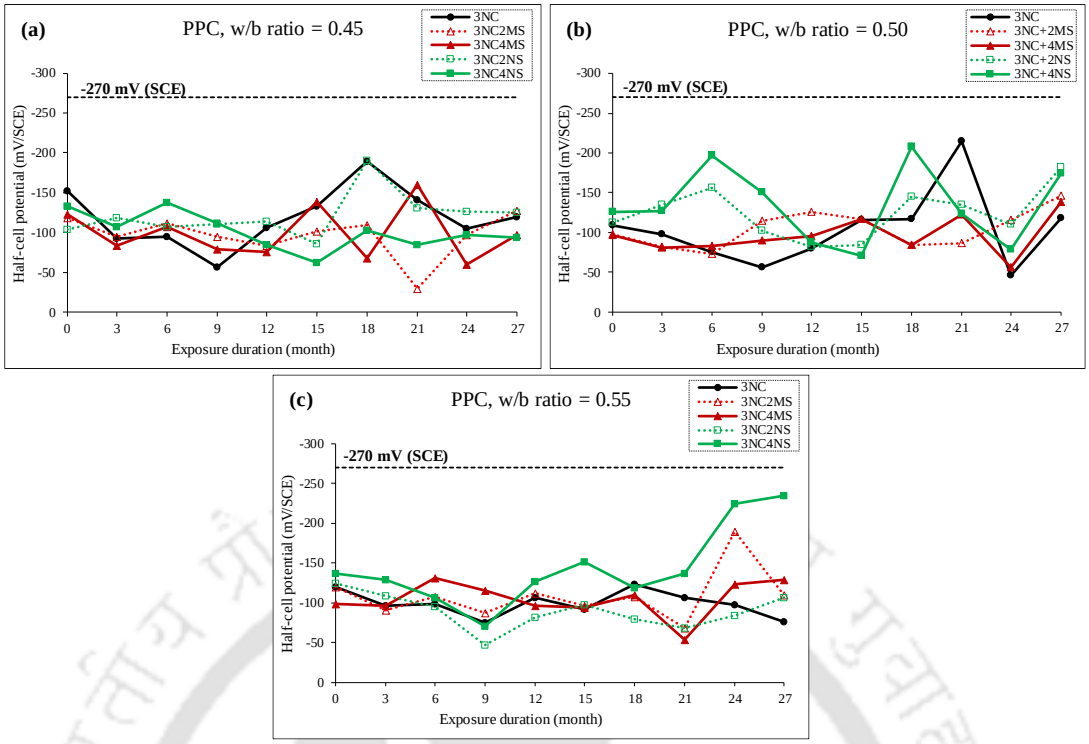

Figure 6.6 Half-cell potential (E_0) of steel bar in concrete made with PPC and exposed to 3% NaCl and respective composite chloride-sulfate solutions: (a) w/b ratio = 0.45, (b) w/b ratio = 0.50, and (c) w/b ratio = 0.55

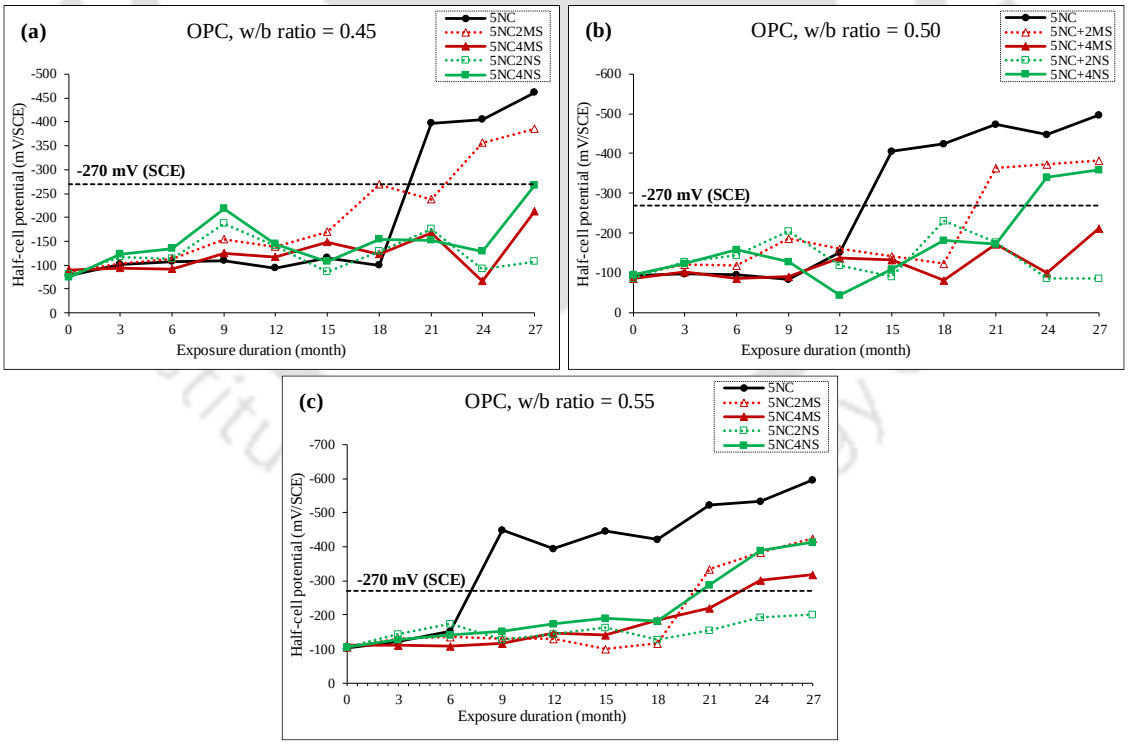

5NC: 5% NaCl, **5NC+2MS:** 5% NaCl + 2% $MgSO_4$, **5NC+4MS:** 5% NaCl + 4% $MgSO_4$
5NC+2NS: 5% NaCl + 2% Na_2SO_4, **5NC+4NS:** 5% NaCl + 4% Na_2SO_4

Figure 6.7 Half-cell potential (E_0) of steel bar in concrete made with OPC and exposed to 5% NaCl and respective composite chloride-sulfate solutions: (a) w/b ratio = 0.45, (b) w/b ratio = 0.50, and (c) w/b ratio = 0.55

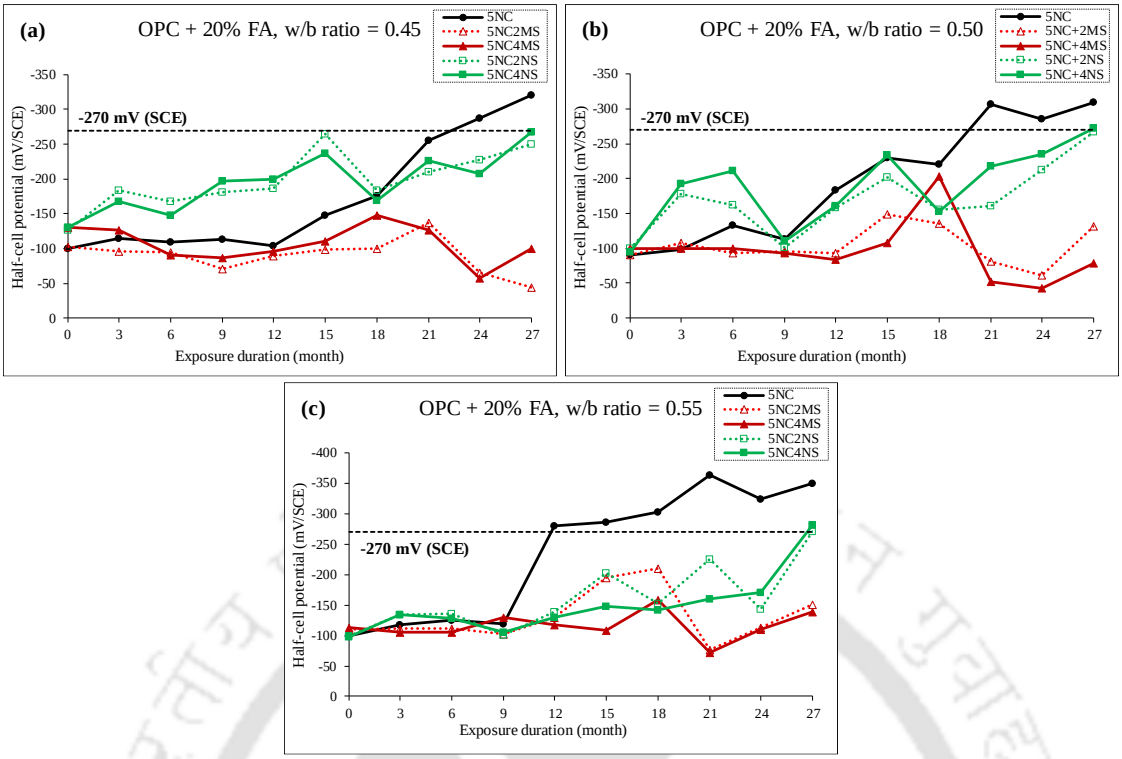

Figure 6.8 Half-cell potential (E_0) of steel bar in concrete made with OPC + 20% FA and exposed to 5% NaCl and respective composite chloride-sulfate solutions: (a) w/b ratio = 0.45, (b) w/b ratio = 0.50, and (c) w/b ratio = 0.55

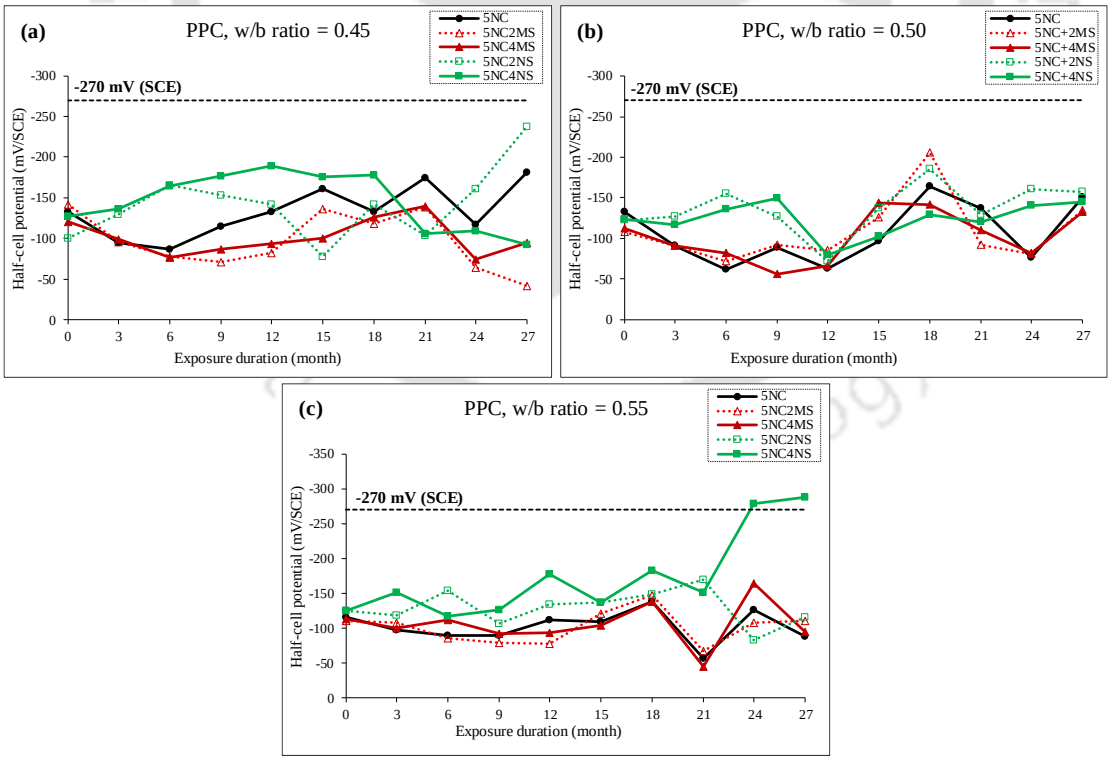

Figure 6.9 Half-cell potential (E_0) of steel bar in concrete made with PPC and exposed to 5% NaCl and respective composite chloride-sulfate solutions: (a) w/b ratio = 0.45, (b) w/b ratio = 0.50, and (c) w/b ratio = 0.55

From Figure 6.1 to 6.9, it is observed that the half-cell potential values of steel bar were mostly more negative in the prismatic reinforced concrete specimens exposed to higher concentration of sodium chloride than those exposed to lower concentration of sodium chloride in chloride as well as in composite chloride-sulfate solutions (irrespective of cation type associated with sulfate ions) for all binders and w/b ratios during the entire exposure period till 27 months. In other words, the more negative potential values were observed in the specimens exposed to 5% NaCl as compared to 3% NaCl followed by 1% NaCl in the exposure solutions. The more negative potential in the specimens exposed to solutions of higher concentration of NaCl may be ascribed to the diffusion of chloride ions in more amount to the rebar level as a result of higher concentration gradient of chloride ions. Further from Figure 6.1 to 6.9, it is inferred that the half-cell potential of steel reinforcement was less negative during the early exposure period whereas it was more negative during the later exposure period for both chloride and composite chloride-sulfate solutions.

Figure 6.1 to Figure 6.3, it is observed that for both chloride and composite chloride-sulfate solutions the half-cell potential values were mostly less negative than -350 mV ($Cu/CuSO_4$ electrode)/ -270 mV (SCE) in all the specimens except in few cases (i.e. for OPC, w/c ratio of 0.50, after 24 months, and OPC, w/c ratio of 0.55, after 21 months) at 1% NaCl concentration in the exposure solution till the exposure period of 27 months. This indicates less than 90% probability of occurrence of steel reinforcement corrosion in concrete as per ASTM C876 [41]. Further, the specimens exposed to composite solutions of 1% NaCl with $MgSO_4$ (both concentrations i.e. 2% and 4%) mostly showed less negative half-cell potential values as compared to 1% NaCl solution for OPC and OPC + 20% FA concrete at all w/b ratios till the exposure period of 27 months (i.e. at all exposure periods till 27 months) as evident from Figure 6.1 and Figure 6.2. The less negative potential value in the specimens exposed to composite solutions of NaCl with $MgSO_4$ is attributed to the availability of lower free chloride content near the rebar level. As already mentioned in Section 4.3.1.2 (Chapter 4), the measured free chloride content was lower at rebar level (i.e. in the depth interval of 20-25 mm from the exposure surface of concrete) in the specimens exposed to composite solutions of NaCl with $MgSO_4$ as compared to those exposed to only chloride (NaCl) solutions. In case of PPC specimens, the potential values were not systematic between exposure solutions of 1% NaCl, and 1% NaCl with $MgSO_4$ (both concentrations i.e. 2% and 4%) at all w/b ratios during the entire exposure period. The unsystematic variation in potential values may be attributed to the effect of alterations

in the availability of oxygen and moisture content at rebar level, although the free chloride content was lower in case of exposure to composite solution of NaCl with $MgSO_4$. Further, there was unsystematic variation in potential values of steel reinforcement between exposure solutions of 1% NaCl, and 1% NaCl with Na_2SO_4 (both concentrations i.e. 2% and 4%) during the early exposure period for all binders and w/b ratios as evident from Figure 6.1 to 6.3. However, during the later exposure period the potential values were mostly more negative in case of exposure to 1% NaCl solution as compared to composite solutions of 1% NaCl with Na_2SO_4 in the prismatic specimens made with OPC, whereas the opposite variation was observed in OPC + 20% FA and PPC specimens wherein the potential values were mostly more negative for composite solutions of 1% NaCl with Na_2SO_4 as compared to 1% NaCl solution. The more negative corrosion potential of steel reinforcement in OPC + 20% FA and PPC concrete exposed to composite solutions of 1% NaCl with Na_2SO_4 (although the free chloride content was lower as compared to NaCl solution) may be ascribed to the significant effect of variation in the amount of oxygen near rebar level in concrete.

From Figure 6.1 to 6.3, it is inferred that there is no systematic variation in half-cell potential of steel reinforcement with increase in concentration of $MgSO_4$ in the composite solutions of 1% NaCl with $MgSO_4$ for all binders and w/b ratios till the exposure period of 27 months. However, in case of composite solutions of NaCl and Na_2SO_4, the potential values became more negative with increase in concentration of Na_2SO_4 in the exposure solutions for prismatic specimens made with OPC, but there is no systematic variation in potential value with increase in concentration of Na_2SO_4 in the exposure solution for the prismatic specimens made with OPC + 20% FA and PPC. These variations in the potential values with increase in concentration $MgSO_4$ or Na_2SO_4 in the composite chloride-sulfate solutions may be attributed to the effect of presence of both chloride and sulfate ions in the electrolytic pore solution of concrete surrounding the steel reinforcement thereby altering the initiation of corrosion activity. On comparing the effect of cation type of associated with sulfate ions on half-cell potential of rebar, it is observed that the potential values were mostly more negative in the prismatic specimens exposed to composite solutions of NaCl with Na_2SO_4 as compared to those exposed to composite solutions of NaCl with $MgSO_4$. From the measured free chloride content (stated in Section 4.3.1.2, Chapter 4), it is observed that the free chloride at rebar level (i.e. in the depth interval of 20-25 mm from the exposure surface of prismatic specimen) was lower in case of specimens exposed to

composite solutions of NaCl with Na_2SO_4 as compared to those exposed to composite solutions of NaCl with $MgSO_4$. The more negative corrosion potential of steel reinforcement in case of exposure to composite solutions of NaCl with Na_2SO_4 (even though the free chloride content was lower) may be attributed to the significant effect of Na^+ ions in the pore solution of concrete surrounding the steel reinforcement that might have increased the conductivity of concrete and increased the extent of occurrence of corrosion activity of rebar.

From Figure 6.4 and Figure 6.5, it is observed that for both chloride and composite chloride-sulfate solutions at 3% NaCl concentration, the half-cell potential of steel reinforcement was less negative than -350 mV ($Cu/CuSO_4$ electrode)/ -270 mV (SCE), and there was no systematic variation in half-cell potential of steel reinforcement among exposure solutions during the early periods of exposure in the specimens made with OPC and OPC + 20% FA for all w/b ratios. Further, minor difference was observed in the potential values between chloride (NaCl) solution and composite chloride-sulfate (both $MgSO_4$ and Na_2SO_4) solutions. However, during the later exposure periods, the half-cell potential of steel reinforcement became more negative in case of exposure to chloride solution as compared to composite chloride-sulfate (both $MgSO_4$ and Na_2SO_4) solutions for OPC and OPC + 20% FA concrete at all w/b ratios. Further, the half-cell potential of steel reinforcement was more negative than -270 mV (SCE) in OPC and OPC + 20% FA specimens in case of exposure to chloride solution during the later exposure period as evident from Figure 6.4 and 6.5, which indicates greater probability of initiation of corrosion of steel reinforcement. The more negative potential of rebar in case of exposure to chloride solution for OPC and OPC + 20% FA concrete is attributed to the presence of higher amount of free chloride near the rebar level as compared to that in case of exposure to composite chloride-sulfate (both $MgSO_4$ and Na_2SO_4) solutions. In case of PPC specimens, the half-cell potential of steel reinforcement was less negative than -350 mV ($Cu/CuSO_4$ electrode)/ -270 mV (SCE) during the entire exposure period for both chloride and composite chloride-sulfate solutions at 3% NaCl concentration for all w/b ratios as evident from Figure 6.6, which indicated lower probability of occurrence of steel reinforcement corrosion in concrete made with PPC. Further, there was no systematic variation in half-cell potential of steel reinforcement with exposure solution. The less negative potential and unsystematic variation in potential of steel reinforcement with exposure solution in case of PPC concrete may be attributed to the effect of presence of

lower free chloride content in concrete in the vicinity of steel reinforcement. While evaluating the effect of cation type associated with sulfate ion, it is observed that there is no systematic variation in half-cell potential of steel reinforcement between composite solutions of NaCl (3%) with Na_2SO_4 (both concentrations, i.e. 2% and 4%), and NaCl (3%) with $MgSO_4$ (both concentrations i.e. 2% and 4%) throughout the entire exposure period for PPC specimens as observed from Figure 6.6. In case of OPC and OPC + 20% FA specimens, there is unsystematic variation in half-cell potential of steel reinforcement between composite solutions of NaCl with Na_2SO_4, and NaCl with $MgSO_4$ during the early exposure periods as evident from Figure 6.4 and Figure 6.5. However, during the later exposure periods, the potential of steel reinforcement was more negative for exposure to composite solutions of NaCl with $MgSO_4$ as compared to composite solutions of NaCl with Na_2SO_4 solution in OPC specimens whereas in OPC + 20% FA specimens, the potential of steel reinforcement was more negative in case of exposure to composite solutions of NaCl with Na_2SO_4 as compared to NaCl with $MgSO_4$ solution, as observed from Figure 6.4 and Figure 6.5. The more negative potential of steel reinforcement in OPC against exposure to composite solution of NaCl with $MgSO_4$ may be attributed to the availability of higher amount of free chloride near the steel bar as compared to that in case of exposure to composite solution of NaCl with Na_2SO_4 solution. It is to be noted that the measured free chloride content was higher in case of exposure to composite solution of NaCl with $MgSO_4$ than that exposed to composite solution of NaCl with Na_2SO_4 (mentioned in Section 4.3.1.2, Chapter 4). In case of OPC + 20% FA specimens, the more negative potential of steel reinforcement against exposure to composite solution of NaCl with Na_2SO_4 (although the measured free chloride content at rebar level was lower in case of exposure to composite solution of NaCl with Na_2SO_4 as compared to composite solution of NaCl with $MgSO_4$) may be attributed to the significant effect of Na^+ ions in the pore solution of concrete that might have altered the conductivity of concrete and increased the extent of initiation of corrosion activity of steel reinforcement. Further, in case of exposure to composite solutions of NaCl with $MgSO_4$, and NaCl with Na_2SO_4, there was no systematic variation in half-cell potential of steel reinforcement with increase in concentration of $MgSO_4$ or Na_2SO_4 in the exposure solution throughout the exposure period for all binders and w/b ratios, as observed from Figure 6.4 to 6.6.

For the specimens exposed to 5% NaCl solution, and composite solutions of 5% NaCl with $MgSO_4$ or Na_2SO_4 (concentrations of 2% and 4%), it is observed that the half-cell potential

of steel reinforcement was mostly more negative in case of exposure to composite solutions of NaCl with Na_2SO_4 as compared to NaCl solution and composite solutions of NaCl with $MgSO_4$ during the early exposure period for all binders and w/b ratios as observed from Figure 6.7 to 6.9. The more negative potential of steel reinforcement in case of exposure to composite solutions of NaCl with Na_2SO_4 during the early exposure period may be ascribed to the variation in conductivity of concrete due to alteration in the electrolytic pore solution of concrete in the presence of Na^+ ions. During the later exposure periods, there was unsystematic variation in potential of steel reinforcement with the exposure solution i.e. chloride and composite chloride-sulfate solutions for PPC at all w/b ratios, which may be attributed to the dominant effect of variations in oxygen and moisture content near the steel reinforcement, which affected the initiation of corrosion activity of steel reinforcement. Further, in case of PPC concrete the corrosion potential of steel reinforcement was mostly less negative than -270 mV (SCE) throughout the entire exposure period irrespective of exposure solution as evident from Figure 6.9. In addition, in PPC concrete, there was no systematic variation in half-cell potential of steel reinforcement with increase in concentration of either $MgSO_4$ or Na_2SO_4 in the composite chloride-sulfate solutions as observed from Figure 6.9. In case of OPC concrete, the potential of steel reinforcement was more negative against exposure to 5% NaCl solution as compared to composite solutions of 5% NaCl with $MgSO_4$ or Na_2SO_4 (concentrations of 2% and 4%) during the later exposures period as evident from Figure 6.7. The more negative potential of steel reinforcement in OPC concrete against 5% NaCl solution is attributed to the influence of higher amount of free chloride near the steel reinforcement as compared to that in case of exposure to composite chloride-sulfate solutions. It may be noted that the higher free chloride content was observed in the depth interval of 20-25 mm from the exposure surface of concrete (i.e. near the rebar level) for exposure to 5% NaCl solution as compared to its companion composite chloride-sulfate solutions (mentioned earlier in Section 4.3.1.2, Chapter 4). Further, during the later exposure periods, the half-cell potential values became more negative than -270 mV (SCE) in case of 5% NaCl and also in majority of the cases for exposure against composite solutions of 5% NaCl with $MgSO_4$ or Na_2SO_4 (concentrations of 2% and 4%) in OPC concrete, as observed from Figure 6.7. This is attributed to the ingress of more amount of chloride ions with increase in exposure period thereby resulting in higher free chloride content near the rebar level as compared to that during the early exposure period. Further from Figure 6.7, it is observed that during later exposure periods, the half-cell potential of steel reinforcement was more negative in case

of exposure to composite solution of 5% NaCl with 2% $MgSO_4$ as compared to composite solution of 5% NaCl with 2% Na_2SO_4, whereas at 4% concentration, the opposite variation was observed i.e. the half-cell potential was more negative against exposure solution of 5% NaCl with 4% Na_2SO_4 as compared to exposure solution of 5% NaCl with 4% $MgSO_4$ in OPC concrete. The more negative potential of steel reinforcement in OPC concrete in case of exposure to composite solution of 5% NaCl with 2% $MgSO_4$ is due to the presence of more amount of free chloride near rebar level as compared to that in case of exposure to composite solution of 5% NaCl with 2% Na_2SO_4. The more negative potential of steel reinforcement in OPC concrete in case of exposure to composite solution of 5% NaCl with 4% Na_2SO_4 (although the free chloride content was lower) as compared to composite solution of 5% NaCl with 4% $MgSO_4$ indicated higher probability of initiation of corrosion activity, which may be attributed to the alteration in the pore solution of concrete surrounding the steel bar due to the effect of combined presence of chloride ions and sulfate ions associated with Na^+ cation. While evaluating the effect of sulfate ion concentration, it is observed that in OPC concrete, the potential of steel reinforcement became more negative with increase in concentration of Na_2SO_4 whereas, it became less negative with increase in concentration of $MgSO_4$ in the respective composite chloride-sulfate solutions as evident from Figure 6.7. This indicates that cation type associated with sulfate ions in the concomitant presence of chloride ions altered the initiation of corrosion activity of steel reinforcement in concrete.

In OPC + 20% FA concrete, during the later exposure periods, the half-cell potential of rebar was more negative in case of exposure to 5% NaCl solution as compared to composite solutions of 5% NaCl with $MgSO_4$ or Na_2SO_4 (concentrations of 2% and 4%) as observed from Figure 6.8. Further, among the exposure solutions, the potential values of steel reinforcement were more negative than -270 mV (SCE) only in case of exposure to chloride solutions during the later exposure periods at all w/b ratios as observed from Figure 6.8, which indicates greater than 90% probability of occurrence of steel reinforcement corrosion [41] in the presence of chloride ions as compared to the combined presence of both chloride and sulfate ions. Further from Figure 6.8, it is inferred that the half-cell potential of steel reinforcement was more negative in case of exposure to composite solutions of 5% NaCl with Na_2SO_4 (both concentrations of 2% and 4%) as compared to composite solutions of 5% NaCl with $MgSO_4$ (both concentrations of 2% and 4%) during later exposure periods in OPC + 20% FA concrete at all w/b ratios. This indicates that the presence of Na^+ cation

associated with sulfate ions had comparatively significant effect on corrosion initiation of steel reinforcement as compared to Mg^{2+} cation associated with sulfate ions even though the free chloride content at rebar level in concrete was higher in case of exposure to composite solutions of NaCl with $MgSO_4$ as compared to composite solutions of NaCl with Na_2SO_4 (Section 4.3.1.2, Chapter 4). In addition, from Figure 6.8, it is noted that there was unsystematic variation as well as minor difference in the half-cell potential values of steel reinforcement with increase in concentration of $MgSO_4$ or Na_2SO_4 in the exposure solutions throughout the exposure period for OPC + 20% FA concrete at all w/b ratios.

6.2.2. Effect of binder type on half-cell potential

From Figure 6.1 to Figure 6.9, it is observed that mostly there was no systematic variation in half-cell potential of steel reinforcement with binder type during the early exposure period irrespective of w/b ratio against chloride exposure. This may be attributed to the effect of penetration of comparatively lower amount of chloride ions, and variations in oxygen and moisture content in the vicinity of steel reinforcement. During the later exposure period, the specimens made with OPC showed more negative half-cell potential values as compared to those made with OPC + 20% FA followed by PPC at all w/b ratios against chloride exposure (1%, 3% and 5% NaCl solutions) till the exposure period of 27 months as observed from Figure 6.1 to 6.9. This is attributed to higher free chloride content near rebar level due to penetration of more amount of chloride ions with increase in exposure period in OPC concrete. The penetration of comparatively lower amount of chloride ions in OPC + 20% FA and PPC concrete during the later exposure period is attributed to the formation of denser microstructure. As reported by Oliveira and Cascudo [154], the concrete made with OPC exhibited more negative half-cell potential as compared to that made with OPC plus 25% fly ash in case of exposure to NaCl solution (NaCl diluted to 5% by mass or 0.855 M) under drying-wetting cycle (1 cycle consist of 2 days of wetting followed by 5 days of drying) till 46 cycles. In case of exposure to composite solutions of NaCl with $MgSO_4$, and NaCl with Na_2SO_4, there was no systematic variation in half-cell potential of steel reinforcement with binder type during the early exposure period. However, during the later exposure periods, the half-cell potential of steel reinforcement was more negative in OPC specimens as compared to that in OPC + 20% FA and PPC specimens against exposure to composite solutions of NaCl with $MgSO_4$, as observed from Figure 6.1 to 6.9, which indicated greater probability of initiation of corrosion activity of rebar in OPC concrete in the combined presence of chloride ions and sulfate ions associated

with Mg^{2+} cation. Similarly from Figure 6.1 to 6.9, it is observed that during the later exposure periods, the half-cell potential of steel reinforcement was mostly more negative in OPC + 20% FA concrete as compared to that in OPC and PPC concrete against exposure to composite solutions of NaCl with Na_2SO_4. It may be noted that the free chloride content near the rebar level (in the depth interval of 20-25 mm from the exposure surface of concrete) was lower in OPC + 20% FA concrete as compared to OPC concrete whereas it was higher as compared to PPC concrete against exposure to composite solutions of NaCl with Na_2SO_4 (Section 4.3.1.3, Chapter 4). The more negative half-cell potential of steel reinforcement in OPC + 20% FA concrete (although the free chloride content was lower) as compared to OPC concrete in case of exposure to NaCl with Na_2SO_4 solution may be ascribed to the effect of variations in the availability of oxygen near rebar level, and alteration in the electrolytic pore solution of concrete due to the combined presence of chloride ions and sulfate ions associated with sodium cation.

To analyze the effect of binder type on initiation of steel reinforcement corrosion in concrete with respect to the threshold potential of -270 mV (SCE), the obtained half-cell potential values were plotted between different binders irrespective of w/b ratio, and exposure solution at different exposure periods, and the plots are shown in Figure 6.10, Figure 6.11 and Figure 6.12 for OPC vs. PPC, OPC vs. OPC + 20% FA, and OPC + 20% FA vs. PPC respectively. These plots can be used to compare the variations in half-cell potential of steel reinforcement with respect to corrosion initiation between two types of binder at different exposure periods.

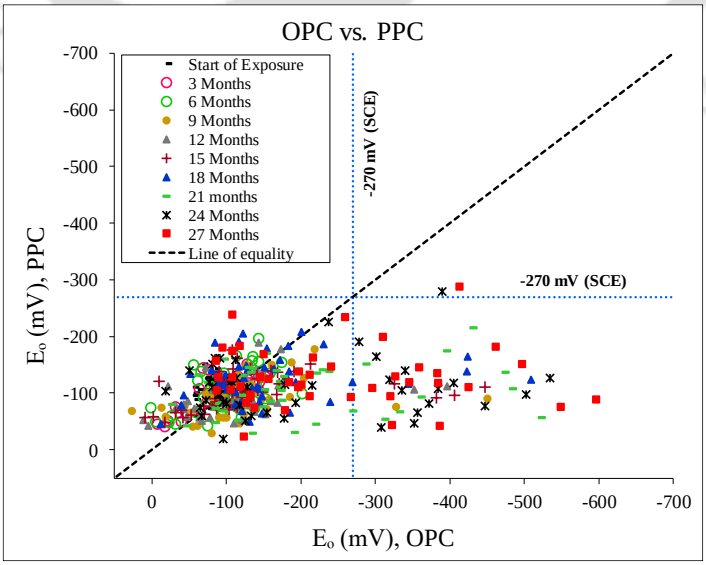

Figure 6.10 Comparison of half-cell potential of steel reinforcement in prismatic reinforced concrete specimens made with OPC and PPC

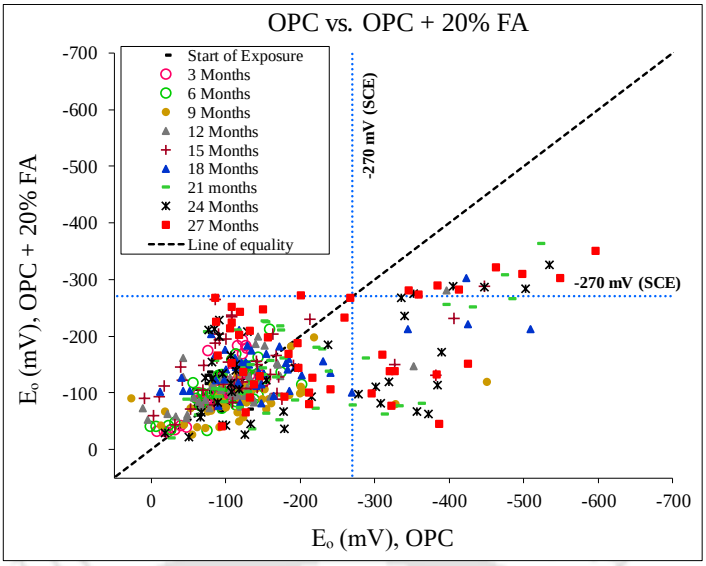

Figure 6.11 Comparison of half-cell potential of steel reinforcement in prismatic reinforced concrete specimens made with OPC and OPC + 20% FA

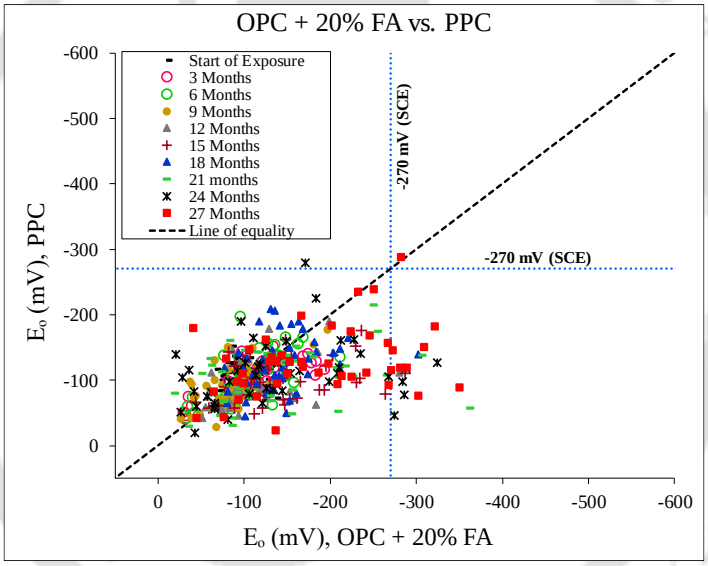

Figure 6.12 Comparison of half-cell potential of steel reinforcement in prismatic reinforced concrete specimens made with OPC + 20% FA and PPC

From Figure 6.10 to Figure 6.12, it is observed that there is no systematic variation in half-cell potential of steel reinforcement with binder type at different exposure periods when the potential values are less negative than -270 mV (SCE). The potential values less negative than -270 mV (SCE) were observed in all the cases irrespective of binder type during the early exposure period and in majority of the cases during the later exposure period. Further from Figure 6.10 to Figure 6.12, it is noted that the half-cell potential values of steel reinforcement were more negative than -270 mV (SCE) in majority of the cases in OPC concrete followed by OPC + 20% FA concrete during the later exposure period. However, in very few cases, the half-cell potential of steel reinforcement was more negative than -

270 mV (SCE) in PPC concrete. This indicated lower probability of corrosion initiation of steel reinforcement in PPC concrete as compared to OPC + 20% FA followed by OPC concrete. Thus, based on the results of half-cell potential measurement, concrete made with PPC showed better performance against corrosion initiation of steel reinforcement as compared to OPC + 20% FA followed by OPC concrete against chloride and composite chloride-sulfate solutions till the exposure period of 27 months.

6.2.3. Effect of w/b ratio on half-cell potential

From Figure 6.1 to Figure 6.9, it is observed that the OPC and OPC + 20% FA specimens exposed to chloride (NaCl) solutions mostly showed more negative potential values at w/b ratio of 0.55 as compared to w/b ratio of 0.50 followed by w/b ratio of 0.45 till the exposure period of 27 months, which is attributed to the presence of higher amount of free chloride near rebar level in the concrete made with higher w/b ratio. However, in case of PPC concrete, there was no systematic variation in half-cell potential of steel reinforcement with w/b ratio against chloride as well as composite chloride-sulfate (for both Mg^{2+} and Na^{+} cations) solutions during the entire exposure period. This may be attributed to the dominant effect of lower free chloride content near rebar level due to penetration of comparatively lower amount of chloride ions into PPC concrete irrespective of w/b ratio as compared to OPC + 20% FA and OPC concrete. As stated earlier in Section 4.3.1.3, Chapter 4, lower free chloride content was observed in PPC concrete in the depth interval of 20-25 mm (i.e. near rebar level) at all w/b ratios (0.45, 0.50 and 0.55) as compared to that in OPC + 20% FA and OPC concrete.

In case of exposure to composite chloride-sulfate (for both Na^{+} and Mg^{2+} cations) solutions, there was no systematic variation in half-cell potential of steel reinforcement with w/b ratio in OPC + 20% FA concrete during the entire exposure period. This indicated that the dominant effect of simultaneous penetration of sulfate ions resulted in a reduction in penetration of chloride ions irrespective of w/b ratio thereby altering the electrolytic pore solution of concrete surrounding the steel reinforcement. In OPC concrete, there was no systematic variation in half-cell potential of steel reinforcement with w/b ratio in case of exposure to composite chloride-sulfate solutions during the early exposure periods, whereas the half-cell potential became more negative with increase in w/b ratio during the later exposure periods. The more negative potential of steel reinforcement at higher w/b ratio during the later exposure periods in OPC concrete against exposure to composite

chloride-sulfate solutions may be ascribed to the ingress of relatively more amount of chloride ions due to formation of a comparatively less denser pore structure at higher w/b ratio, even though there was reduced penetration of chloride ions due to simultaneous ingress of sulfate ions into concrete than exposure to only chloride solution.

In order to evaluate the effect of w/b ratio on initiation of corrosion activity of steel reinforcement in concrete with respect to the threshold potential of -270 mV (SCE), the measured half-cell potential values were plotted between different w/b ratios irrespective of binder type, and exposure solution at different exposure periods, and the plots are shown in Figure 6.13 and Figure 6.14 for w/b ratios of 0.45 vs. 0.50 and 0.50 vs. 0.55 respectively.

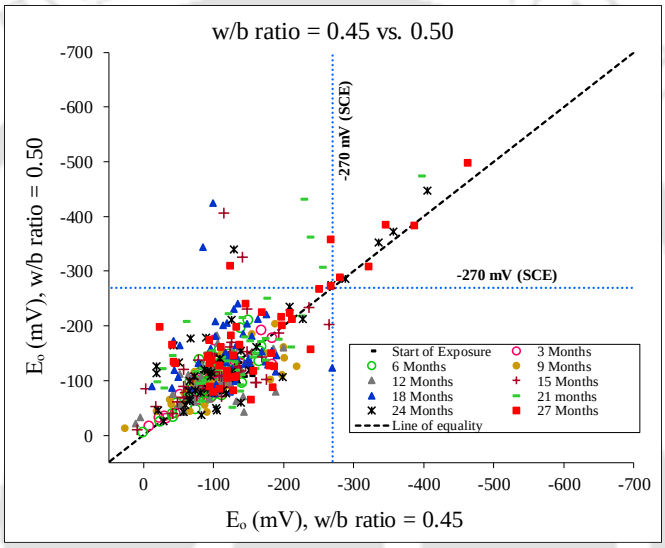

Figure 6.13 Comparison of half-cell potential of steel reinforcement in prismatic reinforced concrete specimens made at w/b ratios of 0.45 and 0.50

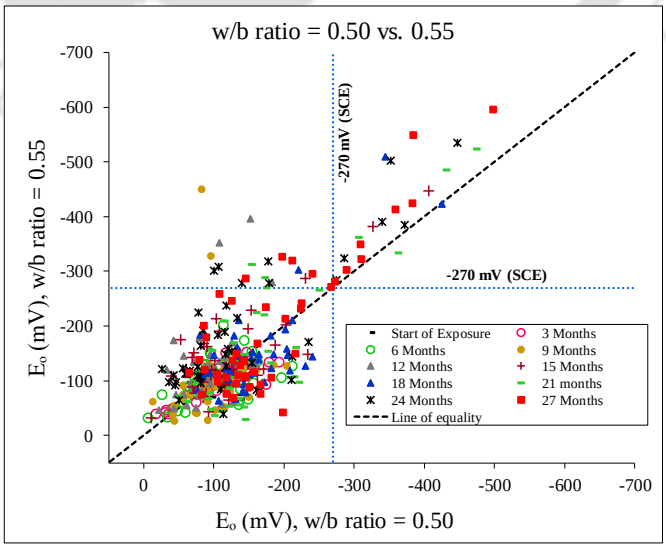

Figure 6.14 Comparison of half-cell potential of steel reinforcement in prismatic reinforced concrete specimens made at w/b ratios of 0.50 and 0.55

From Figure 6.13 and Figure 6.14, it is observed that there is no systematic variation in half-cell potential of steel reinforcement with w/b ratio at different exposure periods when the potential values are less negative than -270 mV (SCE). The potential values less negative than -270 mV (SCE) were observed during the early exposure period in all the specimens, and also during the later exposure period in majority of the specimens irrespective of w/b ratio as evident from Figure 6.13 and 6.14. Further from Figure 6.13 and 6.14, it is observed that out of the total number of specimens those exhibited potential values more negative than -270 mV (SCE), the specimens made with w/b ratio of 0.55 showed potential values more negative than -270 mV (SCE) in more cases as compared to those made with w/b ratio of 0.50 followed by w/b ratio 0.45. Thus, there was lower probability of occurrence of reinforcing steel corrosion in concrete made with lower w/b ratio as compared that made with higher w/b ratio against exposure to chloride and composite chloride-sulfate solutions.

6.3. Corrosion current density of steel reinforcement in concrete

As stated in Chapter 3, linear polarization resistance (LPR) measurement was carried out on the prismatic reinforced concrete specimens to determine the corrosion current density (I_{corr}) of steel reinforcement in concrete exposed to chloride and composite chloride-sulfate solutions for different exposure periods. The LPR measurement was performed on the prismatic specimens at the start of wetting period (of wetting-drying cycle) at every 3-month interval. The reported corrosion current density values at different testing ages of exposure periods are the average values of replicate prismatic specimens.

6.3.1. Effect of exposure solution and cation type associated with sulfate ions on corrosion current density

The obtained values of corrosion current density of steel reinforcement embedded in prismatic reinforced concrete specimens were plotted for chloride solutions, and composite chloride-sulfate solutions against exposure duration as shown in Figure 6.15 to Figure 6.23.

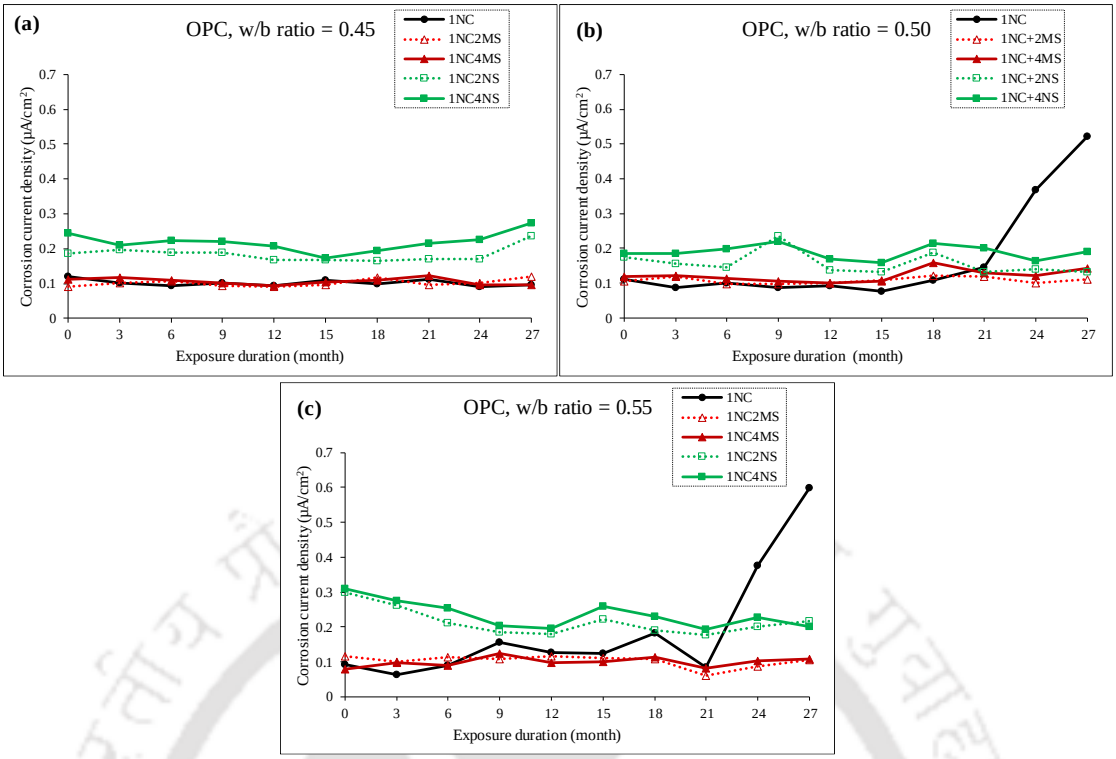

Figure 6.15 Corrosion current density (I_{corr}) of steel bar in concrete made with OPC and exposed to 1% NaCl and respective composite chloride-sulfate solutions: (a) w/b ratio = 0.45 (b) w/b ratio = 0.50, and (c) w/b ratio = 0.55

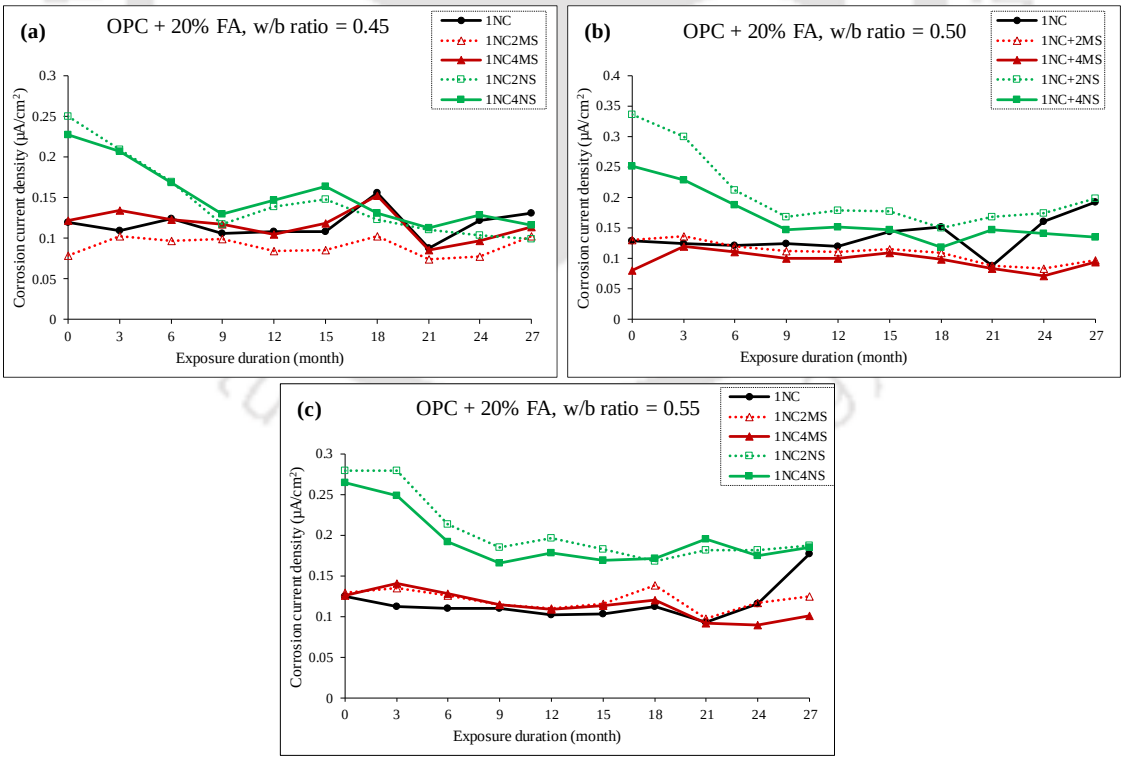

Figure 6.16 Corrosion current density (I_{corr}) of steel bar in concrete made with OPC + 20% FA and exposed to 1% NaCl and respective composite chloride-sulfate solutions: (a) w/b ratio = 0.45 (b) w/b ratio = 0.50, and (c) w/b ratio = 0.55

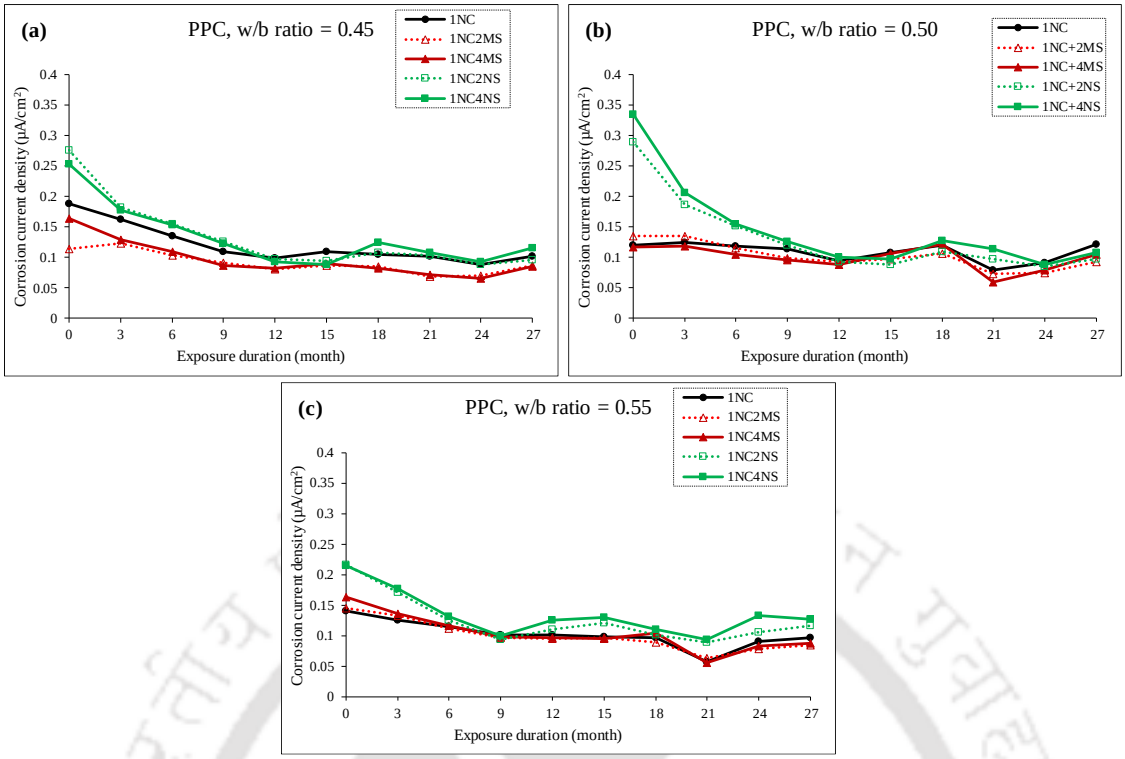

Figure 6.17 Corrosion current density (I_{corr}) of steel bar in concrete made with PPC and exposed to 1% NaCl and respective composite chloride-sulfate solutions: (a) w/b ratio = 0.45 (b) w/b ratio = 0.50, and (c) w/b ratio = 0.55

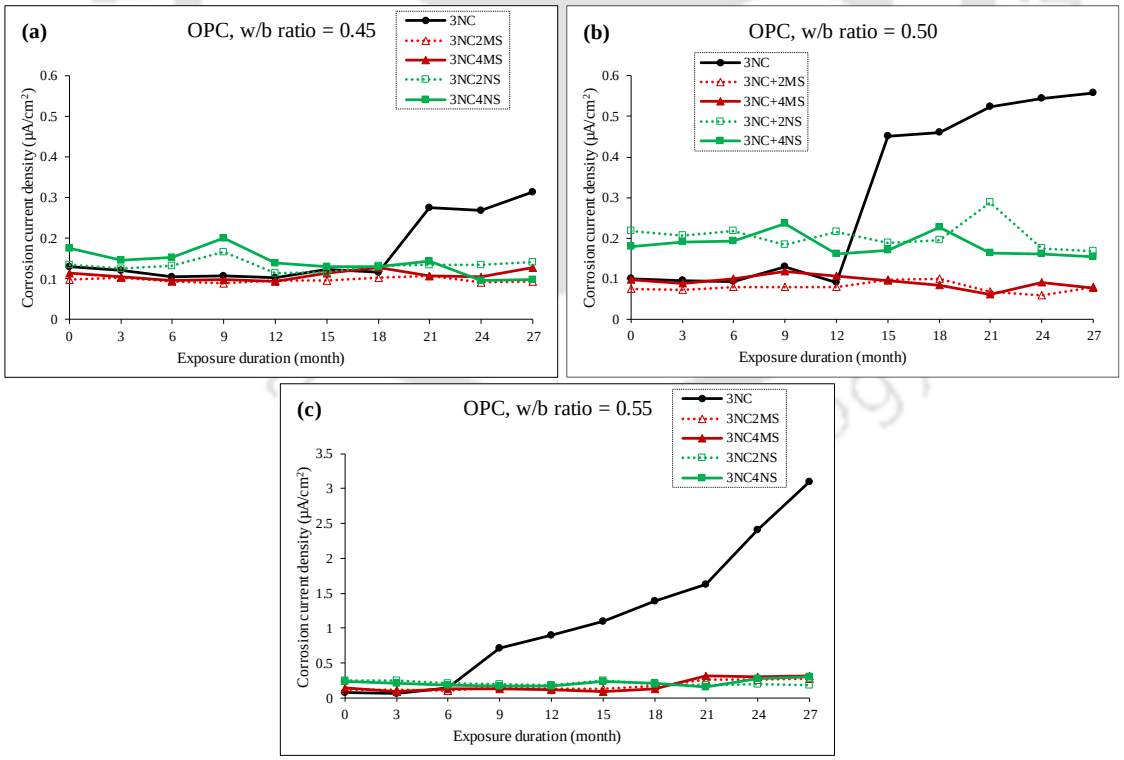

Figure 6.18 Corrosion current density (I_{corr}) of steel bar in concrete made with OPC and exposed to 3% NaCl and respective composite chloride-sulfate solutions: (a) w/b ratio = 0.45 (b) w/b ratio = 0.50, and (c) w/b ratio = 0.55

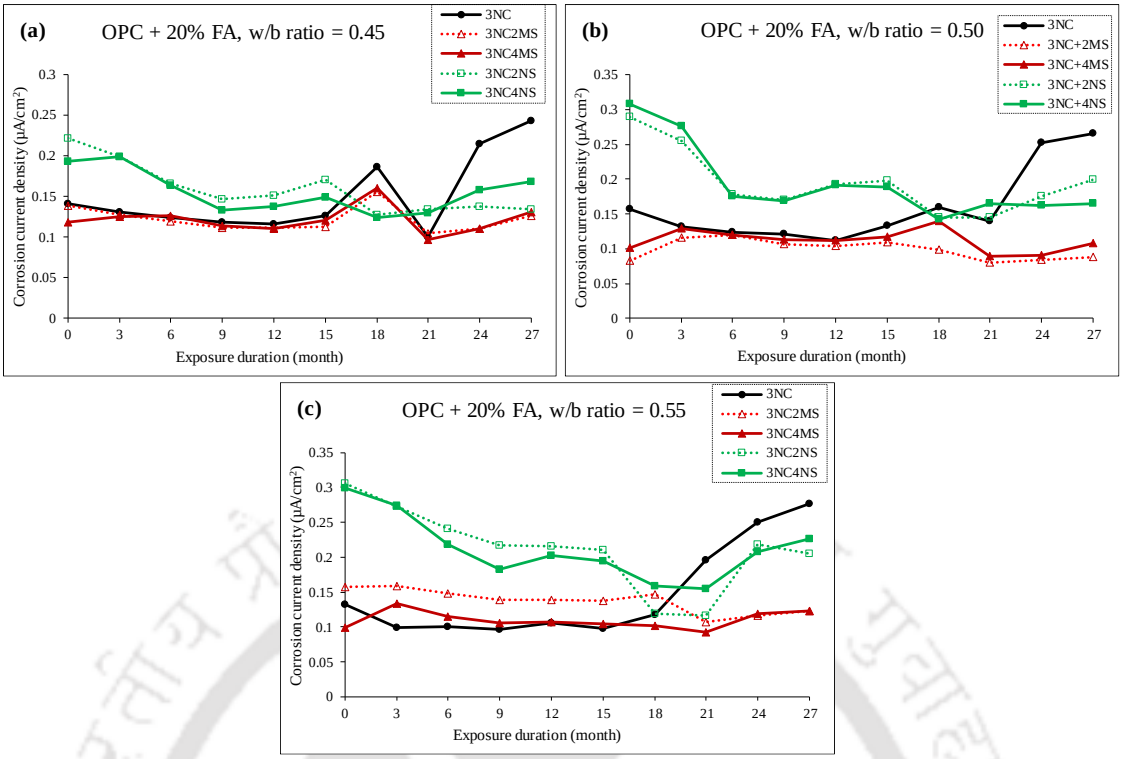

Figure 6.19 Corrosion current density (I_{corr}) of steel bar in concrete made with OPC + 20% FA and exposed to 3% NaCl and respective composite chloride-sulfate solutions: (a) w/b ratio = 0.45 (b) w/b ratio = 0.50, and (c) w/b ratio = 0.55

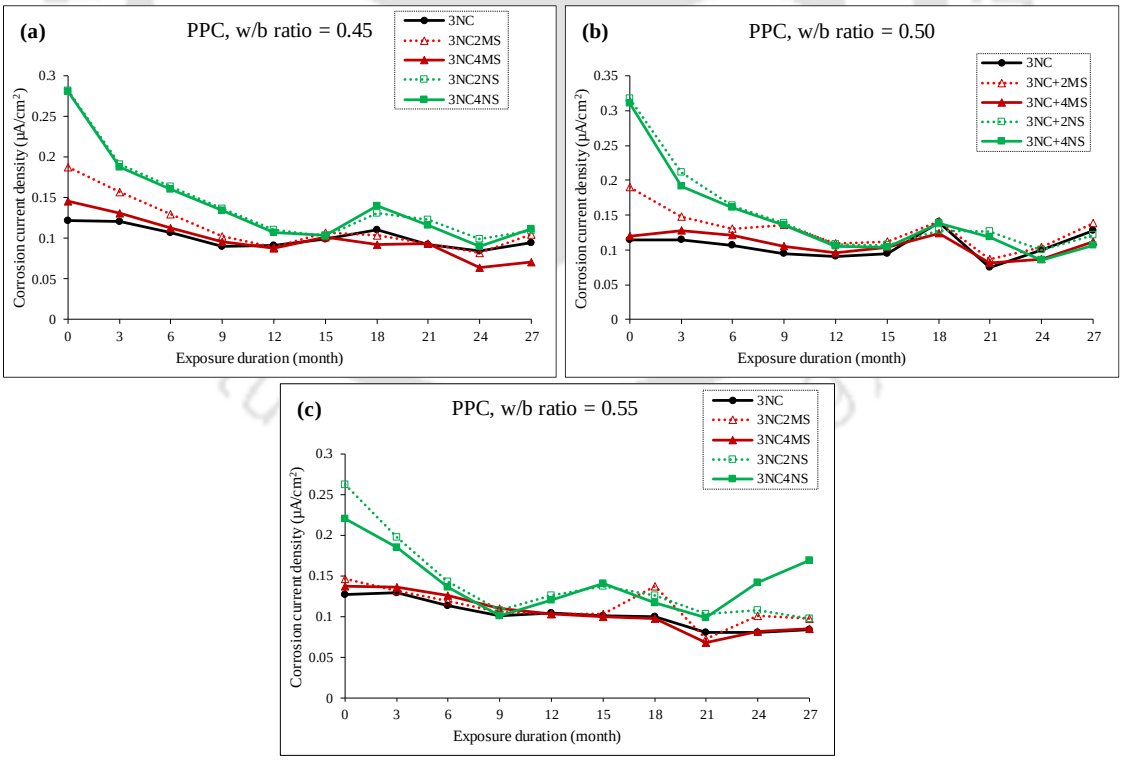

Figure 6.20 Corrosion current density (I_{corr}) of steel bar in concrete made with PPC and exposed to 3% NaCl and respective composite chloride-sulfate solutions: (a) w/b ratio = 0.45 (b) w/b ratio = 0.50, and (c) w/b ratio = 0.55

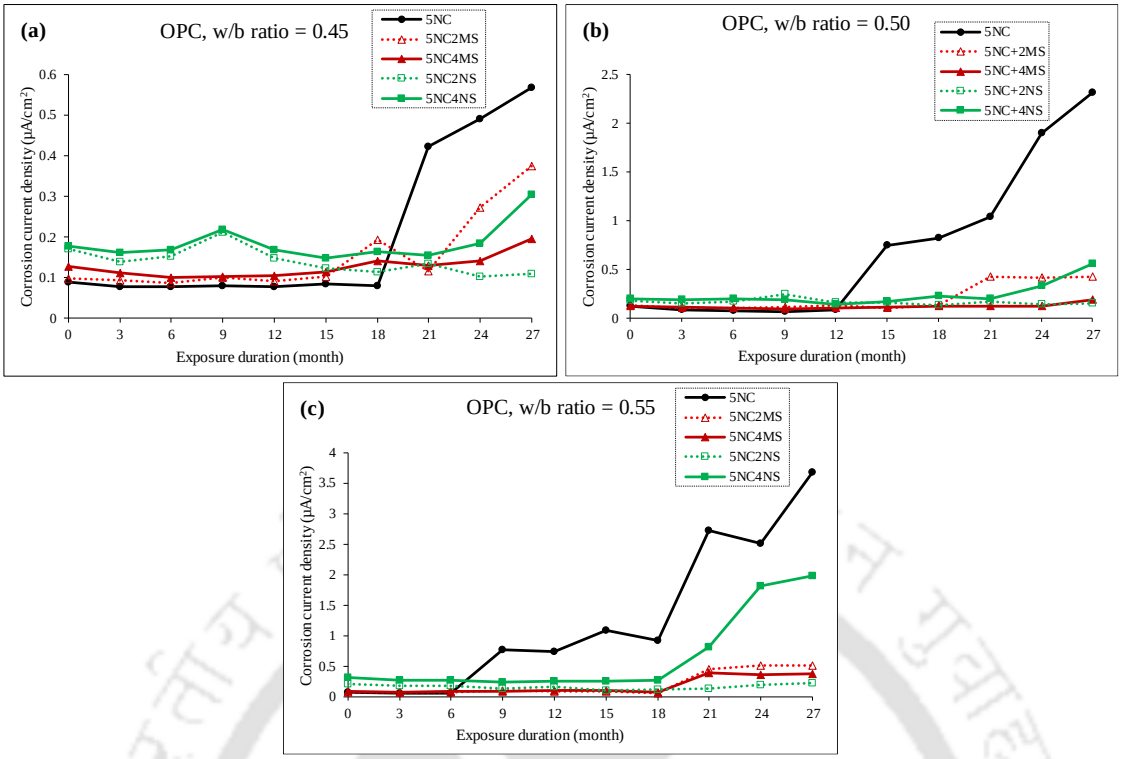

Figure 6.21 Corrosion current density (I_{corr}) of steel bar in concrete made with OPC and exposed to 5% NaCl and respective composite chloride-sulfate solutions: (a) w/b ratio = 0.45 (b) w/b ratio = 0.50, and (c) w/b ratio = 0.55

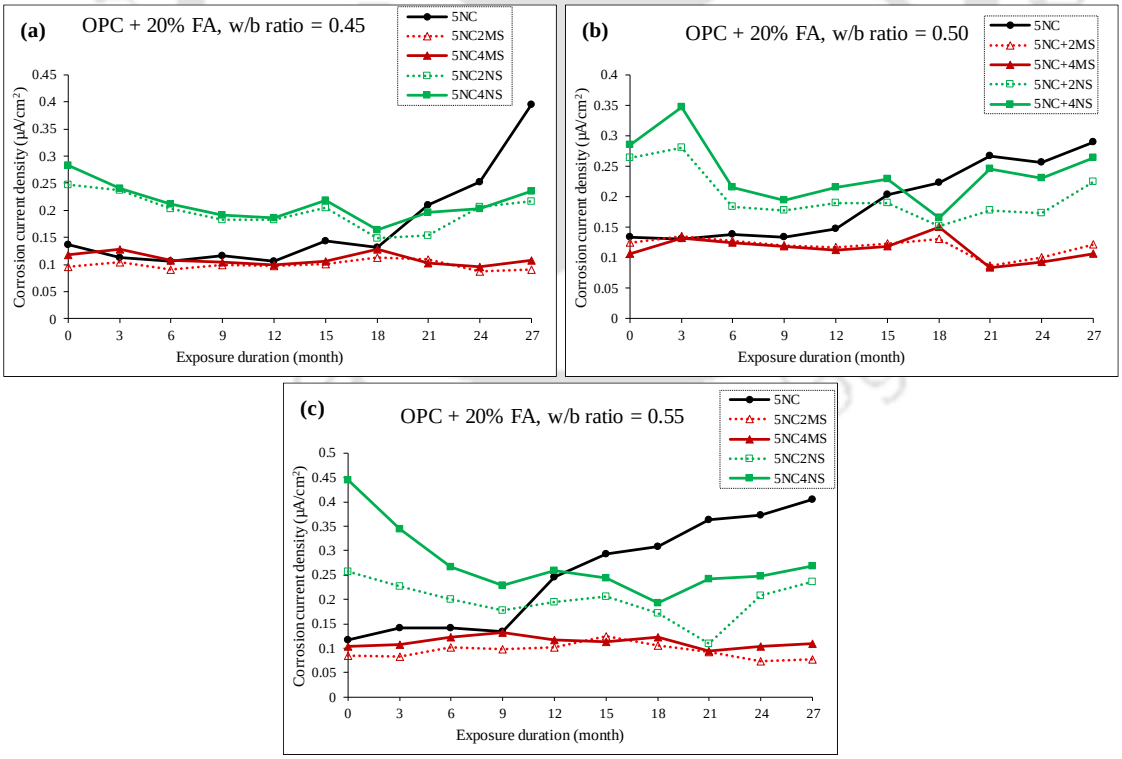

Figure 6.22 Corrosion current density (I_{corr}) of steel bar in concrete made with OPC + 20% FA and exposed to 5% NaCl and respective composite chloride-sulfate solutions: (a) w/b ratio = 0.45 (b) w/b ratio = 0.50, and (c) w/b ratio = 0.55

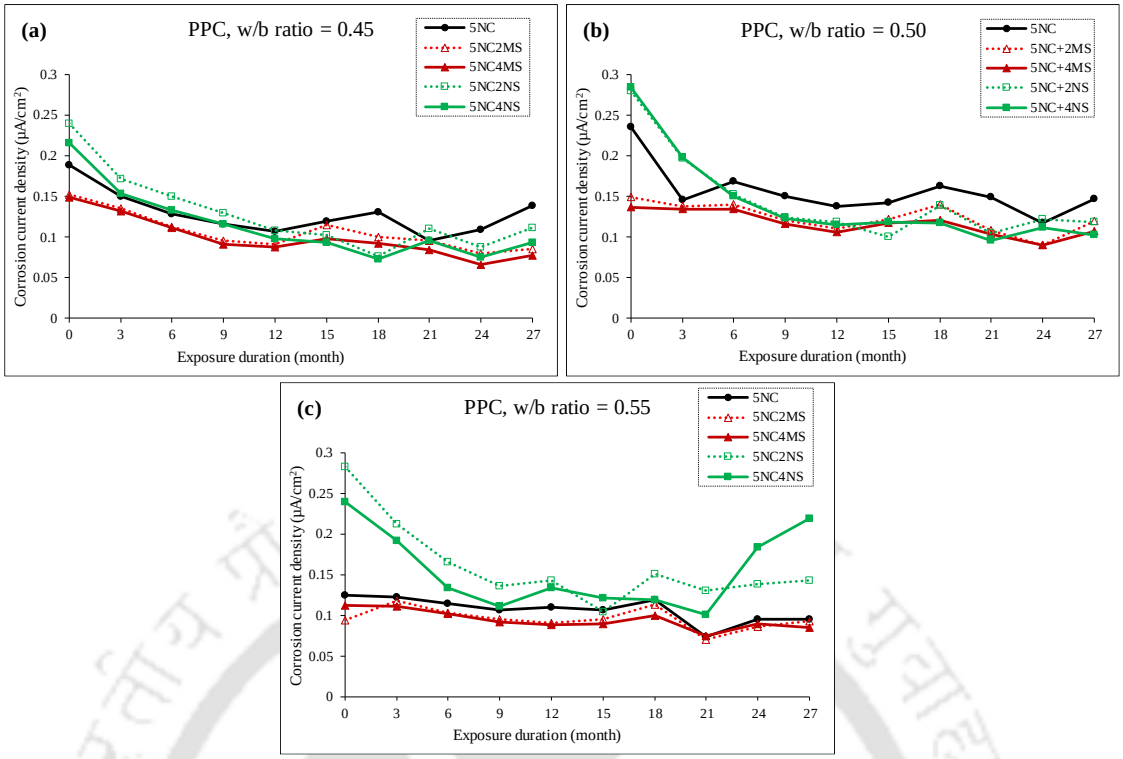

Figure 6.23 Corrosion current density (I_{corr}) of steel bar in concrete made with PPC and exposed to 5% NaCl and respective composite chloride-sulfate solutions: (a) w/b ratio = 0.45 (b) w/b ratio = 0.50, and (c) w/b ratio = 0.55

From Figure 6.15 to 6.23, it is observed that the corrosion current density of steel reinforcement increased with increase in concentration of NaCl in the exposure solution in case of exposure to chloride solutions for all binders (OPC, OPC + 20% FA and PPC) and w/b ratios (0.45, 0.50 and 0.55) during the entire exposure period till 27 months. This is attributed to increase in concentration of free chloride near the steel reinforcement due to penetration of more amount of chloride ions into concrete against exposure to chloride solutions with higher concentration of NaCl. The presence of higher free chloride content at rebar level in the concrete exposed to chloride solutions with higher concentration of NaCl is evident from the results of free chloride content presented in Section 4.3.1.2, Chapter 4. The presence of higher free chloride content increased the conductivity of concrete surrounding the steel reinforcement that resulted in an increase in corrosion current density.

From the specimens exposed to composite solutions of NaCl with $MgSO_4$ or Na_2SO_4 (for both concentrations, i.e. 2% and 4%), it is observed that there is no systematic variation in corrosion current density of steel reinforcement in PPC concrete with increase in concentration of NaCl in the composite solutions throughout the entire exposure period as

evident from Figure 6.17, 6.20 and 6.23. This may be attributed to the dominant effect of lower free chloride content, and also due to the variations in oxygen and moisture content in the vicinity of steel reinforcement in PPC concrete. The lower free chloride content near rebar level (i.e. at depth interval of 20-25 mm from the exposure surface) in PPC concrete is evident from the results of free chloride content presented in Section 4.3.1.2, Chapter 4. In case of OPC and OPC + 20% FA concrete, the variation in corrosion current density with increase in concentration of NaCl in the composite chloride-sulfate ($MgSO_4$ and Na_2SO_4) solutions was unsystematic during the early exposure periods. However, during the later exposure periods the corrosion current density mostly increased with increase in concentration of NaCl in the composite chloride-sulfate solutions. The increase in corrosion current density with increase in concentration of NaCl in the composite solutions in OPC and OPC + 20% FA concrete during the later exposure period may be ascribed to the significant effect of penetration of comparatively higher amount of chloride ions into OPC and OPC + 20% FA concrete during the later exposure period although the penetration of chloride ion was comparatively less in case of exposure to composite chloride-sulfate solutions as compared to only chloride solution for all binders and w/b ratios as result of simultaneous ingress of both chloride and sulfate ions. The lower free chloride content at rebar level in the prismatic specimens exposed to composite chloride-sulfate solutions as compared to only chloride solutions for all binders and w/b ratios is observed from results of free chloride content presented in Section 4.3.1.2, Chapter 4.

While comparing between chloride (NaCl) solution and composite chloride-sulfate (NaCl with $MgSO_4$ or Na_2SO_4) solutions, it is observed that at 1% NaCl concentration, the specimens exposed to composite solution of NaCl with Na_2SO_4 mostly exhibited higher corrosion current density as compared to those exposed to NaCl solution and composite solution of NaCl with $MgSO_4$ for all binders and w/b ratios during the entire exposure period (except in very few cases in OPC concrete during the later exposure period for NaCl solution) as observed from Figure 6.15 to 6.17. However, the free chloride content in the vicinity of steel bar i.e. in the depth interval of 20-25 mm from the exposure surface of prismatic specimen was lower in the specimens exposed to composite solution of NaCl with Na_2SO_4 as compared to those exposed to composite solution of NaCl with $MgSO_4$, and NaCl solution as evident from the results of free chloride content presented in Section 4.3.1.2, Chapter 4. Therefore, higher corrosion current density in the specimens exposed to composite solutions of NaCl with Na_2SO_4 (although free chloride content was lower) may

be attributed to the dominant effect of Na^+ ions in the electrolytic pore solution of concrete that might have increased the conductivity of concrete. Further, there was unsystematic variation as well as minor difference in corrosion current density of steel reinforcement between NaCl solution, and composite solution of NaCl with $MgSO_4$ during the entire exposure period as observed from Figure 6.15 to 6.17. While analyzing the effect of concentration of sulfate ions, it is observed that there is no systematic variation in corrosion current density of steel reinforcement with increase in concentration of $MgSO_4$ (i.e. from 2% to 4%) in the composite solution of 1% NaCl with $MgSO_4$ for all binders and w/b ratios during the entire exposure period as observed from Figure 6.15 to 6.17. In addition, the difference in corrosion current density was very small with increase in concentration of $MgSO_4$ in the composite solution. This indicated that the presence of sulfate ions associated with magnesium cation in the pore solution of concrete did not affect its conductivity. It may also be noted that the free chloride content near steel reinforcement was lower in the concrete exposed to composite solution of NaCl with $MgSO_4$ as compared to NaCl solution. From Figure 6.15 to 6.17, it is noted that the variation in corrosion current density was unsystematic as well as very small with increase in concentration of Na_2SO_4 (i.e. from 2% to 4%) in the composite solution of 1% NaCl with Na_2SO_4 in OPC + 20% FA and PPC concrete. This may be ascribed to the dominant effect of availability of lower free chloride content near rebar level in OPC + 20% FA and PPC concrete exposed to composite solutions of NaCl with Na_2SO_4. However, in OPC concrete the corrosion current density of steel reinforcement increased slightly with increase in concentration of Na_2SO_4 in the composite solution of 1% NaCl with Na_2SO_4 at all w/b ratios during the entire exposure period as observed from Figure 6.15. This indicated that the presence of sulfate ions associated with sodium cation along with the presence of chloride ions increased the conductivity of OPC concrete thereby resulting in slightly higher corrosion current density with increase in concentration of Na_2SO_4 in the composite solution.

At both 3% and 5% NaCl concentrations, the specimens exposed to composite solutions of NaCl with Na_2SO_4 mostly exhibited higher corrosion current density as compared to those exposed to NaCl solutions and composite solutions of NaCl with $MgSO_4$ for OPC and OPC + 20% FA concrete during the early exposure period as observed from Figure 6.18, 6.19, 6.21 and 6.22. Further, during the early exposure period, there was no systematic variation in corrosion current density between NaCl solution, and composite solution of NaCl with $MgSO_4$. However, during the later exposure period, the specimens exposed to NaCl

solutions exhibited significantly higher corrosion current density as compared to those exposed to composite solutions of NaCl (3% and 5%) with Na_2SO_4 (2% and 4%), and NaCl (3% and 5%) with $MgSO_4$ (2% and 4%). The higher corrosion current density in the specimens exposed to NaCl solutions during the later exposure period is attributed to the significant effect of increase in conductivity of concrete due to penetration of higher amount of chloride ions that resulted in higher free chloride content near rebar level. The higher free chloride content near rebar level in the specimens exposed to NaCl solutions as compared to composite solutions of NaCl with $MgSO_4$ and NaCl with Na_2SO_4 is observed from the results of free chloride content presented in Section 4.3.1.2 (Chapter 4).

From Figure 6.20, it is observed that at 3% NaCl concentration, the specimens exposed to composite solutions of NaCl with Na_2SO_4 mostly exhibited higher corrosion current density as compared to those exposed to NaCl solution and composite solutions of NaCl with $MgSO_4$ in PPC concrete at all w/b ratios during the entire exposure period. Between NaCl solution and composite solution of NaCl with $MgSO_4$, the specimens exposed to composite solution of NaCl with $MgSO_4$ exhibited slightly higher corrosion current density as compared to NaCl solution during the early exposure period, however, there was unsystematic variation in corrosion current density between these solutions during the later exposure period as observed from Figure 6.20. It may be noted that the free chloride content at rebar level was higher in the specimens exposed to NaCl solution as compared to composite solution of NaCl with $MgSO_4$ followed by composite solution of NaCl with Na_2SO_4 as observed from the results of free chloride content presented in Section 4.3.1.2, (Chapter 4). Thus, the above mentioned variations in corrosion current density of steel reinforcement in PPC concrete among different exposure solutions may be attributed to the variations in conductivity of concrete due to the combined presence of chloride and sulfate ions, and also due to the effect of cation type associated with sulfate ions that might have altered the electrolytic pore solution of concrete. From Figure 6.23, it is observed that at 5% NaCl concentration, the corrosion current density of steel reinforcement was mostly higher in the specimens exposed to composite solutions of NaCl with Na_2SO_4 as compared to other solutions during the early exposure period in PPC concrete at w/b ratios of 0.45 and 0.50, however, during the later exposure period, the corrosion current density of steel reinforcement was higher in the specimens exposed to NaCl solution as compared to other solutions. Further at w/b ratio of 0.55, the corrosion current density of steel reinforcement was higher in the specimens exposed to composite solution of NaCl with Na_2SO_4 as

compared to NaCl solution followed by composite solution of NaCl with $MgSO_4$ in PPC concrete during the entire exposure period as observed from Figure 6.23 (c). These observations indicated that the variations in corrosion current density of steel reinforcement during early and later exposure periods are dependent on the alterations in the electrolytic pore solution of concrete due to variations in the penetration of chloride and sulfate ions into concrete with change in w/b ratio, and also due to the effect of cation type associated with sulfate ions.

While analyzing the effect of sulfate ion, it is inferred that at 3% NaCl concentration, there was mostly unsystematic variation in corrosion current density of steel reinforcement with increase in concentration of $MgSO_4$ (from 2% to 4%) or Na_2SO_4 (from 2% to 4%) in the respective composite solutions for all binders and w/b ratios during the entire exposure period as observed from Figure. 6.18 to 6.20. In addition, there was minor difference in corrosion current density of steel reinforcement with increase in concentration of $MgSO_4$ or Na_2SO_4 in the respective composite solutions. The unsystematic variation in corrosion current density of steel reinforcement with increase in concentration of $MgSO_4$ or Na_2SO_4 in the composite solutions even at comparatively higher concentration of NaCl, i.e. 3% is attributed to the significant effect of ingress of comparatively lower amount of chloride ions into concrete due to simultaneous ingress of sulfate ions thereby resulting in lower free chloride content near the steel bar in concrete. Further, increase in concentration of sulfate ions might not have significant effect on conductivity of concrete at this concentration of NaCl i.e. 3%.

At 5% NaCl concentration, the variation in corrosion current density of steel reinforcement was mostly unsystematic with increase in concentration of $MgSO_4$ (from 2% to 4%) in the composite solution of NaCl with $MgSO_4$ in OPC + 20% FA and PPC concrete during the entire exposure period as observed from Figure 6.22 and Figure 6.23. In addition, the difference in corrosion current density was also very small. In OPC concrete, the variation in corrosion current density of steel reinforcement was unsystematic as well as very less with increase in concentration of $MgSO_4$ (from 2% to 4%) during the early exposure periods, whereas, during the later exposure period, the corrosion current density decreased with increase in concentration of $MgSO_4$ (from 2% to 4%) in the composite solution 5% NaCl with $MgSO_4$ as observed from Figure 6.21. The higher corrosion current density of steel reinforcement at lower concentration of $MgSO_4$ in the composite solution during the later exposure period in OPC concrete may be attributed to the dominant effect of

penetration of comparatively higher amount of chloride ions to rebar level due to the simultaneous ingress of chloride ions, and lower amount of sulfate ions. It may be noted that higher free chloride content was observed near rebar level in the concrete exposed to composite solution of NaCl with 2% $MgSO_4$ as compared to composite solution of NaCl with 4% $MgSO_4$ (mentioned earlier in Section 4.3.1.2, Chapter 4). While analyzing the effect of Na_2SO_4 concentration, it is observed that at 5% NaCl concentration, there was very less difference in corrosion current density of rebar in OPC concrete with increase in concentration of Na_2SO_4 (from 2% to 4%) in the composite solution of NaCl with Na_2SO_4 during the early exposure period, whereas the corrosion current density increased significantly with increase in concentration of Na_2SO_4 in the composite solution during the later exposure period as evident from Figure 6.21. The higher corrosion current density of steel reinforcement in OPC concrete at higher of concentration of Na_2SO_4 i.e. 4% in the composite solution with 5% NaCl during the later exposure period is attributed to the increase in conductivity of concrete due to the dominant effect of Na^+ ions as well as due to the effect of presence of higher concentration of sulfate ions in the pore solution of concrete as compared to composite solution of 5% NaCl with 2% Na_2SO_4. In PPC concrete, there was mostly unsystematic variation as well as minor difference in corrosion current density of steel reinforcement with increase in concentration of Na_2SO_4 (from 2% to 4%) in the composite solution of 5% NaCl with Na_2SO_4 during the entire exposure period as observed from Figure 6.23. From Figure 6.22, it is inferred that the corrosion current density increased with increase in concentration of Na_2SO_4 in the composite solution of 5% NaCl with Na_2SO_4 during the entire exposure period in OPC + 20% FA concrete, which may be attributed to the alteration in the electrolytic pore solution of concrete due to the presence of Na^+ ions along with the presence of comparatively higher concentration of sulfate ions in the concrete exposed to composite solution of 5% NaCl with 4% Na_2SO_4 as compared to composite solution of 5% NaCl with 2% Na_2SO_4, although there was lower free chloride content near rebar level in the concrete exposed to composite solution of 5% NaCl with 4% Na_2SO_4 as compared to composite solution of 5% NaCl with 2% Na_2SO_4 as observed from the results of free chloride content presented in Section 4.3.1.2, Chapter 4.

6.3.2. Effect of binder type on corrosion current density

From Figure 6.15 to Figure 6.23, it is observed that the corrosion current density of steel reinforcement was mostly higher in the prismatic specimens made with PPC as compared to those made with OPC + 20% FA and OPC during the early exposure periods when

exposed to chloride (NaCl), and composite chloride (NaCl)-sulfate (both Na_2SO_4 and $MgSO_4$) solutions. It may be noted that the free chloride content was lower in PPC concrete at rebar level (i.e. in the depth interval of 20-25 mm from exposure surface) as compared to OPC and OPC + 20% FA concrete. Thus, higher corrosion current density in PPC concrete during the early exposure period may be ascribed to the dominant effect of variations in the oxygen and moisture content near rebar level in concrete. However, during the later exposure periods, the corrosion current density of steel reinforcement was lower in PPC specimens as compared to OPC and OPC + 20% FA specimens against exposure to both chloride and composite chloride-sulfate solutions as observed from Figure 6.15 to Figure 6.23. The lower corrosion current density in PPC specimens during the later exposure period is attributed to the dominant effect of presence of lower amount of free chloride near steel reinforcement in PPC concrete as compared to that in OPC and OPC + 20% FA concrete against exposure to chloride and composite chloride-sulfate solutions for all w/b ratios. Between OPC and OPC + 20% FA, the specimens made with OPC + 20% FA exhibited higher corrosion current density as compared to OPC specimens during the early exposure period for both chloride (NaCl) and composite chloride (NaCl)-sulfate (both Na_2SO_4 and $MgSO_4$) solutions as observed from Figures 6.15, 6.16, 6.18, 6.19, 6.21 and 6.22, although the free chloride content was lower in OPC + 20% FA concrete at rebar level as compared to OPC concrete. However, Oliveira and Cascudo [154] reported that the concrete made with OPC plus 25% fly ash showed lower corrosion current density as compared to that made with OPC in case of exposure to NaCl solution under drying-wetting cycle (1 cycle consist of 2 days of wetting followed by 5 days of drying) till 46 cycles. In the present study, the higher corrosion current density in OPC + 20% FA concrete during the early exposure period may be attributed to the alteration in the electrolytic pore solution of concrete due to variations in oxygen and moisture content in the vicinity of steel reinforcement. However, the specimens made with OPC mostly exhibited higher corrosion current density as compared to those made with OPC + 20% FA against exposure to NaCl solutions and composite solutions of NaCl with $MgSO_4$ during the later exposure period as observed from Figures 6.15, 6.16, 6.18, 6.19, 6.21 and 6.22. The higher corrosion current density of steel reinforcement in OPC is due to the increased conductivity of concrete as result of more free chloride content at rebar level as compared to OPC + 20% FA concrete against exposure to both NaCl solutions and composite solutions of NaCl with $MgSO_4$. In case of exposure to composite solutions of NaCl with Na_2SO_4, the variation in corrosion

current density was not systematic between OPC and OPC + 20% FA concrete during the later exposure period.

While analyzing the variations in corrosion current density of steel reinforcement with exposure period, it is inferred that the variation in corrosion current density with increase in exposure period was very less in OPC concrete when exposed to composite solutions of NaCl with $MgSO_4$ (2% and 4%), and NaCl with Na_2SO_4 (2% and 4%) at 1% and 3% NaCl concentrations as observed from Figure 6.15 and 6.18. In case of exposure to only chloride solutions (i.e. 1% and 3% NaCl concentrations), the variation in corrosion current density with exposure period was very less in OPC concrete during the early exposure periods whereas the corrosion current density of steel reinforcement increased significantly during the later exposure periods. Similarly, at 5% NaCl concentration, the variation in corrosion current density with exposure period was very less during the early exposure periods whereas the corrosion current density increased during the later exposure periods in OPC concrete against all exposure solutions (i.e. both chloride and composite chloride-sulfate solution) as observed from Figure 6.21. However, the increase in corrosion current density was significantly higher in case of exposure to NaCl solution as compared to composite solutions of NaCl with $MgSO_4$ or Na_2SO_4 during the later exposure periods as evident from Figure 6.21. Thus, from the aforementioned observations, it is inferred that the presence of chloride ions had significant effect on variations in corrosion rate of steel reinforcement whereas the presence of sulfate ions (irrespective of associated cation i.e. Na^+ and Mg^{2+}) in the exposure solution (i.e. composite chloride-sulfate solution) hindered the effect of chloride ions on increasing the corrosion rate of steel reinforcement in OPC concrete during the later exposure periods.

In OPC + 20% FA concrete, the variation in corrosion current density of steel reinforcement with exposure period was very less against exposure to composite solutions of NaCl (1%, 3%, and 5% NaCl) with $MgSO_4$ (2% and 4%) as observed from Figure 6.16, 6.19 and 6.22. In case of exposure to composite solutions of NaCl (1%, 3%, and 5%) with Na_2SO_4 (2% and 4%), the corrosion current density of steel reinforcement decreased with increase in exposure during the early period, however, afterward the variation in corrosion current density with exposure period was very less. In case of exposure to chloride solutions, the variation in corrosion current density with exposure period was very less during the early exposure periods, however the corrosion current density increased significantly during the later exposure periods at all concentrations of NaCl i.e. 1%, 3%, and 5% in OPC + 20%

FA concrete as observed from Figure 6.16, 6.19 and 6.22. This indicates that chloride ions had significant effect on variation in corrosion rate of steel reinforcement during the later exposure periods in OPC + 20% FA concrete. However, the effect of chloride ions on increasing the corrosion rate of steel reinforcement was mitigated in the presence of sulfate ions (for both cations i.e. Na^+ and Mg^{2+}) during the later exposure periods in OPC + 20% FA concrete exposed to composite chloride-sulfate solutions.

In PPC concrete, the corrosion current density of steel reinforcement decreased with increase in exposure period for all exposure solutions (i.e. both chloride and composite chloride-sulfate solutions) during the early period, however, afterward the variation in corrosion current density with exposure period was very less as observed from Figure 6.17, 6.20 and 6.23. In few cases, the corrosion current density increased slightly during the later exposure period at 5% NaCl concentration for both chloride and composite chloride-sulfate solutions. The higher corrosion current density in PPC concrete during the early exposure period (although the free chloride content was lower) may be attributed to the dominant effect of variations in oxygen and moisture content in the vicinity of steel reinforcement. The lower corrosion current density in PPC concrete during the later exposure period may be attributed to the dominant effect of very less free chloride content near rebar level (although the free chloride content was comparatively higher during the later exposure period as compared to that during early exposure period). As stated earlier in Section 4.3.1.3, (Chapter 4), the formation of denser microstructure in PPC concrete resulted in penetration of lower amount of chloride ions to higher depth intervals from the exposure surface of concrete during the entire exposure period as compared to other binders against exposure to chloride and composite chloride-sulfate solutions. Therefore, from the aforementioned observations, it is inferred that the chloride ions did not have significant effect on variation in corrosion rate of steel reinforcement in PPC concrete irrespective of exposure solution (i.e. chloride solutions and composite chloride-sulfate solution) as a result of penetration of lower amount of chloride ions.

In order to evaluate the effect of binder type, the obtained corrosion current density values were plotted between different types of binder irrespective of w/b ratio, and exposure solution at different exposure periods, and the plots are shown in Figure 6.24, Figure 6.25 and Figure 6.26 for OPC vs. PPC, OPC vs. OPC + 20% FA, and PPC vs. OPC + 20% FA respectively. These plots can be used to compare the variations in corrosion current density of steel reinforcement between two types of binder at different exposure periods.

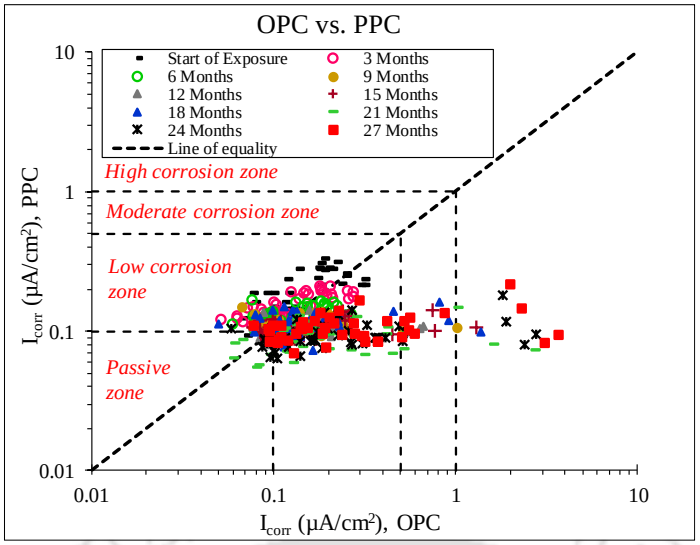

Figure 6.24 Comparison of corrosion current density of steel reinforcement in prismatic reinforced concrete specimens made with OPC, and PPC

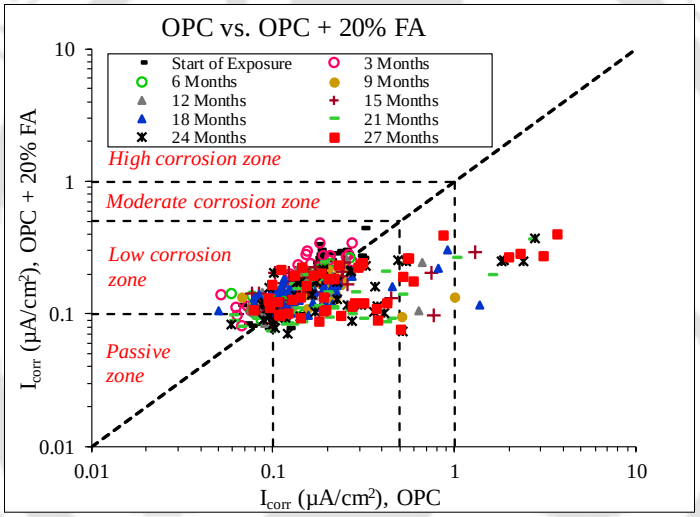

Figure 6.25 Comparison of corrosion current density of steel reinforcement in prismatic reinforced concrete specimens made with OPC, and OPC + 20% FA

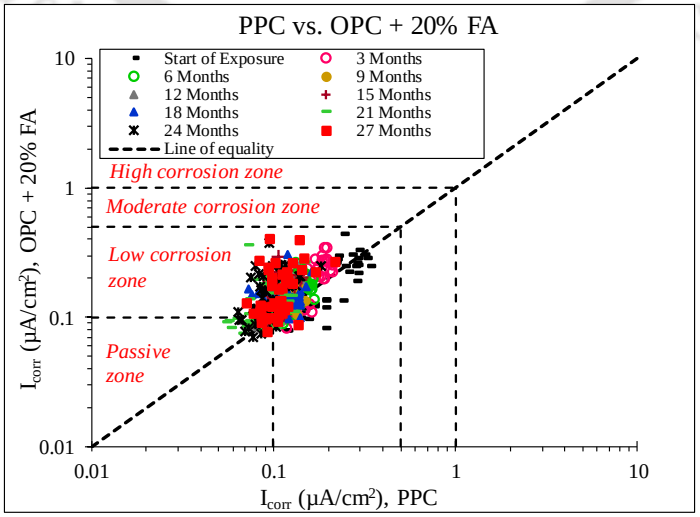

Figure 6.26 Comparison of corrosion current density of steel reinforcement in prismatic reinforced concrete specimens made with PPC, and OPC + 20% FA

From Figure 6.24 to 6.26, it is observed that the corrosion current density (I_{corr}) values lie in different zones with respect to the extent of corrosion such as passive zone (I_{corr}: less than 0.1 µA/cm^2), low corrosion zone (I_{corr}: 0.1 to 0.5 µA/cm^2), moderate corrosion zone (I_{corr}: 0.5 to 1.0 µA/cm^2), and high corrosion zone (I_{corr}: greater than 1 µA/cm^2) [155-157]. From Figure 6.24 and 6.25, it is observed that the corrosion current density values reached up to moderate and high corrosion zones mostly during the later exposure periods in the prismatic reinforced concrete specimens made from OPC against exposure to chloride (NaCl) and composite chloride (NaCl)-sulfate ($MgSO_4$ and Na_2SO_4) solutions. However, for the specimens made from OPC + 20% FA and PPC, the corrosion current density values mostly lie in low corrosion zone against exposure to chloride and composite chloride-sulfate solutions during the entire exposure period. Further, between OPC + 20% FA and PPC, the corrosion current density values were mostly higher in the specimens made from OPC + 20% FA as compared to those made from PPC as observed from Figure 6.26. Thus, from the viewpoint of corrosion current density, the concrete made from PPC performed better as compared to that made from OPC + 20% FA followed by OPC against corrosion of steel reinforcement in concrete exposed to chloride and composite chloride-sulfate solutions.

6.3.3. Effect of w/b ratio on corrosion current density

From Figure 6.17, 6.20 and 6.23, it is observed that in PPC concrete there was no systematic variation in corrosion current density of steel reinforcement with w/b ratio against exposure to both chloride and composite chloride-sulfate (both Mg^{2+} and Na^+ cations) solutions during the entire exposure period. This is attributed to the fact that the formation of denser microstructure in PPC concrete resulted in penetration of comparatively lower amount of chloride ions to higher depth intervals irrespective of w/b ratio as compared to other binders, which resulted in lower free chloride content near rebar level (i.e. in the depth interval of 20-25 mm from exposure surface of concrete). However, in OPC and OPC + 20% FA concrete, the corrosion current density mostly increased with increase in w/b ratio against exposure to chloride (NaCl) solutions throughout the entire exposure period i.e. till the exposure period of 27 months. This is attributed to the presence of higher amount of free chloride near rebar level in the concrete made with higher w/b ratio due to penetration of comparatively more amount of chloride ions.

In OPC + 20% FA concrete, the variation in corrosion current density of steel reinforcement with w/b ratio was not systematic against exposure to composite chloride-sulfate (both Mg^{2+} and Na^{+} cations) solutions throughout the entire exposure period as observed from Figure 6.16, 6.19 and 6.22. This may be due to the fact that the simultaneous ingress of sulfate ions as well as formation of comparatively denser microstructure in OPC + 20% FA concrete resulted in a reduction in penetration of chloride ions to the rebar level irrespective of w/b ratio, which might have altered the conductivity of concrete. In OPC concrete, during the early exposure periods, the variation in corrosion current density with w/b ratio was not systematic against exposure to composite chloride-sulfate (both Mg^{2+} and Na^{+} cations) solutions. However, during the later exposure periods, the corrosion current density increased with increase in w/b ratio as observed from Figure 6.15, 6.18 and 6.21. The higher corrosion current density of steel reinforcement at higher w/b ratio during the later exposure periods when exposed to composite chloride-sulfate (both Mg^{2+} and Na^{+} cations) solutions may be attributed to the increase in conductivity of concrete due to the presence of higher free chloride content near steel reinforcement as a result of ingress of comparatively more amount of chloride ions due to formation of a comparatively less denser pore structure in OPC concrete at higher w/b ratio, although there was comparatively reduced penetration of chloride ions because of simultaneous ingress of sulfate ions into concrete when compared with exposure to only chloride solution.

Similar to binder type, in order to categorize the obtained values of corrosion current density into different corrosion zones, the corrosion current density values were plotted between different w/b ratios irrespective of binder type and exposure solution at different exposure periods. The comparative plots are shown in Figure 6.27 and 6.28 for w/b ratios of 0.45 vs. 0.50, and 0.50 vs. 0.55 respectively. From these figures, it is observed that the corrosion current density values mostly lie in low corrosion zone irrespective of w/b ratio against exposure to chloride and composite chloride-sulfate solutions. However, the corrosion current density values reached up to moderate and high corrosion zones in some of the specimens made with w/b ratios of 0.50 and 0.55 mostly during the later exposure periods as compared to w/b ratio of 0.45 as observed from Figure 6.27 and 6.28. Further, between w/b ratios of 0.50 and 0.55, the corrosion current density of steel reinforcement was mostly higher at w/b ratio of 0.55 as compared to that at w/b ratio of 0.50 as observed from Figure 6.28. Thus, the concrete made with lower w/b ratio showed better performance

as compared to that made with higher w/b ratio against corrosion of steel reinforcement in concrete exposed to chloride and composite chloride-sulfate solutions for all binders.

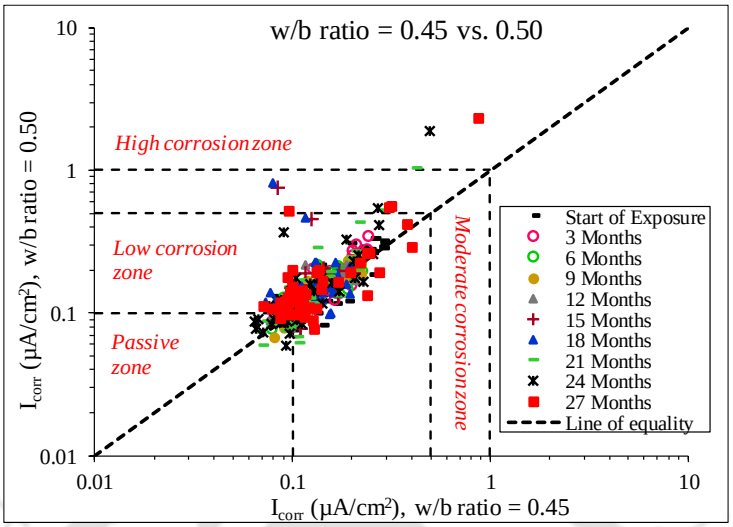

Figure 6.27 Comparison of corrosion current density of steel reinforcement in prismatic reinforced concrete specimens made at w/b ratios of 0.45, and 0.50

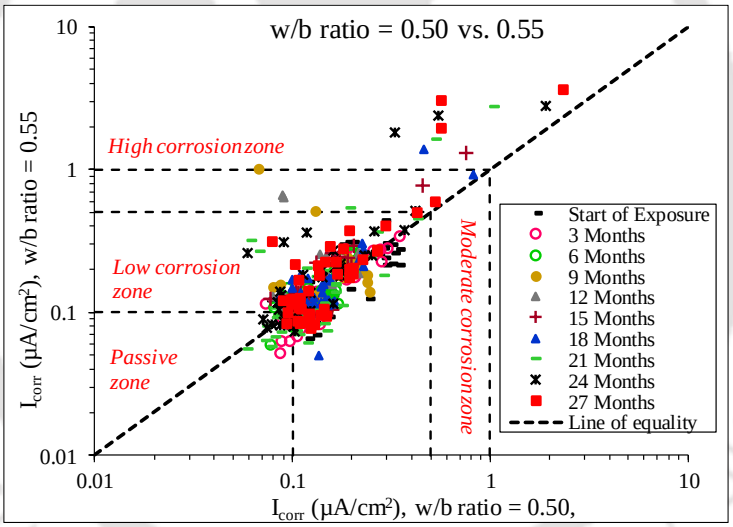

Figure 6.28 Comparison of corrosion current density of steel reinforcement in prismatic reinforced concrete specimens made at w/b ratios of 0.50, and 0.55

6.4. Empirical relationships between durability parameters

The empirical relationships were established between corrosion current density (I_{corr}) and the parameters such as half-cell potential (E_0), apparent chloride diffusion coefficient (D), and rebar surface chloride concentration (C_{rs}) obtained from the same prismatic reinforced concrete specimen for different types of binder and exposure solution. As mentioned earlier in Chapter 3, and Chapter 4, the free chloride content, and apparent chloride diffusion coefficient of concrete were determined at the end of exposure periods of 9, 15, 21, and 27 months in case of exposure to NaCl solutions, and composite solutions of NaCl + $MgSO_4$,

and at the end of exposure periods of 15, 21, and 27 months in case of exposure to composite solutions of NaCl + Na_2SO_4. As observed from the results of corrosion parameters, the variations in both half-cell potential (Figure 6.1 to 6.9) and corrosion current density (Figure 6.15 to 6.23) were less during the early exposure periods whereas the variations in these corrosion parameters were significantly higher during the later exposure periods among various exposure solutions for different types of binder and w/b ratio. Keeping this in view, the values of different parameters i.e. corrosion current density, half-cell potential, apparent chloride diffusion coefficient, and rebar surface chloride concentration obtained at the end of later exposure periods, i.e. 21 months and 27 months were used for developing the empirical relationships.

6.4.1. Empirical relationship between half-cell potential (E_0) and corrosion current density (I_{corr})

The reason for developing the empirical relationship between half-cell potential (E_0) and corrosion current density (I_{corr}) is that for measurement of corrosion current density by polarization resistance technique, there is a need to accurately determine the surface area of the steel bar over which the external perturbation is applied through the auxiliary electrode. Further especially, in case of field measurement of corrosion current density in the existing structures using polarization resistance technique, it is difficult to determine accurately the surface area of steel bar over which the applied perturbation will be confined because of the influence of nearby steel bars on the applied perturbation in the structure, which may result in inaccurate estimation of corrosion current density. However, in case of half-cell potential measurement, it is not required to know the surface area of the steel bar. Thus, when half-cell potential values of steel reinforcement for a given concrete mix are known, it is possible to estimate the corrosion current density of steel reinforcement from the developed empirical relationship for the concrete mix made with same/similar materials without measuring the corrosion current density.

The empirical relationship between the obtained half-cell potential (E_0) and corrosion current density (I_{corr}) was established by the nonlinear least squares regression analysis. First, the relationship was established by taking into account the experimentally obtained values of E_0 and I_{corr} for OPC, PPC, and all w/b ratios with respect to chloride (NaCl), and composite chloride (NaCl)-sulfate ($MgSO_4$ and Na_2SO_4 and) solutions. After that, the established empirical relationship was used for predicting the I_{corr} value of embedded steel

bar in concrete made with OPC + 20% FA from the experimentally obtained E_0 values, followed by comparing the predicted values with the experimentally obtained values of I_{corr} for OPC + 20% FA concrete. For each of the exposure periods of 21 months and 27 months, the relationships were developed for the specimens exposed to NaCl solutions, composite solutions of NaCl with $MgSO_4$, and composite solutions of NaCl with Na_2SO_4. Further, the relationships were established by combining the results of both exposure periods (21 months and 27 months) for chloride and composite chloride-sulfate solutions.

First, the experimentally obtained values of E_0, and I_{corr} for a given exposure period were plotted irrespective of binder type (OPC and PPC), w/b ratio (0.45, 0.50, and 0.55) for a given exposure solution irrespective of its concentration i.e. NaCl concentrations of 1%, 3% and 5% for chloride solutions; NaCl concentrations of 1%, 3% and 5%, and $MgSO_4$ concentrations of 2% and 4% for composite solutions of NaCl + $MgSO_4$; and NaCl concentrations of 1%, 3% and 5%, and Na_2SO_4 concentrations of 2% and 4% for composite solutions of NaCl + Na_2SO_4. The plots are shown in Figure 6.29, 6.30 and 6.31 for NaCl solutions, composite solutions of NaCl + $MgSO_4$, and composite solutions of NaCl + Na_2SO_4 respectively. Using MATLAB [158], the Levenberg-Marquardt algorithm was used for nonlinear least squares technique to establish the relationship between E_0 and I_{corr}. The functions attempted for the empirical relationship were first-degree polynomial, higher-degree polynomial, power function, and exponential function, etc. From among these regressive relationships, the exponential relationship exhibited the best empirical fit. The obtained empirical relationship between E_0 (-mV) and I_{corr} ($\mu A/cm^2$), which is a linear combination of the exponential functions is as follows;

$$I_{corr} = k_1 e^{A_1 E_0} + k_2 e^{A_2 E_0} \quad (6.1)$$

Where k_1 ($\mu A/cm^2$), A_1 (mV^{-1}), k_2 ($\mu A/cm^2$), and A_2 (mV^{-1}) are the coefficients. The fitted relationship between the experimentally obtained E_0 and I_{corr} along with the values of coefficients, and coefficient of correlation (R^2) are shown in Figure 6.29, Figure 6.30 and 6.31. The linear combination of exponential functions covered the large range of E_0 and I_{corr} values, and exhibited a higher value of R^2 than that exhibited by the single exponential relation. After that, the accuracy of this developed empirical formulation was ascertained by using it for predicting the I_{corr} values from the measured values of E_0 of the binder OPC + 20% FA, which are independent of the model development. The variations in the predicted I_{corr} values using the developed empirical model (Equation 6.1) with the measured

I_{corr} of embedded steel bar for OPC + 20% FA are shown in Figure 6.32, 6.33 and 6.34 respectively for NaCl solutions, composite solutions of NaCl with $MgSO_4$, and composite solutions of NaCl and Na_2SO_4 for exposure periods of 21 months, 27 months, and combining the results of both exposure periods i.e. 21 months and 27 months. From Figure 6.32 to 6.34, it is noted that, there is exists a good agreement between the measured and predicted values of I_{corr} of steel reinforcement in the concerete made with OPC + 20% FA as the values are closer towards the line of equality and are lying within ± 30% from it for chloride and composite chloride-sulfate solutions.

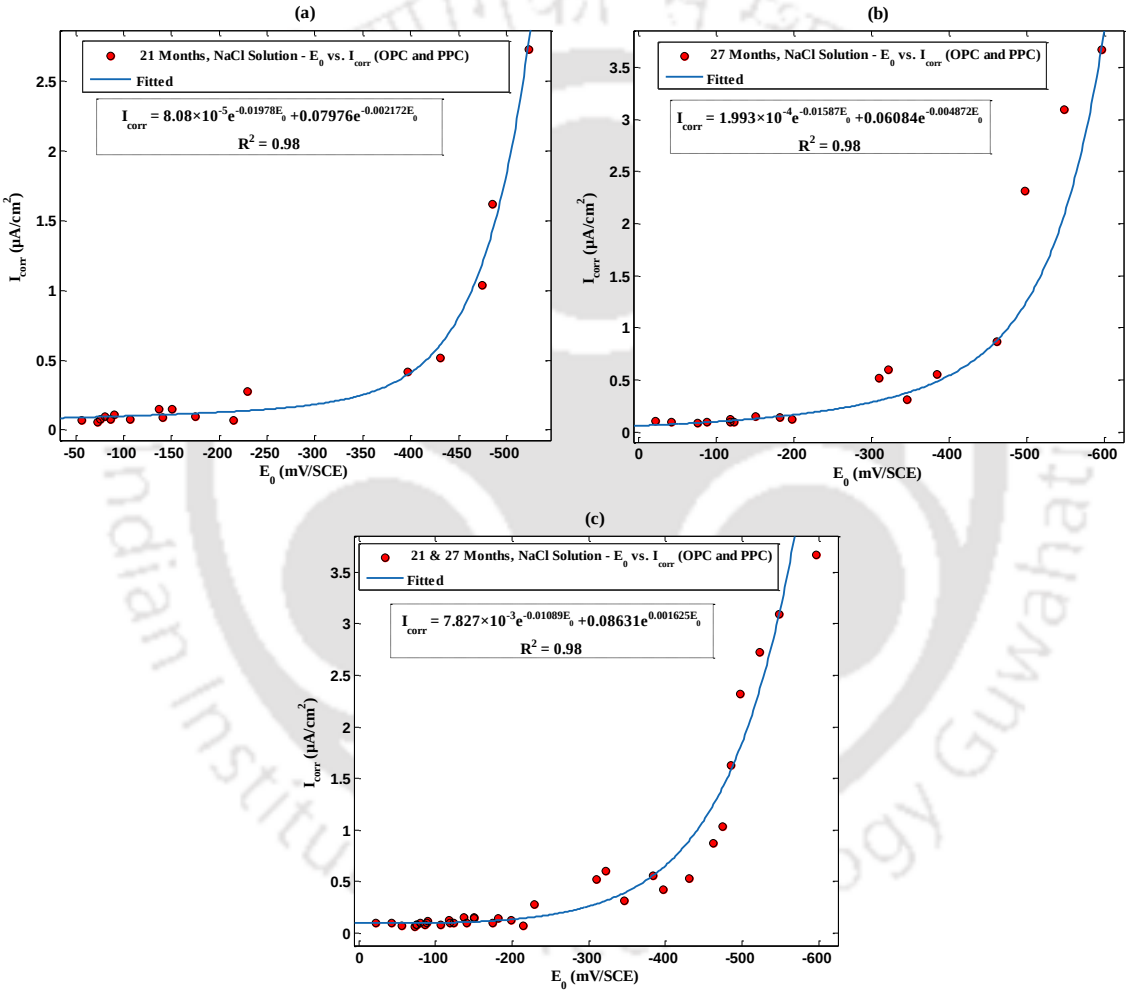

Figure 6.29 Relationship between experimentally obtained half-cell potential (E_0) and corrosion current density (I_{corr}) of rebar in concrete made from OPC and PPC, and exposed to NaCl solutions: (a) exposure period of 21 months, (b) exposure period of 27 months, and (c) combining the results of exposure periods of 21 and 27 months

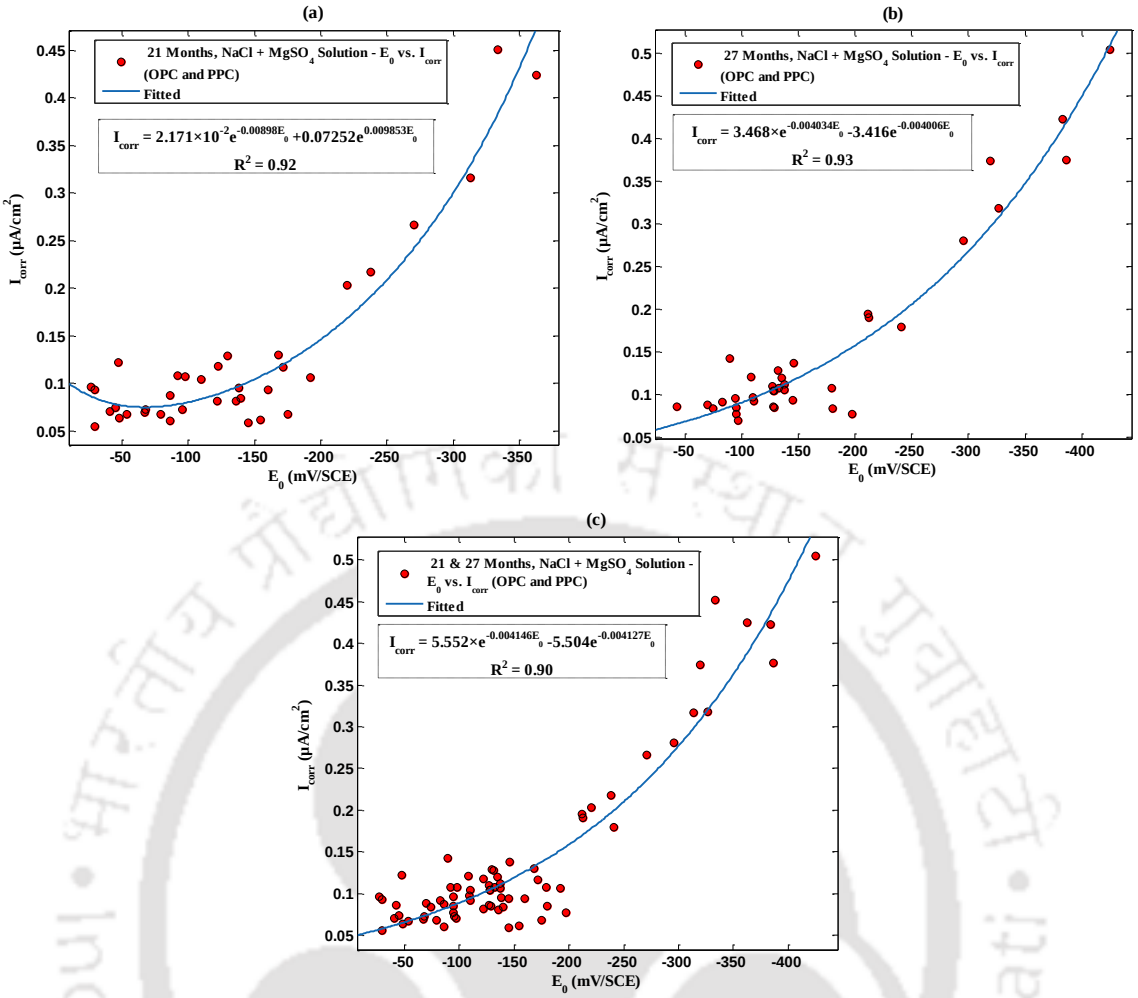

Figure 6.30 Relationship between experimentally obtained half-cell potential (E_0) and corrosion current density (I_{corr}) of rebar in concrete made from OPC and PPC, and exposed to composite solutions of NaCl with $MgSO_4$: (a) exposure period of 21 months, (b) exposure period of 27 months, and (c) combining the results of exposure periods of 21 and 27 months

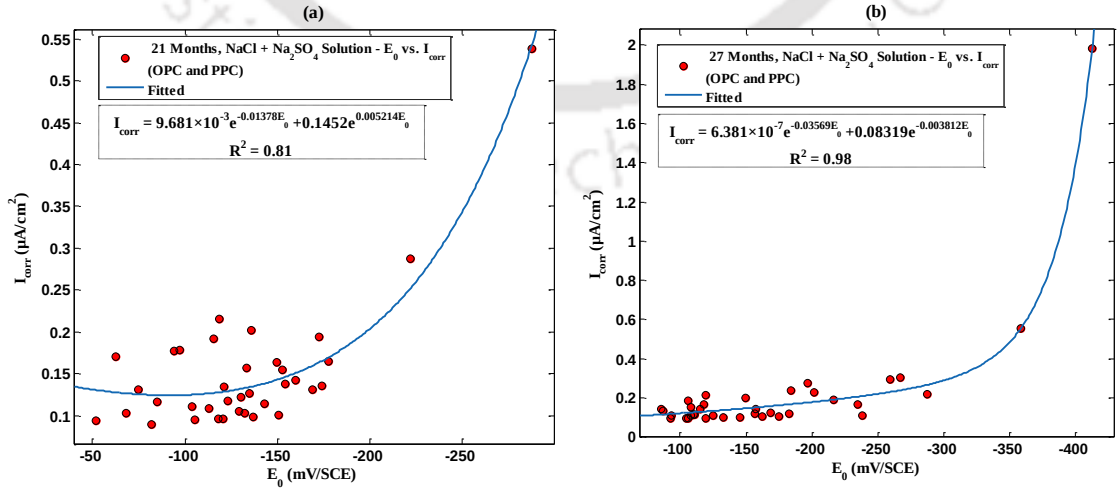

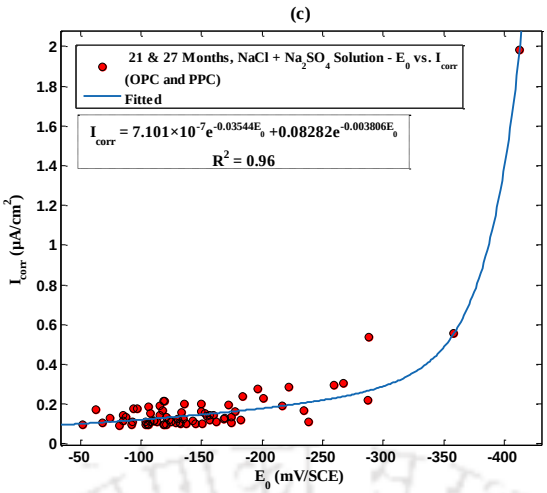

Figure 6.31 Relationship between experimentally obtained half-cell potential (E_0) and corrosion current density (I_{corr}) of rebar in concrete made from OPC and PPC, and exposed to composite solutions of NaCl with Na_2SO_4: (a) exposure period of 21 months, (b) exposure period of 27 months, and (c) combining the results of exposure periods of 21 and 27 months

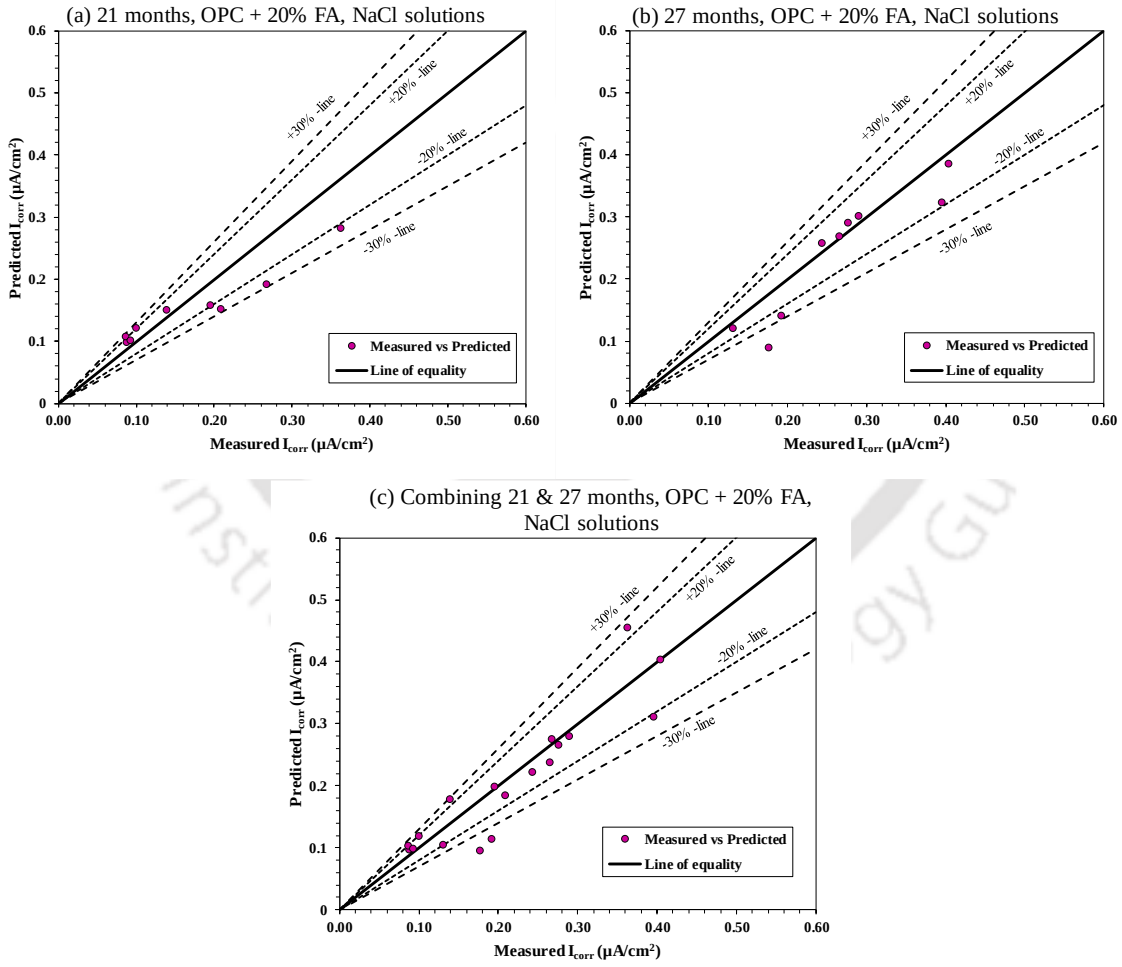

Figure 6.32 Comparison of measured I_{corr} and predicted I_{corr} (using the developed empirical relationship) from half-cell potential of rebar in OPC + 20% FA concrete exposed to NaCl solutions: (a) exposure period of 21 months, (b) exposure period of 27 months, and (c) combining the results of exposure periods of 21 and 27 months

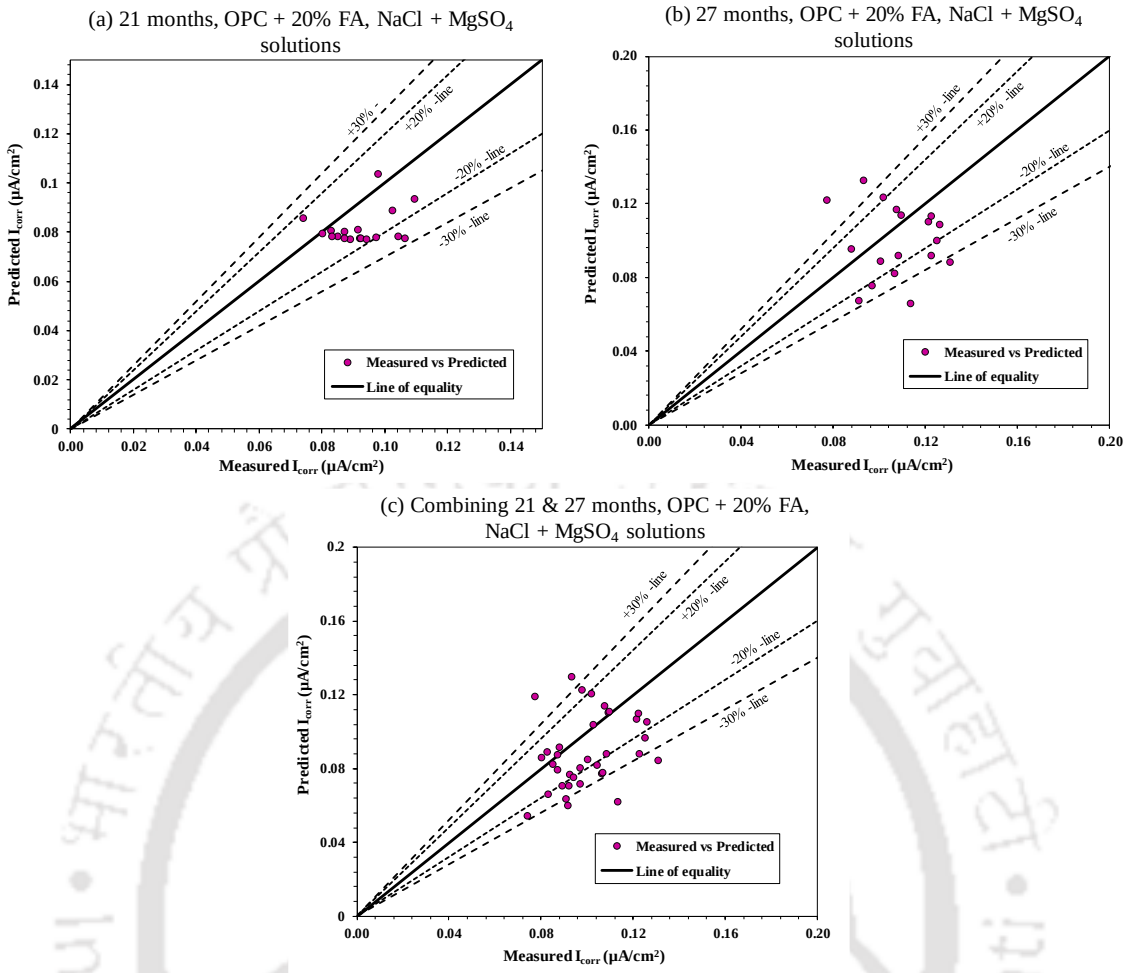

Figure 6.33 Comparison of measured I_{corr} and predicted I_{corr} (using the developed empirical relationship) from half-cell potential of rebar in OPC + 20% FA concrete exposed to composite solutions of NaCl with $MgSO_4$: (a) exposure period of 21 months, (b) exposure period of 27 months, and (c) combining the results of exposure periods of 21 and 27 months

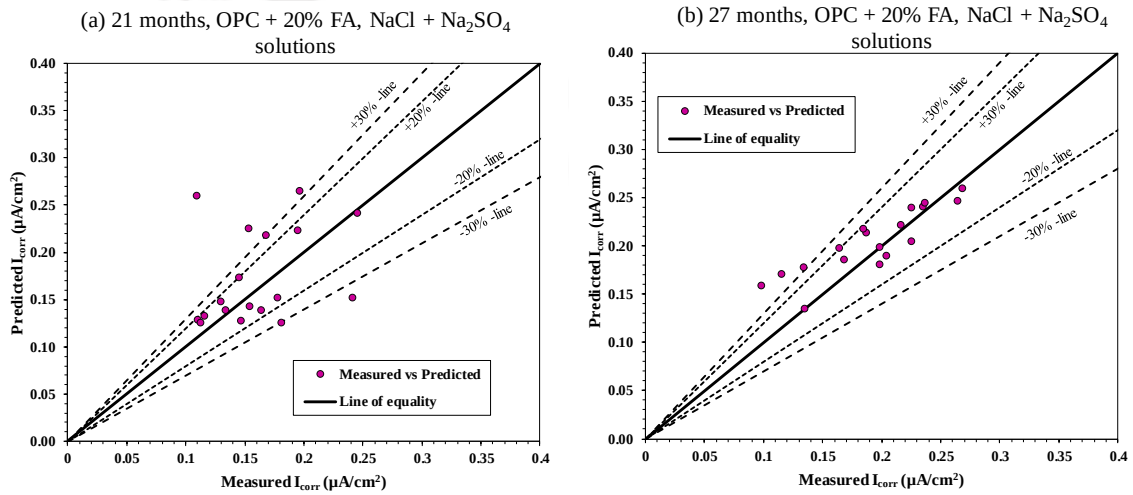

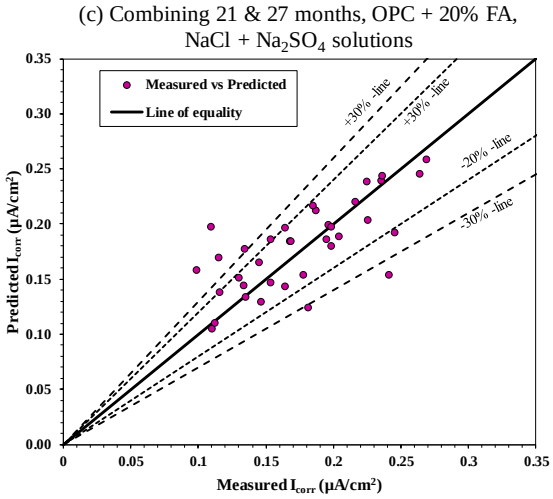

Figure 6.34 Comparison of measured I_{corr} and predicted I_{corr} (using the developed empirical relationship) from half-cell potential of rebar in OPC + 20% FA concrete exposed to composite solutions of NaCl with Na_2SO_4: (a) exposure period of 21 months, (b) exposure period of 27 months, and (c) combining the results of exposure periods of 21 and 27 months

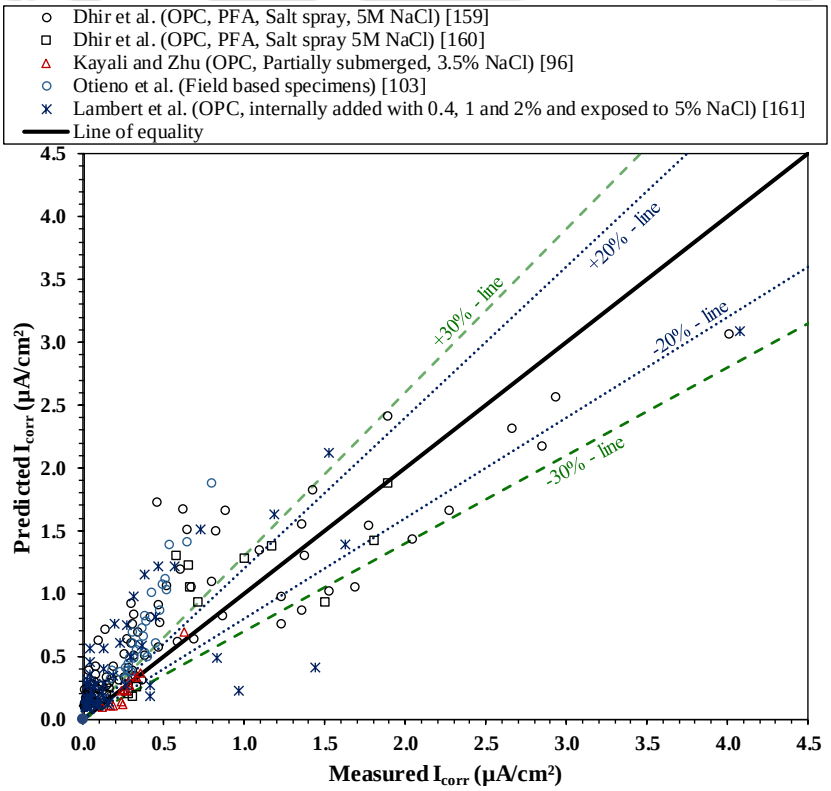

Figure 6.35 Comparison of measured I_{corr} and predicted I_{corr} (using the developed empirical relationship) from half-cell potential of steel based on the data from Dhir et al. [159], Dhir et al. [160], Kayali and Zhu [96], Otieno et al. [103] and Lambert et al. [161]

Further, the empirical exponential relation (Equation 6.1) developed for the case of combining the results of both exposure periods (21 months and 27 months) was used for

predicting the I_{corr} values from the E_0 values reported in the literature by various researchers for chloride exposure conditions [96, 103, 159-161]. The variations in the predicted I_{corr} values using the developed empirical exponential relation with the measured I_{corr} values reported in the literature are shown in Figure 6.35. From this figure, it is noted that a reasonably good agreement exists between the measured and predicted values of I_{corr}, as the values are closer towards the line of equality with majority of them lying within ± 30% from it.

6.4.2. Empirical relationship between apparent chloride diffusion coefficient (D) and corrosion current density (I_{corr})

Similar to the developed empirical relationship between the experimentally obtained half-cell potential (E_0) and corrosion current density (I_{corr}), an empirical relationship was established between apparent chloride diffusion coefficient (D), and corrosion current density (I_{corr}) for the exposure periods of 21 months, 27 months, and combining the results of both the exposure periods i.e. 21 months and 27 months. First, the estimated values of D, and measured values of I_{corr} for a given exposure period were plotted irrespective of binder type (OPC and PPC), and w/b ratio (0.45, 0.50, and 0.55) for a given exposure solution irrespective of its concentration. The plots are shown in Figure 6.36, 6.37 and 6.38 for NaCl solutions, composite solutions of NaCl with $MgSO_4$, and composite solutions of NaCl with Na_2SO_4 respectively. The Levenberg-Marquardt algorithm was used for the nonlinear least squares technique to establish the relationship between D, and I_{corr}. The regressive relationships as mentioned earlier (Section 6.4.1) were tried to establish the relationship, and the power function exhibited the best empirical fit with higher value of coefficient of correlation (R^2) as shown in Figure 6.36 - 6.38. The obtained power function relationship between D (cm^2/s) and I_{corr} ($\mu A/cm^2$) is as follows;

$$I_{corr} = k_3 D^{A_3} + k_4 \quad (6.2)$$

Where, k_3 ($\mu A.s/cm^4$), A_3 and k_4 ($\mu A/cm^2$) are the coefficients. The fitted relationship between D, and I_{corr} along with the values of coefficients and coefficient of correlation (R^2) are shown in Figure 6.36 - 6.38. After that, the accuracy of this developed empirical formulation was determined by using it for predicting the I_{corr} values from the estimated values of D of the binder OPC + 20% FA, which are independent of model development. The variations in the predicted I_{corr} using the developed empirical model (Equation 6.2) with the measured I_{corr} of embedded steel reinforcement for OPC + 20% FA are shown in

Figure 6.39, 6.40 and 6.41 for NaCl solutions, composite solutions of NaCl with $MgSO_4$, and composite solutions of NaCl and Na_2SO_4 respectively. From these figures, it is noted that there exists a good agreement between the measured and predicted values of I_{corr} for OPC + 20% FA concrete.

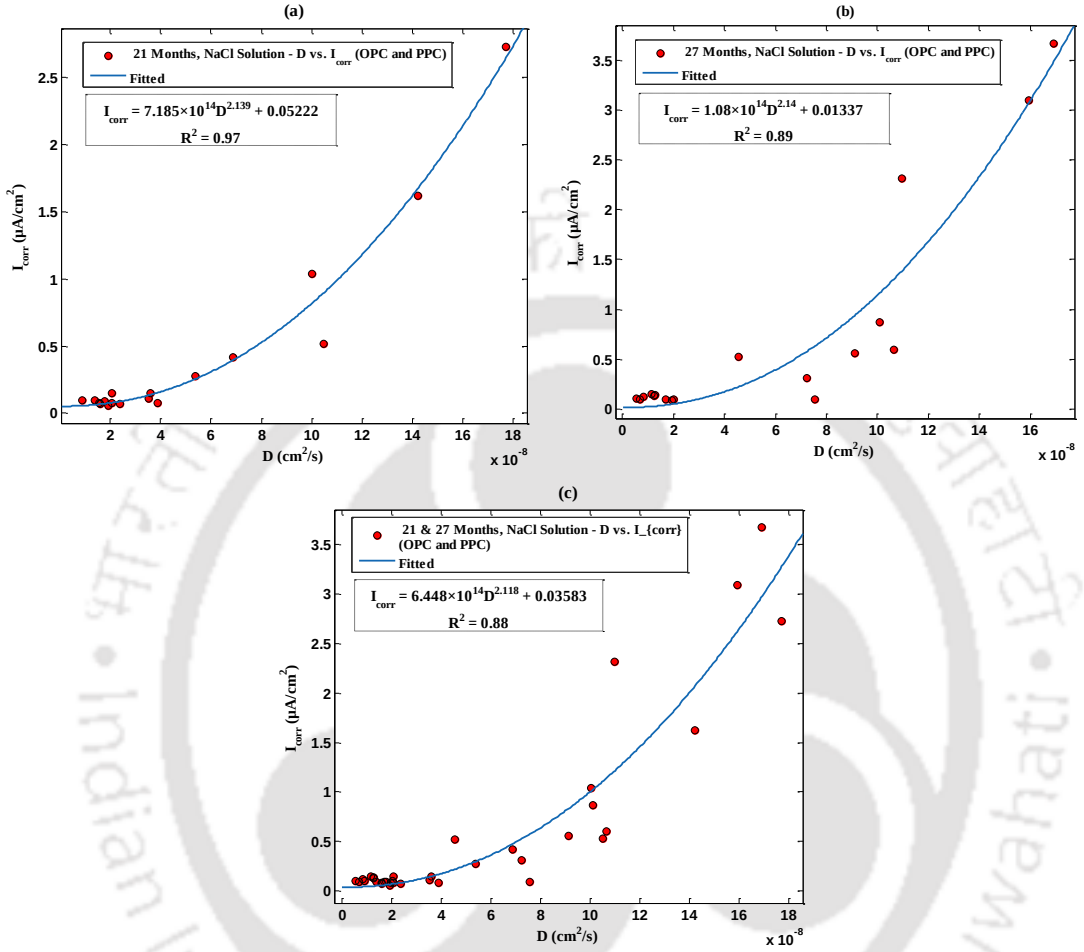

Figure 6.36 Relationship between apparent chloride diffusion coefficient (D) and corrosion current density (I_{corr}) of rebar in concrete made from OPC and PPC, and exposed to NaCl solutions: (a) exposure period of 21 months, (b) exposure period of 27 months, and (c) combining the results of exposure periods of 21 and 27 months

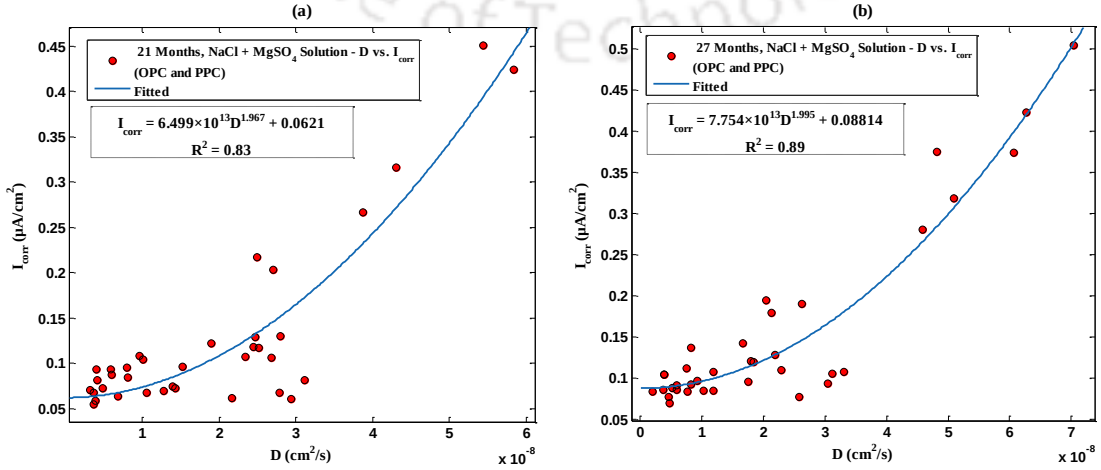

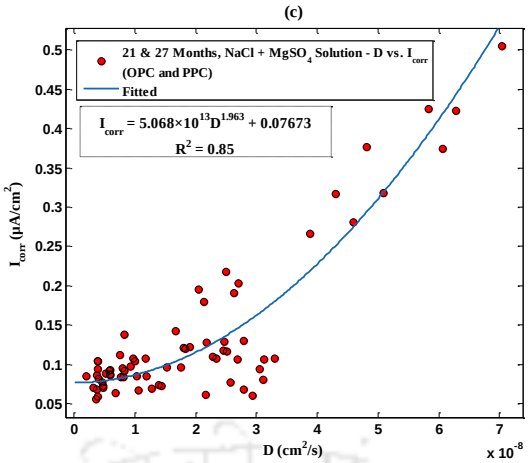

Figure 6.37 Relationship between apparent chloride diffusion coefficient (D) and corrosion current density (I_{corr}) of rebar in concrete made from OPC and PPC, and exposed to composite solutions of NaCl with $MgSO_4$: (a) exposure period of 21 months, (b) exposure period of 27 months, and (c) combining the results of exposure periods of 21 and 27 months

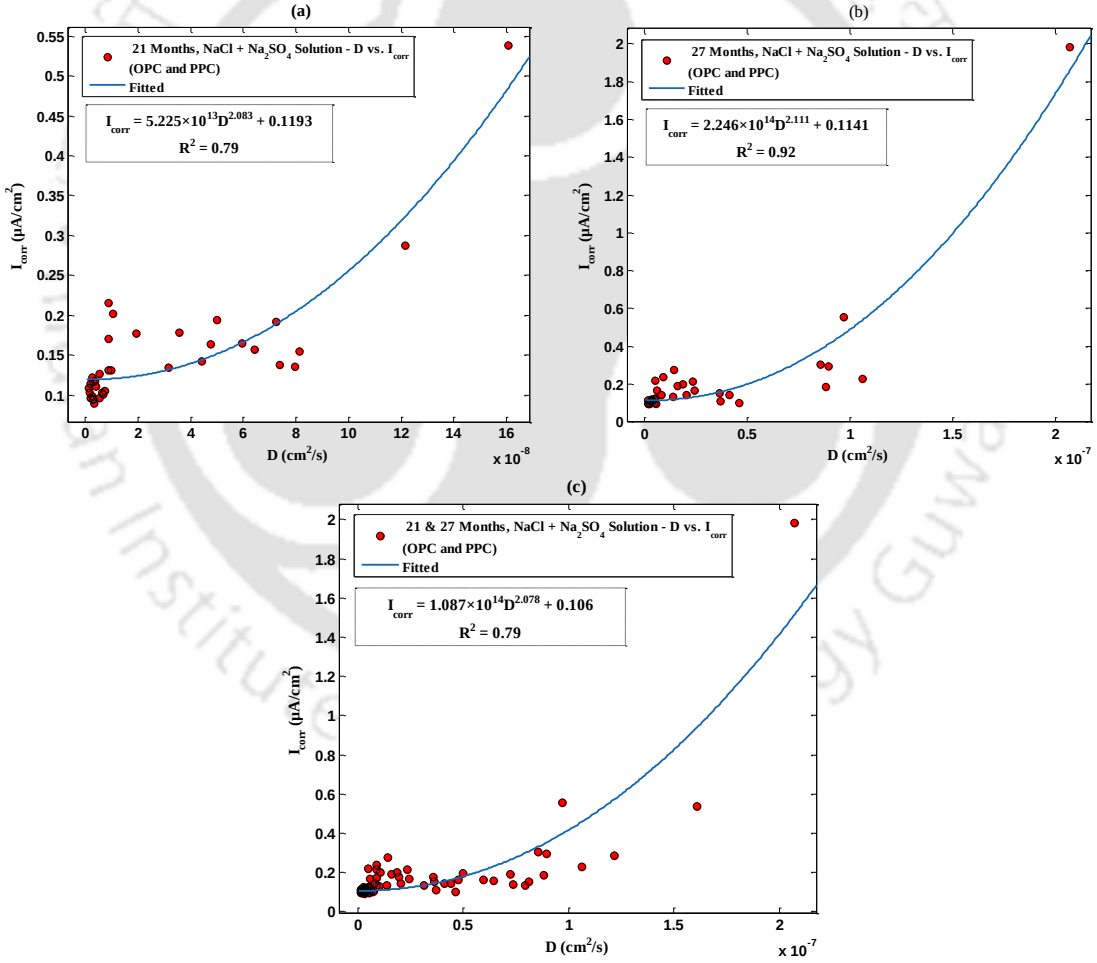

Figure 6.38 Relationship between apparent chloride diffusion coefficient (D) and corrosion current density (I_{corr}) of rebar in concrete made from OPC and PPC, and exposed to composite solutions of NaCl with Na_2SO_4: (a) exposure period of 21 months, (b) exposure period of 27 months, and (c) combining the results of exposure periods of 21 and 27 months

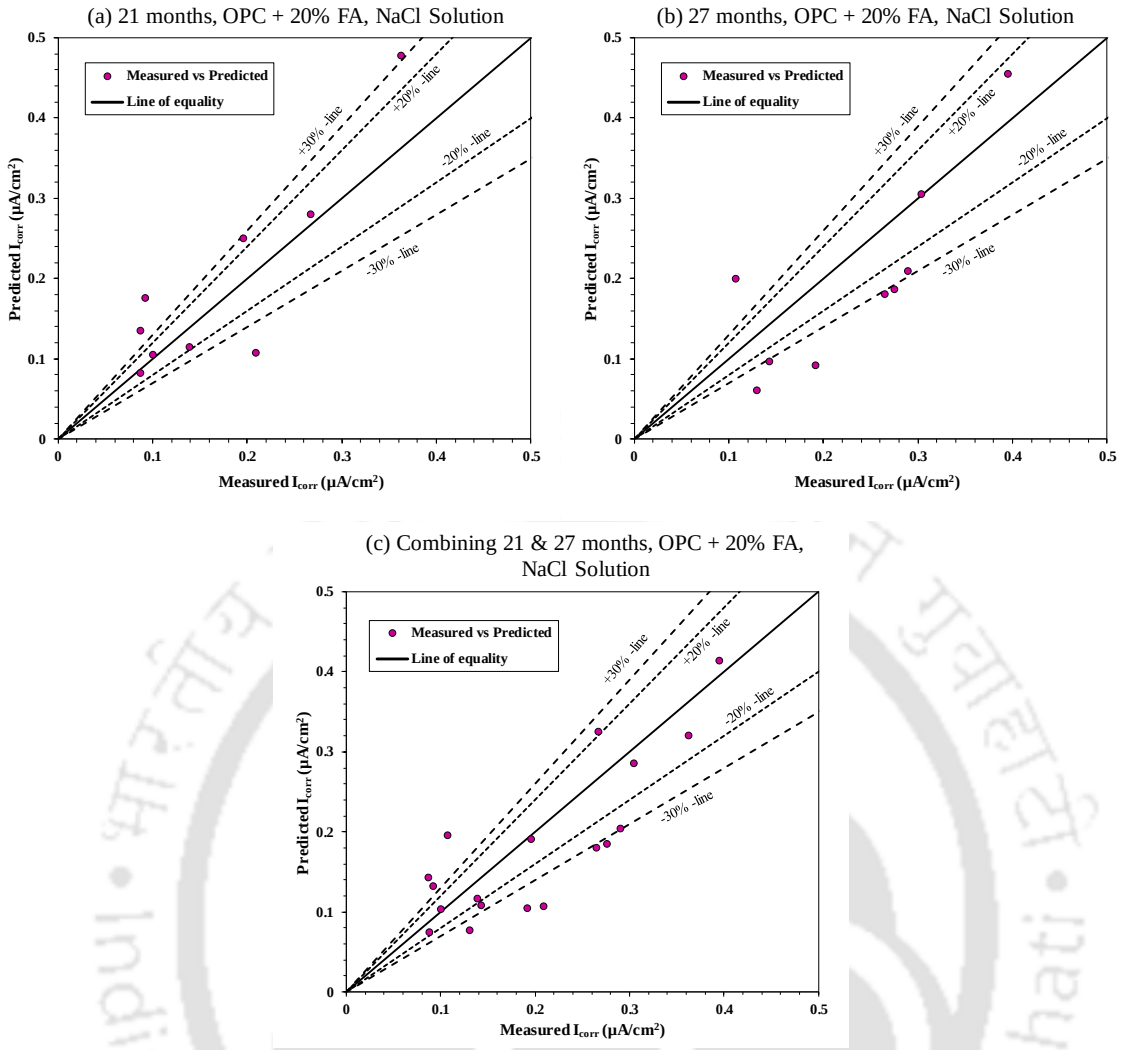

Figure 6.39 Comparison of measured I_{corr} and predicted I_{corr} (using the developed empirical relationship) from apparent chloride diffusion coefficient of OPC + 20% FA concrete exposed to NaCl solutions: (a) exposure period of 21 months, (b) exposure period of 27 months, and (c) combining the results of exposure periods of 21 and 27 months

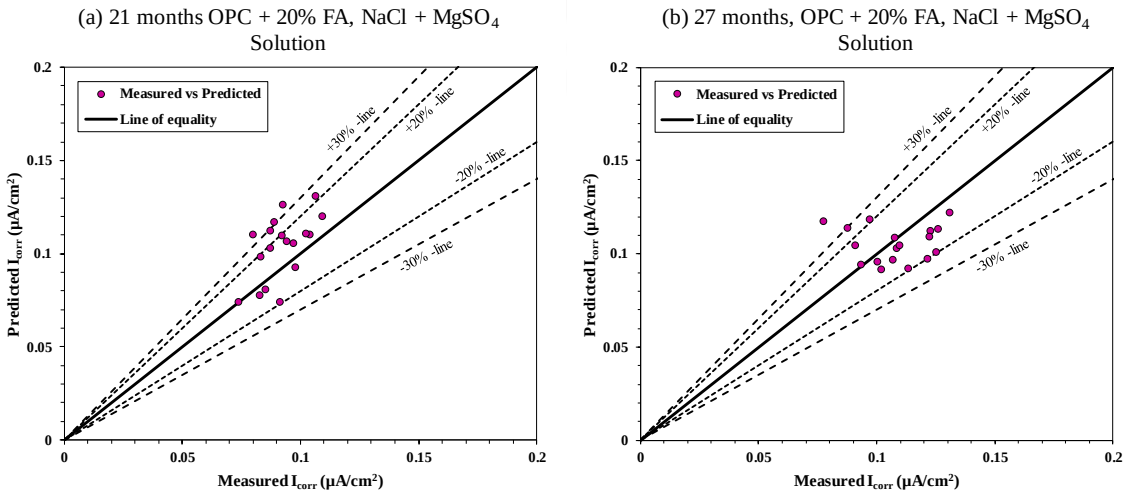

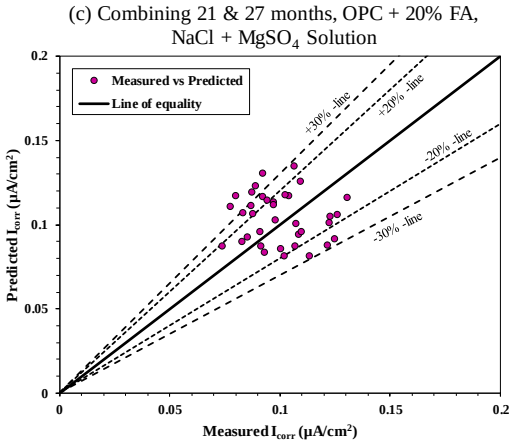

Figure 6.40 Comparison of measured I_{corr} and predicted I_{corr} (using the developed empirical relationship) from apparent chloride diffusion coefficient of OPC + 20% FA concrete exposed to composite solutions of NaCl with $MgSO_4$: (a) exposure period of 21 months, (b) exposure period of 27 months, and (c) combining the results of exposure periods of 21 and 27 months

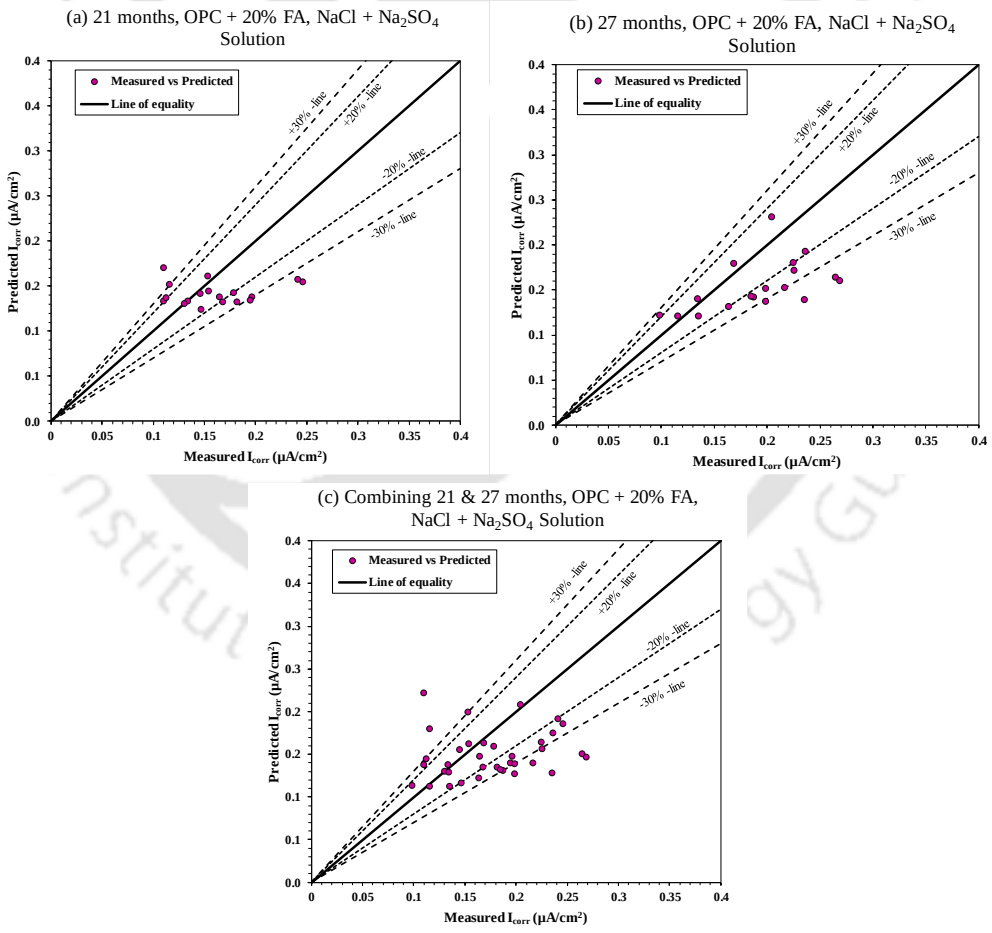

Figure 6.41 Comparison of measured I_{corr} and predicted I_{corr} (using the developed empirical relationship) from apparent chloride diffusion coefficient of OPC + 20% FA concrete exposed to composite solutions of NaCl with Na_2SO_4: (a) exposure period of 21 months, (b) exposure period of 27 months, and (c) combining the results of exposure periods of 21 and 27 months

6.4.3. Empirical relationship between rebar surface chloride concentration (C_{rs}) and corrosion current density (I_{corr})

Similarly, an empirical relationship was established between rebar surface chloride concentration (C_{rs}) and corrosion current density (I_{corr}) for the exposure periods of 21 months, 27 months, and combining the results of both the exposure periods i.e. 21 months and 27 months. The estimated C_{rs} and measured I_{corr} values for a given exposure period were plotted irrespective of binder type (OPC and PPC), and w/b ratio (0.45, 0.50, and 0.55) for a given exposure solution irrespective of its concentration. The plots are shown in Figure 6.42, 6.43 and 6.44 for NaCl solutions, composite solutions of NaCl with $MgSO_4$, and composite solutions of NaCl with Na_2SO_4 respectively. The Levenberg-Marquardt algorithm was used for the nonlinear least squares technique to establish the empirical relationship between C_{rs} and I_{corr}. From among the various regressive relationships tried, the power function exhibited the best empirical fit. The obtained empirical relationship between C_{rs} (% by weight of concrete) and I_{corr} ($\mu A/cm^2$) is as follows;

$$I_{corr} = k_5 C_{rs}^{A_4} + k_6 \quad (6.3)$$

Where, k_5 ($\mu A/cm^2.\%$), A_4 and k_6 ($\mu A/cm^2$) are the coefficients. The fitted relationship between C_{rs} and I_{corr} along with the values of coefficients, and coefficient of correlation (R^2) are shown in Figure 6.42 - 6.44. After that, the accuracy of this developed empirical formulation was ascertained by using it to predict the I_{corr} values from the estimated values of C_{rs} of the binder OPC + 20% FA, which are independent of the model development. The variations in the predicted values of I_{corr} using the developed empirical model (Equation 6.3) with the measured values of I_{corr} of embedded steel reinforcement for OPC + 20% FA are shown in Figure 6.45, 6.46 and 6.47 for NaCl solutions, composite solutions of NaCl with $MgSO_4$, and composite solutions of NaCl with Na_2SO_4 respectively. From these figures, it is inferred that there is a good agreement between the measured and predicted values of I_{corr} for OPC + 20% FA concrete.

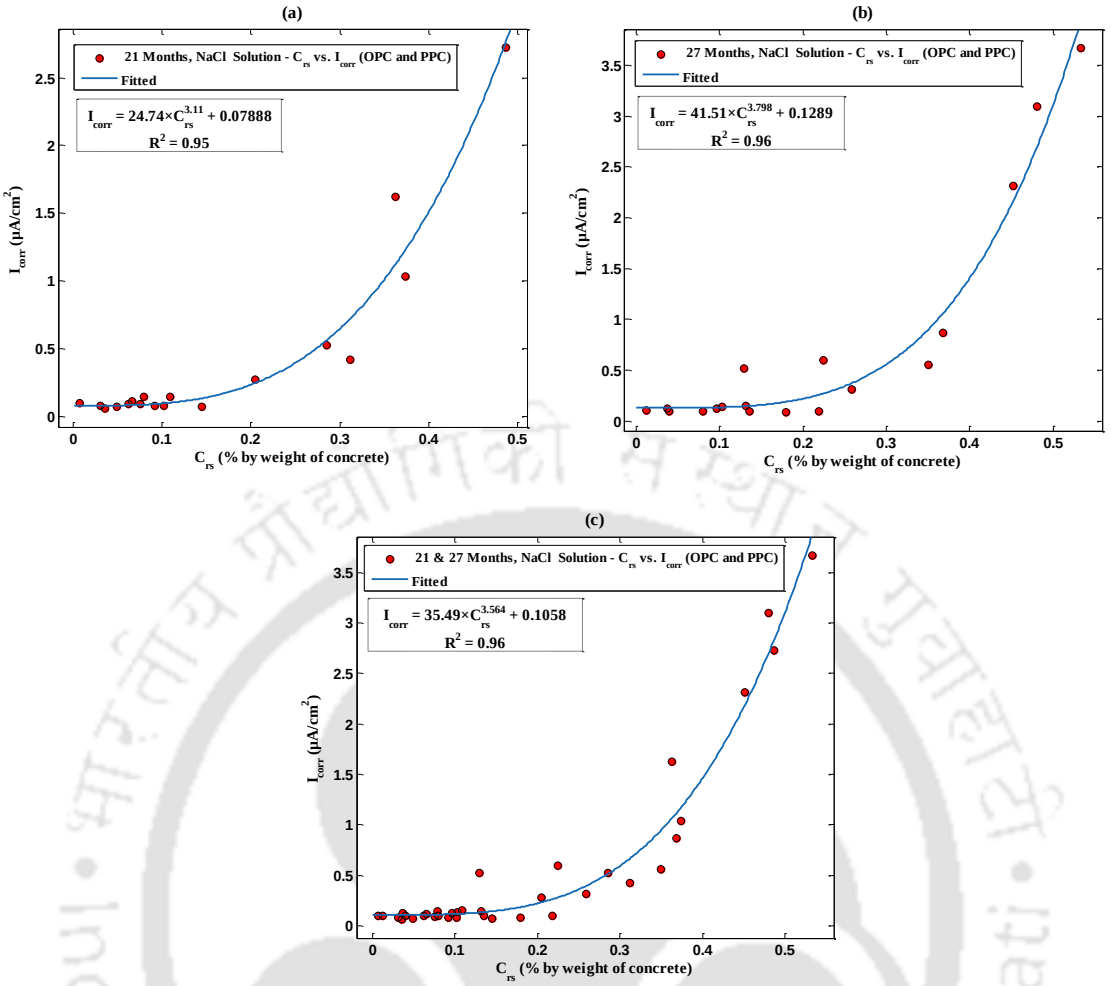

Figure 6.42 Relationship between rebar surface chloride concentration (C_{rs}) and corrosion current density (I_{corr}) of rebar in concrete made from OPC and PPC, and exposed to NaCl solutions: (a) exposure period of 21 months, (b) exposure period of 27 months, and (c) combining the results of exposure periods of 21 and 27 months

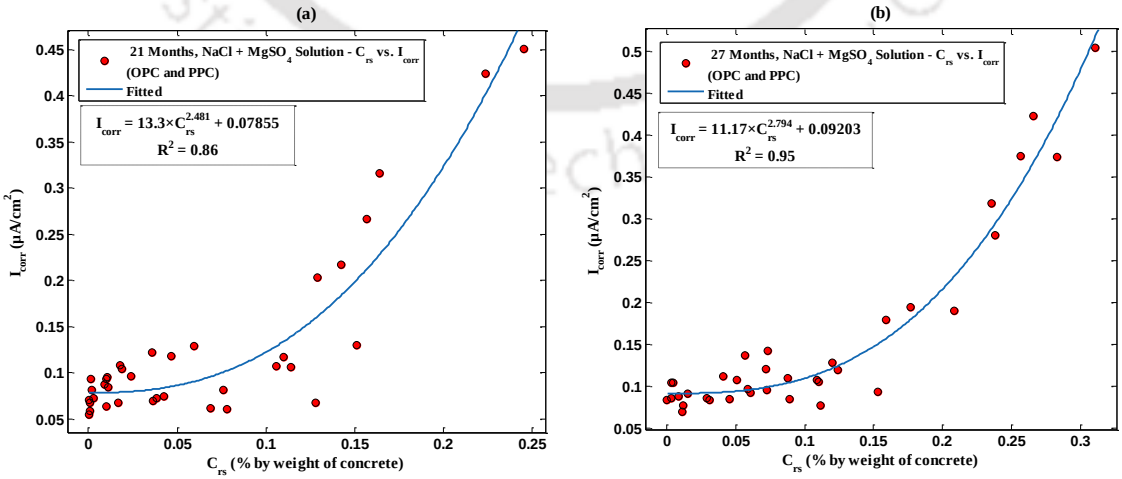

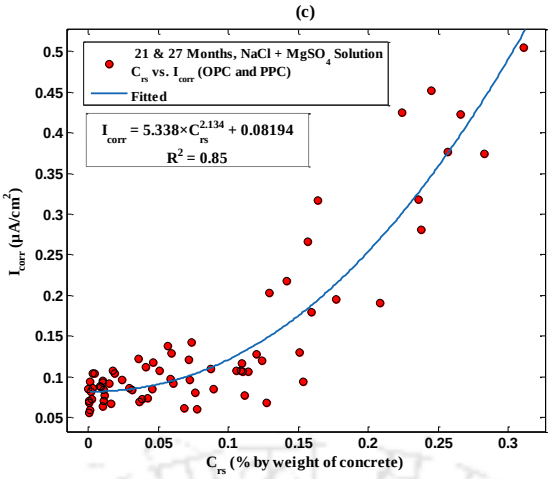

Figure 6.43 Relationship between rebar surface chloride concentration (C_{rs}) and corrosion current density (I_{corr}) of rebar in concrete made from OPC and PPC, and exposed to composite solutions of NaCl with $MgSO_4$: (a) exposure period of 21 months, (b) exposure period of 27 months, and (c) combining the results of exposure periods of 21 and 27 months

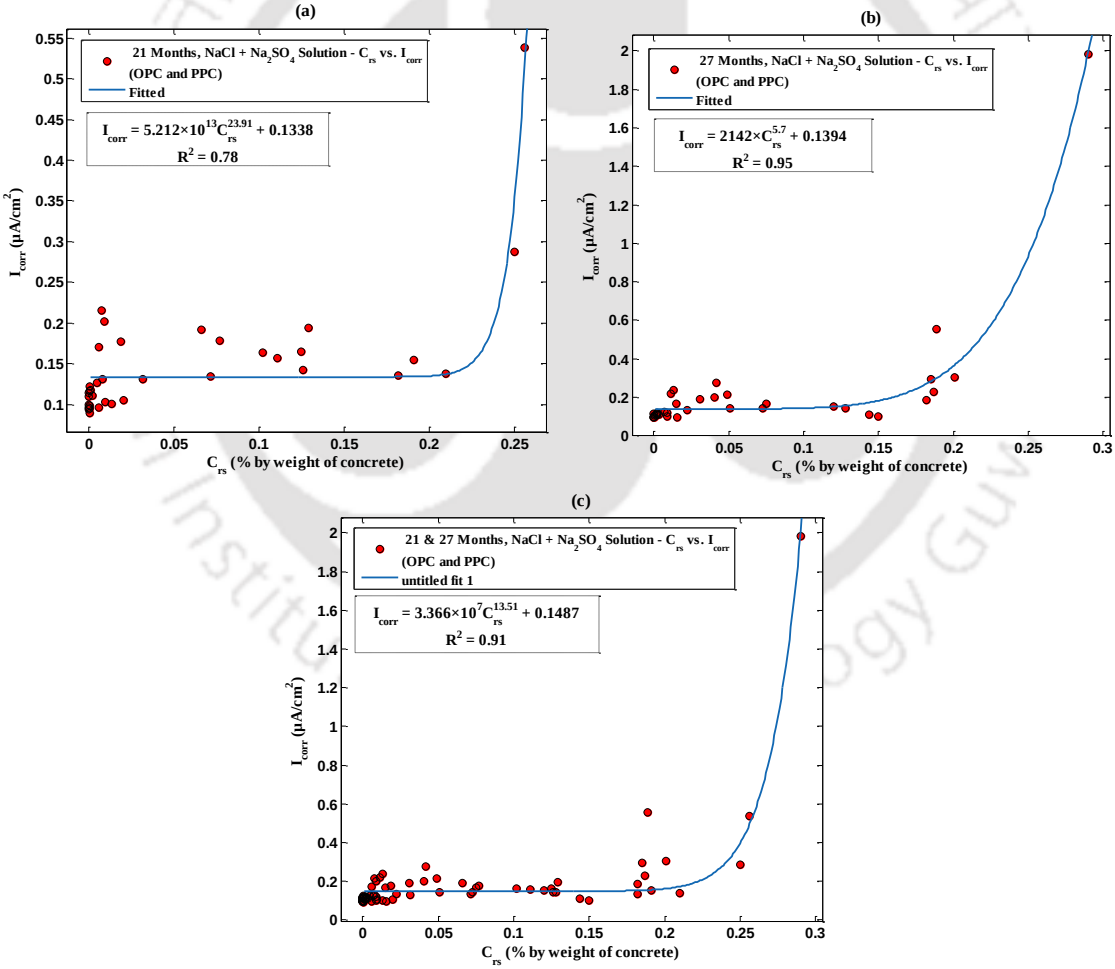

Figure 6.44 Relationship between rebar surface chloride concentration (C_{rs}) and corrosion current density (I_{corr}) of rebar in concrete made from OPC and PPC, and exposed to composite solutions of NaCl with Na_2SO_4: (a) exposure period of 21 months, (b) exposure period of 27 months, and (c) combining the results of exposure periods of 21 and 27 months

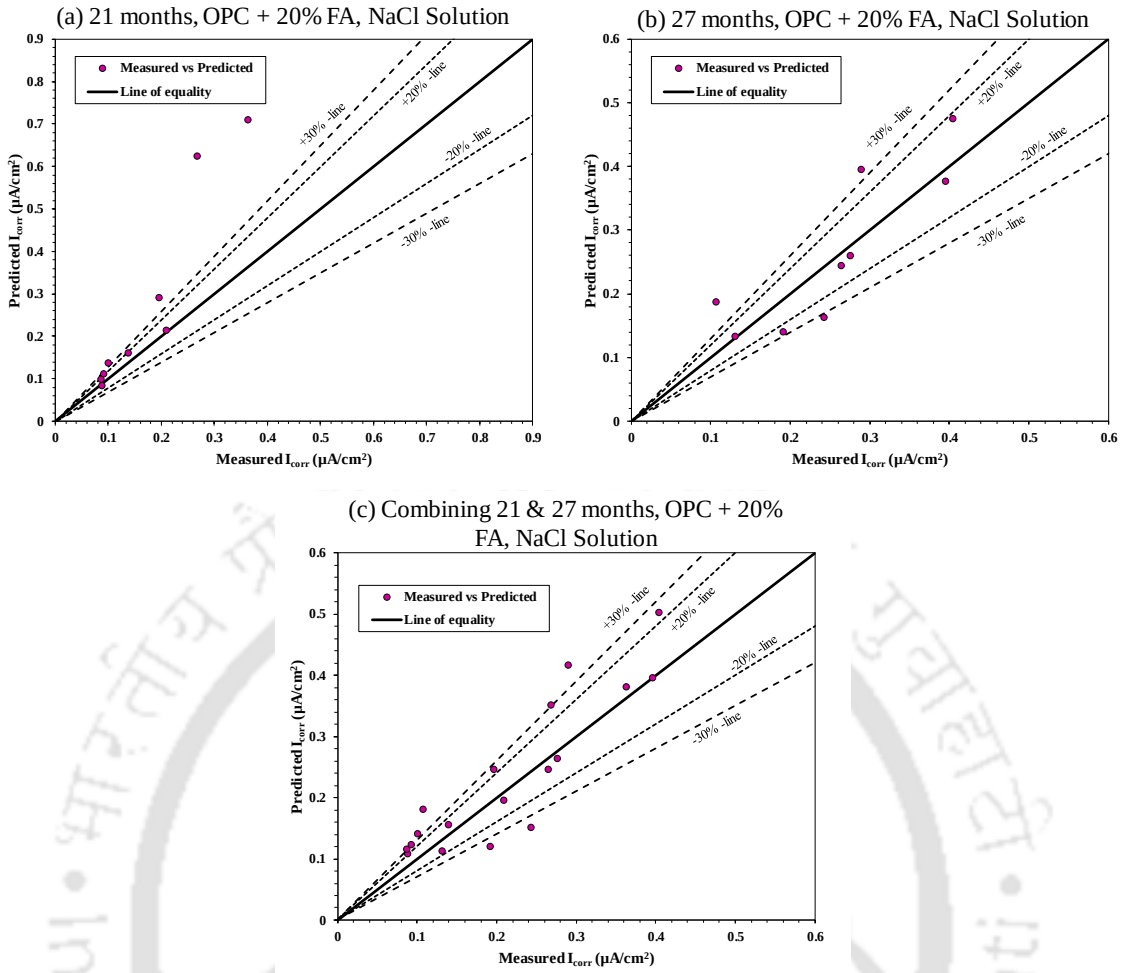

Figure 6.45 Comparison of measured I_{corr} and predicted I_{corr} (using the developed empirical relationship) from rebar surface chloride concentration of OPC + 20% FA concrete exposed to NaCl solutions: (a) exposure period of 21 months, (b) exposure period of 27 months, and (c) combining the results of exposure periods of 21 and 27 months

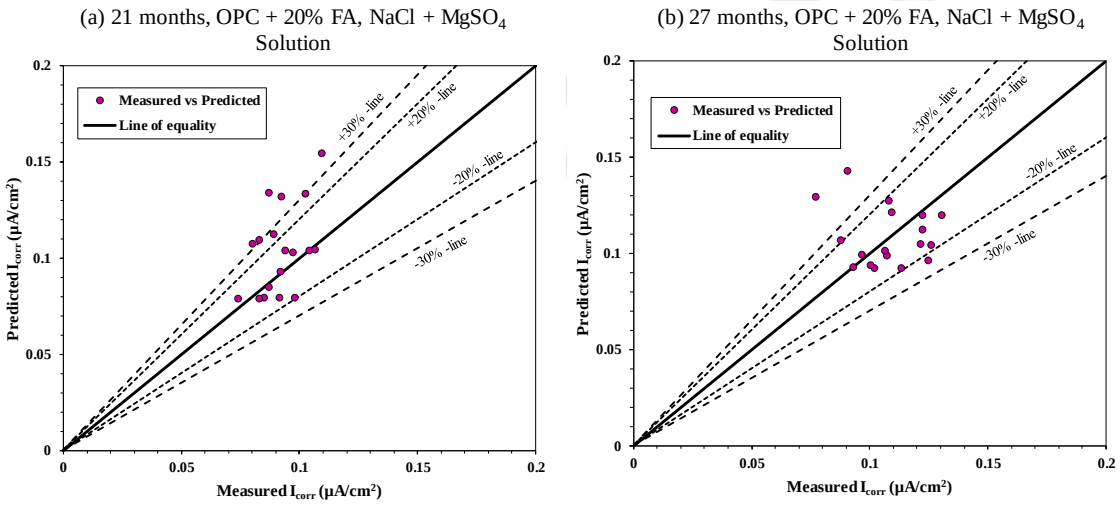

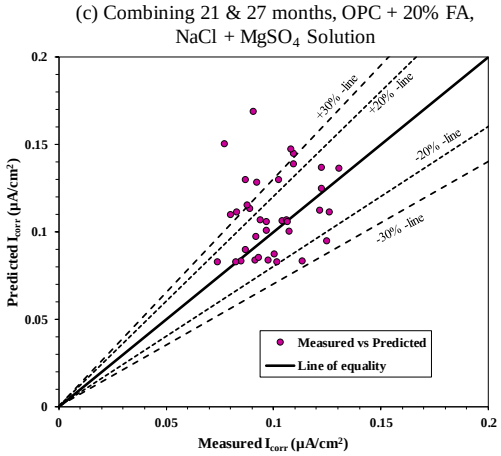

Figure 6.46 Comparison of measured I_{corr} and predicted I_{corr} (using the developed empirical relationship) from rebar surface chloride concentration of OPC + 20% FA concrete exposed to composite solutions of NaCl with $MgSO_4$: (a) exposure period of 21 months, (b) exposure period of 27 months, and (c) combining the results of exposure periods of 21 and 27 months

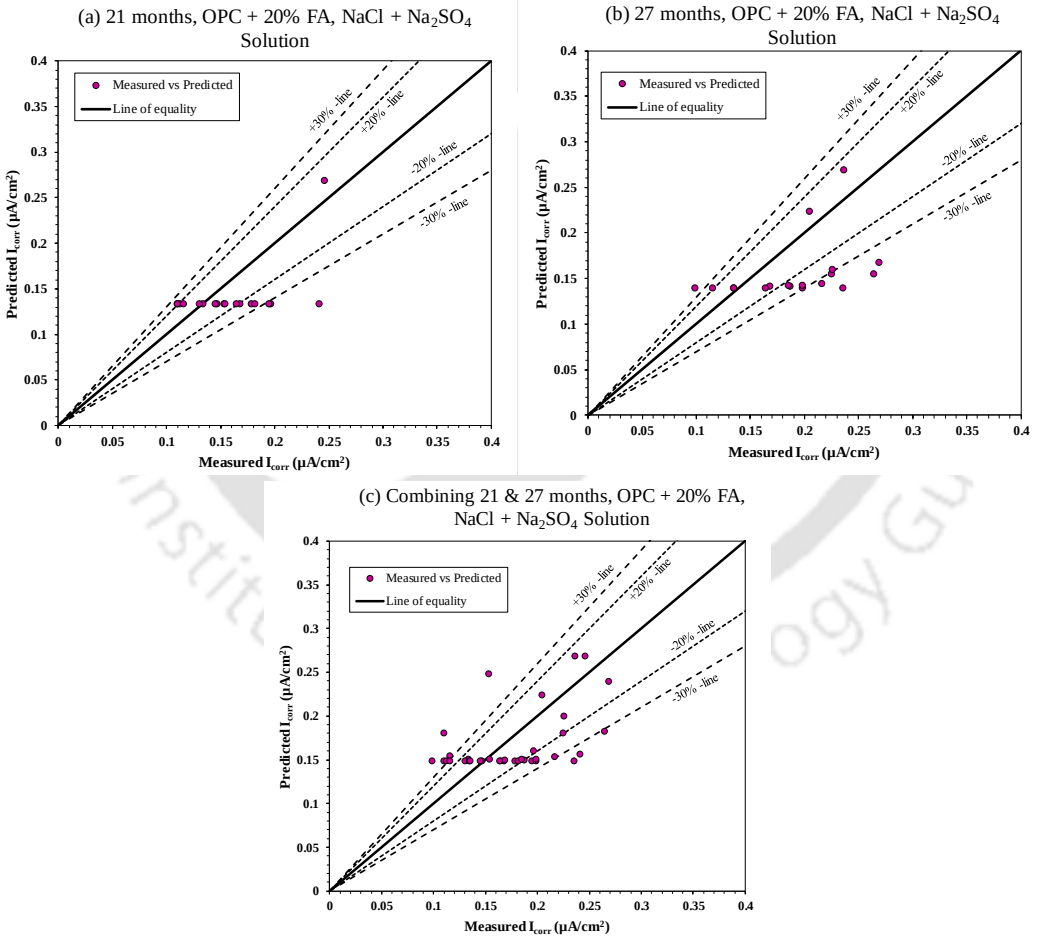

Figure 6.47 Comparison of measured I_{corr} and predicted I_{corr} (using the developed empirical relationship) from rebar surface chloride concentration of OPC + 20% FA concrete exposed to composite solutions of NaCl with Na_2SO_4: (a) exposure period of 21 months, (b) exposure period of 27 months, and (c) combining the results of exposure periods of 21 and 27 months

6.5. Summary

The results of corrosion monitoring of steel reinforcement indicated that the half-cell potential of steel reinforcement was more negative in the prismatic specimens exposed to higher concentration of sodium chloride than those exposed to lower concentration of sodium chloride in chloride and composite chloride-sulfate solutions for all binders and w/b ratios during the entire exposure period. Further, the variation in corrosion potential of steel reinforcement was unsystematic among exposure solutions for OPC and OPC + 20% FA concrete during the early exposure period, however, during the later exposure period, the corrosion potential was more negative in case of exposure to NaCl solutions as compared to composite solutions of NaCl + Na_2SO_4 followed by composite solutions of NaCl + $MgSO_4$ in OPC and OPC + 20% FA concrete. In PPC concrete, the variation in corrosion potential of steel reinforcement was unsystematic among exposure solutions during the entire exposure period. While evaluating the effect of concentration of sulfate ions, it was inferred that the variation in corrosion potential of steel reinforcement was mostly unsystematic with increase in concentration of $MgSO_4$ or Na_2SO_4 in the composite chloride-sulfate solutions for all binders except few cases wherein the corrosion potential became more negative with increase in concentration of Na_2SO_4 in the composite chloride-sulfate solutions for OPC concrete. Further, the corrosion potential values were more negative than -270 mV (SCE) in case of exposure to chloride solutions with higher concentrations of NaCl (i.e. 3% and 5%) in OPC and OPC + 20% FA concrete, and for exposure to composite chloride-sulfate solutions with higher concentration of NaCl (i.e. 5%) in OPC concrete, during the later exposure period thereby indicating greater probability of occurrence of steel reinforcement corrosion in concrete. However, the corrosion potential values were less negative than -270 mV (SCE) in PPC concrete irrespective of NaCl concentration in chloride and composite chloride-sulfate solutions during the entire exposure period, thereby indicating lower probability of occurrence of steel reinforcement corrosion in concrete. Among binder type, it is observed that there was no systematic variation in corrosion potential of steel reinforcement with binder type in chloride as well as composite chloride-sulfate solutions during the early exposure period, however the concrete made with PPC exhibited less negative potential values as compared to that made with OPC + 20% FA and OPC concrete during the later exposure period. While analyzing the effect of w/b ratio, it is inferred that the variation in corrosion potential with w/b ratio was not systematic in PPC concrete for exposure against chloride as well as

composite chloride-sulfate solutions, and in OPC + 20% FA concrete for exposure against composite chloride-sulfate solutions during the entire exposure period. However, the corrosion potential became more negative with increase in w/b ratio in OPC and OPC + 20% FA concrete in case of exposure to chloride solutions during the entire exposure period, and in OPC concrete for exposure against composite chloride-sulfate solutions during the later exposure period.

The results obtained from linear polarization resistance (LPR) test indicated that the corrosion current density of steel reinforcement increased with increase in concentration of NaCl in case of exposure to chloride solutions for all binders and w/b ratios during the entire exposure period. Further, in case of composite chloride-sulfate (both cations i.e. Mg^{2+} and Na^{+}) solutions, there was unsystematic variation in corrosion current density of steel reinforcement with increase in concentration of NaCl in the exposure solution for PPC concrete during the entire exposure period, and for OPC and OPC + 20% FA concrete during the early exposure period. However, during the later exposure period, the corrosion current density of steel reinforcement increased with increase in concentration of NaCl in the composite chloride-sulfate solutions for OPC and OPC + 20% FA concrete. Among exposure solutions, the corrosion current density of steel reinforcement was higher in the concrete exposed to composite solutions of NaCl + Na_2SO_4 as compared to NaCl solution, and composite solutions of NaCl + $MgSO_4$ at lower concentration of NaCl i.e. 1% during the entire exposure period, and at higher concentrations of NaCl i.e. 3% and 5% during the early exposure period for all binders. However, during the later exposure period, the corrosion current density of steel reinforcement was higher in the concrete in case of exposure to NaCl solutions as compared to composite solutions of NaCl + Na_2SO_4, and NaCl + $MgSO_4$ at higher concentrations of NaCl i.e. 3% and 5%. Between composite chloride-sulfate solutions, the corrosion current density was higher in the concrete in case of exposure to composite solutions of NaCl + Na_2SO_4 as compared to composite solutions of NaCl + $MgSO_4$ for all binders and w/b ratios during the entire exposure period. While analyzing the effect of concentration of sulfate ions, there was mostly unsystematic variation as well as minor difference in the corrosion current density with increase in concentration of $MgSO_4$ or Na_2SO_4 in the composite chloride-sulfate solutions for all binders except few cases where the corrosion current density increased with increase in concentration of Na_2SO_4 in the composite chloride-sulfate solution for OPC and OPC + 20% FA concrete whereas it decreased with increase in concentration of $MgSO_4$ in the

composite chloride-sulfate solution for OPC concrete, at higher concentration of NaCl i.e. 5% during the later exposure period. Among binder type, the concrete made with PPC exhibited higher corrosion current density during the early exposure period whereas it showed lower corrosion current density during the later exposure period as compared to that made with OPC and OPC + 20% FA in case of exposure to chloride and composite chloride-sulfate solutions. Further, the variation in corrosion current density of steel reinforcement with exposure period was very less in OPC and OPC + 20% FA concrete during the early exposure period irrespective of exposure solution except in OPC + 20% FA concrete exposed to composite solutions of NaCl with Na_2SO_4 wherein the corrosion current density decreased during the early period. However, during the later exposure period, the corrosion current density increased significantly in case of exposure to chloride solutions for OPC and OPC + 20% FA concrete at all concentrations of NaCl whereas it increased in case of exposure to composite chloride-sulfate (both cations i.e. Mg^{2+} and Na^{+}) solutions containing higher concentration of NaCl i.e. 5% for only OPC concrete. In PPC concrete, the corrosion current density decreased with increase in exposure period irrespective of exposure solution during the early period followed by a very less variation in corrosion current density with exposure duration during the later period. However, in few cases, the corrosion current density in PPC concrete increased slightly for both chloride and composite chloride-sulfate solutions at 5% NaCl concentration during the later exposure period. Among w/b ratios, the variation in corrosion current density with w/b ratio was mostly unsystematic for all binders except the cases wherein, the corrosion current density increased with increase in w/b ratio in case of exposure to chloride solutions during the entire exposure period in OPC and OPC + 20% FA concrete, and for exposure to composite chloride-sulfate solutions during the later exposure period in OPC concrete.

Based on the obtained results corresponding to the exposure periods of 21 months, 27 months, and combining the results of both the exposure periods, the developed empirical relationships between corrosion current density (I_{corr}), and the parameters such as half-cell potential (E_0), apparent chloride diffusion coefficient (D), and rebar surface chloride concentration (C_{rs}) for OPC and PPC concrete predicted the corrosion current density of steel reinforcement with a higher degree of accuracy for OPC + 20% fly ash concrete, which was independent of the empirical model development, in case of exposure to chloride (NaCl) and composite chloride (NaCl)-sulfate ($MgSO_4$ and Na_2SO_4) solutions. In addition, the developed empirical relationship between I_{corr}, and E_0 predicted well the I_{corr} values reported in the literature for chloride exposure conditions.

CHAPTER 7

CONCLUSIONS AND SUGGESTIONS FOR FURTHER STUDY

7.1. General

In this chapter, the conclusions obtained from the present research work are presented. First, the conclusions obtained from the results of compressive strength of concrete made with different types of binder and w/b ratio are presented. Further, the conclusions on the effect of depth from exposure surface of concrete, exposure solution and duration, binder type, and w/b ratio on free chloride content in concrete exposed to chloride and composite chloride-sulfate solutions are presented. In addition, the conclusions on the effect of these parameters on apparent chloride diffusion coefficient, and chloride binding in concrete are also provided. Subsequently, the conclusions on variations in microstructure of concrete with depth from exposure surface of concrete, exposure solution, binder type, and w/b ratio are presented. In addition, the conclusions on the effect of exposure solution, binder type, w/b ratio, and exposure duration on corrosion performance evaluated through half-cell potential, and corrosion current density of steel reinforcement in concrete exposed to chloride and composite chloride-sulfate solutions are presented. Further, the conclusions on the developed relationships between experimentally obtained corrosion current density (I_{corr}), and the parameters i.e. experimentally obtained half-cell potential (E_0), apparent chloride diffusion coefficient (D), and rebar surface chloride concentration (C_{rs}) are also presented in this chapter.

7.2. Conclusions from compressive strength and chloride ingress in concrete

- The compressive strength of OPC concrete was higher as compared to OPC + 20% FA followed by PPC concrete at all w/b ratios and curing ages. However, the rate of increase in compressive strength with curing age was higher in PPC, and OPC + 20% FA concrete as compared to OPC concrete.
- From the obtained free chloride content profile, the convection zone was observed near the exposure surface i.e. in the depth interval of 0-5 mm from exposure surface of concrete exposed to chloride and composite chloride-sulfate solutions with alternate wetting-drying cycles.
- The presence of convection zone in the concrete varied with exposure duration, w/b ratio, binder type, and exposure solution. The formation of convection zone was more

dominant with increase in exposure period, and w/b ratio. Among binder type, the formation of convection zone was more dominant in PPC concrete as compared to OPC + 20% FA followed by OPC concrete. With exposure solution, the formation of convection zone was more in the concrete exposed to NaCl + Na_2SO_4 solutions as compared to NaCl + $MgSO_4$ solutions followed by NaCl solutions.

- The free chloride content decreased with increase in depth from the exposure surface of concrete for all binders, w/b ratios, exposure solutions, and exposure periods except some cases where, the free chloride content in the depth interval of 0-5 mm was less than that in the depth interval of 5-10 mm from the exposure surface. The lower free chloride content near the exposure surface region i.e. in the depth interval of 0-5 mm from the exposure surface of concrete is attributed to the presence of convection zone.
- The free chloride content in concrete increased with an increase in concentration of NaCl in the exposure solution at all depth intervals for both chloride (NaCl), and composite chloride-sulfate (NaCl + $MgSO_4$, and NaCl + Na_2SO_4) solutions.
- The free chloride content was lower in the concrete exposed to composite chloride-sulfate (NaCl + $MgSO_4$, and NaCl + Na_2SO_4) solutions as compared to chloride (NaCl) solutions, and decreased with increase in concentration of $MgSO_4$ or Na_2SO_4 in the exposure solution.
- Between the cation type associated with sulfate ions in the composite chloride-sulfate solutions, the free chloride content was lower in the concrete exposed to composite solutions of NaCl + Na_2SO_4 as compared to composite solutions of NaCl + $MgSO_4$ at all depth intervals for all binders.
- Among binder type, the free chloride content was higher in PPC concrete as compared to OPC + 20% FA followed by OPC concrete at lower depth intervals i.e. near the exposure surface region of concrete. However, at higher depth intervals from exposure surface of concrete, the free chloride content was higher in OPC concrete as compared to OPC + 20% FA followed by PPC concrete.
- It is concluded that the resistance against chloride penetration i.e. rate of decrease of free chloride content with depth from the exposure surface was higher in PPC concrete as compared to OPC + 20% FA followed by OPC concrete against exposure to chloride and composite chloride-sulfate solutions for all w/b ratios and exposure periods. The higher resistance against penetration of chloride ions in PPC and OPC + 20% FA concrete as compared to OPC concrete is attributed to the formation of compacted

microstructure in PPC and OPC + 20% FA concrete due to the production of more amount of C-S-H gel as a result of pozzolanic reaction.

- Among w/b ratio, the concrete made with lower w/b ratio showed higher free chloride content as compared to that made with higher w/b ratio at lower depth intervals from exposure surface of concrete whereas the opposite variation was observed at higher depth intervals i.e. the concrete made with lower w/b ratio showed lower free chloride content as compared to that made with higher w/b ratio for all binders, exposure solutions, and exposure periods.
- The estimated apparent chloride diffusion coefficient was higher in the concrete exposed to chloride and composite chloride-sulfate solutions with higher concentration of NaCl as compared to exposure solutions with lower concentration of NaCl. Further, the estimated apparent chloride diffusion coefficient was mostly lower in the concrete exposed to composite chloride-sulfate solutions as compared to chloride solutions, and the chloride diffusion coefficient decreased with an increase in concentration of sulfate ions for both cations i.e. Mg^{2+} and Na^{+} for the concrete exposed to composite chloride-sulfate solutions.
- Between the cation type associated with sulfate ions, the concrete exposed to composite solutions of NaCl with $MgSO_4$ mostly exhibited higher apparent chloride diffusion coefficient as compared to that exposed to composite solutions of NaCl with Na_2SO_4.
- Among binder type, the concrete made with OPC exhibited higher apparent chloride diffusion coefficient as compared to that made with OPC + 20% FA followed by PPC for all w/b ratios, exposure solutions, and exposure periods. Further, the concrete made with lower w/b ratio exhibited lower apparent chloride diffusion coefficient as compared to that made with higher w/b ratio irrespective of binder type, exposure solution, and exposure period.
- With exposure period, the estimated apparent chloride diffusion coefficient mostly decreased with increase in exposure period in the concrete exposed to composite chloride-sulfate (both cations i.e. Mg^{2+} and Na^{+}) solutions. However, in case of exposure to chloride solutions, the variation in apparent chloride diffusion coefficient was mostly unsystematic with exposure period till 21 months whereas, in majority of the cases, it decreased at the exposure period of 27 months.

7.3. Conclusions from chloride binding in concrete

- From the results of chloride binding, the concrete exposed to composite chloride-sulfate (both cations i.e. Mg^{2+} and Na^{+}) solutions exhibited higher chloride binding as compared to chloride solutions during the early exposure periods (i.e. till 15 months of exposure) whereas the opposite variation was observed during the later exposure periods (after 15 months of exposure).
- Between the cation type associated with sulfate ions, the concrete exposed to composite solutions of NaCl + Na_2SO_4 exhibited higher chloride binding as compared to that exposed to composite solutions of NaCl + $MgSO_4$ at all exposure periods.
- Among binder type, the concrete made with OPC exhibited higher chloride binding as compared to that made with OPC + 20% FA followed by PPC at all exposure periods. However, the variation in chloride binding was mostly unsystematic with change in w/b ratio of concrete.

7.4. Conclusions from variations in microstructure of concrete with depth from exposure surface

- From the microstructure study of concrete at different depth intervals, the results of XRD analysis indicated that the peak intensity and wt. % of calcium hydroxide (CH) were lower near the exposure surface and increased with increase in depth from the exposure surface of concrete exposed to chloride and composite chloride-sulfate solutions. The presence of higher amount of calcium hydroxide at higher depth intervals is attributed to the effect of its leaching in the presence of chloride ions to a lower extent as compared to that at lower depth intervals from the exposure surface of concrete.
- The results of XRD analysis showed that there was no systematic variation in the formation of ettringite (E) with increase in depth from the exposure surface of concrete as indicated by its peak intensity and wt. %. However, the formation of ettringite was mostly higher in the depth interval of 10-15 mm followed by 15-20 mm, and 5-10 mm as compared to other depth intervals from the exposure surface of concrete for all binders, exposure solutions and exposure periods.

- There was no systematic variation in the formation of gypsum (G) with increase in depth from the exposure surface of concrete as indicated by its peak intensity and wt. % for all binders, exposure solutions, and exposure periods.
- The results of XRD analysis indicated the formation of thaumasite (T) at lower depth intervals i.e. till 10 mm from the exposure surface of concrete exposed to composite chloride-sulfate (both cations i.e. Mg^{2+} and Na^{+}) solutions. The formation of thaumasite in concrete near the surface region was also attributed to the presence of calcium carbonate in higher amount in the surface region where the peak intensity and wt. % of calcite (CC) were higher in the depth interval of 0-5 mm from the exposure surface of concrete as compared to other depth intervals.
- There was unsystematic variation as well as minor difference in the peak intensity and wt. % of calcium chloroaluminate (CCA) among different depth intervals for all binders, exposure solutions and exposure periods. However, in majority of the cases, the formation of CCA, as indicated by its peak intensity and wt. %, was slightly higher at lower depth intervals (i.e. till 10 mm from the exposure surface) as compared to higher depth intervals from the exposure surface of concrete.
- The formations of ettringite (E), calcium chloroaluminate (CCA), calcium hydroxide (CH), gypsum (G), and magnesium hydroxide (MH) in the concrete subjected to different exposure solutions, as indicated by the XRD patterns were also confirmed from the obtained FESEM images.

7.5. Conclusions from variations in microstructure of concrete with exposure solution

- The results of XRD analysis indicated the formation of mostly higher amount of ettringite (E) in the concrete exposed to composite solutions of NaCl + Na_2SO_4 as compared to composite solutions of NaCl + $MgSO_4$ followed by NaCl solutions for all concentrations of NaCl, $MgSO_4$, and Na_2SO_4. This variation in the formation of ettringite in concrete with the exposure solution was consistent with the obtained FESEM images.
- The variation in the formation of calcium chloroaluminate (CCA) in concrete with exposure solution was opposite to that of ettringite (E) i.e. the formation of CCA was mostly higher in the concrete exposed to NaCl solutions as compared to composite solutions of NaCl + $MgSO_4$ followed by composite solutions of NaCl + Na_2SO_4 for all

concentrations of NaCl, $MgSO_4$, and Na_2SO_4 as indicated by the peak intensity and wt. % of CCA.

- The results of XRD analysis showed that the peak intensity and wt. % of ettringite mostly decreased whereas that of calcium chloroaluminate mostly increased with increase in concentration of NaCl in chloride as well as composite chloride-sulfate (both cations i.e. Mg^{2+} and Na^{+}) solutions, and with increase in concentration of $MgSO_4$, and Na_2SO_4 in the composite chloride-sulfate solutions.
- The amount of calcium hydroxide (CH) was mostly higher in the concrete exposed to composite solutions of NaCl + Na_2SO_4 as compared to composite solutions of NaCl + $MgSO_4$ followed by NaCl solutions at all depth intervals irrespective of binder type, and concentrations of NaCl, $MgSO_4$, and Na_2SO_4 as observed from the XRD analysis.
- The amount of calcium hydroxide (CH) mostly decreased with increase in concentration of NaCl in chloride as well as composite chloride-sulfate solutions whereas it mostly increased with increase in concentration of $MgSO_4$ in the composite solutions of NaCl + $MgSO_4$ for all binder as indicated by the XRD analysis. However, there was no systematic variation in the peak intensity and wt. % of calcium hydroxide with increase in concentration of Na_2SO_4 in the composite solutions of NaCl + Na_2SO_4.
- The amount of gypsum (G) was mostly higher in the concrete exposed to composite solutions NaCl + $MgSO_4$ as compared to NaCl solutions followed by composite solutions of NaCl + Na_2SO_4 as indicated by the XRD analysis. Further, the results of XRD analysis showed that there was no systematic variation in the amount of gypsum with increase in concentration of NaCl in chloride and composite chloride-sulfate solutions, whereas the amount of gypsum in concrete mostly increased with increase in concentration of $MgSO_4$, and Na_2SO_4 in the composite chloride-sulfate solutions.
- The variations in the formation of ettringite, calcium chloroaluminate, and calcium hydroxide, as observed from the XRD analysis, in the concrete exposed to chloride and composite chloride-sulfate solutions were consistent with the variations in the obtained free chloride content of concrete.

7.6. Conclusions from variations in microstructure of concrete with binder type and w/b ratio

- With binder type, the formation of calcium chloroaluminate (CCA) varied with the depth interval from exposure surface of concrete. The results of XRD analysis showed

that the formation of calcium chloroaluminate was mostly higher in OPC + 20% FA as compared to PPC followed by OPC concrete at lower depth intervals (i.e. till 10 mm from the exposure surface) whereas at higher depth intervals (i.e. beyond 10 mm from the exposure surface), the formation of CCA was mostly higher in OPC as compared to that in OPC + 20% FA followed by PPC concrete for chloride and composite chloride-sulfate solutions.

- The formation of ettringite (E) was lower in OPC concrete as compared to OPC + 20% FA followed by PPC concrete in case of exposure to chloride solutions at all depth intervals as indicated by its peak intensity and wt. % obtained from XRD analysis. However, the formation of ettringite varied with the depth interval from exposure surface of concrete in case of exposure to composite solutions of NaCl + $MgSO_4$ whereas in case of composite solutions of NaCl + Na_2SO_4, the formation of ettringite was higher in PPC concrete as compared to OPC followed by OPC + 20% FA concrete at all depth intervals as observed from the XRD analysis.
- The results of XRD analysis showed lower amount of calcium hydroxide (CH) in OPC + 20% FA, and PPC concrete as compared to OPC concrete at all depth intervals from the exposure surface in case of exposure to composite chloride-sulfate solutions, and at higher depth intervals in case of exposure to chloride solutions as indicated by the results of XRD analysis. However, there was unsystematic variation in the amount of calcium hydroxide with binder type at lower depth intervals in case of exposure to chloride solutions, which may be attributed to the dominant effect of variations in the leaching of calcium hydroxide with respect to binder type near the exposure surface of concrete.
- The formation of compacted microstructure due to production of more amount of C-S-H gel in OPC + 20% FA, and PPC concrete than that in OPC concrete was evident from the obtained FESEM images.
- The results of XRD analysis indicated lower amount of gypsum (G) in PPC concrete as compared to OPC, and OPC + 20% FA concrete when exposed to chloride solutions whereas, there was unsystematic as well as very less variation in the amount of gypsum with binder type in case of exposure to composite chloride-sulfate solutions at all depth intervals from the exposure surface of concrete.

- The formation of magnesium hydroxide (MH) was mostly higher in OPC concrete as compared to OPC + 20% FA followed by PPC concrete exposed to composite solutions of NaCl with $MgSO_4$ as indicated by the XRD analysis.
- The formation of ettringite, calcium chloroaluminate, calcium hydroxide, and gypsum in the concrete exposed to chloride and composite chloride-sulfate solutions varied with w/b ratio as observed from the XRD analysis. The formation of ettringite in concrete increased with increase in w/b ratio, however there was no systematic variation in the formation of gypsum, calcium chloroaluminate, and calcium hydroxide with increase in w/b ratio as indicated by the XRD analysis.

7.7. Conclusions from variations in microstructure of concrete obtained from thermo-gravimetry analysis (TGA)

- The results of thermo-gravimetry analysis (TGA) indicated that the mass loss of concrete associated with the decomposition of various compounds such as C-S-H gel, ettringite, thaumasite, gypsum, calcium chloroaluminate, calcium hydroxide, M-S-H gel, and calcium carbonate, in different temperature ranges varied with the depth interval from exposure surface, exposure solution, binder type, and w/b ratio.
- The total mass loss of concrete was higher in the depth interval of 0-5 mm from the exposure surface as compared to other depth intervals in the concrete exposed to chloride and composite chloride-sulfate solutions.
- The mass loss of concrete due to departure of combined water was mostly higher in the concrete exposed to composite chloride-sulfate (both cations i.e. Mg^{2+} and Na^{+}) solutions as compared to chloride solutions. With binder type, the mass loss due to departure of combined water was mostly higher in the concrete made with OPC as compared to that made with OPC + 20% FA followed by PPC for all exposure solutions.
- The results obtained from TGA indicated that the total mass loss was mostly higher in OPC concrete as compared to OPC + 20% FA, and PPC concrete for exposure against chloride and composite chloride-sulfate (both cations i.e. Mg^{2+} and Na^{+}) solutions.
- The variations in the mass loss of concrete, obtained from TGA, in different temperature ranges due to dehydration of calcium hydroxide, ettringite, calcium chloroaluminate, and gypsum were mostly consistent with the variations in the

formation of these compounds as indicated by the peak intensity and wt. % obtained from the XRD analysis for different binders and exposure solutions.

7.8. Conclusions from corrosion behaviour of steel reinforcement in concrete through half-cell potential

- The obtained results of corrosion monitoring indicated that the half-cell potential of steel reinforcement became more negative with increase in concentration of NaCl in chloride as well as composite chloride-sulfate (both cations i.e. Mg^{2+} and Na^{+}) solutions during the entire exposure period. However, the variation in half-cell potential was mostly unsystematic with increase in concentration of $MgSO_4$ or Na_2SO_4 in the composite chloride-sulfate solutions.
- The variation in corrosion potential of steel reinforcement was unsystematic among exposure solutions during the early exposure period whereas during the later exposure period, the corrosion potential was more negative in case of exposure to NaCl solutions as compared to composite solutions of NaCl with Na_2SO_4 followed by composite solutions of NaCl with $MgSO_4$ for OPC, and OPC + 20% FA concrete. However, in PPC concrete, the variation in corrosion potential was unsystematic among exposure solutions during the entire exposure period.
- The probability of occurrence of reinforcing steel corrosion was greater in OPC, and OPC + 20% FA concrete in case of exposure to chloride solutions with higher concentrations of NaCl i.e. 3% and 5%, and only in OPC concrete in case of exposure to composite chloride-sulfate solutions with higher concentrations of NaCl, during the later exposure period as the corrosion potential values were more negative than -270 mV (SCE). However, in PPC concrete, there was lower probability of occurrence of reinforcing steel corrosion as the corrosion potential values were less negative than -270 mV (SCE) irrespective of exposure solution during the entire exposure period.
- With binder type, the variation in corrosion potential was not systematic during the early exposure period, however, during the later exposure period, the concrete made with PPC exhibited less negative corrosion potential values as compared to OPC + 20% FA, and OPC concrete.
- The variation in corrosion potential was not systematic with w/b ratio in PPC concrete irrespective of exposure solution, and in OPC + 20% FA concrete in case of exposure to composite chloride-sulfate solutions during the entire exposure period. However,

the corrosion potential became more negative with increase in w/b ratio in OPC, and OPC + 20% FA concrete in case of exposure to chloride solutions during the entire exposure period, and only in OPC concrete for exposure to composite chloride-sulfate solutions during the later exposure period.

7.9. Conclusions from corrosion behaviour of steel reinforcement in concrete through corrosion current density

- The results of corrosion monitoring indicated that the corrosion current density of steel reinforcement in concrete increased with increase in concentration of NaCl in chloride solution for all binders, and w/b ratios during the entire exposure period.
- In case of exposure to composite chloride-sulfate (both Mg^{2+} and Na^{+} cations) solutions, the variation in corrosion current density was unsystematic with increase in concentration of NaCl in the exposure solution for PPC concrete during the entire exposure period, and for OPC and OPC + 20% FA concrete during the early exposure period. However, during the later exposure period, the corrosion current density of steel reinforcement increased with increase in concentration of NaCl in the composite chloride-sulfate solutions for OPC, and OPC + 20% FA concrete.
- Among exposure solutions, the corrosion current density was higher in the concrete exposed to composite solutions of NaCl + Na_2SO_4 as compared to NaCl solution, and composite solutions of NaCl + $MgSO_4$ at lower concentration of NaCl i.e. 1% during the entire exposure period, and at higher concentrations of NaCl i.e. 3% and 5% during the early exposure period for all binders. However, during the later exposure period, the concrete exposed to NaCl solutions showed higher corrosion current density as compared to composite solutions of NaCl + Na_2SO_4, and NaCl + $MgSO_4$ at higher concentrations of NaCl i.e. 3% and 5%.
- Between composite chloride-sulfate solutions, the corrosion current density of steel reinforcement was higher in the concrete exposed to composite solutions of NaCl + Na_2SO_4 as compared to composite solutions of NaCl + $MgSO_4$ for all binders, and w/b ratios during the entire exposure period. In other words, the presence of sulfate ions when associated with Na^{+} cation resulted in higher corrosion current density as compared to Mg^{2+} cation in the concomitant presence of chloride ions.
- While evaluating the effect of concentrations of $MgSO_4$ and Na_2SO_4, the variation in corrosion current density was mostly unsystematic as well as very less with increase

in concentration of $MgSO_4$ or Na_2SO_4 in the composite chloride-sulfate solutions for all binders except few cases where the corrosion current density increased with increase in concentration of Na_2SO_4 in the composite solution of NaCl + Na_2SO_4 for OPC, and OPC + 20% FA concrete whereas the corrosion current density decreased with increase in concentration of $MgSO_4$ in the composite solution of NaCl + $MgSO_4$ for OPC concrete, at higher concentration of NaCl (i.e. 5%) during the later exposure period.

- Among binder type, the concrete made with PPC showed higher corrosion current density during early exposure period whereas it showed lower corrosion current density during later exposure period as compared to OPC, and OPC + 20% FA concrete in case of exposure to chloride and composite chloride-sulfate solutions.
- With exposure period, the variation in corrosion current density was very less in OPC, and OPC + 20% FA concrete irrespective of exposure solution during the early period except in OPC + 20% FA concrete exposed to NaCl + Na_2SO_4 solutions where the corrosion current density decreased during the early period. However, during the later exposure period, the corrosion current density increased significantly in case of exposure to chloride solutions at all concentrations of NaCl for OPC, and OPC + 20% FA concrete whereas in case of exposure to composite chloride-sulfate (both cations i.e. Mg^{2+} and Na^{+}) solutions, the corrosion current density increased at higher concentration of NaCl i.e. 5% for only OPC concrete.
- With exposure period, the corrosion current density of steel reinforcement in PPC concrete decreased irrespective of exposure solution during the early period followed by a very less variation in corrosion current density with exposure duration during the later period.
- While evaluating the effect of w/b ratio, the variation in corrosion current density with w/b ratio was mostly unsystematic for all binders except the cases where, the corrosion current density increased with increase in w/b ratio in OPC, and OPC + 20% FA concrete in case of exposure to chloride solutions during the entire exposure period, and in OPC concrete in case of exposure to composite chloride-sulfate solutions during the later exposure period.
- From viewpoint of corrosion behaviour of steel reinforcement in concrete evaluated through half-cell potential, and corrosion current density, the concrete made with PPC

showed better performance as compared to that made with OPC + 20% FA, and OPC in case of exposure to chloride, and composite chloride-sulfate solutions. Similarly, the concrete made with lower w/b ratio showed better corrosion performance as compared to that made with higher w/b ratio for exposure against chloride, and composite chloride-sulfate solutions.

7.10. Conclusions from the developed empirical relationships between durability parameters

- The developed empirical relationships between the obtained corrosion current density (I_{corr}), and the parameters i.e. half-cell potential (E_0), apparent chloride diffusion coefficient (D), and rebar surface chloride concentration (C_{rs}) for OPC and PPC concrete predicted the corrosion current density of steel reinforcement with a higher degree of accuracy for OPC + 20% FA concrete, which was independent of the empirical model development, for exposure against chloride, and composite chloride-sulfate solutions.
- The developed empirical relationship between the obtained corrosion current density (I_{corr}), and half-cell potential (E_0) predicted well the corrosion current density (I_{corr}) values reported in the literature by different researchers for chloride exposure conditions.

7.11. Significance of research outcome from the present study

In the present research work, the influence of mix parameters, exposure solution, and exposure duration on chloride ingress, chloride binding, microstructure, and steel reinforcement corrosion in concrete exposed to chloride, and composite chloride-sulfate solutions were evaluated. The research outcome from the present study provided a detailed insight about the effects of parameters related to the concrete, and that related to the exposure environment on variations in durability properties of concrete. The obtained research outcome on variations in free chloride content, apparent chloride diffusion coefficient, and chloride binding in concrete as well as on corrosion behaviour of steel reinforcement can be used for selecting the mix parameters such as suitable binder type for the construction of reinforced concrete structures in different exposure environment. As observed from the present study, although the concrete made with ordinary Portland cement (OPC) exhibited higher chloride binding, but the concrete made with Portland pozzolana cement (PPC), and OPC plus fly ash showed higher resistance against penetration of

chloride ions into concrete as well as exhibited better corrosion performance as compared to that made with OPC for exposure against chloride, and composite chloride-sulfate solutions. Thus, PPC (fly ash based blended cement) as well as OPC added with fly ash can be recommended as the suitable binder for the preparation of concrete for exposure against aggressive environment. Further, the obtained research outcome from the present study on variations in the microstructure of concrete with depth from exposure surface, exposure solution, binder type, and w/b ratio can be useful in analyzing the durability behaviour of concrete through the variations in the formation of different compounds in the presence of chloride and sulfate ions at various depth intervals from exposure surface of concrete exposed to different exposure environment. The empirical relationships developed, in the present study, between different durability parameters of concrete exposed to chloride, and composite chloride-sulfate environment can be useful in estimating the values of different durability parameters without measuring them from the known values of other relevant durability parameters of concrete.

7.12. Suggestions for further study

The present research work can be extended to evaluate the effect of other types of binder such as Portland slag cement, and OPC added with supplementary cementitious materials namely ground granulated blast furnace slag, silica fume etc. on chloride ingress, chloride binding, microstructure, and reinforcing steel corrosion in concrete exposed to chloride, and composite chloride-sulfate environment. Similarly, the present study can also be extended to evaluate the effect of cation type associated with chloride ions as well as that of different corrosion inhibitors on chloride ingress, chloride binding, microstructure, and reinforcing steel corrosion in concrete subjected to different exposure environment.

REFERENCES

[1] A. M. Neville and J. J. Brooks, “Concrete technology,” 2nd ed., England: Pearson Education Limited, 2010.

[2] P. K. Mehta and P. J. M Monteiro, “Concrete: microstructure, properties, and materials,” New Delhi: Tata McGraw Hill Education Private Limited, 2006.

[3] A.M. Neville, “Properties of concrete,” Fourth Edition, New Delhi: Dorling Kindersley (India) Pvt. Ltd, 2010.

[4] C. E. T. Balestra, T. A. Reichert, W. A. Pansera and G. Savaris, “Chloride profile modeling contemplating the convection zone based on concrete structures present for more than 40 years in different marine aggressive zones," Constr. Build. Mater., vol. 198, pp. 345-358, 2019.

[5] S. Erdogdu, I. L. Kondratova and T. W. Bremner, "Determination of chloride diffusion coefficient of concrete using open-circuit potential measurements," Cem. Concr. Res., vol. 34, pp. 603-609, 2004.

[6] K. Tuutti, "Chloride induced corrosion in marine concrete structures," in durability of concrete on saline environment, Uppsala, 1996, p. 81-93.

[7] J. Crank, “The mathematics of diffusion,” Oxford: Clarendon Press, 1975.

[8] J. Zhang and Z. Lounis, "Sensitivity analysis of simplified diffusion-based corrosion initiation model of concrete structures exposed to chlorides," Cem. Concr. Res., vol. 36, pp. 1312-1323, 2006.

[9] S. Goni and C. Andrade, "Synthetic concrete pore solution chemistry and rebar corrosion rate in the presence of chlorides," Cem. Concr. Res., vol. 20, pp. 525-539, 1990.

[10] V. Baroghel-Bouny, X. Wang, M. Thiery, M. Saillio and F. Barberon, "Prediction of chloride binding isotherms of cementitious materials by analytical model or numerical inverse analysis," Cem. Concr. Res., vol. 42, pp. 1207-1224, 2012.

[11] H. S. Al-alaily and A. A. A. Hassan, "Time-dependence of chloride diffusion for concrete containing metakaolin," J. Build. Eng., vol. 7, pp. 159-169, 2016.

[12] A. Petcherdchoo, "Time dependent models of apparent diffusion coefficient and surface chloride for chloride transport in fly ash concrete," Constr. Build. Mater., vol. 38, pp. 497-507, 2013.

[13] Y. M. Sun, T. P. Chang and M. T. Liang, “Service life prediction for concrete structures by time-depth dependent chloride diffusion coefficient,” ASCE J. Mater. Civ. Eng., vol. 22, pp. 1187-1190, 2010.

[14] W. Chalee, C. Jaturapitakkul and P. Chindaprasirt, "Predicting the chloride penetration of fly ash concrete in seawater," Mar. Struct., vol. 22, pp. 341-353, 2009.

[15] M. D. A. Thomas and P. B. Bamforth, "Modelling chloride diffusion in concrete effect of fly ash and slag," Cem. Concr. Res., vol. 29, pp. 487-495, 1999.

[16] M. Shekarchi, A. Rafiee and H. Layssi, "Long-term chloride diffusion in silica fume concrete in harsh marine climates," Cem. Concr. Compos., vol. 31, pp. 769-775, 2009.

[17] A. Farahani, H. Taghaddos and M. Shekarchi, "Prediction of long-term chloride diffusion in silica fume concrete in a marine environment," Cem. Concr. Compos., vol. 59, pp. 10-17, 2015.

[18] C. Andrade, "Calculation of chloride diffusion coefficient in concrete from ionic migration measurements," Cem. Concr. Res., vol. 23, pp. 724-742, 1993.

[19] M. A. Climent, G. de Vera, J. F. Lopez, E. Viqueira and C. Andrade, "A test method for measuring chloride diffusion coefficients through nonsaturated concrete: Part I. The instantaneous plane source diffusion case," Cem. Concr. Res., vol. 32, pp. 1113-1123, 2002.

[20] G. de Vera, M. A. Climent, E. Viqueira, C. Antón and C. Andrade, "A test method for measuring chloride diffusion coefficients through partially saturated concrete. Part II: The instantaneous plane source diffusion case with chloride binding consideration," Cem. Concr. Res., vol. 37, p. 714-724, 2007.

[21] C. Andrade, R. d'Andrea and N. Rebolledo, "Chloride ion penetration in concrete: The reaction factor in the electrical resistivity model," Cem. Concr. Compos., vol. 47, pp. 41-46, 2014.

[22] F. Pargar, D. A. Koleva and K. van Breugel, "Determination of chloride content in cementitious materials: From fundamental aspects to application of Ag/AgCl chloride sensors," Sensors, vol. 17, p. 2482, 2017.

[23] C. Qiao, W. Ni, Q. Wang and J. Weiss, "Chloride diffusion and wicking in concrete exposed to NaCl and $MgCl_2$ solutions," ASCE J. Mater. Civ. Eng., vol. 30, no. 3, pp. 04018015-1-10, 2018.

[24] Q. Yuan, C. Shi, G. De Schutter, K. Audenaert and D. Deng , "Chloride binding of cement-based materials subjected to external chloride environment - A review," Constr. Build. Mater., vol. 23, pp. 1-13, 2009.

[25] Nicholas J. Carino, "Nondestructive techniques to investigate corrosion status in concrete structures," J. Perfor. Constr. Facil., vol. 13, no. 3, pp. 96-106, 1999.

[26] N. Asrar, A. U. Malik, S. Ahmad and F. S. Mujahid, "Corrosion protection performance of microsilica added concretes in NaCl and seawater environments," Constr. Build. Mater., vol. 13, pp. 213-219, 1999.

[27] T. D. Marcotte and C. M. Hansson, "Corrosion products that form on steel within cement paste," Mater. Struct., vol. 40, pp. 325-340, 2007.

[28] Y. Zhao, X. Zhang and W. Jin, "Influence of environment on the development of corrosion product-filled paste and a corrosion layer at the steel/concrete interface," Corros. Sci., vol. 124, pp. 1-9, 2017.

[29] B. Pradhan and B. Bhattacharjee, "Half-cell potential as an indicator of chloride-induced rebar corrosion initiation in RC," ASCE J. Mater. Civ. Eng., vol. 21, pp. 543-552, 2009.

[30] A. Sarja and E. Vesikari, "Durability design of concrete structures report of RILEM Technical Committee 130-CSL," E & FN Spon, London, 2005.

[31] T. E. l. Maaddawy and K. Soudki , "A model for prediction of time from corrosion initiation to corrosion cracking," Cem. Concr. Compos., vol. 29, pp. 168-175, 2007.

[32] P. W. Brown and S. Badger, "The distributions of bound sulfates and chlorides in concrete subjected to mixed NaCl, $MgSO_4$,Na_2SO_4 attack," Cem. Concr. Res., vol. 30, pp. 1535-1542, 2000.

[33] M. Maes and N. De Belie, "Resistance of concrete and mortar against combined attack of chloride and sodium sulphate," Cem. Concr. Compos., vol. 53, pp. 59-72, 2014.

[34] Z. Yang, J. Jiang, X. Jiang, S. Mu, M. Wu, S. Sui, L. Wang and F. Wang, "The influence of sodium sulfate and magnesium sulfate on the stability of bound chlorides in cement paste," Constr. Build. Mater., vol. 228, p. 116775, 2019.

[35] S. Cheng, Z. Shui, T. Sun, X. Gao and C. Guo, "Effects of sulfate and magnesium ion on the chloride transportation behavior and binding capacity of Portland cement mortar," Constr. Build. Mater., vol. 204, pp. 265-275, 2019.

[36] Y. Cao, L. Guo and B. Chen, "Influence of sulfate on the chloride diffusion mechanism in mortar," Constr. Build. Mater., vol. 197, pp. 398-405, 2019.

[37] K. De Weerdt, B. Lothenbach and M. R. Geiker, "Comparing chloride ingress from seawater and NaCl solution in Portland cement mortar," Cem. Concr. Res., vol. 115, pp. 80-89, 2019.

[38] J. Zuquan, S. Wei, Z. Yunsheng, J. Jinyang and L. Jianzhong, "Interaction between sulfate and chloride solution attack of concretes with and without fly ash," Cem. Concr. Res., vol. 37, pp. 1223-1232, 2007.

[39] V. S. Ramachandran and J. J. Beaudoin, "Handbook of analytical techniques in concrete science and technology," New Jersey, Noyes Publications, 2001, p. 441-504.

[40] H. Song and V. Saraswathy, "Corrosion monitoring of reinforced concrete structures - a review," Int. J. Electrochem. Sci., vol. 2, pp. 1-28, 2007.

[41] ASTM: C876-15, “Standard test method for corrosion potential of unloaded reinforcing steel in concrete,” ASTM Standard, West Conshohocken, PA, 2015.

[42] M. F. Montemor, A. M. P. Simoes and M. G. S Ferreira., "Chloride-induced corrosion on reinforcing steel: from the fundamentals to the monitoring techniques," Cem. Concr. Compos., vol. 25, pp. 491-502, 2003.

[43] Y. S. Choi, J. G. Kim and K. M. Lee, "Corrosion behavior of steel bar embedded in fly ash concrete," Corros. Sci., vol. 48, pp. 1733-1745, 2006.

[44] B. Pradhan, "Corrosion behavior of steel reinforcement in concrete exposed to composite chloride-sulfate environment," Constr. Build. Mater., vol. 72, pp. 398-410, 2014.

[45] O. E. Gjorv and O. Vennesland, "Diffusion of chloride ions from seawater into concrete," Cem. Concr. Res., vol. 9, pp. 229-238, 1979.

[46] H. G. Midgley and J. M. Illston, "The penetration of chloride into hardened cement paste," Cem. Concr. Res., vol. 14, pp. 546 - 558, 1984.

[47] K. Byfors, "Influence of silica fume and flyash on chloride diffusion and pH values in cement paste," Cem. Concr. Res., vol. 17, pp. 115-130, 1987.

[48] C. Arya, N. R. Buenfeld and J. B. Newman, "Factors influencing chloride-binding in concrete," Cem. Concr. Res., vol. 20, pp. 291-300, 1990.

[49] M. D. A. Thomas, M. H. Shehata, S. G. Shashiprakash, D. S. Hopkins and K. Cail, "Use of ternary cementitious systems containing silica fume and fly ash in concrete," Cem. Concr. Res., vol. 29, pp. 1207-1214, 1999.

[50] C. S. Poon, S. C. Kou and L. Lam, "Compressive strength, chloride diffusivity and pore structure of high performance metakaolin and silica fume concrete," Constr. Build. Mater., vol. 20, pp. 858-865, 2006.

[51] C. S. Poon, L. Lam, S. C. Kou, Y. L. Wong and R. Wong, "Rate of pozzolanic reaction of metakaolin in high performance cement pastes," Cem. Concr. Res, vol. 31, pp. 1301-1306, 2001.

[52] P. Chindaprasirt, C. Chotithanorm, H. T. Cao and V. Sirivivatnanon, "Influence of fly ash fineness on the chloride penetration of concrete," Constr. Build. Mater., vol. 21, pp. 356-361, 2007.

[53] H. W. Song, C. H. Lee and K. Y. Ann, "Factors influencing chloride transport in concrete structures exposed to marine environments," Cem. Concr. Compos., vol. 30, pp. 113-121, 2008.

[54] P. S. Mangat and B. T. Molloy, "Predicting of long term chloride concentration in concrete," Mater. Struct., vol. 27, pp. 338-346, 1994.

[55] C. W. Chung, C. S. Shon, Y. S. Kim, "Chloride ion diffusivity of fly ash and silica fume concretes exposed to freeze-thaw cycles," Constr. Build. Mater., vol. 24, pp. 1739-1745, 2010.

[56] T. Cheewaket, C. Jaturapitakkul and W. Chalee, "Long term performance of chloride binding capacity in fly ash concrete in a marine environment," Constr. Build. Mater., vol. 24, pp. 1352-1357, 2010.

[57] D. K. Panesar and S. E. Chidiac, "Effect of cold temperature on the chloride-binding capacity of cement," J. Cold Reg. Eng., vol. 25 (4), pp. 133-144, 2011.

[58] L. Tang and L. O. Nilsson, "Chloride binding capacity and binding isotherms of OPC pastes and mortars," Cem. Concr. Res., vol. 23, pp. 247-253, 1993.

[59] W. Zhang, H. Ba and S. Chen, "Effect of fly ash and repeated loading on diffusion coefficient in chloride migration test," Constr. Build. Mater., vol. 25, pp. 2269-2274, 2011.

[60] M. Radlinski and J. Olek, "Investigation into the synergistic effects in ternary cementitious systems containing Portland cement, fly ash and silica fume," Cem. Concr. Compos., vol. 34, pp. 451-459, 2012.

[61] S. E. Chidiac, D. K. Panesar and H. Zibara, "The effect of short duration NaCl exposure on the surface pore structure of concrete containing GGBFS," Mater. Struct., vol. 45, pp. 1245-1258, 2012.

[62] M. Uysal and V. Akyuncu, "Durability performance of concrete incorporating Class F and Class C fly ashes," Constr. Build. Mater., vol. 34, pp. 170-178, 2012.

[63] T. Simcic, S. Pejovnik, G. De Schutter and V. B. Bosiljkov, "Chloride ion penetration into fly ash modified concrete during wetting-drying cycles," Constr. Build. Mater., vol. 93, pp. 1216-1223, 2015.

[64] M. H. Tadayon, M. Shekarchi and M. Tadayon, "Long-term field study of chloride ingress in concretes containing pozzolans exposed to severe marine tidal zone," Constr. Build. Mater., vol. 123, pp. 611-616, 2016.

[65] P. Gao, J. Wei, T. Zhang, J. Hu and Q. Yu, "Modification of chloride diffusion coefficient of concrete based on the electrical conductivity of pore solution," Constr. Build. Mater., vol. 145, pp. 361-366, 2017.

[66] J. Liu, G. Ou, Q. Qiu, X. Chen, J. Hong and F. Xing, "Chloride transport and microstructure of concrete with/without fly ash under atmospheric chloride condition," Constr. Build. Mater., vol. 146, pp. 493-501, 2017.

[67] J. Zhang, J. Zhao, Y. Zhang, Y. Gao and Y. Zheng, "Instantaneous chloride diffusion coefficient and its time dependency of concrete exposed to a marine tidal environment," Constr. Build. Mater., vol. 167, pp. 225-234, 2018.

[68] D. K. Panesar and G.Y. Ching, "Implications of coupled degradation mechanisms of cement based materials exposed to cold climates," Int. J. Mech. Sci., vol. 144, pp. 865-876, 2018.

[69] J. O. Ukpataa, P.A. M. Basheer and L. Black, "Expansion of CEM I and slag-blended cement mortars exposed to combined chloride-sulphate environments," Cem. Concr. Res., vol. 123, p. 105794, 2019.

[70] J. N. Enevoldsen, C. M. Hansson and B. B. Hope, "Binding of chloride in mortar containing admixed or penetrated chlorides," Cem. Concr. Res., vol. 24, pp. 1525-1533, 1994.

[71] W. A. Al-Khaja, "Influence of temperature, cement type and level of concrete consolidation on chloride ingress in conventional and high-strength concretes," Constr. Build. Mater., vol. 11, pp. 9-13, 1997.

[72] A. K. Suryavanshi, R. N. Swamy and S. McHugh, "Chloride penetration into reinforced concrete slabs," Can. J. Civ. Eng., vol. 25, pp. 87-95, 1998.

[73] A. Costa and J. Appleton, "Chloride penetration into concrete in marine environment - Part 1: Main parameters affecting chloride penetration," Mater. Struct., vol. 32, pp. 252-259, 1999.

[74] K. Hong and R. D. Hooton, "Effects of cyclic chloride exposure on penetration of concrete cover," Cem. Concr. Res., vol. 29, pp. 1379-1386, 1999.

[75] A. T. C. Guimarães, M. A. Climent, G. deVera, F. J. Vicente, F. T. Rodrigues and C. Andrade, "Determination of chloride diffusivity through partially saturated Portland cement concrete by a simplified procedure," Constr. Build. Mater., vol. 25, pp. 785-790, 2011.

[76] K. Sotiriadis, E. Nikolopoulou and S Tsivilis, "Sulfate resistance of limestone cement concrete exposed to combined chloride and sulfate environment at low temperature," Cem. Concr. Compos., vol. 34, pp. 903-910, 2012.

[77] M. Safehian and A. A. Ramezanianpour, "Assessment of service life models for determination of chloride penetration into silica fume concrete in the severe marine environmental condition," Constr. Build. Mater., vol. 48, pp. 287-294, 2013.

[78] J. Xu, C. Zhang, L. Jiang, L. Tang, G. Gao and Y. Xu, "Releases of bound chlorides from chloride-admixed plain and blended cement pastes subjected to sulfate attacks," Constr. Build. Mater., vol. 45, pp. 53-59, 2013.

[79] K. de Weerdt, D. Orsakova and M. R. Geiker, "The impact of sulphate and magnesium on chloride binding in Portland cement paste," Cem. Concr. Res., vol. 65, pp. 30-40, 2014.

[80] Z. Song, L. Jiang, J. Liu and J. Liu, "Influence of cation type on diffusion behavior of chloride ions in concrete," Constr. Build. Mater., vol. 99, pp. 150-158, 2015.

[81] C. Lu, Y. Gao, Z. Cui and R. Liu, "Experimental analysis of chloride penetration into concrete subjected to drying-wetting cycles," ASCE J. Mater. Civ. Eng., vol. 27, no. 12, p. 04015036(10), 2015.

[82] A. V. Saetta, R. V. Scotta and R. V. Vitaliani, "Analysis of chloride diffusion into partially saturated concrete," ACI Mater. J., vol. 90, no. 5, pp. 441-451, 1993.

[83] Y. Chen, J. Gao, L. Tang and X. Li, "Resistance of concrete against combined attack of chloride and sulfate under drying-wetting cycles," Constr. Build. Mater., vol. 106, pp. 650-658, 2016.

[84] L. Wu, W. Li and X. Yu, "Time-dependent chloride penetration in concrete in marine environments," Constr. Build. Mater., vol. 152, pp. 406-413, 2017.

[85] J. Zuquan, Z. Xia, Z. Tiejun and L. Jianqing, "Chloride ions transportation behavior and binding capacity of concrete exposed to different marine corrosion zones," Constr. Build. Mater., vol. 177, pp. 170-183, 2018.

[86] Y. Zhang, H. Zhuang, J. Shi, J. Huang and J. Zhang, "Time-dependent characteristic and similarity of chloride diffusivity in concrete," Mag. Concr. Res., vol. 70, no. 3, pp. 129-137, 2018.

[87] S. Cheng, Z. Shui, T. Sun, X. Gao and C. Guo, "Synergistic effects of sulfate and magnesium ions on chloride diffusion behaviors of Portland cement mortar," Constr. Build. Mater., vol. 229, p. 116878, 2019.

[88] G. Zhao, J. Li, M. Shi, J. Cui and F. Xie, "Degradation of cast-in-situ concrete subjected to sulphate-chloride combined attack," Constr. Build. Mater., vol. 241, p. 117995, 2020.

[89] S. Cheng, Z. Shui, X. Gao, J. Lu, T. Sun and R. Yu, "Degradation progress of Portland cement mortar under the coupled effects of multiple corrosive ions and drying-wetting cycles," Cem. Concr. Comp., vol. 111, p. 103629, 2020.

[90] C. L. Page, N. R. Short and W. R. Holden, "The influence of different cement on chloride-induced corrosion of reinforcing steel," Cem. Concr. Res., vol. 16, pp. 79-86, 1986.

[91] H. T. Cao and V. Sirivivatnanon, "Corrosion of steel in concrete with and without silica fume," Cem. Concr. Res., vol. 21, pp. 316-324, 1991.

[92] P. S. Mangat, J. M. Khatib and B. T. Molloy, "Microstructure, chloride diffusion and reinforcement corrosion in blended cement paste and concrete," Cem. Concr. Compos., vol. 16, pp. 73-81, 1994.

[93] C. Arya and Y. Xu, "Effect of cement type on chloride binding and corrosion of steel in concrete," Cem. Concr. Res., vol. 25, pp. 893-902, 1995.

[94] O. S. B. Al-Amoudi, "Performance of 15 reinforced concrete mixtures in magnesium-sodium sulphate environments," Constr. Build. Mater., vol. 9, no. 3, pp. 149-158, 1995.

[95] O. Kayali and B. Zhu, "Chloride induced reinforcement corrosion in lightweight aggregate high-strength fly ash concrete," Constr. Build. Mater., vol. 19, pp. 327-336, 2005.

[96] O. Kayali and B. Zhu, "Corrosion performance of medium-strength and silica fume high-strength reinforced concrete in a chloride solution," Cem. Concr. Compos., vol. 27, pp. 117-124, 2005.

[97] S. A. Alghamdi and S. Ahmad, "Service life prediction of RC structures based on correlation between electrochemical and gravimetric reinforcement corrosion rates," Cem. Concr. Compos., vol. 47, pp. 64-68, 2014.

[98] T. P. Cheng, J. T. Lee and W. T. Tsai, "Corrosion of reinforcements in artificial sea water and concentrated sulfate solution," Cem. Concr. Res., vol. 20, pp. 243-252, 1990.

[99] A. J. Al-Tayyib and M. S. Khan, "Effect of sulfate ions on the corrosion of rebars embedded in concrete," Cem. Concr. Compos., vol. 13, pp. 123-127, 1991.

[100] O. S. B. Al-Amoudi and M. Maslehuddin, "The effect of chloride and sulfate ions on reinforcement corrosion," Cem. Concr. Res., vol. 23, pp. 139-146, 1993.

[101] H. A. F. Dehwah, M. Maslehuddin and S. A. Austin, "Long-term effect of sulfate ions and associated cation type on chloride-induced reinforcement corrosion in Portland cement concretes," Cem. Concr. Compos., vol. 24, pp. 17-25, 2002.

[102] A. Dousti, M. Moradian, S. R. Taheri, R. Rashetnia and M. Shekarchi, "Corrosion assessment of RC deck in a jetty structure damaged by chloride attack," ASCE J. Perform. Constr. Facil., vol. 27, pp. 519-528, 2013.

[103] M. Otieno, H. Beushausen and M. Alexander, "Chloride-induced corrosion of steel in cracked concrete - Part I: Experimental studies under accelerated and natural marine environments," Cem. Concr. Res., vol. 79, pp. 373-385, 2016.

[104] M. Otieno, H. Beushausen and M. Alexander, "Chloride-induced corrosion of steel in cracked concrete—Part II: Corrosion rate prediction models," Cem. Concr. Res., vol. 79, pp. 386-394, 2016.

[105] R. Liu, L. Jiang, G. Huang, Y. Zhu, X. Liu, H. Chu and C. Xiong, "The effect of carbonate and sulfate ions on chloride threshold level of reinforcement corrosion in mortar with/without fly ash," Constr. Build. Mater., vol. 113, pp. 90-95, 2016.

[106] K. Sotiriadis, E. Rakanta, M. E. Mitzithra, G. Batis and S. Tsivilis, "Influence of sulfates on chloride diffusion and chloride-induced reinforcement corrosion in limestone cement materials at low temperature," ASCE J. Mater. Civ. Eng., vol. 29(8), p. 04017060, 2017.

[107] A. Abdalkader, C. Lynsdale and J. Cripps, "Corrosion behaviour of steel rebar in mortars subjected to magnesium sulfate and sodium chloride mixtures at 5 and 20º C," Constr. Build. Mater., vol. 153, pp. 358-363, 2017.

[108] S. J. Kwon, H. S. Lee, S. Karthick, V. Saraswathy and H. M. Yang, "Long-term corrosion performance of blended cement concrete in the marine environment - A real-time study," Constr. Build. Mater., vol. 154, pp. 349-360, 2017.

[109] IS 8112: 2013, "Ordinary Portland cement, 43 grade - specification (Second revision)," Bureau of Indian Standards, New Delhi, 2013.

[110] ASTM C150/C150M-17, "Standard specification for Portland cement," ASTM International, West Conshohocken, PA, 2017.

[111] IS 1489: 1991, "Specification for Portland pozzolana cement," Bureau of Indian Standard, New Delhi, 1991.

[112] ASTM C595/C595M-17, "Standard specification for blended hydraulic cements," ASTM International, West Conshohocken, PA, 2017.

[113] ASTM C618, "Standard specification for coal fly ash and raw or calcined natural pozzolan for use in concrete," ASTM International, West Conshohocken, PA, 2012.

[114] IS: 2386 (Part-1): 1963 (Reaffirmed 2007), "Method of test for aggregate for concrete, (Part-1 Partical size and shape)," Bureau of Indian Standard, New Delhi, 1963.

[115] ASTM C33/C33M-16, "Standard specification for concrete aggregates," ASTM International, West Conshohocken, PA, 2016.

[116] IS: 383: 1970 (Reaffirmed 2002), "Specification for coarse and fine aggregate from natural sources for concrete," Bureau of Indian Standard, New Delhi, 1993.

[117] IS: 2386 (Part-3): 1963, "Method of test for aggregates for concrete," Bureau of Indian Standard, New Delhi, 1963.

[118] SP23: 1982, “Handbook on concrete mixes (Based on Indian standard),” Bureau of Indian standards, New Delhi, 1990.

[119] IS 456: 2000 (Reaffirmed 2005), "Indian standard plain and reinforced concrete-code for practice," Bureau of Indian Standards, New Delhi, 2000.

[120] B. Pradhan and B. Bhattacharjee, "Performance evaluation of rebar in chloride contaminated concrete by corrosion rate," Constr. Build. Mater., vol. 23, p. 2346-2356, 2009.

[121] B. Pradhan and B. Bhattacharjee, "Corrosion zones of rebar in chloride contaminated concrete through potentiostatic study in concrete powder solution extracts," Corros. Sci., vol. 49, pp. 3935-3952, 2007.

[122] B. Pradhan and B. Bhattacharjee, "Role of steel and cement type on chloride-induced corrosion in concrete," ACI Mater. J, vol. 104, no. 6, pp. 612-619, 2009.

[123] S. Muralidharan, R. Vedalakshmi, V. Saraswathi, J. Joseph and N. Palaniswamy, "Studies on the aspects of chloride ion determination in different types of concrete under macro-cell corrosion conditions," Build. Environ., vol. 40, p. 1275-1281, 2005.

[124] Y. Gao, J. Zhang, S. Zhang and Y. Zhang, "Probability distribution of convection zone depth of chloride in concrete in a marine tidal environment," Constr. Build. Mater., vol. 140, pp. 485-495, 2017.

[125] P. Liu, Z. Yu, Z. Lu, Y. Chen and X. Liu, "Predictive convection zone depth of chloride in concrete under chloride environment," Cem. Concr. Compos., vol. 72, pp. 257-267, 2016.

[126] A. M. Brown, "A step-by-step guide to non-linear regression analysis of experimental data using a Microsoft Excel spreadsheet," Com. Methods Progr. Biomed, vol. 65, pp. 191-200, 2001.

[127] F. H. Chung, "Quantitative interpretation of X-ray diffraction patterns of mixtures. I. Matrix-flushing method for quantitative multicomponent analysis," J. Appl. Cryst., vol. 7, pp. 519-525, 1974.

[128] F. H Chung, "Quantitative interpretation of X-ray diffraction patterns of mixtures. III Simultaneous determination of a set of reference intensities," J. Appl. Cryst. , vol. 8, pp. 17-19, 1975.

[129] F. H. Chung, "Quantitative interpretation of X-ray diffraction patterns, II. Adiabatic principle of X-ray diffraction analysis of mixtures," J. Appl. Cryst, vol. 7, pp. 526-531, 1974.

[130] J. Geng, D. Easterbrook, L. Li and L. Mo, "The stability of bound chlorides in cement paste with sulfate attack," Cem. Concr. Res., vol. 68, pp. 211-222, 2015.

[131] S. Jain and B. Pradhan, "Effect of cement type on hydration, microstructure and thermos-gravimetric behaviour of chloride admixed self-compacting concrete," Constr. Build. Mater., vol. 212, pp. 304-316, 2019.

[132] B. N. Hupp and J. J. Donovan, "Quantitative mineralogy for facies definition in the Marcellus Shale (Appalachian Basin, USA) using XRD-XRF integration," Sedim. Geo., vol. 371, pp. 16-31, 2018.

[133] H. F. W. Taylor, “Cement Chemistry,” Second ed., Thomas Telford, 1997.

[134] H. Ye, X. Jin, C. Fu, N. Jin, Y. Xu and T. Huang, "Chloride penetration in concrete exposed to cyclic drying-wetting and carbonation," Constr. Build. Mater., vol. 112, pp. 457-463, 2016.

[135] H. Ye, N. Jin, X. Jin, C. Fu and W. Chen, "Chloride ingress profiles and binding capacity of mortar in cyclic drying-wetting salt fog environments," Constr. Build. Mater., vol. 127, pp. 733-742, 2016.

[136] A. Delagrave, M. Pigeon, J. Marchand and E. Revertegat, "Influence of chloride ions and pH level on the durability of high performance cement pastes (Part II)," Cem. Concr. Res., vol. 26, pp. 749-760, 1996.

[137] C. Ftikos and G. Parissakis, "The combined action of Mg^{2+} and Cl^{-} ions in cement pastes," Cem. Concr. Res., vol. 15, pp. 593-599, 1985.

[138] H. Lee, R. D. Cody, A. M. Cody and P. G. Spry, "Effects of various deicing chemicals on pavement concrete deterioration," Mid-Cont. Transp. Symp. Proc., pp. 151-155, 2000.

[139] K. A. A. Al-Sodani, M. M. Al-Zahrani, M. M. Maslehuddin, O. S. B. Al-Amoudi and S. U. Al-Dulaijan, "Chloride diffusion models for Type I and fly ash cement concrete exposed to field and laboratory conditions," Mar. Struct., vol. 76, p. 102900, 2021.

[140] Z. Yu, Y. Chen, P. Liu and W. Wang, "Accelerated simulation of chloride ingress into concrete under drying-wetting alternation condition chloride environment," Constr. Build. Mater., vol. 93, pp. 205-213, 2015.

[141] Z. Wang, B. Wang, D. Yang and J. Han, "Research progress on the chloride binding capability of cement-based composites," J. Ceram. Soc. Japan, vol. 128(5), pp. 238-253, 2020.

[142] M. Regourd, H. Hornain, and B. Mortureux, "Microstructure of concrete in aggressive environments," Durab. Build. Mater. Comp., ASTM STP 691, pp. 253-268, 1980.

[143] M. R. Meier and J. Plank, "Crystal growth of $[Ca_3Al(OH)_6{\cdot}12H_2O]_2{\cdot}(SO_4)_3{\cdot}2H_2O$ (ettringite) under microgravity: On the impact of anionicity of polycarboxylate comb polymers," J. Cry. Grow. vol. 446, p. 92.102, 2016.

[144] K. De Weerdt, H. Justnes and M. R. Geiker, "Changes in the phase assemblage of concrete exposed to sea water," Cem. Concr. Compos., vol. 47, pp. 53-63, 2014.

[145] C. Shi, D. Wang and A. Behnood, "Review of thaumasite sulfate attack on cement mortar and concrete," ASCE J. Mater. Civ. Eng., vol. 24, pp. 1450-1460, 2012.

[146] R. Luo, Y. Cai, C. Wang and X. Huang, "Study of chloride binding and diffusion in GGBS concrete," Cem. Concr. Res., vol. 33, pp. 1-7, 2003.

[147] P. E. Grattan-Bellew, "Microstructural investigation of deteriorated Portland cement concretes," Constr. Build. Mater., vol. 10, pp. 3-16, 1996.

[148] T. U. Mohammed, H. Hamada and T. Yamaji, "Concrete after 30 years of exposure—Part I: Mineralogy, microstructures, and interfaces," ACI Mater. J., vol. 101, pp. 3-12, 2004.

[149] N. Xie, Y. Dang and X. Shi, "New insights into how $MgCl_2$ deteriorates Portland cement concrete," Cem. Concr. Res., vol. 120, pp. 244-255, 2019.

[150] B. D. Barnes, S. Diamond and W. L. Dolch, "The contact zone between Portland cement paste and glass "aggregate" surfaces," Cem. Concr. Res., vol. 8, pp. 233-244, 1978.

[151] S. Mirvalad, M. Nokken and D. Banu, "Detection of thaumasite formation using differential scanning calorimetry," ASCE J. Mater. Civ. Eng., vol. 31(9), p. 04019178, 2019.

[152] K. De Weerdt and H. Justnes, "The effect of sea water on the phase assemblage of hydrated cement paste," Cem. Concr. Compos., vol. 55, pp. 215-222, 2015.

[153] N. Marinoni, A. Pavese, M. Voltolini and M. Merlini, "Long-term leaching test in concretes: An X-ray powder diffraction study," Cem. Concr. Compos., vol. 30, pp. 700-705, 2008.

[154] A. M. de Oliveira and O. Cascudo, "Effect of mineral additions incorporated in concrete on thermodynamic and kinetic parameters of chloride-induced reinforcement corrosion," Constr. Build. Mater., vol. 192, pp. 467-477, 2018.

[155] C. Andrade and C. Alonso, "On-site measurements of corrosion rate of reinforcements," Constr. Build. Mater., vol. 15, pp. 141-145, 2001.

[156] S. G. Millard, D. Law, J. H. Bungey and J. Cairns, "Environmental influences on linear polarisation corrosion rate measurement in reinforced concrete," NDT & E Inter., vol. 34, pp. 409-417, 2001.

[157] T. Liu and R. W. Weyers, "Modeling the dynamic corrosion process in chloride contaminated concrete structures," Cem. Concr. Res., vol. 28, no. 3, pp. 365-379, 1998.

[158] MATLAB R2014a, “The MathWorks, Inc.,” Natick, Massachusetts, United States, 2014.

[159] R. K. Dhir, M. R. Jones and M. J. McCarthy, "Quantifying chloride-induced corrosion from half-cell potential," Cem. Concr. Res., vol. 23, pp. 1443-1454, 1993.

[160] R. K. Dhir, M. R. Jones and M. J. McCarthy, "PFA concrete: chloride-induced reinforcement corrosion," Mag. Concr. Res., vol. 46, pp. 269-277, 1994.

[161] P. Lambert, C. L. Page and P. R. W. Vassie, "Investigations of reinforcement corrosion 2. Electrochemical monitoring of steel in chloride-contaminated concrete," Mater. Struct., vol. 24, pp. 351-358, 1991.

APPENDIX A1

Free chloride content profile of concrete exposed to chloride, and composite chloride-sulfate solutions for different exposure periods

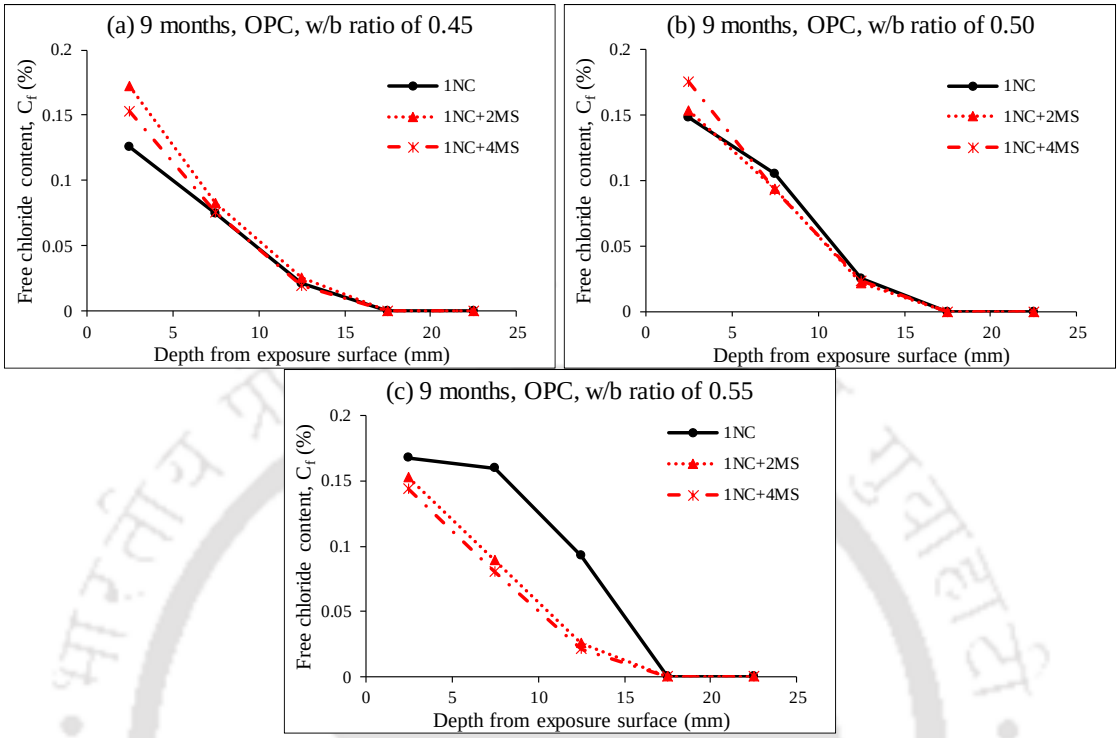

Figure A1 Free chloride content profile of OPC concrete exposed to 1% NaCl and 1% NaCl with $MgSO_4$ solutions for 9 months: (a) w/b ratio of 0.45, (b) w/b ratio of 0.50, and (c) w/b ratio of 0.55

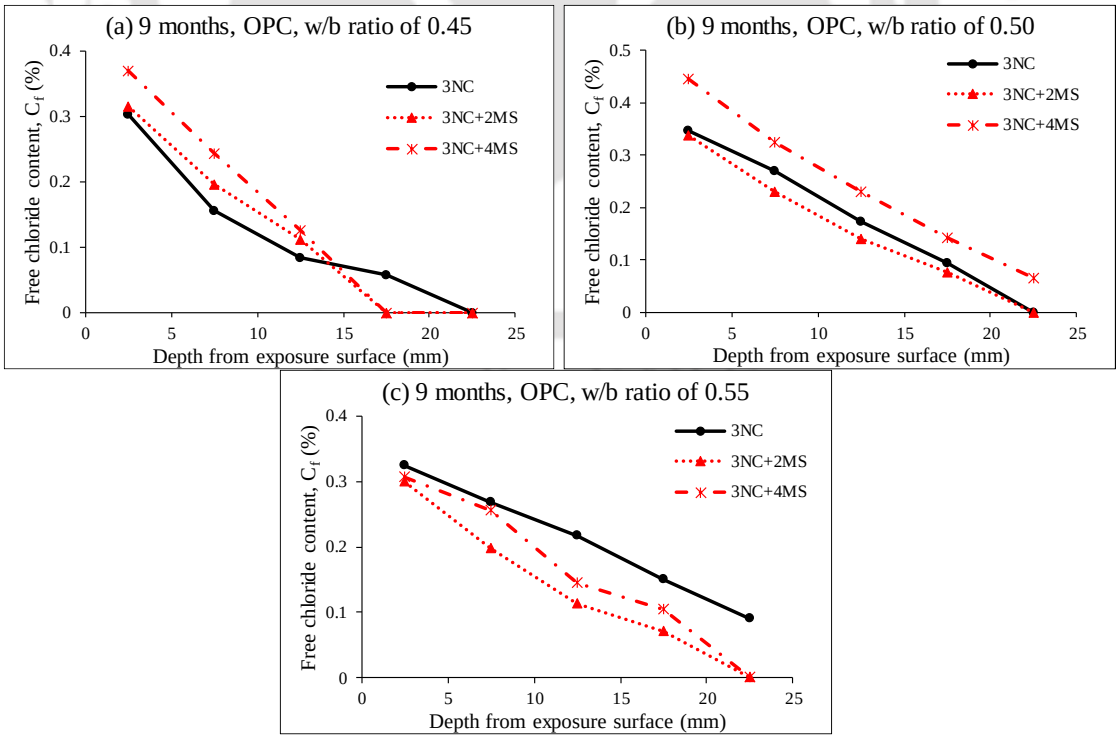

Figure A2 Free chloride content profile of OPC concrete exposed to 3% NaCl and 3% NaCl with $MgSO_4$ solutions for 9 months: (a) w/b ratio of 0.45, (b) w/b ratio of 0.50, and (c) w/b ratio of 0.55

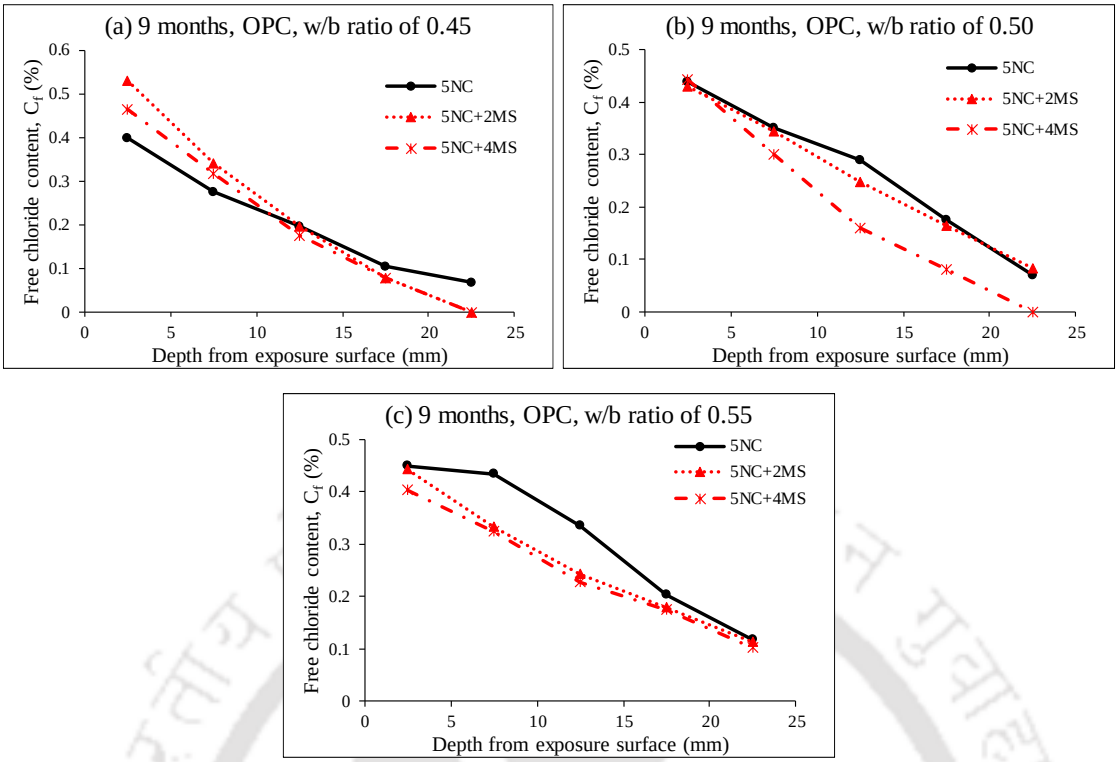

Figure A3 Free chloride content profile of OPC concrete exposed to 5% NaCl and 5% NaCl with $MgSO_4$ solutions for 9 months: (a) w/b ratio of 0.45, (b) w/b ratio of 0.50, and (c) w/b ratio of 0.55

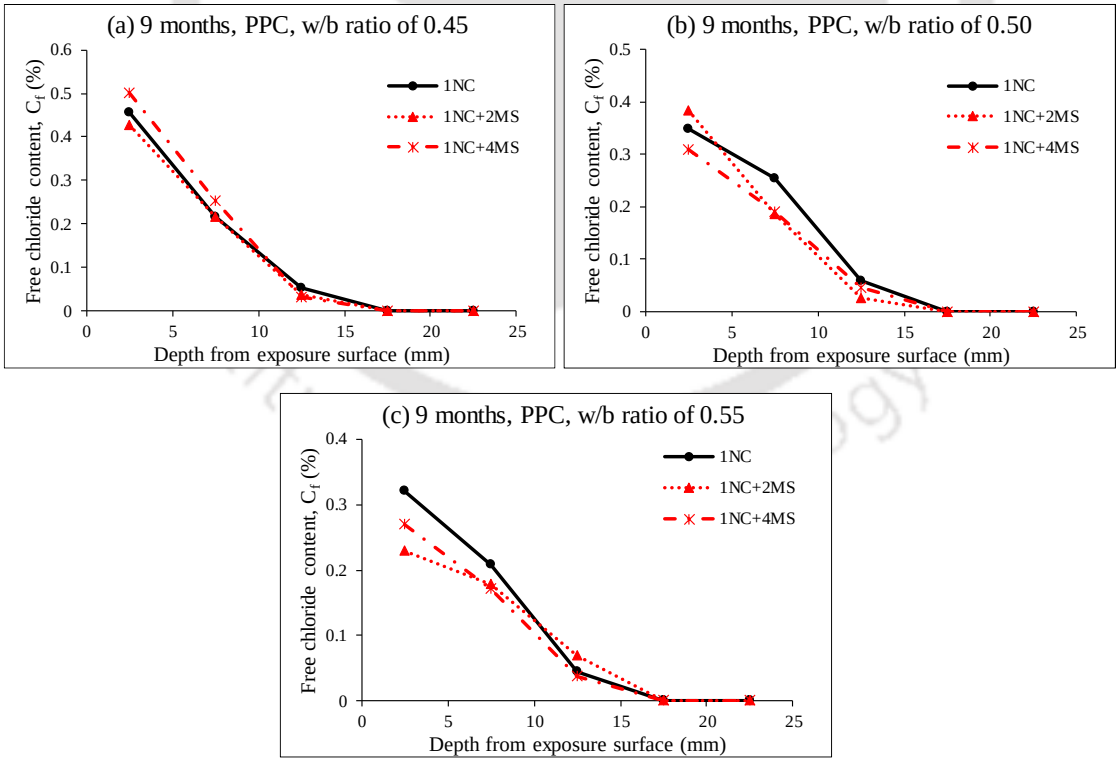

Figure A4 Free chloride content profile of PPC concrete exposed to 1% NaCl and 1% NaCl with $MgSO_4$ solutions for 9 months: (a) w/b ratio of 0.45, (b) w/b ratio of 0.50, and (c) w/b ratio of 0.55

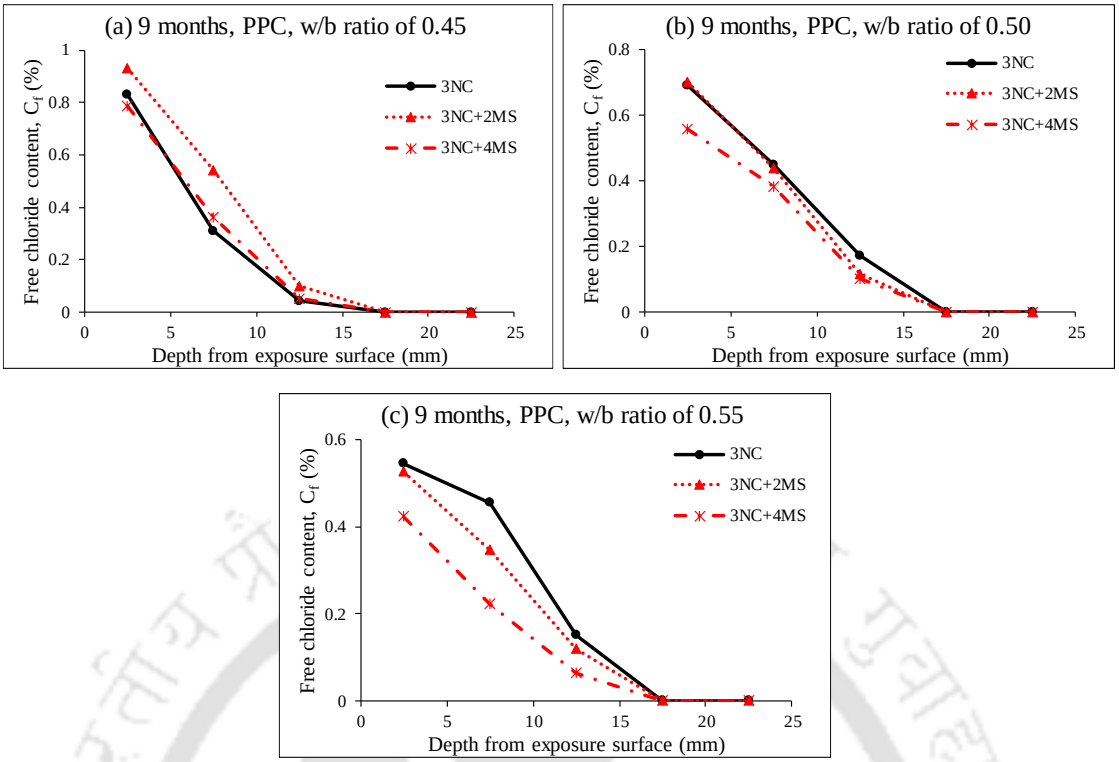

Figure A5 Free chloride content profile of PPC concrete exposed to 3% NaCl and 3% NaCl with $MgSO_4$ solutions for 9 months: (a) w/b ratio of 0.45, (b) w/b ratio of 0.50, and (c) w/b ratio of 0.55

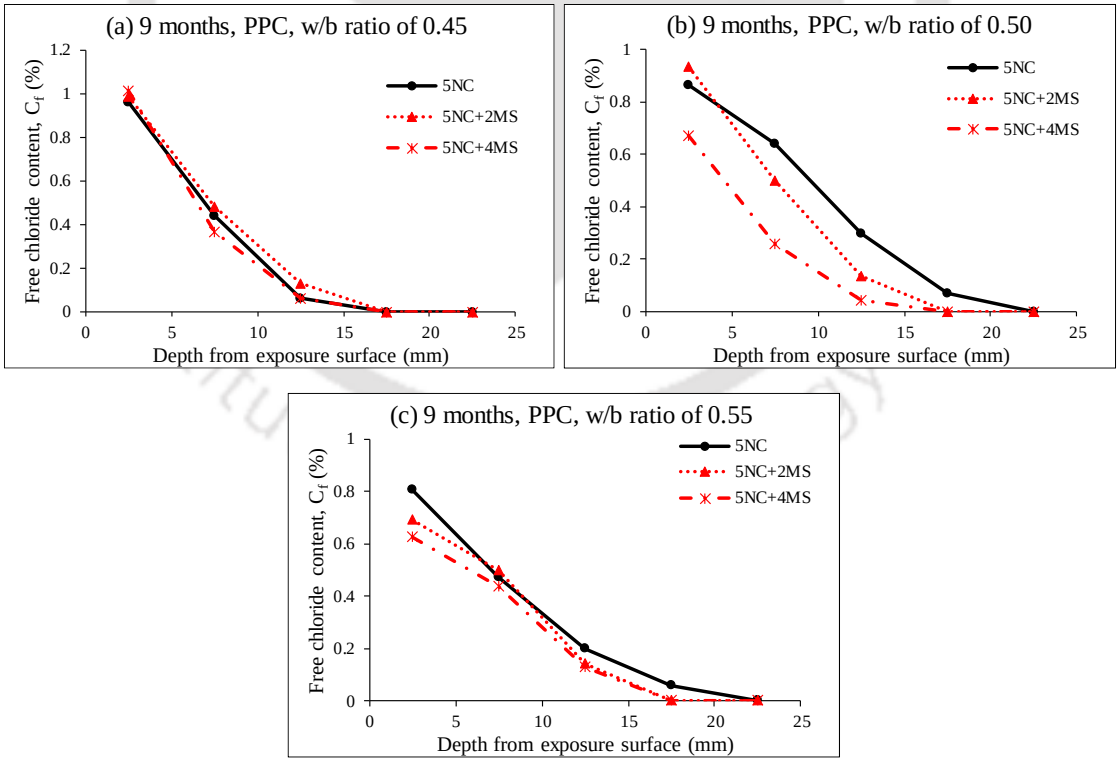

Figure A6 Free chloride content profile of PPC concrete exposed to 5% NaCl and 5% NaCl with $MgSO_4$ solutions for 9 months: (a) w/b ratio of 0.45, (b) w/b ratio of 0.50, and (c) w/b ratio of 0.55

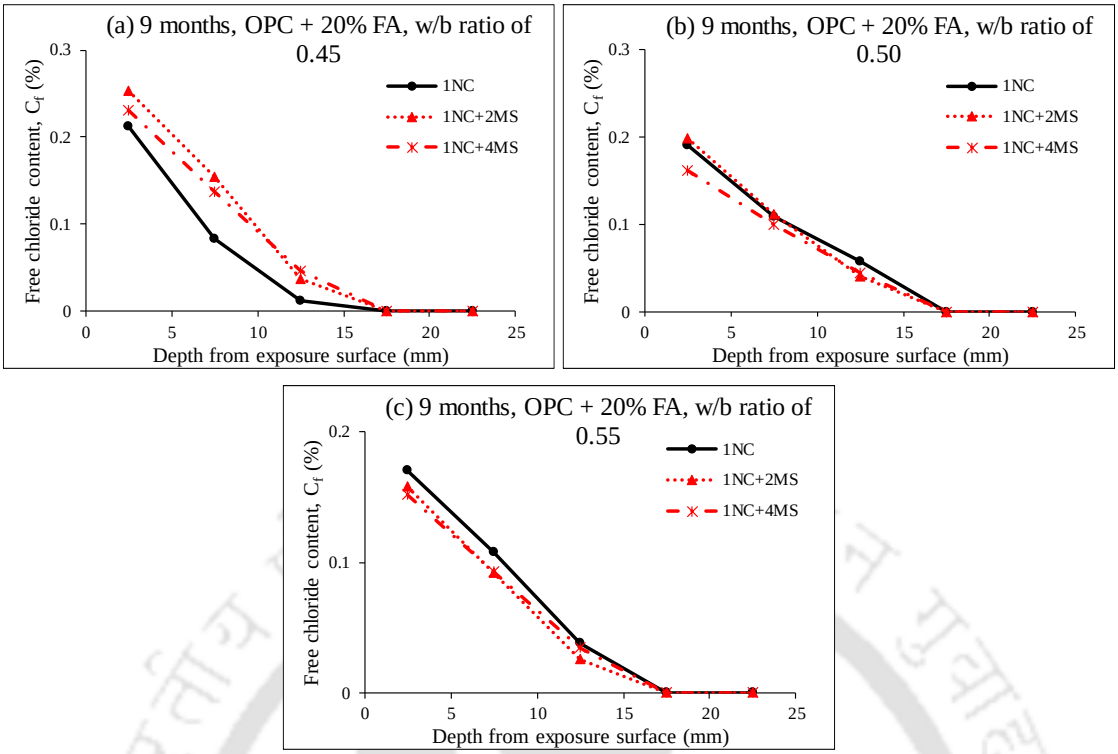

Figure A7 Free chloride content profile of OPC + 20% FA concrete exposed to 1% NaCl and 1% NaCl with $MgSO_4$ solutions for 9 months: (a) w/b ratio of 0.45, (b) w/b ratio of 0.50, and (c) w/b ratio of 0.55

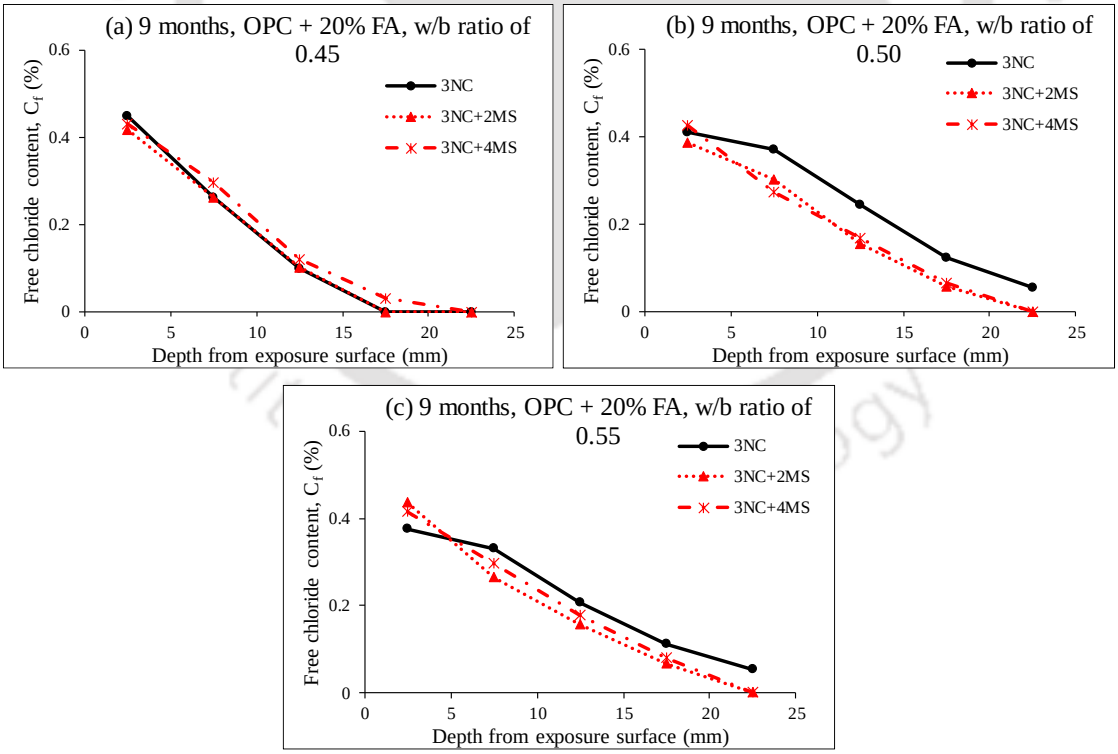

Figure A8 Free chloride content profile of OPC + 20% FA concrete exposed to 3% NaCl and 3% NaCl with $MgSO_4$ solutions for 9 months: (a) w/b ratio of 0.45, (b) w/b ratio of 0.50, and (c) w/b ratio of 0.55

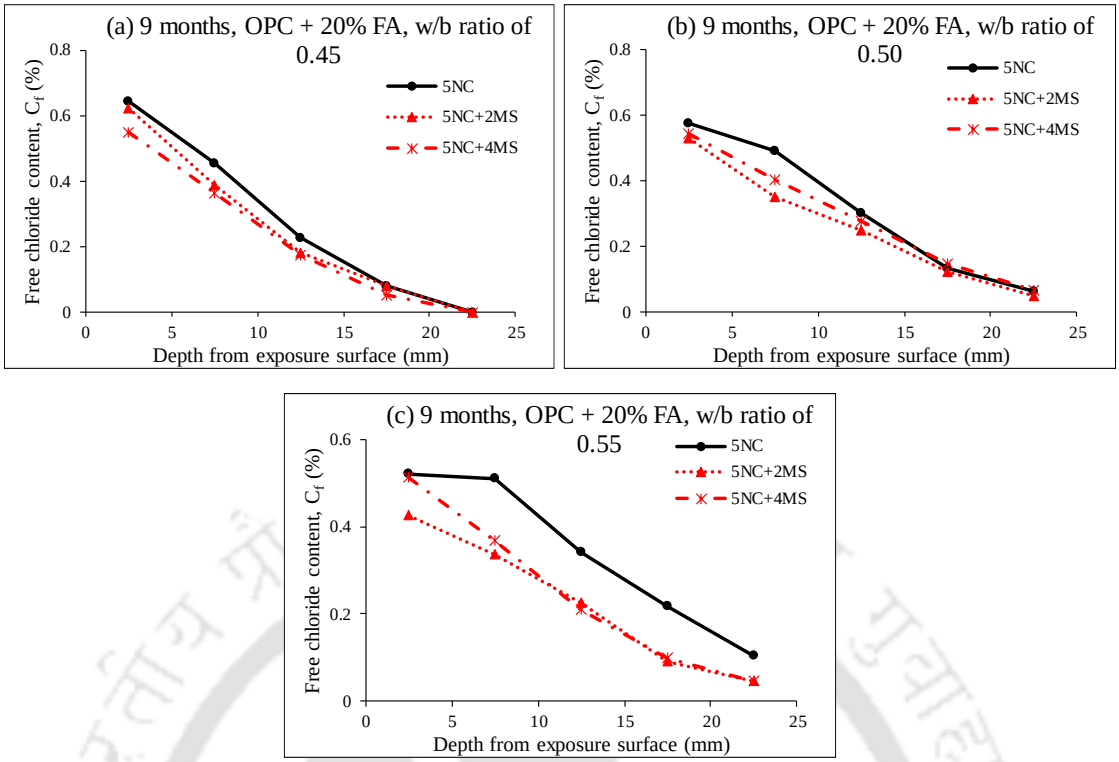

Figure A9 Free chloride content profile of OPC + 20% FA concrete exposed to 5% NaCl and 5% NaCl with $MgSO_4$ solutions for 9 months: (a) w/b ratio of 0.45, (b) w/b ratio of 0.50, and (c) w/b ratio of 0.55

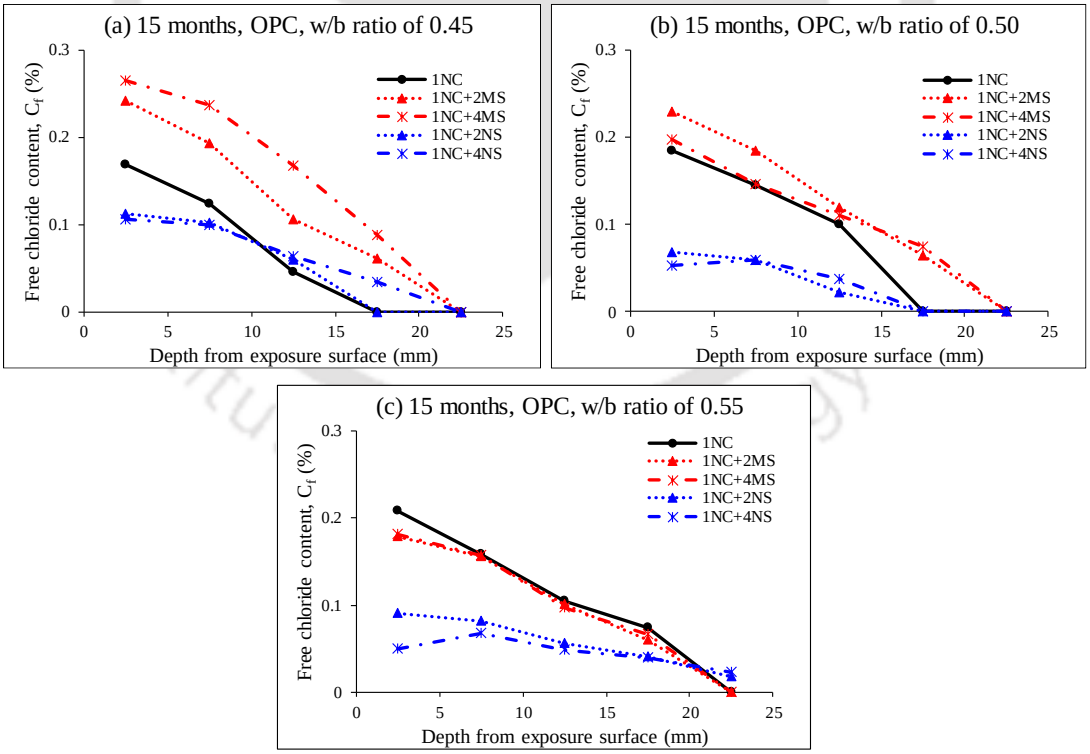

Figure A10 Free chloride content profile of OPC concrete exposed to 1% NaCl and 1% NaCl with $MgSO_4$ or Na_2SO_4 solutions for 15 months: (a) w/b ratio of 0.45, (b) w/b ratio of 0.50, and (c) w/b ratio of 0.55

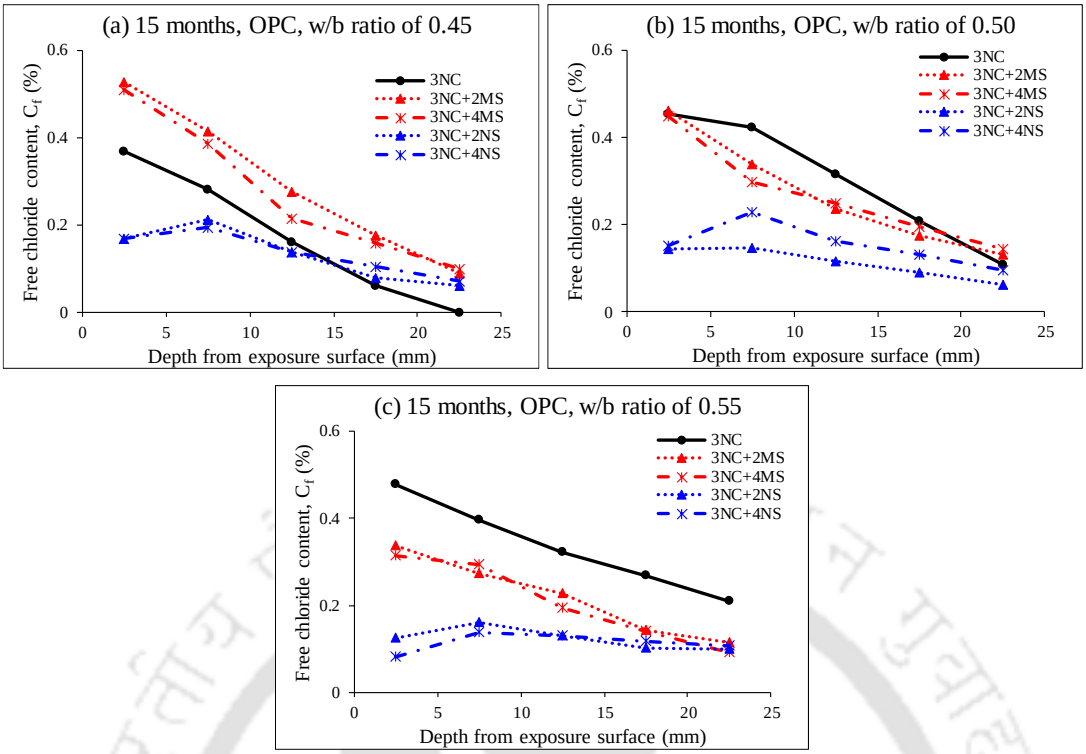

Figure A11 Free chloride content profile of OPC concrete exposed to 3% NaCl and 3% NaCl with $MgSO_4$ or Na_2SO_4 solutions for 15 months: (a) w/b ratio of 0.45, (b) w/b ratio of 0.50, and (c) w/b ratio of 0.55

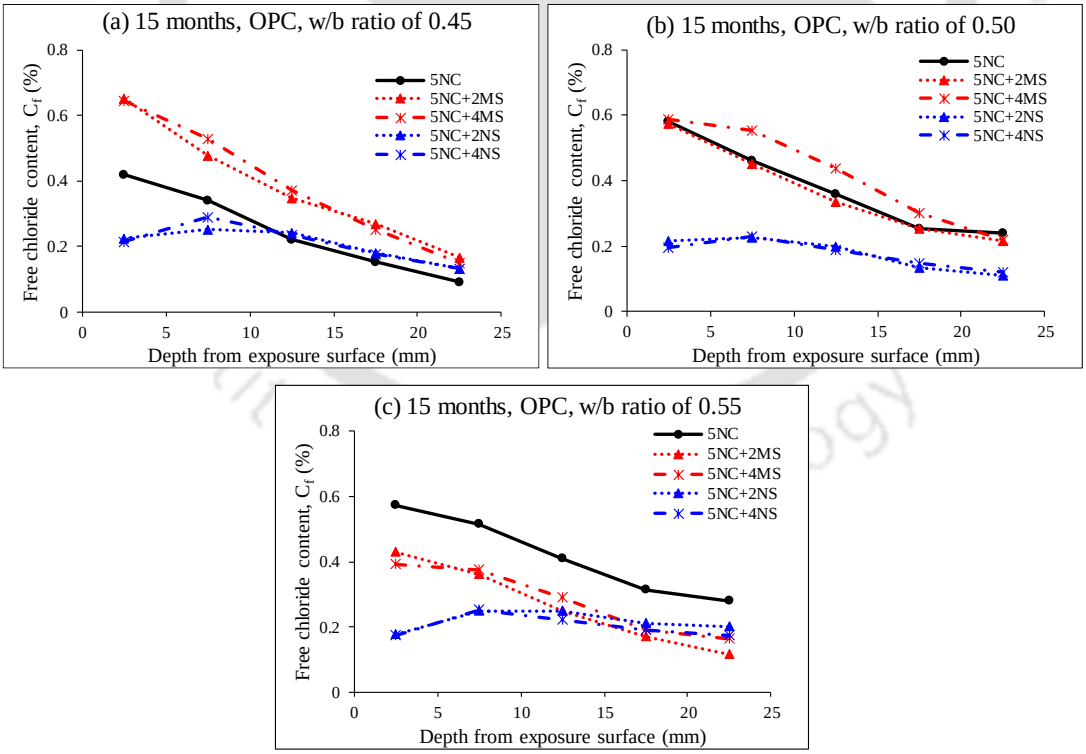

Figure A12 Free chloride content profile of OPC concrete exposed to 5% NaCl and 5% NaCl with $MgSO_4$ or Na_2SO_4 solutions for 15 months: (a) w/b ratio of 0.45, (b) w/b ratio of 0.50, and (c) w/b ratio of 0.55

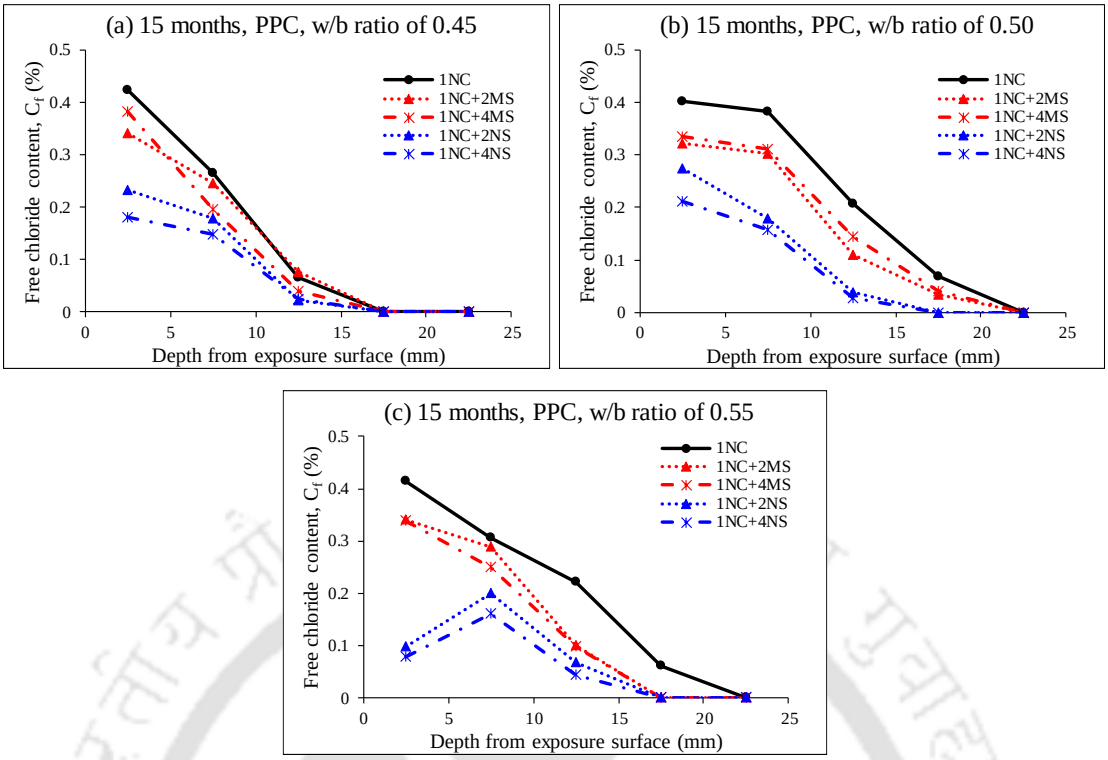

Figure A13 Free chloride content profile of PPC concrete exposed to 1% NaCl and 1% NaCl with $MgSO_4$ or Na_2SO_4 solutions for 15 months: (a) w/b ratio of 0.45, (b) w/b ratio of 0.50, and (c) w/b ratio of 0.55

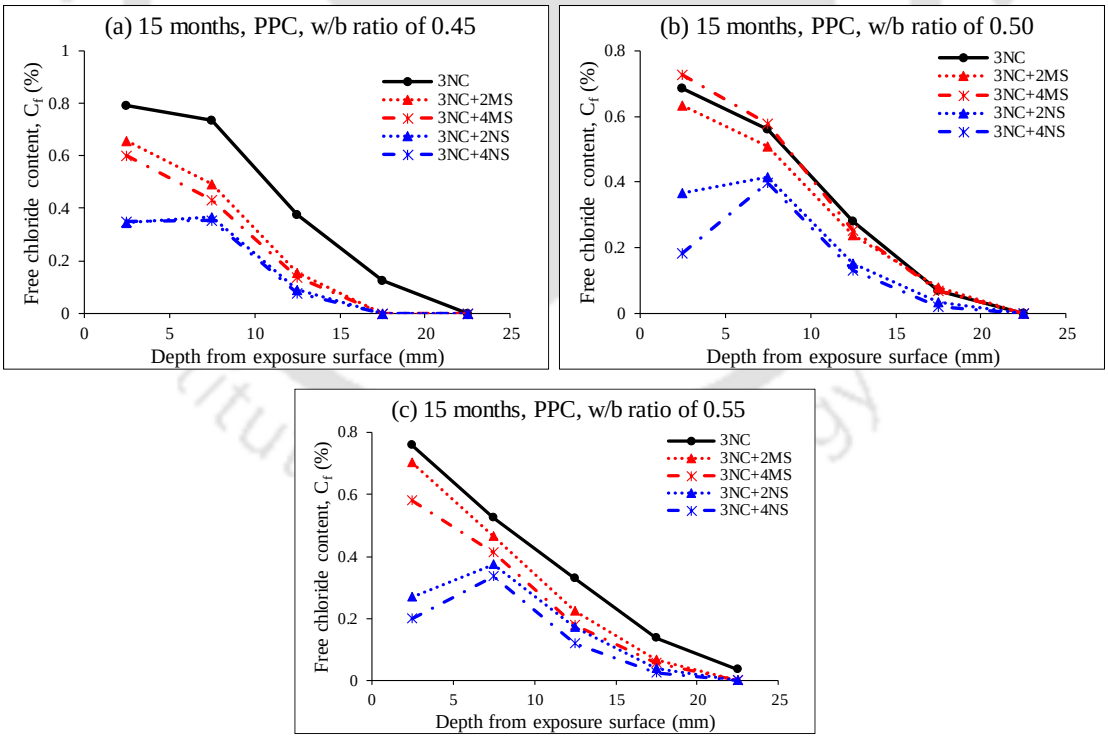

Figure A14 Free chloride content profile of PPC concrete exposed to 3% NaCl and 3% NaCl with $MgSO_4$ or Na_2SO_4 solutions for 15 months: (a) w/b ratio of 0.45, (b) w/b ratio of 0.50, and (c) w/b ratio of 0.55

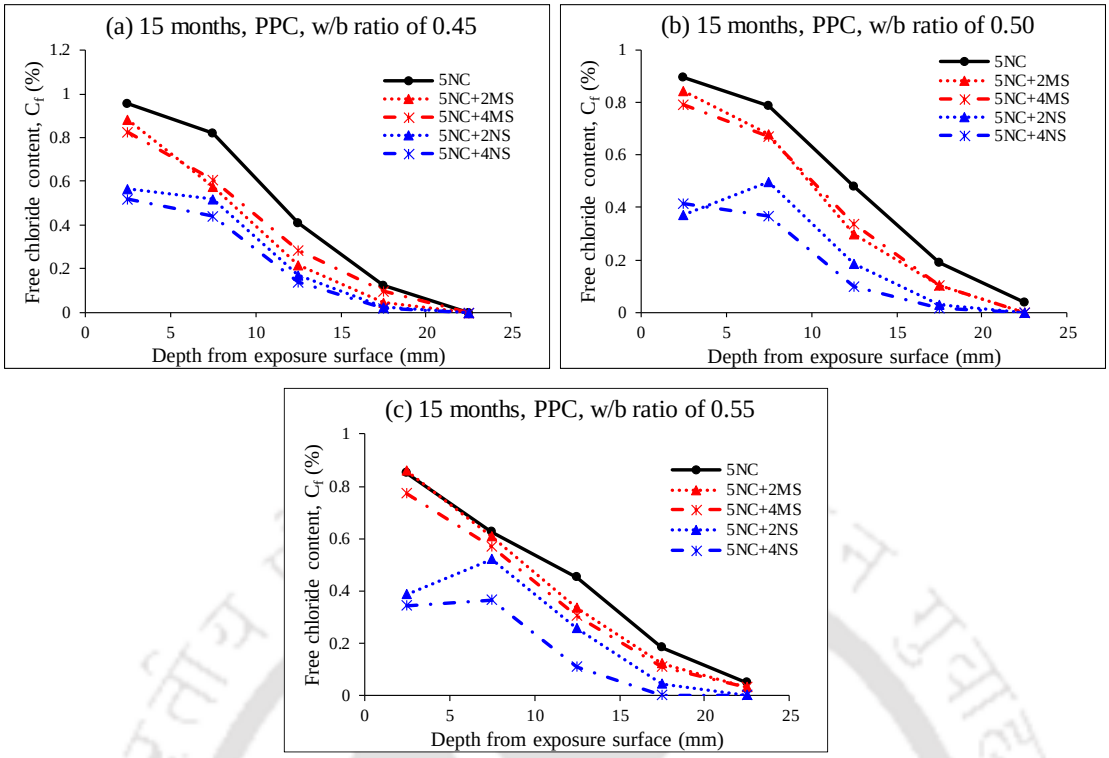

Figure A15 Free chloride content profile of PPC concrete exposed to 5% NaCl and 5% NaCl with $MgSO_4$ or Na_2SO_4 solutions for 15 months: (a) w/b ratio of 0.45, (b) w/b ratio of 0.50, and (c) w/b ratio of 0.55

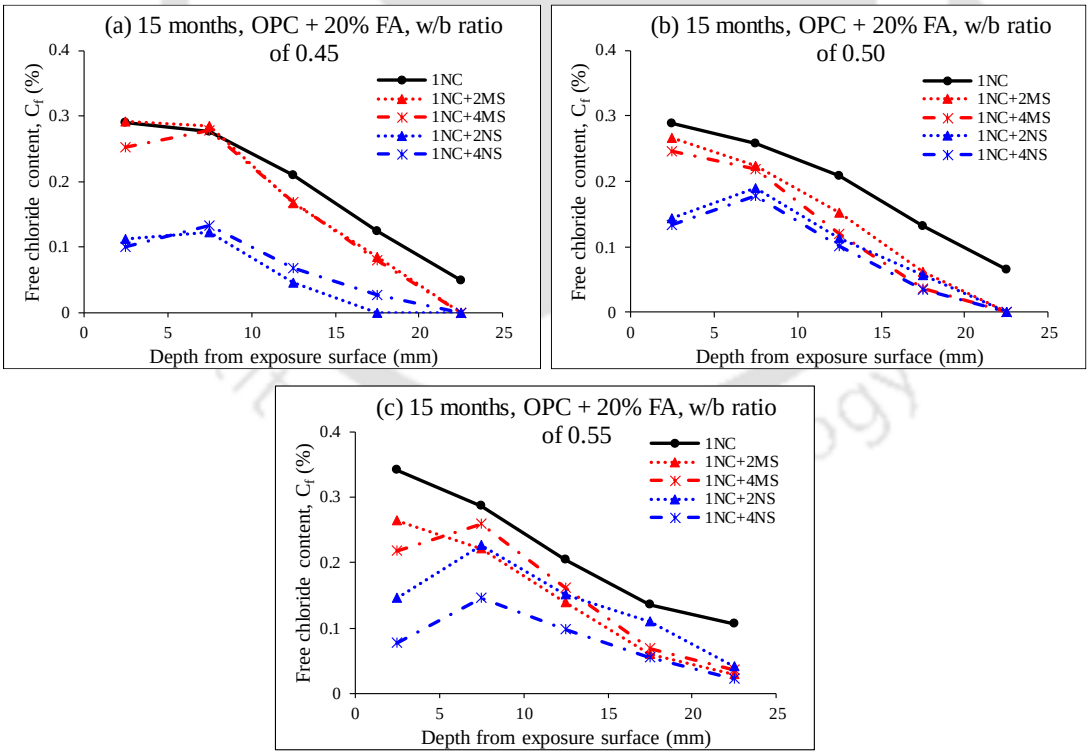

Figure A16 Free chloride content profile of OPC + 20% FA concrete exposed to 1% NaCl and 1% NaCl with $MgSO_4$ or Na_2SO_4 solutions for 15 months: (a) w/b ratio of 0.45, (b) w/b ratio of 0.50, and (c) w/b ratio of 0.55

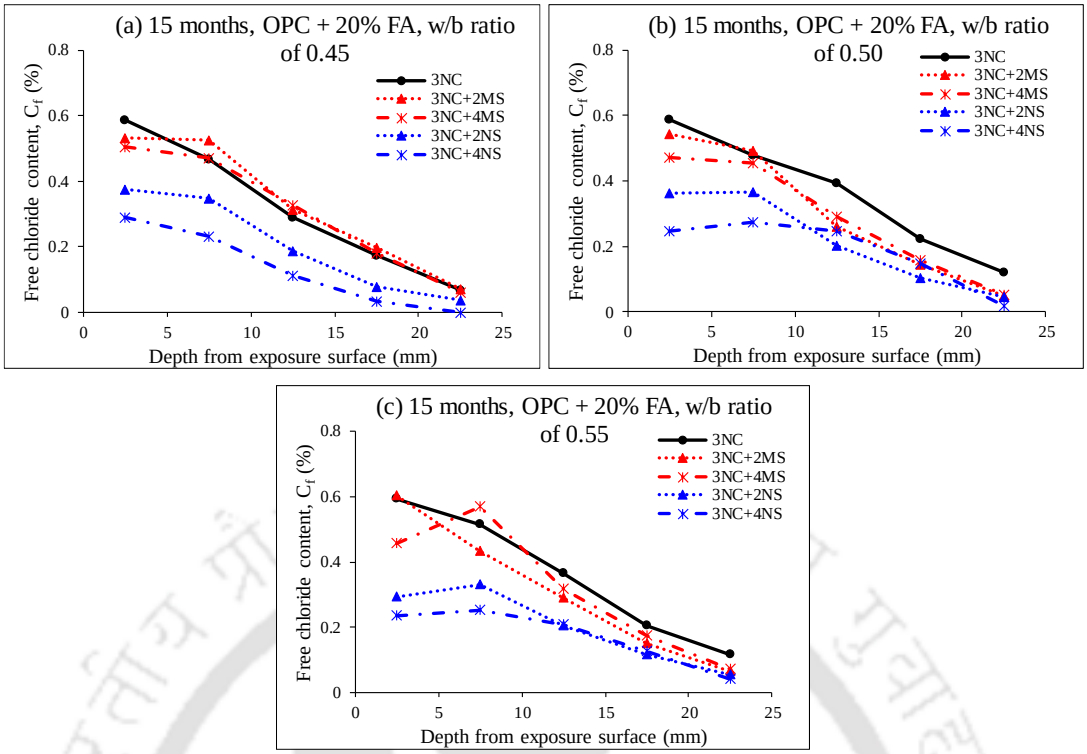

Figure A17 Free chloride content profile of OPC + 20% FA concrete exposed to 3% NaCl and 3% NaCl with $MgSO_4$ or Na_2SO_4 solutions for 15 months: (a) w/b ratio of 0.45, (b) w/b ratio of 0.50, and (c) w/b ratio of 0.55

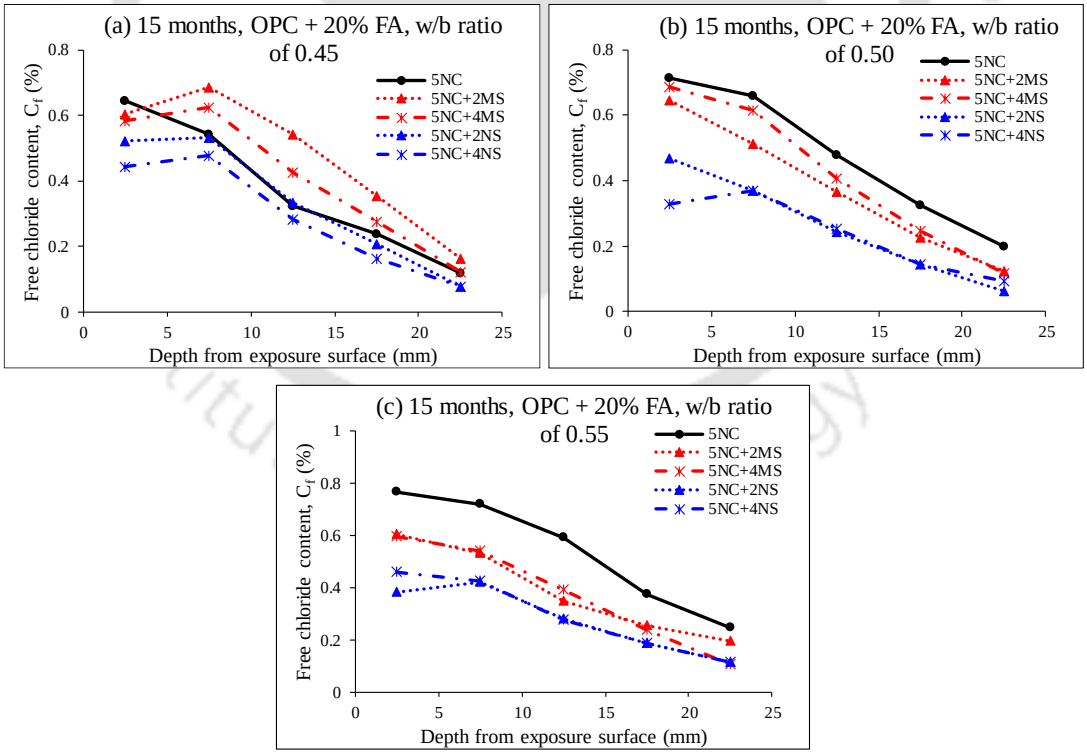

Figure A18 Free chloride content profile of OPC + 20% FA concrete exposed to 5% NaCl and 5% NaCl with $MgSO_4$ or Na_2SO_4 solutions for 15 months: (a) w/b ratio of 0.45, (b) w/b ratio of 0.50, and (c) w/b ratio of 0.55

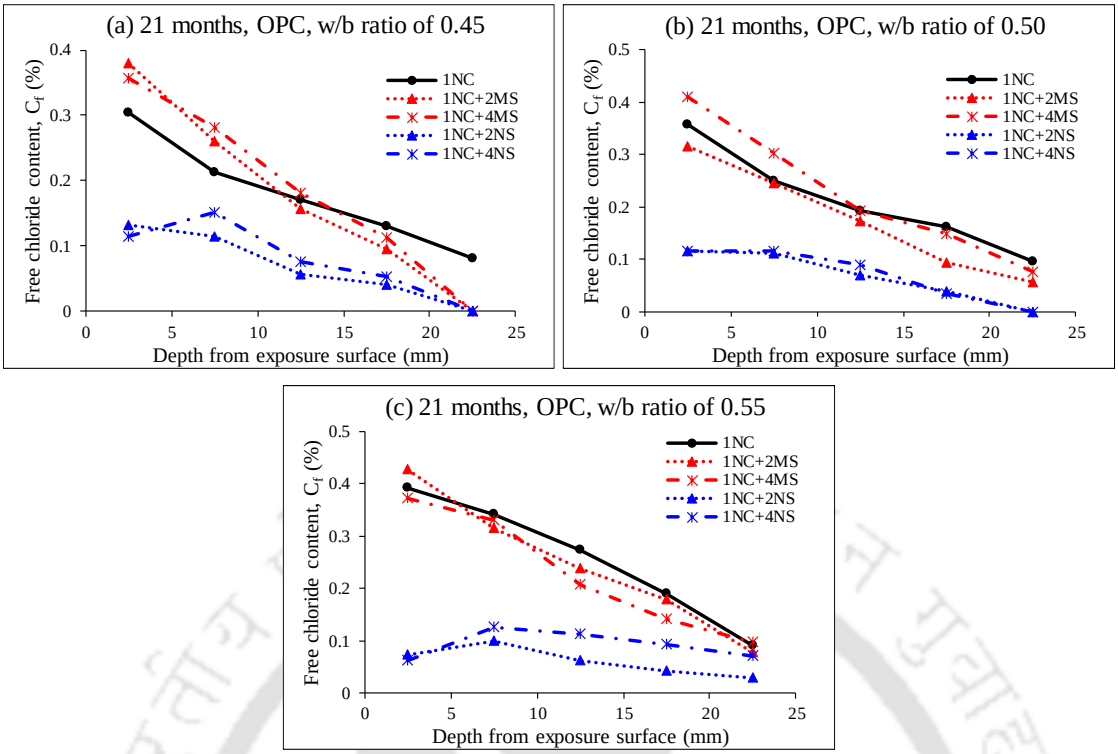

Figure A19 Free chloride content profile of OPC concrete exposed to 1% NaCl and 1% NaCl with $MgSO_4$ or Na_2SO_4 solutions for 21 months: (a) w/b ratio of 0.45, (b) w/b ratio of 0.50, and (c) w/b ratio of 0.55

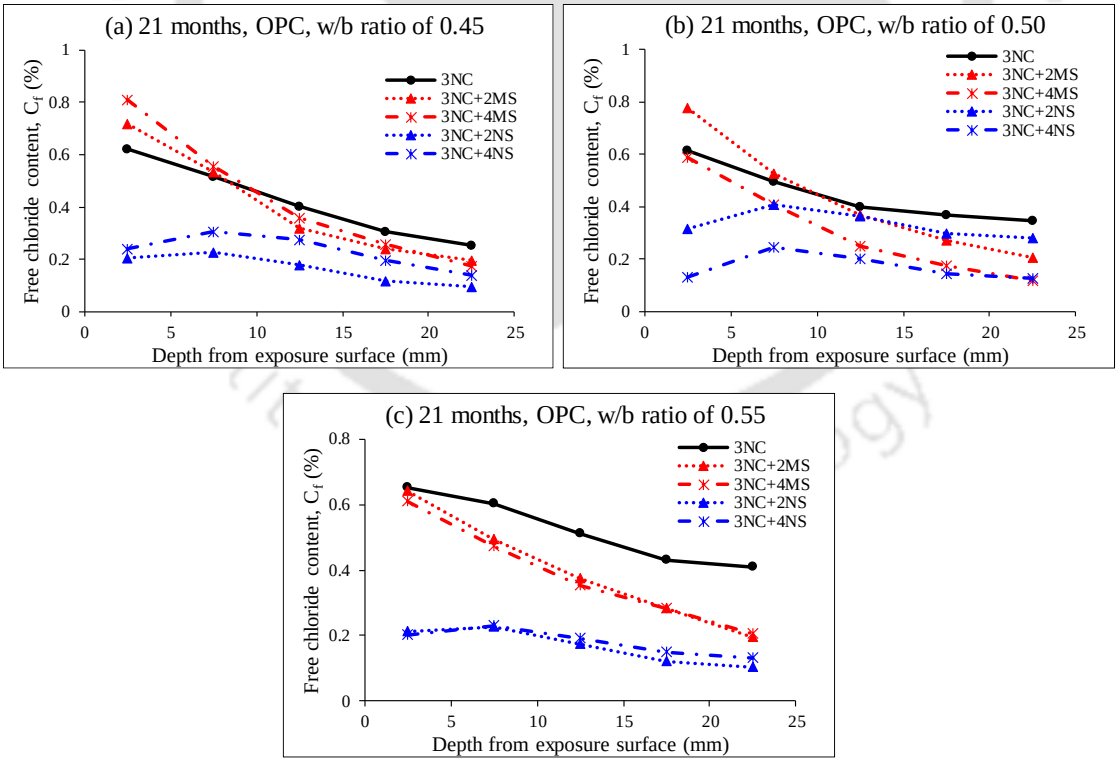

Figure A20 Free chloride content profile of OPC concrete exposed to 3% NaCl and 3% NaCl with $MgSO_4$ or Na_2SO_4 solutions for 21 months: (a) w/b ratio of 0.45, (b) w/b ratio of 0.50, and (c) w/b ratio of 0.55

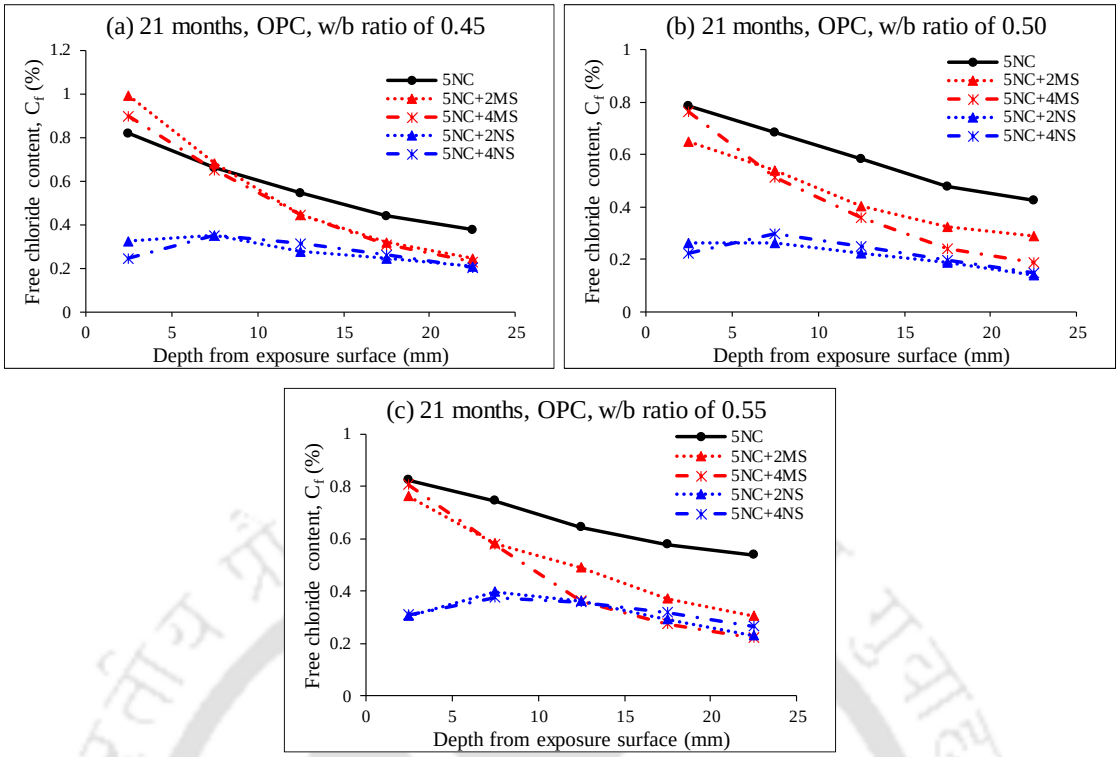

Figure A21 Free chloride content profile of OPC concrete exposed to 5% NaCl and 5% NaCl with $MgSO_4$ or Na_2SO_4 solutions for 21 months: (a) w/b ratio of 0.45, (b) w/b ratio of 0.50, and (c) w/b ratio of 0.55

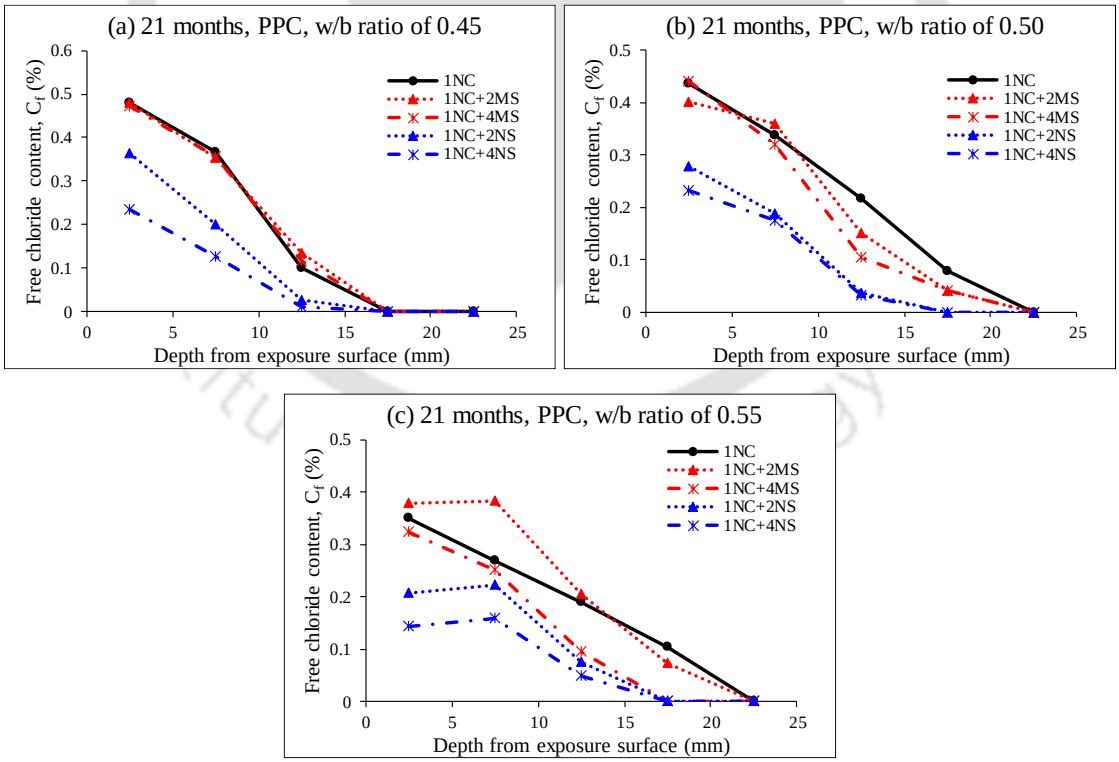

Figure A22 Free chloride content profile of PPC concrete exposed to 1% NaCl and 1% NaCl with $MgSO_4$ or Na_2SO_4 solutions for 21 months: (a) w/b ratio of 0.45, (b) w/b ratio of 0.50, and (c) w/b ratio of 0.55

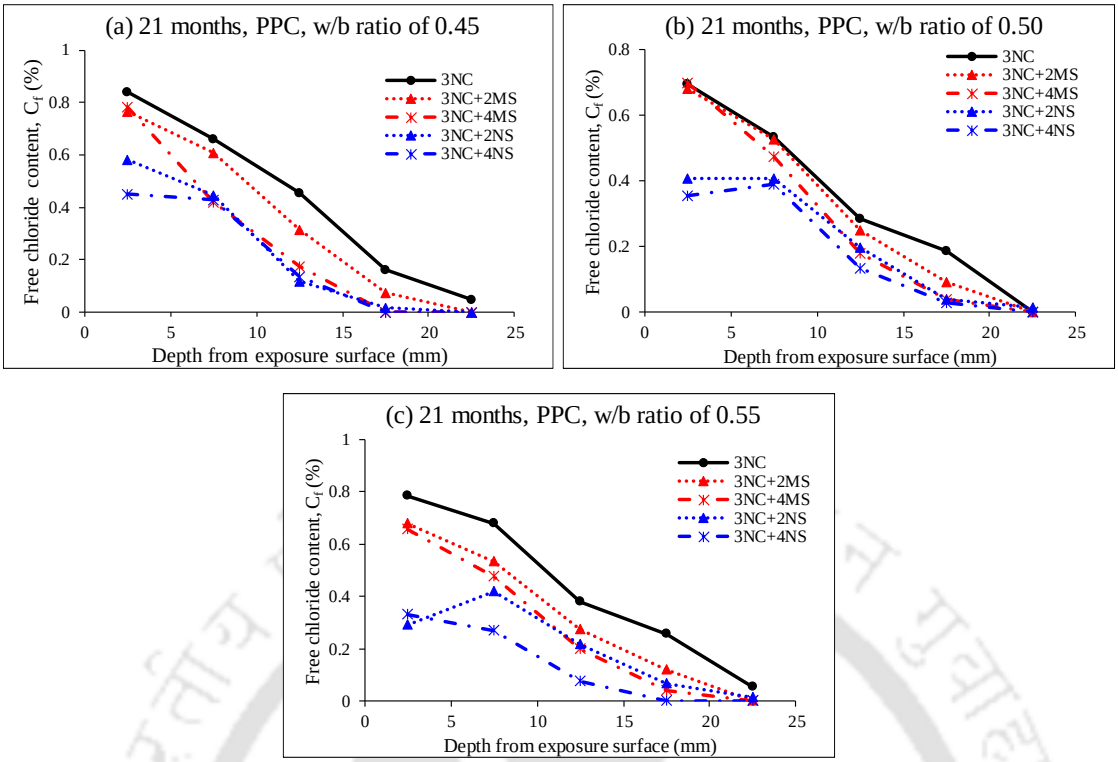

Figure A23 Free chloride content profile of PPC concrete exposed to 3% NaCl and 3% NaCl with $MgSO_4$ or Na_2SO_4 solutions for 21 months: (a) w/b ratio of 0.45, (b) w/b ratio of 0.50, and (c) w/b ratio of 0.55

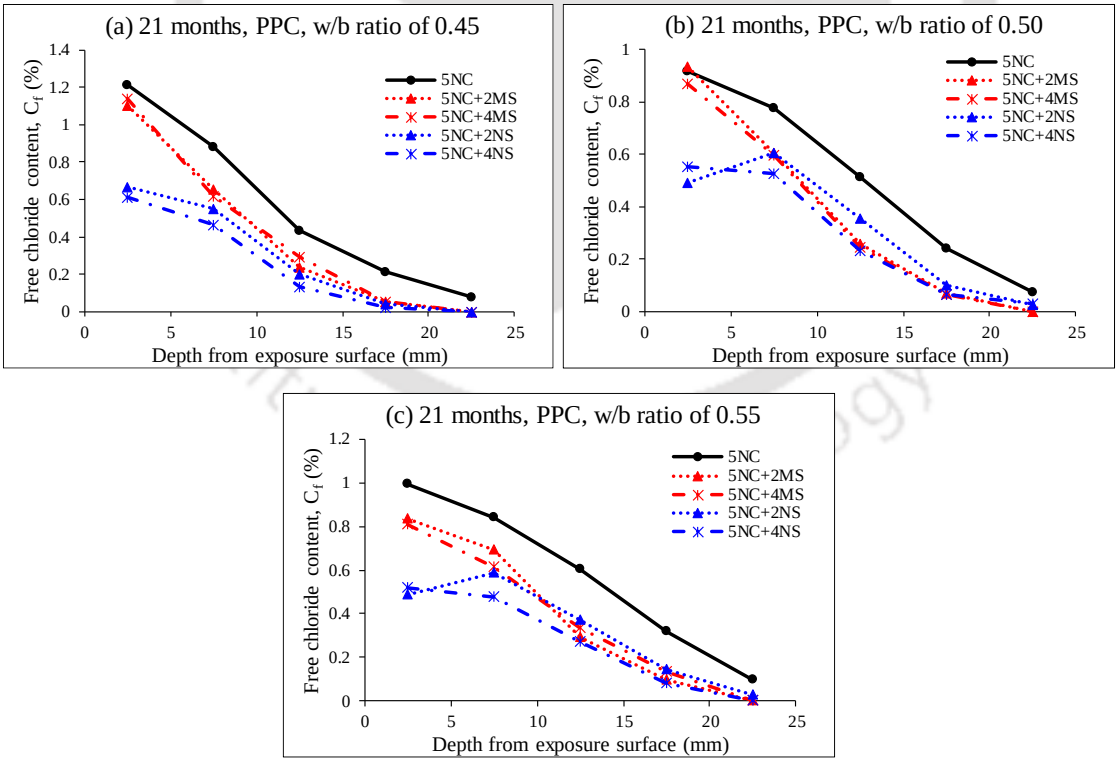

Figure A24 Free chloride content profile of PPC concrete exposed to 5% NaCl and 5% NaCl with $MgSO_4$ or Na_2SO_4 solutions for 21 months: (a) w/b ratio of 0.45, (b) w/b ratio of 0.50, and (c) w/b ratio of 0.55.

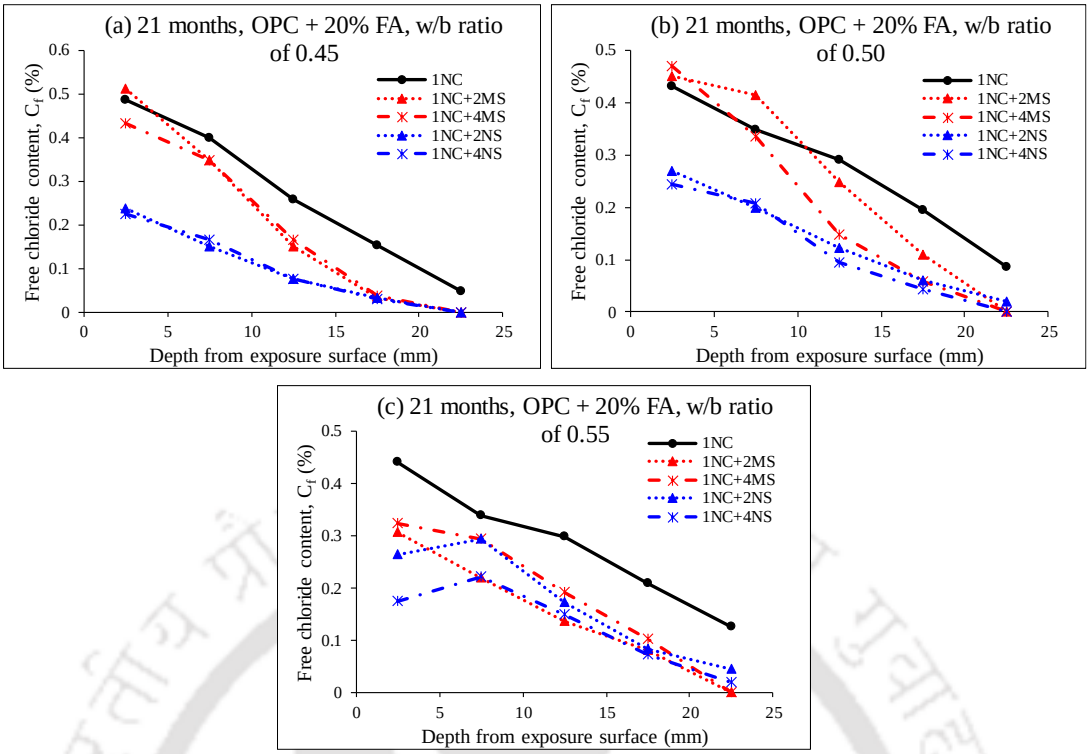

Figure A25 Free chloride content profile of OPC + 20% FA concrete exposed to 1% NaCl and 1% NaCl with $MgSO_4$ or Na_2SO_4 solutions for 21 months: (a) w/b ratio of 0.45, (b) w/b ratio of 0.50, and (c) w/b ratio of 0.55

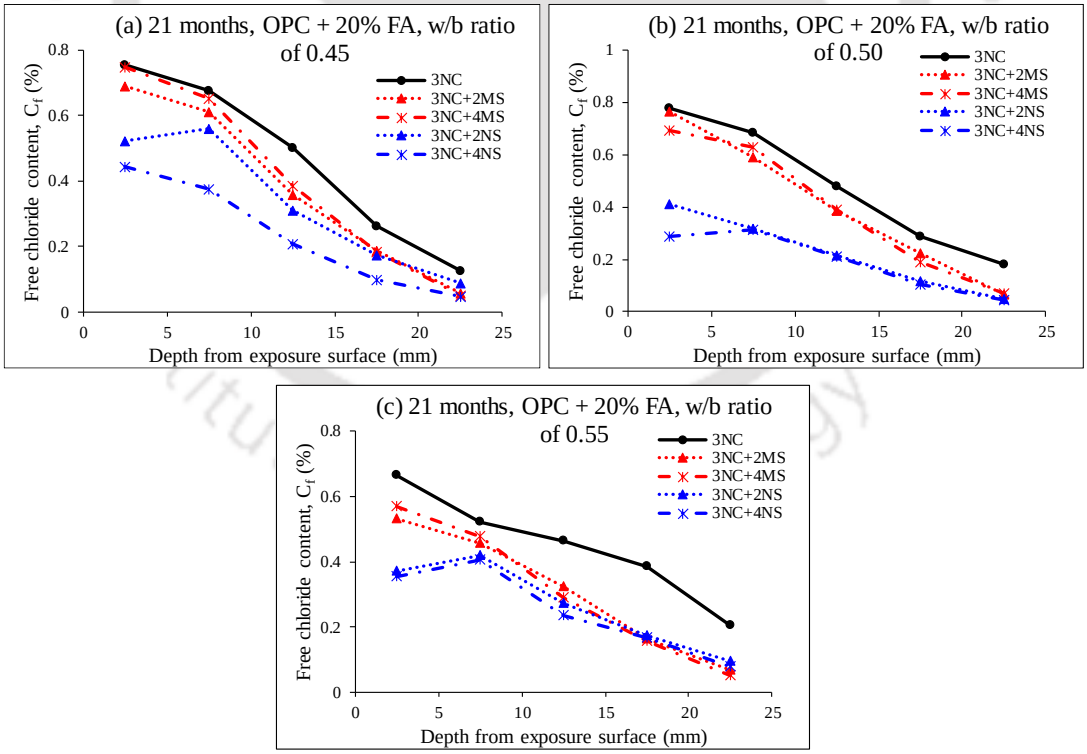

Figure A26 Free chloride content profile of OPC + 20% FA concrete exposed to 3% NaCl and 3% NaCl with $MgSO_4$ or Na_2SO_4 solutions for 21 months: (a) w/b ratio of 0.45, (b) w/b ratio of 0.50, and (c) w/b ratio of 0.55

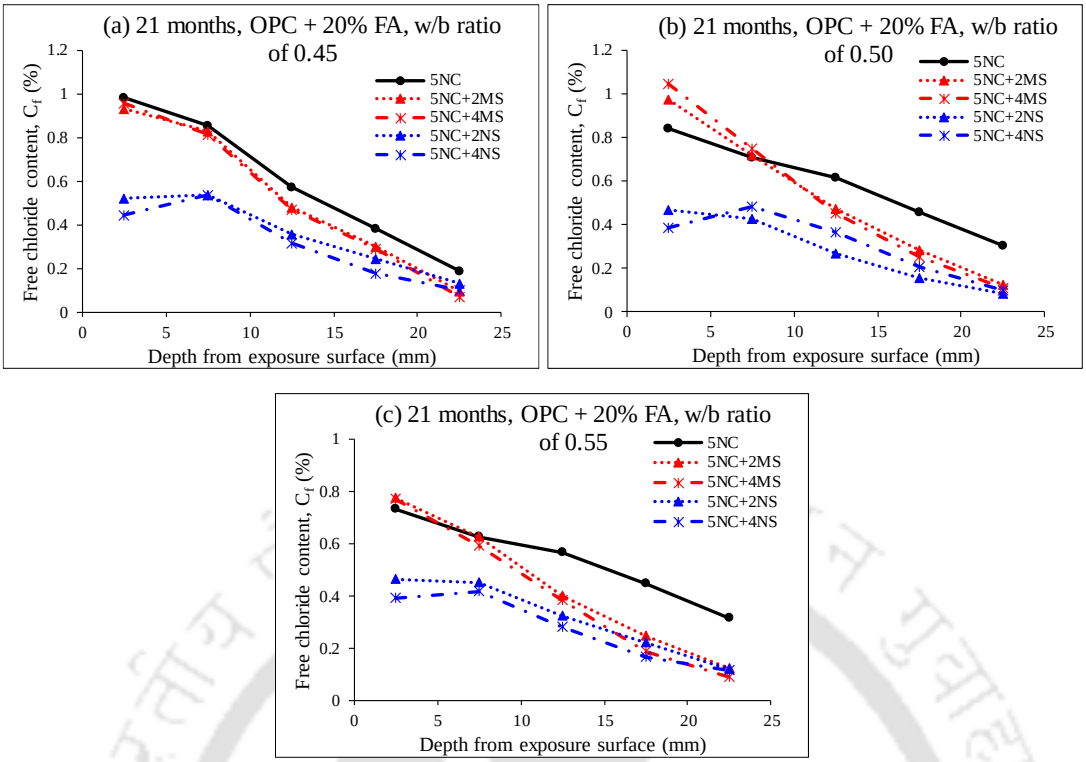

Figure A27 Free chloride content profile of OPC + 20% FA concrete exposed to 5% NaCl and 5% NaCl with $MgSO_4$ or Na_2SO_4 solutions for 21 months: (a) w/b ratio of 0.45, (b) w/b ratio of 0.50, and (c) w/b ratio of 0.55.

APPENDIX A2

Free chloride content (C_f) versus total chloride content (C_t) of concrete

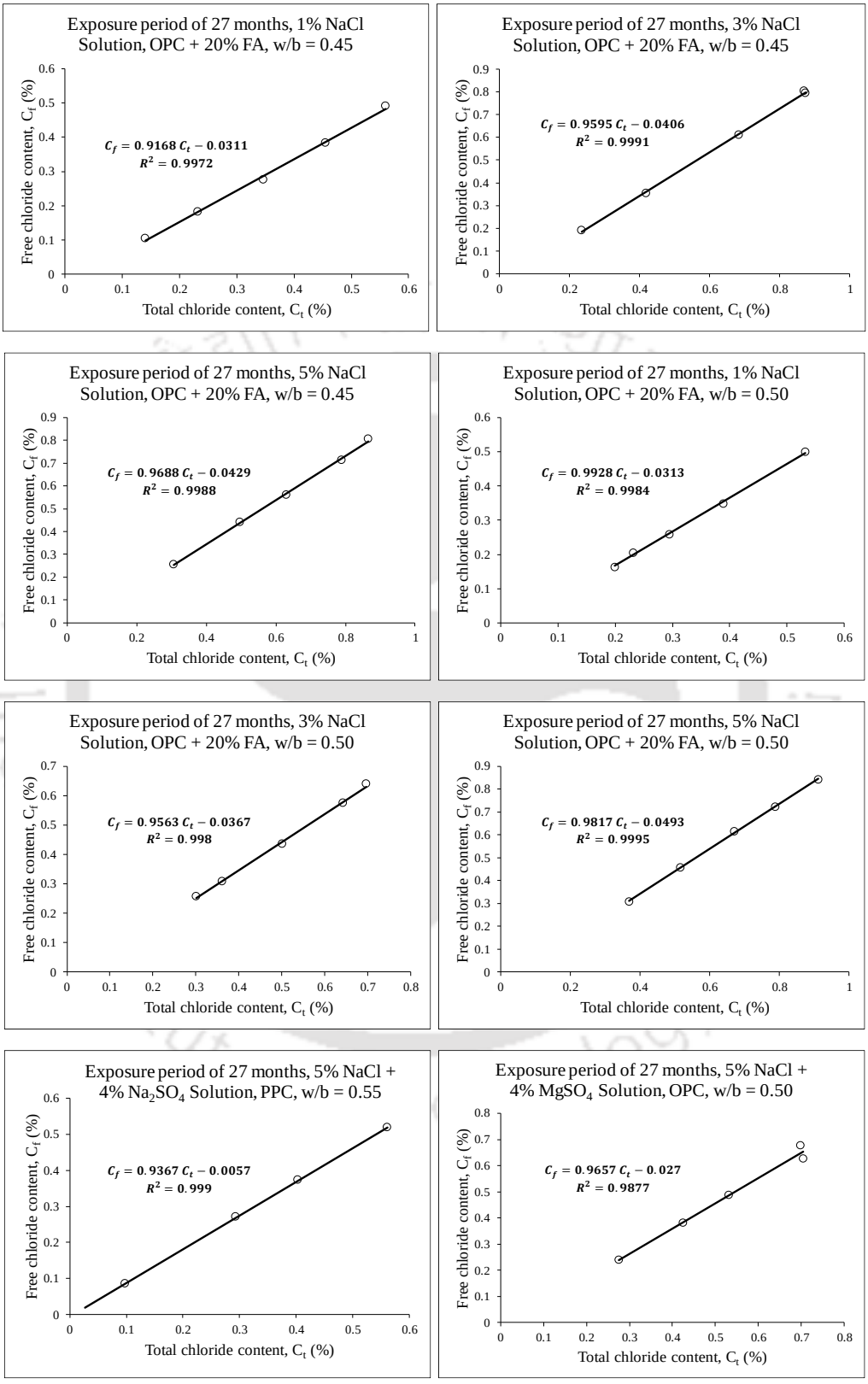

Figure A28 Typical plots of free chloride content versus total chloride content irrespective of depth interval from the exposure surface

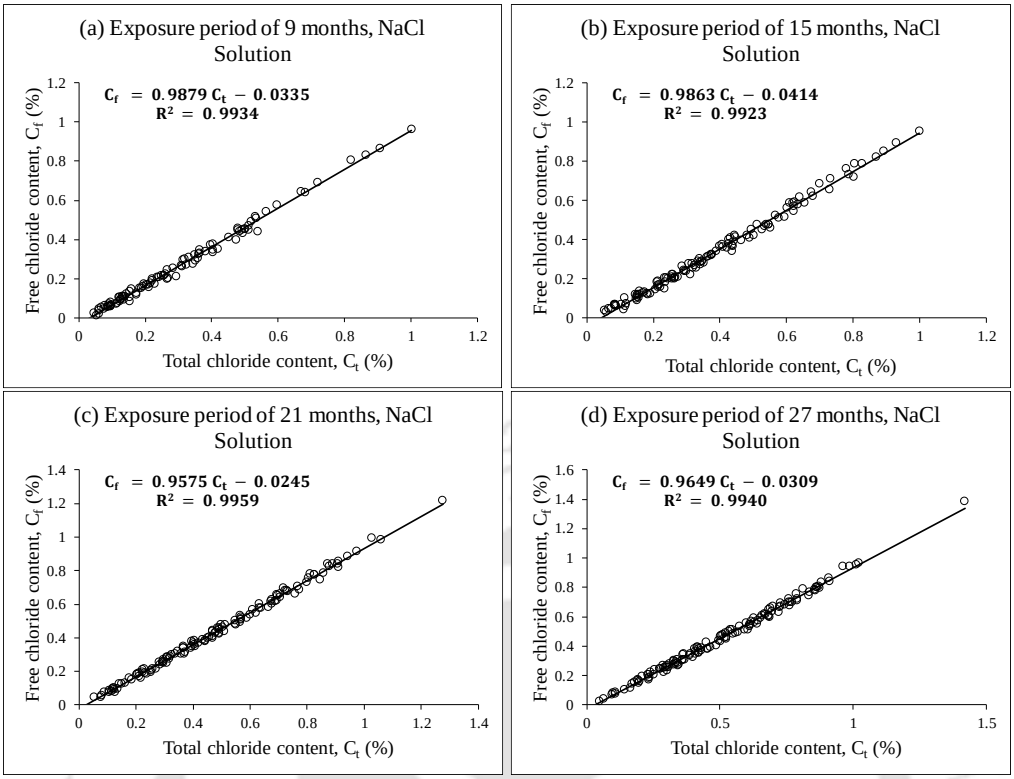

Figure A29 Free chloride versus total chloride content of NaCl solution: (a) 9 months, (b) 15 months, (c) 21 months and (d) 27 months of exposure

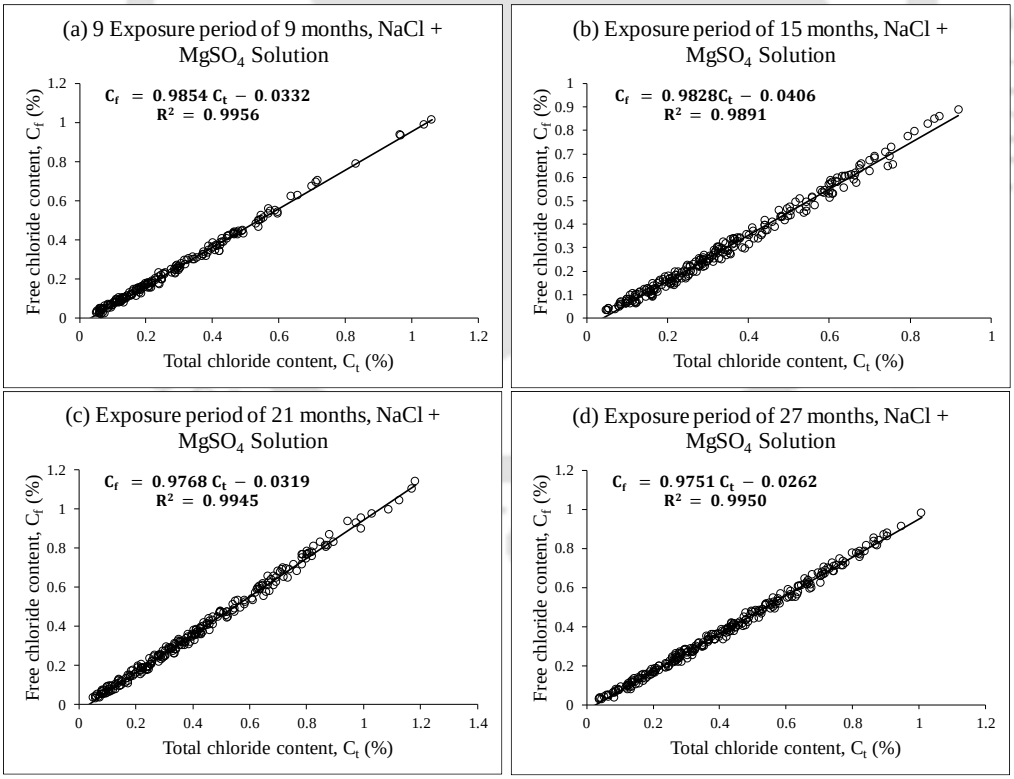

Figure A30 Free chloride versus total chloride content of NaCl + $MgSO_4$ solution: (a) 9 months, (b) 15 months, (c) 21 months and (d) 27 months of exposure

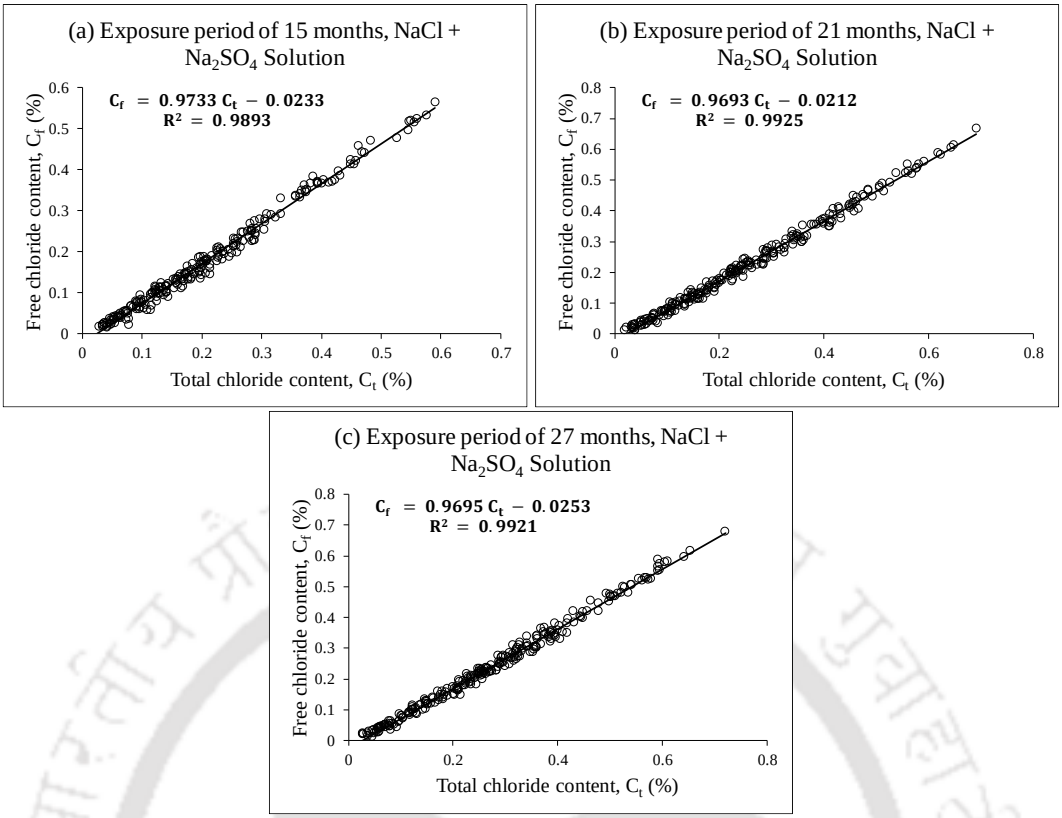

Figure A31 Free chloride versus total chloride content of NaCl + Na_2SO_4 solution: (a) 15 months, (b) 21 months and (c) 27 months of exposure

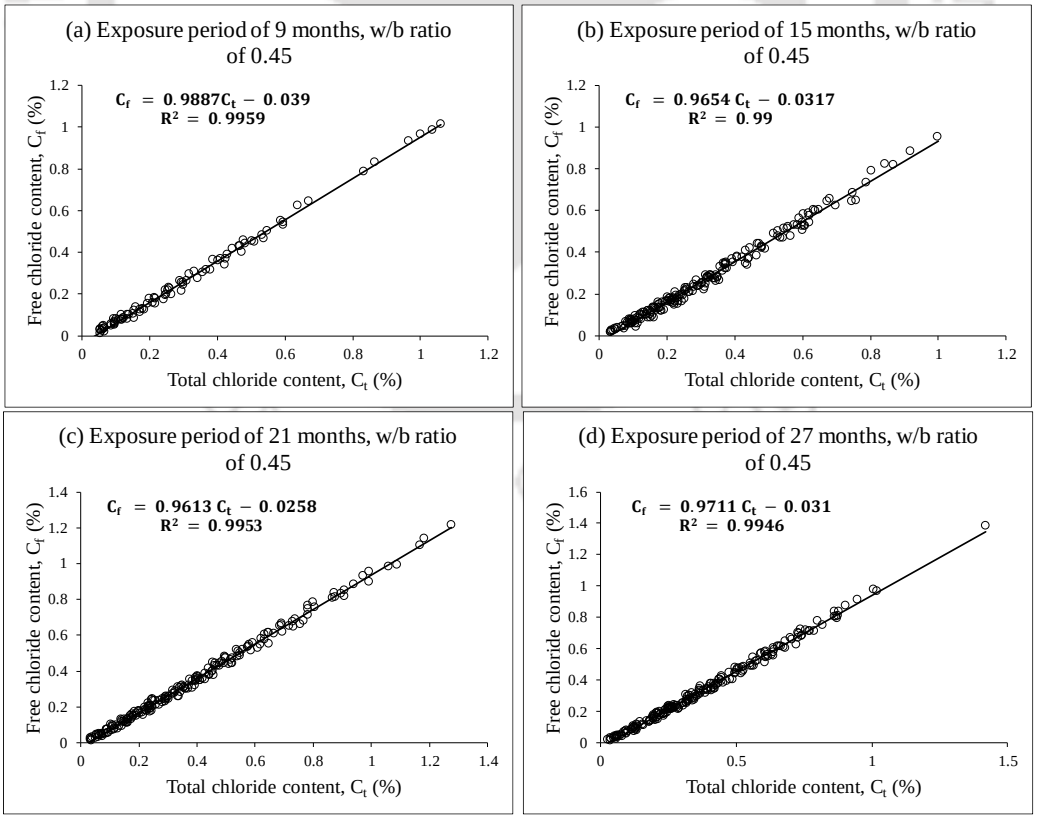

Figure A32 Free chloride versus total chloride content of concrete at w/b ratio of 0.45: (a) 15 months, (b) 21 months and (c) 27 months of exposure

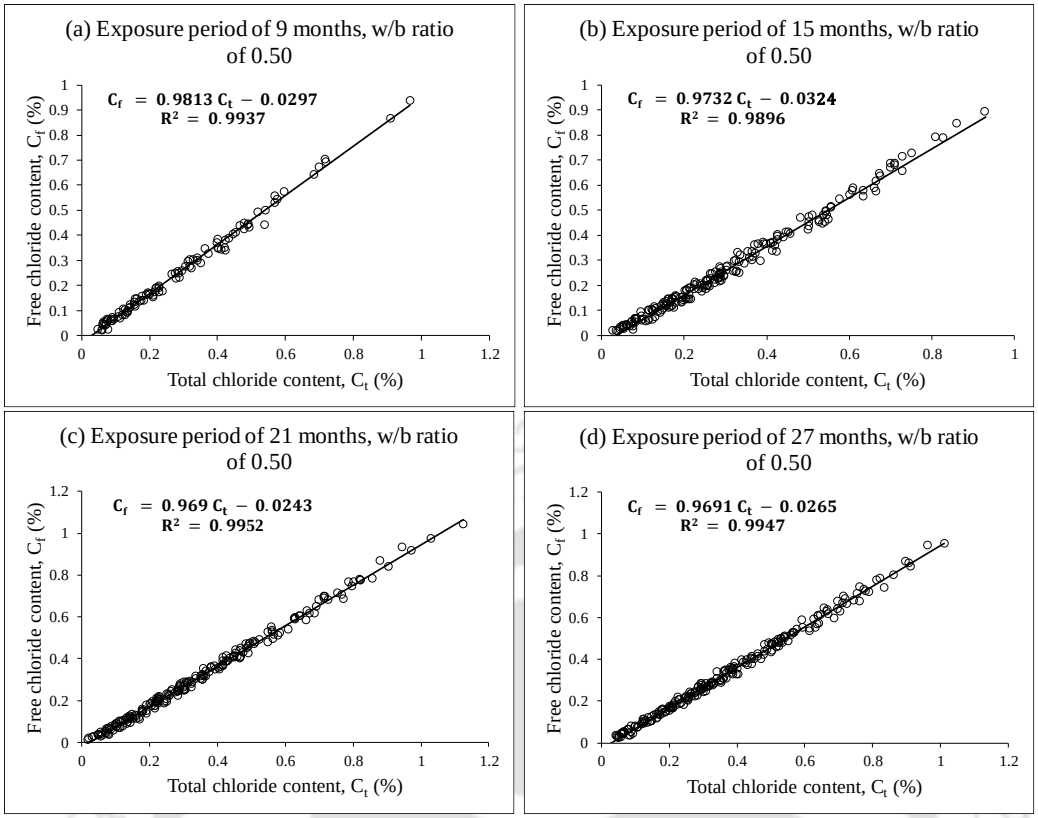

Figure A33 Free chloride versus total chloride content of concrete at w/b ratio of 0.50: (a) 15 months, (b) 21 months and (c) 27 months of exposure

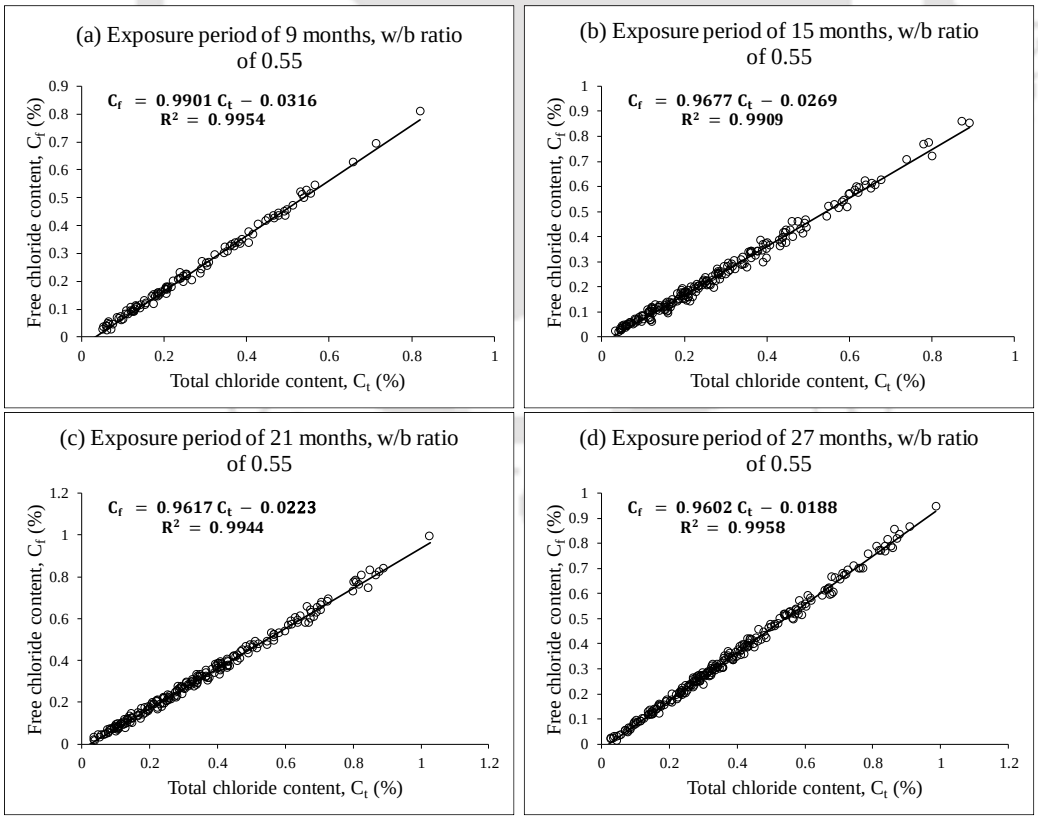

Figure A34 Free chloride versus total chloride content of concrete at w/b ratio of 0.55: (a) 15 months, (b) 21 months and (c) 27 months of exposure

APPENDIX B1

XRD patterns and wt. % of compounds of concrete at different depth intervals from exposure surface

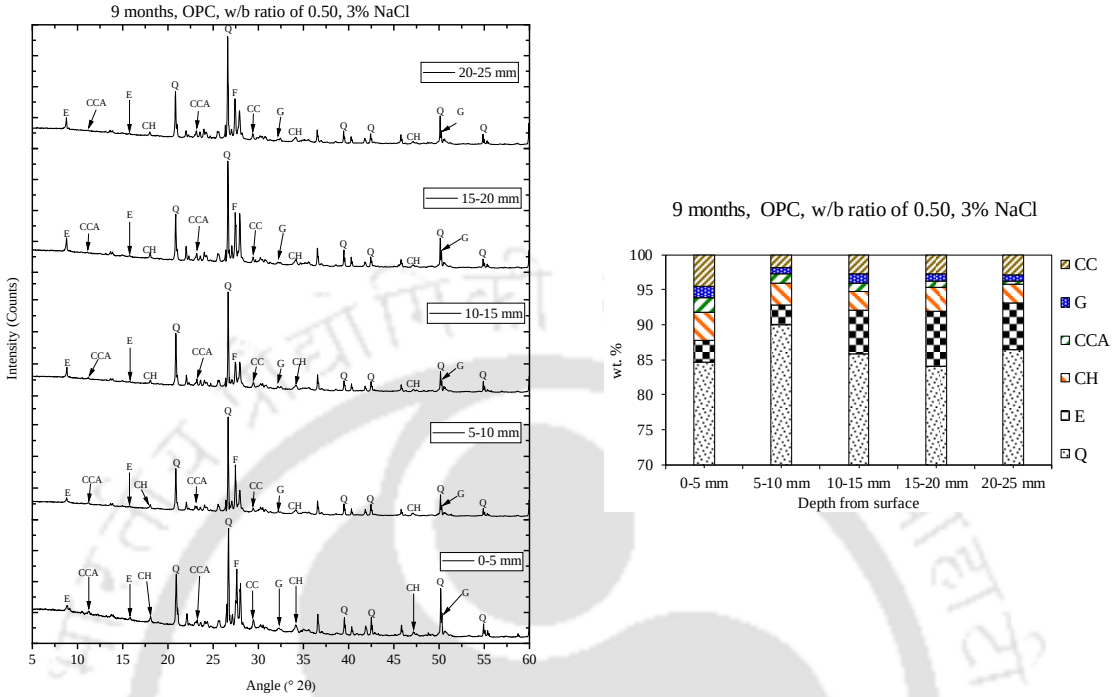

Figure B1 XRD patterns and wt. % of compounds of concrete at depth intervals of 0-5 mm, 5-10 mm, 10-15 mm, 15-20 mm and 20-25 mm from the surface for OPC concrete at w/b ratio of 0.50 and subjected to 3% NaCl solution for 9 months

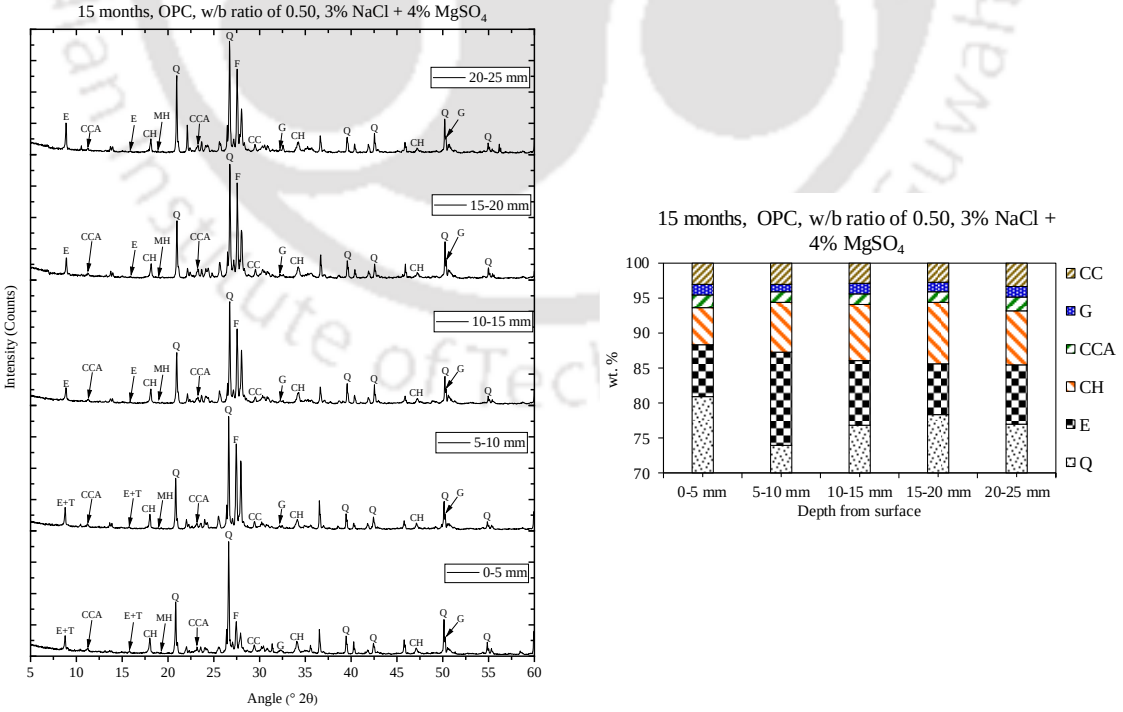

Figure B2 XRD patterns and wt. % of compounds of concrete at depth intervals of 0-5 mm, 5-10 mm, 10-15 mm, 15-20 mm and 20-25 mm from the surface for OPC concrete at w/b ratio of 0.50 and subjected to 3% NaCl + 4% $MgSO_4$ solution for 15 months

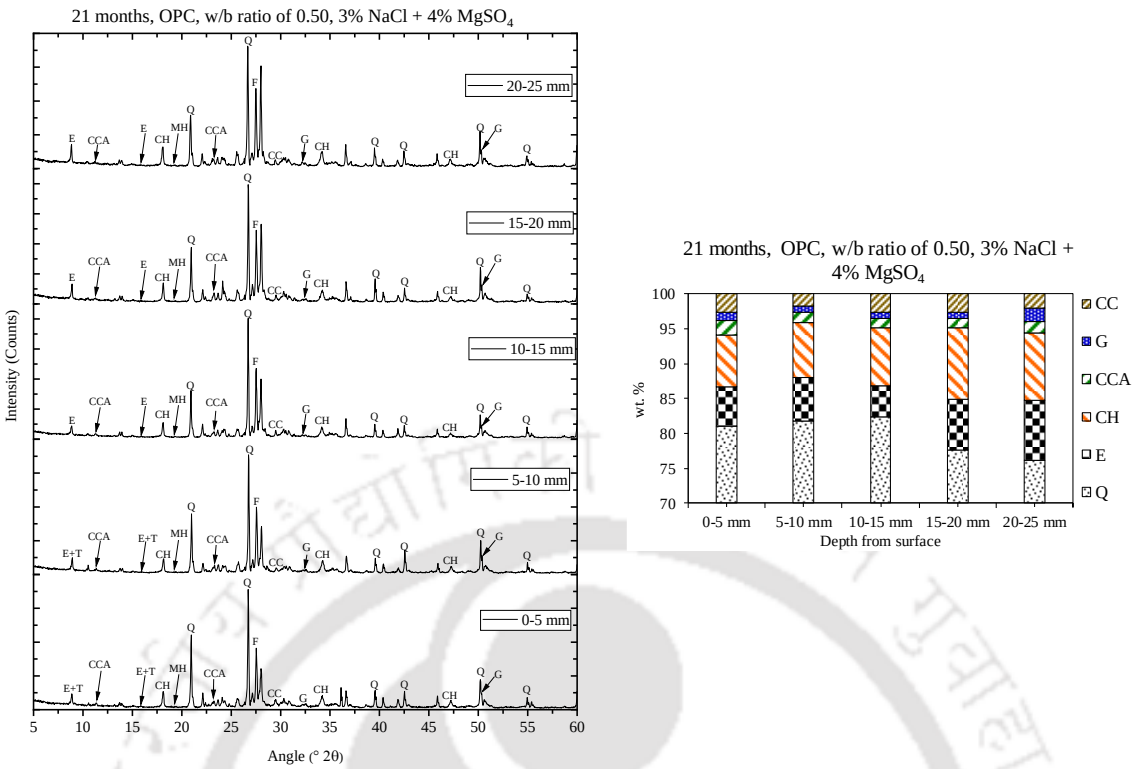

Figure B3 XRD patterns and wt. % of compounds of concrete at depth intervals of 0-5 mm, 5-10 mm, 10-15 mm, 15-20 mm and 20-25 mm from the surface for OPC concrete at w/b ratio of 0.50 and subjected to 3% NaCl + 4% $MgSO_4$ solution for 21 months

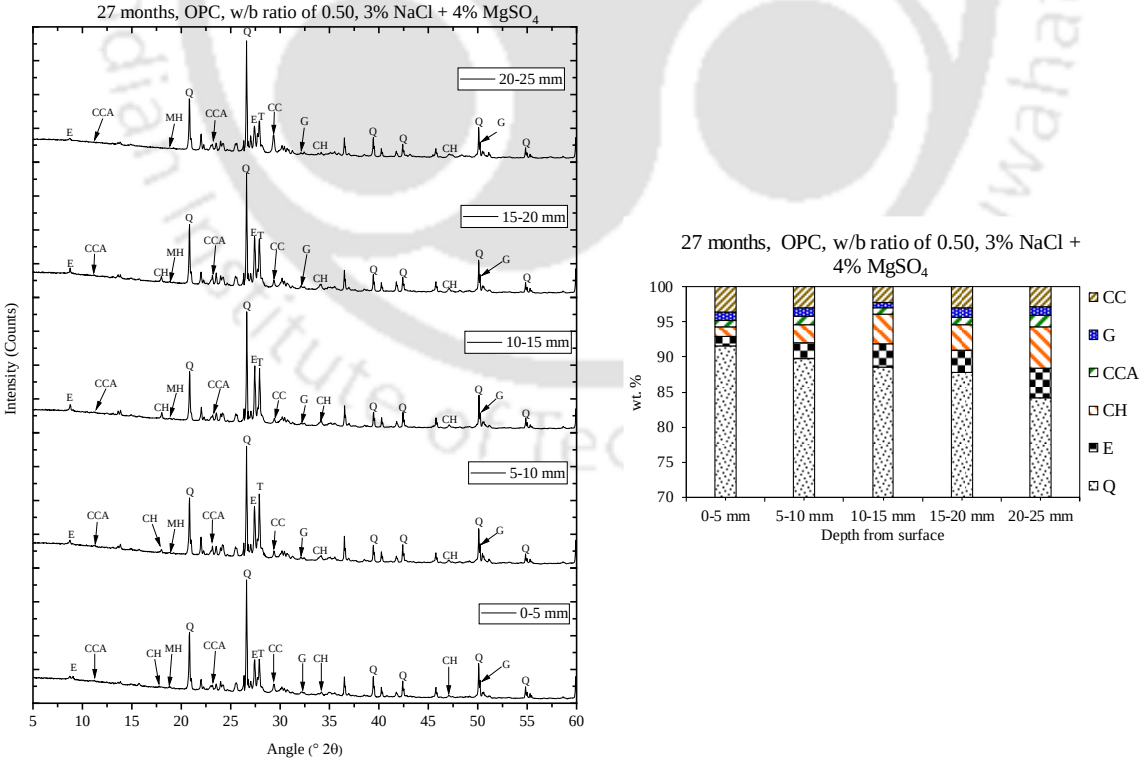

Figure B4 XRD patterns and wt. % of compounds of concrete at depth intervals of 0-5 mm, 5-10 mm, 10-15 mm, 15-20 mm and 20-25 mm from the surface for OPC concrete at w/b ratio of 0.50 and subjected to 3% NaCl + 4% $MgSO_4$ solution for 27 months

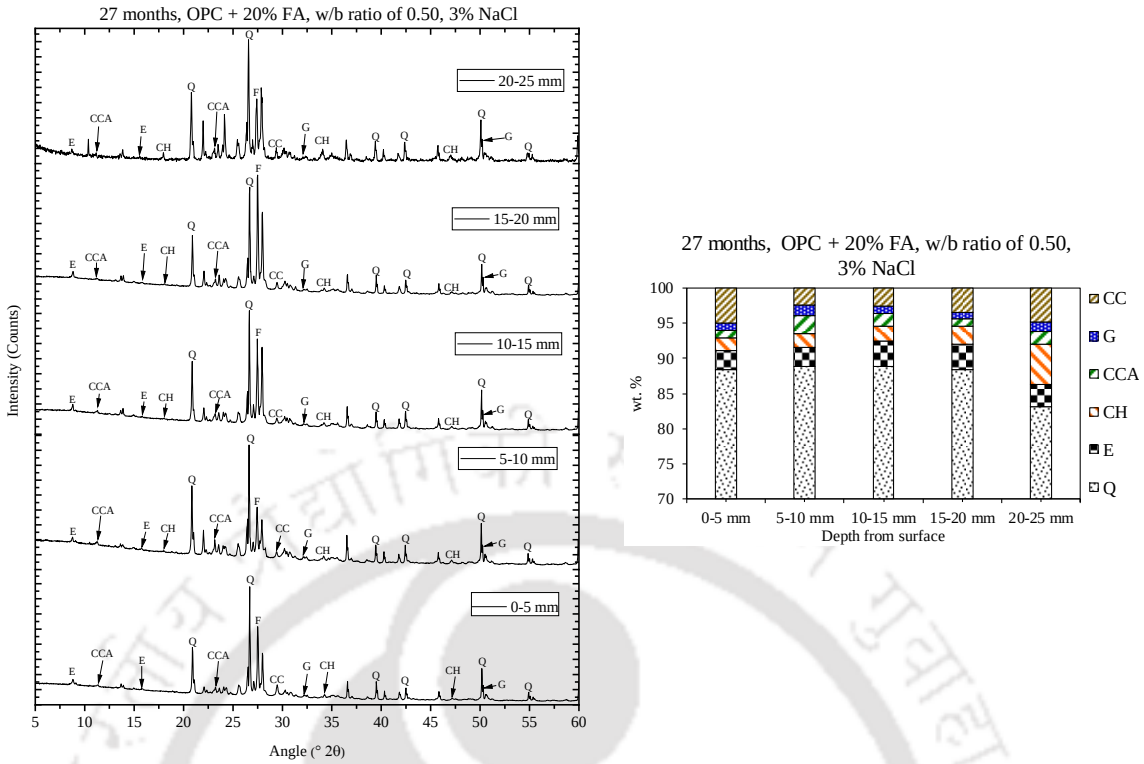

Figure B5 XRD patterns and wt. % of compounds of concrete at depth intervals of 0-5 mm, 5-10 mm, 10-15 mm, 15-20 mm and 20-25 mm from the surface for OPC + 20% FA concrete at w/b ratio of 0.50 and subjected to 3% NaCl solution for 27 months

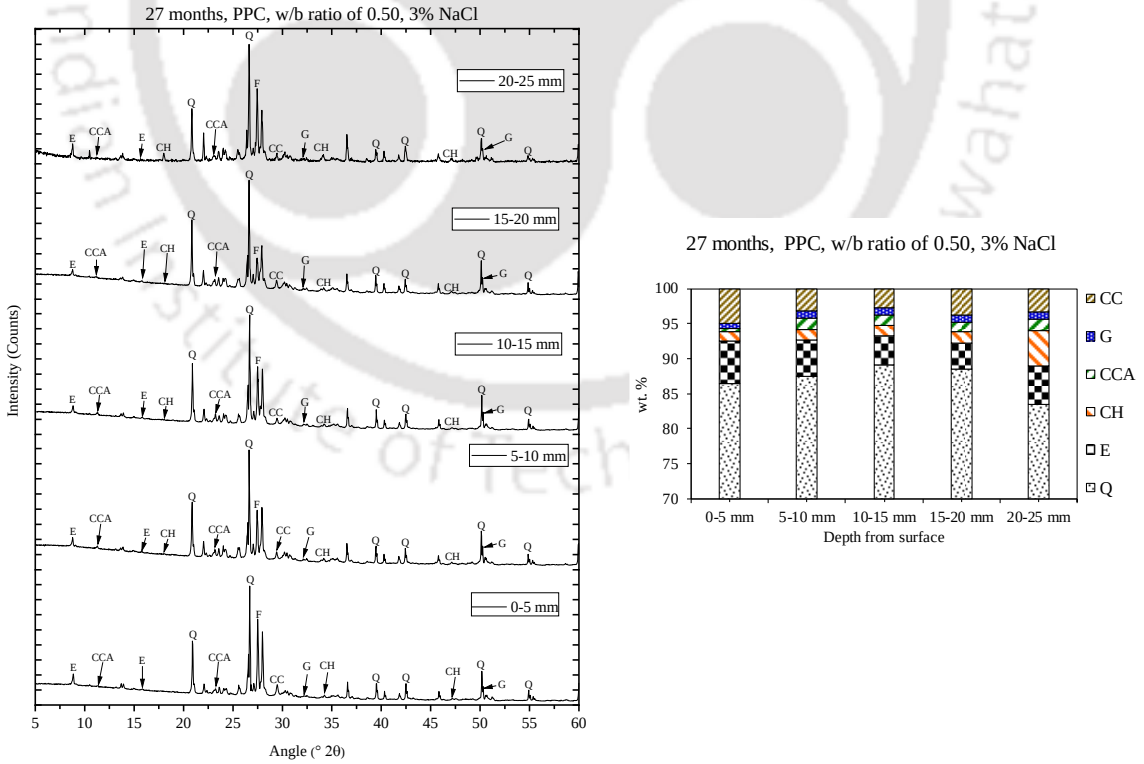

Figure B6 XRD patterns and wt. % of compounds of concrete at depth intervals of 0-5 mm, 5-10 mm, 10-15 mm, 15-20 mm and 20-25 mm from the surface for PPC concrete at w/b ratio of 0.50 and subjected to 3% NaCl solution for 27 months

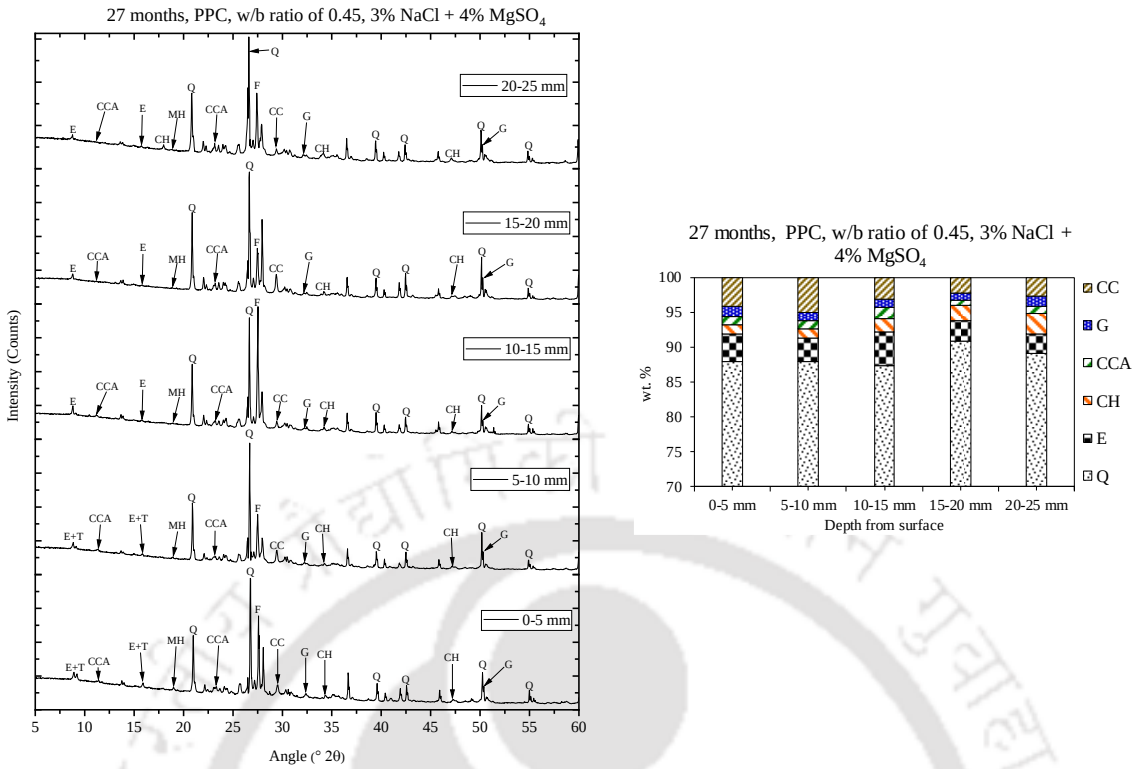

Figure B7 XRD patterns and wt. % of compounds of concrete at depth intervals of 0-5 mm, 5-10 mm, 10-15 mm, 15-20 mm and 20-25 mm from the surface for PPC concrete at w/b ratio of 0.45 and subjected to 3% NaCl + 4% $MgSO_4$ solution for 27 months

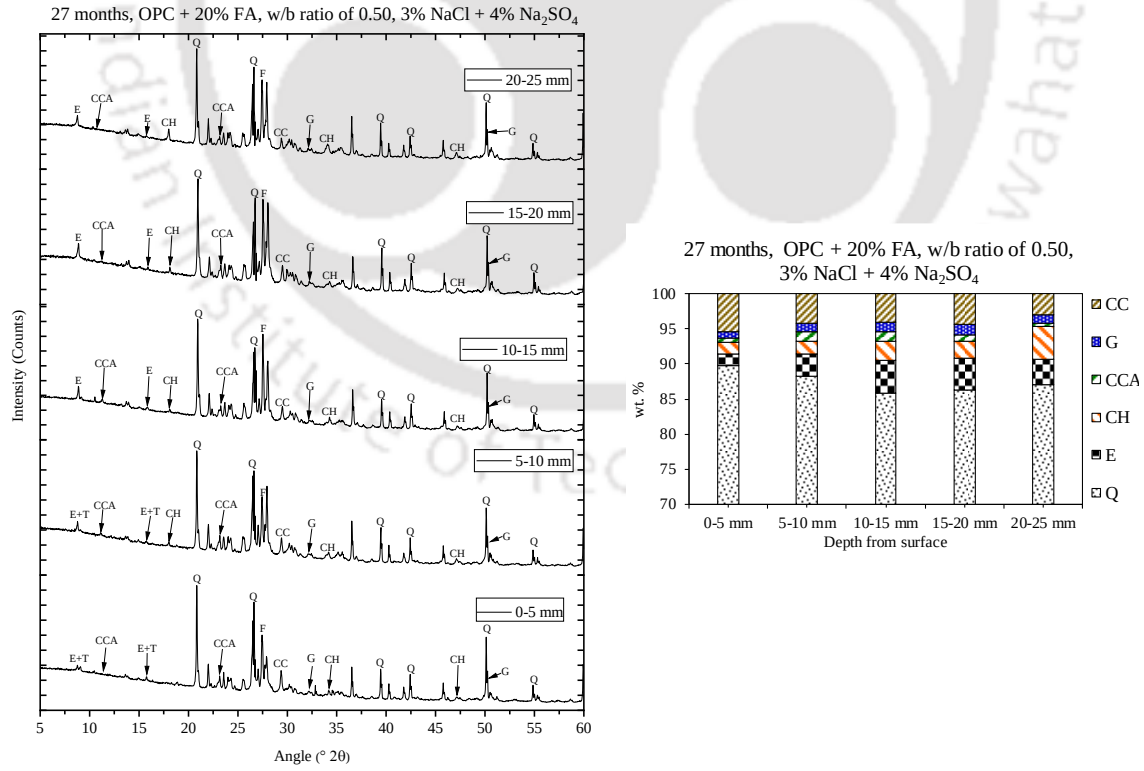

Figure B8 XRD patterns and wt. % of compounds of concrete at depth intervals of 0-5 mm, 5-10 mm, 10-15 mm, 15-20 mm and 20-25 mm from the surface for OPC + 20% FA concrete at w/b ratio of 0.50 and subjected to 3% NaCl + 4% Na_2SO_4 solution for 27 months

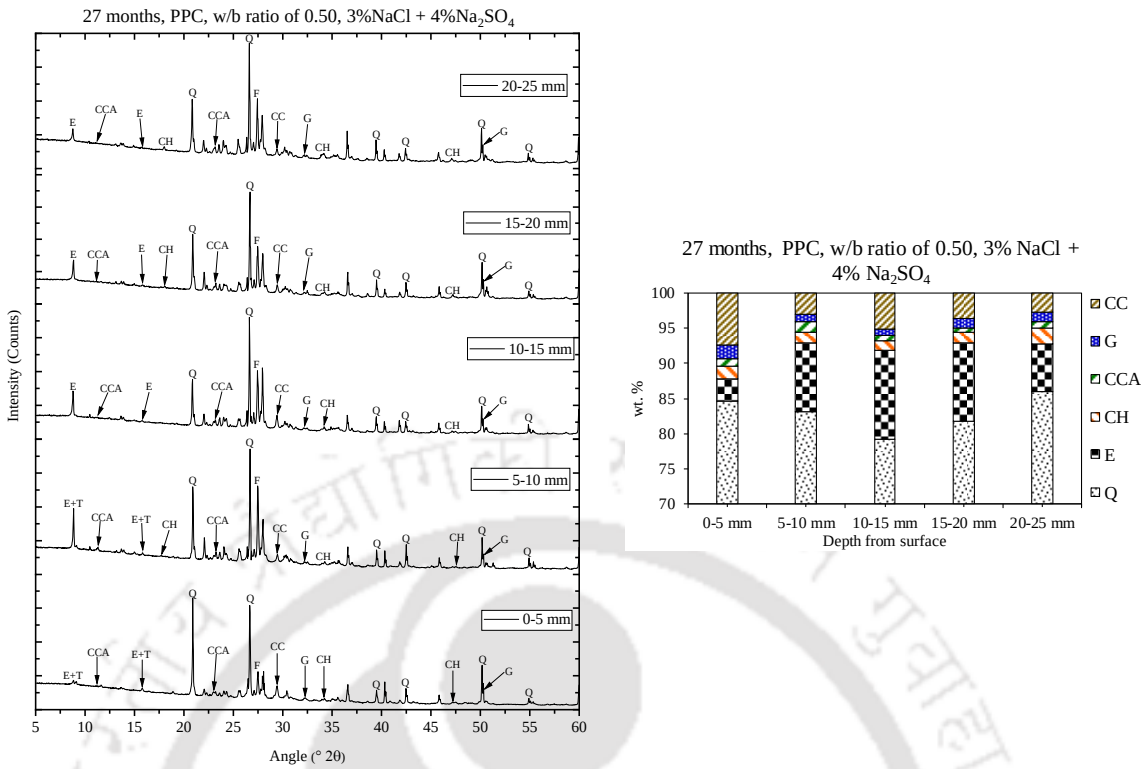

Figure B9 XRD patterns and wt. % of compounds of concrete at depth intervals of 0-5 mm, 5-10 mm, 10-15 mm, 15-20 mm and 20-25 mm from the surface for PPC concrete at w/b ratio of 0.50 and subjected to 3% NaCl + 4% Na_2SO_4 solution for 27 months

APENDIX B2

XRD patterns and wt. % of compounds of concrete exposed to different exposure solutions

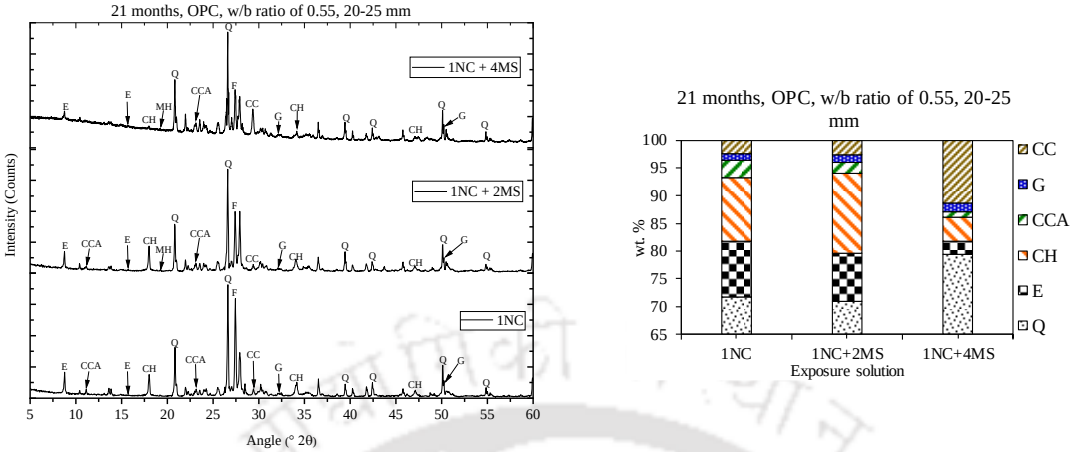

Figure B10 XRD patterns and wt. % of compounds of concrete at a depth interval of 20-25 mm (near rebar) from the surface for OPC at w/b ratio of 0.55 and subjected to 1% NaCl and 1% NaCl with $MgSO_4$ solutions for 21 months

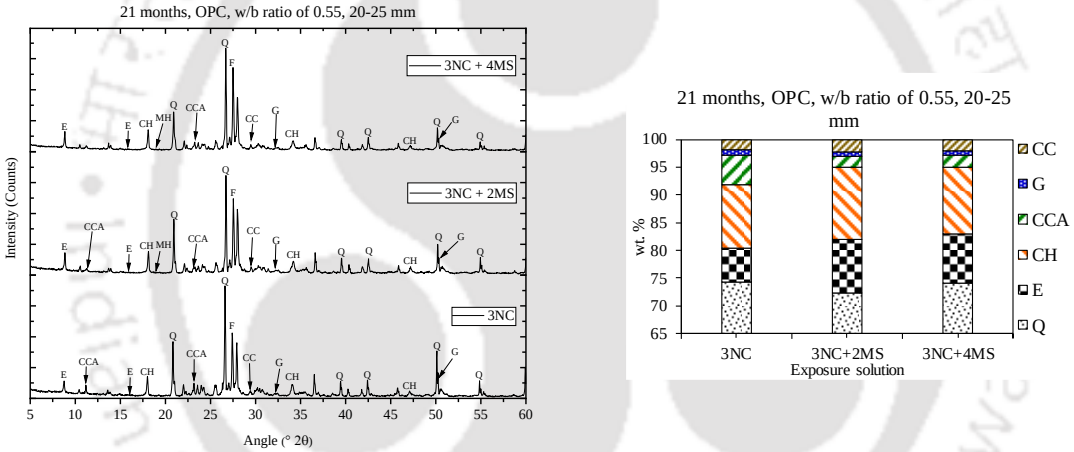

Figure B11 XRD patterns and wt. % of compounds of concrete at a depth interval of 20-25 mm (near rebar) from the surface for OPC at w/b ratio of 0.55 and subjected to 3% NaCl and 3% NaCl with $MgSO_4$ solutions for 21 months

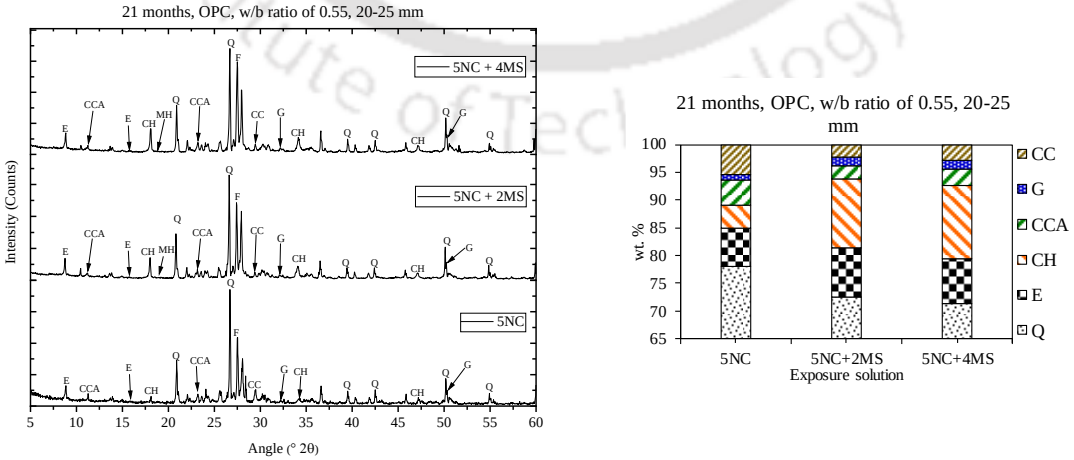

Figure B12 XRD patterns and wt. % of compounds of concrete at a depth interval of 20-25 mm (near rebar) from the surface for OPC at w/b ratio of 0.55 and subjected to 5% NaCl and 5% NaCl with $MgSO_4$ solutions for 21 months

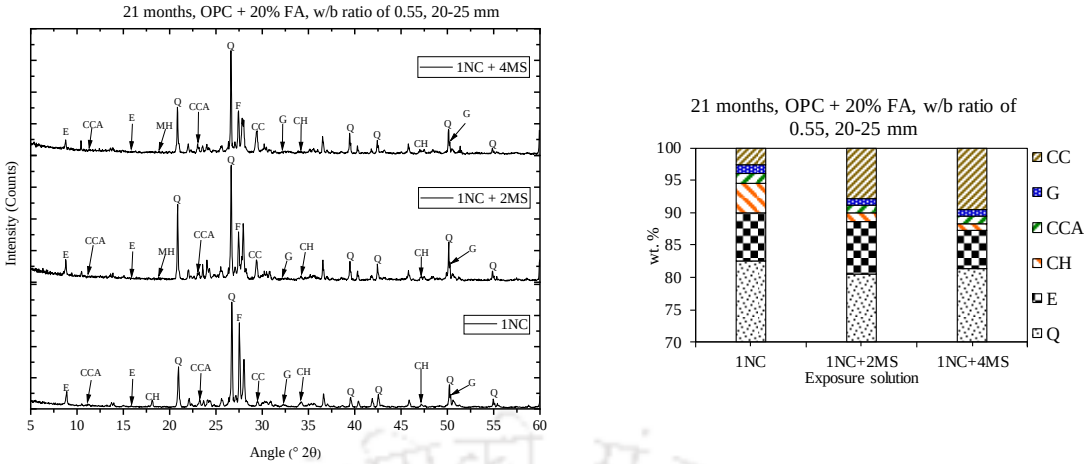

Figure B13 XRD patterns and wt. % of compounds of concrete at a depth interval of 20-25 mm (near rebar) from the surface for OPC + 20% FA at w/b ratio of 0.55 and subjected to 1% NaCl and 1% NaCl with $MgSO_4$ solutions for 21 months

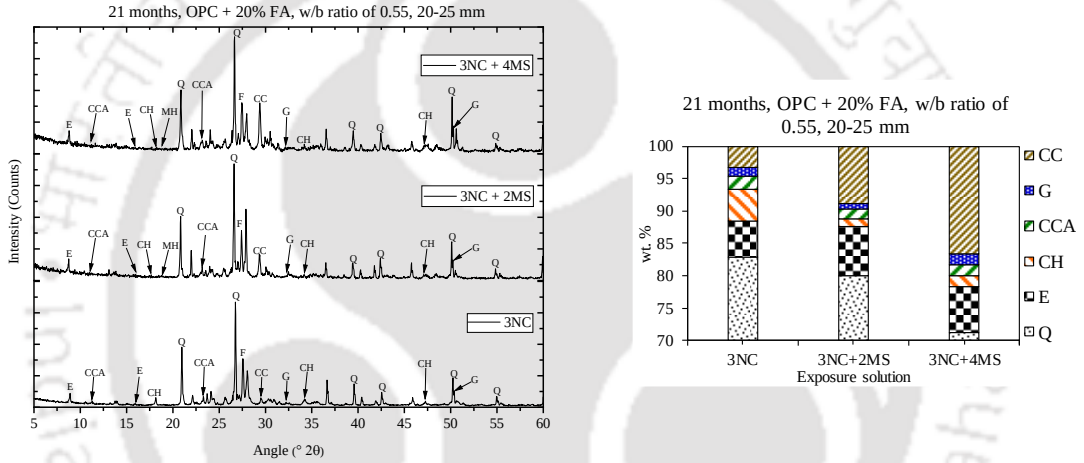

Figure B14 XRD patterns and wt. % of compounds of concrete at a depth interval of 20-25 mm (near rebar) from the surface for OPC + 20% FA at w/b ratio of 0.55 and subjected to 3% NaCl and 3% NaCl with $MgSO_4$ solutions for 21 months

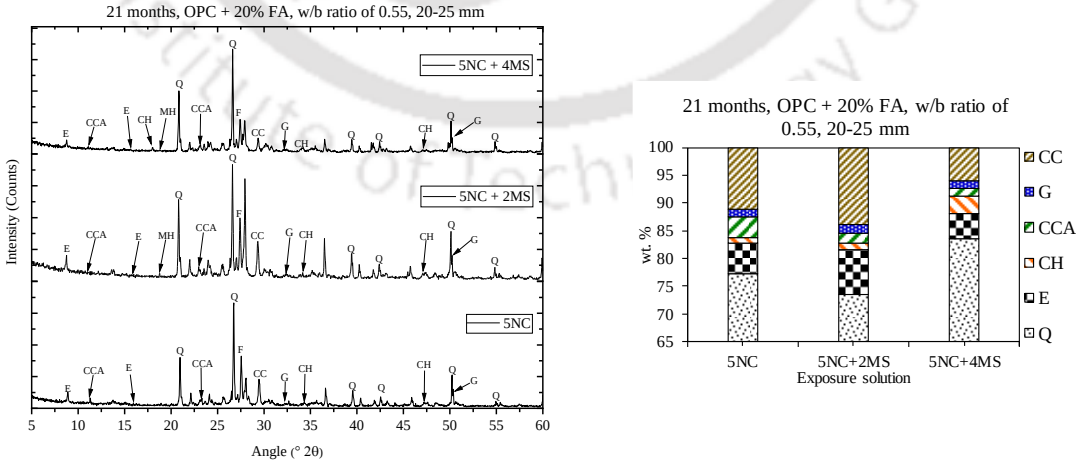

Figure B15 XRD patterns and wt. % of compounds of concrete at a depth interval of 20-25 mm (near rebar) from the surface for OPC + 20% FA at w/b ratio of 0.55 and subjected to 5% NaCl and 5% NaCl with $MgSO_4$ solutions for 21 months

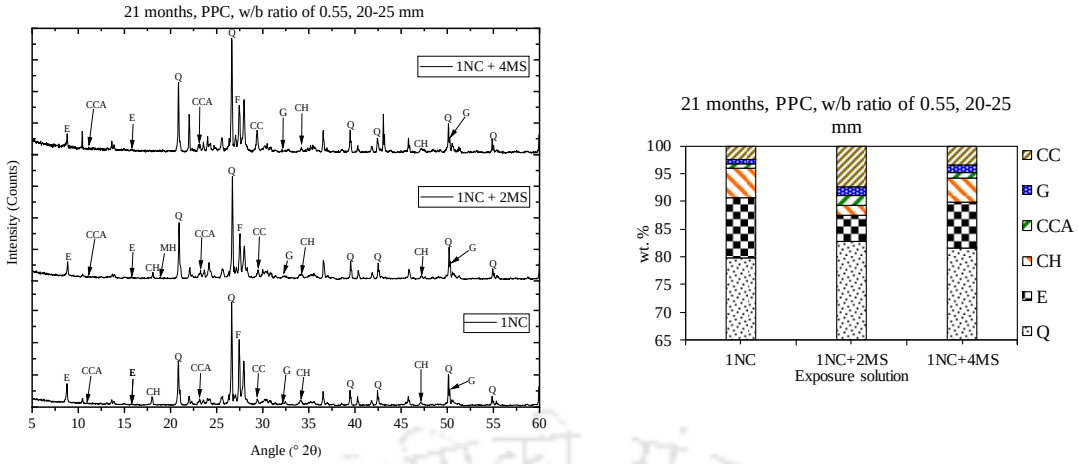

Figure B16 XRD patterns and wt. % of compounds of concrete at a depth interval of 20-25 mm (near rebar) from the surface for PPC at w/b ratio of 0.55 and subjected to 1% NaCl and 1% NaCl with $MgSO_4$ solutions for 21 months

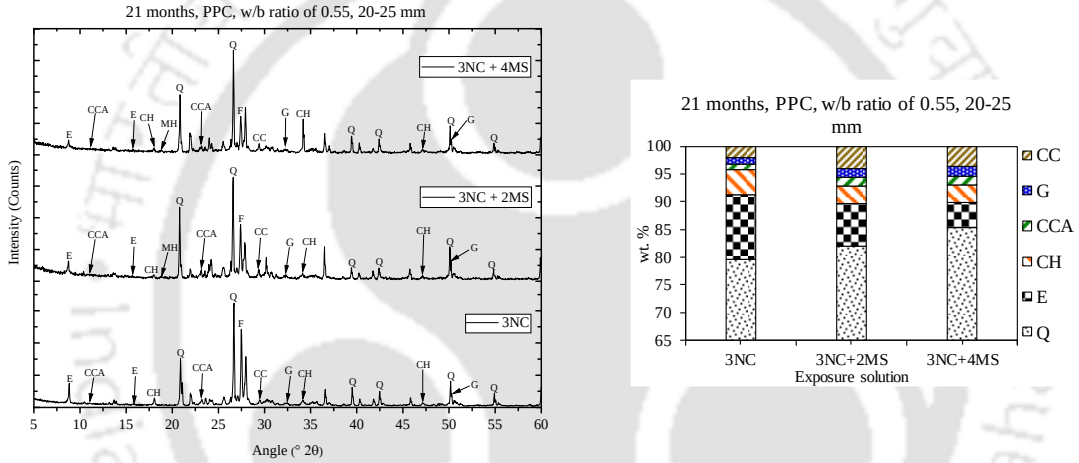

Figure B17 XRD patterns and wt. % of compounds of concrete at a depth interval of 20-25 mm (near rebar) from the surface for PPC at w/b ratio of 0.55 and subjected to 3% NaCl and 3% NaCl with $MgSO_4$ solutions for 21 months

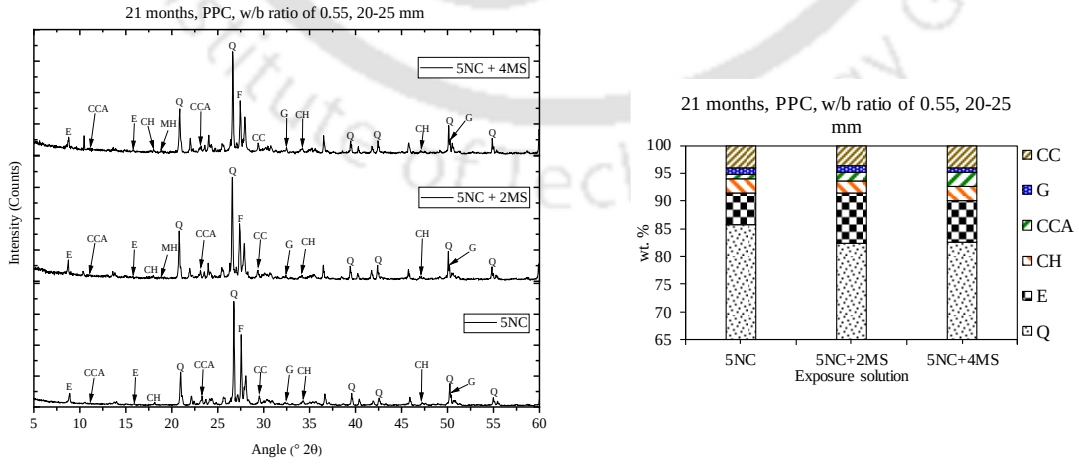

Figure B18 XRD patterns and wt. % of compounds of concrete at a depth interval of 20-25 mm (near rebar) from the surface for PPC at w/b ratio of 0.55 and subjected to 5% NaCl and 5% NaCl with $MgSO_4$ solutions for 21 months

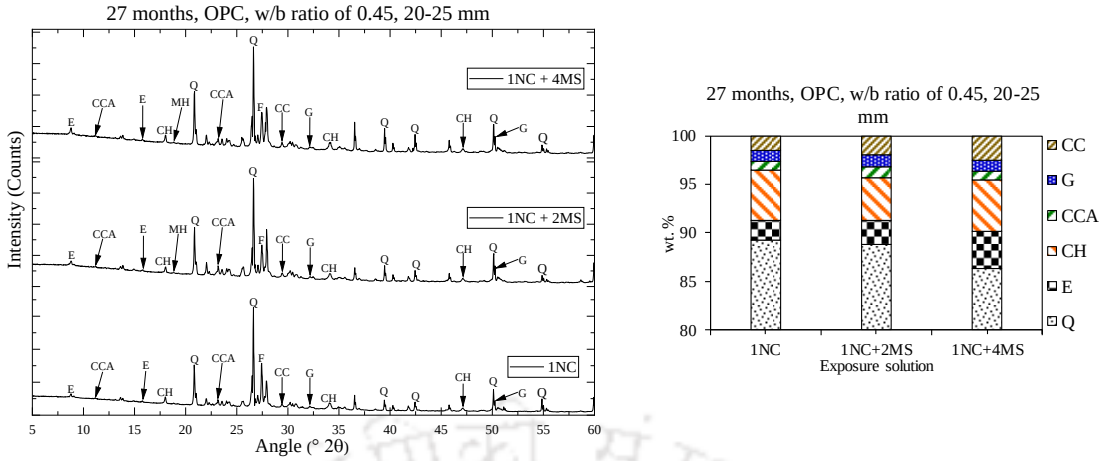

Figure B19 XRD patterns and wt. % of compounds of concrete at a depth interval of 20-25 mm (near rebar) from the surface for OPC at w/b ratio of 0.45 and subjected to 1% NaCl and 1% NaCl with $MgSO_4$ solutions for 27 months

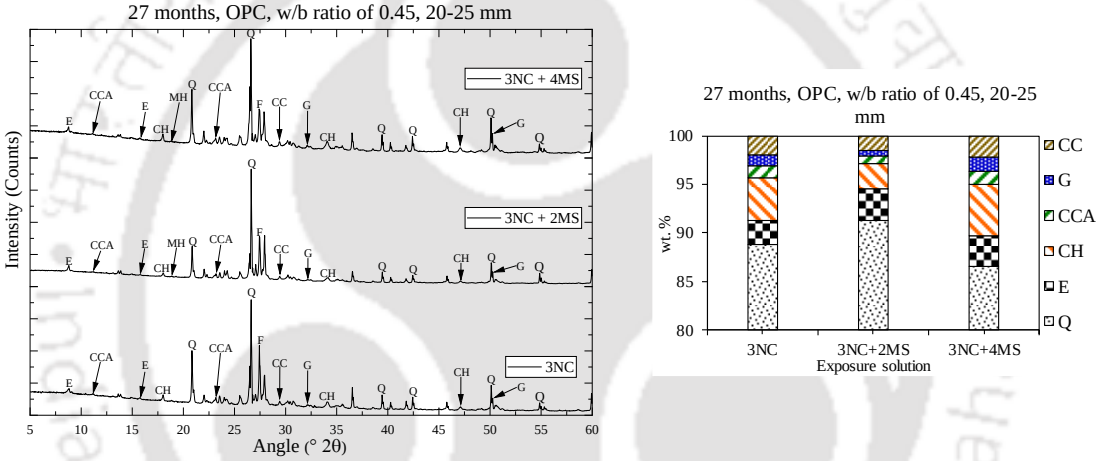

Figure B20 XRD patterns and wt. % of compounds of concrete at a depth interval of 20-25 mm (near rebar) from the surface for OPC at w/b ratio of 0.45 and subjected to 3% NaCl and 3% NaCl with $MgSO_4$ solutions for 27 months

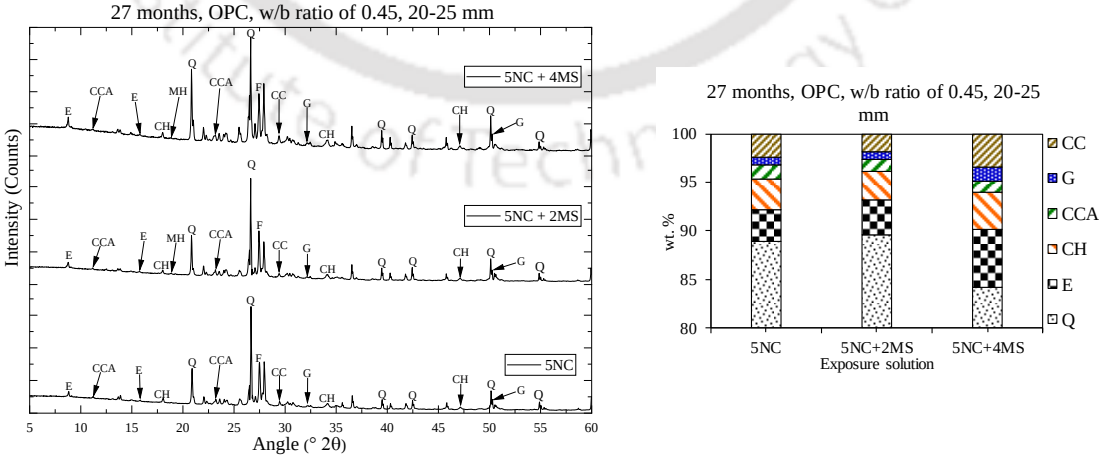

Figure B21 XRD patterns and wt. % of compounds of concrete at a depth interval of 20-25 mm (near rebar) from the surface for OPC at w/b ratio of 0.45 and subjected to 5% NaCl and 5% NaCl with $MgSO_4$ solutions for 27 months

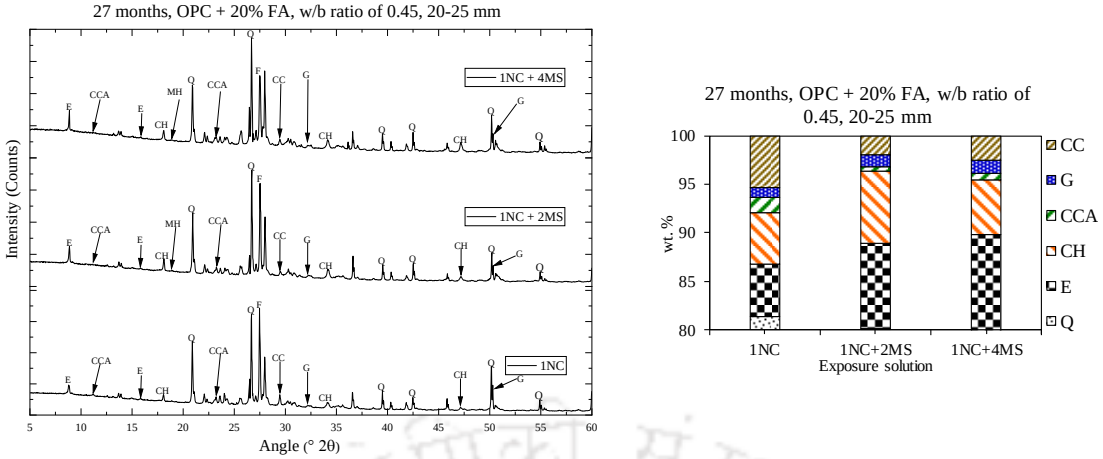

Figure B22 XRD patterns and wt. % of compounds of concrete at a depth interval of 20-25 mm (near rebar) from the surface for OPC + 20% FA at w/b ratio of 0.45 and subjected to 1% NaCl and 1% NaCl with $MgSO_4$ solutions for 27 months

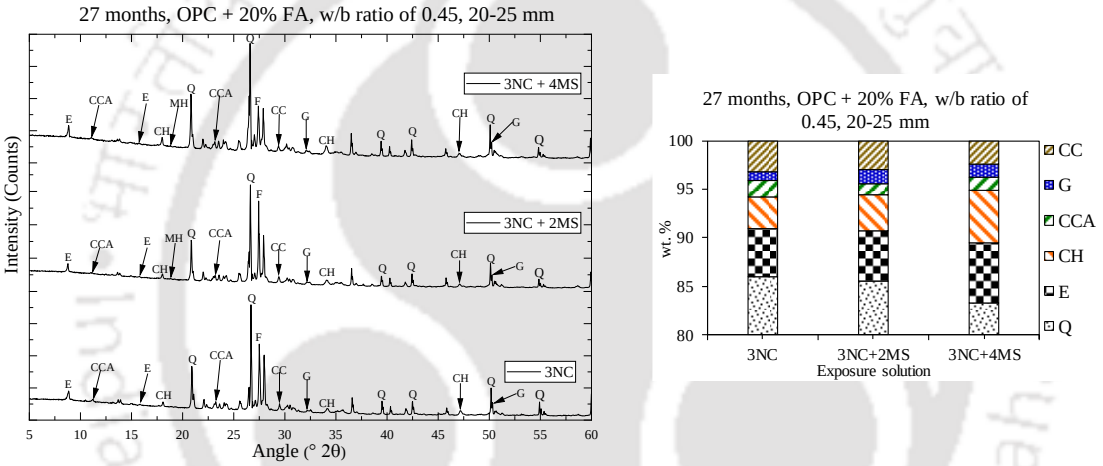

Figure B23 XRD patterns and wt. % of compounds of concrete at a depth interval of 20-25 mm (near rebar) from the surface for OPC + 20% FA at w/b ratio of 0.45 and subjected to 3% NaCl and 3% NaCl with $MgSO_4$ solutions for 27 months

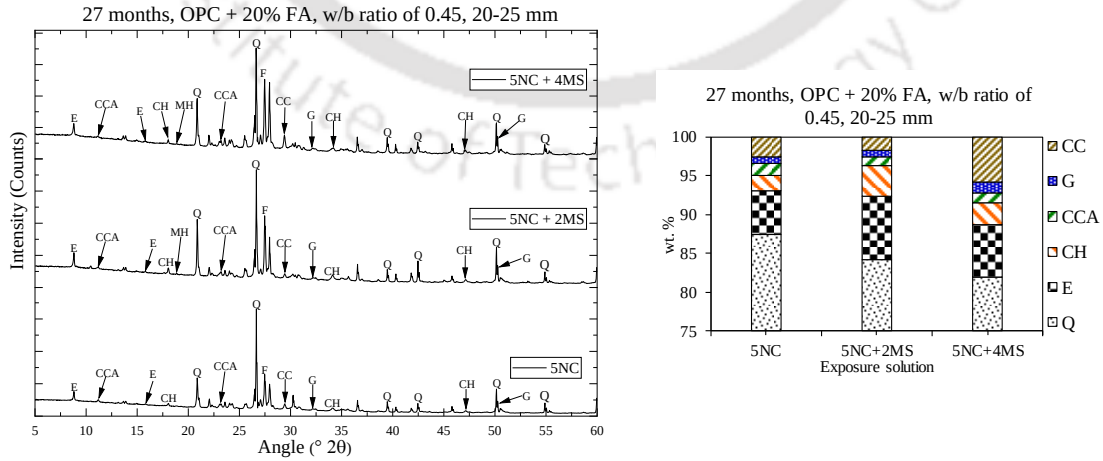

Figure B24 XRD patterns and wt. % of compounds of concrete at a depth interval of 20-25 mm (near rebar) from the surface for OPC + 20% FA at w/b ratio of 0.45 and subjected to 5% NaCl and 5% NaCl with $MgSO_4$ solutions for 27 months

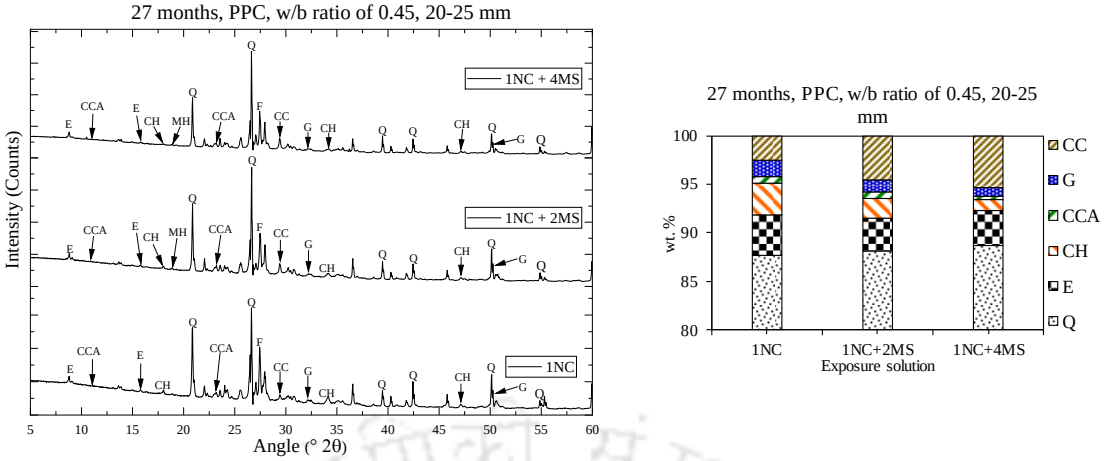

Figure B25 XRD patterns and wt. % of compounds of concrete at a depth interval of 20-25 mm (near rebar) from the surface for PPC at w/b ratio of 0.45 and subjected to 1% NaCl and 1% NaCl with $MgSO_4$ solutions for 27 months

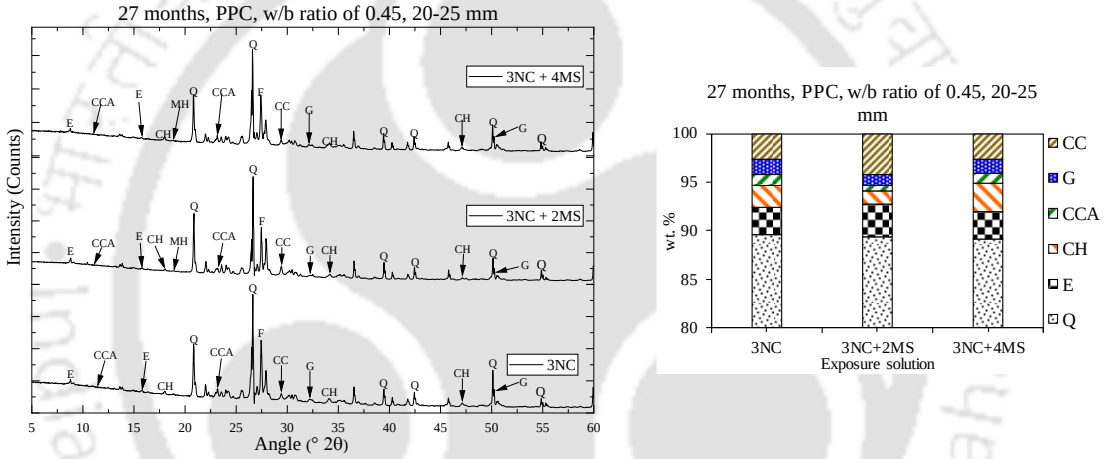

Figure B26 XRD patterns and wt. % of compounds of concrete at a depth interval of 20-25 mm (near rebar) from the surface for PPC at w/b ratio of 0.45 and subjected to 3% NaCl and 3% NaCl with $MgSO_4$ solutions for 27 months

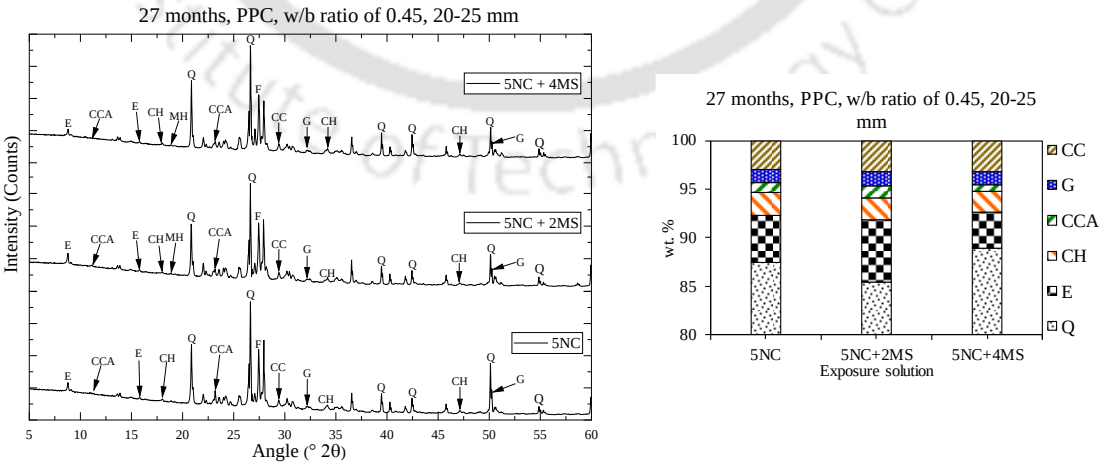

Figure B27 XRD patterns and wt. % of compounds of concrete at a depth interval of 20-25 mm (near rebar) from the surface for PPC at w/b ratio of 0.45 and subjected to 5% NaCl and 5% NaCl with $MgSO_4$ solutions for 27 months

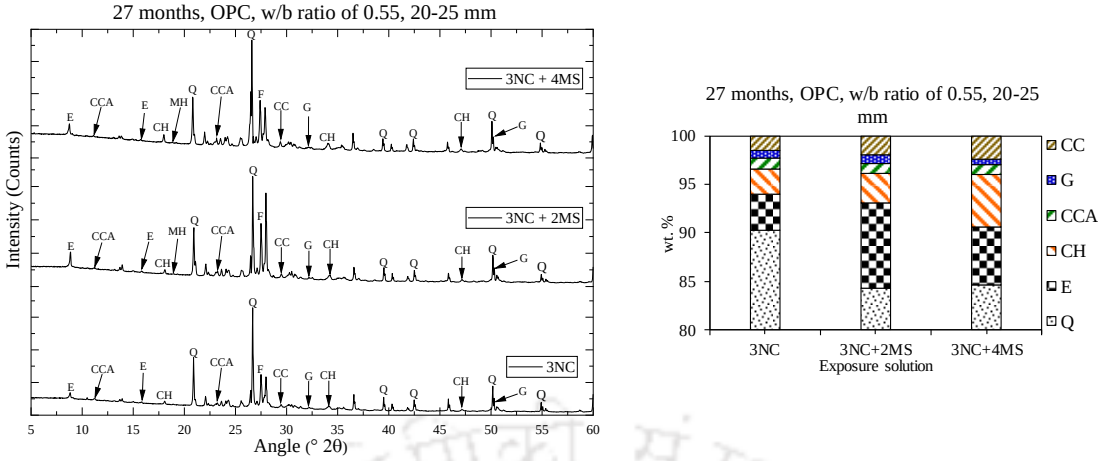

Figure B28 XRD patterns and wt. % of compounds of concrete at a depth interval of 20-25 mm (near rebar) from the surface for OPC at w/b ratio of 0.55 and subjected to 3% NaCl and 3% NaCl with $MgSO_4$ solutions for 27 months

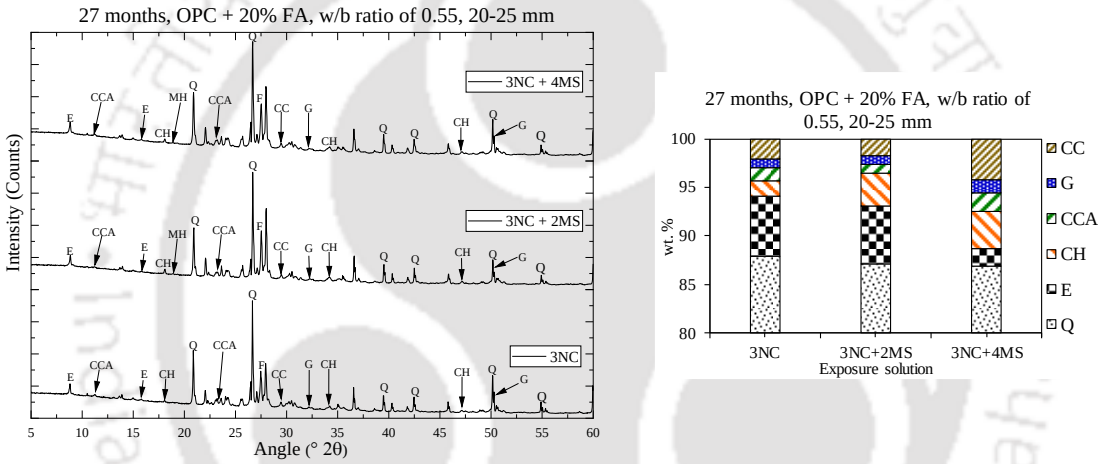

Figure B29 XRD patterns and wt. % of compounds of concrete at a depth interval of 20-25 mm (near rebar) from the surface for OPC + 20% FA at w/b ratio of 0.55 and subjected to 3% NaCl and 3% NaCl with $MgSO_4$ solutions for 27 months

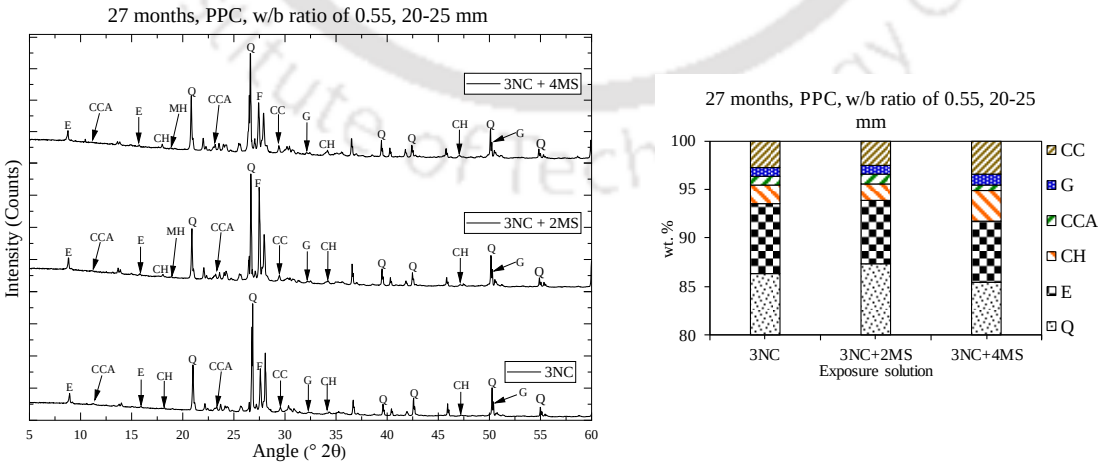

Figure B28 XRD patterns and wt. % of compounds of concrete at a depth interval of 20-25 mm (near rebar) from the surface for PPC at w/b ratio of 0.55 and subjected to 3% NaCl and 3% NaCl with $MgSO_4$ solutions for 27 months

LIST OF PUBLICATIONS

Journals

1. **Arya Anuj Jee** and Bulu Pradhan, Study on development of empirical relationships between durability parameters of concrete made with different types of binder and exposed to chloride environment, *Construction and Building Materials*, vol. 212, pp 799-817, 2019.

Book Chapters

1. **Arya Anuj Jee** and Bulu Pradhan, Durability of fly ash added reinforced concrete in chloride and composite chloride-sulfate environment. In *Recent Advances in Structural Engineering, Volume 1 (pp. 773-785).* Springer, Singapore, 2019.
2. **Arya Anuj Jee** and Bulu Pradhan, Chloride ingress in concrete: effect of mix parameters, heating condition and exposure solution, *International Conference on Advances in Civil Engineering and Sustainable Construction* (pp. 23-29) RILEM publications SARL, *2016.*

Conference

1 Smrati Jain, **Arya Anuj Jee** and Bulu Pradhan, Application of modern techniques to evaluate microstructure of concrete, *International Conference on Sophisticated Instruments in Modern Research, ICSIMR-2017*, IIT Guwahati, June 30 -July 1, 2017.

2 **Arya Anuj Jee** and Bulu Pradhan, Performance of pozzolana blended cement vis-à-vis ordinary Portland cement against chloride ingress in concrete, *UKIERI Concrete Congress*, Jalandhar, *November 2-5, 2015*.